CONTENTS BY TOPIC INDEX TO VOLUME 16

This table is a cumulative topical listing of all the articles contained in Volume 16. The topics are arranged in alphabetical order so that papers dealing with the same subjects are grouped together. Each article may be listed under a maximum of three topics.

Acoustic emission

Characteristics of elastic waves generated by crack initiation in aluminum alloys under fatigue loading . . . Kiwoo Nam *et al.* 1745

Adhesion

Strongly adhering and thick highly tetrahedral amorphous carbon (ta–C) thin films via surface modification by implantation . . . M. Chhowalla *et al.* 5
Adhesion of benzocyclobutene-passivated silicon in epoxy layered structures . . . Robert J. Hohlfelder *et al.* 243
Evaluation of the modified edge lift-off test for adhesion characterization in microelectronic multifilm applications . . . Jack C. Hay *et al.* 385
Molecular dynamics analysis of adhesion strength of interfaces between thin films . . . T. Iwasaki *et al.* 1789

Adhesives

Piezoelectric actuation of crack growth along polymer–metal interfaces in adhesive bonds . . . Tianbao Du *et al.* 2885

Adsorption

Spectroscopic study of a cryptomelane-type manganic acid exchanged by divalent transition-metal cations . . . Masamichi Tsuji *et al.* 108
Comparison of hydrophilic properties of amorphous TiO_x films obtained by radio frequency sputtering and plasma-enhanced chemical vapor deposition . . . Masatoshi Nakamura *et al.* 621

Aerogel

Effect of material properties on integration damage in organosilicate glass films . . . E. Todd Ryan *et al.* 3335

Aging

Infrared optical properties of aged porous GaAs . . . S. Zangooie *et al.* 1241
Water-associated surface degradation of $CsLiB_6O_{10}$ crystal during harmonic generation in the ultraviolet region . . . Yukihiro Morimoto *et al.* 2082
Effects of static thermal aging and thermal cycling on the microstructure and shear strength of $Sn_{95.5}Ag_{3.8}Cu_{0.7}$ solder joints . . . Shawkret Ahat *et al.* 2914

Alloys

Precipitation of icosahedral phase from amorphous $Zr_{65}Cu_{17.5-x}Al_{7.5}Ni_{10}Ag_x$ ($x = 0, 5$) alloys . . . J.K. Lee *et al.* 1311
^{18}O study of the oxidation of reactively sputtered $Ti_{1-x}Al_xN$ barrier . . . M.C. Hugon *et al.* 2591

Alloys, intermetallic

Raman spectroscopic determination of phase evolutions in $LiAl_xCo_{1-x}O_2$ battery materials . . . P.S. Dobal *et al.* 1
The healing of quenched crack in 1045 steel under electropulsing . . . Zhou Yizhou *et al.* 17
Thermal analysis investigation of hydriding properties of nanocrystalline Mg–Ni- and Mg–Fe-based alloys prepared by high-energy ball milling . . . L.E.A. Berlouis *et al.* 45
Formation of intermetallic compounds at eutectic Sn–Zn–Al solder/Cu interface . . . Shan-Pu Yu *et al.* 76
Synthesis and processing of nanocrystalline Ag–Fe–Ni for low thermal expansion–high conductivity thermal management applications . . . J. Stolk *et al.* 340
Site preference of alloying elements in Fe_3Al-based alloys . . . Xiao Dong Ni *et al.* 344
Grain boundary structure in Al–Mg and Al–Mg–Sc alloys after equal-channel angular pressing . . . Keiichiro Oh-ishi *et al.* 583
Magnetic properties, domain structure, and microstructure of anisotropic $SmCo_{6.5}Zr_{0.5}$ ribbons with C addition . . . A-Ru Yan *et al.* 629
Microstructural studies of Cu brazing on AlN . . . Chaoxian Cai *et al.* 670
Effects of preparation processes on structure and magnetic properties of $Nd_2Fe_{14}B/\alpha$–Fe-type nanocomposite magnets . . . Bao-zhi Cui *et al.* 709
Surface studies of phase formation in Co–Ge system: Reactive deposition epitaxy versus solid-phase epitaxy . . . I. Goldfarb *et al.* 744
Tensile fracture during transformation superplasticity of Ti–6Al–4V . . . C. Schuh *et al.* 865
Multifunctional microtruss laminates: Textile synthesis and properties . . . D.J. Sypeck *et al.* 890
Effects of pressure on the solidification of Al–Mn alloy . . . Duanwei He *et al.* 910
Grain growth behavior of a nanostructured 5083 Al–Mg alloy . . . V.L. Tellkamp *et al.* 938
Synthesis of open-cell metal foams by templated directed vapor deposition . . . Douglas T. Queheillalt *et al.* 1028
On some discrepancies in the literature about the formation of icosahedral quasi-crystal in Al–Cu–Fe alloys . . . Jianian Gui *et al.* 1037
Synthesis of $Nd_2Fe_{14}B$ powders by spray-drying and reduction–diffusion processes . . . X.L. Dong *et al.* 1083
Finite element modeling of microscale thermal residual stresses in Al interconnects . . . A. Saerens *et al.* 1112
Orientation dependence of Portevin–Le Châtelier plastic instabilities in depth-sensing microindentation . . . Zs. Kovács *et al.* 1171
Precipitation of icosahedral quasicrystalline phase in $Hf_{69.5}Al_{7.5}Ni_{11}Cu_{12}$ metallic glass . . . Chunfei Li *et al.* 1190
Effects of Cu and Ni additions to eutectic Pb–Sn solders on Au embrittlement of solder interconnections . . . Jong-Hyun Lee *et al.* 1249
Mechanochemistry of the titanium–silicon system: Compositional effects . . . S. Doppiu *et al.* 1266

CONTENTS BY TOPIC INDEX TO VOLUME 16

This table is a cumulative topical listing of all the articles contained in Volume 16. The topics are arranged in alphabetical order so that papers dealing with the same subjects are grouped together. Each article may be listed under a maximum of three topics.

Acoustic emission

Characteristics of elastic waves generated by crack initiation in aluminum alloys under fatigue loading . . . Kiwoo Nam *et al.* 1745

Adhesion

Strongly adhering and thick highly tetrahedral amorphous carbon (ta–C) thin films via surface modification by implantation . . . M. Chhowalla *et al.* 5
Adhesion of benzocyclobutene-passivated silicon in epoxy layered structures . . . Robert J. Hohlfelder *et al.* 243
Evaluation of the modified edge lift-off test for adhesion characterization in microelectronic multifilm applications . . . Jack C. Hay *et al.* 385
Molecular dynamics analysis of adhesion strength of interfaces between thin films . . . T. Iwasaki *et al.* 1789

Adhesives

Piezoelectric actuation of crack growth along polymer–metal interfaces in adhesive bonds . . . Tianbao Du *et al.* 2885

Adsorption

Spectroscopic study of a cryptomelane-type manganic acid exchanged by divalent transition-metal cations . . . Masamichi Tsuji *et al.* 108
Comparison of hydrophilic properties of amorphous TiO_x films obtained by radio frequency sputtering and plasma-enhanced chemical vapor deposition . . . Masatoshi Nakamura *et al.* 621

Aerogel

Effect of material properties on integration damage in organosilicate glass films . . . E. Todd Ryan *et al.* 3335

Aging

Infrared optical properties of aged porous GaAs . . . S. Zangooie *et al.* 1241
Water-associated surface degradation of $CsLiB_6O_{10}$ crystal during harmonic generation in the ultraviolet region . . . Yukihiro Morimoto *et al.* 2082
Effects of static thermal aging and thermal cycling on the microstructure and shear strength of $Sn_{95.5}Ag_{3.8}Cu_{0.7}$ solder joints . . . Shawkret Ahat *et al.* 2914

Alloys

Precipitation of icosahedral phase from amorphous $Zr_{65}Cu_{17.5-x}Al_{7.5}Ni_{10}Ag_x$ ($x = 0, 5$) alloys . . . J.K. Lee *et al.* 1311
^{18}O study of the oxidation of reactively sputtered $Ti_{1-x}Al_xN$ barrier . . . M.C. Hugon *et al.* 2591

Alloys, intermetallic

Raman spectroscopic determination of phase evolutions in $LiAl_xCo_{1-x}O_2$ battery materials . . . P.S. Dobal *et al.* 1
The healing of quenched crack in 1045 steel under electropulsing . . . Zhou Yizhou *et al.* 17
Thermal analysis investigation of hydriding properties of nanocrystalline Mg–Ni- and Mg–Fe-based alloys prepared by high-energy ball milling . . . L.E.A. Berlouis *et al.* 45
Formation of intermetallic compounds at eutectic Sn–Zn–Al solder/Cu interface . . . Shan-Pu Yu *et al.* 76
Synthesis and processing of nanocrystalline Ag–Fe–Ni for low thermal expansion–high conductivity thermal management applications . . . J. Stolk *et al.* 340
Site preference of alloying elements in Fe_3Al-based alloys . . . Xiao Dong Ni *et al.* 344
Grain boundary structure in Al–Mg and Al–Mg–Sc alloys after equal-channel angular pressing . . . Keiichiro Oh-ishi *et al.* 583
Magnetic properties, domain structure, and microstructure of anisotropic $SmCo_{6.5}Zr_{0.5}$ ribbons with C addition . . . A-Ru Yan *et al.* 629
Microstructural studies of Cu brazing on AlN . . . Chaoxian Cai *et al.* 670
Effects of preparation processes on structure and magnetic properties of $Nd_2Fe_{14}B/\alpha$–Fe-type nanocomposite magnets . . . Bao-zhi Cui *et al.* 709
Surface studies of phase formation in Co–Ge system: Reactive deposition epitaxy versus solid-phase epitaxy . . . I. Goldfarb *et al.* 744
Tensile fracture during transformation superplasticity of Ti–6Al–4V . . . C. Schuh *et al.* 865
Multifunctional microtruss laminates: Textile synthesis and properties . . . D.J. Sypeck *et al.* 890
Effects of pressure on the solidification of Al–Mn alloy . . . Duanwei He *et al.* 910
Grain growth behavior of a nanostructured 5083 Al–Mg alloy . . . V.L. Tellkamp *et al.* 938
Synthesis of open-cell metal foams by templated directed vapor deposition . . . Douglas T. Queheillalt *et al.* 1028
On some discrepancies in the literature about the formation of icosahedral quasi-crystal in Al–Cu–Fe alloys . . . Jianian Gui *et al.* 1037
Synthesis of $Nd_2Fe_{14}B$ powders by spray-drying and reduction–diffusion processes . . . X.L. Dong *et al.* 1083
Finite element modeling of microscale thermal residual stresses in Al interconnects . . . A. Saerens *et al.* 1112
Orientation dependence of Portevin–Le Châtelier plastic instabilities in depth-sensing microindentation . . . Zs. Kovács *et al.* 1171
Precipitation of icosahedral quasicrystalline phase in $Hf_{69.5}Al_{7.5}Ni_{11}Cu_{12}$ metallic glass . . . Chunfei Li *et al.* 1190
Effects of Cu and Ni additions to eutectic Pb–Sn solders on Au embrittlement of solder interconnections . . . Jong-Hyun Lee *et al.* 1249
Mechanochemistry of the titanium–silicon system: Compositional effects . . . S. Doppiu *et al.* 1266

Quasicrystalline phase formation in $Al_{62}Cu_{22.5}Fe_{12.5}$ and $Al_{55}Cu_{22.5}Fe_{12.5}Be_7$ alloys . . . S.M. Lee *et al.* 1535
A combinatorial approach for efficient mapping of phase diagrams and properties . . . Ji-Cheng Zhao 1565
Corrosive wear of the Co–Cr–W alloy in liquid zinc . . . Xibao Wang *et al.* 1585
Submicron-grained multiphase TiAlSi alloys: Processing, characterization, and microstructural design . . . R. Bohn *et al.* 1850
Novel hexagonal structure and ultrahigh strength of magnesium solid solution in the Mg–Zn–Y system . . . Akihisa Inoue *et al.* 1894
Microstructural characterization of rapidly solidified Al–Fe–Si, Al–V–Si, and Al–Fe–V–Si alloys . . . A.K. Srivastava *et al.* 2103
Effect of a magnetic field on phase transformation of steel . . . W. Liu *et al.* 2280
Site preference determination in intermetallic compounds by thermal conductivity measurement . . . Yoshihiro Terada *et al.* 2314
Hardness–depth profile of a carbon-implanted Ti–6Al–4V alloy and its relation to composition and microstructure . . . M. Kunert *et al.* 2321
Transient self-dewetting of steels after pulsed electron beam melting . . . N. Mingolo *et al.* 2343
Formation of eutectic RuAl/Ru nanocomposite by mechanical alloying and subsequent annealing . . . K.W. Liu *et al.* 2459
Effect of lead content on vibration fracture behavior of Pb–Sn eutectic solder . . . C.M. Chuang *et al.* 2644
Formation rule for Al-based ternary quasi-crystals: Example of Al–Ni–Fe decagonal phase . . . Jian-Bing Qiang *et al.* 2653
Development of a model for the prediction of the fretting fatigue regimes . . . T.E. Matikas *et al.* 2716
Development of nanocrystalline structure during cryomilling of Inconel 625 . . . Jianhong He *et al.* 2724
Plate domain structure of sintered NdFeB magnets and dependence on compacting mode . . . Zhen Rong Zhang *et al.* 2992
Single-crystal growth of the Al–Cu–Fe icosahedral quasicrystal from the ternary melt . . . J.Q. Guo *et al.* 3038
Preparation of superfine Fe-base alloy by liquidus casting . . . X.F. Pan *et al.* 3459
Origin of the anomalous volume expansion in Al–Si alloys above liquidus . . . W.M. Wang *et al.* 3592

Alloys, semiconductor

Optical and electrical properties of $Ge_{10+x}Se_{40}Te_{50-x}$ thin film . . . S.A. Fayek *et al.* 1549
Development of *p*-type microcrystalline silicon carbon alloy films by the very high frequency plasma-enhanced chemical vapor deposition technique . . . Tapati Jana *et al.* 2130
Effect of *in situ* boron doping on properties of silicon germanium films deposited by chemical vapor deposition at 400 °C . . . Sherif Sedky *et al.* 2607

Aluminum alloy

Characteristics of elastic waves generated by crack initiation in aluminum alloys under fatigue loading . . . Kiwoo Nam *et al.* 1745

Amorphous

Comparison of hydrophilic properties of amorphous TiO_x films obtained by radio frequency sputtering and plasma-enhanced chemical vapor deposition . . . Masatoshi Nakamura *et al.* 621
Precipitation of icosahedral phase from amorphous $Zr_{65}Cu_{17.5-x}Al_{7.5}Ni_{10}Ag_x$ (x = 0, 5) alloys . . . J.K. Lee *et al.* 1311
Entrapment of organosilicon molecules in nonhydrolytic alumina gels and thermal behavior of the resulting composite . . . G.S. Grader *et al.* 1413
Kinetic analysis of solid-state processes . . . Jiří Málek *et al.* 1862
Anelastic behavior of precursor-derived amorphous ceramics in the system Si–B–C–N . . . Martin Christ *et al.* 1994

Annealing

Formation of intermetallic compounds at eutectic Sn–Zn–Al solder/Cu interface . . . Shan-Pu Yu *et al.* 76
Microstructure of (Nd, Eu, Gd)-123 matrix with (Nd, Eu, Gd)-211 inclusions . . . M. Muralidhar *et al.* 407
In situ transmission electron microscopy study of the silicidation process in Co thin films on patterned (001) Si substrates . . . C. Ghica *et al.* 701
Crystallization kinetics of amorphous nanostructured $Pd_{40.5}Ni_{40.5}P_{19}$ alloys . . . H.W. Ngai *et al.* 797
Influence of annealing treatments on microstructure and toughness of liquid-phase-sintered silicon carbide . . . D. Sciti *et al.* 806
Phenomenological description of grain growth stagnation for nanocrystalline films and powders . . . Rand Dannenberg *et al.* 1090
Effect of hydrogen on true leakage current characteristics of $(Pb,La)(Zr,Ti)O_3$ thin-film capacitors with Pt- or Ir-based top electrodes . . . Soon-Gil Yoon *et al.* 1185
Optimization of the annealing process for the $(Ba,Sr)TiO_3$ thin films grown by low-temperature (420 °C) metalorganic chemical vapor deposition . . . Jaehoo Park *et al.* 1363
Intrinsic microcrystalline silicon by postgrowth anneals . . . Jong-Hwan Yoon 1531
Devitrification kinetics and mechanism of Pyrex borosilicate glass . . . Jau-Ho Jean *et al.* 1752
Effects of thermal annealing on the texture of $La_{0.67}Sr_{0.33}MnO_3$ thin films . . . Lamartine Meda *et al.* 1887
Effect of a magnetic field on phase transformation of steel . . . W. Liu *et al.* 2280
Formation of eutectic RuAl/Ru nanocomposite by mechanical alloying and subsequent annealing . . . K.W. Liu *et al.* 2459
Optical and electrochromic properties of heated and annealed MoO_3 thin films . . . Zahid Hussain 2695
Effects of static thermal aging and thermal cycling on the microstructure and shear strength of $Sn_{95.5}Ag_{3.8}Cu_{0.7}$ solder joints . . . Shawkret Ahat *et al.* 2914
Oxygen transport during annealing of $Pb(Zr,Ti)O_3$ thin films in O_2 gas and its effect on their conductivity . . . F. Ayguavives *et al.* 3005

	Structural and electrical properties of strontium barium niobate thin films crystallized by conventional furnace and rapid-thermal annealing process . . . R.G. Mendes *et al.*	3009
	Thermal stability of carbon nitride thin films . . . Niklas Hellgren *et al.*	3188
	Wetting of mullite by Y_2O_3–Al_2O_3–SiO_2 and B_2O_3–SiO_2 glasses . . . T.S. Huang *et al.*	3223
	Impacts of postannealing ambient atmospheres on Pt /$SrBi_{2.2}Ta_2O_9$/Pt capacitors . . . Ai-Dong Li *et al.*	3526
	Scanning probe microscopy generated out-of-plane deformation maps exhibiting heterogeneous nanoscale deformation resulting from thermal cycling of Cu–polyimide damascene interconnects . . . Todd S. Gross *et al.*	3560
Atomic diffusion	Redistribution behavior of constitutional elements at an initial crystallization stage in the $Zr_{65}Al_{7.5}Ni_{10}Cu_{17.5}$ glassy alloy . . . J. Saida *et al.*	28
Atomic force microscopy (AFM)		
	Development of a continuous microscratch technique in an atomic force microscope and its application to study scratch resistance of ultrathin hard amorphous carbon coatings . . . Sriram Sundararajan *et al.*	437
	In situ microscopic surface characterization studies of polymeric thin films during tensile deformation using atomic force microscopy . . . M.S. Bobji *et al.*	844
	Direct measurement of plowing friction and wear of a polymer thin film using the atomic force microscope . . . Binyang Du *et al.*	1487
Attrition	Mechanochemistry of the titanium–silicon system: Compositional effects . . . S. Doppiu *et al.*	1266
	Submicron-grained multiphase TiAlSi alloys: Processing, characterization, and microstructural design . . . R. Bohn *et al.*	1850
	Development of nanocrystalline structure during cryomilling of Inconel 625 . . . Jianhong He *et al.*	2724
Biological materials	Model for the robust mechanical behavior of nacre . . . A.G. Evans *et al.*	2475
	Deformation mechanisms in nacre . . . R.Z. Wang *et al.*	2485
Biological synthesis	Biomimetic model of a sponge-spicular optical fiber—mechanical properties and structure . . . M. Sarikaya *et al.*	1420
Biomedical materials	Strongly adhering and thick highly tetrahedral amorphous carbon (ta–C) thin films via surface modification by implantation . . . M. Chhowalla *et al.*	5
	Rheological characteristics of slurry controlling the microstructure and the compressive strength behavior of biomimetic hydroxyapatite . . . S. Guicciardi *et al.*	163
	Machinable calcium pyrophosphate glass-ceramics . . . Toshihiro Kasuga *et al.*	876
	Mechanochemical-hydrothermal preparation of crystalline hydroxyapatite powders at room temperature . . . Pavel Shuk *et al.*	1231
	Textural properties of $SiO_2 \cdot CaO \cdot P_2O_5$ glasses prepared by the sol-gel method . . . F. Balas *et al.*	1345
	Cracking of porcelain coatings bonded to metal substrates of different modulus and hardness . . . Hong Zhao *et al.*	1471
	Phase transformation effects on the wear properties of alumina gel–polymer matrix nanocomposites . . . Jiazhong Luo *et al.*	1680
	Comparison of crystal structure parameters of natural and synthetic apatites from neutron powder diffraction . . . Th. Leventouri *et al.*	2600
	Processing and characterization of hydroxyapatite coatings on titanium produced by magnetron sputtering . . . T.G. Nieh *et al.*	3238
Bonding	Microstructural studies of Cu brazing on AlN . . . Chaoxian Cai *et al.*	670
	Stability of channels at a scalloplike Cu_6Sn_5 layer in solder interconnections . . . Jong-Hyun Lee *et al.*	1227
	Microstructure and growth of joins in melt-textured $YBa_2Cu_3O_{7-\delta}$ . . . A.D. Bradley *et al.*	2298
Brittle materials	Shear-activated indentation crack in GaAs single crystal . . . Z.C. Li *et al.*	2845
Casting	Formation and properties of $Zr_{48}Nb_8Fe_8Cu_{12}Be_{24}$ bulk metallic glass . . . Yong Zhang *et al.*	1675
	Formation and mechanical properties of Cu–Hf–Ti bulk glassy alloys . . . Akihisa Inoue *et al.*	2836
	Preparation of superfine Fe-base alloy by liquidus casting . . . X.F. Pan *et al.*	3459
Catalytic materials	Optical and structural properties of solid oxide photocatalyst Bi_2FeNbO_7 . . . Zhigang Zou *et al.*	35
	Sol-gel-derived photosensitive TiO_2 and Cu/TiO_2 using homogeneous hydrolysis technique . . . Jeffrey C.S. Wu *et al.*	615
	Photocatalytic activity of TiO_2 prepared at low temperature by a photo-assisted sol-gel method . . . Zi-sheng Guan *et al.*	907
	Combinatorial synthesis of oxide powders . . . H.M. Reichenbach *et al.*	967
	Electrolyte electroreflectance study of TiO_2 films modified with metal nanoparticles . . . A.I. Kulak *et al.*	2357
	Effects of zinc(II) and iron(III) doping of titania films on their photoreactivity to decompose rhodamine B . . . Ying Ma *et al.*	2928
	Processing of mesoporous alumina from a powder precursor . . . J. Wayne Frazee *et al.*	3262
	Hydrodynamic cavitation as a tool to control macro-, micro-, and nano-properties of inorganic materials . . . J. Find *et al.*	3503
	Preparation of nanocrystalline nickel oxide–yttria-stabilized zirconia composite powder by solution combustion with ignition of glycine fuel . . . Sun-Jae Kim *et al.*	3621

Cellular

Patterning of copper particles on polymeric surface . . . . . Arvind Sinha *et al.* **1354**
Solid-state foaming of titanium by superplastic expansion of argon-filled pores . . . . . N.G. Davis *et al.* **1508**
Gradient porosity poly(dicyclopentadiene) . . . . . A. Della Martina *et al.* **2045**

Ceramics

High-strength porous silicon nitride fabricated by the sinter-forging technique . . . . . Naoki Kondo *et al.* **32**
Optical and structural properties of solid oxide photocatalyst Bi_2FeNbO_7 . . . . . Zhigang Zou *et al.* **35**
Macroporous morphology of titania films prepared by sol-gel dip-coating method from a system containing poly(ethylene glycol) and poly(vinylpyrrolidone) . . . . . Koichi Kajihara *et al.* **58**
Enhanced crystallization and phase transformation of amorphous silicon nitride under high pressure . . . . . Ya-Li Li *et al.* **67**
Structure and dielectric properties of pyrochlore–fluorite biphase ceramics in the Bi_2O_3–ZnO–Nb_2O_5 system . . . . . Hong Wang *et al.* **83**
Modeling of wave configuration during electrically ignited combustion synthesis . . . . . O.A. Graeve *et al.* **93**
Spectroscopic study of a cryptomelane-type manganic acid exchanged by divalent transition-metal cations . . . . . Masamichi Tsuji *et al.* **108**
Improvement in oxidation resistance of TiB_2 by formation of protective SiO_2 layer on surface . . . . . Young-Hag Koh *et al.* **132**
Rheological characteristics of slurry controlling the microstructure and the compressive strength behavior of biomimetic hydroxyapatite . . . . . S. Guicciardi *et al.* **163**
Preparation of calcium strontium hydroxyapatites by a new route involving calcium phosphate cements . . . . . L. Leroux *et al.* **171**
Analysis of defect formation in Nb-doped $SrTiO_3$ by impedance spectroscopy . . . . . Seong-Ho Kim *et al.* **192**
$BaTiO_3$ formation by thermal decomposition of a (BaTi)-citrate polyester resin in air . . . . . P. Durán *et al.* **197**
Residual stress in fiber-textured thin films of cubic materials . . . . . P. Scardi *et al.* **233**
Dependence of dielectric and piezoelectric properties on film thickness for highly {100}-oriented lead magnesium niobate–lead titanate (70/30) thin films . . . . . Jeong Hwan Park *et al.* **268**
Sintering and microstructure of glass-coated nanocrystalline yttria-stabilized tetragonal zirconia powder: Effect of the glass . . . . . R. Ramamoorthy *et al.* **296**
Ferroelectric property of epitaxial $Bi_4Ti_3O_{12}$ films prepared by metalorganic chemical vapor deposition . . . . . Takayuki Watanabe *et al.* **303**
Dense, bubble-free ceramic deposits from aqueous suspensions by electrophoretic deposition . . . . . Tetsuo Uchikoshi *et al.* **321**
Erbium doping into lithium niobate and sapphire single crystal wafers . . . . . P. Nekvindova *et al.* **333**
Investigation of some phenomena occurring during continuous ink-jet printing of ceramics . . . . . B.Y. Tay *et al.* **373**
Valence variations in titanium-based perovskite oxides by high-pressure and high-temperature method . . . . . Liping Li *et al.* **417**
Improved tensile creep properties of yttrium- and lanthanum-doped alumina: a solid solution effect . . . . . Junghyun Cho *et al.* **425**
Development of a continuous microscratch technique in an atomic force microscope and its application to study scratch resistance of ultrathin hard amorphous carbon coatings . . . . . Sriram Sundararajan *et al.* **437**
Phase-transformation kinetics in triphasic cordierite gel . . . . . R. Petrović *et al.* **451**
Densification and grain growth of Al-doped ZnO . . . . . Jiaping Han *et al.* **459**
Characterization of bond formation in SiC and Si_3N_4 implanted with Ti, Fe, and Co . . . . . Didier Zanghi *et al.* **512**
Silica particle growth in metastable supersaturation solution . . . . . Kyung-Soo Kim *et al.* **545**
Nonepitaxial heterogeneous nucleation of α-sialon in the Ca-doped system . . . . . Ya-Wen Li *et al.* **578**
Preferred orientation of beta-phase and its mechanisms in a fine-grained silicon-nitride-based ceramic . . . . . Rong-Jun Xie *et al.* **590**
Deposition of epitaxial transition metal carbide films and superlattices by simultaneous direct current metal magnetron sputtering and C_{60} evaporation . . . . . H. Högberg *et al.* **633**
Sol-gel synthesis and the effect of boron addition on the phosphorescent properties of $SrAl_2O_4:Eu^{2+},Dy^{3+}$ phosphors . . . . . I-Cherng Chen *et al.* **644**
Influence of CaO–SiO_2 ratio on the chemistry of intergranular films in liquid-phase sintered alumina and implications for rate of erosive wear . . . . . Rik Brydson *et al.* **652**
Thermodynamic stability of tetragonal zirconia nanocrystallites . . . . . Nae-Lih Wu *et al.* **666**
Thermal conductivity and thermal diffusivity of selected oxide single crystals . . . . . A. Stanimirovic *et al.* **678**
Transient creep in fine-grained polycrystalline Al_2O_3 with Lu^{3+} ion segregation at the grain boundaries . . . . . Hidehiro Yoshida *et al.* **716**
Synthesis and properties of $B_xC_yN_z$ coatings . . . . . M.N. Oliveira *et al.* **734**
Low-temperature fabrication of pyroelectric $Ba_{0.8}Sr_{0.2}TiO_3$ thin films by a sol-gel process . . . . . Jian-Gong Cheng *et al.* **778**
Magnetotransport properties of $La_{0.7}Ca_{0.3}MnO_3$ thick films prepared by spray pyrolysis . . . . . F. Damay *et al.* **784**
Influence of annealing treatments on microstructure and toughness of liquid-phase-sintered silicon carbide . . . . . D. Sciti *et al.* **806**
Effect of bond valence on microwave dielectric properties of $(Pb_{1-x}Ca_x)(Mg_{0.33}Ta_{0.67})O_3$ ceramics . . . . . Heung Soo Park *et al.* **817**
Subsolidus phase relations in the La_2O_3–Fe_2O_3–Al_2O_3 system . . . . . Danjela Kuščer *et al.* **822**
Dielectric properties anomaly of $(1-x)Pb(Ni_{1/3}Nb_{2/3})O_3$–$xPbTiO_3$ ceramics near the morphotropic phase boundary . . . . . Zhenrong Li *et al.* **834**

Machinable calcium pyrophosphate glass-ceramics . . . Toshihiro Kasuga *et al.* **876**
Domain configurations in relaxor ferroelectric single crystals $Pb(Mg_{1/3}Nb_{2/3})O_3$–$PbTiO_3$ . . . Guisheng Xu *et al.* **932**
Combinatorial synthesis of oxide powders . . . H.M. Reichenbach *et al.* **967**
Direct measurement of mechanical properties of $(Pb,La)TiO_3$ ferroelectric thin films using nanoindentation techniques . . . M. Algueró *et al.* **993**
Modification of sol–gel-derived amorphous Al_2O_3 thin films by F_2 excimer laser irradiation at ambient temperature . . . Satoshi Takeda *et al.* **1003**
Fabrication, characterization, and photoluminescence properties of highly ordered TiO_2 nanowire arrays . . . Y. Lei *et al.* **1138**
Structure and phase characteristics of amorphous boron–carbon–nitrogen under high pressure and high temperature . . . Jianyu Huang *et al.* **1178**
Synthesis of $Ba_2Ti_9O_{20}$ via ethylenediaminetetraacetic acid precursor . . . Yebin Xu *et al.* **1195**
Processing effects on the composition and dielectric properties of hydrothermally derived $Ba_xSr_{(1-x)}TiO_3$ thin films . . . Mark A. McCormick *et al.* **1200**
Synthesis of $Zn_{2-x}Mn_xSiO_4$ phosphors using a hydrothermal technique . . . Chulsoo Yoon *et al.* **1210**
Twinning domain in $67Pb(Mg_{1/3}Nb_{2/3})O_3$–$33PbTiO_3$ ferroelectric complex perovskite crystal grown by the Bridgman method . . . Donglin Li *et al.* **1252**
Low-power plasma torch method for the production of crystalline spherical ceramic particles . . . Chun-Kuo Chen *et al.* **1256**
Growth, structure, and mechanical properties of transition metal carbide superlattices . . . H. Högberg *et al.* **1301**
Processing- and composition-dependent characteristics of chemical solution deposited $Bi_{4-x}La_xTi_3O_{12}$ thin films . . . Di Wu *et al.* **1325**
Optimization of the annealing process for the $(Ba,Sr)TiO_3$ thin films grown by low-temperature (420 °C) metalorganic chemical vapor deposition . . . Jaehoo Park *et al.* **1363**
Entrapment of organosilicon molecules in nonhydrolytic alumina gels and thermal behavior of the resulting composite . . . G.S. Grader *et al.* **1413**
Synthesis of dense nanometric $MoSi_2$ through mechanical and field activation . . . R. Orrù *et al.* **1439**
Microwave dielectric properties of $(1-x)Cu_3Nb_2O_8$–$xZn_3Nb_2O_8$ ceramics . . . Dong-Wan Kim *et al.* **1465**
Experimental evidence for space charge segregation in Nb-doped $BaTiO_3$ . . . Seok Hyun Yoon *et al.* **1479**
Polarization reversal and domain anisotropy in flux-grown $KTiOPO_4$ and isomorphic crystals . . . P. Urenski *et al.* **1493**
Synthesis of Al_2O_3–SiC from kyanite precursor . . . A. Amroune *et al.* **1609**
Metal–oxide films with magnetically-modulated nanoporous architectures . . . Craig A. Grimes *et al.* **1686**
Influence of ligand groups in Ti precursors on phase transformation and microstructural evolution of TiO_2 thin films prepared by the wet chemical process . . . Chu-Chi Ting *et al.* **1712**
Structures and microwave dielectric properties of $Ba_{6-3x}(Nd,Bi_y)_{8+2x}Ti_{18}O_{54}$ ($x = \frac{2}{3}$) solid solution . . . Yong Jun Wu *et al.* **1734**
Epitaxial growth of $PbZr_{0.5}Ti_{0.5}O_3$ thin films on $SrRuO_3/SrTiO_3$ substrates using chemical solution deposition: Microstructural and ferroelectric properties . . . J.H. Kim *et al.* **1739**
Influence of sintering atmosphere on the fabrication of SiC ceramics with a powder mixture of sialon composition . . . Jong-Kook Lee *et al.* **1784**
$L1_2$- and $L1_0$-like cation-ordered structures in ZrO_2–Y_2O_3 ceramics . . . J.C. Rao *et al.* **1806**
Packing and solidification in ceramic injection moulding . . . S. Krug *et al.* **1829**
Kinetic analysis of solid-state processes . . . Jiří Málek *et al.* **1862**
Deformation-induced surface corrugation of superplastic ceramics . . . Hiroyuki Muto *et al.* **1879**
Blue photoluminescent properties of pure nanostructured γ–Al_2O_3 . . . Zhong Qing Yu *et al.* **1890**
Additive controlled crystallization of barium titanate powders and their application for thin-film ceramic production: Part I. Powder Synthesis . . . B. Grohe *et al.* **1901**
Additive controlled crystallization of barium titanate powders and their application for thin-film ceramic production: Part II. From nano-sized powders to ceramic thin films . . . B. Grohe *et al.* **1911**
Porosity and microstructure control of porous ceramics by partial hot pressing . . . Jian-Feng Yang *et al.* **1916**
Microstructure and formation mechanism of combustion-synthesized rodlike Ca α-sialon crystals . . . Kexin Chen *et al.* **1928**
Anelastic behavior of precursor-derived amorphous ceramics in the system Si–B–C–N . . . Martin Christ *et al.* **1994**
Transmission electron microscopy study of $n = 1$–5 $Sr_{n+1}Ti_nO_{3n+1}$ epitaxial thin films . . . W. Tian *et al.* **2013**
Study of phase components of $La_{1.5}Ca_{1.5}Mn_2O_7$ . . . J.L. Zhu *et al.* **2027**
Dielectric properties of La-substituted $Pb_{0.5}Ca_{0.5}[(Mg_{1/3}Nb_{2/3})_{0.5}Ti_{0.5}]O_3$ ceramics . . . X.J. Lu *et al.* **2053**
Transformation behavior of yttria stabilized tetragonal zirconia polycrystal–TiB_2 composites . . . B. Basu *et al.* **2158**
Cubic silicon nitride embedded in amorphous silicon dioxide . . . Ming Zhang *et al.* **2179**
Improved creep resistance in anisotropic silicon nitride . . . Naoki Kondo *et al.* **2182**
Transmission electron microscopy observation in a liquid-phase-sintered SiC with oxynitride glass . . . Guo-Dong Zhan *et al.* **2189**
Combustion synthesis of aluminum nitride powder using additives . . . Chun-Nan Lin *et al.* **2200**

Thermal expansion and high-temperature phase transformation of the yttrium silicate Y_2SiO_5 . . . J.W. Nowok *et al.* **2251**
Effect of α/β phase ratio on microstructure and mechanical properties of silicon nitride ceramics . . . Hirokazu Kawaoka *et al.* **2264**
Modeling of electric field induced texture in lead zirconate titanate ceramics . . . Shan Wan *et al.* **2306**
Effect of the calcium dopant on oxide ion diffusion in yttria ceramics . . . Noriko Saito *et al.* **2362**
Precursor scavenging of the resistive grain-boundary phase in 8 mol% yttria-stabilized zirconia: Effect of trace concentrations of SiO_2 . . . Jong-Heun Lee *et al.* **2377**
Thermodynamic analysis of combustion synthesis of Al_2O_3–TiC–ZrO_2 nanoceramics . . . Q. Dong *et al.* **2494**
Flash synthesis of zirconia nanoparticles by microwave forced hydrolysis . . . K. Bellon *et al.* **2619**
Thermochemistry of rare-earth orthophosphates . . . S.V. Ushakov *et al.* **2623**
Thin-film fracture during nanoindentation of a titanium oxide film–titanium system . . . M. Pang *et al.* **2634**
Electric properties of barium–strontium titanate thin films deposited by two-step radio-frequency sputtering . . . J.S. Fang *et al.* **2680**
Mechanical properties of nanocrystalline and epitaxial TiN films on (100) silicon . . . H. Wang *et al.* **2733**
Reaction kinetics and anisothermal effects in microwave fields: The System Y_2O_3–Fe_3O_4 . . . Ramesh D. Peelamedu *et al.* **2770**
Translucent yttrium aluminum garnet: Microwave-assisted route to synthesis and processing . . . M. Panneerselvam *et al.* **2773**
Enthalpies of formation of lanthanide oxyapatite phases . . . A.S. Risbud *et al.* **2780**
Chemical sensors based on dielectric response of functionalized mesoporous silica films . . . Karel Domansky *et al.* **2810**
Electrical and microstructural characteristics of ZnO–Bi_2O_3-based varistors doped with rare-earth oxides . . . Nguyen The Hung *et al.* **2817**
Microwave sintering of ZnO at ultra high heating rates . . . Geng-fu Xu *et al.* **2850**
Structural and dielectric characterization of $Ba_4Nd_2Ti_{4+x}Ta_{6-x}O_{30-x/2}$ nonstoichiometric ceramics . . . X.M. Chen *et al.* **2859**
Microstructures of $La_{1-x}A_x$(A = Ca or Sr)$MnO_{3-\delta}$ thin films by liquid-delivery metalorganic chemical vapor deposition . . . Y. Xin *et al.* **3073**
Nucleation and growth of silicon nitride nanoneedles using microwave plasma heating . . . H. Cui *et al.* **3111**
Parameter effect on the crystallization of Nd:yttrium aluminum garnet laser-ablated TiO_2 thin film . . . Mrinal Pal *et al.* **3158**
Halide removal from BaM ($BaFe_{12}O_{19}$) and SrM ($SrFe_{12}O_{19}$) ferrite fibers via a steaming process . . . R.C. Pullar *et al.* **3162**
Wetting of mullite by Y_2O_3–Al_2O_3–SiO_2 and B_2O_3–SiO_2 glasses . . . T.S. Huang *et al.* **3223**
Dependence of fracture stress on applied stress rate in a Yb_2O_3–SiO_2-doped hot-pressed silicon nitride ceramic . . . Shuqi Guo *et al.* **3254**
Consolidation and crystallization of Si_3N_4/SiC nanocomposites from a poly(urea–silazane) ceramic precursor . . . Julin Wan *et al.* **3274**
Mechanism of improvement of TiN-coated tool life by nitrogen implantation . . . S.J. Bull *et al.* **3293**
Titanium oxide nanotube arrays prepared by anodic oxidation . . . Dawei Gong *et al.* **3331**
Lubricity of zinc oxide thin films: Study of deposition parameters and Si as an additive . . . J.J. Nainaparampil *et al.* **3423**
Raman scattering of cubic boron nitride films deposited from the low-pressure gas phase . . . W.J. Zhang *et al.* **3430**
Formation of Al_2O_3 grains with different sizes and morphologies during the pulse electric current sintering process . . . S.W. Wang *et al.* **3514**
Combustion synthesis method for synthesis of aluminum nitride powder using aluminum containers . . . Chun-Nan Lin *et al.* **3518**
Mechanical and thermal properties of combustion-synthesized perovskites, $La_{1-x}Sr_xCr_{0.2}Fe_{0.8}O_3$ . . . Yeong-Shyung Chou *et al.* **3545**
Minima in the strength of MnZn ferrites . . . M.A.H. Donners *et al.* **3575**

Chemical reaction

Preparation of calcium strontium hydroxyapatites by a new route involving calcium phosphate cements . . . L. Leroux *et al.* **171**
Synthesis of nanoscale particles of Ta and Nb_3Al by homogeneous reduction in liquid ammonia . . . Hongmin Zhu *et al.* **2544**

Chemical synthesis

$BaTiO_3$ formation by thermal decomposition of a (BaTi)-citrate polyester resin in air . . . P. Durán *et al.* **197**
Synthesis and processing of nanocrystalline Ag–Fe–Ni for low thermal expansion–high conductivity thermal management applications . . . J. Stolk *et al.* **340**
Synthesis and characterization of antimony oxide nanoparticles . . . Zaoli Zhang *et al.* **803**
New combustion synthesis technique for the production of $(In_xGa_{1-x})_2O_3$ powders: Hydrazine/metal nitrate method . . . R. García *et al.* **1059**
Synthesis of $Nd_2Fe_{14}B$ powders by spray-drying and reduction–diffusion processes . . . X.L. Dong *et al.* **1083**
Solid-phase synthesis of cupric tungstate . . . Leonid P. Dorfman *et al.* **1096**
Synthesis of $Ba_2Ti_9O_{20}$ via ethylenediaminetetraacetic acid precursor . . . Yebin Xu *et al.* **1195**
Patterning of copper particles on polymeric surface . . . Arvind Sinha *et al.* **1354**
Synthesis of Al_2O_3–SiC from kyanite precursor . . . A. Amroune *et al.* **1609**

Growth of epitaxial GaN on $LiGaO_2$ substrates via a reaction with ammonia . . . . . David Kisailus *et al.* **2077**
Templated growth of a complex nitride island dispersion through an internal nitridation reaction . . . . . M.P. Brady *et al.* **2784**
Preparation and characterization of nanocrystalline PbSe in poly(acrylic acid-*co*-styrene) . . . . . Yangyang Sun *et al.* **2922**
Solvothermal route to Bi_3Se_4 nanorods at low temperature . . . . . Yuan-fang Liu *et al.* **3361**
Cure depth in photopolymerization: Experiments and theory . . . . . Jim H. Lee *et al.* **3536**

Chemical vapor deposition (CVD)

Chemical-vapor-deposition growth and characterization of epitaxial 3C–SiC films on SOI substrates with thin silicon top layers . . . . . C.K. Moon *et al.* **24**
Study of the effects of low-energy electron bombardment during the chemical vapor deposition of diamond . . . . . J.A. González *et al.* **293**
Ferroelectric property of epitaxial $Bi_4Ti_3O_{12}$ films prepared by metalorganic chemical vapor deposition . . . . . Takayuki Watanabe *et al.* **303**
Carrier diffusion characterization in epitaxial 4H–SiC . . . . . Paulius Grivickas *et al.* **524**
Comparison of hydrophilic properties of amorphous TiO_x films obtained by radio frequency sputtering and plasma-enhanced chemical vapor deposition . . . . . Masatoshi Nakamura *et al.* **621**
Synthesis of α–SiO_2 nanowires using Au nanoparticle catalysts on a silicon substrate . . . . . Z.Q. Liu *et al.* **683**
Synthesis and properties of $B_xC_yN_z$ coatings . . . . . M.N. Oliveira *et al.* **734**
Metal-organic vapor phase epitaxial growth of high-quality ZnO films on $Al_2O_3(00{\cdot}1)$ . . . . . W.I. Park *et al.* **1358**
Metalorganic chemical vapor deposition of titanium oxide for microelectronics applications . . . . . Kanchana Vydianathan *et al.* **1838**
Highly (111)-oriented and conformal iridium films by liquid source metalorganic chemical vapor deposition . . . . . Jaydeb Goswami *et al.* **2192**
Phase formation and crystal growth of Sr–Bi–Ta–O thin films grown by metalorganic chemical vapor deposition . . . . . H. Bachhofer *et al.* **2966**
Anode-supported planar solid oxide fuel cells by plasma-enhanced metalorganic chemical vapor deposition (PE-MOCVD) and electrostatic spray deposition (ESD): Fabrication of dense thin layers of yttria-stabilized zirconia by PE-MOCVD . . . . . Gianfranco Di Giuseppe *et al.* **2983**
In situ analysis of gaseous species for chemical vapor deposition diamond synthesis and the possible reaction model . . . . . Mayu Uede *et al.* **3069**
Aligned carbon nanotube growth under oxidative ambient . . . . . Anyuan Cao *et al.* **3107**
Nucleation and growth of silicon nitride nanoneedles using microwave plasma heating . . . . . H. Cui *et al.* **3111**

Coating

Strongly adhering and thick highly tetrahedral amorphous carbon (ta–C) thin films via surface modification by implantation . . . . . M. Chhowalla *et al.* **5**
Formation of intermetallic compounds at eutectic Sn–Zn–Al solder/Cu interface . . . . . Shan-Pu Yu *et al.* **76**
Improvement in oxidation resistance of TiB_2 by formation of protective SiO_2 layer on surface . . . . . Young-Hag Koh *et al.* **132**
Characterization of GaN grown on sapphire by laser-induced molecular beam epitaxy . . . . . H. Zhou *et al.* **261**
Chemical vapor deposition of an aluminum nitride–diamond composite in a triple torch plasma reactor . . . . . Marcus Asmann *et al.* **469**
Misting-free diamond surface created by sheet electron beam irradiation . . . . . Kazuya Oguri *et al.* **553**
Synthesis and properties of $B_xC_yN_z$ coatings . . . . . M.N. Oliveira *et al.* **734**
Rational solvent selection strategies to combat striation formation during spin coating of thin films . . . . . Dunbar P. Birnie, III **1145**
Chemical sensors based on dielectric response of functionalized mesoporous silica films . . . . . Karel Domansky *et al.* **2810**
Use of combined elastic modulus in the analysis of depth-sensing indentation data . . . . . A.C. Fischer-Cripps **3050**
Direct writing of polymer thick film resistors using a novel laser transfer technique . . . . . R. Modi *et al.* **3214**
Processing and characterization of hydroxyapatite coatings on titanium produced by magnetron sputtering . . . . . T.G. Nieh *et al.* **3238**
Effect of material properties on integration damage in organosilicate glass films . . . . . E. Todd Ryan *et al.* **3335**
Properties of $YBa_2Cu_3O_{7-\delta}$ multilayer films from the fluoride-based sol-gel process . . . . . M.P. Siegal *et al.* **3339**
Highly oriented diamond growth on positively biased Si substrates . . . . . Te-Fu Chang *et al.* **3351**
Nondestructive measurement of striation defect spacing using laser diffraction . . . . . Dylan E. Haas *et al.* **3355**
Microstructural and mechanical characterization of carbon coatings on SiC fibers . . . . . K.L. Kendig *et al.* **3366**
Adhesion of polymer–inorganic interfaces by nanoindentation . . . . . Min Li *et al.* **3378**
Structural characterization of laser-treated Cr_3C_2–NiCr coatings . . . . . P. Serra *et al.* **3416**

Cold isostatic pressing (CIP)

Size effects in powder compaction . . . . . J. Gil Sevillano **1238**

Combinatorial synthesis

Combinatorial synthesis of oxide powders . . . . . H.M. Reichenbach *et al.* **967**

Combustion synthesis

Modeling of wave configuration during electrically ignited combustion synthesis . . . . . O.A. Graeve *et al.* **93**
Fractal aggregates of lanthanide-doped Y_2O_3 nanoparticles obtained by propellant synthesis . . . . . Stefano Polizzi *et al.* **146**
Synthesis of dense nanometric $MoSi_2$ through mechanical and field activation . . . . . R. Orrù *et al.* **1439**
Mechanistic studies in combustion synthesis of $NiAl–TiB_2$ composites: Effects of gravity . . . . . Cheryl Lau *et al.* **1614**
Combustion synthesis of aluminum nitride powder using additives . . . . . Chun-Nan Lin *et al.* **2200**
Thermodynamic analysis of combustion synthesis of $Al_2O_3–TiC–ZrO_2$ nanoceramics . . . . . Q. Dong *et al.* **2494**
Combustion synthesis method for synthesis of aluminum nitride powder using aluminum containers . . . . . Chun-Nan Lin *et al.* **3518**

Composites

Metal/ceramic interface in an *in situ* synthesized Ti/TiC_p composite coating by laser processing . . . . . R. Yu *et al.* **9**
Strength prediction of partially aligned discontinuous fiber-reinforced composites . . . . . Rex J. Kuriger *et al.* **226**
Designing composite microstructures with targeted properties . . . . . S. Hyun *et al.* **280**
Carbonization behavior of polyimide film containing iron complex in relation to magnetic properties . . . . . Y. Kaburagi *et al.* **352**
Joining characteristics of oxidized SiC particles reinforced Al–Mg matrix composite prepared by reaction infiltration processing . . . . . Zhongliang Shi *et al.* **400**
Chemical vapor deposition of an aluminum nitride–diamond composite in a triple torch plasma reactor . . . . . Marcus Asmann *et al.* **469**
Thermal stability of nanocrystalline WC–Co powder synthesized by using mechanical milling at low temperature . . . . . Jianhong He *et al.* **478**
Analysis of a ceramic/metal laminate under thermal shock . . . . . D. Sherman *et al.* **753**
Precipitation of multilayered core–shell TiO_2 composite nanoparticles onto polymer layers . . . . . Mingtai Wang *et al.* **765**
Synthesis of nano-AgI arrays and their optical properties . . . . . Yinhai Wang *et al.* **990**
Creep and toughness of cryomilled NiAl containing Cr . . . . . J. Daniel Whittenberger *et al.* **1333**
Patterning of copper particles on polymeric surface . . . . . Arvind Sinha *et al.* **1354**
Damping behavior of *in situ* Al–(graphite, Al_4C_3) composites produced by reciprocating extrusion . . . . . Hsu-Shen Chu *et al.* **1372**
Synthesis of coaxial nanotubes: Titanium oxide sheathed with silicon oxide . . . . . Ming Zhang *et al.* **1408**
Mechanistic studies in combustion synthesis of $NiAl–TiB_2$ composites: Effects of gravity . . . . . Cheryl Lau *et al.* **1614**
Electrical conductivity of vapor-grown carbon fiber/thermoplastic composites . . . . . Ioana C. Finegan *et al.* **1668**
Phase transformation effects on the wear properties of alumina gel–polymer matrix nanocomposites . . . . . Jiazhong Luo *et al.* **1680**
Dielectric properties of oxide structures by a laser-based direct-writing method . . . . . D. Young *et al.* **1720**
Effects of whisker content and dimensions on the *R*-curve behavior of an alumina matrix composite reinforced with silicon carbide whiskers . . . . . Takashi Akatsu *et al.* **1919**
Increased fracture toughness in nanoporous silica–polyimide matrix composites . . . . . Shiling Ruan *et al.* **1975**
Piezoresistivity of conducting polyaniline/$BaTiO_3$ composites . . . . . R.C. Patil *et al.* **1982**
Rectifying and thermocouple junctions based on Portland cement . . . . . Sihai Wen *et al.* **1989**
Photoinduced condensation of sol-gel hybrid glass films doped with benzildimethylketal . . . . . Oun-Ho Park *et al.* **2143**
Dye-doped sol-gel coatings for near-infrared laser protection . . . . . T. Kololuoma *et al.* **2186**
Fabrication of heteropolyoxometalate-based photochromic inorganic–organic nanocomposites . . . . . Tie Rui Zhang *et al.* **2256**
Interface structure and solute segregation behavior in SiC/2124 and SiC/6061 Al composites exhibiting high-strain-rate superplasticity . . . . . Woo-Jin Kim *et al.* **2429**
Two-dimensional simulation of mass transport in polymer removal from a powder injection molding compact by thermal debinding . . . . . Ying Shengjie *et al.* **2436**
Freeform fabrication of aluminum metal-matrix composites . . . . . C.W. Souvignier *et al.* **2613**
Nanocrystals in crystalline silicon: Void formation and hollow particles . . . . . A. Meldrum *et al.* **2670**
Templated growth of a complex nitride island dispersion through an internal nitridation reaction . . . . . M.P. Brady *et al.* **2784**
Microprobe fluorescence spectroscopy evaluation of stress fields developed along a propagating crack in an $Al_2O_3/CaO \cdot 6Al_2O_3$ ceramic composite . . . . . O. Sbaizero *et al.* **2798**
Preparation, structure, and magnetic properties of cobalt nanoparticles in carbon fibers . . . . . I. Bashmakov *et al.* **2832**
Piezoelectric actuation of crack growth along polymer–metal interfaces in adhesive bonds . . . . . Tianbao Du *et al.* **2885**
A new technique for pressureless infiltration of Al alloys into Al_2O_3 preforms . . . . . B. Srinivasa Rao *et al.* **2906**
Preparation and characterization of nanocrystalline PbSe in poly(acrylic acid-*co*-styrene) . . . . . Yangyang Sun *et al.* **2922**
Formation and characterization of high-density silver nanoparticles embedded in silica thin films by "*in situ*" self-reduction . . . . . G. Compagnini *et al.* **2934**
Silicalite/poly(dimethylsiloxane) nanocomposite pervaporation membranes for acetic acid/water separation . . . . . Shih-Yuan Lu *et al.* **3053**

Low-resistance films of polyimides with impregnated copper sulfide . . . R.V.A. Rowe *et al.* **3097**
Structural characterization of laser-treated Cr_3C_2–NiCr coatings . . . P. Serra *et al.* **3416**

Compositions

Determination of optical constants of Si/ZnO polycrystalline nanocomposites by spectroscopic ellipsometry . . . J. García-Serrano *et al.* **3554**

Compound semiconductors

Characterization of GaN grown on sapphire by laser-induced molecular beam epitaxy . . . H. Zhou *et al.* **261**
Preparation of $Cu(In,Ga)Se_2$ thin films at low substrate temperatures . . . S. Nishiwaki *et al.* **394**
Quantification and effects of molecular oxygen and water in zinc phthalocyanine layers . . . H.R. Kerp *et al.* **503**
Carrier diffusion characterization in epitaxial 4H–SiC . . . Paulius Grivickas *et al.* **524**
Synthesis and characterization of antimony oxide nanoparticles . . . Zaoli Zhang *et al.* **803**
Effects of Ce filling fraction and Fe content on the thermoelectric properties of Co-rich $Ce_yFe_xCo_{4-x}Sb_{12}$ . . . Xinfeng Tang *et al.* **837**
Photocatalytic activity of TiO_2 prepared at low temperature by a photo-assisted sol-gel method . . . Zi-sheng Guan *et al.* **907**
Epitaxial stabilization of orthorhombic cuprous oxide films on MgO(110) . . . Paul R. Markworth *et al.* **914**
Infrared optical properties of aged porous GaAs . . . S. Zangooie *et al.* **1241**
Deep center luminescence versus surface preparation of ZnSe single crystals . . . J.A. Garcia *et al.* **1245**
Characterization of NO_x sensor using doped In_2O_3 . . . Shinichiro Tanaka *et al.* **1389**
Third-order nonlinear optical response in PbS-coated CdS nanocomposites . . . Bing Liu *et al.* **1644**
X-ray scattering study on the structural evolution of AlN/sapphire(0001) films during radiofrequency sputter growth . . . H.C. Kang *et al.* **1814**
X-ray photoelectron spectroscopy of electrodeposited cadmium mercury telluride thin films and their native surface oxides . . . J. Ramiro *et al.* **1942**
Growth of epitaxial GaN on $LiGaO_2$ substrates via a reaction with ammonia . . . David Kisailus *et al.* **2077**
Temperature dependence of the optical properties in p-$Cd_{0.96}Zn_{0.04}Te$ single crystals . . . H.Y. Lee *et al.* **2196**
Epitaxial growth of skutterudite ($CoSb_3$) thin films on (001) InSb by pulsed laser deposition . . . J.C. Caylor *et al.* **2467**
Preparation and characterization of $CuInS_2$ nanorods and nanotubes from an elemental solvothermal reaction . . . Yang Jiang *et al.* **2805**
High-temperature thermoelectric properties of *n*-type $Ba_xNi_yCo_{4-x}Sb_{12}$ . . . X.F. Tang *et al.* **3343**
Preparation and phase control of nanocrystalline silver indium sulfides via a hydrothermal route . . . J.Q. Hu *et al.* **3411**

Computer simulation

Modeling of wave configuration during electrically ignited combustion synthesis . . . O.A. Graeve *et al.* **93**
Designing composite microstructures with targeted properties . . . S. Hyun *et al.* **280**
Site preference of alloying elements in Fe_3Al-based alloys . . . Xiao Dong Ni *et al.* **344**
Glass-forming ability of the Ni–Zr and Ni–Ti systems determined by interatomic potentials . . . W.S. Lai *et al.* **446**
Small correction required when applying the Hertzian contact model to instrumented indentation data . . . J.L. Hay *et al.* **1280**
Delamination of a strong film from a ductile substrate during indentation unloading . . . A. Abdul-Baqi *et al.* **1396**
Molecular dynamics analysis of adhesion strength of interfaces between thin films . . . T. Iwasaki *et al.* **1789**
Topological transformation of grains in three-dimensional normal grain growth . . . F. Wakai *et al.* **2136**
Two-dimensional simulation of mass transport in polymer removal from a powder injection molding compact by thermal debinding . . . Ying Shengjie *et al.* **2436**
Quantum atomistic simulations of silicon and germanium . . . Carlos P. Herrero **2505**
Embedded-atom-method functions for the body-centered-cubic iron and hydrogen . . . Mao Wen *et al.* **3496**

Conductors, ionic

Oxygen self-diffusion in cerium oxide doped with Nd . . . Michiyo Kamiya *et al.* **179**
Synthesis and characterization of partially and fully stabilized zirconia fibers made from an inorganic precursor . . . A. Hartridge *et al.* **2384**
Solid solubility and transport properties of $Ce_{1-x}Nd_xO_{2-\delta}$ nanocrystalline solid solutions by a sol-gel route . . . Liping Li *et al.* **3207**

Conductors, metallic

Sintering of screen-printed platinum thick films for electrode applications . . . J.B. Véchembre *et al.* **922**
Superplasticicity of Cu–16 at.% Ag microcomposites . . . S.I. Hong *et al.* **1822**
Electromigration properties of multigrain aluminum thin film conductors as influenced by grain boundary structure . . . O.V. Kononenko *et al.* **2124**

Conductors, transparent

New combustion synthesis technique for the production of $(In_xGa_{1-x})_2O_3$ powders: Hydrazine/metal nitrate method . . . R. García *et al.* **1059**
Dependence of structural, electrical, and optical properties of ZnO:Al films on substrate temperature . . . M. Chen *et al.* **2118**
Highly textured nanostructure of pulsed laser deposited IrO_2 thin films as investigated by transmission electron microscopy . . . A.M. Serventi *et al.* **2336**

Corrosion

Corrosive wear of the Co–Cr–W alloy in liquid zinc . . . Xibao Wang *et al.* **1585**
Wetting of mullite by Y_2O_3–Al_2O_3–SiO_2 and B_2O_3–SiO_2 glasses . . . T.S. Huang *et al.* **3223**

Crystal (single)

Phase transition, growth, and optical properties of $Nd_xLa_{1-x}Sc_3(BO_3)_4$ crystals . . . Yunkui Li *et al.* **38**
Atomic structure of YB_{56} studied by digital high-resolution electron microscopy and electron diffraction . . . Takeo Oku *et al.* **101**
Effective symmetry and physical properties of twinned perovskite ferroelectric single crystals . . . Jiří Erhart *et al.* **570**
Thermal conductivity and thermal diffusivity of selected oxide single crystals . . . A. Stanimirovic *et al.* **678**
Electron backscatter diffraction analysis of $Pb(Mg_{1/3}Nb_{2/3})O_3$–35mol%$PbTiO_3$ single crystals grown by seeded polycrystal conversion . . . Ajmal Khan *et al.* **694**
Domain configurations in relaxor ferroelectric single crystals $Pb(Mg_{1/3}Nb_{2/3})O_3$–$PbTiO_3$ . . . Guisheng Xu *et al.* **932**
Growth of melt-textured Nd-123 by hot seeding under reduced oxygen partial pressure . . . M. Kambara *et al.* **1163**
Deep center luminescence versus surface preparation of ZnSe single crystals . . . J.A. Garcia *et al.* **1245**
Photoluminescence spectra of undoped and Sm^{3+}-doped $BaAl_2S_4$ and $BaAl_2Se_4$ single crystals . . . Moon-Seog Jin *et al.* **1520**
Ordered structure formation in the flux-grown $Ba(Mg_{1/3}Ta_{2/3})O_3$ single crystals . . . Yu-Chang Lee *et al.* **1593**
Water-associated surface degradation of $CsLiB_6O_{10}$ crystal during harmonic generation in the ultraviolet region . . . Yukihiro Morimoto *et al.* **2082**
Elastic constants of polycrystalline Al and TiN calculated by an *ab initio* method within the local-density approximation . . . Ming Zhang *et al.* **2293**
Electron microscopy of high-temperature and high-pressure as-grown diamond crystals . . . Long-Wei Yin *et al.* **3023**

Crystal growth

Texture analysis of grain refinement in undercooled $Ni_{99.45}B_{0.55}$ . . . K.L. Lee *et al.* **1434**
Initial growth mechanism of $YBa_2Cu_3O_y$ crystal on MgO substrate by liquid-phase epitaxy . . . Katsumi Nomura *et al.* **2947**

Crystallographic structure

Optical and structural properties of solid oxide photocatalyst Bi_2FeNbO_7 . . . Zhigang Zou *et al.* **35**
Atomic structure of YB_{56} studied by digital high-resolution electron microscopy and electron diffraction . . . Takeo Oku *et al.* **101**
Valence variations in titanium-based perovskite oxides by high-pressure and high-temperature method . . . Liping Li *et al.* **417**
Transmission electron microscopy study of (103)-oriented epitaxial $SrBi_2Nb_2O_9$ films grown on (111) $SrTiO_3$ and (111) $SrRuO_3$/(111) $SrTiO_3$ . . . M.A. Zurbuchen *et al.* **489**
Synthesis of $Zn_{1-x}Mg_xO$ and its structural characterization . . . M.S. Tomar *et al.* **903**
Epitaxial stabilization of orthorhombic cuprous oxide films on MgO(110) . . . Paul R. Markworth *et al.* **914**
Processing of highly oriented lithium niobate films through chemical solution deposition . . . Satomi Ono *et al.* **1155**
Ordered structure formation in the flux-grown $Ba(Mg_{1/3}Ta_{2/3})O_3$ single crystals . . . Yu-Chang Lee *et al.* **1593**
Growth study of epitaxial $Fe_xZn_{1-x}F_2$ thin films . . . J. McChesney *et al.* **1769**
Microstructural analysis of high-pressure compressed C_{60} . . . K. Miyazawa *et al.* **1960**
Crystallography and structural evolution of $LiNbO_3$ and $LiNb_{1-x}Ta_xO_3$ films on sapphire prepared by high-rate thermal plasma spray chemical vapor deposition . . . D.V. Shtansky *et al.* **2271**
Ferroelectric domain structure of epitaxial $(Pb,Sr)TiO_3$ thin films . . . Yong Kwan Kim *et al.* **2463**
Epitaxial growth of skutterudite ($CoSb_3$) thin films on (001) InSb by pulsed laser deposition . . . J.C. Caylor *et al.* **2467**
Quantum atomistic simulations of silicon and germanium . . . Carlos P. Herrero **2505**
Comparison of crystal structure parameters of natural and synthetic apatites from neutron powder diffraction . . . Th. Leventouri *et al.* **2600**
Formation of quasi-one-dimensional carbon chains in cubic nanocrystals by photon-breaking of C–S bonds in polythiophene . . . Z.M. Ren *et al.* **2793**
Investigation of crystal properties of TmP/GaAs and GaAs/TmP/GaAs heterostructures grown by molecular beam epitaxy . . . C.H. Lin *et al.* **3266**
Structure and thc nonlinearity of lithium triborate studied by Raman and infrared reflectivity spectroscopy . . . H.R. Xia *et al.* **3464**

Czochralski growth

Formation of $Nd_{1+x}(Ba_{1-y}Sr_y)_{2-x}Cu_3O_{7\pm\delta}$ solid solutions by crystal pulling . . . Xin Yao *et al.* **529**

Defects

The healing of quenched crack in 1045 steel under electropulsing . . . Zhou Yizhou *et al.* **17**
Deep center luminescence versus surface preparation of ZnSe single crystals . . . J.A. Garcia *et al.* **1245**
Packing and solidification in ceramic injection moulding . . . S. Krug *et al.* **1829**
Threading dislocations with edge components in GaN epilayers grown on Al_2O_3 substrates . . . Junyong Kang *et al.* **2550**
Mass density of glassy $Pd_{80}Si_{20}$ during low-temperature light ion irradiation . . . G. Schumacher *et al.* **2788**
Aligned carbon nanotube growth under oxidative ambient . . . Anyuan Cao *et al.* **3107**

Dielectric properties

Microwave dielectric properties of $(1 - x)Cu_3Nb_2O_8$–$xZn_3Nb_2O_8$ ceramics . . . . . Dong-Wan Kim *et al.* **1465**
Metalorganic chemical vapor deposition of titanium oxide for microelectronics applications . . . . . Kanchana Vydianathan *et al.* **1838**

Dielectrics

Microwave dielectric properties of $(1 - x)Cu_3Nb_2O_8$–$xZn_3Nb_2O_8$ ceramics . . . . . Dong-Wan Kim *et al.* **1465**

Diffusion

Oxygen self-diffusion in cerium oxide doped with Nd . . . . . Michiyo Kamiya *et al.* **179**
Diffusion of oxygen and silicon in silicon: Silicon monoxide model . . . . . Robert H. Doremus **185**
Erbium doping into lithium niobate and sapphire single crystal wafers . . . . . P. Nekvindova *et al.* **333**
Modeling of the effects of crystallographic orientation on electromigration-limited reliability of interconnects with bamboo grain structures . . . . . W.R. Fayad *et al.* **413**
Quantification and effects of molecular oxygen and water in zinc phthalocyanine layers . . . . . H.R. Kerp *et al.* **503**
Electronic paramagnetic resonance study of Cu^{2+} ions in copper ion-exchanged layers of lithium niobate crystals . . . . . F. Caccavale *et al.* **1554**
Chemical stresses induced by grain-boundary diffusion in thin films . . . . . W.L. Wang *et al.* **1967**
Effect of the calcium dopant on oxide ion diffusion in yttria ceramics . . . . . Noriko Saito *et al.* **2362**
Analysis of interdiffusion of Dy, Nd, and Pr in Mg . . . . . Y. Xu *et al.* **3287**

Directional solidification

Role of the primary phase particles during the peritectic solidification of Y-123 superconducting oxides . . . . . M. Kambara *et al.* **2229**

Elastic properties

Optical evaluation of the flexural rigidity and residual stress in thin membranes: Picosecond transient grating measurements of the dispersion of the lowest-order Lamb acoustic waveguide mode . . . . . John A. Rogers *et al.* **217**
Effective symmetry and physical properties of twinned perovskite ferroelectric single crystals . . . . . Jiří Erhart *et al.* **570**
Elastic properties of anisotropic monolithic samples of compressed expanded graphite studied with ultrasounds . . . . . M. Krzesińska *et al.* **606**
Small correction required when applying the Hertzian contact model to instrumented indentation data . . . . . J.L. Hay *et al.* **1280**
Determination of the elastic properties of glasses and polymers exploiting the resonant characteristic of depth-sensing indentation tests . . . . . D. Lorenz *et al.* **1776**
Size effect on the mechanical properties of microfabricated polysilicon thin films . . . . . J.N. Ding *et al.* **2223**
Elastic constants of polycrystalline Al and TiN calculated by an *ab initio* method within the local-density approximation . . . . . Ming Zhang *et al.* **2293**
Simplified method for analyzing nanoindentation data and evaluating performance of nanoindentation instruments . . . . . Takeshi Sawa *et al.* **3084**

Electrical materials

Structure and dielectric properties of pyrochlore–fluorite biphase ceramics in the Bi_2O_3–ZnO–Nb_2O_5 system . . . . . Hong Wang *et al.* **83**
Analysis of defect formation in Nb-doped $SrTiO_3$ by impedance spectroscopy . . . . . Seong-Ho Kim *et al.* **192**
Analysis of phase distributions in the Li_2O–Nb_2O_5–TiO_2 system by piezoresponse imaging . . . . . Albina Y. Borisevich *et al.* **329**
Transmission electron microscopy study of (103)-oriented epitaxial $SrBi_2Nb_2O_9$ films grown on (111) $SrTiO_3$ and (111) $SrRuO_3$/(111) $SrTiO_3$ . . . . . M.A. Zurbuchen *et al.* **489**
Effective symmetry and physical properties of twinned perovskite ferroelectric single crystals . . . . . Jiří Erhart *et al.* **570**
Electron backscatter diffraction analysis of $Pb(Mg_{1/3}Nb_{2/3})O_3$–35mol%$PbTiO_3$ single crystals grown by seeded polycrystal conversion . . . . . Ajmal Khan *et al.* **694**
Low-temperature fabrication of pyroelectric $Ba_{0.8}Sr_{0.2}TiO_3$ thin films by a sol-gel process . . . . . Jian-Gong Cheng *et al.* **778**
Effect of bond valence on microwave dielectric properties of $(Pb_{1-x}Ca_x)(Mg_{0.33}Ta_{0.67})O_3$ ceramics . . . . . Heung Soo Park *et al.* **817**
Dielectric properties anomaly of (1–x)$Pb(Ni_{1/3}Nb_{2/3})O_3$–x$PbTiO_3$ ceramics near the morphotropic phase boundary . . . . . Zhenrong Li *et al.* **834**
Solid-phase synthesis of cupric tungstate . . . . . Leonid P. Dorfman *et al.* **1096**
Effect of hydrogen on true leakage current characteristics of $(Pb,La)(Zr,Ti)O_3$ thin-film capacitors with Pt- or Ir-based top electrodes . . . . . Soon-Gil Yoon *et al.* **1185**
Processing effects on the composition and dielectric properties of hydrothermally derived $Ba_xSr_{(1-x)}TiO_3$ thin films . . . . . Mark A. McCormick *et al.* **1200**
Effects of Cu and Ni additions to eutectic Pb–Sn solders on Au embrittlement of solder interconnections . . . . . Jong-Hyun Lee *et al.* **1249**
Twinning domain in $67Pb(Mg_{1/3}Nb_{2/3})O_3$–$33PbTiO_3$ ferroelectric complex perovskite crystal grown by the Bridgman method . . . . . Donglin Li *et al.* **1252**
Generation of circular and hexagonal microholes in a graphite surface . . . . . Hidefumi Hiura **1287**
Processing- and composition-dependent characteristics of chemical solution deposited $Bi_{4-x}La_xTi_3O_{12}$ thin films . . . . . Di Wu *et al.* **1325**
Phase formation and reactions in the Bi_2O_3–ZnO–Nb_2O_5–Ag pyrochlore system . . . . . Juan C. Nino *et al.* **1460**
Experimental evidence for space charge segregation in Nb-doped $BaTiO_3$ . . . . . Seok Hyun Yoon *et al.* **1479**

Polarization reversal and domain anisotropy in flux-grown $KTiOPO_4$ and isomorphic crystals . . . . P. Urenski *et al.* **1493**
Ordered structure formation in the flux-grown $Ba(Mg_{1/3}Ta_{2/3})O_3$ single crystals . . . . . Yu-Chang Lee *et al.* **1593**
$Pb(Zr_xTi_{1-x})O_3$ ceramics via reactive sintering of partially reacted mixture produced by a high-energy ball milling process . . . . L.B. Kong *et al.* **1636**
Electrical conductivity of vapor-grown carbon fiber/thermoplastic composites . . . . . Ioana C. Finegan *et al.* **1668**
Ferroelectric $SrBi_2Ta_2O_9$ single-crystal growth and characterization . . . . B. Sih *et al.* **1726**
Epitaxial growth of $PbZr_{0.5}Ti_{0.5}O_3$ thin films on $SrRuO_3/SrTiO_3$ substrates using chemical solution deposition: Microstructural and ferroelectric properties . . . . J.H. Kim *et al.* **1739**
Low-temperature crystallization induced by excimer laser irradiation of $SrBi_2Ta_2O_9$ films . . . . Kwang Soo Seol *et al.* **1883**
Effects of thermal annealing on the texture of $La_{0.67}Sr_{0.33}MnO_3$ thin films . . . . . Lamartine Meda *et al.* **1887**
Additive controlled crystallization of barium titanate powders and their application for thin-film ceramic production: Part I. Powder Synthesis . . . . B. Grohe *et al.* **1901**
Additive controlled crystallization of barium titanate powders and their application for thin-film ceramic production: Part II. From nano-sized powders to ceramic thin films . . . . B. Grohe *et al.* **1911**
Nonisothermal phase formation kinetics in sol-gel-derived strontium bismuth tantalate . . . . Yun-Mo Sung **2039**
Crystallization and dielectric properties of $SrO–BaO–Nb_2O_5–GeO_2$ tungsten–bronze glass–ceramics . . . . Jiin-Jyh Shyu *et al.* **2057**
Thermal and structural characterization of the $ZrO_{2-x}(OH)_{2x}$ to ZrO_2 transition . . . . E. Torres-García *et al.* **2209**
Piezoresistivity in ruthenium-based metal–insulator–metal structures . . . . Ahmed Amin **2239**
Modeling of electric field induced texture in lead zirconate titanate ceramics . . . . Shan Wan *et al.* **2306**
Chemical structure evolution and orientation selection in sol-gel-prepared ferroelectric $Pb(Zr,Ti)O_3$ thin films . . . . L. Fè *et al.* **2499**
Annealing effect on in-plane alignment and surface morphology of epitaxial $Bi_4Ti_3O_{12}$ thin films prepared by the chemical solution deposition . . . . K. Hwang *et al.* **2519**
Purification of single-walled carbon nanotubes synthesized by the hydrogen arc-discharge method . . . . Pengxiang Hou *et al.* **2526**
Mechanical stress of the electrical performance of polycrystalline-silicon resistors . . . . N. Nakabayashi *et al.* **2579**
Flash synthesis of zirconia nanoparticles by microwave forced hydrolysis . . . . K. Bellon *et al.* **2619**
Precipitate splitting in $Pb_{0.91}La_{0.09}Zr_{0.65}Ti_{0.35}O_3$ films . . . . Bahadir Tunaboylu *et al.* **2763**
Phase formation and crystal growth of Sr–Bi–Ta–O thin films grown by metalorganic chemical vapor deposition . . . . H. Bachhofer *et al.* **2966**
Oxygen transport during annealing of $Pb(Zr,Ti)O_3$ thin films in O_2 gas and its effect on their conductivity . . . . F. Ayguavives *et al.* **3005**
Microstructures of $La_{1-x}A_x(A = Ca \text{ or } Sr)MnO_{3-\delta}$ thin films by liquid-delivery metalorganic chemical vapor deposition . . . . Y. Xin *et al.* **3073**
Single-layer submicron-thick $BaTiO_3$ coatings from poly(vinylpyrrolidone)-containing sols: Gel-to-ceramic film conversion, densification, and dielectric properties . . . . Hiromitsu Kozuka *et al.* **3116**
Formation and characteristics of highly *c*-axis-oriented $Bi_{3.25}La_{0.75}Ti_3O_{12}$ thin films on $SiO_2/Si(100)$ and $Pt/Ti/SiO_2/Si(100)$ substrates . . . . Uong Chon *et al.* **3124**
Novel synthesis of AlN nanowires with controlled diameters . . . . Jun Liu *et al.* **3133**
Relation between tolerance factor and T_c in Aurivillius compounds . . . . Donají Y. Suárez *et al.* **3139**
Direct writing of polymer thick film resistors using a novel laser transfer technique . . . . R. Modi *et al.* **3214**
Effect of material properties on integration damage in organosilicate glass films . . . . E. Todd Ryan *et al.* **3335**
Solvothermal route to Bi_3Se_4 nanorods at low temperature . . . . Yuan-fang Liu *et al.* **3361**
Microstructure and misfit relaxation in $SrTiO_3/SrRuO_3$ bilayer films on $LaAlO_3(100)$ substrates . . . . J.S. Wu *et al.* **3443**
Bulk- or interface-limited electrical conductions in $IrO_2/(Ba,Sr)TiO_3/IrO_2$ thin film capacitors . . . . Cheol Seong Hwang **3476**
Impacts of postannealing ambient atmospheres on $Pt/SrBi_{2.2}Ta_2O_9/Pt$ capacitors . . . . Ai-Dong Li *et al.* **3526**

Electrical properties

High J_c $YBa_2Cu_3O_{7-\delta}$ films via rapid, low pO_2 pyrolysis . . . . J.T. Dawley *et al.* **13**
Structure and dielectric properties of pyrochlore–fluorite biphase ceramics in the $Bi_2O_3–ZnO–Nb_2O_5$ system . . . . Hong Wang *et al.* **83**
Analysis of defect formation in Nb-doped $SrTiO_3$ by impedance spectroscopy . . . . Seong-Ho Kim *et al.* **192**
Dependence of dielectric and piezoelectric properties on film thickness for highly {100}-oriented lead magnesium niobate–lead titanate (70/30) thin films . . . . Jeong Hwan Park *et al.* **268**
Ferroelectric property of epitaxial $Bi_4Ti_3O_{12}$ films prepared by metalorganic chemical vapor deposition . . . . Takayuki Watanabe *et al.* **303**
Carrier diffusion characterization in epitaxial 4H–SiC . . . . Paulius Grivickas *et al.* **524**
Electrical transport properties of single-crystalline Mn–Zn ferrous ferrite . . . . Yong-Chae Chung *et al.* **774**
Magnetotransport properties of $La_{0.7}Ca_{0.3}MnO_3$ thick films prepared by spray pyrolysis . . . . F. Damay *et al.* **784**
Effect of bond valence on microwave dielectric properties of $(Pb_{1-x}Ca_x)(Mg_{0.33}Ta_{0.67})O_3$ ceramics . . . . Heung Soo Park *et al.* **817**

Dielectric properties anomaly of (1–x)$Pb(Ni_{1/3}Nb_{2/3})O_3$–x$PbTiO_3$ ceramics near the morphotropic phase boundary . . . Zhenrong Li *et al.* **834**
Effects of Ce filling fraction and Fe content on the thermoelectric properties of Co-rich $Ce_yFe_xCo_{4-x}Sb_{12}$ . . . Xinfeng Tang *et al.* **837**
Domain configurations in relaxor ferroelectric single crystals $Pb(Mg_{1/3}Nb_{2/3})O_3$–$PbTiO_3$ . . . Guisheng Xu *et al.* **932**
Alternating current conductivity of the interfacial phase in copper oxide–silica gel nanocomposites . . . D. Das *et al.* **1047**
Effect of hydrogen on true leakage current characteristics of (Pb,La)(Zr,Ti)O_3 thin-film capacitors with Pt- or Ir-based top electrodes . . . Soon-Gil Yoon *et al.* **1185**
High-T_c superconducting NbN films with low particulate density grown at 25 °C using pulsed laser deposition . . . Anupama B. Kaul *et al.* **1223**
Optimization of the annealing process for the (Ba,Sr)TiO_3 thin films grown by low-temperature (420 °C) metalorganic chemical vapor deposition . . . Jaehoo Park *et al.* **1363**
Experimental evidence for space charge segregation in Nb-doped $BaTiO_3$ . . . Seok Hyun Yoon *et al.* **1479**
Polarization reversal and domain anisotropy in flux-grown $KTiOPO_4$ and isomorphic crystals . . . P. Urenski *et al.* **1493**
Intrinsic microcrystalline silicon by postgrowth anneals . . . Jong-Hwan Yoon **1531**
Electrical conductivity of vapor-grown carbon fiber/thermoplastic composites . . . Ioana C. Finegan *et al.* **1668**
Dielectric properties of oxide structures by a laser-based direct-writing method . . . D. Young *et al.* **1720**
Structures and microwave dielectric properties of $Ba_{6-3x}(Nd,Bi_y)_{8+2x}Ti_{18}O_{54}$ ($x = \frac{2}{3}$) solid solution . . . Yong Jun Wu *et al.* **1734**
Piezoresistivity of conducting polyaniline/$BaTiO_3$ composites . . . R.C. Patil *et al.* **1982**
Rectifying and thermocouple junctions based on Portland cement . . . Sihai Wen *et al.* **1989**
Dielectric properties of La-substituted $Pb_{0.5}Ca_{0.5}[(Mg_{1/3}Nb_{2/3})_{0.5}Ti_{0.5}]O_3$ ceramics . . . X.J. Lu *et al.* **2053**
Dependence of structural, electrical, and optical properties of ZnO:Al films on substrate temperature . . . M. Chen *et al.* **2118**
Electromigration properties of multigrain aluminum thin film conductors as influenced by grain boundary structure . . . O.V. Kononenko *et al.* **2124**
Development of *p*-type microcrystalline silicon carbon alloy films by the very high frequency plasma-enhanced chemical vapor deposition technique . . . Tapati Jana *et al.* **2130**
High critical current density $YBa_2Cu_3O_{7-\delta}$ thick films using ion beam assisted deposition MgO bi-axially oriented template layers on nickel-based superalloy substrates . . . J.R. Groves *et al.* **2175**
Piezoresistivity in ruthenium-based metal–insulator–metal structures . . . Ahmed Amin **2239**
Precursor scavenging of the resistive grain-boundary phase in 8 mol% yttria-stabilized zirconia: Effect of trace concentrations of SiO_2 . . . Jong-Heun Lee *et al.* **2377**
Mechanical stress of the electrical performance of polycrystalline-silicon resistors . . . N. Nakabayashi *et al.* **2579**
Growth and characterization of conductive $SrRuO_3$ and $LaNiO_3$ multilayers on textured Ni tapes for high-J_c $YBa_2Cu_3O_{7-\delta}$ coated conductors . . . T. Aytug *et al.* **2661**
Electric properties of barium–strontium titanate thin films deposited by two-step radio-frequency sputtering . . . J.S. Fang *et al.* **2680**
Space-charge concepts on grain boundary impedance of a high-purity yttria-stabilized tetragonal zirconia polycrystal . . . Jong-Sook Lee *et al.* **2739**
Chemical sensors based on dielectric response of functionalized mesoporous silica films . . . Karel Domansky *et al.* **2810**
Electrical and microstructural characteristics of ZnO–Bi_2O_3-based varistors doped with rare-earth oxides . . . Nguyen The Hung *et al.* **2817**
Structural and dielectric characterization of $Ba_4Nd_2Ti_{4+x}Ta_{6-x}O_{30-x/2}$ nonstoichiometric ceramics . . . X.M. Chen *et al.* **2859**
Oxygen transport during annealing of Pb(Zr,Ti)O_3 thin films in O_2 gas and its effect on their conductivity . . . F. Ayguavives *et al.* **3005**
Low-resistance films of polyimides with impregnated copper sulfide . . . R.V.A. Rowe *et al.* **3097**
Solid solubility and transport properties of $Ce_{1-x}Nd_xO_{2-\delta}$ nanocrystalline solid solutions by a sol-gel route . . . Liping Li *et al.* **3207**
Direct writing of polymer thick film resistors using a novel laser transfer technique . . . R. Modi *et al.* **3214**
Photovoltaic effect of $Sn_2P_2S_6$ ferroelectric crystal and ceramics . . . Y.W. Cho *et al.* **3317**
High-temperature thermoelectric properties of *n*-type $Ba_yNi_xCo_{4-x}Sb_{12}$ . . . X.F. Tang *et al.* **3343**
Bulk- or interface-limited electrical conductions in IrO_2/(Ba,Sr)TiO_3/IrO_2 thin film capacitors . . . Cheol Seong Hwang **3476**
Impacts of postannealing ambient atmospheres on Pt/$SrBi_{2.2}Ta_2O_9$/Pt capacitors . . . Ai-Dong Li *et al.* **3526**

Electro-optical materials

Relationship between the microstructure and nanoindentation hardness of thermally evaporated and magnetron-sputtered electrochromic tungsten oxide films . . . C.W. Ong *et al.* **1541**
Structural and electrical properties of strontium barium niobate thin films crystallized by conventional furnace and rapid-thermal annealing process . . . R.G. Mendes *et al.* **3009**
Novel route for the epitaxial growth of (SrBa)Nb_2O_6 thick films by the sol-gel method using a self-template layer . . . A-D. Li *et al.* **3179**

Electrodeposition

Dense, bubble-free ceramic deposits from aqueous suspensions by electrophoretic deposition . . . Tetsuo Uchikoshi *et al.* **321**
Fabrication and characterization of microscale sandwich beams . . . Francisco Arias *et al.* **597**
X-ray photoelectron spectroscopy of electrodeposited cadmium mercury telluride thin films and their native surface oxides . . . J. Ramiro *et al.* **1942**

Electron energy-loss spectroscopy (EELS)

Structure and phase characteristics of amorphous boron–carbon–nitrogen under high pressure and high temperature . . . Jianyu Huang *et al.* **1178**

Electron irradiation

Study of the effects of low-energy electron bombardment during the chemical vapor deposition of diamond . . . J.A. González *et al.* **293**
Misting-free diamond surface created by sheet electron beam irradiation . . . Kazuya Oguri *et al.* **553**
Generation of circular and hexagonal microholes in a graphite surface . . . Hidefumi Hiura **1287**
Transient self-dewetting of steels after pulsed electron beam melting . . . N. Mingolo *et al.* **2343**

Electron spin resonance

Spectroscopic study of a cryptomelane-type manganic acid exchanged by divalent transition-metal cations . . . Masamichi Tsuji *et al.* **108**
Electronic paramagnetic resonance study of Cu^{2+} ions in copper ion-exchanged layers of lithium niobate crystals . . . F. Caccavale *et al.* **1554**

Electron-beam irradiation

High fracture resistance of carbon fiber treated by electron beam irradiation . . . Yoshitake Nishi *et al.* **1632**

Electron-phonon interactions

Influence of compositional disorder on optical absorption processes in $Cu_6P(S_{1-x}Se_x)_5I$ crystals . . . I.P. Studenyak *et al.* **1600**

Electronic materials

Adhesion of benzocyclobutene-passivated silicon in epoxy layered structures . . . Robert J. Hohlfelder *et al.* **243**
Gas flow effects on the structure and composition of $SiN_x/Si/SiN_x$ films prepared by radio-frequency magnetron sputtering . . . Wentao Xu *et al.* **308**
Evaluation of the modified edge lift-off test for adhesion characterization in microelectronic multifilm applications . . . Jack C. Hay *et al.* **385**
Modeling of the effects of crystallographic orientation on electromigration-limited reliability of interconnects with bamboo grain structures . . . W.R. Fayad *et al.* **413**
Field-activated combustion synthesis of Ta–Si intermetallic compounds . . . F. Maglia *et al.* **534**
In situ transmission electron microscopy study of the silicidation process in Co thin films on patterned (001) Si substrates . . . C. Ghica *et al.* **701**
Effects of Ce filling fraction and Fe content on the thermoelectric properties of Co-rich $Ce_xFe_xCo_{4-x}Sb_{12}$ . . . Xinfeng Tang *et al.* **837**
Alternating current conductivity of the interfacial phase in copper oxide–silica gel nanocomposites . . . D. Das *et al.* **1047**
Finite element modeling of microscale thermal residual stresses in Al interconnects . . . A. Saerens *et al.* **1112**
Rational solvent selection strategies to combat striation formation during spin coating of thin films . . . Dunbar P. Birnie, III **1145**
Synthesis of $Ba_2Ti_9O_{20}$ via ethylenediaminetetraacetic acid precursor . . . Yebin Xu *et al.* **1195**
Stability of channels at a scalloplike Cu_6Sn_5 layer in solder interconnections . . . Jong-Hyun Lee *et al.* **1227**
Characterization of NO_x sensor using doped In_2O_3 . . . Shinichiro Tanaka *et al.* **1389**
Production and characterization of titanium and iron oxide nano-sized thin films . . . E. Comini *et al.* **1559**
Interfacial embrittlement by bismuth segregation in copper/tin–bismuth Pb-free solder interconnect . . . P.L. Liu *et al.* **1651**
Influence of ligand groups in Ti precursors on phase transformation and microstructural evolution of TiO_2 thin films prepared by the wet chemical process . . . Chu-Chi Ting *et al.* **1712**
Metalorganic chemical vapor deposition of titanium oxide for microelectronics applications . . . Kanchana Vydianathan *et al.* **1838**
Piezoresistivity of conducting polyaniline/$BaTiO_3$ composites . . . R.C. Patil *et al.* **1982**
Growth behavior and defects in conductive $SrRuO_3$ thin films grown on a Si(100) substrate by sputtering . . . Sang Ho Oh *et al.* **1998**
Solid-state reaction mechanism for the formation of $Ba_{6-x}Ln_{8+2\,x/3}Ti_{18}O_{54}$ (Ln = Nd, Sm) solid solutions . . . Anatolii G. Belous *et al.* **2350**
Effect of lead content on vibration fracture behavior of Pb–Sn eutectic solder . . . C.M. Chuang *et al.* **2644**
Effects of static thermal aging and thermal cycling on the microstructure and shear strength of $Sn_{95.5}Ag_{3.8}Cu_{0.7}$ solder joints . . . Shawkret Ahat *et al.* **2914**
Effect of oxygen on the reactions in the Si/Ta/Cu metallization system . . . Tomi Laurila *et al.* **2939**
Growth and characterization of aligned carbon nanotubes from patterned nickel nanodots and uniform thin films . . . J.G. Wen *et al.* **3246**
Scanning probe microscopy generated out-of-plane deformation maps exhibiting heterogeneous nanoscale deformation resulting from thermal cycling of Cu–polyimide damascene interconnects . . . Todd S. Gross *et al.* **3560**

Electronic structure

Preliminary study on alternating thienylene/phenylene copolymers functionalized with an electron-donating or -withdrawing group . . . J.M. Xu *et al.* **1235**
Electrolyte electroreflectance study of TiO_2 films modified with metal nanoparticles . . . A.I. Kulak *et al.* **2357**

Elemental semiconductors

Diffusion of oxygen and silicon in silicon: Silicon monoxide model . . . Robert H. Doremus **185**
Planar oxidation of strained silicon substrates . . . M-T. Lin *et al.* **728**
Mechanical deformation in silicon by micro-indentation . . . J.E. Bradby *et al.* **1500**
Analysis and modeling of residual stress in diamond thin film deposited by the hot-filament chemical vapor deposition process . . . Seung I. Cha *et al.* **1953**
Size effect on the mechanical properties of microfabricated polysilicon thin films . . . J.N. Ding *et al.* **2223**
Quantum atomistic simulations of silicon and germanium . . . Carlos P. Herrero **2505**
Mechanical stress of the electrical performance of polycrystalline-silicon resistors . . . N. Nakabayashi *et al.* **2579**
Synthesis of silicon microwire . . . J.J. Petrovic *et al.* **2777**
Observations of structural order in ion-implanted amorphous silicon . . . Ju-Yin Cheng *et al.* **3030**
Defect formation due to the crystallisation of deep amorphous volumes formed in silicon by mega electron volt (*MeV*) ion implantation . . . A.C.Y. Liu *et al.* **3229**
Highly oriented diamond growth on positively biased Si substrates . . . Te-Fu Chang *et al.* **3351**
Laser-induced surface perturbations in silicon . . . A.J. Pedraza *et al.* **3599**

Embrittlement

Site preference of alloying elements in Fe_3Al-based alloys . . . Xiao Dong Ni *et al.* **344**
Effects of Cu and Ni additions to eutectic Pb–Sn solders on Au embrittlement of solder interconnections . . . Jong-Hyun Lee *et al.* **1249**

Energy-storage materials

Raman spectroscopic determination of phase evolutions in $LiAl_xCo_{1-x}O_2$ battery materials . . . P.S. Dobal *et al.* **1**
Thermal analysis investigation of hydriding properties of nanocrystalline Mg–Ni- and Mg–Fe-based alloys prepared by high-energy ball milling . . . L.E.A. Berlouis *et al.* **45**
Study of the activation process of Mg-based hydrogen storage materials modified by graphite and other carbonaceous compounds . . . S. Bouaricha *et al.* **2893**
Anode-supported planar solid oxide fuel cells by plasma-enhanced metalorganic chemical vapor deposition (PE-MOCVD) and electrostatic spray deposition (ESD): Fabrication of dense thin layers of yttria-stabilized zirconia by PE-MOCVD . . . Gianfranco Di Giuseppe *et al.* **2983**
Morphological effect on the electrochemical behavior of electric double-layer capacitors . . . M. Endo *et al.* **3402**

Environmentally protective materials

Preparation of calcium strontium hydroxyapatites by a new route involving calcium phosphate cements . . . L. Leroux *et al.* **171**
Microscopic effects of self-radiation damage in ^{244}Cm-doped $LuPO_4$ crystals . . . J.S. Luo *et al.* **366**

Er:Yb:Glasses

Investigation of optical waveguide formed in Er:Yb:phosphate glass by MeV He^+ implantation . . . Zhuang Zhuo *et al.* **1135**

Extended x-ray absorption fine structure (EXAFS)

CsCl-modified Ga_2S_3–La_2S_3 glasses: Structural approach by x-ray absorption spectroscopy . . . A.Y. Ramos *et al.* **1349**

Extrusion

Damping behavior of *in situ* Al–(graphite, Al_4C_3) composites produced by reciprocating extrusion . . . Hsu-Shen Chu *et al.* **1372**

Fatigue

Piezoelectric actuation of crack growth along polymer–metal interfaces in adhesive bonds . . . Tianbao Du *et al.* **2885**

Ferroelectrics

Growth of (111)-oriented $Pb(Zr,Ti)O_3$ layers on nanocrystalline RuO_2 electrodes using the sol-gel technique . . . G.J. Norga *et al.* **828**
Metalorganic chemical vapor deposition of very thin $Pb(Zr,Ti)O_3$ thin films at low temperatures for high-density ferroelectric memory applications . . . Hye Ryoung Kim *et al.* **3583**

Fiber

Morphological effect on the electrochemical behavior of electric double-layer capacitors . . . M. Endo *et al.* **3402**

Filamentary

Multifunctional microtruss laminates: Textile synthesis and properties . . . D.J. Sypeck *et al.* **890**
Synthesis of Al_2O_3–SiC from kyanite precursor . . . A. Amroune *et al.* **1609**
Synthesis and characterization of partially and fully stabilized zirconia fibers made from an inorganic precursor . . . A. Hartridge *et al.* **2384**
Synthesis of silicon microwire . . . J.J. Petrovic *et al.* **2777**
Microstructure studies of potassium hexatitanate whiskers . . . G.L. Li *et al.* **3614**

Film

Relationship between the microstructure and nanoindentation hardness of thermally evaporated and magnetron-sputtered electrochromic tungsten oxide films . . . . . C.W. Ong *et al.* **1541**
Molecular dynamics analysis of adhesion strength of interfaces between thin films . . . . . T. Iwasaki *et al.* **1789**
Silicalite/poly(dimethylsiloxane) nanocomposite pervaporation membranes for acetic acid/water separation . . . . . Shih-Yuan Lu *et al.* **3053**
Aligned carbon nanotube growth under oxidative ambient . . . . . Anyuan Cao *et al.* **3107**

Firing

Two-dimensional simulation of mass transport in polymer removal from a powder injection molding compact by thermal debinding . . . . . Ying Shengjie *et al.* **2436**

Flux growth

Ferroelectric $SrBi_2Ta_2O_9$ single-crystal growth and characterization . . . . . B. Sih *et al.* **1726**

Foam

Synthesis of open-cell metal foams by templated directed vapor deposition . . . Douglas T. Queheillalt *et al.* **1028**

Forging

High-strength porous silicon nitride fabricated by the sinter-forging technique . . . . . Naoki Kondo *et al.* **32**

Four-point bending test

Dependence of fracture stress on applied stress rate in a Yb_2O_3–SiO_2-doped hot-pressed silicon nitride ceramic . . . . . Shuqi Guo *et al.* **3254**

Fracture

Contact fracture of brittle bilayer coatings on soft substrates . . . . . Pedro Miranda *et al.* **115**
High fracture resistance of carbon fiber treated by electron beam irradiation . . . . . Yoshitake Nishi *et al.* **1632**
Interfacial embrittlement by bismuth segregation in copper/tin–bismuth Pb-free solder interconnect . . . . . P.L. Liu *et al.* **1651**
Increased fracture toughness in nanoporous silica–polyimide matrix composites . . . . . Shiling Ruan *et al.* **1975**
Microprobe fluorescence spectroscopy evaluation of stress fields developed along a propagating crack in an $Al_2O_3/CaO \cdot 6Al_2O_3$ ceramic composite . . . . . O. Sbaizero *et al.* **2798**
Shear-activated indentation crack in GaAs single crystal . . . . . Z.C. Li *et al.* **2845**
Evaluation of the impactive-surface-fracture behavior of glass plates using a back-surface strain measurement . . . . . Hyoung-Gu Kim *et al.* **3042**
Dependence of fracture stress on applied stress rate in a Yb_2O_3–SiO_2-doped hot-pressed silicon nitride ceramic . . . . . Shuqi Guo *et al.* **3254**
Minima in the strength of MnZn ferrites . . . . . M.A.H. Donners *et al.* **3575**

Fracture and fatigue

Characteristics of elastic waves generated by crack initiation in aluminum alloys under fatigue loading . . . . . Kiwoo Nam *et al.* **1745**

Gas chromatography

In situ analysis of gaseous species for chemical vapor deposition diamond synthesis and the possible reaction model . . . . . Mayu Uede *et al.* **3069**

Glass

Formation of $NdBa_2Cu_3O_{7-\delta}$ amorphous phase by combining aero-acoustic levitation and splat quenching . . . . . K. Nagashio *et al.* **138**
Devitrification kinetics and mechanism of Pyrex borosilicate glass . . . . . Jau-Ho Jean *et al.* **1752**
Crystallization kinetics of yttrium aluminum garnet ($Y_3Al_5O_{12}$) . . . . . Bradley R. Johnson *et al.* **1795**
Crystallization and dielectric properties of SrO–BaO–Nb_2O_5–GeO_2 tungsten–bronze glass–ceramics . . . . . Jiin-Jyh Shyu *et al.* **2057**
Photoinduced condensation of sol-gel hybrid glass films doped with benzildimethylketal . . . . . Oun-Ho Park *et al.* **2143**

Glasses

Relaxation of ultraviolet-radiation-induced structure and long-lasting phosphorescence in Eu^{2+}-doped strontium aluminosilicate glasses . . . . . Jianrong Qiu *et al.* **88**
Thermally reversible γ-ray-induced redox reaction between substitutional iron and aluminum impurity centers in a silica glass . . . . . Radhaballabh Debnath **127**
Coordination structures of implanted Fe, Co, and Ni ions in silica glass by x-ray absorption fine structure spectroscopy . . . . . Kohei Fukumi *et al.* **155**
Enhancement of the 1.31-μm emission properties of Dy^{3+}-doped Ge–Ga–S glasses with the addition of alkali halides . . . . . Yong Beom Shin *et al.* **1318**
Textural properties of $SiO_2 \cdot CaO \cdot P_2O_5$ glasses prepared by the sol-gel method . . . . . F. Balas *et al.* **1345**
CsCl-modified Ga_2S_3–La_2S_3 glasses: Structural approach by x-ray absorption spectroscopy . . . . . A.Y. Ramos *et al.* **1349**
Effect of composition on the thermal properties and spontaneous emission probabilities of Tm^{3+}-doped TeO_2–LiCl glass . . . . . G. Özen *et al.* **1381**
Phase separation in SiO_2–TiO_2 gel and glassy films studied by atomic force microscopy and transmission electron microscopy . . . . . A. Karthikeyan *et al.* **1626**
Determination of the elastic properties of glasses and polymers exploiting the resonant characteristic of depth-sensing indentation tests . . . . . D. Lorenz *et al.* **1776**
Structure of heat-treated sol-gel SiO_2 glasses containing silver . . . . . M.G. Garníca-Romo *et al.* **2007**
Glass transformation in vitreous As_2Se_3 studied by conventional and temperature-modulated differential scanning calorimetry . . . . . S.O. Kasap *et al.* **2399**
Explanation of the effects of gravity on crystallization of ZrF_2–BaF_2–LaF_3–AlF_3–NaF glass . . . . . Dennis S. Tucker *et al.* **3027**
Evaluation of the impactive-surface-fracture behavior of glass plates using a back-surface strain measurement . . . . . Hyoung-Gu Kim *et al.* **3042**

Glasses, metallic

Formation of icosahedral quasicrystal by crystallization of $Zr_{70}(Ni, Cu, Pd)_{30}$ amorphous alloys . . . T. Zhang *et al.* **20**
Redistribution behavior of constitutional elements at an initial crystallization stage in the $Zr_{65}Al_{7.5}Ni_{10}Cu_{17.5}$ glassy alloy . . . J. Saida *et al.* **28**
Glass-forming ability of the Ni–Zr and Ni–Ti systems determined by interatomic potentials . . . W.S. Lai *et al.* **446**
Crystallization kinetics of amorphous nanostructured $Pd_{40.5}Ni_{40.5}P_{19}$ alloys . . . H.W. Ngai *et al.* **797**
Formation and properties of $Zr_{48}Nb_8Fe_8Cu_{12}Be_{24}$ bulk metallic glass . . . Yong Zhang *et al.* **1675**
In situ transmission electron microscopy studies of shear bands in a bulk metallic glass based composite . . . E. Pekarskaya *et al.* **2513**
Compaction of bulk ferromagnetic $Fe_{80}P_{13}C_7$ amorphous alloys . . . F.W. Chan *et al.* **2767**
Mass density of glassy $Pd_{80}Si_{20}$ during low-temperature light ion irradiation . . . G. Schumacher *et al.* **2788**
Formation and mechanical properties of Cu–Hf–Ti bulk glassy alloys . . . Akihisa Inoue *et al.* **2836**
Change in local atomic structure during formation of the icosahedral quasicrystalline phase in $Zr_{70}Pd_{30}$ glassy alloy . . . Muneyuki Imafuku *et al.* **3046**
Investigation of the stability of glassy state in the Zr- and Hf-based glassy alloys correlated with their transformation behavior . . . Junji Saida *et al.* **3389**

Grain growth

Microwave sintering of ZnO at ultra high heating rates . . . Geng-fu Xu *et al.* **2850**
Formation of Al_2O_3 grains with different sizes and morphologies during the pulse electric current sintering process . . . S.W. Wang *et al.* **3514**

Hardness testing

Small correction required when applying the Hertzian contact model to instrumented indentation data . . . J.L. Hay *et al.* **1280**
Study of analysis methods of depth-sensing indentation test data for spherical indenters . . . A.C. Fischer-Cripps **1579**
Analysis of depth-sensing indentation tests with a Knoop indenter . . . L. Riester *et al.* **1660**
Measurement of residual stress by load and depth sensing indentation with spherical indenters . . . J.G. Swadener *et al.* **2091**
Simulation of sub-micron indentation tests with spherical and Berkovich indenters . . . A.C. Fischer-Cripps **2149**
Methods of correction for analysis of depth-sensing indentation test data for spherical indenters . . . A.C. Fischer-Cripps *et al.* **2244**
Identification of the constitutive equation by the indentation technique using plural indenters with different apex angles . . . Masatoshi Futakawa *et al.* **2283**
Thin-film fracture during nanoindentation of a titanium oxide film–titanium system . . . M. Pang *et al.* **2634**
Numerical study on the measurement of thin film mechanical properties by means of nanoindentation . . . Xi Chen *et al.* **2974**
Use of combined elastic modulus in the analysis of depth-sensing indentation data . . . A.C. Fischer-Cripps **3050**
Substrate effects on indentation plastic zone development in thin soft films . . . D.E. Kramer *et al.* **3150**
Derivation of plastic stress–strain relationship from ball indentations: Examination of strain definition and pileup effect . . . Jeong-Hoon Ahn *et al.* **3170**
Alternative technique for analyzing instrumented indentation data . . . W.C. Oliver **3202**

Hopping conductivity

Electrical transport properties of single-crystalline Mn–Zn ferrous ferrite . . . Yong-Chae Chung *et al.* **774**

Hot isostatic pressing (HIP)

Preferred orientation of beta-phase and its mechanisms in a fine-grained silicon-nitride-based ceramic . . . Rong-Jun Xie *et al.* **590**
Structure and phase characteristics of amorphous boron–carbon–nitrogen under high pressure and high temperature . . . Jianyu Huang *et al.* **1178**
Porosity and microstructure control of porous ceramics by partial hot pressing . . . Jian-Feng Yang *et al.* **1916**
Transmission electron microscopy observation in a liquid-phase-sintered SiC with oxynitride glass . . . Guo-Dong Zhan *et al.* **2189**

Hot pressing

Enhanced crystallization and phase transformation of amorphous silicon nitride under high pressure . . . Ya-Li Li *et al.* **67**
Compaction of bulk ferromagnetic $Fe_{80}P_{13}C_7$ amorphous alloys . . . F.W. Chan *et al.* **2767**

Hydrothermal

Mechanochemical-hydrothermal preparation of crystalline hydroxyapatite powders at room temperature . . . Pavel Shuk *et al.* **1231**

Hydrothermal synthesis

Processing effects on the composition and dielectric properties of hydrothermally derived $Ba_xSr_{(1-x)}TiO_3$ thin films . . . Mark A. McCormick *et al.* **1200**
Synthesis of $Zn_{2-x}Mn_xSiO_4$ phosphors using a hydrothermal technique . . . Chulsoo Yoon *et al.* **1210**
Preparation and phase control of nanocrystalline silver indium sulfides via a hydrothermal route . . . J.Q. Hu *et al.* **3411**

Impact testing

Evaluation of the impactive-surface-fracture behavior of glass plates using a back-surface strain measurement . . . Hyoung-Gu Kim *et al.* **3042**

Infiltration

Single-domain $YBa_2Cu_3O_y$ thick films and fabrics prepared by an infiltration and growth process . . . E. Sudhakar Reddy *et al.* **955**
A new technique for pressureless infiltration of Al alloys into Al_2O_3 preforms . . . . . B. Srinivasa Rao *et al.* **2906**
Novel synthesis of AlN nanowires with controlled diameters . . . Jun Liu *et al.* **3133**

Ink-jet printing

Investigation of some phenomena occurring during continuous ink-jet printing of ceramics . . . B.Y. Tay *et al.* **373**

Ion implantation

Coordination structures of implanted Fe, Co, and Ni ions in silica glass by x-ray absorption fine structure spectroscopy . . . Kohei Fukumi *et al.* **155**
Refractive index profile and attenuation measurement in $KTiOPO_4$ waveguide by megaelectronvolt He ions . . . Ke-Ming Wang *et al.* **276**
Characterization of bond formation in SiC and Si_3N_4 implanted with Ti, Fe, and Co . . . Didier Zanghi *et al.* **512**
Investigation of optical waveguide formed in Er:Yb:phosphate glass by MeV He^+ implantation . . . Zhuang Zhuo *et al.* **1135**
Hardness–depth profile of a carbon-implanted Ti–6Al–4V alloy and its relation to composition and microstructure . . . M. Kunert *et al.* **2321**
Nanocrystals in crystalline silicon: Void formation and hollow particles . . . A. Meldrum *et al.* **2670**
Observations of structural order in ion-implanted amorphous silicon . . . Ju-Yin Cheng *et al.* **3030**
Defect formation due to the crystallisation of deep amorphous volumes formed in silicon by mega electron volt (*MeV*) ion implantation . . . A.C.Y. Liu *et al.* **3229**
Mechanism of improvement of TiN-coated tool life by nitrogen implantation . . . S.J. Bull *et al.* **3293**
Effect of ion implant dose on the mechanical properties of polyethersulfone films . . . Manuel Luis B. Palacio *et al.* **3628**

Ion irradiation

Mass density of glassy $Pd_{80}Si_{20}$ during low-temperature light ion irradiation . . . G. Schumacher *et al.* **2788**

Ionic conductors

Influence of compositional disorder on optical absorption processes in $Cu_6P(S_{1-x}Se_x)_5I$ crystals . . . I.P. Studenyak *et al.* **1600**
Space-charge concepts on grain boundary impedance of a high-purity yttria-stabilized tetragonal zirconia polycrystal . . . Jong-Sook Lee *et al.* **2739**

Kinetic properties

$BaTiO_3$ formation by thermal decomposition of a (BaTi)-citrate polyester resin in air . . . P. Durán *et al.* **197**
Grain growth behavior of a nanostructured 5083 Al–Mg alloy . . . V.L. Tellkamp *et al.* **938**
Combustion synthesis of mechanically activated powders in the Ti–Si system . . . F. Maglia *et al.* **1074**
Growth of melt-textured Nd-123 by hot seeding under reduced oxygen partial pressure . . . M. Kambara *et al.* **1163**
Crystallization kinetics of yttrium aluminum garnet ($Y_3Al_5O_{12}$) . . . Bradley R. Johnson *et al.* **1795**
Kinetic analysis of solid-state processes . . . Jiří Málek *et al.* **1862**
Topological transformation of grains in three-dimensional normal grain growth . . . F. Wakai *et al.* **2136**
Effects of zinc(II) and iron(III) doping of titania films on their photoreactivity to decompose rhodamine B . . . Ying Ma *et al.* **2928**
Thermal stability of carbon nitride thin films . . . Niklas Hellgren *et al.* **3188**
High grain size stability of nanocrystalline Al prepared by mechanical attrition . . . F. Zhou *et al.* **3451**

Kinetics

Characterization of the induction period in tricalcium silicate hydration by nuclear resonance reaction analysis . . . R.A. Livingston *et al.* **687**
Nonisothermal phase formation kinetics in sol-gel-derived strontium bismuth tantalate . . . Yun-Mo Sung **2039**

Laminate

Statistical behavior and misfit stresses in ceramic and metal laminated system . . . D. Sherman *et al.* **721**
Delamination of a strong film from a ductile substrate during indentation unloading . . . A. Abdul-Baqi *et al.* **1396**
Analysis of interdiffusion of Dy, Nd, and Pr in Mg . . . Y. Xu *et al.* **3287**

Laser ablation

Epitaxial growth of skutterudite ($CoSb_3$) thin films on (001) InSb by pulsed laser deposition . . . J.C. Caylor *et al.* **2467**

Laser annealing

Low-temperature crystallization induced by excimer laser irradiation of $SrBi_2Ta_2O_9$ films . . . Kwang Soo Seol *et al.* **1883**

Laser irradiation

Modification of sol–gel-derived amorphous Al_2O_3 thin films by F_2 excimer laser irradiation at ambient temperature . . . Satoshi Takeda *et al.* **1003**
Direct laser writing of self-developed waveguides in benzyldimethylketal-doped sol-gel hybrid glass . . . Byeong-Soo Bae *et al.* **3184**
Laser-induced surface perturbations in silicon . . . A.J. Pedraza *et al.* **3599**

Layered structure

Contact fracture of brittle bilayer coatings on soft substrates . . . Pedro Miranda *et al.* **115**
Evaluation of the modified edge lift-off test for adhesion characterization in microelectronic multifilm applications . . . Jack C. Hay *et al.* **385**
Analysis of a ceramic/metal laminate under thermal shock . . . D. Sherman *et al.* **753**
Growth, structure, and mechanical properties of transition metal carbide superlattices . . . H. Högberg *et al.* **1301**
Texture in Ti/Al and Nb/Al multilayer thin films: Role of Cu . . . G. Lucadamo *et al.* **1449**

	Cracking of porcelain coatings bonded to metal substrates of different modulus and hardness . . . Hong Zhao *et al.*	1471
	Compositional distributions in nanoscale metallic multilayers studied using x-ray mapping . . . V.J. Keast *et al.*	2032
	Effect of annealing on microstructure, residual stress, and hardness of Al–Ti multilayered films . . . R. Mitra *et al.*	2064
	Characterization of mechanical properties of tungsten carbide/carbon multilayers: Cross-sectional electron microscopy and nanoindentation observations . . . N.J.M. Carvalho *et al.*	2213
	Growth and characterization of conductive $SrRuO_3$ and $LaNiO_3$ multilayers on textured Ni tapes for high-J_c $YBa_2Cu_3O_{7-\delta}$ coated conductors . . . T. Aytug *et al.*	2661
	Bulk- or interface-limited electrical conductions in IrO_2/(Ba,Sr)TiO_3/IrO_2 thin film capacitors . . . Cheol Seong Hwang	3476
Liquid	Origin of the anomalous volume expansion in Al–Si alloys above liquidus . . . W.M. Wang *et al.*	3592
Liquid-phase epitaxy (LPE)	Preferential growth mechanism of $REBa_2Cu_3O_y$ (RE = Y, Nd) crystal on MgO substrate by liquid phase epitaxy . . . Katsumi Nomura *et al.*	979
	Initial growth mechanism of $YBa_2Cu_3O_y$ crystal on MgO substrate by liquid-phase epitaxy . . . Katsumi Nomura *et al.*	2947
Lubricants	Impression creep of a viscous layer . . . Hong Chen *et al.*	2709
	Fretting wear rate of sulphur deficient MoS_x coatings based on dissipated energy . . . Xiaoling Zhang *et al.*	3567
Luminescence	Photoluminescence behavior of Al^{3+}, Pr^{3+} doped perovskite $La_{2/3}TiO_3$ and pyrochlore $La_2Ti_2O_7$ . . . J.K. Park *et al.*	2568
Magnetic materials	Formation and characterization of crystalline iron oxide films on self-assembled organic monolayers and their *in situ* patterning . . . Hyunjung Shin *et al.*	564
	Electrical transport properties of single-crystalline Mn–Zn ferrous ferrite . . . Yong-Chae Chung *et al.*	774
	Growth study of epitaxial $Fe_xZn_{1-x}F_2$ thin films . . . J. McChesney *et al.*	1769
	Low-temperature growth of *c*-axis-oriented Y-type hexagonal ferrite thin films by the polymeric precursor method . . . Tatsuo Fujii *et al.*	2471
	Metastable solidification of NdFeB alloys by drop-tube processing . . . Jianrong Gao *et al.*	2562
	Microstructure of $La_{1-x}Ca_xMnO_3$ studied by transmission electron microscopy . . . Q. Chen *et al.*	2959
	Halide removal from BaM ($BaFe_{12}O_{19}$) and SrM ($SrFe_{12}O_{19}$) ferrite fibers via a steaming process . . . R.C. Pullar *et al.*	3162
	Preparation of γ–Fe_2O_3 nanoparticles from a nonaqueous precursor . . . P. Deb *et al.*	3471
Magnetic properties	Thermally reversible γ-ray-induced redox reaction between substitutional iron and aluminum impurity centers in a silica glass . . . Radhaballabh Debnath	127
	Carbonization behavior of polyimide film containing iron complex in relation to magnetic properties . . . Y. Kaburagi *et al.*	352
	Magnetic properties, domain structure, and microstructure of anisotropic $SmCo_{6.5}Zr_{0.5}$ ribbons with C addition . . . A-Ru Yan *et al.*	629
	Effects of preparation processes on structure and magnetic properties of $Nd_2Fe_{14}B$/α–Fe-type nanocomposite magnets . . . Bao-zhi Cui *et al.*	709
	Plate domain structure of sintered NdFeB magnets and dependence on compacting mode . . . Zhen Rong Zhang *et al.*	2992
Marangoni effect	Transient self-dewetting of steels after pulsed electron beam melting . . . N. Mingolo *et al.*	2343
Mechanical properties	High-strength porous silicon nitride fabricated by the sinter-forging technique . . . Naoki Kondo *et al.*	32
	Rheological characteristics of slurry controlling the microstructure and the compressive strength behavior of biomimetic hydroxyapatite . . . S. Guicciardi *et al.*	163
	Strength prediction of partially aligned discontinuous fiber-reinforced composites . . . Rex J. Kuriger *et al.*	226
	Residual stress in fiber-textured thin films of cubic materials . . . P. Scardi *et al.*	233
	A note on a common mistake in the analysis of nanoindentation data . . . M. Munawar Chaudhri	336
	Improved tensile creep properties of yttrium- and lanthanum-doped alumina: a solid solution effect . . . Junghyun Cho *et al.*	425
	Development of a continuous microscratch technique in an atomic force microscope and its application to study scratch resistance of ultrathin hard amorphous carbon coatings . . . Sriram Sundararajan *et al.*	437
	Characterization and modeling of specific strain gradient modulus of epoxy . . . D.C.C. Lam *et al.*	558
	Fabrication and characterization of microscale sandwich beams . . . Francisco Arias *et al.*	597
	Transient creep in fine-grained polycrystalline Al_2O_3 with Lu^{3+} ion segregation at the grain boundaries . . . Hidehiro Yoshida *et al.*	716
	Statistical behavior and misfit stresses in ceramic and metal laminated system . . . D. Sherman *et al.*	721
	Analysis of a ceramic/metal laminate under thermal shock . . . D. Sherman *et al.*	753
	Influence of annealing treatments on microstructure and toughness of liquid-phase-sintered silicon carbide . . . D. Sciti *et al.*	806

In situ microscopic surface characterization studies of polymeric thin films during tensile deformation using atomic force microscopy . . . M.S. Bobji *et al.* **844**
Effects of strain hardenability and strain-rate sensitivity on the plastic flow and deformation homogeneity during equal channel angular pressing . . . Hyoung Seop Kim *et al.* **856**
Machinable calcium pyrophosphate glass-ceramics . . . Toshihiro Kasuga *et al.* **876**
Multifunctional microtruss laminates: Textile synthesis and properties . . . D.J. Sypeck *et al.* **890**
Ultrathin TiB_2 protective films . . . Feng Huang *et al.* **945**
Direct measurement of mechanical properties of $(Pb,La)TiO_3$ ferroelectric thin films using nanoindentation techniques . . . M. Algueró *et al.* **993**
Effect of process variables on the structure, residual stress, and hardness of sputtered nanocrystalline nickel films . . . R. Mitra *et al.* **1010**
Torsion and bending of micron-scaled structures . . . A.C.M. Chong *et al.* **1052**
Influence of thermal history on morphology and viscoelastic behavior of ethylene–1-octene copolymers synthesized with metallocene catalysts . . . M.L. Cerrada *et al.* **1103**
Finite element modeling of microscale thermal residual stresses in Al interconnects . . . A. Saerens *et al.* **1112**
Orientation dependence of Portevin–Le Châtelier plastic instabilities in depth-sensing microindentation . . . Zs. Kovács *et al.* **1171**
Growth, structure, and mechanical properties of transition metal carbide superlattices . . . H. Högberg *et al.* **1301**
Creep and toughness of cryomilled NiAl containing Cr . . . J. Daniel Whittenberger *et al.* **1333**
Damping behavior of *in situ* Al–(graphite, Al_4C_3) composites produced by reciprocating extrusion . . . Hsu-Shen Chu *et al.* **1372**
Delamination of a strong film from a ductile substrate during indentation unloading . . . A. Abdul-Baqi *et al.* **1396**
Biomimetic model of a sponge-spicular optical fiber—mechanical properties and structure . . . M. Sarikaya *et al.* **1420**
Cracking of porcelain coatings bonded to metal substrates of different modulus and hardness . . . Hong Zhao *et al.* **1471**
Direct measurement of plowing friction and wear of a polymer thin film using the atomic force microscope . . . Binyang Du *et al.* **1487**
Mechanical deformation in silicon by micro-indentation . . . J.E. Bradby *et al.* **1500**
Solid-state foaming of titanium by superplastic expansion of argon-filled pores . . . N.G. Davis *et al.* **1508**
Relationship between the microstructure and nanoindentation hardness of thermally evaporated and magnetron-sputtered electrochromic tungsten oxide films . . . C.W. Ong *et al.* **1541**
Study of analysis methods of depth-sensing indentation test data for spherical indenters . . . A.C. Fischer-Cripps **1579**
Interfacial embrittlement by bismuth segregation in copper/tin–bismuth Pb-free solder interconnect . . . P.L. Liu *et al.* **1651**
Analysis of depth-sensing indentation tests with a Knoop indenter . . . L. Riester *et al.* **1660**
Formation and properties of $Zr_{48}Nb_8Fe_8Cu_{12}Be_{24}$ bulk metallic glass . . . Yong Zhang *et al.* **1675**
Superplasticicity of Cu–16 at.% Ag microcomposites . . . S.I. Hong *et al.* **1822**
Novel hexagonal structure and ultrahigh strength of magnesium solid solution in the Mg–Zn–Y system . . . Akihisa Inoue *et al.* **1894**
Effects of whisker content and dimensions on the *R*-curve behavior of an alumina matrix composite reinforced with silicon carbide whiskers . . . Takashi Akatsu *et al.* **1919**
Analysis and modeling of residual stress in diamond thin film deposited by the hot-filament chemical vapor deposition process . . . Seung I. Cha *et al.* **1953**
Anelastic behavior of precursor-derived amorphous ceramics in the system Si–B–C–N . . . Martin Christ *et al.* **1994**
Effect of annealing on microstructure, residual stress, and hardness of Al–Ti multilayered films . . . R. Mitra *et al.* **2064**
Measurement of residual stress by load and depth sensing indentation with spherical indenters . . . J.G. Swadener *et al.* **2091**
Simulation of sub-micron indentation tests with spherical and Berkovich indenters . . . A.C. Fischer-Cripps **2149**
Improved creep resistance in anisotropic silicon nitride . . . Naoki Kondo *et al.* **2182**
Characterization of mechanical properties of tungsten carbide/carbon multilayers: Cross-sectional electron microscopy and nanoindention observations . . . N.J.M. Carvalho *et al.* **2213**
Methods of correction for analysis of depth-sensing indentation test data for spherical indenters . . . A.C. Fischer-Cripps *et al.* **2244**
Effect of α/β phase ratio on microstructure and mechanical properties of silicon nitride ceramics . . . Hirokazu Kawaoka *et al.* **2264**
Identification of the constitutive equation by the indentation technique using plural indenters with different apex angles . . . Masatoshi Futakawa *et al.* **2283**
Hardness–depth profile of a carbon-implanted Ti–6Al–4V alloy and its relation to composition and microstructure . . . M. Kunert *et al.* **2321**
Synthesis and characterization of partially and fully stabilized zirconia fibers made from an inorganic precursor . . . A. Hartridge *et al.* **2384**
Controlled preparation and characterization of multilayer sol-gel zirconia dip-coatings . . . Ricardo Caruso *et al.* **2391**
Model for the robust mechanical behavior of nacre . . . A.G. Evans *et al.* **2475**

Deformation mechanisms in nacre . . . R.Z. Wang *et al.* **2485**
Freeform fabrication of aluminum metal-matrix composites . . . C.W. Souvignier *et al.* **2613**
Thin-film fracture during nanoindentation of a titanium oxide film–titanium system . . . M. Pang *et al.* **2634**
Effect of lead content on vibration fracture behavior of Pb–Sn eutectic solder . . . C.M. Chuang *et al.* **2644**
Impression creep of a viscous layer . . . Hong Chen *et al.* **2709**
Development of a model for the prediction of the fretting fatigue regimes . . . T.E. Matikas *et al.* **2716**
Mechanical properties of nanocrystalline and epitaxial TiN films on (100) silicon . . . H. Wang *et al.* **2733**
Formation and mechanical properties of Cu–Hf–Ti bulk glassy alloys . . . Akihisa Inoue *et al.* **2836**
Numerical study on the measurement of thin film mechanical properties by means of nanoindentation . . . Xi Chen *et al.* **2974**
Thermal stress in a polymer-coated optical glass fiber with a low-modulus coating at the ends . . . E. Suhir **2996**
Ion energy dependence of film properties for diamond-like carbon prepared with plasma-assisted deposition . . . Cao Zexian **3034**
Use of combined elastic modulus in the analysis of depth-sensing indentation data . . . A.C. Fischer-Cripps **3050**
Substrate effects on indentation plastic zone development in thin soft films . . . D.E. Kramer *et al.* **3150**
Derivation of plastic stress–strain relationship from ball indentations: Examination of strain definition and pileup effect . . . Jeong-Hoon Ahn *et al.* **3170**
Alternative technique for analyzing instrumented indentation data . . . W.C. Oliver **3202**
Processing and characterization of hydroxyapatite coatings on titanium produced by magnetron sputtering . . . T.G. Nieh *et al.* **3238**
Mechanism of improvement of TiN-coated tool life by nitrogen implantation . . . S.J. Bull *et al.* **3293**
Deformation under nanoindents in Si, Ge, and GaAs examined through transmission electron microscopy . . . S.J. Lloyd *et al.* **3347**
Adhesion of polymer–inorganic interfaces by nanoindentation . . . Min Li *et al.* **3378**
Lubricity of zinc oxide thin films: Study of deposition parameters and Si as an additive . . . J.J. Nainaparampil *et al.* **3423**
Embedded-atom-method functions for the body-centered-cubic iron and hydrogen . . . Mao Wen *et al.* **3496**
Mechanical and thermal properties of combustion-synthesized perovskites, $La_{1-x}Sr_xCr_{0.2}Fe_{0.8}O_3$ . . . Yeong-Shyung Chou *et al.* **3545**
Fretting wear rate of sulphur deficient MoS_x coatings based on dissipated energy . . . Xiaoling Zhang *et al.* **3567**
Effect of ion implant dose on the mechanical properties of polyethersulfone films . . . Manuel Luis B. Palacio *et al.* **3628**

Metalorganic chemical vapor deposition (MOCVD)

Metalorganic chemical vapor deposition of very thin $Pb(Zr,Ti)O_3$ thin films at low temperatures for high-density ferroelectric memory applications . . . Hye Ryoung Kim *et al.* **3583**

Metals

Effect of process variables on the structure, residual stress, and hardness of sputtered nanocrystalline nickel films . . . R. Mitra *et al.* **1010**
Torsion and bending of micron-scaled structures . . . A.C.M. Chong *et al.* **1052**
Chemical–mechanical polishing of copper and tantalum with silica abrasives . . . Y. Li *et al.* **1066**
Texture analysis of grain refinement in undercooled $Ni_{99.45}B_{0.55}$ . . . K.L. Lee *et al.* **1434**
Texture in Ti/Al and Nb/Al multilayer thin films: Role of Cu . . . G. Lucadamo *et al.* **1449**
Solid-state foaming of titanium by superplastic expansion of argon-filled pores . . . N.G. Davis *et al.* **1508**
Compositional distributions in nanoscale metallic multilayers studied using x-ray mapping . . . V.J. Keast *et al.* **2032**
Effect of annealing on microstructure, residual stress, and hardness of Al–Ti multilayered films . . . R. Mitra *et al.* **2064**
Measurement of residual stress by load and depth sensing indentation with spherical indenters . . . J.G. Swadener *et al.* **2091**
Highly (111)-oriented and conformal iridium films by liquid source metalorganic chemical vapor deposition . . . Jaydeb Goswami *et al.* **2192**
Moving the pulsed heating technique beyond monolithic specimens: Experiments with coated wires . . . D. Josell *et al.* **2421**
Synthesis of nanoscale particles of Ta and Nb_3Al by homogeneous reduction in liquid ammonia . . . Hongmin Zhu *et al.* **2544**
Combustion of zirconium foils in oxygen . . . K.H. Ewald *et al.* **2687**
Study of the activation process of Mg-based hydrogen storage materials modified by graphite and other carbonaceous compounds . . . S. Bouaricha *et al.* **2893**
Analysis of interdiffusion of Dy, Nd, and Pr in Mg . . . Y. Xu *et al.* **3287**
Comparison of different models for melting point change of metallic nanocrystals . . . M. Zhao *et al.* **3304**
High grain size stability of nanocrystalline Al prepared by mechanical attrition . . . F. Zhou *et al.* **3451**
Origins of stored enthalpy in cryomilled nanocrystalline Zn . . . Xinghang Zhang *et al.* **3485**
Embedded-atom-method functions for the body-centered-cubic iron and hydrogen . . . Mao Wen *et al.* **3496**

Micron-scale

Torsion and bending of micron-scaled structures . . . A.C.M. Chong *et al.* **1052**

Microstructural

Microstructural studies of Cu brazing on AlN . . . Chaoxian Cai *et al.* **670**

Epitaxial growth of $PbZr_{0.5}Ti_{0.5}O_3$ thin films on $SrRuO_3/SrTiO_3$ substrates using chemical solution deposition: Microstructural and ferroelectric properties . . . J.H. Kim *et al.* **1739**

X-ray scattering study on the structural evolution of AlN/sapphire(0001) films during radiofrequency sputter growth . . . H.C. Kang *et al.* **1814**

Formation and characteristics of highly *c*-axis-oriented $Bi_{3.25}La_{0.75}Ti_3O_{12}$ thin films on $SiO_2/Si(100)$ and $Pt/Ti/SiO_2/Si(100)$ substrates . . . Uong Chon *et al.* **3124**

Microstructure

Metal/ceramic interface in an *in situ* synthesized Ti/TiC_p composite coating by laser processing . . . R. Yu *et al.* **9**

Chemical-vapor-deposition growth and characterization of epitaxial 3C–SiC films on SOI substrates with thin silicon top layers . . . C.K. Moon *et al.* **24**

Macroporous morphology of titania films prepared by sol-gel dip-coating method from a system containing poly(ethylene glycol) and poly(vinylpyrrolidone) . . . Koichi Kajihara *et al.* **58**

Formation of $NdBa_2Cu_3O_{7-\delta}$ amorphous phase by combining aero-acoustic levitation and splat quenching . . . K. Nagashio *et al.* **138**

Coordination structures of implanted Fe, Co, and Ni ions in silica glass by x-ray absorption fine structure spectroscopy . . . Kohei Fukumi *et al.* **155**

Combined out-of-plane and in-plane texture control in thin films using ion beam assisted deposition . . . L. Dong *et al.* **210**

Chemical reaction at the interface between $(Hg_{0.9}Re_{0.1})Ba_2CaCu_2O_y$ thin film and $SrTiO_3$ substrate . . . Xiao-Jing Wu *et al.* **256**

Characterization of GaN grown on sapphire by laser-induced molecular beam epitaxy . . . H. Zhou *et al.* **261**

Designing composite microstructures with targeted properties . . . S. Hyun *et al.* **280**

Surface effects in field-assisted sintering . . . J.R. Groza *et al.* **286**

Sintering and microstructure of glass-coated nanocrystalline yttria-stabilized tetragonal zirconia powder: Effect of the glass . . . R. Ramamoorthy *et al.* **296**

Microscopic effects of self-radiation damage in ^{244}Cm-doped $LuPO_4$ crystals . . . J.S. Luo *et al.* **366**

Joining characteristics of oxidized SiC particles reinforced Al–Mg matrix composite prepared by reaction infiltration processing . . . Zhongliang Shi *et al.* **400**

Microstructure of (Nd, Eu, Gd)-123 matrix with (Nd, Eu, Gd)-211 inclusions . . . M. Muralidhar *et al.* **407**

Densification and grain growth of Al-doped ZnO . . . Jiaping Han *et al.* **459**

Thermal stability of nanocrystalline WC–Co powder synthesized by using mechanical milling at low temperature . . . Jianhong He *et al.* **478**

Nonepitaxial heterogeneous nucleation of α-sialon in the Ca-doped system . . . Ya-Wen Li *et al.* **578**

Grain boundary structure in Al–Mg and Al–Mg–Sc alloys after equal-channel angular pressing . . . Keiichiro Oh-ishi *et al.* **583**

Preferred orientation of beta-phase and its mechanisms in a fine-grained silicon-nitride-based ceramic . . . Rong-Jun Xie *et al.* **590**

Deposition of epitaxial transition metal carbide films and superlattices by simultaneous direct current metal magnetron sputtering and C_{60} evaporation . . . H. Högberg *et al.* **633**

Influence of $CaO–SiO_2$ ratio on the chemistry of intergranular films in liquid-phase sintered alumina and implications for rate of erosive wear . . . Rik Brydson *et al.* **652**

Electron backscatter diffraction analysis of $Pb(Mg_{1/3}Nb_{2/3})O_3$–35mol%$PbTiO_3$ single crystals grown by seeded polycrystal conversion . . . Ajmal Khan *et al.* **694**

Single-domain $YBa_2Cu_3O_y$ thick films and fabrics prepared by an infiltration and growth process . . . E. Sudhakar Reddy *et al.* **955**

New combustion synthesis technique for the production of $(In_xGa_{1-x})_2O_3$ powders: Hydrazine/metal nitrate method . . . R. García *et al.* **1059**

Synthesis of $Nd_2Fe_{14}B$ powders by spray-drying and reduction–diffusion processes . . . X.L. Dong *et al.* **1083**

Phenomenological description of grain growth stagnation for nanocrystalline films and powders . . . Rand Dannenberg *et al.* **1090**

Stability of channels at a scalloplike Cu_6Sn_5 layer in solder interconnections . . . Jong-Hyun Lee *et al.* **1227**

Twinning domain in $67Pb(Mg_{1/3}Nb_{2/3})O_3$–$33PbTiO_3$ ferroelectric complex perovskite crystal grown by the Bridgman method . . . Donglin Li *et al.* **1252**

Texture in Ti/Al and Nb/Al multilayer thin films: Role of Cu . . . G. Lucadamo *et al.* **1449**

Production and characterization of titanium and iron oxide nano-sized thin films . . . E. Comini *et al.* **1559**

Metal–oxide films with magnetically-modulated nanoporous architectures . . . Craig A. Grimes *et al.* **1686**

Melt processing of Ba_2CuO_3: Textured precursor for the fabrication of $HgBa_2CuO_y$ superconductor . . . E. Sudhakar Reddy *et al.* **1759**

Influence of sintering atmosphere on the fabrication of SiC ceramics with a powder mixture of sialon composition . . . Jong-Kook Lee *et al.* **1784**

$L1_2$- and $L1_0$-like cation-ordered structures in $ZrO_2–Y_2O_3$ ceramics . . . J.C. Rao *et al.* **1806**

Submicron-grained multiphase TiAlSi alloys: Processing, characterization, and microstructural design . . . R. Bohn *et al.* **1850**

Effects of thermal annealing on the texture of $La_{0.67}Sr_{0.33}MnO_3$ thin films . . . Lamartine Meda *et al.* **1887**

Porosity and microstructure control of porous ceramics by partial hot pressing . . . Jian-Feng Yang *et al.* **1916**

Microstructure and formation mechanism of combustion-synthesized rodlike Ca α-sialon crystals . . . Kexin Chen *et al.* **1928**

Influence of antiphase boundaries on critical current densities in $YBa_2Cu_3O_{7-y}$ single crystals . . . Junko Shibata *et al.* **1935**

Growth behavior and defects in conductive $SrRuO_3$ thin films grown on a Si(100) substrate by sputtering . . . Sang Ho Oh *et al.* **1998**

Transmission electron microscopy study of $n = 1–5$ $Sr_{n+1}Ti_nO_{3n+1}$ epitaxial thin films . . . W. Tian *et al.* **2013**

Study of phase components of $La_{1.5}Ca_{1.5}Mn_2O_7$ . . . J.L. Zhu *et al.* **2027**

Gradient porosity poly(dicyclopentadiene) . . . A. Della Martina *et al.* **2045**

Microstructural characterization of rapidly solidified Al–Fe–Si, Al–V–Si, and Al–Fe–V–Si alloys . . . A.K. Srivastava *et al.* **2103**

Cubic silicon nitride embedded in amorphous silicon dioxide . . . Ming Zhang *et al.* **2179**

Effect of a magnetic field on phase transformation of steel . . . W. Liu *et al.* **2280**

Microstructure and growth of joins in melt-textured $YBa_2Cu_3O_{7-\delta}$ . . . A.D. Bradley *et al.* **2298**

Modeling of electric field induced texture in lead zirconate titanate ceramics . . . Shan Wan *et al.* **2306**

Solid-state reaction mechanism for the formation of $Ba_{6-x}Ln_{8+2\,x/3}Ti_{18}O_{54}$ (Ln = Nd, Sm) solid solutions . . . Anatolii G. Belous *et al.* **2350**

^{29}Si nuclear-magnetic-resonance and vibrational spectroscopy studies of SiO_2–TiO_2 powders prepared by the sol-gel process . . . J.P. Rainho *et al.* **2369**

Interface structure and solute segregation behavior in SiC/2124 and SiC/6061 Al composites exhibiting high-strain-rate superplasticity . . . Woo-Jin Kim *et al.* **2429**

Formation of eutectic RuAl/Ru nanocomposite by mechanical alloying and subsequent annealing . . . K.W. Liu *et al.* **2459**

Chemical structure evolution and orientation selection in sol-gel-prepared ferroelectric $Pb(Zr,Ti)O_3$ thin films . . . L. Fè *et al.* **2499**

In situ transmission electron microscopy studies of shear bands in a bulk metallic glass based composite . . . E. Pekarskaya *et al.* **2513**

Annealing effect on in-plane alignment and surface morphology of epitaxial $Bi_4Ti_3O_{12}$ thin films prepared by the chemical solution deposition . . . K. Hwang *et al.* **2519**

Metastable solidification of NdFeB alloys by drop-tube processing . . . Jianrong Gao *et al.* **2562**

Effect of *in situ* boron doping on properties of silicon germanium films deposited by chemical vapor deposition at 400 °C . . . Sherif Sedky *et al.* **2607**

Precipitate splitting in $Pb_{0.91}La_{0.09}Zr_{0.65}Ti_{0.35}O_3$ films . . . Bahadir Tunaboylu *et al.* **2763**

Synthesis of silicon microwire . . . J.J. Petrovic *et al.* **2777**

Preparation, structure, and magnetic properties of cobalt nanoparticles in carbon fibers . . . I. Bashmakov *et al.* **2832**

Excellent buffer layer for growing high-quality Y–Ba–Cu–O thin films . . . W.H. Tang *et al.* **2864**

Nucleation and growth of $YBa_2Cu_3O_x$ on $SrTiO_3$ and CeO_2 by a BaF_2 postdeposition reaction process . . . L. Wu *et al.* **2869**

Formation and characterization of high-density silver nanoparticles embedded in silica thin films by "*in situ*" self-reduction . . . G. Compagnini *et al.* **2934**

Microstructure of $La_{1-x}Ca_xMnO_3$ studied by transmission electron microscopy . . . Q. Chen *et al.* **2959**

Phase formation and crystal growth of Sr–Bi–Ta–O thin films grown by metalorganic chemical vapor deposition . . . H. Bachhofer *et al.* **2966**

Electron microscopy of high-temperature and high-pressure as-grown diamond crystals . . . Long-Wei Yin *et al.* **3023**

Observations of structural order in ion-implanted amorphous silicon . . . Ju-Yin Cheng *et al.* **3030**

Microstructures of $La_{1-x}A_x$(A = Ca or Sr)$MnO_{3-\delta}$ thin films by liquid-delivery metalorganic chemical vapor deposition . . . Y. Xin *et al.* **3073**

Growth and characterization of aligned carbon nanotubes from patterned nickel nanodots and uniform thin films . . . J.G. Wen *et al.* **3246**

Processing of mesoporous alumina from a powder precursor . . . J. Wayne Frazee *et al.* **3262**

Consolidation and crystallization of Si_3N_4/SiC nanocomposites from a poly(urea–silazane) ceramic precursor . . . Julin Wan *et al.* **3274**

Microstructure of laser-ablated superconducting $La_2CuO_4F_x$ thin films on $SrTiO_3$ . . . G. Kong *et al.* **3309**

Titanium oxide nanotube arrays prepared by anodic oxidation . . . Dawei Gong *et al.* **3331**

Highly oriented diamond growth on positively biased Si substrates . . . Te-Fu Chang *et al.* **3351**

Microstructural and mechanical characterization of carbon coatings on SiC fibers . . . K.L. Kendig *et al.* **3366**

Morphological effect on the electrochemical behavior of electric double-layer capacitors . . . M. Endo *et al.* **3402**

Structural characterization of laser-treated Cr_3C_2–NiCr coatings . . . P. Serra *et al.* **3416**

Microstructure and misfit relaxation in $SrTiO_3$/$SrRuO_3$ bilayer films on $LaAlO_3$(100) substrates . . . J.S. Wu *et al.* **3443**

Preparation of superfine Fe-base alloy by liquidus casting . . . X.F. Pan *et al.* **3459**

Scanning probe microscopy generated out-of-plane deformation maps exhibiting heterogeneous nanoscale deformation resulting from thermal cycling of Cu–polyimide damascene interconnects . . . Todd S. Gross *et al.* **3560**

Laser-induced surface perturbations in silicon . . . A.J. Pedraza *et al.* **3599**

Microstructure studies of potassium hexatitanate whiskers . . . G.L. Li *et al.* **3614**

Preparation of nanocrystalline nickel oxide–yttria-stabilized zirconia composite powder by solution combustion with ignition of glycine fuel . . . Sun-Jae Kim *et al.* **3621**

Micro wear test

Phase transformation effects on the wear properties of alumina gel–polymer matrix nanocomposites . . . Jiazhong Luo *et al.* **1680**

Microwave heating

Reaction kinetics and anisothermal effects in microwave fields: The System Y_2O_3–Fe_3O_4 . . . . Ramesh D. Peelamedu *et al.* **2770**

Microwave sintering

Microwave sintering of ZnO at ultra high heating rates . . . . Geng-fu Xu *et al.* **2850**

Mixed oxide

Coherent island formation of Cu_2O films grown by chemical vapor deposition on MgO(110) . . . . P.R. Markworth *et al.* **2408**

Molding

Packing and solidification in ceramic injection moulding . . . . S. Krug *et al.* **1829**

Nanocomposites

Alternating current conductivity of the interfacial phase in copper oxide–silica gel nanocomposites . . . . D. Das *et al.* **1047**

Nanocrystal

Thermal analysis investigation of hydriding properties of nanocrystalline Mg–Ni- and Mg–Fe-based alloys prepared by high-energy ball milling . . . . L.E.A. Berlouis *et al.* **45**

Additive controlled crystallization of barium titanate powders and their application for thin-film ceramic production: Part I. Powder Synthesis . . . . B. Grohe *et al.* **1901**

Additive controlled crystallization of barium titanate powders and their application for thin-film ceramic production: Part II. From nano-sized powders to ceramic thin films . . . . B. Grohe *et al.* **1911**

Control growth of PbS quantum dots doped sono-ormosil . . . . R. Erce-Montilla *et al.* **2572**

Nanocrystals in crystalline silicon: Void formation and hollow particles . . . . A. Meldrum *et al.* **2670**

Comparison of different models for melting point change of metallic nanocrystals . . . . M. Zhao *et al.* **3304**

Nanoindentation

A note on a common mistake in the analysis of nanoindentation data . . . . M. Munawar Chaudhri **336**

Characterization and modeling of specific strain gradient modulus of epoxy . . . . D.C.C. Lam *et al.* **558**

Determination of the elastic properties of glasses and polymers exploiting the resonant characteristic of depth-sensing indentation tests . . . . D. Lorenz *et al.* **1776**

Simplified method for analyzing nanoindentation data and evaluating performance of nanoindentation instruments . . . . Takeshi Sawa *et al.* **3084**

Nanoparticle

Third-order nonlinear optical response in PbS-coated CdS nanocomposites . . . . Bing Liu *et al.* **1644**

Nanophase

Sintering and microstructure of glass-coated nanocrystalline yttria-stabilized tetragonal zirconia powder: Effect of the glass . . . . R. Ramamoorthy *et al.* **296**

Synthesis and processing of nanocrystalline Ag–Fe–Ni for low thermal expansion–high conductivity thermal management applications . . . . J. Stolk *et al.* **340**

Thermal stability of nanocrystalline WC–Co powder synthesized by using mechanical milling at low temperature . . . . Jianhong He *et al.* **478**

Sol-gel-derived photosensitive TiO_2 and Cu/TiO_2 using homogeneous hydrolysis technique . . . . Jeffrey C.S. Wu *et al.* **615**

Thermodynamic stability of tetragonal zirconia nanocrystallites . . . . Nae-Lih Wu *et al.* **666**

Synthesis of α–SiO_2 nanowires using Au nanoparticle catalysts on a silicon substrate . . . . Z.Q. Liu *et al.* **683**

Precipitation of multilayered core–shell TiO_2 composite nanoparticles onto polymer layers . . . . Mingtai Wang *et al.* **765**

Synthesis and characterization of antimony oxide nanoparticles . . . . Zaoli Zhang *et al.* **803**

Grain growth behavior of a nanostructured 5083 Al–Mg alloy . . . . V.L. Tellkamp *et al.* **938**

Synthesis of nano-AgI arrays and their optical properties . . . . Yinhai Wang *et al.* **990**

Effect of process variables on the structure, residual stress, and hardness of sputtered nanocrystalline nickel films . . . . R. Mitra *et al.* **1010**

Fabrication, characterization, and photoluminescence properties of highly ordered TiO_2 nanowire arrays . . . . Y. Lei *et al.* **1138**

Synthesis of coaxial nanotubes: Titanium oxide sheathed with silicon oxide . . . . Ming Zhang *et al.* **1408**

Synthesis of dense nanometric $MoSi_2$ through mechanical and field activation . . . . R. Orrù *et al.* **1439**

Blue photoluminescent properties of pure nanostructured γ–Al_2O_3 . . . . Zhong Qing Yu *et al.* **1890**

Increased fracture toughness in nanoporous silica–polyimide matrix composites . . . . Shiling Ruan *et al.* **1975**

Cubic silicon nitride embedded in amorphous silicon dioxide . . . . Ming Zhang *et al.* **2179**

Thermal and structural characterization of the $ZrO_{2-x}(OH)_{2x}$ to ZrO_2 transition . . . . E. Torres-García *et al.* **2209**

Purification of single-walled carbon nanotubes synthesized by the hydrogen arc-discharge method . . . . Pengxiang Hou *et al.* **2526**

Synthesis of nanoscale particles of Ta and Nb_3Al by homogeneous reduction in liquid ammonia . . . . Hongmin Zhu *et al.* **2544**

Flash synthesis of zirconia nanoparticles by microwave forced hydrolysis . . . . K. Bellon *et al.* **2619**

Development of nanocrystalline structure during cryomilling of Inconel 625 . . . . Jianhong He *et al.* **2724**

Templated growth of a complex nitride island dispersion through an internal nitridation reaction . . . . M.P. Brady *et al.* **2784**

Preparation and characterization of $CuInS_2$ nanorods and nanotubes from an elemental solvothermal reaction . . . . Yang Jiang *et al.* **2805**

	Preparation, structure, and magnetic properties of cobalt nanoparticles in carbon fibers	I. Bashmakov *et al.*	2832
	Preparation and characterization of nanocrystalline PbSe in poly(acrylic acid-*co*-styrene)	Yangyang Sun *et al.*	2922
	Nucleation and growth of silicon nitride nanoneedles using microwave plasma heating	H. Cui *et al.*	3111
	Novel synthesis of AlN nanowires with controlled diameters	Jun Liu *et al.*	3133
	Growth and characterization of aligned carbon nanotubes from patterned nickel nanodots and uniform thin films	J.G. Wen *et al.*	3246
	Titanium oxide nanotube arrays prepared by anodic oxidation	Dawei Gong *et al.*	3331
	Solvothermal route to Bi_3Se_4 nanorods at low temperature	Yuan-fang Liu *et al.*	3361
	Preparation and phase control of nanocrystalline silver indium sulfides via a hydrothermal route	J.Q. Hu *et al.*	3411
	High grain size stability of nanocrystalline Al prepared by mechanical attrition	F. Zhou *et al.*	3451
	Preparation of γ–Fe_2O_3 nanoparticles from a nonaqueous precursor	P. Deb *et al.*	3471
	Origins of stored enthalpy in cryomilled nanocrystalline Zn	Xinghang Zhang *et al.*	3485
	Preparation and characterization of nanocrystalline potassium lithium niobate powders and films	H.X. Zhang *et al.*	3609
	Preparation of nanocrystalline nickel oxide–yttria-stabilized zirconia composite powder by solution combustion with ignition of glycine fuel	Sun-Jae Kim *et al.*	3621
Neutron scattering	Comparison of crystal structure parameters of natural and synthetic apatites from neutron powder diffraction	Th. Leventouri *et al.*	2600
Nuclear reaction analysis	^{18}O study of the oxidation of reactively sputtered $Ti_{1-x}Al_xN$ barrier	M.C. Hugon *et al.*	2591
Optical	Growth, defects, and properties of $GdCa_4O(BO_3)_3$ and $Nd:GdCa_4O(BO_3)_3$ crystals	Jiyang Wang *et al.*	790
	Photoluminescence behavior of Al^{3+}, Pr^{3+} doped perovskite $La_{2/3}TiO_3$ and pyrochlore $La_2Ti_2O_7$	J.K. Park *et al.*	2568
Optical absorption spectroscopy	Absorption spectra of Co^{2+} in $AgInS_2$ orthorhombic single crystals	Hidong Kim *et al.*	975
Optical diffraction	Nondestructive measurement of striation defect spacing using laser diffraction	Dylan E. Haas *et al.*	3355
Optical materials	Phase transition, growth, and optical properties of $Nd_xLa_{1-x}Sc_3(BO_3)_4$ crystals	Yunkui Li *et al.*	38
	Thermally reversible γ-ray-induced redox reaction between substitutional iron and aluminum impurity centers in a silica glass	Radhaballabh Debnath	127
	Fractal aggregates of lanthanide-doped Y_2O_3 nanoparticles obtained by propellant synthesis	Stefano Polizzi *et al.*	146
	Refractive index profile and attenuation measurement in $KTiOPO_4$ waveguide by megaelectronvolt He ions	Ke-Ming Wang *et al.*	276
	Erbium doping into lithium niobate and sapphire single crystal wafers	P. Nekvindova *et al.*	333
	Preparation and characteristics of seeded epitaxial $(Sr,Ba)Nb_2O_6$ optical waveguide thin films using sol-gel method	Junmo Koo *et al.*	430
	Misting-free diamond surface created by sheet electron beam irradiation	Kazuya Oguri *et al.*	553
	Synthesis of α–SiO_2 nanowires using Au nanoparticle catalysts on a silicon substrate	Z.Q. Liu *et al.*	683
	Luminescence and decay behaviors of Tb-doped yttrium silicate	Yoon Young Choi *et al.*	881
	Effect of host compositions on the afterglow properties of phosphorescent strontium aluminate phosphors derived from the sol-gel method	I-Cherng Chen *et al.*	1293
	Biomimetic model of a sponge-spicular optical fiber—mechanical properties and structure	M. Sarikaya *et al.*	1420
	Eu^{+3} and Cr^{+3} doping for red cathodoluminescence in $ZnGa_2O_4$	Philip D. Rack *et al.*	1429
	Electronic paramagnetic resonance study of Cu^{2+} ions in copper ion-exchanged layers of lithium niobate crystals	F. Caccavale *et al.*	1554
	Correlation of the Raman spectra with the thermal conductivity of a set of diamond wafers prepared by chemical vapor deposition	Edgar S. Etz *et al.*	1694
	Crystallization kinetics of yttrium aluminum garnet ($Y_3Al_5O_{12}$)	Bradley R. Johnson *et al.*	1795
	Water-associated surface degradation of $CsLiB_6O_{10}$ crystal during harmonic generation in the ultraviolet region	Yukihiro Morimoto *et al.*	2082
	Dye-doped sol-gel coatings for near-infrared laser protection	T. Kololuoma *et al.*	2186
	Fabrication of heteropolyoxometalate-based photochromic inorganic–organic nanocomposites	Tie Rui Zhang *et al.*	2256
	Control growth of PbS quantum dots doped sono-ormosil	R. Erce-Montilla *et al.*	2572
	Optical and electrochromic properties of heated and annealed MoO_3 thin films	Zahid Hussain	2695
	Translucent yttrium aluminum garnet: Microwave-assisted route to synthesis and processing	M. Panneerselvam *et al.*	2773
	Enthalpies of formation of lanthanide oxyapatite phases	A.S. Risbud *et al.*	2780
	Formation and characterization of high-density silver nanoparticles embedded in silica thin films by "*in situ*" self-reduction	G. Compagnini *et al.*	2934
	Thermal stress in a polymer-coated optical glass fiber with a low-modulus coating at the ends	E. Suhir	2996
	Explanation of the effects of gravity on crystallization of ZrF_2–BaF_2–LaF_3–AlF_3–NaF glass	Dennis S. Tucker *et al.*	3027

Direct laser writing of self-developed waveguides in benzyldimethylketal-doped sol-gel hybrid glass . . . Byeong-Soo Bae *et al.* **3184**
Structure and the nonlinearity of lithium triborate studied by Raman and infrared reflectivity spectroscopy . . . H.R. Xia *et al.* **3464**

Optical properties

Relaxation of ultraviolet-radiation-induced structure and long-lasting phosphorescence in Eu^{2+}-doped strontium aluminosilicate glasses . . . Jianrong Qiu *et al.* **88**
Refractive index profile and attenuation measurement in $KTiOPO_4$ waveguide by megaelectronvolt He ions . . . Ke-Ming Wang *et al.* **276**
Novel photoluminescence from hydrogenated amorphous carbon films prepared by using xylene source . . . Jun Xu *et al.* **325**
Sol-gel synthesis and the effect of boron addition on the phosphorescent properties of $SrAl_2O_4:Eu^{2+},Dy^{3+}$ phosphors . . . I-Cherng Chen *et al.* **644**
Luminescence and decay behaviors of Tb-doped yttrium silicate . . . Yoon Young Choi *et al.* **881**
Absorption spectra of Co^{2+} in $AgInS_2$ orthorhombic single crystals . . . Hidong Kim *et al.* **975**
Synthesis of nano-AgI arrays and their optical properties . . . Yinhai Wang *et al.* **990**
Investigation of optical waveguide formed in Er:Yb:phosphate glass by MeV He^+ implantation . . . Zhuang Zhuo *et al.* **1135**
Fabrication, characterization, and photoluminescence properties of highly ordered TiO_2 nanowire arrays . . . Y. Lei *et al.* **1138**
Synthesis of $Zn_{2-x}Mn_xSiO_4$ phosphors using a hydrothermal technique . . . Chulsoo Yoon *et al.* **1210**
Effect of host compositions on the afterglow properties of phosphorescent strontium aluminate phosphors derived from the sol-gel method . . . I-Cherng Chen *et al.* **1293**
Enhancement of the 1.31-μm emission properties of Dy^{3+}-doped Ge–Ga–S glasses with the addition of alkali halides . . . Yong Beom Shin *et al.* **1318**
Metal-organic vapor phase epitaxial growth of high-quality ZnO films on $Al_2O_3(00{\cdot}1)$ . . . W.I. Park *et al.* **1358**
Effect of composition on the thermal properties and spontaneous emission probabilities of Tm^{3+}-doped TeO_2–LiCl glass . . . G. Özen *et al.* **1381**
Eu^{+3} and Cr^{+3} doping for red cathodoluminescence in $ZnGa_2O_4$ . . . Philip D. Rack *et al.* **1429**
Optical and electrical properties of $Ge_{10+x}Se_{40}Te_{50-x}$ thin film . . . S.A. Fayek *et al.* **1549**
Influence of compositional disorder on optical absorption processes in $Cu_6P(S_{1-x}Se_x)_5I$ crystals . . . I.P. Studenyak *et al.* **1600**
Third-order nonlinear optical response in PbS-coated CdS nanocomposites . . . Bing Liu *et al.* **1644**
Blue photoluminescent properties of pure nanostructured γ–Al_2O_3 . . . Zhong Qing Yu *et al.* **1890**
Dye-doped sol-gel coatings for near-infrared laser protection . . . T. Kololuoma *et al.* **2186**
Temperature dependence of the optical properties in p-$Cd_{0.96}Zn_{0.04}Te$ single crystals . . . H.Y. Lee *et al.* **2196**
Optical and electrochromic properties of heated and annealed MoO_3 thin films . . . Zahid Hussain **2695**
Determination of optical constants of Si/ZnO polycrystalline nanocomposites by spectroscopic ellipsometry . . . J. García-Serrano *et al.* **3554**
Preparation and characterization of nanocrystalline potassium lithium niobate powders and films . . . H.X. Zhang *et al.* **3609**

Optical spectroscopy

Optical evaluation of the flexural rigidity and residual stress in thin membranes: Picosecond transient grating measurements of the dispersion of the lowest-order Lamb acoustic waveguide mode . . . John A. Rogers *et al.* **217**
Infrared optical properties of aged porous GaAs . . . S. Zangooie *et al.* **1241**

Optoelectronic materials

Novel photoluminescence from hydrogenated amorphous carbon films prepared by using xylene source . . . Jun Xu *et al.* **325**
Precipitation of multilayered core–shell TiO_2 composite nanoparticles onto polymer layers . . . Mingtai Wang *et al.* **765**
Synthesis of $Zn_{1-x}Mg_xO$ and its structural characterization . . . M.S. Tomar *et al.* **903**
CsCl-modified Ga_2S_3–La_2S_3 glasses: Structural approach by x-ray absorption spectroscopy . . . A.Y. Ramos *et al.* **1349**
Metal-organic vapor phase epitaxial growth of high-quality ZnO films on $Al_2O_3(00{\cdot}1)$ . . . W.I. Park *et al.* **1358**
Photoluminescence spectra of undoped and Sm^{3+}-doped $BaAl_2S_4$ and $BaAl_2Se_4$ single crystals . . . Moon-Seog Jin *et al.* **1520**
Crystallography and structural evolution of $LiNbO_3$ and $LiNb_{1-x}Ta_xO_3$ films on sapphire prepared by high-rate thermal plasma spray chemical vapor deposition . . . D.V. Shtansky *et al.* **2271**
^{29}Si nuclear-magnetic-resonance and vibrational spectroscopy studies of SiO_2–TiO_2 powders prepared by the sol-gel process . . . J.P. Rainho *et al.* **2369**
Study of the mechanism for controlled crystallization of BaF_2 under two kinds of monolayers . . . L. Lu *et al.* **2415**
Ferroelectric domain structure of epitaxial (Pb,Sr)TiO_3 thin films . . . Yong Kwan Kim *et al.* **2463**
X-ray reflectivity spectra of ultrathin films and nanometric multilayers: Experiment and simulation . . . E. Bontempi *et al.* **2556**

Calorimetric determination of the enthalpy of formation of InN and comparison with AlN and GaN . . . M.R. Ranade *et al.* **2824**
Photovoltaic effect of $Sn_2P_2S_6$ ferroelectric crystal and ceramics . . . Y.W. Cho *et al.* **3317**
Preparation and characterization of nanocrystalline potassium lithium niobate powders and films . . . H.X. Zhang *et al.* **3609**

Oxidation

Improvement in oxidation resistance of TiB_2 by formation of protective SiO_2 layer on surface . . . Young-Hag Koh *et al.* **132**
Planar oxidation of strained silicon substrates . . . M-T. Lin *et al.* **728**
^{18}O study of the oxidation of reactively sputtered $Ti_{1-x}Al_xN$ barrier . . . M.C. Hugon *et al.* **2591**
Combustion of zirconium foils in oxygen . . . K.H. Ewald *et al.* **2687**

Phase equilibria

Formation of $Nd_{1+x}(Ba_{1-y}Sr_y)_{2-x}Cu_3O_{7\pm\delta}$ solid solutions by crystal pulling . . . Xin Yao *et al.* **529**
Thermodynamic analysis of combustion synthesis of Al_2O_3–TiC–ZrO_2 nanoceramics . . . Q. Dong *et al.* **2494**

Phase transformation

Raman spectroscopic determination of phase evolutions in $LiAl_xCo_{1-x}O_2$ battery materials . . . P.S. Dobal *et al.* **1**
Formation of icosahedral quasicrystal by crystallization of $Zr_{70}(Ni, Cu, Pd)_{30}$ amorphous alloys . . . T. Zhang *et al.* **20**
Redistribution behavior of constitutional elements at an initial crystallization stage in the $Zr_{65}Al_{7.5}Ni_{10}Cu_{17.5}$ glassy alloy . . . J. Saida *et al.* **28**
Phase transition, growth, and optical properties of $Nd_xLa_{1-x}Sc_3(BO_3)_4$ crystals . . . Yunkui Li *et al.* **38**
Enhanced crystallization and phase transformation of amorphous silicon nitride under high pressure . . . Ya-Li Li *et al.* **67**
Analysis of phase distributions in the Li_2O–Nb_2O_5–TiO_2 system by piezoresponse imaging . . . Albina Y. Borisevich *et al.* **329**
Phase-transformation kinetics in triphasic cordierite gel . . . R. Petrović *et al.* **451**
Characterization of bond formation in SiC and Si_3N_4 implanted with Ti, Fe, and Co . . . Didier Zanghi *et al.* **512**
Thermodynamic stability of tetragonal zirconia nanocrystallites . . . Nae-Lih Wu *et al.* **666**
In situ transmission electron microscopy study of the silicidation process in Co thin films on patterned (001) Si substrates . . . C. Ghica *et al.* **701**
Surface studies of phase formation in Co–Ge system: Reactive deposition epitaxy versus solid-phase epitaxy . . . I. Goldfarb *et al.* **744**
Subsolidus phase relations in the La_2O_3–Fe_2O_3–Al_2O_3 system . . . Danjela Kuščer *et al.* **822**
Tensile fracture during transformation superplasticity of Ti–6Al–4V . . . C. Schuh *et al.* **865**
Effects of pressure on the solidification of Al–Mn alloy . . . Duanwei He *et al.* **910**
On some discrepancies in the literature about the formation of icosahedral quasi-crystal in Al–Cu–Fe alloys . . . Jianian Gui *et al.* **1037**
Directional solidification and microstructural studies of the peritectic Y_2BaCuO_5 phase . . . E. Sudhakar Reddy *et al.* **1123**
Precipitation of icosahedral quasicrystalline phase in $Hf_{69.5}Al_{7.5}Ni_{11}Cu_{12}$ metallic glass . . . Chunfei Li *et al.* **1190**
Precipitation of icosahedral phase from amorphous $Zr_{65}Cu_{17.5-x}Al_{7.5}Ni_{10}Ag_x$ (x = 0, 5) alloys . . . J.K. Lee *et al.* **1311**
Phase formation and reactions in the Bi_2O_3–ZnO–Nb_2O_5–Ag pyrochlore system . . . Juan C. Nino *et al.* **1460**
A combinatorial approach for efficient mapping of phase diagrams and properties . . . Ji-Cheng Zhao **1565**
Influence of ligand groups in Ti precursors on phase transformation and microstructural evolution of TiO_2 thin films prepared by the wet chemical process . . . Chu-Chi Ting *et al.* **1712**
Devitrification kinetics and mechanism of Pyrex borosilicate glass . . . Jau-Ho Jean *et al.* **1752**
Low-temperature crystallization induced by excimer laser irradiation of $SrBi_2Ta_2O_9$ films . . . Kwang Soo Seol *et al.* **1883**
Structure of heat-treated sol-gel SiO_2 glasses containing silver . . . M.G. Garníca-Romo *et al.* **2007**
Crystallization and dielectric properties of SrO–BaO–Nb_2O_5–GeO_2 tungsten–bronze glass–ceramics . . . Jiin-Jyh Shyu *et al.* **2057**
Transformation behavior of yttria stabilized tetragonal zirconia polycrystal–TiB_2 composites . . . B. Basu *et al.* **2158**
Transmission electron microscopy observation in a liquid-phase-sintered SiC with oxynitride glass . . . Guo-Dong Zhan *et al.* **2189**
Thermal and structural characterization of the $ZrO_{2-x}(OH)_{2x}$ to ZrO_2 transition . . . E. Torres-García *et al.* **2209**
Study of the mechanism for controlled crystallization of BaF_2 under two kinds of monolayers . . . L. Lu *et al.* **2415**
Moving the pulsed heating technique beyond monolithic specimens: Experiments with coated wires . . . D. Josell *et al.* **2421**
Effect of pressure on the structure of Fe–N alloys formed by solid-state reaction . . . B. Yao *et al.* **2583**
Formation rule for Al-based ternary quasi-crystals: Example of Al–Ni–Fe decagonal phase . . . Jian-Bing Qiang *et al.* **2653**
Effect of oxygen on the reactions in the Si/Ta/Cu metallization system . . . Tomi Laurila *et al.* **2939**
Structural and electrical properties of strontium barium niobate thin films crystallized by conventional furnace and rapid-thermal annealing process . . . R.G. Mendes *et al.* **3009**

	Explanation of the effects of gravity on crystallization of ZrF_2–BaF_2–LaF_3–AlF_3–NaF glass . . . Dennis S. Tucker *et al.*	3027
	Single-crystal growth of the Al–Cu–Fe icosahedral quasicrystal from the ternary melt . . . J.Q. Guo *et al.*	3038
	Change in local atomic structure during formation of the icosahedral quasicrystalline phase in $Zr_{70}Pd_{30}$ glassy alloy . . . Muneyuki Imafuku *et al.*	3046
	Relation between tolerance factor and T_c in Aurivillius compounds . . . Donají Y. Suárez *et al.*	3139
	Parameter effect on the crystallization of Nd:yttrium aluminum garnet laser-ablated TiO_2 thin film . . . Mrinal Pal *et al.*	3158
	Defect formation due to the crystallisation of deep amorphous volumes formed in silicon by mega electron volt (*MeV*) ion implantation . . . A.C.Y. Liu *et al.*	3229
	Comparison of different models for melting point change of metallic nanocrystals . . . M. Zhao *et al.*	3304
	Investigation of the stability of glassy state in the Zr- and Hf-based glassy alloys correlated with their transformation behavior . . . Junji Saida *et al.*	3389
Phase transition	Glass-forming ability of the Ni–Zr and Ni–Ti systems determined by interatomic potentials . . . W.S. Lai *et al.*	446
	Silica particle growth in metastable supersaturation solution . . . Kyung-Soo Kim *et al.*	545
	Crystallization kinetics of amorphous nanostructured $Pd_{40.5}Ni_{40.5}P_{19}$ alloys . . . H.W. Ngai *et al.*	797
	Quasicrystalline phase formation in $Al_{62}Cu_{22.5}Fe_{12.5}$ and $Al_{55}Cu_{22.5}Fe_{12.5}Be_7$ alloys . . . S.M. Lee *et al.*	1535
	Phase separation in SiO_2–TiO_2 gel and glassy films studied by atomic force microscopy and transmission electron microscopy . . . A. Karthikeyan *et al.*	1626
Photochemical processing	Cure depth in photopolymerization: Experiments and theory . . . Jim H. Lee *et al.*	3536
Photoluminescence	Enhancement of the 1.31-μm emission properties of Dy^{3+}-doped Ge–Ga–S glasses with the addition of alkali halides . . . Yong Beom Shin *et al.*	1318
	Photoluminescence spectra of undoped and Sm^{3+}-doped $BaAl_2S_4$ and $BaAl_2Se_4$ single crystals . . . Moon-Seog Jin *et al.*	1520
	Temperature dependence of the optical properties in p-$Cd_{0.96}Zn_{0.04}Te$ single crystals . . . H.Y. Lee *et al.*	2196
Physical vapor deposition (PVD)	Combined out-of-plane and in-plane texture control in thin films using ion beam assisted deposition . . . L. Dong *et al.*	210
	Preparation of Cu(In,Ga)Se_2 thin films at low substrate temperatures . . . S. Nishiwaki *et al.*	394
	Deposition of epitaxial transition metal carbide films and superlattices by simultaneous direct current metal magnetron sputtering and C_{60} evaporation . . . H. Högberg *et al.*	633
	Ultrathin TiB_2 protective films . . . Feng Huang *et al.*	945
	Synthesis of open-cell metal foams by templated directed vapor deposition . . . Douglas T. Queheillalt *et al.*	1028
	High-T_c superconducting NbN films with low particulate density grown at 25 °C using pulsed laser deposition . . . Anupama B. Kaul *et al.*	1223
	Dielectric properties of oxide structures by a laser-based direct-writing method . . . D. Young *et al.*	1720
	Dependence of structural, electrical, and optical properties of ZnO:Al films on substrate temperature . . . M. Chen *et al.*	2118
	Highly textured nanostructure of pulsed laser deposited IrO_2 thin films as investigated by transmission electron microscopy . . . A.M. Serventi *et al.*	2336
	Electric properties of barium–strontium titanate thin films deposited by two-step radio-frequency sputtering . . . J.S. Fang *et al.*	2680
	Growth mechanism of superconducting MgB_2 films prepared by various methods . . . H.Y. Zhai *et al.*	2759
	Nucleation and growth of $YBa_2Cu_3O_x$ on $SrTiO_3$ and CeO_2 by a BaF_2 postdeposition reaction process . . . L. Wu *et al.*	2869
	Ion energy dependence of film properties for diamond-like carbon prepared with plasma-assisted deposition . . . Cao Zexian	3034
Piezoresponse	Analysis of phase distributions in the Li_2O–Nb_2O_5–TiO_2 system by piezoresponse imaging . . . Albina Y. Borisevich *et al.*	329
Plasma deposition	Gas flow effects on the structure and composition of SiN_x/Si/SiN_x films prepared by radio-frequency magnetron sputtering . . . Wentao Xu *et al.*	308
	Chemical vapor deposition of an aluminum nitride–diamond composite in a triple torch plasma reactor . . . Marcus Asmann *et al.*	469
	Low–power plasma torch method for the production of crystalline spherical ceramic particles . . . Chun-Ku Chen *et al.*	1256
	X-ray scattering study on the structural evolution of AlN/sapphire(0001) films during radiofrequency sputter growth . . . H.C. Kang *et al.*	1814
Plasma-enhanced CVD (PECVD)	Coherent island formation of Cu_2O films grown by chemical vapor deposition on MgO(110) . . . P.R. Markworth *et al.*	2408

Polishing

Chemical–mechanical polishing of copper and tantalum with silica abrasives . . . . . Y. Li *et al.* **1066**

Polycrystal

Topological transformation of grains in three-dimensional normal grain growth . . . . . F. Wakai *et al.* **2136**

Polymers

Characterization and modeling of specific strain gradient modulus of epoxy . . . . . D.C.C. Lam *et al.* **558**

Influence of thermal history on morphology and viscoelastic behavior of ethylene–1-octene copolymers synthesized with metallocene catalysts . . . . . M.L. Cerrada *et al.* **1103**

Preliminary study on alternating thienylene/phenylene copolymers functionalized with an electron-donating or -withdrawing group . . . . . J.M. Xu *et al.* **1235**

Direct measurement of plowing friction and wear of a polymer thin film using the atomic force microscope . . . . . Binyang Du *et al.* **1487**

Microstructural analysis of high-pressure compressed C_{60} . . . . . K. Miyazawa *et al.* **1960**

Gradient porosity poly(dicyclopentadiene) . . . . . A. Della Martina *et al.* **2045**

Formation of quasi-one-dimensional carbon chains in cubic nanocrystals by photon-breaking of C–S bonds in polythiophene . . . . . Z.M. Ren *et al.* **2793**

Adhesion of polymer–inorganic interfaces by nanoindentation . . . . . Min Li *et al.* **3378**

Cure depth in photopolymerization: Experiments and theory . . . . . Jim H. Lee *et al.* **3536**

Effect of ion implant dose on the mechanical properties of polyethersulfone films . . . . . Manuel Luis B. Palacio *et al.* **3628**

Powder

Fractal aggregates of lanthanide-doped Y_2O_3 nanoparticles obtained by propellant synthesis . . . . . Stefano Polizzi *et al.* **146**

Investigation of some phenomena occurring during continuous ink-jet printing of ceramics . . . . . B.Y. Tay *et al.* **373**

Mechanochemical-hydrothermal preparation of crystalline hydroxyapatite powders at room temperature . . . . . Pavel Shuk *et al.* **1231**

Size effects in powder compaction . . . . . J. Gil Sevillano **1238**

Low–power plasma torch method for the production of crystalline spherical ceramic particles . . . . . Chun-Ku Chen *et al.* **1256**

Study of phase components of $La_{1.5}Ca_{1.5}Mn_2O_7$ . . . . . J.L. Zhu *et al.* **2027**

Combustion synthesis of aluminum nitride powder using additives . . . . . Chun-Nan Lin *et al.* **2200**

Photoluminescence behavior of Al^{3+}, Pr^{3+} doped perovskite $La_{2/3}TiO_3$ and pyrochlore $La_2Ti_2O_7$ . . . . . J.K. Park *et al.* **2568**

Reaction kinetics and anisothermal effects in microwave fields: The System Y_2O_3–Fe_3O_4 . . . . . Ramesh D. Peelamedu *et al.* **2770**

Combustion synthesis method for synthesis of aluminum nitride powder using aluminum containers . . . . . Chun-Nan Lin *et al.* **3518**

Powder metallurgy

Creep and toughness of cryomilled NiAl containing Cr . . . . . J. Daniel Whittenberger *et al.* **1333**

Powder processing

Mechanochemistry of the titanium–silicon system: Compositional effects . . . . . S. Doppiu *et al.* **1266**

Study of the activation process of Mg-based hydrogen storage materials modified by graphite and other carbonaceous compounds . . . . . S. Bouaricha *et al.* **2893**

Pulsed heating

Moving the pulsed heating technique beyond monolithic specimens: Experiments with coated wires . . . . . D. Josell *et al.* **2421**

Purification

Purification of single-walled carbon nanotubes synthesized by the hydrogen arc-discharge method . . . . . Pengxiang Hou *et al.* **2526**

Pyrolysis

Carbonization behavior of polyimide film containing iron complex in relation to magnetic properties . . . . . Y. Kaburagi *et al.* **352**

Low-temperature growth of *c*-axis-oriented Y-type hexagonal ferrite thin films by the polymeric precursor method . . . . . Tatsuo Fujii *et al.* **2471**

Quasicrystal

Formation of icosahedral quasicrystal by crystallization of $Zr_{70}(Ni, Cu, Pd)_{30}$ amorphous alloys . . . . . T. Zhang *et al.* **20**

On some discrepancies in the literature about the formation of icosahedral quasi-crystal in Al–Cu–Fe alloys . . . . . Jianian Gui *et al.* **1037**

Precipitation of icosahedral quasicrystalline phase in $Hf_{69.5}Al_{7.5}Ni_{11}Cu_{12}$ metallic glass . . . . . Chunfei Li *et al.* **1190**

Quasicrystalline phase formation in $Al_{62}Cu_{22.5}Fe_{12.5}$ and $Al_{55}Cu_{22.5}Fe_{12.5}Be_7$ alloys . . . . . S.M. Lee *et al.* **1535**

Formation rule for Al-based ternary quasi-crystals: Example of Al–Ni–Fe decagonal phase . . . . . Jian-Bing Qiang *et al.* **2653**

Single-crystal growth of the Al–Cu–Fe icosahedral quasicrystal from the ternary melt . . . . . J.Q. Guo *et al.* **3038**

Raman spectroscopy

Correlation of the Raman spectra with the thermal conductivity of a set of diamond wafers prepared by chemical vapor deposition . . . . . Edgar S. Etz *et al.* **1694**

Microprobe fluorescence spectroscopy evaluation of stress fields developed along a propagating crack in an $Al_2O_3/CaO \cdot 6Al_2O_3$ ceramic composite . . . . . O. Sbaizero *et al.* **2798**

Raman scattering of cubic boron nitride films deposited from the low-pressure gas phase . . . . . W.J. Zhang *et al.* **3430**

Structure and the nonlinearity of lithium triborate studied by Raman and infrared reflectivity spectroscopy . . . . . H.R. Xia *et al.* **3464**

Scanning tunneling microscopy (STM)

Surface studies of phase formation in Co–Ge system: Reactive deposition epitaxy versus solid-phase epitaxy . . . I. Goldfarb *et al.* **744**
Generation of circular and hexagonal microholes in a graphite surface . . . Hidefumi Hiura **1287**

Screen printing

Sintering of screen-printed platinum thick films for electrode applications . . . J.B. Véchembre *et al.* **922**

Self-propagating high-temperature synthesis (SHS)

Field-activated combustion synthesis of Ta–Si intermetallic compounds . . . F. Maglia *et al.* **534**
Combustion synthesis of mechanically activated powders in the Ti–Si system . . . F. Maglia *et al.* **1074**
Microstructure and formation mechanism of combustion-synthesized rodlike Ca α-sialon crystals . . . Kexin Chen *et al.* **1928**
Effect of mechanical alloying on combustion synthesis of $MoSi_2$ . . . Hyung-Sang Park *et al.* **3060**

Semiconductors

Chemical-vapor-deposition growth and characterization of epitaxial 3C–SiC films on SOI substrates with thin silicon top layers . . . C.K. Moon *et al.* **24**
Absorption spectra of Co^{2+} in $AgInS_2$ orthorhombic single crystals . . . Hidong Kim *et al.* **975**
Intrinsic microcrystalline silicon by postgrowth anneals . . . Jong-Hwan Yoon **1531**
Chemical stresses induced by grain-boundary diffusion in thin films . . . W.L. Wang *et al.* **1967**
Electrolyte electroreflectance study of TiO_2 films modified with metal nanoparticles . . . A.I. Kulak *et al.* **2357**
Threading dislocations with edge components in GaN epilayers grown on Al_2O_3 substrates . . . Junyong Kang *et al.* **2550**
Investigation of crystal properties of TmP/GaAs and GaAs/TmP/GaAs heterostructures grown by molecular beam epitaxy . . . C.H. Lin *et al.* **3266**
Deformation under nanoindents in Si, Ge, and GaAs examined through transmission electron microscopy . . . S.J. Lloyd *et al.* **3347**

Separation material

Silicalite/poly(dimethylsiloxane) nanocomposite pervaporation membranes for acetic acid/water separation . . . Shih-Yuan Lu *et al.* **3053**

Shock synthesis

Hydrodynamic cavitation as a tool to control macro-, micro-, and nano-properties of inorganic materials . . . J. Find *et al.* **3503**

Single crystal

Ferroelectric $SrBi_2Ta_2O_9$ single-crystal growth and characterization . . . B. Sih *et al.* **1726**

Sintering

Densification and grain growth of Al-doped ZnO . . . Jiaping Han *et al.* **459**
Sintering of screen-printed platinum thick films for electrode applications . . . J.B. Véchembre *et al.* **922**
$Pb(Zr_xTi_{1-x})O_3$ ceramics via reactive sintering of partially reacted mixture produced by a high-energy ball milling process . . . L.B. Kong *et al.* **1636**
Influence of sintering atmosphere on the fabrication of SiC ceramics with a powder mixture of sialon composition . . . Jong-Kook Lee *et al.* **1784**
Effect of α/β phase ratio on microstructure and mechanical properties of silicon nitride ceramics . . . Hirokazu Kawaoka *et al.* **2264**
Solid-state reaction mechanism for the formation of $Ba_{6-x}Ln_{8+2x/3}Ti_{18}O_{54}$ (Ln = Nd, Sm) solid solutions . . . Anatolii G. Belous *et al.* **2350**
Freeform fabrication of aluminum metal-matrix composites . . . C.W. Souvignier *et al.* **2613**
Compaction of bulk ferromagnetic $Fe_{80}P_{13}C_7$ amorphous alloys . . . F.W. Chan *et al.* **2767**
Translucent yttrium aluminum garnet: Microwave-assisted route to synthesis and processing . . . M. Panneerselvam *et al.* **2773**
Consolidation and crystallization of Si_3N_4/SiC nanocomposites from a poly(urea–silazane) ceramic precursor . . . Julin Wan *et al.* **3274**
Formation of Al_2O_3 grains with different sizes and morphologies during the pulse electric current sintering process . . . S.W. Wang *et al.* **3514**

Sintering (powder metallurgy)

Surface effects in field-assisted sintering . . . J.R. Groza *et al.* **286**

Sol-gel

High J_c $YBa_2Cu_3O_{7-\delta}$ films via rapid, low pO_2 pyrolysis . . . J.T. Dawley *et al.* **13**
Macroporous morphology of titania films prepared by sol-gel dip-coating method from a system containing poly(ethylene glycol) and poly(vinylpyrrolidone) . . . Koichi Kajihara *et al.* **58**
Preparation and characteristics of seeded epitaxial $(Sr,Ba)Nb_2O_6$ optical waveguide thin films using sol-gel method . . . Junmo Koo *et al.* **430**
Phase-transformation kinetics in triphasic cordierite gel . . . R. Petrović *et al.* **451**
Silica particle growth in metastable supersaturation solution . . . Kyung-Soo Kim *et al.* **545**
Sol-gel-derived photosensitive TiO_2 and Cu/TiO_2 using homogeneous hydrolysis technique . . . Jeffrey C.S. Wu *et al.* **615**
Sol-gel synthesis and the effect of boron addition on the phosphorescent properties of $SrAl_2O_4:Eu^{2+},Dy^{3+}$ phosphors . . . I-Cherng Chen *et al.* **644**
Low-temperature fabrication of pyroelectric $Ba_{0.8}Sr_{0.2}TiO_3$ thin films by a sol-gel process . . . Jian-Gong Cheng *et al.* **778**
Growth of (111)-oriented $Pb(Zr,Ti)O_3$ layers on nanocrystalline RuO_2 electrodes using the sol-gel technique . . . G.J. Norga *et al.* **828**

	Photocatalytic activity of TiO_2 prepared at low temperature by a photo-assisted sol-gel method	Zi-sheng Guan *et al.*	907
	Effect of host compositions on the afterglow properties of phosphorescent strontium aluminate phosphors derived from the sol-gel method	I-Cherng Chen *et al.*	1293
	Textural properties of $SiO_2 \cdot CaO \cdot P_2O_5$ glasses prepared by the sol-gel method	F. Balas *et al.*	1345
	Synthesis of coaxial nanotubes: Titanium oxide sheathed with silicon oxide	Ming Zhang *et al.*	1408
	Entrapment of organosilicon molecules in nonhydrolytic alumina gels and thermal behavior of the resulting composite	G.S. Grader *et al.*	1413
	Phase separation in SiO_2–TiO_2 gel and glassy films studied by atomic force microscopy and transmission electron microscopy	A. Karthikeyan *et al.*	1626
	Metal–oxide films with magnetically-modulated nanoporous architectures	Craig A. Grimes *et al.*	1686
	Structure of heat-treated sol-gel SiO_2 glasses containing silver	M.G. Garnica-Romo *et al.*	2007
	Nonisothermal phase formation kinetics in sol-gel-derived strontium bismuth tantalate	Yun-Mo Sung	2039
	Photoinduced condensation of sol-gel hybrid glass films doped with benzildimethylketal	Oun-Ho Park *et al.*	2143
	Fabrication of heteropolyoxometalate-based photochromic inorganic–organic nanocomposites	Tie Rui Zhang *et al.*	2256
	^{29}Si nuclear-magnetic-resonance and vibrational spectroscopy studies of SiO_2–TiO_2 powders prepared by the sol-gel process	J.P. Rainho *et al.*	2369
	Controlled preparation and characterization of multilayer sol-gel zirconia dip-coatings	Ricardo Caruso *et al.*	2391
	Chemical structure evolution and orientation selection in sol-gel-prepared ferroelectric $Pb(Zr,Ti)O_3$ thin films	L. Fè *et al.*	2499
	Control growth of PbS quantum dots doped sono-ormosil	R. Erce-Montilla *et al.*	2572
	Single-layer submicron-thick $BaTiO_3$ coatings from poly(vinylpyrrolidone)-containing sols: Gel-to-ceramic film conversion, densification, and dielectric properties	Hiromitsu Kozuka *et al.*	3116
	Formation and characteristics of highly *c*-axis-oriented $Bi_{3.25}La_{0.75}Ti_3O_{12}$ thin films on SiO_2/Si(100) and Pt/Ti/SiO_2/Si(100) substrates	Uong Chon *et al.*	3124
	Halide removal from BaM ($BaFe_{12}O_{19}$) and SrM ($SrFe_{12}O_{19}$) ferrite fibers via a steaming process	R.C. Pullar *et al.*	3162
	Novel route for the epitaxial growth of $(SrBa)Nb_2O_6$ thick films by the sol-gel method using a self-template layer	A-D. Li *et al.*	3179
	Direct laser writing of self-developed waveguides in benzyldimethylketal-doped sol-gel hybrid glass	Byeong-Soo Bae *et al.*	3184
	Solid solubility and transport properties of $Ce_{1-x}Nd_xO_{2-\delta}$ nanocrystalline solid solutions by a sol-gel route	Liping Li *et al.*	3207
	Processing of mesoporous alumina from a powder precursor	J. Wayne Frazee *et al.*	3262
	Properties of $YBa_2Cu_3O_{7-\delta}$ multilayer films from the fluoride-based sol-gel process	M.P. Siegal *et al.*	3339
Solution	Study of the mechanism for controlled crystallization of BaF_2 under two kinds of monolayers	L. Lu *et al.*	2415
Solution deposition	Processing of highly oriented lithium niobate films through chemical solution deposition	Satomi Ono *et al.*	1155
Solvent deposition	Processing- and composition-dependent characteristics of chemical solution deposited $Bi_{4-x}La_xTi_3O_{12}$ thin films	Di Wu *et al.*	1325
Spinning	Nondestructive measurement of striation defect spacing using laser diffraction	Dylan E. Haas *et al.*	3355
Spray pyrolysis	Magnetotransport properties of $La_{0.7}Ca_{0.3}MnO_3$ thick films prepared by spray pyrolysis	F. Damay *et al.*	784
Stress modeling	Statistical behavior and misfit stresses in ceramic and metal laminated system	D. Sherman *et al.*	721
Stress/strain relationship measurements	Deformation-induced surface corrugation of superplastic ceramics	Hiroyuki Muto *et al.*	1879
Structural materials	Study of the effects of low-energy electron bombardment during the chemical vapor deposition of diamond	J.A. González *et al.*	293
	Fabrication and characterization of microscale sandwich beams	Francisco Arias *et al.*	597
	Characterization of the induction period in tricalcium silicate hydration by nuclear resonance reaction analysis	R.A. Livingston *et al.*	687
	Combustion synthesis of mechanically activated powders in the Ti–Si system	F. Maglia *et al.*	1074
	A combinatorial approach for efficient mapping of phase diagrams and properties	Ji-Cheng Zhao	1565
	Rectifying and thermocouple junctions based on Portland cement	Sihai Wen *et al.*	1989
	Transformation behavior of yttria stabilized tetragonal zirconia polycrystal–TiB_2 composites	B. Basu *et al.*	2158
	Characterization of mechanical properties of tungsten carbide/carbon multilayers: Cross-sectional electron microscopy and nanoindentation observations	N.J.M. Carvalho *et al.*	2213

	Controlled preparation and characterization of multilayer sol-gel zirconia dip-coatings	Ricardo Caruso *et al.*	2391
	Effect of pressure on the structure of Fe–N alloys formed by solid-state reaction	B. Yao *et al.*	2583
	Mechanical properties of nanocrystalline and epitaxial TiN films on (100) silicon	H. Wang *et al.*	2733
	Electron microscopy of high-temperature and high-pressure as-grown diamond crystals	Long-Wei Yin *et al.*	3023
	Ion energy dependence of film properties for diamond-like carbon prepared with plasma-assisted deposition	Cao Zexian	3034
	Effect of mechanical alloying on combustion synthesis of $MoSi_2$	Hyung-Sang Park *et al.*	3060
	Derivation of plastic stress–strain relationship from ball indentations: Examination of strain definition and pileup effect	Jeong-Hoon Ahn *et al.*	3170
	Thermal stability of carbon nitride thin films	Niklas Hellgren *et al.*	3188
	Microstructure studies of potassium hexatitanate whiskers	G.L. Li *et al.*	3614
Superconductors	High J_c $YBa_2Cu_3O_{7-\delta}$ films via rapid, low pO_2 pyrolysis	J.T. Dawley *et al.*	13
	Formation of $NdBa_2Cu_3O_{7-\delta}$ amorphous phase by combining aero-acoustic levitation and splat quenching	K. Nagashio *et al.*	138
	Chemical reaction at the interface between $(Hg_{0.9}Re_{0.1})Ba_2CaCu_2O_y$ thin film and $SrTiO_3$ substrate	Xiao-Jing Wu *et al.*	256
	Microstructure of (Nd, Eu, Gd)-123 matrix with (Nd, Eu, Gd)-211 inclusions	M. Muralidhar *et al.*	407
	Formation of Nd_{1+x} $(Ba_{1-y}Sr_y)_{2-x}$ $Cu_3O_{7\pm\delta}$ solid solutions by crystal pulling	Xin Yao *et al.*	529
	Single-domain $YBa_2Cu_3O_y$ thick films and fabrics prepared by an infiltration and growth process	E. Sudhakar Reddy *et al.*	955
	Preferential growth mechanism of $REBa_2Cu_3O_y$ (RE = Y, Nd) crystal on MgO substrate by liquid phase epitaxy	Katsumi Nomura *et al.*	979
	Directional solidification and microstructural studies of the peritectic Y_2BaCuO_5 phase	E. Sudhakar Reddy *et al.*	1123
	Growth of melt-textured Nd-123 by hot seeding under reduced oxygen partial pressure	M. Kambara *et al.*	1163
	High-T_c superconducting NbN films with low particulate density grown at 25 °C using pulsed laser deposition	Anupama B. Kaul *et al.*	1223
	Melt processing of Ba_2CuO_3: Textured precursor for the fabrication of $HgBa_2CuO_y$ superconductor	E. Sudhakar Reddy *et al.*	1759
	Influence of antiphase boundaries on critical current densities in $YBa_2Cu_3O_{7-y}$ single crystals	Junko Shibata *et al.*	1935
	High critical current density $YBa_2Cu_3O_{7-\delta}$ thick films using ion beam assisted deposition MgO bi-axially oriented template layers on nickel-based superalloy substrates	J.R. Groves *et al.*	2175
	Role of the primary phase particles during the peritectic solidification of Y-123 superconducting oxides	M. Kambara *et al.*	2229
	Microstructure and growth of joins in melt-textured $YBa_2Cu_3O_{7-\delta}$	A.D. Bradley *et al.*	2298
	Growth and characterization of conductive $SrRuO_3$ and $LaNiO_3$ multilayers on textured Ni tapes for high-J_c $YBa_2Cu_3O_{7-\delta}$ coated conductors	T. Aytug *et al.*	2661
	Growth mechanism of superconducting MgB_2 films prepared by various methods	H.Y. Zhai *et al.*	2759
	Excellent buffer layer for growing high-quality Y–Ba–Cu–O thin films	W.H. Tang *et al.*	2864
	Nucleation and growth of $YBa_2Cu_3O_x$ on $SrTiO_3$ and CeO_2 by a BaF_2 postdeposition reaction process	L. Wu *et al.*	2869
	Initial growth mechanism of $YBa_2Cu_3O_y$ crystal on MgO substrate by liquid-phase epitaxy	Katsumi Nomura *et al.*	2947
	Microstructure of laser-ablated superconducting $La_2CuO_4F_x$ thin films on $SrTiO_3$	G. Kong *et al.*	3309
	Properties of $YBa_2Cu_3O_{7-\delta}$ multilayer films from the fluoride-based sol-gel process	M.P. Siegal *et al.*	3339
Superplasticity	Deformation-induced surface corrugation of superplastic ceramics	Hiroyuki Muto *et al.*	1879
	Interface structure and solute segregation behavior in SiC/2124 and SiC/6061 Al composites exhibiting high-strain-rate superplasticity	Woo-Jin Kim *et al.*	2429
Theory	Strength prediction of partially aligned discontinuous fiber-reinforced composites	Rex J. Kuriger *et al.*	226
	Elastic constants of polycrystalline Al and TiN calculated by an *ab initio* method within the local-density approximation	Ming Zhang *et al.*	2293
	Impression creep of a viscous layer	Hong Chen *et al.*	2709
	Space-charge concepts on grain boundary impedance of a high-purity yttria-stabilized tetragonal zirconia polycrystal	Jong-Sook Lee *et al.*	2739
Thermodynamic properties	Thermal conductivity and thermal diffusivity of selected oxide single crystals	A. Stanimirovic *et al.*	678
	Correlation of the Raman spectra with the thermal conductivity of a set of diamond wafers prepared by chemical vapor deposition	Edgar S. Etz *et al.*	1694
	Thermal expansion and high-temperature phase transformation of the yttrium silicate Y_2SiO_5	J.W. Nowok *et al.*	2251
	Site preference determination in intermetallic compounds by thermal conductivity measurement	Yoshihiro Terada *et al.*	2314
	Glass transformation in vitreous As_2Se_3 studied by conventional and temperature-modulated differential scanning calorimetry	S.O. Kasap *et al.*	2399

Measurement of the thermal conductivity of thin layers using a scanning thermal microscope . . . Erwin R. Meinders **2530**
Thermochemistry of rare-earth orthophosphates . . . S.V. Ushakov *et al.* **2623**
Enthalpies of formation of lanthanide oxyapatite phases . . . A.S. Risbud *et al.* **2780**
Calorimetric determination of the enthalpy of formation of InN and comparison with AlN and GaN . . . M.R. Ranade *et al.* **2824**
Origins of stored enthalpy in cryomilled nanocrystalline Zn . . . Xinghang Zhang *et al.* **3485**

Thin film

Combined out-of-plane and in-plane texture control in thin films using ion beam assisted deposition . . . L. Dong *et al.* **210**
Optical evaluation of the flexural rigidity and residual stress in thin membranes: Picosecond transient grating measurements of the dispersion of the lowest-order Lamb acoustic waveguide mode . . . John A. Rogers *et al.* **217**
Residual stress in fiber-textured thin films of cubic materials . . . P. Scardi *et al.* **233**
Chemical reaction at the interface between $(Hg_{0.9}Re_{0.1})Ba_2CaCu_2O_y$ thin film and $SrTiO_3$ substrate . . . Xiao-Jing Wu *et al.* **256**
Dependence of dielectric and piezoelectric properties on film thickness for highly {100}-oriented lead magnesium niobate–lead titanate (70/30) thin films . . . Jeong Hwan Park *et al.* **268**
Gas flow effects on the structure and composition of $SiN_x/Si/SiN_x$ films prepared by radio-frequency magnetron sputtering . . . Wentao Xu *et al.* **308**
Novel photoluminescence from hydrogenated amorphous carbon films prepared by using xylene source . . . Jun Xu *et al.* **325**
Preparation of $Cu(In,Ga)Se_2$ thin films at low substrate temperatures . . . S. Nishiwaki *et al.* **394**
Modeling of the effects of crystallographic orientation on electromigration-limited reliability of interconnects with bamboo grain structures . . . W.R. Fayad *et al.* **413**
Preparation and characteristics of seeded epitaxial $(Sr,Ba)Nb_2O_6$ optical waveguide thin films using sol-gel method . . . Junmo Koo *et al.* **430**
Quantification and effects of molecular oxygen and water in zinc phthalocyanine layers . . . H.R. Kerp *et al.* **503**
Formation and characterization of crystalline iron oxide films on self-assembled organic monolayers and their *in situ* patterning . . . Hyunjung Shin *et al.* **564**
Growth of (111)-oriented $Pb(Zr,Ti)O_3$ layers on nanocrystalline RuO_2 electrodes using the sol-gel technique . . . G.J. Norga *et al.* **828**
In situ microscopic surface characterization studies of polymeric thin films during tensile deformation using atomic force microscopy . . . M.S. Bobji *et al.* **844**
Epitaxial stabilization of orthorhombic cuprous oxide films on MgO(110) . . . Paul R. Markworth *et al.* **914**
Ultrathin TiB_2 protective films . . . Feng Huang *et al.* **945**
Direct measurement of mechanical properties of $(Pb,La)TiO_3$ ferroelectric thin films using nanoindentation techniques . . . M. Algueró *et al.* **993**
Modification of sol–gel-derived amorphous Al_2O_3 thin films by F_2 excimer laser irradiation at ambient temperature . . . Satoshi Takeda *et al.* **1003**
Processing of highly oriented lithium niobate films through chemical solution deposition . . . Satomi Ono *et al.* **1155**
Optical and electrical properties of $Ge_{10+x}Se_{40}Te_{50-x}$ thin film . . . S.A. Fayek *et al.* **1549**
Production and characterization of titanium and iron oxide nano-sized thin films . . . E. Comini *et al.* **1559**
Study of analysis methods of depth-sensing indentation test data for spherical indenters . . . A.C. Fischer-Cripps **1579**
Growth study of epitaxial $Fe_xZn_{1-x}F_2$ thin films . . . J. McChesney *et al.* **1769**
Analysis and modeling of residual stress in diamond thin film deposited by the hot-filament chemical vapor deposition process . . . Seung I. Cha *et al.* **1953**
Chemical stresses induced by grain-boundary diffusion in thin films . . . W.L. Wang *et al.* **1967**
Growth behavior and defects in conductive $SrRuO_3$ thin films grown on a Si(100) substrate by sputtering . . . Sang Ho Oh *et al.* **1998**
Transmission electron microscopy study of $n = 1$–5 $Sr_{n+1}Ti_nO_{3n+1}$ epitaxial thin films . . . W. Tian *et al.* **2013**
Growth of epitaxial GaN on $LiGaO_2$ substrates via a reaction with ammonia . . . David Kisailus *et al.* **2077**
Electromigration properties of multigrain aluminum thin film conductors as influenced by grain boundary structure . . . O.V. Kononenko *et al.* **2124**
Development of *p*-type microcrystalline silicon carbon alloy films by the very high frequency plasma-enhanced chemical vapor deposition technique . . . Tapati Jana *et al.* **2130**
Highly (111)-oriented and conformal iridium films by liquid source metalorganic chemical vapor deposition . . . Jaydeb Goswami *et al.* **2192**
Size effect on the mechanical properties of microfabricated polysilicon thin films . . . J.N. Ding *et al.* **2223**
Methods of correction for analysis of depth-sensing indentation test data for spherical indenters . . . A.C. Fischer-Cripps *et al.* **2244**
Crystallography and structural evolution of $LiNbO_3$ and $LiNb_{1-x}Ta_xO_3$ films on sapphire prepared by high-rate thermal plasma spray chemical vapor deposition . . . D.V. Shtansky *et al.* **2271**
Highly textured nanostructure of pulsed laser deposited IrO_2 thin films as investigated by transmission electron microscopy . . . A.M. Serventi *et al.* **2336**
Coherent island formation of Cu_2O films grown by chemical vapor deposition on MgO(110) . . . P.R. Markworth *et al.* **2408**
Ferroelectric domain structure of epitaxial $(Pb,Sr)TiO_3$ thin films . . . Yong Kwan Kim *et al.* **2463**

Low-temperature growth of *c*-axis-oriented Y-type hexagonal ferrite thin films by the polymeric precursor method . . . Tatsuo Fujii *et al.* **2471**
Annealing effect on in-plane alignment and surface morphology of epitaxial $Bi_4Ti_3O_{12}$ thin films prepared by the chemical solution deposition . . . K. Hwang *et al.* **2519**
Measurement of the thermal conductivity of thin layers using a scanning thermal microscope . . . Erwin R. Meinders **2530**
X-ray reflectivity spectra of ultrathin films and nanometric multilayers: Experiment and simulation . . . E. Bontempi *et al.* **2556**
Effect of *in situ* boron doping on properties of silicon germanium films deposited by chemical vapor deposition at 400 °C . . . Sherif Sedky *et al.* **2607**
Growth mechanism of superconducting MgB_2 films prepared by various methods . . . H.Y. Zhai *et al.* **2759**
Precipitate splitting in $Pb_{0.91}La_{0.09}Zr_{0.65}Ti_{0.35}O_3$ films . . . Bahadir Tunaboylu *et al.* **2763**
Formation of quasi-one-dimensional carbon chains in cubic nanocrystals by photon-breaking of C–S bonds in polythiophene . . . Z.M. Ren *et al.* **2793**
Excellent buffer layer for growing high-quality Y–Ba–Cu–O thin films . . . W.H. Tang *et al.* **2864**
Effect of oxygen on the reactions in the Si/Ta/Cu metallization system . . . Tomi Laurila *et al.* **2939**
Numerical study on the measurement of thin film mechanical properties by means of nanoindentation . . . Xi Chen *et al.* **2974**
Anode-supported planar solid oxide fuel cells by plasma-enhanced metalorganic chemical vapor deposition (PE-MOCVD) and electrostatic spray deposition (ESD): Fabrication of dense thin layers of yttria-stabilized zirconia by PE-MOCVD . . . Gianfranco Di Giuseppe *et al.* **2983**
In situ analysis of gaseous species for chemical vapor deposition diamond synthesis and the possible reaction model . . . Mayu Uede *et al.* **3069**
Single-layer submicron-thick $BaTiO_3$ coatings from poly(vinylpyrrolidone)-containing sols: Gel-to-ceramic film conversion, densification, and dielectric properties . . . Hiromitsu Kozuka *et al.* **3116**
Substrate effects on indentation plastic zone development in thin soft films . . . D.E. Kramer *et al.* **3150**
Parameter effect on the crystallization of Nd:yttrium aluminum garnet laser-ablated TiO_2 thin film . . . Mrinal Pal *et al.* **3158**
Microstructure of laser-ablated superconducting $La_2CuO_4F_x$ thin films on $SrTiO_3$ . . . G. Kong *et al.* **3309**
Lubricity of zinc oxide thin films: Study of deposition parameters and Si as an additive . . . J.J. Nainaparampil *et al.* **3423**
Raman scattering of cubic boron nitride films deposited from the low-pressure gas phase . . . W.J. Zhang *et al.* **3430**
Microstructure and misfit relaxation in $SrTiO_3/SrRuO_3$ bilayer films on $LaAlO_3(100)$ substrates . . . J.S. Wu *et al.* **3443**
Determination of optical constants of Si/ZnO polycrystalline nanocomposites by spectroscopic ellipsometry . . . J. García-Serrano *et al.* **3554**
Metalorganic chemical vapor deposition of very thin $Pb(Zr,Ti)O_3$ thin films at low temperatures for high-density ferroelectric memory applications . . . Hye Ryoung Kim *et al.* **3583**

Transmission electron microscopy (TEM)

Atomic structure of YB_{56} studied by digital high-resolution electron microscopy and electron diffraction . . . Takeo Oku *et al.* **101**
Transmission electron microscopy study of (103)-oriented epitaxial $SrBi_2Nb_2O_9$ films grown on (111) $SrTiO_3$ and (111) $SrRuO_3$/(111) $SrTiO_3$ . . . M.A. Zurbuchen *et al.* **489**
Grain boundary structure in Al–Mg and Al–Mg–Sc alloys after equal-channel angular pressing . . . Keiichiro Oh-ishi *et al.* **583**
Mechanical deformation in silicon by micro-indentation . . . J.E. Bradby *et al.* **1500**
$L1_2$- and $L1_0$-like cation-ordered structures in ZrO_2–Y_2O_3 ceramics . . . J.C. Rao *et al.* **1806**
Influence of antiphase boundaries on critical current densities in $YBa_2Cu_3O_{7-y}$ single crystals . . . Junko Shibata *et al.* **1935**
Microstructural analysis of high-pressure compressed C_{60} . . . K. Miyazawa *et al.* **1960**
Compositional distributions in nanoscale metallic multilayers studied using x-ray mapping . . . V.J. Keast *et al.* **2032**
Threading dislocations with edge components in GaN epilayers grown on Al_2O_3 substrates . . . Junyong Kang *et al.* **2550**
Shear-activated indentation crack in GaAs single crystal . . . Z.C. Li *et al.* **2845**
Microstructure of $La_{1-x}Ca_xMnO_3$ studied by transmission electron microscopy . . . Q. Chen *et al.* **2959**
Relation between tolerance factor and T_c in Aurivillius compounds . . . Donají Y. Suárez *et al.* **3139**
Investigation of crystal properties of TmP/GaAs and GaAs/TmP/GaAs heterostructures grown by molecular beam epitaxy . . . C.H. Lin *et al.* **3266**
Microstructural and mechanical characterization of carbon coatings on SiC fibers . . . K.L. Kendig *et al.* **3366**
Investigation of the stability of glassy state in the Zr- and Hf-based glassy alloys correlated with their transformation behavior . . . Junji Saida *et al.* **3389**

Two-body-interaction calculation

Thermal stress in a polymer-coated optical glass fiber with a low-modulus coating at the ends . . . E. Suhir **2996**

Waste management

Thermochemistry of rare-earth orthophosphates . . . S.V. Ushakov *et al.* **2623**

X-ray diffraction (XRD)

Growth, defects, and properties of $GdCa_4O(BO_3)_3$ and $Nd:GdCa_4O(BO_3)_3$ crystals . . . . . Jiyang Wang *et al.* **790**
Synthesis of $Zn_{1-x}Mg_xO$ and its structural characterization . . . . . M.S. Tomar *et al.* **903**
Texture analysis of grain refinement in undercooled $Ni_{99.45}B_{0.55}$ . . . . . K.L. Lee *et al.* **1434**
Thermal expansion and high-temperature phase transformation of the yttrium silicate Y_2SiO_5 . . . . . J.W. Nowok *et al.* **2251**
Change in local atomic structure during formation of the icosahedral quasicrystalline phase in $Zr_{70}Pd_{30}$ glassy alloy . . . . . Muneyuki Imafuku *et al.* **3046**
Novel route for the epitaxial growth of $(SrBa)Nb_2O_6$ thick films by the sol-gel method using a self-template layer . . . . . A-D. Li *et al.* **3179**
Preparation of γ–Fe_2O_3 nanoparticles from a nonaqueous precursor . . . . . P. Deb *et al.* **3471**
Origin of the anomalous volume expansion in Al–Si alloys above liquidus . . . . . W.M. Wang *et al.* **3592**

X-ray photoelectron spectroscopy (XPS)

X-ray photoelectron spectroscopy of electrodeposited cadmium mercury telluride thin films and their native surface oxides . . . . . J. Ramiro *et al.* **1942**

X-ray reflectivity

X-ray reflectivity spectra of ultrathin films and nanometric multilayers: Experiment and simulation . . . . . E. Bontempi *et al.* **2556**

MATERIALS INDEX TO VOLUME 16

This table is a cumulative listing of all the articles in Volume 16 classified according to the specific material(s) for which data and/or calculations are reported. For materials studied in physical combination, the type of combinations is indicated using several formats. Components of a true alloy are separated by dashes (i.e., Al–Zn or W–Ti–Cu). In general, the most abundant component is listed first. The notation (AB) or (ABC) is used to denote A_xB_{1-x} or $(A_xB_{1-x})_yC_{1-y}$, respectively, as well as for the more general pseudoalloys and mixtures. Symbols for trace elements are appended to the host material by a colon such as in CdS:Na for sodium-doped cadmium sulfide. Elements within parentheses separated by a comma indicate the simultaneous presence of both as in Si:(Ga,B) for silicon doped with both gallium and boron. A semicolon refers to each item in the set separately so that Al_2O_3:(Cr;Fe) indicates alumina doped with chromium or alumina doped with iron. The intimate juxtaposition of components, such as in thin-film couples, is indicated by a slash as in SiO_2/Si or Au/Ni/Cu. When the allotropic form of a material is vital to its identification, a parenthetic reference is provided [e.g., $C_{(diamond)}$ versus $C_{(graphite)}$].

Activated carbon

- Morphological effect on the electrochemical behavior of electric double-layer capacitors.–M. Endo, Y.J. Kim, T. Maeda, K. Koshiba, K. Katayam, and M.S. Dresselhaus; **16**(12), 3402–3410.

Activated milled mesophase carbon fiber

- Morphological effect on the electrochemical behavior of electric double-layer capacitors.–M. Endo, Y.J. Kim, T. Maeda, K. Koshiba, K. Katayam, and M.S. Dresselhaus; **16**(12), 3402–3410.

Ag–Fe–Ni

- Synthesis and processing of nanocrystalline Ag–Fe–Ni for low thermal expansion–high conductivity thermal management applications.–J. Stolk, M. Gross, D. Stolk, and A. Manthiram; **16**(2), 340–343.

Ag–In–S

- Preparation and phase control of nanocrystalline silver indium sulfides via a hydrothermal route.–J.Q. Hu, B. Deng, K.B. Tang, C.R. Wang, and Y.T. Qian; **16**(12), 3411–3415.

AgI/Al_2O_3

- Synthesis of nano-AgI arrays and their optical properties.–Yinhai Wang, Jimei Mo, Weili Cai, Lianzeng Yao, and Lide Zhang; **16**(4), 990–992.

$AgInS_2$

- Absorption spectra of Co^{2+} in $AgInS_2$ orthorhombic single crystals.–Hidong Kim, Seok-Joo Lee, Jae-Eun Kim, Hae Yong Park, Seok-Kyun Oh, and Wha-Tek Kim; **16**(4), 975–978.

$AgInS_2$:Co^{2+}

- Absorption spectra of Co^{2+} in $AgInS_2$ orthorhombic single crystals.–Hidong Kim, Seok-Joo Lee, Jae-Eun Kim, Hae Yong Park, Seok-Kyun Oh, and Wha-Tek Kim; **16**(4), 975–978.

Al

- Combined out-of-plane and in-plane texture control in thin films using ion beam assisted deposition.–L. Dong, D.J. Srolovitz, G.S. Was, Q. Zhao, and A.D. Rollett; **16**(1), 210–216.
- Modeling of the effects of crystallographic orientation on electromigration-limited reliability of interconnects with bamboo grain structures.–W.R. Fayad, V.K. Andleigh, and C.V. Thompson; **16**(2), 413–416.
- Measurement of residual stress by load and depth sensing indentation with spherical indenters.–J.G. Swadener, B. Taljat, and G.M. Pharr; **16**(7), 2091–2102.
- Electromigration properties of multigrain aluminum thin film conductors as influenced by grain boundary structure.–O.V. Kononenko, V.N. Matveev, and D.P. Field; **16**(7), 2124–2129.
- Elastic constants of polycrystalline Al and TiN calculated by an *ab initio* method within the local-density approximation.–Ming Zhang, Jiang Shen, and Jiawen He; **16**(8), 2293–2297.
- Measurement of the thermal conductivity of thin layers using a scanning thermal microscope.–Erwin R. Meinders; **16**(9), 2530–2543.
- Piezoelectric actuation of crack growth along polymer–metal interfaces in adhesive bonds.–Tianbao Du, Ming Liu, Steve Seghi, K.J. Hsia, J. Economy, and J.K. Shang; **16**(10), 2885–2892.
- High grain size stability of nanocrystalline Al prepared by mechanical attrition.–F. Zhou, J. Lee, S. Dallek, and E.J. Lavernia; **16**(12), 3451–3458.
- Combustion synthesis method for synthesis of aluminum nitride powder using aluminum containers.–Chun-Nan Lin and Shyan-Lung Chung; **16**(12), 3518–3525.

2024 Al-alloy

- Characteristics of elastic waves generated by crack initiation in aluminum alloys under fatigue loading.–Kiwoo Nam and Ajit Mal; **16**(6), 1745–1751.

5052 Al-alloy

- Characteristics of elastic waves generated by crack initiation in aluminum alloys under fatigue loading.–Kiwoo Nam and Ajit Mal; **16**(6), 1745–1751.

Al/Al_2O_3

- New technique for pressureless infiltration of Al alloys into Al_2O_3 preforms.–B. Srinivasa Rao and V. Jayaram; **16**(10), 2906–2913.
- Substrate effects on indentation plastic zone development in thin soft films.–D.E. Kramer, A.A. Volinsky, N.R. Moody, and W.W. Gerberich; **16**(11), 3150–3157.

Al/$C_{(graphite)}$

- Damping behavior of *in situ* Al–(graphite, Al_4C_3) composites produced by reciprocating extrusion.–Hsu-Shen Chu, Kuo-Shung Liu, and Jien-Wei Yeh; **16**(5), 1372–1380.

Al/Si

- Substrate effects on indentation plastic zone development in thin soft films.–D.E. Kramer, A.A. Volinsky, N.R. Moody, and W.W. Gerberich; **16**(11), 3150–3157.

Al–Cu–Fe

- On some discrepancies in the literature about the formation of icosahedral quasi-crystal in Al–Cu–Fe alloys.–Jianian Gui, Jianbo Wang, Renhui Wang, Dahai Wang, Jing Liu, and Fangyu Chen; **16**(4), 1037–1046.
- Single-crystal growth of the Al–Cu–Fe icosahedral quasicrystal from the ternary melt.–J.Q. Guo and A.P. Tsai; **16**(11), 3038–3041.

Al–Cu–Fe–Be

- Quasicrystalline phase formation in $Al_{62}Cu_{22.5}Fe_{12.5}$ and $Al_{55}Cu_{22.5}Fe_{12.5}Be_7$ alloys.–S.M. Lee, B.H. Kim, D.H. Kim, and W.T. Kim; **16**(6), 1535–1540.

Al–Cu–Mg/SiC

- Interface structure and solute segregation behavior in SiC/2124 and SiC/6061 Al composites exhibiting high-strain-rate superplasticity.–Woo-Jin Kim, Dong-Wha Kum, and Ha-Guk Jeong; **16**(8), 2429–2435.

Al–Fe–V–Si

– Microstructural characterization of rapidly solidified Al–Fe–Si, Al–V–Si, and Al–Fe–V–Si alloys.–A.K. Srivastava and S. Ranganathan; **16**(7), 2103–2117.

Al–Mg

– Grain growth behavior of a nanostructured 5083 Al–Mg alloy.–V.L. Tellkamp, S. Dallek, D. Cheng, and E.J. Lavernia; **16**(4), 938–944.

Al–Mg/SiC

– Joining characteristics of oxidized SiC particles reinforced Al–Mg matrix composite prepared by reaction infiltration processing.–Zhongliang Shi, Shijiro Ochiai, Masaki Hojo, Jaechul Lee, Mingyuan Gu, and Hoin Lee; **16**(2), 400–406.

Al–Mg–Sc

– Grain boundary structure in Al–Mg and Al–Mg–Sc alloys after equal-channel angular pressing.–Keiichiro Oh-ishi, Zenji Horita, David J. Smith, and Terence G. Langdon; **16**(2), 583–589.

Al–Mg–Sn/Al

– Freeform fabrication of aluminum metal-matrix composites.–C.W. Souvignier, T.B. Sercombe, S.H. Huo, P. Calvert, and G.B. Schaffer; **16**(9), 2613–2618.

Al–Mg–Sn/C

– Freeform fabrication of aluminum metal-matrix composites.–C.W. Souvignier, T.B. Sercombe, S.H. Huo, P. Calvert, and G.B. Schaffer; **16**(9), 2613–2618.

Al–Mg–Sn/SiC

– Freeform fabrication of aluminum metal-matrix composites.–C.W. Souvignier, T.B. Sercombe, S.H. Huo, P. Calvert, and G.B. Schaffer; **16**(9), 2613–2618.

Al–Mn

– Effects of pressure on the solidification of Al–Mn alloy.–Duanwei He, M. He, C.S. Kiminami, F.X. Zhang, Y.F. Xu, W.K. Wang, and K.H. Kuo; **16**(4), 910–913.

Al–Ni–Fe

– Formation rule for Al-based ternary quasi-crystals: Example of Al–Ni–Fe decagonal phase.–Jian-Bing Qiang, De-He Wang, Cui-Min Bao, Ying-Min Wang, Wei-Ping Xu, Mei-Li Song, and Chuang Dong; **16**(9), 2653–2660.

Al–Si

– Origin of the anomalous volume expansion in Al–Si alloys above liquidus.–W.M. Wang, X.F. Bian, H.R. Wang, Zhen Wang, L. Zhang, Z.G. Liu, and J-M. Liu; **16**(12), 3592–3598.

Al–Si–Cu

– Finite element modeling of microscale thermal residual stresses in Al interconnects.–A. Saerens, P. Van Houtte, and S.R. Kalidindi; **16**(4), 1112–1122.

Al–Si–Mg/SiC

– Interface structure and solute segregation behavior in SiC/2124 and SiC/6061 Al composites exhibiting high-strain-rate superplasticity.–Woo-Jin Kim, Dong-Wha Kum, and Ha-Guk Jeong; **16**(8), 2429–2435.

Al–Ti

– Effect of annealing on microstructure, residual stress, and hardness of Al–Ti multilayered films.–R. Mitra, A. Madan, R.A. Hoffman, W-A. Chiou, and J.R. Weertman; **16**(7), 2064–2076.

Al–Zn–Mg–Cu

– Orientation dependence of Portevin–Le Châtelier plastic instabilities in depth-sensing microindentation.–Zs. Kovács, N.Q. Chinh, and J. Lendvai; **16**(4), 1171–1177.

AlN

– Surface effects in field-assisted sintering.–J.R. Groza, M. Garcia, and J.A. Schneider; **16**(1), 286–292.

– Combustion synthesis of aluminum nitride powder using additives.–Chun-Nan Lin and Shyan-Lung Chung; **16**(8), 2200–2208.

– Combustion synthesis method for synthesis of aluminum nitride powder using aluminum containers.–Chun-Nan Lin and Shyan-Lung Chung; **16**(12), 3518–3525.

AlN$_{(filamentary)}$

– Novel synthesis of AlN nanowires with controlled diameters.–Jun Liu, X. Zhang, Yingjiu Zhang, Rongrui He, and Jing Zhu; **16**(11), 3133–3138.

AlN/Al_2O_3 (sapphire)

– X-ray scattering study on the structural evolution of AlN/sapphire(0001) films during radiofrequency sputter growth.–H.C. Kang, S.H. Seo, and D.Y. Noh; **16**(6), 1814–1821.

AlN/C$_{(diamond)}$

– Chemical vapor deposition of an aluminum nitride–diamond composite in a triple torch plasma reactor.–Marcus Asmann, Robert F. Cook, Joachim V. Heberlein, and Emil Pfender; **16**(2), 469–477.

Al_2O_3

– Dense, bubble-free ceramic deposits from aqueous suspensions by electrophoretic deposition.–Tetsuo Uchikoshi, Kiyoshi Ozawa, Benjamin D. Hatton, and Yoshio Sakka; **16**(2), 321–324.

– Modification of sol–gel-derived amorphous Al_2O_3 thin films by F_2 excimer laser irradiation at ambient temperature.–Satoshi Takeda, Yoshiaki Ikuta, Masahiro Hirano, and Hideo Hosono; **16**(4), 1003–1009.

– Low-power plasma torch method for the production of crystalline spherical ceramic particles.–Chun-Ku Chen, Seth Gleiman, and Jonathan Phillips; **16**(5), 1256–1265.

– Analysis of depth-sensing indentation tests with a Knoop indenter.–L. Riester, T.J. Bell, and A.C. Fischer-Cripps; **16**(6), 1660–1667.

– Metal–oxide films with magnetically-modulated nanoporous architectures.–Craig A. Grimes, R. Suresh Singh, Elizabeth C. Dickey, and Oomman K. Varghese; **16**(6), 1686–1693.

– Packing and solidification in ceramic injection moulding.–S. Krug, J.R.G. Evans, and J.H.H. ter Maat; **16**(6), 1829–1837.

– Blue photoluminescent properties of pure nanostructured γ–Al_2O_3.–Zhong Qing Yu, Dao Chang, Cun Li, Ning Zhang, Yu Ying Feng, and You Yuan Dai; **16**(7), 1890–1893.

– Threading dislocations with edge components in GaN epilayers grown on Al_2O_3 substrates.–Junyong Kang and Tomoya Ogawa; **16**(9), 2550–2555.

– Processing of mesoporous alumina from a powder precursor.–J. Wayne Frazee and Thomas M. Harris; **16**(11), 3262–3265.

– Simplified method for analyzing nanoindentation data and evaluating performance of nanoindentation instruments.–Takeshi Sawa and Kohichi Tanaka; **16**(11), 3084–3096.

– Formation of Al_2O_3 grains with different sizes and morphologies during the pulse electric current sintering process.–S.W. Wang, L.D. Chen, T. Hirai, and Jingkun Guo; **16**(12), 3514–3517.

Al_2O_3:Er

– Erbium doping into lithium niobate and sapphire single crystal wafers.–P. Nekvindova, J. Spirkova-Hradilova, J. Schröfel, and V. Perina; **16**(2), 333–335.

Al_2O_3:Lu

– Transient creep in fine-grained polycrystalline Al_2O_3 with Lu^{3+} ion segregation at the grain boundaries.–Hidehiro Yoshida, Yuichi Ikuhara, and Taketo Sakuma; **16**(3), 716–720.

Al_2O_3:(Y_2O_3;La_2O_3)

– Improved tensile creep properties of yttrium- and lanthanum-doped alumina: a solid solution effect.–Junghyun Cho, Chong Min Wang, Helen M. Chan, J.M. Rickman, and Martin P. Harmer; **16**(2), 425–429.

$Al_2O_3/CaAl_{12}O_{19}$

- Microprobe fluorescence spectroscopy evaluation of stress fields developed along a propagating crack in an $Al_2O_3/CaO \cdot 6Al_2O_3$ ceramic composite.–O. Sbaizero, S. Maschio, G. Pezzotti, and I.J. Davies; **16**(10), 2798–2804.

Al_2O_3/SiC

- Synthesis of Al_2O_3–SiC from kyanite precursor.–A. Amroune and G. Fantozzi; **16**(6), 1609–1613.
- Effects of whisker content and dimensions on the *R*-curve behavior of an alumina matrix composite reinforced with silicon carbide whiskers.–Takashi Akatsu, Minoru Suzuki, Yasuhiro Tanabe, and Eiichi Yasuda; **16**(7), 1919–1927.

Al_2O_3–$AlCl_3$:$(C_3H_7)_2O$

- Entrapment of organosilicon molecules in nonhydrolytic alumina gels and thermal behavior of the resulting composite.–G.S. Grader, S.A. Melchior, Y. De-Hazan, S. Melamed, and G.E. Shter; **16**(5), 1413–1419.

Al_2O_3–CaO–SiO_2

- Influence of CaO–SiO_2 ratio on the chemistry of intergranular films in liquid-phase sintered alumina and implications for rate of erosive wear.–Rik Brydson, Peter C. Twigg, Fiona Loughran, and Frank L. Riley; **16**(3), 652–665.

$3Al_2O_3$–$2SiO_2$/B_2O_3–SiO_2

- Wetting of mullite by Y_2O_3–Al_2O_3–SiO_2 and B_2O_3–SiO_2 glasses.–T.S. Huang, M.N. Rahaman, B.T. Eldred, and P.D. Ownby; **16**(11), 3223–3228.

$3Al_2O_3$–$2SiO_2$/Y_2O_3–Al_2O_3–SiO_2

- Wetting of mullite by Y_2O_3–Al_2O_3–SiO_2 and B_2O_3–SiO_2 glasses.–T.S. Huang, M.N. Rahaman, B.T. Eldred, and P.D. Ownby; **16**(11), 3223–3228.

Al_2O_3–SrO–SiO_2:(Eu,Dy)

- Relaxation of ultraviolet-radiation-induced structure and long-lasting phosphorescence in Eu^{2+}-doped strontium aluminosilicate glasses.–Jianrong Qiu, Y. Shimizugawa, K. Kojima, K. Tanaka, and K. Hirao; **16**(1), 88–92.

Al_2O_3–TiC–IrO_2

- Thermodynamic analysis of combustion synthesis of Al_2O_3–TiC–ZrO_2 nanoceramics.–Q. Dong, Q. Tang, W.C. Li, and D.Y. Wu; **16**(9), 2494–2498.

Γ-alumina

- Phase transformation effects on the wear properties of alumina gel–polymer matrix nanocomposites.–Jiazhong Luo, John Lannutti, and Robert Seghi; **16**(6), 1680–1685.

Alumina gel

- Phase transformation effects on the wear properties of alumina gel–polymer matrix nanocomposites.–Jiazhong Luo, John Lannutti, and Robert Seghi; **16**(6), 1680–1685.

δ-alumina monohydrate

- Phase transformation effects on the wear properties of alumina gel–polymer matrix nanocomposites.–Jiazhong Luo, John Lannutti, and Robert Seghi; **16**(6), 1680–1685.

Aluminum alloys

- Characteristics of elastic waves generated by crack initiation in aluminum alloys under fatigue loading.–Kiwoo Nam and Ajit Mal; **16**(6), 1745–1751.

As_2Se_3

- Glass transformation in vitreous As_2Se_3 studied by conventional and temperature-modulated differential scanning calorimetry.–S.O. Kasap and D. Tonchev; **16**(8), 2399–2407.

Au-Porcelain

- Cracking of porcelain coatings bonded to metal substrates of different modulus and hardness.–Hong Zhao, Xiaozhi Hu, Mark B. Bush, and Brian R. Lawn; **16**(5), 1471–1478.

B–C–N

- Synthesis and properties of $B_xC_yN_z$ coatings.–M.N. Oliveira and O. Conde; **16**(3), 734–743.
- Structure and phase characteristics of amorphous boron–carbon–nitrogen under high pressure and high temperature.–Jianyu Huang, Yuntian T. Zhu, and Hirotaro Mori; **16**(4), 1178–1184.

Ba–Nd–Ti–O

- Solid-state reaction mechanism for the formation of $Ba_{6-x}Ln_{8+2x/3}Ti_{18}O_{54}$ (Ln = Nd, Sm) solid solutions.–Anatolii G. Belous, Oleg V. Ovchar, Matjaz Valant, and Danilo Suvorov; **16**(8), 2350–2356.

Ba–(Nd,Bc)–Ti–O

- Structures and microwave dielectric properties of $Ba_{6-3x}(Nd,Bi_x)_{8+2x}Ti_{18}O_{54}$ ($x = \frac{2}{3}$) solid solution.–Yong Jun Wu and Xiang Ming Chen; **16**(6), 1734–1738.

$(Ba,Nd)TiO_3$

- Solid-state reaction mechanism for the formation of $Ba_{6-x}Ln_{8+2x/3}Ti_{18}O_{54}$ (Ln = Nd, Sm) solid solutions.–Anatolii G. Belous, Oleg V. Ovchar, Matjaz Valant, and Danilo Suvorov; **16**(8), 2350–2356.

$(Ba,Sr)TiO_3$

- Low-temperature fabrication of pyroelectric $Ba_{0.8}Sr_{0.2}TiO_3$ thin films by a sol-gel process.–Jian-Gong Cheng, Jun Tang, Shao-Ling Guo, and Jun-Hao Chu; **16**(3), 778–783.
- Processing effects on the composition and dielectric properties of hydrothermally derived $Ba_xSr_{(1-x)}TiO_3$ thin films.–Mark A. McCormick, Ryan K. Roeder, and Elliott B. Slamovich; **16**(4), 1200–1209.
- Optimization of the annealing process for the $(Ba,Sr)TiO_3$ thin films grown by low-temperature (420 °C) metalorganic chemical vapor deposition.–Jaehoo Park, Cheol Seong Hwang, and Doo Young Yang; **16**(5), 1363–1371.
- Electric properties of barium–strontium titanate thin films deposited by two-step radio-frequency sputtering.–J.S. Fang, C.T. Chang, and T.S. Chin; **16**(9), 2680–2686.

$BaAl_2S_4$:Sm

- Photoluminescence spectra of undoped and Sm^{3+}-doped $BaAl_2S_4$ and $BaAl_2Se_4$ single crystals.–Moon-Seog Jin, Choong-Il Lee, Chang-Sun Yoon, Chang-Dae Kim, Jae-Mo Goh, and Wha-Tek Kim; **16**(5), 1520–1524.

$BaAl_2Se_4$

- Photoluminescence spectra of undoped and Sm^{3+}-doped $BaAl_2S_4$ and $BaAl_2Se_4$ single crystals.–Moon-Seog Jin, Choong-Il Lee, Chang-Sun Yoon, Chang-Dae Kim, Jae-Mo Goh, and Wha-Tek Kim; **16**(5), 1520–1524.

BaF_2

- Study of the mechanism for controlled crystallization of BaF_2 under two kinds of monolayers.–L. Lu, H. Cui, W. Li, H. Zhang, and S. Xi; **16**(8), 2415–2420.

$BaFe_{12}O_{19}$

- Halide removal from BaM ($BaFe_{12}O_{19}$) and SrM ($SrFe_{12}O_{19}$) ferrite fibers via a steaming process.–R.C. Pullar, M.D. Taylor, and A.K. Bhattacharya; **16**(11), 3162–3169.

$Ba(Mg,Ta)O_3$

- Ordered structure formation in the flux-grown $Ba(Mg_{1/3}Ta_{2/3})O_3$ single crystals.–Yu-Chang Lee, Chen-Chia Chou, and Dah-Shyang Tsai; **16**(6), 1593–1599.

$Ba_4Nd_2Ti_4Ta_6O_{30}$

- Structural and dielectric characterization of $Ba_4Nd_2Ti_{4+x}Ta_{6-x}O_{30-x/2}$ nonstoichiometric ceramics.–X.M. Chen, X.H. Zheng, and J. Wang; **16**(10), 2859–2863.

$Ba_x(Ni,Co)Sb_3$

- High-temperature thermoelectric properties of *n*-type $Ba_xNi_xCo_{4-x}Sb_{12}$.–X.F. Tang, L.M. Zhang, R.Z. Yuan, L.D. Chen, T. Goto, T. Hirai, J.S. Dyck, W. Chen, and C. Uher; **16**(12), 3343–3346.

$BaTiO_3$

- $BaTiO_3$ formation by thermal decomposition of a (BaTi)-citrate polyester resin in air.–P. Durán, F. Capel, J. Tartaj, and C. Moure; **16**(1), 197–209.
- Effective symmetry and physical properties of twinned perovskite ferroelectric single crystals.–Jiří Erhart and Wenwu Cao; **16**(2), 570–577.
- Additive controlled crystallization of barium titanate powders and their application for thin-film ceramic production: Part I. Powder Synthesis.–B. Grohe, G. Miehe, and G. Wegner; **16**(7), 1901–1910.
- Additive controlled crystallization of barium titanate powders and their application for thin-film ceramic production: Part II. From nano-sized powders to ceramic thin films.–B. Grohe, G. Miehe, and G. Wegner; **16**(7), 1911–1915.
- Single-layer submicron-thick $BaTiO_3$ coatings from poly(vinylpyrrolidone)-containing sols: Gel-to-ceramic film conversion, densification, and dielectric properties.–Hiromitsu Kozuka and Atsushi Higuchi; **16**(11), 3116–3123.

$Ba_2Ti_9O_{20}$

- Synthesis of $Ba_2Ti_9O_{20}$ via ethylenediaminetetraacetic acid precursor.–Yebin Xu, Yanyan He, and Liangbin Wang; **16**(4), 1195–1199.

$BaTiO_3$:Nb

- Experimental evidence for space charge segregation in Nb-doped $BaTiO_3$.–Seok Hyun Yoon and Hwan Kim; **16**(5), 1479–1486.

$BaTiO_3$–SiO_2–TiO_2

- Dielectric properties of oxide structures by a laser-based direct-writing method.–D. Young, H.D. Wu, R.C.Y. Auyeung, R. Modi, J. Fitz-Gerald, A. Pique, D.B. Chrisey, P. Atanassova, and T. Kodas; **16**(6), 1720–1725.

$Ba_2Zn_2Fe_{12}O_{22}$

- Low-temperature growth of *c*-axis-oriented Y-type hexagonal ferrite thin films by the polymeric precursor method.–Tatsuo Fujii, Aiko Harano, Makoto Nakanishi, and Jun Takada; **16**(9), 2471–2474.

Benzyldimethylketal

- Photoinduced condensation of sol-gel hybrid glass films doped with benzildimethylketal.–Oun-Ho Park, Ji-In Jung, and Byeong-Soo Bae; **16**(7), 2143–2148.
- Direct laser writing of self-developed waveguides in benzyldimethylketal-doped sol-gel hybrid glass.–Byeong-Soo Bae, Oun-Ho Park, Robbie Charters, Barry Luther-Davies, and Graham R. Atkins; **16**(11), 3184–3187.

$(Bi,La)_4Ti_3O_{12}$

- Processing- and composition-dependent characteristics of chemical solution deposited $Bi_{4-x}La_xTi_3O_{12}$ thin films.–Di Wu, Aidong Li, Tao Zhu, Zhifeng Li, Zhiguo Liu, and Naiben Ming; **16**(5), 1325–1332.

$(Bi,La)_4Ti_3O_{12}/SiO_2/Si$

- Formation and characteristics of highly *c*-axis-oriented $Bi_{3.25}La_{0.75}Ti_3O_{12}$ thin films on SiO_2/Si(100) and Pt/Ti/SiO_2/Si(100) substrates.–Uong Chon, Hyun M. Jang, Sun-Hwa Lee, and Gyu-Chul Yi; **16**(11), 3124–3132.

Bi_2FeNbO_7

- Optical and structural properties of solid oxide photocatalyst Bi_2FeNbO_7.–Zhigang Zou, Jinhua Ye, and Hironori Arakawa; **16**(1), 35–37.

Bi_2O_3–ZnO–Nb_2O_5

- Structure and dielectric properties of pyrochlore–fluorite biphase ceramics in the Bi_2O_3–ZnO–Nb_2O_5 system.–Hong Wang and Xi Yao; **16**(1), 83–87.

Bi_2O_3–ZnO_2–Nb_2O_5–Ag

- Phase formation and reactions in the Bi_2O_3–ZnO–Nb_2O_5–Ag pyrochlore system.–Juan C. Nino, Michael T. Lanagan, and Clive A. Randall; **16**(5), 1460–1464.

Bi_3Se_4

- Solvothermal route to Bi_3Se_4 nanorods at low temperature.–Yuanfang Liu, Jing-hui Zeng, Wei-xin Zhang, Wei-chao Yu, Yi-tai Qian, Jin-bo Cao, and Wan-qun Zhang; **16**(12), 3361–3365.

$Bi_4Ti_3O_{12}/CaRuO_3/SrTiO_3$

- Ferroelectric property of epitaxial $Bi_4Ti_3O_{12}$ films prepared by metalorganic chemical vapor deposition.–Takayuki Watanabe, Hiroshi Funakubo, and Keisuke Saito; **16**(1), 303–307.

$Bi_4Ti_3O_{12}/SrTiO_3$

- Annealing effect on in-plane alignment and surface morphology of epitaxial $Bi_4Ti_3O_{12}$ thin films prepared by the chemical solution deposition.–K. Hwang and Y. Park; **16**(9), 2519–2525.

Bis-GMA {2,2-bis[4-(2-hydroxy-3-methacryloxypropoxy)phenyl]propane}

- Cure depth in photopolymerization: Experiments and theory.–Jim H. Lee, Robert K. Prud'homme, and Ilhan A. Aksay; **16**(12), 3536–3544.

BN

- Raman scattering of cubic boron nitride films deposited from the low-pressure gas phase.–W.J. Zhang and S. Matsumoto; **16**(12), 3430–3442.

Borate glass BK7

- Determination of the elastic properties of glasses and polymers exploiting the resonant characteristic of depth-sensing indentation tests.–D. Lorenz, W. Fränzel, M. Einax, P. Grau, and G. Berg; **16**(6), 1776–1783.

C

- Formation of quasi-one-dimensional carbon chains in cubic nanocrystals by photon-breaking of C–S bonds in polythiophene.–Z.M. Ren, Y.F. Lu, H.W. Choy, T.C. Chong, S.C. Ng, and P. Miao; **16**(10), 2793–2797.
- Microstructural and mechanical characterization of carbon coatings on SiC fibers.–K.L. Kendig, R. Gibala, and D.B. Miracle; **16**(12), 3366–3377.

C_{60}

- Deposition of epitaxial transition metal carbide films and superlattices by simultaneous direct current metal magnetron sputtering and C_{60} evaporation.–H. Högberg, J. Birch, M.P. Johansson, L. Hultman, and U. Jansson; **16**(3), 633–643.
- Microstructural analysis of high-pressure compressed C_{60}.–K. Miyazawa, H. Satsuki, M. Kuwabara, and M. Akaishi; **16**(7), 1960–1966.

$C_{(amorphous)}$

- Strongly adhering and thick highly tetrahedral amorphous carbon (ta–C) thin films via surface modification by implantation.–M. Chhowalla and G.A.J. Amaratunga; **16**(1), 5–8.

$C_{(diamond)}$

- Study of the effects of low-energy electron bombardment during the chemical vapor deposition of diamond.–J.A. González, O.L. Figueroa, B.R. Weiner, and G. Morell; **16**(1), 293–295.
- Misting-free diamond surface created by sheet electron beam irradiation.–Kazuya Oguri, Nobuhiro Iwataka, Akira Tonegawa, Yoichi Hirose, Kazuo Takayama, and Yoshitake Nishi; **16**(2), 553–557.
- Correlation of the Raman spectra with the thermal conductivity of a set of diamond wafers prepared by chemical vapor deposition.–Edgar S. Etz, Wilbur S. Hurst, and Albert Feldman; **16**(6), 1694–1711.
- Analysis and modeling of residual stress in diamond thin film deposited by the hot-filament chemical vapor deposition process.–Seung I. Cha and Soon H. Hong; **16**(7), 1953–1959.

– Electron microscopy of high-temperature and high-pressure as-grown diamond crystals.–Long-Wei Yin, Mu-Sen Li, Jian-Jun Cui, Bin Xu, Jian-Hong Gong, Zhao-Yin Hao, and Jiong-Fa Zhang; **16**(11), 3023–3026.

– *In situ* analysis of gaseous species for chemical vapor deposition diamond synthesis and the possible reaction model.–Mayu Uede and Yoshiki Takagi; **16**(11), 3069–3072.

– Highly oriented diamond growth on positively biased Si substrates.–Te-Fu Chang and Li Chang; **16**(12), 3351–3354.

$C_{(diamond\text{-}like)}$

– Ion energy dependence of film properties for diamond-like carbon prepared with plasma-assisted deposition.–Cao Zexian; **16**(11), 3034–3037.

$C_{(filamentary)}$

– Purification of single-walled carbon nanotubes synthesized by the hydrogen arc-discharge method.–Pengxiang Hou, Chang Liu, Yu Tong, Shitao Xu, Min Liu, and Huiming Cheng; **16**(9), 2526–2529.

– Growth and characterization of aligned carbon nanotubes from patterned nickel nanodots and uniform thin films.–J.G. Wen, Z.P. Huang, D.Z. Wang, J.H. Chen, S.X. Yang, Z.F. Ren, J.H. Wang, L.E. Calvet, J. Chen, J.F. Klemic, and M.A. Reed; **16**(11), 3246–3253.

$C_{(graphite)}$

– Elastic properties of anisotropic monolithic samples of compressed expanded graphite studied with ultrasounds.–M. Krzesińska, A. Celzard, J.F. Marêché, and S. Puricelli; **16**(2), 606–614.

– Generation of circular and hexagonal microholes in a graphite surface.–Hidefumi Hiura; **16**(5), 1287–1292.

– *In situ* analysis of gaseous species for chemical vapor deposition diamond synthesis and the possible reaction model.–Mayu Uede and Yoshiki Takagi; **16**(11), 3069–3072.

$C_{(nanotubes)}$

– Aligned carbon nanotube growth under oxidative ambient.–Anyuan Cao, Xianfeng Zhang, Cailu Xu, Ji Liang, Dehai Wu, and Bingqing Wei; **16**(11), 3107–3110.

C:H

– Novel photoluminescence from hydrogenated amorphous carbon films prepared by using xylene source.–Jun Xu, Wei Li, Tianfu Ma, Zhifeng Li, Li Wang, and Kunji Chen; **16**(2), 325–328.

$C_{(fiber)}$/Nylon

– Electrical conductivity of vapor-grown carbon fiber/thermoplastic composites.–Ioana C. Finegan and Gary G. Tibbetts; **16**(6), 1668–1674.

$C_{(fiber)}$/polypropylene

– Electrical conductivity of vapor-grown carbon fiber/thermoplastic composites.–Ioana C. Finegan and Gary G. Tibbetts; **16**(6), 1668–1674.

C–H

– Development of a continuous microscratch technique in an atomic force microscope and its application to study scratch resistance of ultrathin hard amorphous carbon coatings.–Sriram Sundararajan and Bharat Bhushan; **16**(2), 437–445.

C–N

– Thermal stability of carbon nitride thin films.–Niklas Hellgren, Nian Lin, Esteban Broitman, Virginie Serin, Stefano E. Grillo, Ray Twesten, Ivan Petrov, Christian Colliex, Lars Hultman, and Jan-Eric Sundgren; **16**(11), 3188–3201.

CH_3COOH

– Silicalite/poly(dimethylsiloxane) nanocomposite pervaporation membranes for acetic acid/water separation.–Shih-Yuan Lu, Hsiang-Yuan Huang, and Kwen-Hua Wu; **16**(11), 3053–3059.

$C_5(PO_4)_3F$

– Comparison of crystal structure parameters of natural and synthetic apatites from neutron powder diffraction.–Th. Leventouri, B.C. Chakoumakos, N. Papanearchou, and V. Perdikatsis; **16**(9), 2600–2606.

$C_5(PO_4)_3OH$

– Comparison of crystal structure parameters of natural and synthetic apatites from neutron powder diffraction.–Th. Leventouri, B.C. Chakoumakos, N. Papanearchou, and V. Perdikatsis; **16**(9), 2600–2606.

Ca–Ni–O/Polyethylene trepthalate

– *In situ* microscopic surface characterization studies of polymeric thin films during tensile deformation using atomic force microscopy.–M.S. Bobji and Bharat Bhushan; **16**(3), 844–855.

Ca–Si–Al–O–N

– Nonepitaxial heterogeneous nucleation of α-sialon in the Ca-doped system.–Ya-Wen Li, Pei-Ling Wang, Wei-Wu Chen, Jing-Wei Feng, Yi-Bing Cheng, and Dong-Sheng Yan; **16**(2), 578–582.

$CaCO_3$/polymers

– Deformation mechanisms in nacre.–R.Z. Wang, Z. Suo, A.G. Evans, N. Yao, and I.A. Aksay; **16**(9), 2485–2493.

$Ca_2P_2O_7$–(Ca–P_2O_5–TiO_2–Na_2O)

– Machinable calcium pyrophosphate glass-ceramics.–Toshihiro Kasuga, Miwako Terada, Masayuki Nogami, and Mitsuo Niinomi; **16**(3), 876–880.

$Ca_{10}(PO_4)_6(OH)_2$

– Mechanochemical-hydrothermal preparation of crystalline hydroxyapatite powders at room temperature.–Pavel Shuk, Wojciech L. Suchanek, Tian Hao, Eric Gulliver, Richard E. Riman, Mamoru Senna, Kevor S. TenHuisen, and Victor F. Janas; **16**(5), 1231–1234.

$Ca_{10}(PO_4)_6(OH)_2$/Ti

– Processing and characterization of hydroxyapatite coatings on titanium produced by magnetron sputtering.–T.G. Nieh, A.F. Jankowski, and J. Koike; **16**(11), 3238–3245.

Ca_3SiO_5–H_2O

– Characterization of the induction period in tricalcium silicate hydration by nuclear resonance reaction analysis.–R.A. Livingston, J.S. Schweitzer, C. Rolfs, H-W. Becker, and S. Kubsky; **16**(3), 687–693.

$(CaSr)_{10}(PO_4)_6(OH)_2$

– Preparation of calcium strontium hydroxyapatites by a new route involving calcium phosphate cements.–L. Leroux and J.L. Lacout; **16**(1), 171–178.

Carbon fiber

– High fracture resistance of carbon fiber treated by electron beam irradiation.–Yoshitake Nishi, Takashi Toriyama, Kazuya Oguri, Akira Tonegawa, and Kazuo Takayama; **16**(6), 1632–1635.

(Cd,Hg)Te

– X-ray photoelectron spectroscopy of electrodeposited cadmium mercury telluride thin films and their native surface oxides.–J. Ramiro, L. Galán, E. García Camarero, I. Montero, and Y. Laaziz; **16**(7), 1942–1952.

(Cd,Zn)Te

– Temperature dependence of the optical properties in p-$Cd_{0.96}Zn_{0.04}Te$ single crystals.–H.Y. Lee, T.W. Kang, and T.W. Kim; **16**(8), 2196–2199.

CdS

– Third-order nonlinear optical response in PbS-coated CdS nanocomposites.–Bing Liu, Chwee Har Chew, Leong Ming Gan, Guo Qin Xu, Heping Li, Yee Loy Lam, Chan Hin Kam, and Wen Xiu Que; **16**(6), 1644–1650.

$(Ce,Nb)O_{2-x}$

– Solid solubility and transport properties of $Ce_{1-x}Nd_xO_{2-\delta}$ nanocrystalline solid solutions by a sol-gel route.–Liping Li, Xiaomin Lin, Guangshe Li, and Hiroshi Inomata; **16**(11), 3207–3213.

$Ce_x(Fe,Co)_4Sb_{12}$

– Effects of Ce filling fraction and Fe content on the thermoelectric properties of Co-rich $Ce_xFe_xCo_{4-x}Sb_{12}$.–Xinfeng Tang, Lidong Chen, Takashi Goto, and Toshio Hirai; **16**(3), 837–843.

CeO_2:Nd

– Oxygen self-diffusion in cerium oxide doped with Nd.–Michiyo Kamiya, Eriko Shimada, Yasuro Ikuma, Manabu Komatsu, Hajime Haneda, Soichiro Sameshima, and Yoshihiro Hirata; **16**(1), 179–184.

$CePO_4$

– Thermochemistry of rare-earth orthophosphates.–S.V. Ushakov, K.B. Helean, A. Navrotsky, and L.A. Boatner; **16**(9), 2623–2633.

Co-Porcelain

– Cracking of porcelain coatings bonded to metal substrates of different modulus and hardness.–Hong Zhao, Xiaozhi Hu, Mark B. Bush, and Brian R. Lawn; **16**(5), 1471–1478.

$Co/C_{(filamentary)}$

– Preparation, structure, and magnetic properties of cobalt nanoparticles in carbon fibers.–I. Bashmakov, V. Dorosinez, M. Lukashevich, A. Mazanik, T. Tihonova, T. Zabel, B. Wiedenhorst, and H. Micklitz; **16**(10), 2832–2835.

Co/Si

– *In situ* transmission electron microscopy study of the silicidation process in Co thin films on patterned (001) Si substrates.–C. Ghica, L. Nistor, H. Bender, A. Steegen, A. Lauwers, K. Maex, and J. Van Landuyt; **16**(3), 701–708.

Co–Cr–W/Zn

– Corrosive wear of the Co–Cr–W alloy in liquid zinc.–Xibao Wang and Yong Liang; **16**(6), 1585–1592.

Co–Ge

– Surface studies of phase formation in Co–Ge system: Reactive deposition epitaxy versus solid-phase epitaxy.–I. Goldfarb and G.A.D. Briggs; **16**(3), 744–752.

$CoSb_3$/InSb

– Epitaxial growth of skutterudite ($CoSb_3$) thin films on (001) InSb by pulsed laser deposition.–J.C. Caylor, M.S. Sander, A.M. Stacy, J.S. Harper, R. Gronsky, and T. Sands; **16**(9), 2467–2470.

Cr

– Moving the pulsed heating technique beyond monolithic specimens: Experiments with coated wires.–D. Josell, D. Basak, J.L. McClure, U.R. Kattner, M.E. Williams, W.J. Boettinger, and M. Rappaz; **16**(8), 2421–2428.

Cr_3C_2/Ni–Cr

– Structural characterization of laser-treated Cr_3C_2–NiCr coatings.–P. Serra, J.M. Miguel, J.L. Morenza, and J.M. Guilemany; **16**(12), 3416–3422.

Cr_3PtN/Cr_2N

– Templated growth of a complex nitride island dispersion through an internal nitridation reaction.–M.P. Brady, D.T. Hoelzer, E.A. Payzant, P.F. Tortorelli, J.A. Horton, I.M. Anderson, L.R. Walker, and S.K. Wrobel; **16**(10), 2784–2787.

Cr_3PtN/CrPt

– Templated growth of a complex nitride island dispersion through an internal nitridation reaction.–M.P. Brady, D.T. Hoelzer, E.A. Payzant, P.F. Tortorelli, J.A. Horton, I.M. Anderson, L.R. Walker, and S.K. Wrobel; **16**(10), 2784–2787.

$CsLiB_6O_{10}$

– Water-associated surface degradation of $CsLiB_6O_{10}$ crystal during harmonic generation in the ultraviolet region.–Yukihiro Morimoto, Shintaro Miyazawa, Yoshio Kagebayashi, Naoki Kitatochi, Toshio Yokota, and Jun Sakuma; **16**(7), 2082–2090.

Cu

– Modeling of the effects of crystallographic orientation on electromigration-limited reliability of interconnects with bamboo grain structures.–W.R. Fayad, V.K. Andleigh, and C.V. Thompson; **16**(2), 413–416.

– Torsion and bending of micron-scaled structures.–A.C.M. Chong, F. Yang, D.C.C. Lam, and P. Tong; **16**(4), 1052–1058.

– Chemical–mechanical polishing of copper and tantalum with silica abrasives.–Y. Li, M. Hariharaputhiran, and S.V. Babu; **16**(4), 1066–1073.

Cu alloy

– Formation and mechanical properties of Cu–Hf–Ti bulk glassy alloys.–Akihisa Inoue, Wei Zhang, Tao Zhang, and Kei Kurosaka; **16**(10), 2836–2844.

Cu/Cr

– Compositional distributions in nanoscale metallic multilayers studied using x-ray mapping.–V.J. Keast, A. Misra, H. Kung, and T.E. Mitchell; **16**(7), 2032–2038.

Cu/Nb

– Compositional distributions in nanoscale metallic multilayers studied using x-ray mapping.–V.J. Keast, A. Misra, H. Kung, and T.E. Mitchell; **16**(7), 2032–2038.

Cu/Polyimide

– Scanning probe microscopy generated out-of-plane deformation maps exhibiting heterogeneous nanoscale deformation resulting from thermal cycling of Cu–polyimide damascene interconnects.–Todd S. Gross, Nazri bin Kamsah, and I. Tsukrov; **16**(12), 3560–3566.

Cu/Sn–Bi

– Interfacial embrittlement by bismuth segregation in copper/tin–bismuth Pb-free solder interconnect.–P.L. Liu and J.K. Shang; **16**(6), 1651–1659.

Cu/Ta/Si

– Effect of oxygen on the reactions in the Si/Ta/Cu metallization system.–Tomi Laurila, Kejun Zeng, Jorma K. Kivilahti, Jyriki Molarius, and Ilkka Suni; **16**(10), 2939–2946.

Cu/TiO_2

– Sol-gel-derived photosensitive TiO_2 and Cu/TiO_2 using homogeneous hydrolysis technique.–Jeffrey C.S. Wu and Chih-Yang Yeh; **16**(2), 615–620.

Cu–Ag

– Superplasticicity of Cu–16 at.% Ag microcomposites.–S.I. Hong and H.J. Kwon; **16**(6), 1822–1828.

Cu–Ag–Ti

– Microstructural studies of Cu brazing on AlN.–Chaoxian Cai and Janet K. Lumpp; **16**(3), 670–677.

Cu–Be

– Simplified method for analyzing nanoindentation data and evaluating performance of nanoindentation instruments.–Takeshi Sawa and Kohichi Tanaka; **16**(11), 3084–3096.

Cu–Ce–O

– Combinatorial synthesis of oxide powders.–H.M. Reichenbach and P.J. McGinn; **16**(4), 967–974.

Cu–Hf–Ti

– Formation and mechanical properties of Cu–Hf–Ti bulk glassy alloys.–Akihisa Inoue, Wei Zhang, Tao Zhang, and Kei Kurosaka; **16**(10), 2836–2844.

Cu–polyvinylalcohol

– Patterning of copper particles on polymeric surface.–Arvind Sinha, Swapan Kumar Das, V. Rao, and P. Ramachandrarao; **16**(5), 1354–1357.

Cu,Al

– Molecular dynamics analysis of adhesion strength of interfaces between thin films.–T. Iwasaki and H. Miura; **16**(6), 1789–1794.

$Cu(In,Ga)Se_2$

– Preparation of $Cu(In,Ga)Se_2$ thin films at low substrate temperatures.–S. Nishiwaki, T. Satoh, Y. Hashimoto, T. Negami, and T. Wada; **16**(2), 394–399.

$CuInS_2$

– Preparation and characterization of $CuInS_2$ nanorods and nanotubes from an elemental solvothermal reaction.–Yang Jiang, Yue Wu, Shengwen Yuan, Bo Xie, Shuyuan Zhang, and Yitai Qian; **16**(10), 2805–2809.

$Cu_3Nb_2O_8$

– Microwave dielectric properties of $(1 - x)Cu_3Nb_2O_8$–$xZn_3Nb_2O_8$ ceramics.–Dong-Wan Kim, In-Tae Kim, Byungwoo Park, Kug Sun Hong, and Jong-Hee Kim; **16**(5), 1465–1470.

Cu_2O

– Coherent island formation of Cu_2O films grown by chemical vapor deposition on MgO(110).–P.R. Markworth, X. Liu, J.Y. Dai, W. Fan, T.J. Marks, and R.P.H. Chang; **16**(8), 2408–2414.

Cu_2O/MgO

– Epitaxial stabilization of orthorhombic cuprous oxide films on MgO(110).–Paul R. Markworth, R.P.H. Chang, Y. Sun, G.K. Wong, and J.B. Ketterson; **16**(4), 914–921.

CuO–Cu_2O

– Alternating current conductivity of the interfacial phase in copper oxide–silica gel nanocomposites.–D. Das and D. Chakravorty; **16**(4), 1047–1051.

CuO · SiO_2

– Alternating current conductivity of the interfacial phase in copper oxide–silica gel nanocomposites.–D. Das and D. Chakravorty; **16**(4), 1047–1051.

$Cu_6P(S,Se)_5I$

– Influence of compositional disorder on optical absorption processes in $Cu_6P(S_{1-x}Se_x)_5I$ crystals.–I.P. Studenyak, M. Kranjčec, Gy.Sh. Kovacs, I.D. Desnica-Franković, V.V. Panko, and V.Yu. Slivka; **16**(6), 1600–1608.

$CuWO_4$

– Solid-phase synthesis of cupric tungstate.–Leonid P. Dorfman, David L. Houck, Michael J. Scheithauer, Jeffrey N. Dann, and Harry O. Fassett; **16**(4), 1096–1102.

DBMP [2-benzyl-2-N,N-dimethylamino-1-(4-morpholinophenyl)-1-butanone]

– Cure depth in photopolymerization: Experiments and theory.–Jim H. Lee, Robert K. Prud'homme, and Ilhan A. Aksay; **16**(12), 3536–3544.

Epoxy

– Piezoelectric actuation of crack growth along polymer–metal interfaces in adhesive bonds.–Tianbao Du, Ming Liu, Steve Seghi, K.J. Hsia, J. Economy, and J.K. Shang; **16**(10), 2885–2892.

Epoxy/C/Ag

– Direct writing of polymer thick film resistors using a novel laser transfer technique.–R. Modi, H.D. Wu, R.C.Y. Auyeung, C.M. Gilmore, and D.B. Chrisey; **16**(11), 3214–3222.

Epoxy resin

– Characterization and modeling of specific strain gradient modulus of epoxy.–D.C.C. Lam and A.C.M. Chong; **16**(2), 558–563.

Epoxy resin/Benzocyclobutene/Si

– Adhesion of benzocyclobutene-passivated silicon in epoxy layered structures.–Robert J. Hohlfelder, Daniel A. Maidenberg, Reinhold H. Dauskardt, Yueguang Wei, and John W. Hutchinson; **16**(1), 243–255.

Epoxy resin/Ni

– Fabrication and characterization of microscale sandwich beams.–Francisco Arias, Paul J.A. Kenis, Bing Xu, Tao Deng, Olivier J.A. Schueller, George M. Whitesides, Yuki Sugimura, and Anthony G. Evans; **16**(2), 597–605.

Epoxy resin/Si_3N_4/Si

– Evaluation of the modified edge lift-off test for adhesion characterization in microelectronic multifilm applications.–Jack C. Hay, Eric G. Liniger, and Xiao Hu Liu; **16**(2), 385–393.

$(Eu,Ba)TiO_3$

– Valence variations in titanium-based perovskite oxides by high-pressure and high-temperature method.–Liping Li, Guangshe Li, Jipeng Miao, Wenhui Su, and Hiroshi Inomata; **16**(2), 417–424.

$(Eu,K)TiO_3$

– Valence variations in titanium-based perovskite oxides by high-pressure and high-temperature method.–Liping Li, Guangshe Li, Jipeng Miao, Wenhui Su, and Hiroshi Inomata; **16**(2), 417–424.

Fe:H

– Embedded-atom-method functions for the body-centered-cubic iron and hydrogen.–Mao Wen, Xue-Jun Xu, Seiji Fukuyama, and Kiyoshi Yokogawa; **16**(12), 3496–3502.

$Fe/C_{(graphite)}$

– Carbonization behavior of polyimide film containing iron complex in relation to magnetic properties.–Y. Kaburagi, T. Toriyama, A. Yoshida, H. Wakabayashi, Y. Hishiyama, and M. Inagaki; **16**(2), 352–365.

Fe–B–Si–Mo

– Preparation of superfine Fe-base alloy by liquidus casting.–X.F. Pan, H.F. Zhang, A.M. Wang, B.Z. Ding, and Z.Q. Hu; **16**(12), 3459–3463.

Fe–B–Zr–Nb

– Preparation of superfine Fe-base alloy by liquidus casting.–X.F. Pan, H.F. Zhang, A.M. Wang, B.Z. Ding, and Z.Q. Hu; **16**(12), 3459–3463.

Fe–C

– Simplified method for analyzing nanoindentation data and evaluating performance of nanoindentation instruments.–Takeshi Sawa and Kohichi Tanaka; **16**(11), 3084–3096.

$Fe–C_{(steel)}$

– Transient self-dewetting of steels after pulsed electron beam melting.–N. Mingolo, A.N. Roviglione, and O.E. Martínez; **16**(8), 2343–2349.

Fe–Mn–Ni–V

– Effect of a magnetic field on phase transformation of steel.–W. Liu, D.R. Ou, H.H. Zhou, G.Y. Tang, and F. Wu; **16**(8), 2280–2282.

Fe–N

– Effect of pressure on the structure of Fe–N alloys formed by solid-state reaction.–B. Yao, L. Liu, S.E. Liu, X. Hu, and W.H. Su; **16**(9), 2583–2590.

Fe–P–C

– Compaction of bulk ferromagnetic $Fe_{80}P_{13}C_7$ amorphous alloys.–F.W. Chan, N.G. Ma, and H.W. Kui; **16**(10), 2767–2769.

$(Fe,Zn)F_2/MgF_2$

– Growth study of epitaxial $Fe_xZn_{1-x}F_2$ thin films.–J. McChesney, M. Hetzer, H. Shi, T. Charlton, and D. Lederman; **16**(6), 1769–1775.

Fe_3Al(Cr;Mn;Ni;SiTi;Mo)

– Site preference of alloying elements in Fe_3Al-based alloys.–Xiao Dong Ni, Nan Xian Chen, Jiang Shen, Zu Qing Sun, and Wang Yue Yang; **16**(2), 344–351.

Fe_2O_3

– Formation and characterization of crystalline iron oxide films on self-assembled organic monolayers and their *in situ* patterning.–Hyunjung Shin, Jong Up Jeon, Y. Eugene Pak, Hyejin Im, and Eung Soo Kim; **16**(2), 564–569.

– Preparation of γ–Fe_2O_3 nanoparticles from a nonaqueous precursor.–P. Deb and A. Basumallick; **16**(12), 3471–3475.

Fullerene

– Microstructural analysis of high-pressure compressed C_{60}.–K. Miyazawa, H. Satsuki, M. Kuwabara, and M. Akaishi; **16**(7), 1960–1966.

GaAs

– Infrared optical properties of aged porous GaAs.–S. Zangooie, M. Schubert, T.E. Tiwald, and J.A. Woollam; **16**(5), 1241–1244.

– Shear-activated indentation crack in GaAs single crystal.–Z.C. Li, L. Liu, L.L. He, Y.B. Xu, and X. Wu; **16**(10), 2845–2849.

– Deformation under nanoindents in Si, Ge, and GaAs examined through transmission electron microscopy.–S.J. Lloyd, J.M. Molina-Aldareguia, and W.J. Clegg; **16**(12), 3347–3350.

GaAs/TmP/GaAs

– Investigation of crystal properties of TmP/GaAs and GaAs/TmP/GaAs heterostructures grown by molecular beam epitaxy.–C.H. Lin, R.J. Hwu, and L.P. Sadwick; **16**(11), 3266–3273.

GaN

– Threading dislocations with edge components in GaN epilayers grown on Al_2O_3 substrates.–Junyong Kang and Tomoya Ogawa; **16**(9), 2550–2555.

GaN/Al_2O_3

– Characterization of GaN grown on sapphire by laser-induced molecular beam epitaxy.–H. Zhou, A. Rühm, N.Y. Jin-Phillipp, F. Phillipp, M. Gross, and H. Schröder; **16**(1), 261–267.

GaN/$LiGaO_2$

– Growth of epitaxial GaN on $LiGaO_2$ substrates via a reaction with ammonia.–David Kisailus and F.F. Lange; **16**(7), 2077–2081.

Ga_2S_3–La_2S_3–CsCl

– CsCl-modified Ga_2S_3–La_2S_3 glasses: Structural approach by x-ray absorption spectroscopy.–A.Y. Ramos, M. Grisolía Cardona, H.C.N. Tolentino, M.C.M. Alves, N. Watanabe, O.L. Alves, and L.C. Barbosa; **16**(5), 1349–1353.

$GdCa_4O(BO_3)_3$

– Growth, defects, and properties of $GdCa_4O(BO_3)_3$ and Nd:$GdCa_4O(BO_3)_3$ crystals.–Jiyang Wang, Xiaobo Hu, Xin Yin, Renbo Song, Jingqian Wei, Zongsu Shao, Yaogang Liu, Minhua Jiang, Yulian Tian, Jianhua Jiang, and Wanxia Huang; **16**(3), 790–796.

Ge

– Quantum atomistic simulations of silicon and germanium.–Carlos P. Herrero; **16**(9), 2505–2512.

– Deformation under nanoindents in Si, Ge, and GaAs examined through transmission electron microscopy.–S.J. Lloyd, J.M. Molina-Aldareguia, and W.J. Clegg; **16**(12), 3347–3350.

Ge–Ga–S

– Enhancement of the 1.31-μm emission properties of Dy^{3+}-doped Ge–Ga–S glasses with the addition of alkali halides.–Yong Beom Shin, Jong Heo, and Hyoun Soo Kim; **16**(5), 1318–1324.

Ge–Ga–S–(KI;CsI):Dy^{3+}

– Enhancement of the 1.31-μm emission properties of Dy^{3+}-doped Ge–Ga–S glasses with the addition of alkali halides.–Yong Beom Shin, Jong Heo, and Hyoun Soo Kim; **16**(5), 1318–1324.

Ge–Ga–S(CsBr;KBr):Dy^{3+}

– Enhancement of the 1.31-μm emission properties of Dy^{3+}-doped Ge–Ga–S glasses with the addition of alkali halides.–Yong Beom Shin, Jong Heo, and Hyoun Soo Kim; **16**(5), 1318–1324.

Ge–Se–Te

– Optical and electrical properties of $Ge_{10+x}Se_{40}Te_{50-x}$ thin film.–S.A. Fayek, M. El-Ocker, and A.S. Hassanien; **16**(6), 1549–1553.

Glass fabric/epoxy lamina

– Evaluation of the impactive-surface-fracture behavior of glass plates using a back-surface strain measurement.–Hyoung-Gu Kim, Nak-Sam Choi, and Nahmgyoo Cho; **16**(11), 3042–3045.

$H_3PMo_{12}O_{40}$

– Fabrication of heteropolyoxometalate-based photochromic inorganic–organic nanocomposites.–Tie Rui Zhang, Wei Feng, Chun Yan Bao, Ran Lu, Xin Tong Zhang, Tie Jin Li, Ying Ying Zhao, and Jian Nian Yao; **16**(8), 2256–2263.

$H_3PW_{12}O_{40}$

– Fabrication of heteropolyoxometalate-based photochromic inorganic–organic nanocomposites.–Tie Rui Zhang, Wei Feng, Chun Yan Bao, Ran Lu, Xin Tong Zhang, Tie Jin Li, Ying Ying Zhao, and Jian Nian Yao; **16**(8), 2256–2263.

$H_4SiW_{12}O_{40}$

– Fabrication of heteropolyoxometalate-based photochromic inorganic–organic nanocomposites.–Tie Rui Zhang, Wei Feng, Chun Yan Bao, Ran Lu, Xin Tong Zhang, Tie Jin Li, Ying Ying Zhao, and Jian Nian Yao; **16**(8), 2256–2263.

Hf–Al–Ni–Cu

– Investigation of the stability of glassy state in the Zr- and Hf-based glassy alloys correlated with their transformation behavior.–Junji Saida, Chunfei Li, Mitsuhide Matsushita, and Akihisa Inoue; **16**(12), 3389–3401.

Hf–Cu–Pd

– Precipitation of icosahedral quasicrystalline phase in $Hf_{69.5}Al_{7.5}Ni_{11}Cu_{12}$ metallic glass.–Chunfei Li and Akihisa Inoue; **16**(4), 1190–1194.

Hg–Ba–Cu–O

– Melt processing of Ba_2CuO_3: Textured precursor for the fabrication of $HgBa_2CuO_y$ superconductor.–E. Sudhakar Reddy, T. Murakami, Y. Nakayama, J. Shimoyama, and K. Kishio; **16**(6), 1759–1768.

(Hg,Re)$Ba_2CaCu_2O_x$/$SrTiO_3$

– Chemical reaction at the interface between $(Hg_{0.9}Re_{0.1})Ba_2CaCu_2O_y$ thin film and $SrTiO_3$ substrate.–Xiao-Jing Wu, N. Inoue, T. Sugano, T. Morishita, and K. Tanabe; **16**(1), 256–260.

Hydroxyapatite

– Rheological characteristics of slurry controlling the microstructure and the compressive strength behavior of biomimetic hydroxyapatite.–S. Guicciardi, C. Galassi, E. Landi, A. Tampieri, K. Satou, and G. Pezzotti; **16**(1), 163–170.

$(In,Ga)_2O_3$

– New combustion synthesis technique for the production of $(In_xGa_{1-x})_2O_3$ powders: Hydrazine/metal nitrate method.–R. García, G.A. Hirata, and J. McKittrick; **16**(4), 1059–1065.

InN

– Calorimetric determination of the enthalpy of formation of InN and comparison with AlN and GaN.–M.R. Ranade, F. Tessier, A. Navrotsky, and R. Marchand; **16**(10), 2824–2831.

In_2O_3;(Mg;Ba)

– Characterization of NO_x sensor using doped In_2O_3.–Shinichiro Tanaka and Takao Esaka; **16**(5), 1389–1395.

Ir

– Metalorganic chemical vapor deposition of very thin $Pb(Zr,Ti)O_3$ thin films at low temperatures for high-density ferroelectric memory applications.–Hye Ryoung Kim, Seehwa Jeong, Chung Bae Jeon, Oh Seong Kwon, Cheol Seong Hwang, Young Ki Han, Doo Young Yang, and Ki Young Oh; **16**(12), 3583–3591.

Ir/SiO_2

– Highly (111)-oriented and conformal iridium films by liquid source metalorganic chemical vapor deposition.–Jaydeb Goswami, Chang-Gong Wang, Prashant Majhi, Yong-Wook Shin, and Sandwip K. Dey; **16**(8), 2192–2195.

Ir/TiN

– Highly (111)-oriented and conformal iridium films by liquid source metalorganic chemical vapor deposition.–Jaydeb Goswami, Chang-Gong Wang, Prashant Majhi, Yong-Wook Shin, and Sandwip K. Dey; **16**(8), 2192–2195.

IrO_2

– Highly textured nanostructure of pulsed laser deposited IrO_2 thin films as investigated by transmission electron microscopy.–A.M. Serventi, M.A. El Khakani, R.G. Saint-Jacques, and D.G. Rickerby; **16**(8), 2336–2342.

IrO_2/(Ba,Sr)TiO_3/IrO_2

– Bulk- or interface-limited electrical conductions in IrO_2/(Ba,Sr)TiO_3/IrO_2 thin film capacitors.–Cheol Seong Hwang; **16**(12), 3476–3484.

IR 165 dye/polyceram

– Dye-doped sol-gel coatings for near-infrared laser protection.–T. Kololuoma, J.A.I. Oksanen, P. Raerinne, and J.T. Rantala; **16**(8), 2186–2188.

$K_3Li_2Nb_5O_{15}$

– Preparation and characterization of nanocrystalline potassium lithium niobate powders and films.–H.X. Zhang, C.H. Kam, Y. Zhou, X.Q. Han, S.D. Cheng, C.Y. Chan, and Y.L. Lam; **16**(12), 3609–3613.

$KNbO_3$

– Effective symmetry and physical properties of twinned perovskite ferroelectric single crystals.–Jiří Erhart and Wenwu Cao; **16**(2), 570–577.

$K_2Ti_6O_{13}$

– Microstructure studies of potassium hexatitanate whiskers.–G.L. Li, M. Liu, and G.H. Wang; **16**(12), 3614–3620.

$KTiOAsO_4$

– Polarization reversal and domain anisotropy in flux-grown $KTiOPO_4$ and isomorphic crystals.–P. Urenski, G. Rosenman, and M. Molotskii; **16**(5), 1493–1499.

$KTiOPO_4$

– Refractive index profile and attenuation measurement in $KTiOPO_4$ waveguide by megaelectronvolt He ions.–Ke-Ming Wang, Hiu Hu, Fei Lu, Feng Chen, Bo-Rong Shi, Yao-Gang Liu, Ding-Yu Shen, and Xie-Mei Wang; **16**(1), 276–279.

– Polarization reversal and domain anisotropy in flux-grown $KTiOPO_4$ and isomorphic crystals.–P. Urenski, G. Rosenman, and M. Molotskii; **16**(5), 1493–1499.

La–Fe–Al–O

– Subsolidus phase relations in the La_2O_3–Fe_2O_3–Al_2O_3 system.–Danjela Kuščer, Slavko Bernik, Marko Hrovat, and Janez Holc; **16**(3), 822–827.

La–Sr–Co–O

– Combinatorial synthesis of oxide powders.–H.M. Reichenbach and P.J. McGinn; **16**(4), 967–974.

(La,Ca)MnO_3

– Magnetotransport properties of $La_{0.7}Ca_{0.3}MnO_3$ thick films prepared by spray pyrolysis.–F. Damay, J.L. MacManus-Driscoll, and L.F. Cohen; **16**(3), 784–789.

– Microstructure of $La_{1-x}Ca_xMnO_3$ studied by transmission electron microscopy.–Q. Chen, J. Tao, J.M. Zuo, and J.C.H. Spence; **16**(10), 2959–2965.

– Microstructures of $La_{1-x}A_x$(A = Ca or Sr)$MnO_{3-\delta}$ thin films by liquid-delivery metalorganic chemical vapor deposition.–Y. Xin, K. Han, N. Mateeva, H. Garmestani, P.N. Kalu, and K-H. Dahmen; **16**(11), 3073–3083.

[La,(Na,K)]TiO_3

– Valence variations in titanium-based perovskite oxides by high-pressure and high-temperature method.–Liping Li, Guangshe Li, Jipeng Miao, Wenhui Su, and Hiroshi Inomata; **16**(2), 417–424.

(La,Sr)(Cr,Fe)O_3

– Mechanical and thermal properties of combustion-synthesized perovskites, $La_{1-x}Sr_xCr_{0.2}Fe_{0.8}O_3$.–Yeong-Shyung Chou, K. Kerstetter, L.R. Pederson, and R.E. Williford; **16**(12), 3545–3553.

(La,Sr)FeO_3

– Hydrodynamic cavitation as a tool to control macro-, micro-, and nano-properties of inorganic materials.–J. Find, S.C. Emerson, I.M. Krausz, and W.R. Moser; **16**(12), 3503–3513.

(La,Sr)MnO_3

– Effects of thermal annealing on the texture of $La_{0.67}Sr_{0.33}MnO_3$ thin films.–Lamartine Meda, LaQuita Kennon, Cristiane Bacaltchuk, Hamid Garmestani, and Klaus H. Dahmen; **16**(7), 1887–1889.

– Microstructures of $La_{1-x}A_x$(A = Ca or Sr)$MnO_{3-\delta}$ thin films by liquid-delivery metalorganic chemical vapor deposition.–Y. Xin, K. Han, N. Mateeva, H. Garmestani, P.N. Kalu, and K-H. Dahmen; **16**(11), 3073–3083.

$LaAlO_3$

– Thermal conductivity and thermal diffusivity of selected oxide single crystals.–A. Stanimirovic, N.M. Balzaretti, A. Feldman, and J.E. Graebner; **16**(3), 678–682.

$La_3Ca_3Mn_4O_{14}$

– Study of phase components of $La_{1.5}Ca_{1.5}Mn_2O_7$.–J.L. Zhu, R.C. Yu, F.Y. Li, C.Q. Jin, and Z. Zhang; **16**(7), 2027–2031.

$La_2CuO_4F_x$/$SrTiO_3$

– Microstructure of laser-ablated superconducting $La_2CuO_4F_x$ thin films on $SrTiO_3$.–G. Kong, M.O. Jones, J.S. Abell, P.P. Edwards, S.T. Lees, K.E. Gibbons, I. Gameson, and M. Aindow; **16**(11), 3309–3315.

$LaPO_4$

– Thermochemistry of rare-earth orthophosphates.–S.V. Ushakov, K.B. Helean, A. Navrotsky, and L.A. Boatner; **16**(9), 2623–2633.

$La_x(SiO_4)_6O_2$

– Enthalpies of formation of lanthanide oxyapatite phases.–A.S. Risbud, K.B. Helean, M.C. Wilding, P. Lu, and A. Navrotsky; **16**(10), 2780–2783.

$La_2Ti_2O_9$

– Photoluminescence behavior of Al^{3+}, Pr^{3+} doped perovskite $La_{2/3}TiO_3$ and pyrochlore $La_2Ti_2O_7$.–J.K. Park, C.H. Kim, K.J. Choi, H.D. Park, and S.Y. Choi; **16**(9), 2568–2571.

$La_{2/3}TiO_3$

– Photoluminescence behavior of Al^{3+}, Pr^{3+} doped perovskite $La_{2/3}TiO_3$ and pyrochlore $La_2Ti_2O_7$.–J.K. Park, C.H. Kim, K.J. Choi, H.D. Park, and S.Y. Choi; **16**(9), 2568–2571.

$LiAlCoO_2$

– Raman spectroscopic determination of phase evolutions in $LiAl_xCo_{1-x}O_2$ battery materials.–P.S. Dobal, R.S. Katiyar, M.S. Tomar, and A. Hidalgo; **16**(1), 1–4.

$LiAlSi_2O_6$

– Deformation-induced surface corrugation of superplastic ceramics.–Hiroyuki Muto, Takatoshi Futami, and Motosugu Sakai; **16**(7), 1879–1882.

LiB_3O_5

– Structure and the nonlinearity of lithium triborate studied by Raman and infrared reflectivity spectroscopy.–H.R. Xia, L.X. Li, H. Yu, S.M. Dong, J.Y. Wang, Q.M. Lu, C.Q. Ma, and X.N. Wang; **16**(12), 3464–3470.

$Li(Nb,Ta)O_3/Al_2O_3$

– Crystallography and structural evolution of $LiNbO_3$ and $LiNb_{1-x}Ta_xO_3$ films on sapphire prepared by high-rate thermal plasma spray chemical vapor deposition.–D.V. Shtansky, S.A. Kulinich, K. Terashima, T. Yoshida, and Y. Ikuhara; **16**(8), 2271–2279.

$LiNbO_3$

– Effective symmetry and physical properties of twinned perovskite ferroelectric single crystals.–Jiří Erhart and Wenwu Cao; **16**(2), 570–577.

– Processing of highly oriented lithium niobate films through chemical solution deposition.–Satomi Ono and Shin-ichi Hirano; **16**(4), 1155–1162.

$LiNbO_3$:Cu

– Electronic paramagnetic resonance study of Cu^{2+} ions in copper ion-exchanged layers of lithium niobate crystals.–F. Caccavale, C. Sada, F. Segato, L.D. Bogomolova, V.A. Jachkin, and N.A. Krasil'nikova; **16**(6), 1554–1558.

$LiNbO_3$:Er

– Erbium doping into lithium niobate and sapphire single crystal wafers.–P. Nekvindova, J. Spirkova-Hradilova, J. Schröfel, and V. Perina; **16**(2), 333–335.

$Li_2O–TiO_2–Nb_2O_5$

– Analysis of phase distributions in the $Li_2O–Nb_2O_5–TiO_2$ system by piezoresponse imaging.–Albina Y. Borisevich, Sergei V. Kalinin, Dawn A. Bonnell, and Peter K. Davies; **16**(2), 329–332.

$LuPO_4$:Cm

– Microscopic effects of self-radiation damage in ^{244}Cm-doped $LuPO_4$ crystals.–J.S. Luo and G.K. Liu; **16**(2), 366–372.

Methylsilsesquioxane

– Effect of material properties on integration damage in organosilicate glass films.–E. Todd Ryan, Jeremy Martin, Kurt Junker, Jeff Wetzel, David W. Gidley, and Jianing Sun; **16**(12), 3335–3338.

Mg/Dy

– Analysis of interdiffusion of Dy, Nd, and Pr in Mg.–Y. Xu, L.S. Chumbley, G.A. Weigelt, and F.C. Laabs; **16**(11), 3287–3292.

Mg/Nd

– Analysis of interdiffusion of Dy, Nd, and Pr in Mg.–Y. Xu, L.S. Chumbley, G.A. Weigelt, and F.C. Laabs; **16**(11), 3287–3292.

Mg/Pr

– Analysis of interdiffusion of Dy, Nd, and Pr in Mg.–Y. Xu, L.S. Chumbley, G.A. Weigelt, and F.C. Laabs; **16**(11), 3287–3292.

Mg/V

– Study of the activation process of Mg-based hydrogen storage materials modified by graphite and other carbonaceous compounds.–S. Bouaricha, J-P. Dodelet, D. Guay, J. Huot, and R. Schulz; **16**(10), 2893–2905.

Mg–Fe

– Thermal analysis investigation of hydriding properties of nanocrystalline Mg–Ni- and Mg–Fe-based alloys prepared by high-energy ball milling.–L.E.A. Berlouis, E. Cabrera, E. Hall-Barientos, P.J. Hall, S.B. Dodd, S. Morris, and M.A. Imam; **16**(1), 45–57.

Mg–Ni

– Thermal analysis investigation of hydriding properties of nanocrystalline Mg–Ni- and Mg–Fe-based alloys prepared by high-energy ball milling.–L.E.A. Berlouis, E. Cabrera, E. Hall-Barientos, P.J. Hall, S.B. Dodd, S. Morris, and M.A. Imam; **16**(1), 45–57.

Mg–Zn–Y

– Novel hexagonal structure and ultrahigh strength of magnesium solid solution in the Mg–Zn–Y system.–Akihisa Inoue, Yoshihito Kawamura, Mitsuhide Matsushita, Kentaro Hayashi, and Junichi Koike; **16**(7), 1894–1900.

$Mg_2Al_3(AlSi_5O_{18})$

– Phase-transformation kinetics in triphasic cordierite gel.–R. Petrović, Dj. Janacković, S. Zec, S. Drmanić, and Lj. Kostić-Gvozdenović; **16**(2), 451–458.

MgB_2/Al_2O_3

– Growth mechanism of superconducting MgB_2 films prepared by various methods.–H.Y. Zhai, H.M. Christen, L. Zhang, M. Paranthaman, C. Cantoni, B.C. Sales, P.H. Fleming, D.K. Christen, and D.H. Lowndes; **16**(10), 2759–2762.

MgB_2/Si

– Growth mechanism of superconducting MgB_2 films prepared by various methods.–H.Y. Zhai, H.M. Christen, L. Zhang, M. Paranthaman, C. Cantoni, B.C. Sales, P.H. Fleming, D.K. Christen, and D.H. Lowndes; **16**(10), 2759–2762.

MgO

– Preferential growth mechanism of $REBa_2Cu_3O_y$ (RE = Y, Nd) crystal on MgO substrate by liquid phase epitaxy.–Katsumi Nomura, Saburo Hoshi, Xin Yao, Kazuomi Kakimoto, Yuichi Nakamura, Teruo Izumi, and Yuh Shiohara; **16**(4), 979–989.

– Coherent island formation of Cu_2O films grown by chemical vapor deposition on MgO(110).–P.R. Markworth, X. Liu, J.Y. Dai, W. Fan, T.J. Marks, and R.P.H. Chang; **16**(8), 2408–2414.

– Initial growth mechanism of $YBa_2Cu_3O_y$ crystal on MgO substrate by liquid-phase epitaxy.–Katsumi Nomura, Saburo Hoshi, Yuichi Nakamura, Teruo Izumi, and Yuh Shiohara; **16**(10), 2947–2958.

$(Mn,Zn)Fe_2O_4$

– Electrical transport properties of single-crystalline Mn–Zn ferrous ferrite.–Yong-Chae Chung and Han-Ill Yoo; **16**(3), 774–777.

– Minima in the strength of MnZn ferrites.–M.A.H. Donners, L.J.M.G. Dortmans, G. de With, and M.J.M. de Graaf; **16**(12), 3575–3582.

MnO_2 (cryptomelane)

– Spectroscopic study of a cryptomelane-type manganic acid exchanged by divalent transition-metal cations.–Masamichi Tsuji and Yasuo Tanaka; **16**(1), 108–114.

MoO_3

– Optical and electrochromic properties of heated and annealed MoO_3 thin films.–Zahid Hussain; **16**(9), 2695–2708.

MoS_x

– Fretting wear rate of sulphur deficient MoS_x coatings based on dissipated energy.–Xiaoling Zhang, W. Lauwerens, L. Stals, Jiawen He, and J-P. Celis; **16**(12), 3567–3574.

$MoSi_2$

– Modeling of wave configuration during electrically ignited combustion synthesis.–O.A. Graeve, E.M. Carrillo-Heian, A. Feng, and Z.A. Munir; **16**(1), 93–100.

– Synthesis of dense nanometric $MoSi_2$ through mechanical and field activation.–R. Orrù, J. Woolman, G. Cao, and Z.A. Munir; **16**(5), 1439–1448.

– Effect of mechanical alloying on combustion synthesis of $MoSi_2$.–Hyung-Sang Park, Kwang-Seon Shin, and Yong-Seog Kim; **16**(11), 3060–3068.

MPTMS (methacryloxypropyltrimethoxysilane)

– Direct laser writing of self-developed waveguides in benzyldimethylketal-doped sol-gel hybrid glass.–Byeong-Soo Bae, Oun-Ho Park, Robbie Charters, Barry Luther-Davies, and Graham R. Atkins; **16**(11), 3184–3187.

NH_4Cl

– Combustion synthesis method for synthesis of aluminum nitride powder using aluminum containers.–Chun-Nan Lin and Shyan-Lung Chung; **16**(12), 3518–3525.

$NaBH_4$

– Patterning of copper particles on polymeric surface.–Arvind Sinha, Swapan Kumar Das, V. Rao, and P. Ramachandrarao; **16**(5), 1354–1357.

Nacre

– Model for the robust mechanical behavior of nacre.–A.G. Evans, Z. Suo, R.Z. Wang, I.A. Aksay, M.Y. He, and J.W. Hutchinson; **16**(9), 2475–2484.

Nb/(Al:Cu)

– Texture in Ti/Al and Nb/Al multilayer thin films: Role of Cu.–G. Lucadamo, K. Barmak, and K.P. Rodbell; **16**(5), 1449–1459.

Nb_3Al

– Synthesis of nanoscale particles of Ta and Nb_3Al by homogeneous reduction in liquid ammonia.–Hongmin Zhu and Donald R. Sadoway; **16**(9), 2544–2549.

NbN

– High-T_c superconducting NbN films with low particulate density grown at 25 °C using pulsed laser deposition.–Anupama B. Kaul, Timothy D. Sands, and Theodore Van Duzer; **16**(5), 1223–1226.

Nd:$GdCa_4O(BO_3)_3$

– Growth, defects, and properties of $GdCa_4O(BO_3)_3$ and Nd:$GdCa_4O(BO_3)_3$ crystals.–Jiyang Wang, Xiaobo Hu, Xin Yin, Renbo Song, Jingqian Wei, Zongsu Shao, Yaogang Liu, Minhua Jiang, Yulian Tian, Jianhua Jiang, and Wanxia Huang; **16**(3), 790–796.

Nd–Fe–B

– Synthesis of $Nd_2Fe_{14}B$ powders by spray-drying and reduction–diffusion processes.–X.L. Dong, B.K. Kim, C.J. Choi, K.S. Park, and Z.D. Zhang; **16**(4), 1083–1089.

– Metastable solidification of NdFeB alloys by drop-tube processing.–Jianrong Gao, Th. Volkmann, and D.M. Herlach; **16**(9), 2562–2567.

– Plate domain structure of sintered NdFeB magnets and dependence on compacting mode.–Zhen Rong Zhang, Bao Shan Han, Ye Qing He, and Shou Zeng Zhou; **16**(10), 2992–2995.

Nd–Fe–Mo–B

– Effects of preparation processes on structure and magnetic properties of $Nd_2Fe_{14}B$/α–Fe-type nanocomposite magnets.–Bao-zhi Cui, X.K. Sun, L.Y. Xiong, Wei Liu, Zhi-dong Zhang, Zhi-qing Yang, Ai-min Wang, and Jiang-ning Deng; **16**(3), 709–715.

(Nd,Eu,Gd)$Ba_2Cu_3O_{7-x}$

– Microstructure of (Nd, Eu, Gd)-123 matrix with (Nd, Eu, Gd)-211 inclusions.–M. Muralidhar, M. Jirsa, K. Iida, N. Sakai, and M. Murakami; **16**(2), 407–412.

(Nd,La)$Sc_3(BO_3)_4$

– Phase transition, growth, and optical properties of $Nd_xLa_{1-x}Sc_3(BO_3)_4$ crystals.–Yunkui Li, G. Aka, A. Kahn-Harari, and D. Vivien; **16**(1), 38–44.

$NdBa_2Cu_3O_y$

– Preferential growth mechanism of $REBa_2Cu_3O_y$ (RE = Y, Nd) crystal on MgO substrate by liquid phase epitaxy.–Katsumi Nomura, Saburo Hoshi, Xin Yao, Kazuomi Kakimoto, Yuichi Nakamura, Teruo Izumi, and Yuh Shiohara; **16**(4), 979–989.

$NdBa_2Cu_3O_{7-x}$

– Formation of $NdBa_2Cu_3O_{7-\delta}$ amorphous phase by combining aero-acoustic levitation and splat quenching.–K. Nagashio, W.H. Hofmeister, D.E. Gustafson, A. Altgilbers, R.J. Bayuzick, and K. Kuribayashi; **16**(1), 138–145.

$NdBa_2Cu_3O_x$:Sr

– Formation of $Nd_{1+x}(Ba_{1-y}Sr_y)_{2-x}Cu_3O_{7\pm\delta}$ solid solutions by crystal pulling.–Xin Yao, E.A. Goodilin, Teruo Izumi, and Yuh Shiohara; **16**(2), 529–533.

$NdGaO_3$

– Thermal conductivity and thermal diffusivity of selected oxide single crystals.–A. Stanimirovic, N.M. Balzaretti, A. Feldman, and J.E. Graebner; **16**(3), 678–682.

Nd(Nd,Ba)Cu_3O_{7-x}

– Growth of melt-textured Nd-123 by hot seeding under reduced oxygen partial pressure.–M. Kambara, N. Hari Babu, Y.H. Shi, and D.A. Cardwell; **16**(4), 1163–1170.

NH_4Cl

– Combustion synthesis method for synthesis of aluminum nitride powder using aluminum containers.–Chun-Nan Lin and Shyan-Lung chung; **16**(12), 3518–3525.

Ni

– Surface effects in field-assisted sintering.–J.R. Groza, M. Garcia, and J.A. Schneider; **16**(1), 286–292.

– Fabrication and characterization of microscale sandwich beams.–Francisco Arias, Paul J.A. Kenis, Bing Xu, Tao Deng, Olivier J.A. Schueller, George M. Whitesides, Yuki Sugimura, and Anthony G. Evans; **16**(2), 597–605.

– Effect of process variables on the structure, residual stress, and hardness of sputtered nanocrystalline nickel films.–R. Mitra, R.A. Hoffman, A. Madan, and J.R. Weertman; **16**(4), 1010–1027.

– Torsion and bending of micron-scaled structures.–A.C.M. Chong, F. Yang, D.C.C. Lam, and P. Tong; **16**(4), 1052–1058.

Ni–Al

– A combinatorial approach for efficient mapping of phase diagrams and properties.–Ji-Cheng Zhao; **16**(6), 1565–1578.

Ni–B

– Texture analysis of grain refinement in undercooled $Ni_{99.45}B_{0.55}$.–K.L. Lee, C.H. Shek, and H. Yang; **16**(5), 1434–1438.

Ni–Cr–Fe

– Multifunctional microtruss laminates: Textile synthesis and properties.–D.J. Sypeck and H.N.G. Wadley; **16**(3), 890–897.

Ni–Cr–Mo–Nb

– Development of nanocrystalline structure during cryomilling of Inconel 625.–Jianhong He and Enrique J. Lavernia; **16**(9), 2724–2732.

Ni–Cr–P

– Synthesis of open-cell metal foams by templated directed vapor deposition.–Douglas T. Queheillalt, Derek D. Hass, David J. Sypeck, and Haydn N.G. Wadley; **16**(4), 1028–1036.

Ni–Fe–Cr–Al–Ti–Ta–Nb

– A combinatorial approach for efficient mapping of phase diagrams and properties.–Ji-Cheng Zhao; **16**(6), 1565–1578.

Ni–Ti

– Glass-forming ability of the Ni–Zr and Ni–Ti systems determined by interatomic potentials.–W.S. Lai and B.X. Liu; **16**(2), 446–450.

Ni–Zr

– Glass-forming ability of the Ni–Zr and Ni–Ti systems determined by interatomic potentials.–W.S. Lai and B.X. Liu; **16**(2), 446–450.

Ni_3Al

– Site preference determination in intermetallic compounds by thermal conductivity measurement.–Yoshihiro Terada, Kenji Ohkubo, Tetsuo Mohri, and Tomoo Suzuki; **16**(8), 2314–2320.

NiAl–AlN–Cr

– Creep and toughness of cryomilled NiAl containing Cr.–J. Daniel Whittenberger, Beverly Aikin, and Jon Salem; **16**(5), 1333–1344.

NiAl–TiB_2

– Mechanistic studies in combustion synthesis of NiAl–TiB_2 composites: Effects of gravity.–Cheryl Lau, Alexander Mukasyan, Aleksey Pelekh, and Arvind Varma; **16**(6), 1614–1625.

$Ni_{99.45}B_{0.55}$

– Texture analysis of grain refinement in undercooled $Ni_{99.45}B_{0.55}$.–K.L. Lee, C.H. Shek, and H. Yang; **16**(5), 1434–1438.

NiO–YSZ

– Anode-supported planar solid oxide fuel cells by plasma-enhanced metalorganic chemical vapor deposition (PE-MOCVD) and electrostatic spray deposition (ESD): Fabrication of dense thin layers of yttria-stabilized zirconia by PE-MOCVD.–Gianfranco Di Giuseppe and J. Robert Selman; **16**(10), 2983–2991.

$NiO–ZrO_2$

– Preparation of nanocrystalline nickel oxide–yttria-stabilized zirconia composite powder by solution combustion with ignition of glycine fuel.–Sun-Jae Kim, Wonhee Lee, Won-Jun Lee, Soon Dong Park, Jae Sung Song, and Eun Gu Lee; **16**(12), 3621–3627.

Pb–Sn

– Effect of lead content on vibration fracture behavior of Pb–Sn eutectic solder.–C.M. Chuang, T.S. Lui, and L.H. Chen; **16**(9), 2644–2652.

Pb–Sn/Cu

– Stability of channels at a scalloplike Cu_6Sn_5 layer in solder interconnections.–Jong-Hyun Lee, Jong-Hwan Park, Yong-Ho Lee, Yong-Seog Kim, and Dong Hyuk Shin; **16**(5), 1227–1230.

$(Pb,Ca)(Mg,Nb,Ti)O_3$

– Dielectric properties of La-substituted $Pb_{0.5}Ca_{0.5}[(Mg_{1/3}Nb_{2/3})_{0.5}Ti_{0.5}]O_3$ ceramics.–X.J. Lu and X.M. Chen; **16**(7), 2053–2056.

$(Pb,Ca)(Mg,Ta)O_3$

– Effect of bond valence on microwave dielectric properties of $(Pb_{1-x}Ca_x)(Mg_{0.33}Ta_{0.67})O_3$ ceramics.–Heung Soo Park, Ki Hyun Yoon, and Eung Soo Kim; **16**(3), 817–821.

$(Pb,La)TiO_3$

– Direct measurement of mechanical properties of $(Pb,La)TiO_3$ ferroelectric thin films using nanoindentation techniques.–M. Algueró, A.J. Bushby, and M.J. Reece; **16**(4), 993–1002.

$(Pb,La)(Zr,Ti)O_3/Al_2O_3$

– Precipitate splitting in $Pb_{0.91}La_{0.09}Zr_{0.65}Ti_{0.35}O_3$ films.–Bahadir Tunaboylu, Ken Ring, Sadik C. Esener, Cengiz Ozkan, and Ali Ata; **16**(10), 2763–2766.

$(Pb,La)(Zr,Ti)O_3/Pt$

– Effect of hydrogen on true leakage current characteristics of $(Pb,La)(Zr,Ti)O_3$ thin-film capacitors with Pt- or Ir-based top electrodes.–Soon-Gil Yoon, Dwi Wicaksana, Dong-Joo Kim, Seung-Hyun Kim, and A.I. Kingon; **16**(4), 1185–1189.

$(Pb,Mg)Nb_2O_6–PbTiO_3$

– Dependence of dielectric and piezoelectric properties on film thickness for highly {100}-oriented lead magnesium niobate–lead titanate (70/30) thin films.–Jeong Hwan Park and Susan Trolier-McKinstry; **16**(1), 268–275.

$(Pb,Sr)TiO_3$

– Ferroelectric domain structure of epitaxial $(Pb,Sr)TiO_3$ thin films.–Yong Kwan Kim, Kyeong Seok Lee, and Sunggi Baik; **16**(9), 2463–2466.

$Pb(Mg,Nb)O_3–PbTiO_3$

– Electron backscatter diffraction analysis of $Pb(Mg_{1/3}Nb_{2/3})O_3$–35mol%$PbTiO_3$ single crystals grown by seeded polycrystal conversion.–Ajmal Khan, Derrick T. Carpenter, Adam M. Scotch, Helen M. Chan, and Martin P. Harmer; **16**(3), 694–700.

– Domain configurations in relaxor ferroelectric single crystals $Pb(Mg_{1/3}Nb_{2/3})O_3–PbTiO_3$.–Guisheng Xu, Haosu Luo, Zhenyi Qi, Haiqing Xu, and Zhiwen Yin; **16**(4), 932–937.

– Twinning domain in $67Pb(Mg_{1/3}Nb_{2/3})O_3–33PbTiO_3$ ferroelectric complex perovskite crystal grown by the Bridgman method.–Donglin Li, Pingchu Wang, Xiaoming Pan, Haosu Luo, and Zhiwen Yin; **16**(5), 1252–1255.

$Pb(Ni_{1/3}Nb_{2/3})O_3$

– Dielectric properties anomaly of $(1–x)Pb(Ni_{1/3}Nb_{2/3})O_3–xPbTiO_3$ ceramics near the morphotropic phase boundary.–Zhenrong Li, Liangying Zhang, and Xi Yao; **16**(3), 834–836.

PbS

– Third-order nonlinear optical response in PbS-coated CdS nanocomposites.–Bing Liu, Chwee Har Chew, Leong Ming Gan, Guo Qin Xu, Heping Li, Yee Loy Lam, Chan Hin Kam, and Wen Xiu Que; **16**(6), 1644–1650.

PbS/SiO_2

– Control growth of PbS quantum dots doped sono-ormosil.–R. Erce-Montilla, M. Piñero, N. de la Rosa-Fox, A. Santos, and L. Esquivias; **16**(9), 2572–2578.

PbSe/Polyacrylic acid-styrene

– Preparation and characterization of nanocrystalline PbSe in poly(acrylic acid-*co*-styrene).–Yangyang Sun, Xuefeng Qian, Jie Yin, Junchao Huang, Xiaodong Ma, and Zikang Zhu; **16**(10), 2922–2927.

$PbTiO_3$

– Dielectric properties anomaly of $(1–x)Pb(Ni_{1/3}Nb_{2/3})O_3–xPbTiO_3$ ceramics near the morphotropic phase boundary.–Zhenrong Li, Liangying Zhang, and Xi Yao; **16**(3), 834–836.

$Pb(Zr,Ti)O_3$

– Growth of (111)-oriented $Pb(Zr,Ti)O_3$ layers on nanocrystalline RuO_2 electrodes using the sol-gel technique.–G.J. Norga, S. Jin, Laura Fè, D.J. Wouters, H. Bender, and H.E. Maes; **16**(3), 828–833.

– $Pb(Zr_xTi_{1-x})O_3$ ceramics via reactive sintering of partially reacted mixture produced by a high-energy ball milling process.–L.B. Kong, J. Ma, T.S. Zhang, W. Zhu, and O.K. Tan; **16**(6), 1636–1643.

– Modeling of electric field induced texture in lead zirconate titanate ceramics.–Shan Wan and Keith Bowman; **16**(8), 2306–2313.

– Chemical structure evolution and orientation selection in sol-gel-prepared ferroelectric $Pb(Zr,Ti)O_3$ thin films.–L. Fè, G.J. Norga, D.J. Wouters, H.E. Maes, and G. Maes; **16**(9), 2499–2504.

– Oxygen transport during annealing of $Pb(Zr,Ti)O_3$ thin films in O_2 gas and its effect on their conductivity.–F. Ayguavives, B. Agius, B. Ea-Kim, and I. Vickridge; **16**(10), 3005–3008.

– Hydrodynamic cavitation as a tool to control macro-, micro-, and nano-properties of inorganic materials.–J. Find, S.C. Emerson, I.M. Krausz, and W.R. Moser; **16**(12), 3503–3513.

– Metalorganic chemical vapor deposition of very thin $Pb(Zr,Ti)O_3$ thin films at low temperatures for high-density ferroelectric memory applications.–Hye Ryoung Kim, Seehwa Jeong, Chung Bae Jeon, Oh Seong Kwon, Cheol Seong Hwang, Young Ki Han, Doo Young Yang, and Ki Young Oh; **16**(12), 3583–3591.

$Pb(Zr,Ti)O_3/SrRuO_3$

– Epitaxial growth of $PbZr_{0.5}Ti_{0.5}O_3$ thin films on $SrRuO_3/SrTiO_3$ substrates using chemical solution deposition: Microstructural and ferroelectric properties.–J.H. Kim, Youngman Kim, A.T. Chien, and F.F. Lange; **16**(6), 1739–1744.

Pd–Ni–P

– Crystallization kinetics of amorphous nanostructured $Pd_{40.5}Ni_{40.5}P_{19}$ alloys.–H.W. Ngai, C.C. Leung, W.H. Guo, and H.W. Kui; **16**(3), 797–802.

Pd–S

– Mass density of glassy $Pd_{80}Si_{20}$ during low-temperature light ion irradiation.–G. Schumacher, R.C. Birtcher, and L.E. Rehn; **16**(10), 2788–2792.

Pd-Porcelain

– Cracking of porcelain coatings bonded to metal substrates of different modulus and hardness.–Hong Zhao, Xiaozhi Hu, Mark B. Bush, and Brian R. Lawn; **16**(5), 1471–1478.

PDMS

– Silicalite/poly(dimethylsiloxane) nanocomposite pervaporation membranes for acetic acid/water separation.–Shih-Yuan Lu, Hsiang-Yuan Huang, and Kwen-Hua Wu; **16**(11), 3053–3059.

Phosphate glass:(Er,Yb)

– Investigation of optical waveguide formed in Er:Yb:phosphate glass by MeV He^+ implantation.–Zhuang Zhuo, Edwin Yue Bun Pun, Sun Fat Wong, and Ying Zhou; **16**(4), 1135–1137.

PMMA

– Determination of the elastic properties of glasses and polymers exploiting the resonant characteristic of depth-sensing indentation tests.–D. Lorenz, W. Fränzel, M. Einax, P. Grau, and G. Berg; **16**(6), 1776–1783.

Polyalphamethylstyrene/Fe

– Two-dimensional simulation of mass transport in polymer removal from a powder injection molding compact by thermal debinding.–Ying Shengjie, Y.C. Lam, S.C.M. Yu, and K.C. Tam; **16**(8), 2436–2451.

Polyaniline/$BaTiO_3$

– Piezoresistivity of conducting polyaniline/$BaTiO_3$ composites.–R.C. Patil, S. Radhakrishnan, Sushama Pethkar, and K. Vijaymohanan; **16**(7), 1982–1988.

Polycarbonate

– Direct measurement of plowing friction and wear of a polymer thin film using the atomic force microscope.–Binyang Du, Mark R. VanLandingham, Qingling Zhang, and Tianbai He; **16**(5), 1487–1492.

Poly(dicyclopentadiene)

– Gradient porosity poly(dicyclopentadiene).–A. Della Martina and J.G. Hilborn; **16**(7), 2045–2052.

Polyethersulfone

– Effect of ion implant dose on the mechanical properties of polyethersulfone films.–Manuel Luis B. Palacio, Yongquiang Wang, and William W. Gerberich; **16**(12), 3628–3635.

Poly(ethylene–octene)

– Influence of thermal history on morphology and viscoelastic behavior of ethylene–1-octene copolymers synthesized with metallocene catalysts.–M.L. Cerrada, R. Benavente, and E. Pérez; **16**(4), 1103–1111.

Polyimide/SiO_2

– Increased fracture toughness in nanoporous silica–polyimide matrix composites.–Shiling Ruan, John J. Lannutti, Stan Prybyla, and Robert R. Seghi; **16**(7), 1975–1981.

Polymethyl methacrylate

– Optical evaluation of the flexural rigidity and residual stress in thin membranes: Picosecond transient grating measurements of the dispersion of the lowest-order Lamb acoustic waveguide mode.–John A. Rogers and Gregory R. Bogart; **16**(1), 217–225.

Polymides/CuS

– Low-resistance films of polyimides with impregnated copper sulfide.–R.V.A. Rowe, M.H. Kunita, M.F. Porto, E.C. Muniz, A.F. Rubira, R.C. Nery, E. Radovanovic, L.T. Taylor, and N. Nazem; **16**(11), 3097–3106.

Polypropylene/$C_{(filamentary)}$

– Strength prediction of partially aligned discontinuous fiber-reinforced composites.–Rex J. Kuriger, M. Khairul Alam, and David P. Anderson; **16**(1), 226–232.

Polystyrene/soda glass

– Adhesion of polymer–inorganic interfaces by nanoindentation.–Min Li, C. Barry Carter, Marc A. Hillmyer, and William W. Gerberich; **16**(12), 3378–3388.

Poly(thienylene-phenylene)

– Preliminary study on alternating thienylene/phenylene copolymers functionalized with an electron-donating or -withdrawing group.–J.M. Xu, S.C. Ng, and H.S.O. Chan; **16**(5), 1235–1237.

Portland Cement

– Characterization of the induction period in tricalcium silicate hydration by nuclear resonance reaction analysis.–R.A. Livingston, J.S. Schweitzer, C. Rolfs, H-W. Becker, and S. Kubsky; **16**(3), 687–693.

– Rectifying and thermocouple junctions based on Portland cement.–Sihai Wen and D.D.L. Chung; **16**(7), 1989–1993.

2-propanol

– Gradient porosity poly(dicyclopentadiene).–A. Della Martina and J.G. Hilborn; **16**(7), 2045–2052.

Pt

– Sintering of screen-printed platinum thick films for electrode applications.–J.B. Véchembre and G.R. Fox; **16**(4), 922–931.

– Metalorganic chemical vapor deposition of very thin $Pb(Zr,Ti)O_3$ thin films at low temperatures for high-density ferroelectric memory applications.–Hye Ryoung Kim, Seehwa Jeong, Chung Bae Jeon, Oh Seong Kwon, Cheol Seong Hwang, Young Ki Han, Doo Young Yang, and Ki Young Oh; **16**(12), 3583–3591.

PZT

– Piezoelectric actuation of crack growth along polymer–metal interfaces in adhesive bonds.–Tianbao Du, Ming Liu, Steve Seghi, K.J. Hsia, J. Economy, and J.K. Shang; **16**(10), 2885–2892.

$RBTiOPO_4$

– Polarization reversal and domain anisotropy in flux-grown $KTiOPO_4$ and isomorphic crystals.–P. Urenski, G. Rosenman, and M. Molotskii; **16**(5), 1493–1499.

Ru–Al

– Formation of eutectic RuAl/Ru nanocomposite by mechanical alloying and subsequent annealing.–K.W. Liu, F. Mücklich, and R. Birringer; **16**(9), 2459–2462.

RuO_2

– Growth of (111)-oriented $Pb(Zr,Ti)O_3$ layers on nanocrystalline RuO_2 electrodes using the sol-gel technique.–G.J. Norga, S. Jin, Laura Fè, D.J. Wouters, H. Bender, and H.E. Maes; **16**(3), 828–833.

– Kinetic analysis of solid-state processes.–Jiří Málek, Takefumi Mitsuhashi, and José Manuel Criado; **16**(6), 1862–1871.

$Ru_2O_3/SiO_2/Ru_2O_3$

– Piezoresistivity in ruthenium-based metal–insulator–metal structures.–Ahmed Amin; **16**(8), 2239–2243.

SAN

– Determination of the elastic properties of glasses and polymers exploiting the resonant characteristic of depth-sensing indentation tests.–D. Lorenz, W. Fränzel, M. Einax, P. Grau, and G. Berg; **16**(6), 1776–1783.

Sb_2O_3

– Synthesis and characterization of antimony oxide nanoparticles.–Zaoli Zhang, Lin Guo, and Wendong Wang; **16**(3), 803–805.

$ScAlMgO_4$

– Thermal conductivity and thermal diffusivity of selected oxide single crystals.–A. Stanimirovic, N.M. Balzaretti, A. Feldman, and J.E. Graebner; **16**(3), 678–682.

Si

– Development of a continuous microscratch technique in an atomic force microscope and its application to study scratch resistance of ultrathin hard amorphous carbon coatings.–Sriram Sundararajan and Bharat Bhushan; **16**(2), 437–445.

– Planar oxidation of strained silicon substrates.–M-T. Lin, R.J. Jaccodine, and T.J. Delph; **16**(3), 728–733.

– Mechanical deformation in silicon by micro-indentation.–J.E. Bradby, J.S. Williams, J. Wong-Leung, M.V. Swain, and P. Munroe; **16**(5), 1500–1507.

– Size effect on the mechanical properties of microfabricated polysilicon thin films.–J.N. Ding, Y.G. Meng, and S.Z. Wen; **16**(8), 2223–2228.

– Quantum atomistic simulations of silicon and germanium.–Carlos P. Herrero; **16**(9), 2505–2512.

– Mechanical stress of the electrical performance of polycrystalline-silicon resistors.–N. Nakabayashi, H. Ohyama, E. Simoen, M. Ikegami, C. Claeys, K. Kobayashi, M. Yoneoka, and K. Miyahara; **16**(9), 2579–2582.

– Defect formation due to the crystallization of deep amorphous volumes formed in silicon by mega electron volt (*MeV*) ion implantation.–A.C.Y. Liu, J.C. McCallum, and J. Wong-Leung; **16**(11), 3229–3237.

– Observations of structural order in ion-implanted amorphous silicon.–Ju-Yin Cheng, J.M. Gibson, and D.C. Jacobson; **16**(11), 3030–3033.

– Deformation under nanoindents in Si, Ge, and GaAs examined through transmission electron microscopy.–S.J. Lloyd, J.M. Molina-Aldareguia, and W.J. Clegg; **16**(12), 3347–3350.

– Nondestructive measurement of striation defect spacing using laser diffraction.–Dylan E. Haas and Dunbar P. Birnie III; **16**(12), 3355–3360.

– Laser-induced surface perturbations in silicon.–A.J. Pedraza, S. Jesse, Y.F. Guan, and J.D. Fowlkes; **16**(12), 3599–3608.

Si:H

– Intrinsic microcrystalline silicon by postgrowth anneals.–Jong-Hwan Yoon; **16**(6), 1531–1534.

Si:O

– Diffusion of oxygen and silicon in silicon: Silicon monoxide model.–Robert H. Doremus; **16**(1), 185–191.

Si/Cd

– Nanocrystals in crystalline silicon: Void formation and hollow particles.–A. Meldrum, S. Honda, C.W. White, R.A. Zuhr, and L.A. Boatner; **16**(9), 2670–2679.

Si/Se

– Nanocrystals in crystalline silicon: Void formation and hollow particles.–A. Meldrum, S. Honda, C.W. White, R.A. Zuhr, and L.A. Boatner; **16**(9), 2670–2679.

Si/SiO_2

– Synthesis of silicon microwire.–J.J. Petrovic, R.C. Hoover, R.D. Field, and K. Han; **16**(10), 2777–2779.

Si/Zn

– Nanocrystals in crystalline silicon: Void formation and hollow particles.–A. Meldrum, S. Honda, C.W. White, R.A. Zuhr, and L.A. Boatner; **16**(9), 2670–2679.

Si/ZnO

– Determination of optical constants of Si/ZnO polycrystalline nanocomposites by spectroscopic ellipsometry.–J. García-Serrano, N. Koshizaki, T. Sasaki, G. Martínez-Montes, and U. Pal; **16**(12), 3554–3559.

Si–Al–O–N

– Microstructure and formation mechanism of combustion-synthesized rodlike Ca α-sialon crystals.–Kexin Chen, Haibo Jin, M. Oliveira, Heping Zhou, and J.M.F. Ferreira; **16**(7), 1928–1934.

Si–B–C–N

– Anelastic behavior of precursor-derived amorphous ceramics in the system Si–B–C–N.–Martin Christ, André Zimmermann, and Fritz Aldinger; **16**(7), 1994–1997.

Si–C:H

– Development of *p*-type microcrystalline silicon carbon alloy films by the very high frequency plasma-enhanced chemical vapor deposition technique.–Tapati Jana, Arup Dasgupta, and Swati Ray; **16**(7), 2130–2135.

Si–N:H

– X-ray reflectivity spectra of ultrathin films and nanometric multilayers: Experiment and simulation.–E. Bontempi, L.E. Depero, L. Sangaletti, F. Giorgis, and C.F. Pirri; **16**(9), 2556–2561.

Si–N/SiO_2

– Cubic silicon nitride embedded in amorphous silicon dioxide.–Ming Zhang, Hongliang He, F.F. Xu, T. Sekine, T. Kobayashi, and Y. Bando; **16**(8), 2179–2181.

Si–Ti

– Mechanochemistry of the titanium–silicon system: Compositional effects.–S. Doppiu, M. Monagheddu, G. Cocco, F. Maglia, U. Anselmi-Tamburini, and Z.A. Munir; **16**(5), 1266–1279.

Si · Ge:B

– Effect of *in situ* boron doping on properties of silicon germanium films deposited by chemical vapor deposition at 400 °C.–Sherif Sedky, Ann Witvrouw, Annelies Saerens, Paul Van Houtte, Jef Poortmans, and Kris Baert; **16**(9), 2607–2612.

SiC

– Modeling of wave configuration during electrically ignited combustion synthesis.–O.A. Graeve, E.M. Carrillo-Heian, A. Feng, and Z.A. Munir; **16**(1), 93–100.

– Carrier diffusion characterization in epitaxial 4H–SiC.–Paulius Grivickas, Jan Linnros, and Vytautas Grivickas; **16**(2), 524–528.

– Influence of annealing treatments on microstructure and toughness of liquid-phase-sintered silicon carbide.–D. Sciti and A. Bellosi; **16**(3), 806–816.

– Porosity and microstructure control of porous ceramics by partial hot pressing.–Jian-Feng Yang, Guo-Jun Zhang, and Tatsuki Ohji; **16**(7), 1916–1918.

– Microstructural and mechanical characterization of carbon coatings on SiC fibers.–K.L. Kendig, R. Gibala, and D.B. Miracle; **16**(12), 3366–3377.

SiC:(Ti;Fe;Co)

– Characterization of bond formation in SiC and Si_3N_4 implanted with Ti, Fe, and Co.–Didier Zanghi, Agnès Traverse, Sébastien Gautrot, and Odile Kaïtasov; **16**(2), 512–523.

SiC/C

– Microstructural and mechanical characterization of carbon coatings on SiC fibers.–K.L. Kendig, R. Gibala, and D.B. Miracle; **16**(12), 3366–3377.

SiC/Si

– Chemical-vapor-deposition growth and characterization of epitaxial 3C–SiC films on SOI substrates with thin silicon top layers.–C.K. Moon, H.J. Song, J.K. Kim, J.H. Park, S.J. Jang, J-B. Yoo, H-R. Park, and Byung-Teak Lee; **16**(1), 24–27.

SiC/Y–Mg–Si–Al–O–N

– Transmission electron microscopy observation in a liquid-phase-sintered SiC with oxynitride glass.–Guo-Dong Zhan, Mamoru Mitomo, Young-Wook Kim, Rong-Jun Xie, and Amiya K. Mukherjee; **16**(8), 2189–2191.

SiC–(Y_2O_3+AlN–Si_3N_4)

– Influence of sintering atmosphere on the fabrication of SiC ceramics with a powder mixture of sialon composition.–Jong-Kook Lee, Jong-Gon Park, Eun-Gu Lee, and Kyung-Seok Kim; **16**(6), 1784–1788.

SiN_x

– Gas flow effects on the structure and composition of SiN_x/Si/SiN_x films prepared by radio-frequency magnetron sputtering.–Wentao Xu, Boquan Li, Toshiyuki Fujimoto, and Isao Kojima; **16**(1), 308–313.

Si_3N_4

– Enhanced crystallization and phase transformation of amorphous silicon nitride under high pressure.–Ya-Li Li, Yong Liang, Fen Zheng, Xian-Feng Ma, Suo-Jing Cui, and Liling Sun; **16**(1), 67–75.

– Optical evaluation of the flexural rigidity and residual stress in thin membranes: Picosecond transient grating measurements of the dispersion of the lowest-order Lamb acoustic waveguide mode.–John A. Rogers and Gregory R. Bogart; **16**(1), 217–225.

– Surface effects in field-assisted sintering.–J.R. Groza, M. Garcia, and J.A. Schneider; **16**(1), 286–292.

– Preferred orientation of beta-phase and its mechanisms in a fine-grained silicon-nitride-based ceramic.–Rong-Jun Xie, Mamoru Mitomo, Wonjoong Kim, Young-Wook Kim, and Guo-Dong Zhan; **16**(2), 590–596.

– Porosity and microstructure control of porous ceramics by partial hot pressing.–Jian-Feng Yang, Guo-Jun Zhang, and Tatsuki Ohji; **16**(7), 1916–1918.

– Effect of α/β phase ratio on microstructure and mechanical properties of silicon nitride ceramics.–Hirokazu Kawaoka, Tomohiko Adachi, Tohru Sekino, Yong-Ho Choa, Lian Gao, and Koichi Niihara; **16**(8), 2264–2270.

– Improved creep resistance in anisotropic silicon nitride.–Naoki Kondo, Yoshikazu Suzuki, Manuel E. Brito, and Tatsuki Ohji; **16**(8), 2182–2185.

– Dependence of fracture stress on applied stress rate in a Yb_2O_3–SiO_2-doped hot-pressed silicon nitride ceramic.–Shuqi Guo, Naoto Hirosaki, Yoshinobu Yamamoto, Toshiyuki Nishimura, and Mamoru Mitomo; **16**(11), 3254–3261.

– Nucleation and growth of silicon nitride nanoneedles using microwave plasma heating.–H. Cui and B.R. Stoner; **16**(11), 3111–3115.

Si_3N_4:(Ti;Fe;Co)

– Characterization of bond formation in SiC and Si_3N_4 implanted with Ti, Fe, and Co.–Didier Zanghi, Agnès Traverse, Sébastien Gautrot, and Odile Kaïtasov; **16**(2), 512–523.

SiN_x/Si/SiN_x

– Gas flow effects on the structure and composition of SiN_x/Si/SiN_x films prepared by radio-frequency magnetron sputtering.–Wentao Xu, Boquan Li, Toshiyuki Fujimoto, and Isao Kojima; **16**(1), 308–313.

Si_3N_4/SiC

– Consolidation and crystallization of Si_3N_4/SiC nanocomposites from a poly(urea–silazane) ceramic precursor.–Julin Wan, Matt J. Gasch, and Amiya K. Mukherjee; **16**(11), 3274–3286.

SiO_2

– Silica particle growth in metastable supersaturation solution.–Kyung-Soo Kim, Jun-Kyung Kim, and Woo-Sik Kim; **16**(2), 545–552.

– Analysis of depth-sensing indentation tests with a Knoop indenter.–L. Riester, T.J. Bell, and A.C. Fischer-Cripps; **16**(6), 1660–1667.

– Molecular dynamics analysis of adhesion strength of interfaces between thin films.–T. Iwasaki and H. Miura; **16**(6), 1789–1794.

– Simulation of sub-micron indentation tests with spherical and Berkovich indenters.–A.C. Fischer-Cripps; **16**(7), 2149–2157.

– Chemical sensors based on dielectric response of functionalized mesoporous silica films.–Karel Domansky, Jun Liu, Li-Qiong Wang, Mark H. Engelhard, and Suresh Baskaran; **16**(10), 2810–2816.

– Alternative technique for analyzing instrumented indentation data.–W.C. Oliver; **16**(11), 3202–3206.

– Dependence of fracture stress on applied stress rate in a Yb_2O_3–SiO_2-doped hot-pressed silicon nitride ceramic.–Shuqi Guo, Naoto Hirosaki, Yoshinobu Yamamoto, Toshiyuki Nishimura, and Mamoru Mitomo; **16**(11), 3254–3261.

– Direct laser writing of self-developed waveguides in benzyldimethylketal-doped sol-gel hybrid glass.–Byeong-Soo Bae, Oun-Ho Park, Robbie Charters, Barry Luther-Davies, and Graham R. Atkins; **16**(11), 3184–3187.

(SiO_2)

– Alternating current conductivity of the interfacial phase in copper oxide–silica gel nanocomposites.–D. Das and D. Chakravorty; **16**(4), 1047–1051.

$SiO_{2(Filamentary)}$

– Synthesis of α–SiO_2 nanowires using Au nanoparticle catalysts on a silicon substrate.–Z.Q. Liu, S.S. Xie, L.F. Sun, D.S. Tang, W.Y. Zhou, C.Y. Wang, W. Liu, Y.B. Li, X.P. Zou, and G. Wang; **16**(3), 683–686.

SiO_2:Ag

– Structure of heat-treated sol-gel SiO_2 glasses containing silver.–M.G. Garníca-Romo, J. González-Hernández, M.A. Hernández-Landaverde, Y.V. Vorobiev, F. Ruiz, and J.R. Martínez; **16**(7), 2007–2012.

SiO_2/Ag

– Formation and characterization of high-density silver nanoparticles embedded in silica thin films by "*in situ*" self-reduction.–G. Compagnini, M.E. Fragalà, L. D'Urso, C. Spinella, and O. Puglisi; **16**(10), 2934–2938.

SiO_2:(Fe,Al)

– Thermally reversible γ-ray-induced redox reaction between substitutional iron and aluminum impurity centers in a silica glass.–Radhaballabh Debnath; **16**(1), 127–131.

SiO_2:(Fe;Co;Ni)

– Coordination structures of implanted Fe, Co, and Ni ions in silica glass by x-ray absorption fine structure spectroscopy.–Kohei Fukumi, Akiyoshi Chayahara, Kohei Kadono, Hiroyuki Kageyama, Tomoko Akai, Hiroshi Mizoguchi, Naoyuki Kitamura, Masaki Makihara, Yuji Horino, and Kanenaga Fujii; **16**(1), 155–162.

SiO_2/Polymethacrylate

– Photoinduced condensation of sol-gel hybrid glass films doped with benzildimethylketal.–Oun-Ho Park, Ji-In Jung, and Byeong-Soo Bae; **16**(7), 2143–2148.

SiO_2–B_2O_3–Na_2O–Al_2O_3

– Devitrification kinetics and mechanism of Pyrex borosilicate glass.–Jau-Ho Jean and Yu-Ching Fang; **16**(6), 1752–1758.

SiO_2–Na_2O–SrOglass/ZrO_2

– Sintering and microstructure of glass-coated nanocrystalline yttria-stabilized tetragonal zirconia powder: Effect of the glass.–R. Ramamoorthy and R. Chaim; **16**(1), 296–302.

SiO_2–TiO_2

– Phase separation in SiO_2–TiO_2 gel and glassy films studied by atomic force microscopy and transmission electron microscopy.–A. Karthikeyan and Rui M. Almeida; **16**(6), 1626–1631.

– ^{29}Si nuclear-magnetic-resonance and vibrational spectroscopy studies of SiO_2–TiO_2 powders prepared by the sol-gel process.–J.P. Rainho, J. Rocha, L.D. Carlos, and R.M. Almeida; **16**(8), 2369–2376.

$SiO_2 \cdot CaO \cdot P_2O_5$

– Textural properties of $SiO_2 \cdot CaO \cdot P_2O_5$ glasses prepared by the sol-gel method.–F. Balas, D. Arcos, J. Pérez-Pariente, and M. Vallet-Regí; **16**(5), 1345–1348.

$SiO_2 \cdot H_2O$

– Biomimetic model of a sponge-spicular optical fiber—mechanical properties and structure.–M. Sarikaya, H. Fong, N. Sunderland, B.D. Flinn, G. Mayer, A. Mescher, and E. Gaino; **16**(5), 1420–1428.

Silica glass/organic polymer

– Thermal stress in a polymer-coated optical glass fiber with a low-modulus coating at the ends.–E. Suhir; **16**(10), 2996–3004.

Silicalite

– Silicalite/poly(dimethylsiloxane) nanocomposite pervaporation membranes for acetic acid/water separation.–Shih-Yuan Lu, Hsiang-Yuan Huang, and Kwen-Hua Wu; **16**(11), 3053–3059.

Silicon nitride

– High-strength porous silicon nitride fabricated by the sinter-forging technique.–Naoki Kondo, Yoshikazu Suzuki, and Tatsuki Ohji; **16**(1), 32–34.

Silicon substrate

– Metalorganic chemical vapor deposition of titanium oxide for microelectronics applications.–Kanchana Vydianathan, Guillermo Nuesca, Gregory Peterson, Eric T. Eisenbraun, Alain E. Kaloyeros, John J. Sullivan, and Bin Han; **16**(6), 1838–1849.

Sm–Co–Zr

– Magnetic properties, domain structure, and microstructure of anisotropic $SmCo_{6.5}Zr_{0.5}$ ribbons with C addition.–A-Ru Yan, Zhi-Gang Sun, Wen-Yong Zhang, Hong-Wei Zhang, and Bao-Gen Shen; **16**(3), 629–632.

Sm–Co–Zr–C

– Magnetic properties, domain structure, and microstructure of anisotropic $SmCo_{6.5}Zr_{0.5}$ ribbons with C addition.–A-Ru Yan, Zhi-Gang Sun, Wen-Yong Zhang, Hong-Wei Zhang, and Bao-Gen Shen; **16**(3), 629–632.

$Sm_x(SiO_x)_6O_2$

– Enthalpies of formation of lanthanide oxyapatite phases.–A.S. Risbud, K.B. Helean, M.C. Wilding, P. Lu, and A. Navrotsky; **16**(10), 2780–2783.

Sn–Ag/Cu

– Stability of channels at a scalloplike Cu_6Sn_5 layer in solder interconnections.–Jong-Hyun Lee, Jong-Hwan Park, Yong-Ho Lee, Yong-Seog Kim, and Dong Hyuk Shin; **16**(5), 1227–1230.

Sn–Ag–Cu/Cu

– Effects of static thermal aging and thermal cycling on the microstructure and shear strength of $Sn_{95.5}Ag_{3.8}Cu_{0.7}$ solder joints.–Shawkret Ahat, Mei Sheng, and Le Luo; **16**(10), 2914–2921.

Sn–Ag–Cu/Ni–P

– Effects of static thermal aging and thermal cycling on the microstructure and shear strength of $Sn_{95.5}Ag_{3.8}Cu_{0.7}$ solder joints.–Shawkret Ahat, Mei Sheng, and Le Luo; **16**(10), 2914–2921.

Sn–Bi

– Interfacial embrittlement by bismuth segregation in copper/tin–bismuth Pb-free solder interconnect.–P.L. Liu and J.K. Shang; **16**(6), 1651–1659.

Sn–Pb–Cu/Au/NiCu

– Effects of Cu and Ni additions to eutectic Pb–Sn solders on Au embrittlement of solder interconnections.–Jong-Hyun Lee, Jong-Hwan Park, Yong-Ho Lee, and Yong-Seog Kim; **16**(5), 1249–1251.

Sn–Pb–Ni/Au/Ni/Cu

– Effects of Cu and Ni additions to eutectic Pb–Sn solders on Au embrittlement of solder interconnections.–Jong-Hyun Lee, Jong-Hwan Park, Yong-Ho Lee, and Yong-Seog Kim; **16**(5), 1249–1251.

Sn–Zn–Al/Cu

– Formation of intermetallic compounds at eutectic Sn–Zn–Al solder/Cu interface.–Shan-Pu Yu, Moo-Chin Wang, and Min-Hsiung Hon; **16**(1), 76–82.

SnO_2

– Metal–oxide films with magnetically-modulated nanoporous architectures.–Craig A. Grimes, R. Suresh Singh, Elizabeth C. Dickey, and Oomman K. Varghese; **16**(6), 1686–1693.

$Sn_2P_2S_6$

– Photovoltaic effect of $Sn_2P_2S_6$ ferroelectric crystal and ceramics.–Y.W. Cho, S.K. Choi, and Yu.M. Vysochanskii; **16**(11), 3317–3322.

Soda glass/Al_2O_3/polycarbonate resin

– Contact fracture of brittle bilayer coatings on soft substrates.–Pedro Miranda, Antonia Pajares, Fernando Guiberteau, Francisco L. Cumbrera, and Brian R. Lawn; **16**(1), 115–126.

Soda-lime glass

– Evaluation of the impactive-surface-fracture behavior of glass plates using a back-surface strain measurement.–Hyoung-Gu Kim, Nak-Sam Choi, and Nahmgyoo Cho; **16**(11), 3042–3045.

(SOG) spin-on-glass precursor

– Nondestructive measurement of striation defect spacing using laser diffraction.–Dylan E. Haas and Dunbar P. Birnie III; **16**(12), 3355–3360.

Sol-gel hybrid glass (SGHG)

– Photoinduced condensation of sol-gel hybrid glass films doped with benzildimethylketal.–Oun-Ho Park, Ji-In Jung, and Byeong-Soo Bae; **16**(7), 2143–2148.

Sr-doped Le manganite

– Anode-supported planar solid oxide fuel cells by plasma-enhanced metalorganic chemical vapor deposition (PE-MOCVD) and electrostatic spray deposition (ESD): Fabrication of dense thin layers of yttria-stabilized zirconia by PE-MOCVD.–Gianfranco Di Giuseppe and J. Robert Selman; **16**(10), 2983–2991.

Sr–Bi–Ta–O

– Phase formation and crystal growth of Sr–Bi–Ta–O thin films grown by metalorganic chemical vapor deposition.–H. Bachhofer, H. von Philipsborn, W. Hartner, C. Dehm, B. Jobst, A. Kiendl, H. Schroeder, and R. Waser; **16**(10), 2966–2973.

Sr–Ti–O/$SrTiO_3$

– Transmission electron microscopy study of $n = 1$–5 $Sr_{n+1}Ti_nO_{3n+1}$ epitaxial thin films.–W. Tian, X.Q. Pan, J.H. Haeni, and D.G. Schlom; **16**(7), 2013–2026.

(Sr,Ba,Ca,Pb)$Bi_2Nb_2O_9$

– Relation between tolerance factor and T_c in Aurivillius compounds.–Donají Y. Suárez, Ian M. Reaney, and William E. Lee; **16**(11), 3139–3149.

(Sr,Ba,Ca,Pb)$Bi_4Ti_4O_{15}$

– Relation between tolerance factor and T_c in Aurivillius compounds.–Donají Y. Suárez, Ian M. Reaney, and William E. Lee; **16**(11), 3139–3149.

(Sr,Ba,Ca,Pb)$_2Bi_4Ti_5O_{18}$

– Relation between tolerance factor and T_c in Aurivillius compounds.–Donají Y. Suárez, Ian M. Reaney, and William E. Lee; **16**(11), 3139–3149.

(Sr,Ba)Nb_2O_4/MgO

– Preparation and characteristics of seeded epitaxial (Sr,Ba)Nb_2O_6 optical waveguide thin films using sol-gel method.–Junmo Koo, Jae Hyeok Jang, and Byeong-Soo Bae; **16**(2), 430–436.

(Sr,Ba)Nb_2O_6

– Structural and electrical properties of strontium barium niobate thin films crystallized by conventional furnace and rapid-thermal annealing process.–R.G. Mendes, E.B. Araújo, and J.A. Eiras; **16**(10), 3009–3013.

– Novel route for the epitaxial growth of (SrBa)Nb_2O_6 thick films by the sol-gel method using a self-template layer.–A-D. Li, C.L. Mak, K.H. Wong, D. Wu, and Naiben Ming; **16**(11), 3179–3183.

$SrAl_2O_4$:(Eu,Dy)

– Sol-gel synthesis and the effect of boron addition on the phosphorescent properties of $SrAl_2O_4$:Eu^{2+},Dy^{3+} phosphors.–I-Cherng Chen and Teng-Ming Chen; **16**(3), 644–651.

– Effect of host compositions on the afterglow properties of phosphorescent strontium aluminate phosphors derived from the sol-gel method.–I-Cherng Chen and Teng-Ming Chen; **16**(5), 1293–1300.

$SrBi_2Nb_2O_9$/$SrTiO_3$

– Transmission electron microscopy study of (103)-oriented epitaxial $SrBi_2Nb_2O_9$ films grown on (111) $SrTiO_3$ and (111) $SrRuO_3$/(111) $SrTiO_3$.–M.A. Zurbuchen, J. Lettieri, Y. Jia, D.G. Schlom, S.K. Streiffer, and M.E. Hawley; **16**(2), 489–502.

$SrBi_2Ta_2O_9$

– Ferroelectric $SrBi_2Ta_2O_9$ single-crystal growth and characterization.–B. Sih, J. Tang, M. Dong, and Z-G. Ye; **16**(6), 1726–1733.

– Low-temperature crystallization induced by excimer laser irradiation of $SrBi_2Ta_2O_9$ films.–Kwang Soo Seol, Hironao Hiramatsu, Yoshimichi Ohki, In-Hoon Choi, and Yong-Tea Kim; **16**(7), 1883–1886.

– Nonisothermal phase formation kinetics in sol-gel-derived strontium bismuth tantalate.–Yun-Mo Sung; **16**(7), 2039–2044.

– Impacts of postannealing ambient atmospheres on Pt/$SrBi_{2.2}Ta_2O_9$/Pt capacitors.–Ai-Dong Li, Tao Yu, Hui-Qin Ling, Di Wu, Zhi-Guo Liu, and Nai-Ben Ming; **16**(12), 3526–3535.

$SrBi_2Ta_2O_9/SrRuO_3$

– Transmission electron microscopy study of (103)-oriented epitaxial $SrBi_2Nb_2O_9$ films grown on (111) $SrTiO_3$ and (111) $SrRuO_3$/(111) $SrTiO_3$.–M.A. Zurbuchen, J. Lettieri, Y. Jia, D.G. Schlom, S.K. Streiffer, and M.E. Hawley; **16**(2), 489–502.

$SrFe_{12}O_{19}$

– Halide removal from BaM ($BaFe_{12}O_{19}$) and SrM ($SrFe_{12}O_{19}$) ferrite fibers via a steaming process.–R.C. Pullar, M.D. Taylor, and A.K. Bhattacharya; **16**(11), 3162–3169.

$SrO–BaO–Nb_2O_5–GeO_2$

– Crystallization and dielectric properties of $SrO–BaO–Nb_2O_5–GeO_2$ tungsten–bronze glass–ceramics.–Jiin-Jyh Shyu and Hsin-Wei Peng; **16**(7), 2057–2063.

$SrRuO_3/Si$

– Growth behavior and defects in conductive $SrRuO_3$ thin films grown on a Si(100) substrate by sputtering.–Sang Ho Oh and Chan-Gyung Park; **16**(7), 1998–2006.

$SrTiO_3$:Nb

– Analysis of defect formation in Nb-doped $SrTiO_3$ by impedance spectroscopy.–Seong-Ho Kim, Jung-Ho Moon, Jae-Hwan Park, Jae-Gwan Park, and Yoonho Kim; **16**(1), 192–196.

$SrTiO_3/SrRaO_3$

– Microstructure and misfit relaxation in $SrTiO_3/SrRuO_3$ bilayer films on $LaAlO_3$(100) substrates.–J.S. Wu, C.L. Jia, K. Urban, J.H. Hao, and X.X. Xi; **16**(12), 3443–3450.

Steel

– The healing of quenched crack in 1045 steel under electropulsing.–Zhou Yizhou, Zeng You, He Guanhu, and Zhou Benlian; **16**(1), 17–19.

– Analysis of depth-sensing indentation tests with a Knoop indenter.–L. Riester, T.J. Bell, and A.C. Fischer-Cripps; **16**(6), 1660–1667.

– Simulation of sub-micron indentation tests with spherical and Berkovich indenters.–A.C. Fischer-Cripps; **16**(7), 2149–2157.

– Derivation of plastic stress–strain relationship from ball indentations: Examination of strain definition and pileup effect.–Jeong-Hoon Ahn and Dongil Kwon; **16**(11), 3170–3178.

Ta

– Chemical–mechanical polishing of copper and tantalum with silica abrasives.–Y. Li, M. Hariharaputhiran, and S.V. Babu; **16**(4), 1066–1073.

– Synthesis of nanoscale particles of Ta and Nb_3Al by homogeneous reduction in liquid ammonia.–Hongmin Zhu and Donald R. Sadoway; **16**(9), 2544–2549.

Ta–Si

– Field-activated combustion synthesis of Ta–Si intermetallic compounds.–F. Maglia, U. Anselmi-Tamburini, N. Bertolino, C. Milanese, and Z.A. Munir; **16**(2), 534–544.

– Combustion synthesis of mechanically activated powders in the Ti–Si system.–F. Maglia, U. Anselmi-Tamburini, G. Cocco, M. Monagheddu, N. Bertolino, and Z.A. Munir; **16**(4), 1074–1082.

$TeO_2–LiCl$:Tm

– Effect of composition on the thermal properties and spontaneous emission probabilities of Tm^{3+}-doped $TeO_2–LiCl$ glass.–G. Özen, B. Demirata, and M.L. Öveçoğlu; **16**(5), 1381–1388.

Ti

– Solid-state foaming of titanium by superplastic expansion of argon-filled pores.–N.G. Davis, J. Teisen, C. Schuh, and D.C. Dunand; **16**(5), 1508–1519.

– Moving the pulsed heating technique beyond monolithic specimens: Experiments with coated wires.–D. Josell, D. Basak, J.L. McClure, U.R. Kattner, M.E. Williams, W.J. Boettinger, and M. Rappaz; **16**(8), 2421–2428.

Ti/(Al:Cu)

– Texture in Ti/Al and Nb/Al multilayer thin films: Role of Cu.–G. Lucadamo, K. Barmak, and K.P. Rodbell; **16**(5), 1449–1459.

Ti/TiC

– Metal/ceramic interface in an *in situ* synthesized Ti/TiC_p composite coating by laser processing.–R. Yu, S. Zhang, L.L. He, W.T. Wu, and H.Q. Ye; **16**(1), 9–12.

Ti–Al

– Moving the pulsed heating technique beyond monolithic specimens: Experiments with coated wires.–D. Josell, D. Basak, J.L. McClure, U.R. Kattner, M.E. Williams, W.J. Boettinger, and M. Rappaz; **16**(8), 2421–2428.

Ti–Al–Si

– Submicron-grained multiphase TiAlSi alloys: Processing, characterization, and microstructural design.–R. Bohn, G. Fanta, T. Klassen, and R. Bormann; **16**(6), 1850–1861.

Ti–Al–V

– Tensile fracture during transformation superplasticity of Ti–6Al–4V.–C. Schuh and D.C. Dunand; **16**(3), 865–875.

– Development of a model for the prediction of the fretting fatigue regimes.–T.E. Matikas and P.D. Nicolaou; **16**(9), 2716–2723.

Ti–Al–V:C

– Hardness–depth profile of a carbon-implanted Ti–6Al–4V alloy and its relation to composition and microstructure.–M. Kunert, O. Kienzle, B. Baretzky, S.P. Baker, and E.J. Mittemeijer; **16**(8), 2321–2335.

TiAlN

– ^{18}O study of the oxidation of reactively sputtered $Ti_{1-x}Al_xN$ barrier.–M.C. Hugon, F. Varniere, F. Letendu, B. Agius, I. Vickridge, and A.I. Kingon; **16**(9), 2591–2599.

TiB_2

– Ultrathin TiB_2 protective films.–Feng Huang, John A. Barnard, and Mark L. Weaver; **16**(4), 945–954.

TiB_2/Co

– Ultrathin TiB_2 protective films.–Feng Huang, John A. Barnard, and Mark L. Weaver; **16**(4), 945–954.

TiB_2/Si

– Ultrathin TiB_2 protective films.–Feng Huang, John A. Barnard, and Mark L. Weaver; **16**(4), 945–954.

$TiB_2/Ti_2O_3–B_2O_3/SiO_2$

– Improvement in oxidation resistance of TiB_2 by formation of protective SiO_2 layer on surface.–Young-Hag Koh, Hae-Won Kim, and Hyoun-Ee Kim; **16**(1), 132–137.

TiC

– Deposition of epitaxial transition metal carbide films and superlattices by simultaneous direct current metal magnetron sputtering and C_{60} evaporation.–H. Högberg, J. Birch, M.P. Johansson, L. Hultman, and U. Jansson; **16**(3), 633–643.

TiC/VC

– Growth, structure, and mechanical properties of transition metal carbide superlattices.–H. Högberg, J. Birch, M. Odén, J-O. Malm, L. Hultman, and U. Jansson; **16**(5), 1301–1310.

TiN

– Residual stress in fiber-textured thin films of cubic materials.–P. Scardi and Y.H. Dong; **16**(1), 233–242.

– Elastic constants of polycrystalline Al and TiN calculated by an *ab initio* method within the local-density approximation.–Ming Zhang, Jiang Shen, and Jiawen He; **16**(8), 2293–2297.

TiN:N

– Mechanism of improvement of TiN-coated tool life by nitrogen implantation.–S.J. Bull, Yu.P. Sharkeev, S.V. Fortuna, I.A. Shulepov, and A.J. Perry; **16**(11), 3293–3303.

TiN/Si(100)

– Mechanical properties of nanocrystalline and epitaxial TiN films on (100) silicon.–H. Wang, A. Sharma, A. Kvit, Q. Wei, X. Zhang, C.C. Koch, and J. Narayan; **16**(9), 2733–2738.

TiO

– Titanium oxide nanotube arrays prepared by anodic oxidation.–Dawei Gong, Craig A. Grimes, Oomman K. Varghese, R.S. Singh, Wenchong Hu, Zhi Chen, and Elizabeth C. Dickey; **16**(12), 3331–3334.

TiO_2

– Macroporous morphology of titania films prepared by sol-gel dip-coating method from a system containing poly(ethylene glycol) and poly(vinylpyrrolidone).–Koichi Kajihara and Kazuki Nakanishi; **16**(1), 58–66.

– Sol-gel-derived photosensitive TiO_2 and Cu/TiO_2 using homogeneous hydrolysis technique.–Jeffrey C.S. Wu and Chih-Yang Yeh; **16**(2), 615–620.

– Photocatalytic activity of TiO_2 prepared at low temperature by a photo-assisted sol-gel method.–Zi-sheng Guan, Xin-tong Zhang, Ying Ma, Ya-an Cao, and Jian-nian Yao; **16**(4), 907–909.

– Metal–oxide films with magnetically-modulated nanoporous architectures.–Craig A. Grimes, R. Suresh Singh, Elizabeth C. Dickey, and Oomman K. Varghese; **16**(6), 1686–1693.

– Influence of ligand groups in Ti precursors on phase transformation and microstructural evolution of TiO_2 thin films prepared by the wet chemical process.–Chu-Chi Ting and San-Yuan Chen; **16**(6), 1712–1719.

– Parameter effect on the crystallization of Nd:yttrium aluminum garnet laser-ablated TiO_2 thin film.–Mrinal Pal, Aiko Narazaki, Takeshi Sasaki, and Naoto Koshizaki; **16**(11), 3158–3161.

– Titanium oxide nanotube arrays prepared by anodic oxidation.–Dawei Gong, Craig A. Grimes, Oomman K. Varghese, R.S. Singh, Wenchong Hu, Zhi Chen, and Elizabeth C. Dickey; **16**(12), 3331–3334.

– Hydrodynamic cavitation as a tool to control macro-, micro-, and nano-properties of inorganic materials.–J. Find, S.C. Emerson, I.M. Krausz, and W.R. Moser; **16**(12), 3503–3513.

TiO_x

– Comparison of hydrophilic properties of amorphous TiO_x films obtained by radio frequency sputtering and plasma-enhanced chemical vapor deposition.–Masatoshi Nakamura, Toru Aoki, Yoshinori Hatanaka, Dariusz Korzec, and Jurgen Engemann; **16**(2), 621–626.

– Metalorganic chemical vapor deposition of titanium oxide for microelectronics applications.–Kanchana Vydianathan, Guillermo Nuesca, Gregory Peterson, Eric T. Eisenbraun, Alain E. Kaloyeros, John J. Sullivan, and Bin Han; **16**(6), 1838–1849.

TiO_2:(Zn;Fe)

– Effects of zinc(II) and iron(III) doping of titania films on their photoreactivity to decompose rhodamine B.–Ying Ma, Xin-tong Zhang, Zi-sheng Guan, Ya-an Cao, and Jian-nian Yao; **16**(10), 2928–2933.

TiO_2/Ag

– Electrolyte electroreflectance study of TiO_2 films modified with metal nanoparticles.–A.I. Kulak, A.I. Kokorin, and D.V. Sviridov; **16**(8), 2357–2361.

TiO_2/Cu

– Electrolyte electroreflectance study of TiO_2 films modified with metal nanoparticles.–A.I. Kulak, A.I. Kokorin, and D.V. Sviridov; **16**(8), 2357–2361.

TiO_2/Fe_2O_3

– Production and characterization of titanium and iron oxide nanosized thin films.–E. Comini, G. Sberveglieri, M. Ferroni, V. Guidi, C. Frigeri, and D. Boscarino; **16**(6), 1559–1564.

TiO_2/Pd

– Electrolyte electroreflectance study of TiO_2 films modified with metal nanoparticles.–A.I. Kulak, A.I. Kokorin, and D.V. Sviridov; **16**(8), 2357–2361.

TiO_2/SiO_2 (nanotube)

– Synthesis of coaxial nanotubes: Titanium oxide sheathed with silicon oxide.–Ming Zhang, Y. Bando, and K. Wada; **16**(5), 1408–1412.

TiO_2/Ti

– Thin-film fracture during nanoindentation of a titanium oxide film–titanium system.–M. Pang and D.F. Bahr; **16**(9), 2634–2643.

TiO_2–Al–C–ZrO_2

– Thermodynamic analysis of combustion synthesis of Al_2O_3–TiC–ZrO_2 nanoceramics.–Q. Dong, Q. Tang, W.C. Li, and D.Y. Wu; **16**(9), 2494–2498.

TiO_2 (filamentary)

– Fabrication, characterization, and photoluminescence properties of highly ordered TiO_2 nanowire arrays.–Y. Lei and L.D. Zhang; **16**(4), 1138–1144.

TiO_2(poly/styrene–maleic anhydride)

– Precipitation of multilayered core–shell TiO_2 composite nanoparticles onto polymer layers.–Mingtai Wang and Lide Zhang; **16**(3), 765–773.

TmP/GaAs

– Investigation of crystal properties of TmP/GaAs and GaAs/TmP/GaAs heterostructures grown by molecular beam epitaxy.–C.H. Lin, R.J. Hwu, and L.P. Sadwick; **16**(11), 3266–3273.

Trichloroethylene

– Cure depth in photopolymerization: Experiments and theory.–Jim H. Lee, Robert K. Prud'homme, and Ilhan A. Aksay; **16**(12), 3536–3544.

VC

– Deposition of epitaxial transition metal carbide films and superlattices by simultaneous direct current metal magnetron sputtering and C_{60} evaporation.–H. Högberg, J. Birch, M.P. Johansson, L. Hultman, and U. Jansson; **16**(3), 633–643.

W

– Optical evaluation of the flexural rigidity and residual stress in thin membranes: Picosecond transient grating measurements of the dispersion of the lowest-order Lamb acoustic waveguide mode.–John A. Rogers and Gregory R. Bogart; **16**(1), 217–225.

– Alternative technique for analyzing instrumented indentation data.–W.C. Oliver; **16**(11), 3202–3206.

W/C

– Solid-phase synthesis of cupric tungstate.–Leonid P. Dorfman, David L. Houck, Michael J. Scheithauer, Jeffrey N. Dann, and Harry O. Fassett; **16**(4), 1096–1102.

W,TiN

– Molecular dynamics analysis of adhesion strength of interfaces between thin films.–T. Iwasaki and H. Miura; **16**(6), 1789–1794.

WC/C

– Characterization of mechanical properties of tungsten carbide/carbon multilayers: Cross-sectional electron microscopy and nanoindentation observations.–N.J.M. Carvalho and J.Th.M. De Hosson; **16**(8), 2213–2222.

WC–Co

– Thermal stability of nanocrystalline WC–Co powder synthesized by using mechanical milling at low temperature.–Jianhong He, Leoanardo Ajdelsztajn, and Enrique J. Lavernia; **16**(2), 478–488.

(WO)

– Relationship between the microstructure and nanoindentation hardness of thermally evaporated and magnetron-sputtered electrochromic tungsten oxide films.–C.W. Ong, H.Y. Wong, G.K.H. Pang, K.Z. Baba-Kishi, and C.L. Choy; **16**(6), 1541–1548.

Y–Ba–Cu–O

– Directional solidification and microstructural studies of the peritectic Y_2BaCuO_5 phase.–E. Sudhakar Reddy, J.G. Noudem, M. Tarka, and G.J. Schmitz; **16**(4), 1123–1134.

$Y_3Al_5O_{12}$

– Crystallization kinetics of yttrium aluminum garnet ($Y_3Al_5O_{12}$).–Bradley R. Johnson and Waltraud M. Kriven; **16**(6), 1795–1805.

– Translucent yttrium aluminum garnet: Microwave-assisted route to synthesis and processing.–M. Panneerselvam, G.N. Subanna, and K.J. Rao; **16**(10), 2773–2776.

YB_{56}

– Atomic structure of YB_{56} studied by digital high-resolution electron microscopy and electron diffraction.–Takeo Oku, Jan-Olov Bovin, Iwami Higashi, Takaho Tanaka, and Yoshio Ishizawa; **16**(1), 101–107.

$YBa_2Cu_3O_y$

– Preferential growth mechanism of $REBa_2Cu_3O_y$ (RE = Y, Nd) crystal on MgO substrate by liquid phase epitaxy.–Katsumi Nomura, Saburo Hoshi, Xin Yao, Kazuomi Kakimoto, Yuichi Nakamura, Teruo Izumi, and Yuh Shiohara; **16**(4), 979–989.

– Initial growth mechanism of $YBa_2Cu_3O_y$ crystal on MgO substrate by liquid-phase epitaxy.–Katsumi Nomura, Saburo Hoshi, Yuichi Nakamura, Teruo Izumi, and Yuh Shiohara; **16**(10), 2947–2958.

$YBa_2Cu_3O_{7-x}$

– High J_c $YBa_2Cu_3O_{7-\delta}$ films via rapid, low pO_2 pyrolysis.–J.T. Dawley, P.G. Clem, M.P. Siegal, and D.L. Overmyer; **16**(1), 13–16.

– Single-domain $YBa_2Cu_3O_y$ thick films and fabrics prepared by an infiltration and growth process.–E. Sudhakar Reddy, J.G. Noudem, M. Tarka, and G.J. Schmitz; **16**(4), 955–966.

– Influence of antiphase boundaries on critical current densities in $YBa_2Cu_3O_{7-y}$ single crystals.–Junko Shibata, Akihiro Oka, Teruo Izumi, Yuh Shiohara, Tsukasa Hirayama, and Yuichi Ikuhara; **16**(7), 1935–1941.

– Role of the primary phase particles during the peritectic solidification of Y-123 superconducting oxides.–M. Kambara, M. Yoshizumi, T. Umeda, K. Miyake, K. Murata, T. Izumi, and Y. Shiohara; **16**(8), 2229–2238.

– Microstructure and growth of joins in melt-textured $YBa_2Cu_3O_{7-\delta}$.–A.D. Bradley, W. Lo, M. Mironova, N.H. Babu, D.A. Cardwell, A.M. Campbell, and K. Salama; **16**(8), 2298–2305.

– Properties of $YBa_2Cu_3O_{7-\delta}$ multilayer films from the fluoride-based sol-gel process.–M.P. Siegal, J.T. Dawley, and D.L. Overmyer; **16**(12), 3339–3342.

$YBa_2Cu_3O_{7-x}/CeO_2$

– Nucleation and growth of $YBa_2Cu_3O_x$ on $SrTiO_3$ and CeO_2 by a BaF_2 postdeposition reaction process.–L. Wu, Y. Zhu, V.F. Solovyov, H.J. Wiesmann, A.R. Moodenbaugh, R.L. Sabatini, and M. Suenaga; **16**(10), 2869–2884.

$YBa_2Cu_3O_{7-x}/Eu_2CuO_4/SrTiO_3$

– Excellent buffer layer for growing high-quality Y–Ba–Cu–O thin films.–W.H. Tang, J. Gao, C.X. Liu, and Z.H. Mai; **16**(10), 2864–2868.

$YBa_2Cu_3O_{7-x}/MgO$

– High critical current density $YBa_2Cu_3O_{7-\delta}$ thick films using ion beam assisted deposition MgO bi-axially oriented template layers on nickel-based superalloy substrates.–J.R. Groves, P.N. Arendt, S.R. Foltyn, Q.X. Jia, T.G. Holesinger, H. Kung, E.J. Peterson, R.F. DePaula, P.C. Dowden, L. Stan, and L.A. Emmert; **16**(8), 2175–2178.

$YBa_2Cu_3O_{7-x}/SrRuO_3/LaNiO_3$

– Growth and characterization of conductive $SrRuO_3$ and $LaNiO_3$ multilayers on textured Ni tapes for high-J_c $YBa_2Cu_3O_{7-\delta}$ coated conductors.–T. Aytug, B.W. Kang, C. Cantoni, E.D. Specht, M. Paranthaman, A. Goyal, D.K. Christen, D.T. Verebelyi, J.Z. Wu, R.E. Ericson, C.L. Thomas, C-Y. Yang, and S.E. Babcock; **16**(9), 2661–2669.

$YBa_2Cu_3O_{7-x}/SrTiO_3$

– Nucleation and growth of $YBa_2Cu_3O_x$ on $SrTiO_3$ and CeO_2 by a BaF_2 postdeposition reaction process.–L. Wu, Y. Zhu, V.F. Solovyov, H.J. Wiesmann, A.R. Moodenbaugh, R.L. Sabatini, and M. Suenaga; **16**(10), 2869–2884.

Y_2O_3:Ca

– Effect of the calcium dopant on oxide ion diffusion in yttria ceramics.–Noriko Saito, Hajime Haneda, Isao Sakaguchi, and Takayasu Ikegami; **16**(8), 2362–2368.

Y_2O_3:La

– Fractal aggregates of lanthanide-doped Y_2O_3 nanoparticles obtained by propellant synthesis.–Stefano Polizzi, Giuliano Fagherazzi, Marino Battagliarin, Marco Bettinelli, and Adolfo Speghini; **16**(1), 146–154.

Y_2O_3–Fe_3O_4

– Reaction kinetics and anisothermal effects in microwave fields: System Y_2O_3–Fe_3O_4.–Ramesh D. Peelamedu, Rustum Roy, and Dinesh K. Agrawal; **16**(10), 2770–2772.

YPO_4

– Thermochemistry of rare-earth orthophosphates.–S.V. Ushakov, K.B. Helean, A. Navrotsky, and L.A. Boatner; **16**(9), 2623–2633.

Y_2SiO_5

– Thermal expansion and high-temperature phase transformation of the yttrium silicate Y_2SiO_5.–J.W. Nowok, J.P. Kay, and R.J. Kulas; **16**(8), 2251–2255.

Y_2SiO_5:Tb

– Luminescence and decay behaviors of Tb-doped yttrium silicate.–Yoon Young Choi, Kee-Sun Sohn, Hee Dong Park, and Se Young Choi; **16**(3), 881–889.

Yb_2O_3

– Dependence of fracture stress on applied stress rate in a Yb_2O_3–SiO_2-doped hot-pressed silicon nitride ceramic.–Shuqi Guo, Naoto Hirosaki, Yoshinobu Yamamoto, Toshiyuki Nishimura, and Mamoru Mitomo; **16**(11), 3254–3261.

Yttria-stabilized zirconia

– Anode-supported planar solid oxide fuel cells by plasma-enhanced metalorganic chemical vapor deposition (PE-MOCVD) and electrostatic spray deposition (ESD): Fabrication of dense thin layers of yttria-stabilized zirconia by PE-MOCVD.–Gianfranco Di Giuseppe and J. Robert Selman; **16**(10), 2983–2991.

Zirconia

– Investigation of some phenomena occurring during continuous ink-jet printing of ceramics.–B.Y. Tay and M.J. Edirisinghe; **16**(2), 373–384.

Zn

– Origins of stored enthalpy in cryomilled nanocrystalline Zn.–Xinghang Zhang, Haiyan Wang, Magdy Kassem, Jagdish Narayan, and Carl C. Koch; **16**(12), 3485–3495.

Zn phthalocyanine/O_2,H_2O

– Quantification and effects of molecular oxygen and water in zinc phthalocyanine layers.–H.R. Kerp, K.T. Westerduin, A.T. van Veen, and E.E. van Faassen; **16**(2), 503–511.

(Zn,Mg)O

– Synthesis of $Zn_{1-x}Mg_xO$ and its structural characterization.–M.S. Tomar, R. Melgarejo, P.S. Dobal, and R.S. Katiyar; **16**(4), 903–906.

$(Zn,Mn)_2SiO_4$

– Synthesis of $Zn_{2-x}Mn_xSiO_4$ phosphors using a hydrothermal technique.–Chulsoo Yoon and Shinhoo Kang; **16**(4), 1210–1216.

$ZnGa_2O_4$:(Eu,Cr)

– Eu^{+3} and Cr^{+3} doping for red cathodoluminescence in $ZnGa_2O_4$.–Philip D. Rack, Jeffrey J. Peterson, Michael D. Potter, and Wounjhang Park; **16**(5), 1429–1433.

$Zn_3Nb_2O_8$

– Microwave dielectric properties of $(1 - x)Cu_3Nb_2O_8$–$xZn_3Nb_2O_8$ ceramics.–Dong-Wan Kim, In-Tae Kim, Byungwoo Park, Kug Sun Hong, and Jong-Hee Kim; **16**(5), 1465–1470.

ZnO

– Microwave sintering of ZnO at ultra high heating rates.–Geng-fu Xu, Isabel K. Lloyd, Yuval Carmel, Tayo Olorunyolemi, and Otto C. Wilson, Jr.; **16**(10), 2850–2858.

ZnO:Al

– Densification and grain growth of Al-doped ZnO.–Jiaping Han, P.Q. Mantas, and A.M.R. Senos; **16**(2), 459–468.

– Dependence of structural, electrical, and optical properties of ZnO:Al films on substrate temperature.–M. Chen, Z.L. Pei, X. Wang, C. Sun, and L.S. Wen; **16**(7), 2118–2123.

ZnO:Si

– Lubricity of zinc oxide thin films: Study of deposition parameters and Si as an additive.–J.J. Nainaparampil and J.S. Zabinski; **16**(12), 3423–3429.

ZnO/Al_2O_3

– Metal-organic vapor phase epitaxial growth of high-quality ZnO films on $Al_2O_3(00{\cdot}1)$.–W.I. Park, S-J. An, Gyu-Chul Yi, and Hyun M. Jang; **16**(5), 1358–1362.

$ZnO–Sb_2O_3–Bi_2O_3$:(Pr,Nb)

– Electrical and microstructural characteristics of $ZnO–Bi_2O_3$-based varistors doped with rare-earth oxides.–Nguyen The Hung, Nguyen Dinh Quang, and Slavko Bernik; **16**(10), 2817–2823.

$ZnS–SiO_2$

– Measurement of the thermal conductivity of thin layers using a scanning thermal microscope.–Erwin R. Meinders; **16**(9), 2530–2543.

ZnSe

– Deep center luminescence versus surface preparation of ZnSe single crystals.–J.A. Garcia, V. Muñoz, C. Martinez-Tomas, and J.J.S. Garitaonandia; **16**(5), 1245–1248.

Zr

– Combustion of zirconium foils in oxygen.–K.H. Ewald, U. Anselmi-Tamburini, and Z.A. Munir; **16**(9), 2687–2694.

Zr–Al–Ni–Cu

– Redistribution behavior of constitutional elements at an initial crystallization stage in the $Zr_{65}Al_{7.5}Ni_{10}Cu_{17.5}$ glassy alloy.–J. Saida, M. Matsushita, and A. Inoue; **16**(1), 28–31.

– Investigation of the stability of glassy state in the Zr- and Hf-based glassy alloys correlated with their transformation behavior.–Junji Saida, Chunfei Li, Mitsuhide Matsushita, and Akihisa Inoue; **16**(12), 3389–3401.

Zr–Cu–Al–Ni–Ag

– Precipitation of icosahedral phase from amorphous $Zr_{65}Cu_{17.5-x}Al_{7.5}Ni_{10}Ag_x$ (x = 0, 5) alloys.–J.K. Lee, G. Choi, W.T. Kim, and D.H. Kim; **16**(5), 1311–1317.

Zr–Cu–Pd

– Formation of icosahedral quasicrystal by crystallization of $Zr_{70}(Ni, Cu, Pd)_{30}$ amorphous alloys.–T. Zhang, A. Inoue, M. Matsushita, and J. Saida; **16**(1), 20–23.

Zr–Nb–Cu–Fe–Be

– Formation and properties of $Zr_{48}Nb_8Fe_8Cu_{12}Be_{24}$ bulk metallic glass.–Yong Zhang, D.Q. Zhao, B.C. Wei, P. Wen, M.X. Pan, and W.H. Wang; **16**(6), 1675–1679.

Zr–Ni–Pd

– Formation of icosahedral quasicrystal by crystallization of $Zr_{70}(Ni, Cu, Pd)_{30}$ amorphous alloys.–T. Zhang, A. Inoue, M. Matsushita, and J. Saida; **16**(1), 20–23.

Zr–Pd

– Formation of icosahedral quasicrystal by crystallization of $Zr_{70}(Ni, Cu, Pd)_{30}$ amorphous alloys.–T. Zhang, A. Inoue, M. Matsushita, and J. Saida; **16**(1), 20–23.

Zr–Ti–Be–Cu–Ni–Nb

– *In situ* transmission electron microscopy studies of shear bands in a bulk metallic glass based composite.–E. Pekarskaya, C.P. Kim, and W.L. Johnson; **16**(9), 2513–2518.

$ZrF_4–BaF_2–LaF_3–AlF_3–NaF$

– Explanation of the effects of gravity on crystallization of $ZrF_2–BaF_2–LaF_3–AlF_3–NaF$ glass.–Dennis S. Tucker and Edwin C. Ethridge; **16**(11), 3027–3029.

Zr_2Ni

– Redistribution behavior of constitutional elements at an initial crystallization stage in the $Zr_{65}Al_{7.5}Ni_{10}Cu_{17.5}$ glassy alloy.–J. Saida, M. Matsushita, and A. Inoue; **16**(1), 28–31.

ZrO_2

– Dense, bubble-free ceramic deposits from aqueous suspensions by electrophoretic deposition.–Tetsuo Uchikoshi, Kiyoshi Ozawa, Benjamin D. Hatton, and Yoshio Sakka; **16**(2), 321–324.

– Investigation of some phenomena occurring during continuous ink-jet printing of ceramics.–B.Y. Tay and M.J. Edirisinghe; **16**(2), 373–384.

– Thermodynamic stability of tetragonal zirconia nanocrystallites.–Nae-Lih Wu, Ton-Fon Wu, and Irene A. Rusakova; **16**(3), 666–669.

– Kinetic analysis of solid-state processes.–Jiří Málek, Takefumi Mitsuhashi, and José Manuel Criado; **16**(6), 1862–1871.

– Thermal and structural characterization of the $ZrO_{2-x}(OH)_{2x}$ to ZrO_2 transition.–E. Torres-García, A. Peláiz-Barranco, C. Vázquez-Ramos, and G.A. Fuentes; **16**(8), 2209–2212.

– Flash synthesis of zirconia nanoparticles by microwave forced hydrolysis.–K. Bellon, D. Chaumont, and D. Stuerga; **16**(9), 2619–2622.

ZrO_2 (tetragonal):Y_2O_3

– Deformation-induced surface corrugation of superplastic ceramics.–Hiroyuki Muto, Takatoshi Futami, and Motosugu Sakai; **16**(7), 1879–1882.

$ZrO_2–Y_2O_3$

– $L1_2$- and $L1_0$-like cation-ordered structures in $ZrO_2–Y_2O_3$ ceramics.–J.C. Rao, Y. Zhou, and D.X. Li; **16**(6), 1806–1813.

– Synthesis and characterization of partially and fully stabilized zirconia fibers made from an inorganic precursor.–A. Hartridge, M.D. Taylor, and A.K. Bhattacharya; **16**(8), 2384–2390.

– Space-charge concepts on grain boundary impedance of a high-purity yttria-stabilized tetragonal zirconia polycrystal.–Jong-Sook Lee and Doh-Yeon Kim; **16**(9), 2739–2751.

$(ZrO_2–Y_2O_3):SiO_2$

– Precursor scavenging of the resistive grain-boundary phase in 8 mol% yttria-stabilized zirconia: Effect of trace concentrations of SiO_2.–Jong-Heun Lee, Toshiyuki Mori, Ji-Guang Li, Takayasu Ikegami, John Drennan, and Doh-Yeon Kim; **16**(8), 2377–2383.

$ZrO_2–Y_2O_3$/stainless steel

– Controlled preparation and characterization of multilayer sol-gel zirconia dip-coatings.–Ricardo Caruso, Antonio Díaz-Parralejo, Pedro Miranda, and Fernando Guiberteau; **16**(8), 2391–2398.

$(ZrO_2–Y_2O_3)–TiB_2$

– Transformation behavior of yttria stabilized tetragonal zirconia polycrystal–TiB_2 composites.–B. Basu, J. Vleugels, and O. Van Der Biest; **16**(7), 2158–2169.

$Zr_{70}Pd_{30}$

– Change in local atomic structure during formation of the icosahedral quasicrystalline phase in $Zr_{70}Pd_{30}$ glassy alloy.–Muneyuki Imafuku, Junji Saida, and Akihisa Inoue; **16**(11), 3046–3049.

AUTHOR INDEX TO VOLUME 16

All authors of papers published in Volume 16 are listed alphabetically with the issue and page number following the dash. References with (L) are Communications. References with (E) are Errata. References with (A) are Addenda. References with (R) are Commentaries and Reviews. References with (C) are Comments and Reply. Page numbers are cited in ascending order.

A

Abdul-Baqi, A.–Delamination of a strong film from a ductile substrate during indentation unloading.–A. Abdul-Baqi and E. Van der Giessen; **16**(5), 1396–1407.

Abell, J.S.–Microstructure of laser-ablated superconducting $La_2CuO_4F_x$ thin films on $SrTiO_3$.–G. Kong, M.O. Jones, J.S. Abell, P.P. Edwards, S.T. Lees, K.E. Gibbons, I. Gameson, and M. Aindow; **16**(11), 3309–3316.

Adachi, Tomohiko–Effect of α/β phase ratio on microstructure and mechanical properties of silicon nitride ceramics.–Hirokazu Kawaoka, Tomohiko Adachi, Tohru Sekino, Yong-Ho Choa, Lian Gao, and Koichi Niihara; **16**(8), 2264–2270.

Agius, B.–^{18}O study of the oxidation of reactively sputtered $Ti_{1-x}Al_xN$ barrier.–M.C. Hugon, F. Varniere, F. Letendu, B. Agius, I. Vickridge, and A.I. Kingon; **16**(9), 2591–2599.

–Oxygen transport during annealing of $Pb(Zr,Ti)O_3$ thin films in O_2 gas and its effect on their conductivity.–F. Ayguavives, B. Agius, B. Ea-Kim, and I. Vickridge; **16**(10), 3005–3008.

Agrawal, Dinesh K.–Reaction kinetics and anisothermal effects in microwave fields: The System Y_2O_3–Fe_3O_4.–Ramesh D. Peelamedu, Rustum Roy, and Dinesh K. Agrawal; **16**(10), 2770–2772(L).

Ahat, Shawkret–Effects of static thermal aging and thermal cycling on the microstructure and shear strength of $Sn_{95.5}Ag_{3.8}Cu_{0.7}$ solder joints.–Shawkret Ahat, Mei Sheng, and Le Luo; **16**(10), 2914–2921.

Ahn, Jeong-Hoon–Derivation of plastic stress–strain relationship from ball indentations: Examination of strain definition and pileup effect.–Jeong-Hoon Ahn and Dongil Kwon; **16**(11), 3170–3178.

Aikin, Beverly–Creep and toughness of cryomilled NiAl containing Cr.–J. Daniel Whittenberger, Beverly Aikin, and Jon Salem; **16**(5), 1333–1344.

Aindow, M.–Microstructure of laser-ablated superconducting $La_2CuO_4F_x$ thin films on $SrTiO_3$.–G. Kong, M.O. Jones, J.S. Abell, P.P. Edwards, S.T. Lees, K.E. Gibbons, I. Gameson, and M. Aindow; **16**(11), 3309–3316.

Ajdelsztajn, Leoanardo–Thermal stability of nanocrystalline WC–Co powder synthesized by using mechanical milling at low temperature.–Jianhong He, Leoanardo Ajdelsztajn, and Enrique J. Lavernia; **16**(2), 478–488.

Aka, G.–Phase transition, growth, and optical properties of $Nd_xLa_{1-x}Sc_3(BO_3)_4$ crystals.–Yunkui Li, G. Aga, A. Kahn-Harari, and D. Vivien; **16**(1), 38–44.

Akai, Tomoko–Coordination structures of implanted Fe, Co, and Ni ions in silica glass by x-ray absorption fine structure spectroscopy.–Kohei Fukumi, Akiyoshi Chayahara, Kohei Kadono, Hiroyuki Kageyama, Tomoko Akai, Hiroshi Mizoguchi, Naoyuki Kitamura, Masaki Makihara, Yuji Horino, and Kanenaga Fujii; **16**(1), 155–162.

Akaishi, M.–Microstructural analysis of high-pressure compressed C_{60}.–K. Miyazawa, H. Satsuki, M. Kuwabara, and M. Akaishi; **16**(7), 1960–1966.

Akatsu, Takashi–Effects of whisker content and dimensions on the *R*-curve behavior of an alumina matrix composite reinforced with silicon carbide whiskers.–Takashi Akatsu, Minoru Suzuki, Yasuhiro Tanabe, and Eiichi Yasuda; **16**(7), 1919–1927.

Aksay, I.A.–Model for the robust mechanical behavior of nacre.–A.G. Evans, Z. Suo, R.Z. Wang, I.A. Aksay, M.Y. He, and J.W. Hutchinson; **16**(9), 2475–2484.

–Deformation mechanisms in nacre.–R.Z. Wang, Z. Suo, A.G. Evans, N. Yao, I.A. Aksay; **16**(9), 2485–2493.

–Cure depth in photopolymerization: Experiments and theory.–Jim H. Lee, Robert K. Prud'homme, and Ilhan A. Aksay; **16**(12), 3536–3544.

Alam, M. Khairul–Strength prediction of partially aligned discontinuous fiber-reinforced composites.–Rex J. Kuriger, M. Khairul Alam, and David P. Anderson; **16**(1), 226–232.

Aldinger, Fritz–Anelastic behavior of precursor-derived amorphous ceramics in the system Si–B–C–N.–Martin Christ, André Zimmermann, and Fritz Aldinger; **16**(7), 1994–1997.

Algueró, M.–Direct measurement of mechanical properties of (Pb, La)TiO_3 ferroelectric thin films using nanoindentation techniques.–M. Algueró, A.J. Bushby, and M.J. Reece; **16**(4), 993–1002.

Almeida, R.M.–Phase separation in SiO_2–TiO_2 gel and glassy films studied by atomic force microscopy and transmission electron microscopy.–A. Karthikeyan and Rui M. Almeida; **16**(6), 1626–1631.

–^{29}Si nuclear-magnetic-resonance and vibrational spectroscopy studies of SiO_2–TiO_2 powders prepared by the sol-gel process.–J.P. Rainho, J. Rocha, L.D. Carlos, and R.M. Almeida; **16**(8), 2369–2376.

Altgilbers, A.–Formation of $NdBa_2Cu_3O_{7-\delta}$ amorphous phase by combining aero-acoustic levitation and splat quenching.–K. Nagashio, W.H. Hofmeister, D.E. Gustafson, A. Altgilbers, R.J. Bayuzick, and K. Kuribayashi; **16**(1), 138–145.

Alves, M.C.M.–CsCl-modified Ga_2S_3–La_2S_3 glasses: Structural approach by x-ray absorption spectroscopy.–A.Y. Ramos, M. Grisolía Cardona, H.C.N. Tolentino, M.C.M. Alves, N. Watanabe, O.L. Alves, and L.C. Barbosa; **16**(5), 1349–1353.

Alves, O.L.–CsCl-modified Ga_2S_3–La_2S_3 glasses: Structural approach by x-ray absorption spectroscopy.–A.Y. Ramos, M. Grisolía Cardona, H.C.N. Tolentino, M.C.M. Alves, N. Watanabe, O.L. Alves, and L.C. Barbosa; **16**(5), 1349–1353.

Amaratunga, G.A.J.–Strongly adhering and thick highly tetrahedral amorphous carbon (ta–C) thin films via surface modification by implantation.–M. Chhowalla and G.A.J. Amaratunga; **16**(1), 5–8(L).

Amin, Ahmed–Piezoresistivity in ruthenium-based metal–insulator–metal structures.–Ahmed Amin; **16**(8), 2239–2243.

Amroune, A.–Synthesis of Al_2O_3–SiC from kyanite precursor.–A. Amroune and G. Fantozzi; **16**(6), 1609–1613.

An, S-J.–Metal-organic vapor phase epitaxial growth of high-quality ZnO films on $Al_2O_3(00{\cdot}1)$.–W.I. Park, S-J. An, Gyu-Chul Yi, and Hyun M. Jang; **16**(5), 1358–1362.

Anderson, David P.–Strength prediction of partially aligned discontinuous fiber-reinforced composites.–Rex J. Kuriger, M. Khairul Alam, and David P. Anderson; **16**(1), 226–232.

Anderson, I.M.–Templated growth of a complex nitride island dispersion through an internal nitridation reaction.–M.P. Brady, D.T. Hoelzer, E.A. Payzant, P.F. Tortorelli, J.A. Horton, I.M. Anderson, L.R. Walker, and S.K. Wrobel; **16**(10), 2784–2787(L).

Andleigh, V.K.–Modeling of the effects of crystallographic orientation on electromigration-limited reliability of interconnects with bamboo grain structures.–W.R. Fayad, V.K. Andleigh, and C.V. Thompson; **16**(2), 413–416.

Anselmi-Tamburini, U.–Field-activated combustion synthesis of Ta–Si intermetallic compounds.–F. Maglia, U. Anselmi-Tamburini, N. Bertolino, C. Milanese, and Z.A. Munir; **16**(2), 534–544.

–Combustion synthesis of mechanically activated powders in the Ti–Si system.–F. Maglia, U. Anselmi-Tamburini, G. Cocco, M. Monagheddu, N. Bertolino, and Z.A. Munir; **16**(4), 1074–1082.

–Mechanochemistry of the titanium–silicon system: Compositional effects.–S. Doppiu, M. Monagheddu, G. Cocco, F. Maglia, U. Anselmi-Tamburini, and Z.A. Munir; **16**(5), 1266–1279.

–Combustion of zirconium foils in oxygen.–K.H. Ewald, U. Anselmi-Tamburini, and Z.A. Munir; **16**(9), 2687–2694.

Aoki, Toru–Comparison of hydrophilic properties of amorphous TiO_x films obtained by radio frequency sputtering and plasma-enhanced chemical vapor deposition.–Masatoshi Nakamura, Toru Aoki, Yoshinori Hatanaka, Dariusz Korzec, and Jurgen Engemann; **16**(2), 621–626.

Arakawa, Hironori–Optical and structural properties of solid oxide photocatalyst Bi_2FeNbO_7.–Zhigang Zou, Jinhua Ye, and Hironori Arakawa; **16**(1), 35–37(L).

Araújo, E.B.–Structural and electrical properties of strontium barium niobate thin films crystallized by conventional furnace and rapid-thermal annealing process.–R.G. Mendes, E.B. Araújo, and J.A. Eiras; **16**(10), 3009–3013.

Arcos, D.–Textural properties of $SiO_2 \cdot CaO \cdot P_2O_5$ glasses prepared by the sol-gel method.–F. Balas, D. Arcos, J. Pérez-Pariente, and M. Vallet-Regí; **16**(5), 1345–1348.

Arendt, P.N.–High critical current density $YBa_2Cu_3O_{7-\delta}$ thick films using ion beam assisted deposition MgO bi-axially oriented template layers on nickel-based superalloy substrates.–J.R. Groves, P.N. Arendt, S.R. Foltyn, Q.X. Jia, T.G. Holesinger, H. Kung, E.J. Peterson, R.F. DePaula, P.C. Dowden, L. Stan, and L.A. Emmert; **16**(8), 2175–2178(L).

Arias, Francisco–Fabrication and characterization of microscale sandwich beams.–Francisco Arias, Paul J.A. Kenis, Bing Xu, Tao Deng, Olivier J.A. Schueller, George M. Whitesides, Yuki Sugimura, and Anthony G. Evans; **16**(2), 597–605.

Asmann, Marcus–Chemical vapor deposition of an aluminum nitride–diamond composite in a triple torch plasma reactor.–Marcus Asmann, Robert F. Cook, Joachim V. Heberlein, and Emil Pfender; **16**(2), 469–477.

Ata, Ali–Precipitate splitting in $Pb_{0.91}La_{0.09}Zr_{0.65}Ti_{0.35}O_3$ films.–Bahadir Tunaboylu, Ken Ring, Sadik C. Esener, Cengiz Ozkan, Ali Ata; **16**(10), 2763–2766(L).

Atanassova, P.–Dielectric properties of oxide structures by a laser-based direct-writing method.–D. Young, H.D. Wu, R.C.Y. Auyeung, R. Modi, J. Fitz-Gerald, A. Pique, D.B. Chrisey, P. Atanassova, and T. Kodas; **16**(6), 1720–1725.

Atkins, Graham R.–Direct laser writing of self-developed waveguides in benzyldimethylketal-doped sol-gel hybrid glass.–Byeong-Soo Bae, Oun-Ho Park, Robbie Charters, Barry Luther-Davies, Graham R. Atkins; **16**(11), 3184–3187.

Auyeung, R.C.Y.–Dielectric properties of oxide structures by a laser-based direct-writing method.–D. Young, H.D. Wu, R.C.Y. Auyeung, R. Modi, J. Fitz-Gerald, A. Pique, D.B. Chrisey, P. Atanassova, and T. Kodas; **16**(6), 1720–1725.

–Direct writing of polymer thick film resistors using a novel laser transfer technique.–R. Modi, H.D. Wu, R.C.Y. Auyeung, C.M. Gilmore, and D.B. Chrisey; **16**(11), 3214–3222.

Ayguavives, F.–Oxygen transport during annealing of $Pb(Zr,Ti)O_3$ thin films in O_2 gas and its effect on their conductivity.–F. Ayguavives, B. Agius, B. Ea-Kim, and I. Vickridge; **16**(10), 3005–3008.

Aytug, T.–Growth and characterization of conductive $SrRuO_3$ and $LaNiO_3$ multilayers on textured Ni tapes for high-J_c $YBa_2Cu_3O_{7-\delta}$ coated conductors.–T. Aytug, B.W. Kang, C. Cantoni, E.D. Specht, M. Paranthaman, A. Goyal, D.K. Christen, D.T. Verebelyi, J.Z. Wu, R.E. Ericson, C.L. Thomas, C-Y.Yang, and S.E. Babcock; **16**(9), 2661–2669.

B

Baba-Kishi, K.Z.–Relationship between the microstructure and nanoindentation hardness of thermally evaporated and magnetron-sputtered electrochromic tungsten oxide films.–C.W. Ong, H.Y. Wong, G.K.H. Pang, K.Z. Baba-Kishi, and C.L. Choy; **16**(6), 1541–1548.

Babcock, S.E.–Growth and characterization of conductive $SrRuO_3$ and $LaNiO_3$ multilayers on textured Ni tapes for high-J_c $YBa_2Cu_3O_{7-\delta}$ coated conductors.–T. Aytug, B.W. Kang, C. Cantoni, E.D. Specht, M. Paranthaman, A. Goyal, D.K. Christen, D.T. Verebelyi, J.Z. Wu, R.E. Ericson, C.L. Thomas, C-Y.Yang, and S.E. Babcock; **16**(9), 2661–2669.

Babu, N.H.–Microstructure and growth of joins in melt-textured $YBa_2Cu_3O_{7-\delta}$.–A.D. Bradley, W. Lo, M. Mironova, N.H. Babu, D.A. Cardwell, A.M. Campbell, and K. Salama; **16**(8), 2298–2305.

Babu, S.V.–Chemical–mechanical polishing of copper and tantalum with silica abrasives.–Y. Li, M. Hariharaputhiran, and S.V. Babu; **16**(4), 1066–1073.

Bacaltchuk, Cristiane–Effects of thermal annealing on the texture of $La_{0.67}Sr_{0.33}MnO_3$ thin films.–Lamartine Meda, LaQuita Kennon, Cristiane Bacaltchuk, Hamid Garmestani, and Klaus H. Dahmen; **16**(7), 1887–1889(L).

Bachhofer, H.–Phase formation and crystal growth of Sr–Bi–Ta–O thin films grown by metalorganic chemical vapor deposition.–H. Bachhofer, H. von Philipsborn, W. Hartner, C. Dehm, B. Jobst, A. Kiendl, H. Schroeder, and R. Waser; **16**(10), 2966–2973.

Bae, Byeong-Soo–Preparation and characteristics of seeded epitaxial $(Sr,Ba)Nb_2O_6$ optical waveguide thin films using sol-gel method.–Junmo Koo, Jae Hyeok Jang, and Byeong-Soo Bae; **16**(2), 430–436.

–Photoinduced condensation of sol-gel hybrid glass films doped with benzildimethylketal.–Oun-Ho Park, Ji-In Jung, and Byeong-Soo Bae; **16**(7), 2143–2148.

–Direct laser writing of self-developed waveguides in benzyldimethylketal-doped sol-gel hybrid glass.–Byeong-Soo Bae, Oun-Ho Park, Robbie Charters, Barry Luther-Davies, and Graham R. Atkins; **16**(11), 3184–3187.

Baert, Kris–Effect of *in situ* boron doping on properties of silicon germanium films deposited by chemical vapor deposition at 400 °C.–Sherif Sedky, Ann Witvrouw, Annelies Saerens, Paul Van Houtte, Jef Poortmans, and Kris Baert; **16**(9), 2607–2612.

Bahr, D.F.–Thin-film fracture during nanoindentation of a titanium oxide film–titanium system.–M. Pang and D.F. Bahr; **16**(9), 2634–2643.

Baik, Sunggi–Ferroelectric domain structure of epitaxial $(Pb,Sr)TiO_3$ thin films.–Yong Kwan Kim, Kyeong Seok Lee, and Sunggi Baik; **16**(9), 2463–2466(L).

Baker, S.P.–Hardness–depth profile of a carbon-implanted Ti–6Al–4V alloy and its relation to composition and microstructure.–M. Kunert, O. Kienzle, B. Baretzky, S.P. Baker, and E.J. Mittemeijer; **16**(8), 2321–2335.

Balas, F.–Textural properties of $SiO_2 \cdot CaO \cdot P_2O_5$ glasses prepared by the sol-gel method.–F. Balas, D. Arcos, J. Pérez-Pariente, and M. Vallet-Regí; **16**(5), 1345–1348.

Balzaretti, N.M.–Thermal conductivity and thermal diffusivity of selected oxide single crystals.–A. Stanimirovic, N.M. Balzaretti, A. Feldman, and J.E. Graebner; **16**(3), 678–682.

Bando, Y.–Synthesis of coaxial nanotubes: Titanium oxide sheathed with silicon oxide.–Ming Zhang, Y. Bando, and K. Wada; **16**(5), 1408–1412.

–Cubic silicon nitride embedded in amorphous silicon dioxide.–Ming Zhang, Hongliang He, F.F. Xu, T. Sekine, T. Kobayashi, and Y. Bando; **16**(8), 2179–2181(L).

Bao, Chun Yan–Fabrication of heteropolyoxometalate-based photochromic inorganic–organic nanocomposites.–Tie Rui Zhang, Wei Feng, Chun Yan Bao, Ran Lu, Xin Tong Zhang, Tie Jin Li, Ying Ying Zhao, and Jian Nian Yao; **16**(8), 2256–2263.

Bao, Cui-Min–Formation rule for Al-based ternary quasi-crystals: Example of Al–Ni–Fe decagonal phase.–Jian-Bing Qiang, De-He Wang, Cui-Min Bao, Ying-Min Wang, Wei-Ping Xu, Mei-Li Song, and Chuang Dong; **16**(9), 2653–2660.

Barbosa, L.C.–CsCl-modified Ga_2S_3–La_2S_3 glasses: Structural approach by x-ray absorption spectroscopy.–A.Y. Ramos, M. Grisolía Cardona, H.C.N. Tolentino, M.C.M. Alves, N. Watanabe, O.L. Alves, and L.C. Barbosa; **16**(5), 1349–1353.

Baretzky, B.–Hardness–depth profile of a carbon-implanted Ti–6Al–4V alloy and its relation to composition and microstructure.–M. Kunert, O. Kienzle, B. Baretzky, S.P. Baker, and E.J. Mittemeijer; **16**(8), 2321–2335.

Barmak, K.–Texture in Ti/Al and Nb/Al multilayer thin films: Role of Cu.–G. Lucadamo, K. Barmak, and K.P. Rodbell; **16**(5), 1449–1459.

Barnard, John A.–Ultrathin TiB_2 protective films.–Feng Huang, John A. Barnard, and Mark L. Weaver; **16**(4), 945–954.

Basak, D.–Moving the pulsed heating technique beyond monolithic specimens: Experiments with coated wires.–D. Josell, D. Basak, J.L. McClure, U.R. Kattner, M.E. Williams, W.J. Boettinger, and M. Rappaz; **16**(8), 2421–2428.

Bashmakov, I.–Preparation, structure, and magnetic properties of cobalt nanoparticles in carbon fibers.–I. Bashmakov, V. Dorosinez, M. Lukashevich, A. Mazanik, T. Tihonova, T. Zabel, B. Wiedenhorst, and H. Micklitz; **16**(10), 2832–2835.

Baskaran, Suresh–Chemical sensors based on dielectric response of functionalized mesoporous silica films.–Karel Domansky, Jun Liu, Li-Qiong Wang, Mark H. Engelhard, Suresh Baskaran; **16**(10), 2810–2816.

Basu, B.–Transformation behavior of yttria stabilized tetragonal zirconia polycrystal–TiB_2 composites.–B. Basu, J. Vleugels, and O. Van Der Biest; **16**(7), 2158–2169.

Basumallick, A.–Preparation of γ-Fe_2O_3 nanoparticles from a non-aqueous precursor.–P. Deb and A. Basumallick; **16**(12), 3471–3475.

Battagliarin, Marino–Fractal aggregates of lanthanide-doped Y_2O_3 nanoparticles obtained by propellant synthesis.–Stefano Polizzi, Giuliano Fagherazzi, Marino Battagliarin, Marco Bettinelli, and Adolfo Speghini; **16**(1), 146–154.

Bayuzick, R.J.–Formation of $NdBa_2Cu_3O_{7-\delta}$ amorphous phase by combining aero-acoustic levitation and splat quenching.–K. Nagashio, W.H. Hofmeister, D.E. Gustafson, A. Altgilbers, R.J. Bayuzick, and K. Kuribayashi; **16**(1), 138–145.

Becker, H-W.–Characterization of the induction period in tricalcium silicate hydration by nuclear resonance reaction analysis.–R.A. Livingston, J.S. Schweitzer, C. Rolfs, H-W. Becker, and S. Kubsky; **16**(3), 687–693.

Bell, T.J.–Analysis of depth-sensing indentation tests with a Knoop indenter.–L. Riester, T.J. Bell, and A.C. Fischer-Cripps; **16**(6), 1660–1667.

–Methods of correction for analysis of depth-sensing indentation test data for spherical indenters.–A.C. Fischer-Cripps, A. Bendeli, T.J. Bell, J.S. Field, and A.K. Jamting; **16**(8), 2244–2250.

Bellon, K.–Flash synthesis of zirconia nanoparticles by microwave forced hydrolysis.–K. Bellon, D. Chaumont, and D. Stuerga; **16**(9), 2619–2622.

Bellosi, A.–Influence of annealing treatments on microstructure and toughness of liquid-phase-sintered silicon carbide.–D. Sciti and A. Bellosi; **16**(3), 806–816.

Belous, Anatolii G.–Solid-state reaction mechanism for the formation of $Ba_{6-x}Ln_{8+2\ x/3}Ti_{18}O_{54}$ (Ln = Nd, Sm) solid solutions.–Anatolii G. Belous, Oleg V. Ovchar, Matjaz Valant, and Danilo Suvorov; **16**(8), 2350–2356.

Benavente, R.–Influence of thermal history on morphology and viscoelastic behavior of ethylene–1-octene copolymers synthesized with metallocene catalysts.–M.L. Cerrada, R. Benavente, and E. Pérez; **16**(4), 1103–1111.

Bendeli, A.–Methods of correction for analysis of depth-sensing indentation test data for spherical indenters.–A.C. Fischer-Cripps, A. Bendeli, T.J. Bell, J.S. Field, and A.K. Jamting; **16**(8), 2244–2250.

Bender, H.–*In situ* transmission electron microscopy study of the silicidation process in Co thin films on patterned (001) Si substrates.–C. Ghica, L. Nistor, H. Bender, A. Steegen, A. Lauwers, K. Maex, and J. Van Landuyt; **16**(3), 701–708.

–Growth of (111)-oriented $Pb(Zr,Ti)O_3$ layers on nanocrystalline RuO_2 electrodes using the sol-gel technique.–G.J. Norga, S. Jin, Laura Fè, D.J. Wouters, H. Bender, and H.E. Maes; **16**(3), 828–833.

Benlian, Zhou–The healing of quenched crack in 1045 steel under electropulsing.–Zhou Yizhou, Zeng You, He Guanhu, and Zhou Benlian; **16**(1), 17–19(L).

Berg, G.–Determination of the elastic properties of glasses and polymers exploiting the resonant characteristic of depth-sensing indentation tests.–D. Lorenz, W. Fränzel, M. Einax, P. Grau, G. Berg; **16**(6), 1776–1783.

Berlouis, L.E.A.–Thermal analysis investigation of hydriding properties of nanocrystalline Mg–Ni- and Mg–Fe-based alloys prepared by high-energy ball milling.–L.E.A. Berlouis, E. Cabrera, E. Hall-Barientos, P.J. Hall, S.B. Dodd, S. Morris, and M.A. Imam; **16**(1), 45–57.

Bernik, Slavko–Subsolidus phase relations in the La_2O_3–Fe_2O_3–Al_2O_3 system.–Danjela Kuščer, Slavko Bernik, Marko Hrovat, and Janez Holc; **16**(3), 822–827.

–Electrical and microstructural characteristics of ZnO–Bi_2O_3-based varistors doped with rare-earth oxides.–Nguyen The Hung, Nguyen Dinh Quang, and Slavko Bernik; **16**(10), 2817–2823.

Bertolino, N.–Field-activated combustion synthesis of Ta–Si intermetallic compounds.–F. Maglia, U. Anselmi-Tamburini, N. Bertolino, C. Milanese, and Z.A. Munir; **16**(2), 534–544.

–Combustion synthesis of mechanically activated powders in the Ti–Si system.–F. Maglia, U. Anselmi-Tamburini, G. Cocco, M. Monagheddu, N. Bertolino, and Z.A. Munir; **16**(4), 1074–1082.

Bettinelli, Marco–Fractal aggregates of lanthanide-doped Y_2O_3 nanoparticles obtained by propellant synthesis.–Stefano Polizzi, Giuliano Fagherazzi, Marino Battagliarin, Marco Bettinelli, and Adolfo Speghini; **16**(1), 146–154.

Bhattacharya, A.K.–Synthesis and characterization of partially and fully stabilized zirconia fibers made from an inorganic precursor.–A. Hartridge, M.D. Taylor, and A.K. Bhattacharya; **16**(8), 2384–2390.

–Halide removal from BaM ($BaFe_{12}O_{19}$) and SrM ($SrFe_{12}O_{19}$) ferrite fibers via a steaming process.–R.C. Pullar, M.D. Taylor, and A.K. Bhattacharya; **16**(11), 3162–3169.

Bhushan, Bharat–Development of a continuous microscratch technique in an atomic force microscope and its application to study scratch resistance of ultrathin hard amorphous carbon coatings.–Sriram Sundararajan and Bharat Bhushan; **16**(2), 437–445.

–*In situ* microscopic surface characterization studies of polymeric thin films during tensile deformation using atomic force microscopy.–M.S. Bobji and Bharat Bhushan; **16**(3), 844–855.

Bian, X.F.–Origin of the anomalous volume expansion in Al–Si alloys above liquidus.–W.M. Wang, X.F. Bian, H.R. Wang, Zhen Wang, L. Zhang, Z.G. Liu, and J-M. Liu; **16**(12), 3592–3598.

Birch, J.–Deposition of epitaxial transition metal carbide films and superlattices by simultaneous direct current metal magnetron sputtering and C_{60} evaporation.–H. Högberg, J. Birch, M.P. Johansson, L. Hultman, and U. Jansson; **16**(3), 633–643.

–Growth, structure, and mechanical properties of transition metal carbide superlattices.–H. Högberg, J. Birch, M. Odén, J-O. Malm, L. Hultman, and U. Jansson; **16**(5), 1301–1310.

Birnie, Dunbar P., III–Rational solvent selection strategies to combat striation formation during spin coating of thin films.–Dunbar P. Birnie, III; **16**(4), 1145–1154.

–Nondestructive measurement of striation defect spacing using laser diffraction.–Dylan E. Haas, Dunbar P. Birnie, III; **16**(12), 3355–3360.

Birringer, R.–Formation of eutectic RuAl/Ru nanocomposite by mechanical alloying and subsequent annealing.–K.W. Liu, F. Mücklich, and R. Birringer; **16**(9), 2459–2462(L).

Birtcher, R.C.–Mass density of glassy $Pd_{80}Si_{20}$ during low-temperature light ion irradiation.–G. Schumacher, R.C. Birtcher, and L.E. Rehn; **16**(10), 2788–2792.

Boatner, L.A.–Thermochemistry of rare-earth orthophosphates.–S.V. Ushakov, K.B. Helean, A. Navrotsky, and L.A. Boatner; **16**(9), 2623–2633.

–Nanocrystals in crystalline silicon: Void formation and hollow particles.–A. Meldrum, S. Honda, C.W. White, R.A. Zuhr, L.A. Boatner; **16**(9), 2670–2679.

Bobji, M.S.–*In situ* microscopic surface characterization studies of polymeric thin films during tensile deformation using atomic force microscopy.–M.S. Bobji and Bharat Bhushan; **16**(3), 844–855.

Boettinger, W.J.–Moving the pulsed heating technique beyond monolithic specimens: Experiments with coated wires.–D. Josell, D. Basak, J.L. McClure, U.R. Kattner, M.E. Williams, W.J. Boettinger, and M. Rappaz; **16**(8), 2421–2428.

Bogart, Greg R.–Optical evaluation of the flexural rigidity and residual stress in thin membranes: Picosecond transient grating measurements of the dispersion of the lowest-order Lamb acoustic waveguide mode.–John A. Rogers and Greg R. Bogart; **16**(1), 217–225.

Bogomolova, L.D.–Electronic paramagnetic resonance study of Cu^{2+} ions in copper ion-exchanged layers of lithium niobate crystals.–F. Caccavale, C. Sada, F. Segato, L.D. Bogomolova, V.A. Jachkin, and N.A. Krasil'nikova; **16**(6), 1554–1558.

Bohn, R.–Submicron-grained multiphase TiAlSi alloys: Processing, characterization, and microstructural design.–R. Bohn, G. Fanta, T. Klassen, and R. Bormann; **16**(6), 1850–1861.

Bonnell, Dawn A.–Analysis of phase distributions in the Li_2O–Nb_2O_5–TiO_2 system by piezoresponse imaging.–Albina Y. Borisevich, Sergei V. Kalinin, Dawn A. Bonnell, and Peter K. Davies; **16**(2), 329–332(L).

Bontempi, E.–X-ray reflectivity spectra of ultrathin films and nanometric multilayers: Experiment and simulation.–E. Bontempi, L.E. Depero, L. Sangaletti, F. Giorgis, and C.F. Pirri; **16**(9), 2556–2561.

Borisevich, Albina Y.–Analysis of phase distributions in the Li_2O–Nb_2O_5–TiO_2 system by piezoresponse imaging.–Albina Y. Borisevich, Sergei V. Kalinin, Dawn A. Bonnell, and Peter K. Davies; **16**(2), 329–332(L).

Bormann, R.–Submicron-grained multiphase TiAlSi alloys: Processing, characterization, and microstructural design.–R. Bohn, G. Fanta, T. Klassen, and R. Bormann; **16**(6), 1850–1861.

Boscarino, D.–Production and characterization of titanium and iron oxide nano-sized thin films.–E. Comini, G. Sberveglieri, M. Ferroni, V. Guidi, C. Frigeri, and D. Boscarino; **16**(6), 1559–1564.

Bouaricha, S.–Study of the activation process of Mg-based hydrogen storage materials modified by graphite and other carbonaceous compounds.–S. Bouaricha, J-P. Dodelet, D. Guay, J. Huot, and R. Schulz; **16**(10), 2893–2905.

Bovin, Jan-Olov–Atomic structure of YB_{56} studied by digital high-resolution electron microscopy and electron diffraction.–Takeo Oku, Jan-Olov Bovin, Iwami Higashi, Takaho Tanaka, and Yoshio Ishizawa; **16**(1), 101–107.

Bowman, Keith–Modeling of electric field induced texture in lead zirconate titanate ceramics.–Shan Wan and Keith Bowman; **16**(8), 2306–2313.

Bradby, J.E.–Mechanical deformation in silicon by micro-indentation.–J.E. Bradby, J.S. Williams, J. Wong-Leung, M.V. Swain, and P. Munroe; **16**(5), 1500–1507.

Bradley, A.D.–Microstructure and growth of joins in melt-textured $YBa_2Cu_3O_{7-\delta}$.–A.D. Bradley, W. Lo, M. Mironova, N.H. Babu, D.A. Cardwell, A.M. Campbell, and K. Salama; **16**(8), 2298–2305.

Brady, M.P.–Templated growth of a complex nitride island dispersion through an internal nitridation reaction.–M.P. Brady, D.T. Hoelzer, E.A. Payzant, P.F. Tortorelli, J.A. Horton, I.M. Anderson, L.R. Walker, and S.K. Wrobel; **16**(10), 2784–2787(L).

Briggs, G.A.D.–Surface studies of phase formation in Co–Ge system: Reactive deposition epitaxy versus solid-phase epitaxy.–I. Goldfarb and G.A.D. Briggs; **16**(3), 744–752.

Brito, Manuel E.–Improved creep resistance in anisotropic silicon nitride.–Naoki Kondo, Yoshikazu Suzuki, Manuel E. Brito, and Tatsuki Ohji; **16**(8), 2182–2185(L).

Broitman, Esteban–Thermal stability of carbon nitride thin films.–Niklas Hellgren, Nian Lin, Esteban Broitman, Virginie Serin, Stefano E. Grillo, Ray Twesten, Ivan Petrov, Christian Colliex, Lars Hultman, and Jan-Eric Sundgren; **16**(11), 3188–3201.

Brydson, Rik–Influence of CaO–SiO_2 ratio on the chemistry of intergranular films in liquid-phase sintered alumina and implications for rate of erosive wear.–Rik Brydson, Peter C. Twigg, Fiona Loughran, and Frank L. Riley; **16**(3), 652–665.

Bull, S.J.–Mechanism of improvement of TiN-coated tool life by nitrogen implantation.–S.J. Bull, Yu.P. Sharkeev, S.V. Fortuna, I.A. Shulepov, and A.J. Perry; **16**(11), 3293–3303.

Bush, Mark B.–Cracking of porcelain coatings bonded to metal substrates of different modulus and hardness.–Hong Zhao, Xiaozhi Hu, Mark B. Bush, and Brian R. Lawn; **16**(5), 1471–1478.

Bushby, A.J.–Direct measurement of mechanical properties of (Pb, La)TiO_3 ferroelectric thin films using nanoindentation techniques.–M. Algueró, A.J. Bushby, and M.J. Reece; **16**(4), 993–1002.

C

Cabrera, E.–Thermal analysis investigation of hydriding properties of nanocrystalline Mg–Ni- and Mg–Fe-based alloys prepared by high-energy ball milling.–L.E.A. Berlouis, E. Cabrera, E. Hall-Barientos, P.J. Hall, S.B. Dodd, S. Morris, and M.A. Imam; **16**(1), 45–57.

Caccavale, F.–Electronic paramagnetic resonance study of Cu^{2+} ions in copper ion-exchanged layers of lithium niobate crystals.–F. Caccavale, C. Sada, F. Segato, L.D. Bogomolova, V.A. Jachkin, and N.A. Krasil'nikova; **16**(6), 1554–1558.

Cai, Chaoxian–Microstructural studies of Cu brazing on AlN.–Chaoxian Cai and Janet K. Lumpp; **16**(3), 670–677.

Cai, Weili–Synthesis of nano-AgI arrays and their optical properties.–Yinhai Wang, Jimei Mo, Weili Cai, Lianzeng Yao, and Lide Zhang; **16**(4), 990–992.

Calvert, P.–Freeform fabrication of aluminum metal-matrix composites.–C.W. Souvignier, T.B. Sercombe, S.H. Huo, P. Calvert, and G.B. Schaffer; **16**(9), 2613–2618.

Calvet, L.E.–Growth and characterization of aligned carbon nanotubes from patterned nickel nanodots and uniform thin films.–J.G. Wen, Z.P. Huang, D.Z. Wang, J.H. Chen, S.X. Yang, Z.F. Ren, J.H. Wang, L.E. Calvet, J. Chen, J.F. Klemic, and M.A. Reed; **16**(11), 3246–3253.

Camarero, E. García–X-ray photoelectron spectroscopy of electrodeposited cadmium mercury telluride thin films and their native surface oxides.–J. Ramiro, L. Galán, E. García Camarero, I. Montero, and Y. Laaziz; **16**(7), 1942–1952.

Campbell, A.M.–Microstructure and growth of joins in melt-textured $YBa_2Cu_3O_{7-\delta}$.–A.D. Bradley, W. Lo, M. Mironova, N.H. Babu, D.A. Cardwell, A.M. Campbell, and K. Salama; **16**(8), 2298–2305.

Cantoni, C.–Growth and characterization of conductive $SrRuO_3$ and $LaNiO_3$ multilayers on textured Ni tapes for high-J_c $YBa_2Cu_3O_{7-\delta}$ coated conductors.–T. Aytug, B.W. Kang, C. Cantoni, E.D. Specht, M. Paranthaman, A. Goyal, D.K. Christen, D.T. Verebelyi, J.Z. Wu, R.E. Ericson, C.L. Thomas, C-Y.Yang, and S.E. Babcock; **16**(9), 2661–2669.

–Growth mechanism of superconducting MgB_2 films prepared by various methods.–H.Y. Zhai, H.M. Christen, L. Zhang, M. Paranthaman, C. Cantoni, B.C. Sales, P.H. Fleming, D.K. Christen, and D.H. Lowndes; **16**(10), 2759–2762(L).

Cao, Anyuan–Aligned carbon nanotube growth under oxidative ambient.–Anyuan Cao, Xianfeng Zhang, Cailu Xu, Ji Liang, Dehai Wu, and Bingqing Wei; **16**(11), 3107–3110.

Cao, G.–Synthesis of dense nanometric $MoSi_2$ through mechanical and field activation.–R. Orrù, J. Woolman, G. Cao, and Z.A. Munir; **16**(5), 1439–1448.

Cao, Jin-bo–Solvothermal route to Bi_3Se_4 nanorods at low temperature.–Yuan-fang Liu, Jing-hui Zeng, Wei-xin Zhang, Wei-chao Yu, Yi-tai Qian, Jin-bo Cao, and Wan-qun Zhang; **16**(12), 3361–3365.

Cao, Wenwu–Effective symmetry and physical properties of twinned perovskite ferroelectric single crystals.–Jiří Erhart and Wenwu Cao; **16**(2), 570–577.

Cao, Ya-an–Photocatalytic activity of TiO_2 prepared at low temperature by a photo-assisted sol-gel method.–Zi-sheng Guan, Xin-tong Zhang, Ying Ma, Ya-an Cao, and Jian-nian Yao; **16**(4), 907–909(L).

–Effects of zinc(II) and iron(III) doping of titania films on their photoreactivity to decompose rhodamine B.–Ying Ma, Xin-tong Zhang, Zi-sheng Guan, Ya-an Cao, and Jian-nian Yao; **16**(10), 2928–2933.

Capel, F.–$BaTiO_3$ formation by thermal decomposition of a (BaTi)-citrate polyester resin in air.–P. Durán, F. Capel, J. Tartaj, and C. Moure; **16**(1), 197–209.

Cardona, M. Grisolía–CsCl-modified Ga_2S_3–La_2S_3 glasses: Structural approach by x-ray absorption spectroscopy.–A.Y. Ramos, M. Grisolía Cardona, H.C.N. Tolentino, M.C.M. Alves, N. Watanabe, O.L. Alves, and L.C. Barbosa; **16**(5), 1349–1353.

Cardwell, D.A.–Growth of melt-textured Nd-123 by hot seeding under reduced oxygen partial pressure.–M. Kambara, N. Hari Babu, Y.H. Shi, and D.A. Cardwell; **16**(4), 1163–1170.

–Microstructure and growth of joins in melt-textured $YBa_2Cu_3O_{7-\delta}$.–A.D. Bradley, W. Lo, M. Mironova, N.H. Babu, D.A. Cardwell, A.M. Campbell, and K. Salama; **16**(8), 2298–2305.

Carlos, L.D.–^{29}Si nuclear-magnetic-resonance and vibrational spectroscopy studies of SiO_2–TiO_2 powders prepared by the sol-gel process.–J.P. Rainho, J. Rocha, L.D. Carlos, and R.M. Almeida; **16**(8), 2369–2376.

Carmel, Yuval–Microwave sintering of ZnO at ultra high heating rates.–Geng-fu Xu, Isabel K. Lloyd, Yuval Carmel, Tayo Olorunyolemi, Otto C. Wilson, Jr.; **16**(10), 2850–2858.

Carpenter, Derrick T.–Electron backscatter diffraction analysis of $Pb(Mg_{1/3}Nb_{2/3})O_3$–35mol%$PbTiO_3$ single crystals grown by seeded polycrystal conversion.–Ajmal Khan, Derrick T. Carpenter, Adam M. Scotch, Helen M. Chan, and Martin P. Harmer; **16**(3), 694–700.

Carrillo-Heian, E.M.–Modeling of wave configuration during electrically ignited combustion synthesis.–O.A. Graeve, E.M. Carrillo-Heian, A. Feng, and Z.A. Munir; **16**(1), 93–100.

Carter, C. Barry–Adhesion of polymer–inorganic interfaces by nanoindentation.–Min Li, C. Barry Carter, Marc A. Hillmyer, and William W. Gerberich; **16**(12), 3378–3388.

Caruso, Ricardo–Controlled preparation and characterization of multilayer sol-gel zirconia dip-coatings.–Ricardo Caruso, Antonio Díaz-Parralejo, Pedro Miranda, and Fernando Guiberteau; **16**(8), 2391–2398.

Carvalho, N.J.M.–Characterization of mechanical properties of tungsten carbide/carbon multilayers: Cross-sectional electron microscopy and nanoindentation observations.–N.J.M. Carvalho and J.Th.M. De Hosson; **16**(8), 2213–2222.

Caylor, J.C.–Epitaxial growth of skutterudite ($CoSb_3$) thin films on (001) InSb by pulsed laser deposition.–J.C. Caylor, M.S. Sander, A.M. Stacy, J.S. Harper, R. Gronsky, and T. Sands; **16**(9), 2467–2470(L).

Celis, J-P.–Fretting wear rate of sulphur deficient MoS_x coatings based on dissipated energy.–Xiaoling Zhang, W. Lauwerens, L. Stals, Jiawen He, J-P. Celis; **16**(12), 3567–3574.

Celzard, A.–Elastic properties of anisotropic monolithic samples of compressed expanded graphite studied with ultrasounds.–M. Krzesińska, A. Celzard, J.F. Marêché, and S. Puricelli; **16**(2), 606–614.

Cerrada, M.L.–Influence of thermal history on morphology and viscoelastic behavior of ethylene–1-octene copolymers synthesized with metallocene catalysts.–M.L. Cerrada, R. Benavente, and E. Pérez; **16**(4), 1103–1111.

Cha, Seung I.–Analysis and modeling of residual stress in diamond thin film deposited by the hot-filament chemical vapor deposition process.–Seung I. Cha and Soon H. Hong; **16**(7), 1953–1959.

Chaim, R.–Sintering and microstructure of glass-coated nanocrystalline yttria-stabilized tetragonal zirconia powder: Effect of the glass.–R. Ramamoorthy and R. Chaim; **16**(1), 296–302.

Chakoumakos, B.C.–Comparison of crystal structure parameters of natural and synthetic apatites from neutron powder diffraction.–Th. Leventouri, B.C. Chakoumakos, N. Papanearchou, and V. Perdikatsis; **16**(9), 2600–2606.

Chakravorty, D.–Alternating current conductivity of the interfacial phase in copper oxide–silica gel nanocomposites.–D. Das and D. Chakravorty; **16**(4), 1047–1051.

Chan, C.Y.–Preparation and characterization of nanocrystalline potassium lithium niobate powders and films.–H.X. Zhang, C.H. Kam, Y. Zhou, X.Q. Han, S.D. Cheng, C.Y. Chan, and Y.L. Lam; **16**(12), 3609–3613.

Chan, F.W.–Compaction of bulk ferromagnetic $Fe_{80}P_{13}C_7$ amorphous alloys.–F.W. Chan, N.G. Ma, and H.W. Kui; **16**(10), 2767–2769(L).

Chan, H.S.O.–Preliminary study on alternating thienylene/phenylene copolymers functionalized with an electron-donating or -withdrawing group.–J.M. Xu, S.C. Ng, and H.S.O. Chan; **16**(5), 1235–1237(L).

Chan, Helen M.–Improved tensile creep properties of yttrium- and lanthanum-doped alumina: a solid solution effect.–Junghyun Cho, Chong Min Wang, Helen M. Chan, J.M. Rickman, and Martin P. Harmer; **16**(2), 425–429.

–Electron backscatter diffraction analysis of $Pb(Mg_{1/3}Nb_{2/3})O_3$–35mol%$PbTiO_3$ single crystals grown by seeded polycrystal conversion.–Ajmal Khan, Derrick T. Carpenter, Adam M. Scotch, Helen M. Chan, and Martin P. Harmer; **16**(3), 694–700.

Chang, C.T.–Electric properties of barium–strontium titanate thin films deposited by two-step radio-frequency sputtering.–J.S. Fang, C.T. Chang, and T.S. Chin; **16**(9), 2680–2686.

Chang, Dao–Blue photoluminescent properties of pure nanostructured γ–Al_2O_3.–Zhong Qing Yu, Dao Chang, Cun Li, Ning Zhang, Yu Ying Feng, and You Yuan Dai; **16**(7), 1890–1893(L).

Chang, Li–Highly oriented diamond growth on positively biased Si substrates.–Te-Fu Chang and Li Chang; **16**(12), 3351–3354(L).

Chang, R.P.H.–Epitaxial stabilization of orthorhombic cuprous oxide films on MgO(110).–Paul R. Markworth, R.P.H. Chang, Y. Sun, G.K. Wong, and J.B. Ketterson; **16**(4), 914–921.

–Coherent island formation of Cu_2O films grown by chemical vapor deposition on MgO(110).–P.R. Markworth, X. Liu, J.Y. Dai, W. Fan, T.J. Marks, and R.P.H. Chang; **16**(8), 2408–2414.

Chang, Te-Fu–Highly oriented diamond growth on positively biased Si substrates.–Te-Fu Chang and Li Chang; **16**(12), 3351–3354(L).

Charlton, T.–Growth study of epitaxial $Fe_xZn_{1-x}F_2$ thin films.–J. McChesney, M. Hetzer, H. Shi, T. Charlton, and D. Lederman; **16**(6), 1769–1775.

Charters, Robbie–Direct laser writing of self-developed waveguides in benzyldimethylketal-doped sol-gel hybrid glass.–Byeong-Soo Bae, Oun-Ho Park, Robbie Charters, Barry Luther-Davies, and Graham R. Atkins; **16**(11), 3184–3187.

Chaudhri, M. Munawar–A note on a common mistake in the analysis of nanoindentation data.–M. Munawar Chaudhri; **16**(2), 336–339(L).

Chaumont, D.–Flash synthesis of zirconia nanoparticles by microwave forced hydrolysis.–K. Bellon, D. Chaumont, and D. Stuerga; **16**(9), 2619–2622.

Chayahara, Akiyoshi–Coordination structures of implanted Fe, Co, and Ni ions in silica glass by x-ray absorption fine structure spectroscopy.–Kohei Fukumi, Akiyoshi Chayahara, Kohei Kadono, Hiroyuki Kageyama, Tomoko Akai, Hiroshi Mizoguchi, Naoyuki Kitamura, Masaki Makihara, Yuji Horino, and Kanenaga Fujii; **16**(1), 155–162.

Chen, Chun-Ku–Low-power plasma torch method for the production of crystalline spherical ceramic particles.–Chun-Ku Chen, Seth Gleiman, and Jonathan Phillips; **16**(5), 1256–1265.

Chen, Fangyu–On some discrepancies in the literature about the formation of icosahedral quasi-crystal in Al–Cu–Fe alloys.–Jianian Gui, Jianbo Wang, Renhui Wang, Dahai Wang, Jing Liu, and Fangyu Chen; **16**(4), 1037–1046.

Chen, Feng–Refractive index profile and attenuation measurement in $KTiOPO_4$ waveguide by megaelectronvolt He ions.–Ke-Ming Wang, Hiu Hu, Fei Lu, Feng Chen, Bo-Rong Shi, Yao-Gang Liu, Ding-Yu Shen, and Xie-Mei Wang; **16**(1), 276–279.

Chen, Hong–Impression creep of a viscous layer.–Hong Chen and J.C.M. Li; **16**(9), 2709–2715.

Chen, I-Cherng–Sol-gel synthesis and the effect of boron addition on the phosphorescent properties of $SrAl_2O_4$:Eu^{2+},Dy^{3+} phosphors.–I-Cherng Chen and Teng-Ming Chen; **16**(3), 644–651.

–Effect of host compositions on the afterglow properties of phosphorescent strontium aluminate phosphors derived from the sol-gel method.–I-Cherng Chen and Teng-Ming Chen; **16**(5), 1293–1300.

Chen, J.–Growth and characterization of aligned carbon nanotubes from patterned nickel nanodots and uniform thin films.–J.G. Wen, Z.P. Huang, D.Z. Wang, J.H. Chen, S.X. Yang, Z.F. Ren, J.H. Wang, L.E. Calvet, J. Chen, J.F. Klemic, and M.A. Reed; **16**(11), 3246–3253.

Chen, J.H.–Growth and characterization of aligned carbon nanotubes from patterned nickel nanodots and uniform thin films.–J.G. Wen, Z.P. Huang, D.Z. Wang, J.H. Chen, S.X. Yang, Z.F. Ren, J.H. Wang, L.E. Calvet, J. Chen, J.F. Klemic, and M.A. Reed; **16**(11), 3246–3253.

Chen, Kexin–Microstructure and formation mechanism of combustion-synthesized rodlike Ca α-sialon crystals.–Kexin Chen, Haibo Jin, M. Oliveira, Heping Zhou, and J.M.F. Ferreira; **16**(7), 1928–1934.

Chen, Kunji–Novel photoluminescence from hydrogenated amorphous carbon films prepared by using xylene source.–Jun Xu, Wei Li, Tianfu Ma, Zhifeng Li, Li Wang, and Kunji Chen; **16**(2), 325–328(L).

Chen, L.D.–High-temperature thermoelectric properties of *n*-type $Ba_yNi_xCo_{4-x}Sb_{12}$.–X.F. Tang, L.M. Zhang, R.Z. Yuan, L.D. Chen, T. Goto, T. Hirai, J.S. Dyck, W. Chen, and C. Uher; **16**(12), 3343–3346(L).

–Formation of Al_2O_3 grains with different sizes and morphologies during the pulse electric current sintering process.–S.W. Wang, L.D. Chen, T. Hirai, and Jingkun Guo; **16**(12), 3514–3517.

Chen, L.H.–Effect of lead content on vibration fracture behavior of Pb–Sn eutectic solder.–C.M. Chuang, T.S. Lui, and L.H. Chen; **16**(9), 2644–2652.

Chen, Lidong–Effects of Ce filling fraction and Fe content on the thermoelectric properties of Co-rich $Ce_yFe_xCo_{4-x}Sb_{12}$.–Xinfeng Tang, Lidong Chen, Takashi Goto, and Toshio Hirai; **16**(3), 837–843.

Chen, M.–Dependence of structural, electrical, and optical properties of ZnO:Al films on substrate temperature.–M. Chen, Z.L. Pei, X. Wang, C. Sun, and L.S. Wen; **16**(7), 2118–2123.

Chen, Nan Xian–Site preference of alloying elements in Fe_3Al-based alloys.–Xiao Dong Ni, Nan Xian Chen, Jiang Shen, Zu Qing Sun, and Wang Yue Yang; **16**(2), 344–351.

Chen, Q.–Microstructure of $La_{1-x}Ca_xMnO_3$ studied by transmission electron microscopy.–Q. Chen, J. Tao, J.M. Zuo, and J.C.H. Spence; **16**(10), 2959–2965.

Chen, San-Yuan–Influence of ligand groups in Ti precursors on phase transformation and microstructural evolution of TiO_2 thin films prepared by the wet chemical process.–Chu-Chi Ting and San-Yuan Chen; **16**(6), 1712–1719.

Chen, Teng-Ming–Sol-gel synthesis and the effect of boron addition on the phosphorescent properties of $SrAl_2O_4$:Eu^{2+},Dy^{3+} phosphors.–I-Cherng Chen and Teng-Ming Chen; **16**(3), 644–651.

–Effect of host compositions on the afterglow properties of phosphorescent strontium aluminate phosphors derived from the sol-gel method.–I-Cherng Chen and Teng-Ming Chen; **16**(5), 1293–1300.

Chen, W.–High-temperature thermoelectric properties of *n*-type $Ba_yNi_xCo_{4-x}Sb_{12}$.–X.F. Tang, L.M. Zhang, R.Z. Yuan, L.D. Chen, T. Goto, T. Hirai, J.S. Dyck, W. Chen, and C. Uher; **16**(12), 3343–3346(L).

Chen, Wei-Wu–Nonepitaxial heterogeneous nucleation of α-sialon in the Ca-doped system.–Ya-Wen Li, Pei-Ling Wang, Wei-Wu Chen, Jing-Wei Feng, Yi-Bing Cheng, and Dong-Sheng Yan; **16**(2), 578–582.

Chen, X.M.–Structures and microwave dielectric properties of $Ba_{6-3x}(Nd,Bi_y)_{8+2x}Ti_{18}O_{54}$ ($x = \frac{2}{3}$) solid solution.–Yong Jun Wu and Xiang Ming Chen; **16**(6), 1734–1738.

–Dielectric properties of La-substituted $Pb_{0.5}Ca_{0.5}[(Mg_{1/3}Nb_{2/3})_{0.5}Ti_{0.5}]O_3$ ceramics.–X.J. Lu and X.M. Chen; **16**(7), 2053–2056.

–Structural and dielectric characterization of $Ba_4Nd_2Ti_{4+x}Ta_{6-x}O_{30-x/2}$ nonstoichiometric ceramics.–X.M. Chen, X.H. Zheng, and J. Wang; **16**(10), 2859–2863.

Chen, Xi–Numerical study on the measurement of thin film mechanical properties by means of nanoindentation.–Xi Chen and Joost J. Vlassak; **16**(10), 2974–2982.

Chen, Zhi–Titanium oxide nanotube arrays prepared by anodic oxidation.–Dawei Gong, Craig A. Grimes, Oomman K. Varghese, R.S. Singh, Wenchong Hu, Zhi Chen, and Elizabeth C. Dickey; **16**(12), 3331–3334(L).

Cheng, D.–Grain growth behavior of a nanostructured 5083 Al–Mg alloy.–V.L. Tellkamp, S. Dallek, D. Cheng, and E.J. Lavernia; **16**(4), 938–944.

Cheng, Huiming–Purification of single-walled carbon nanotubes synthesized by the hydrogen arc-discharge method.–Pengxiang Hou, Chang Liu, Yu Tong, Shitao Xu, Min Liu, and Huiming Cheng; **16**(9), 2526–2529.

Cheng, Jian-Gong–Low-temperature fabrication of pyroelectric $Ba_{0.8}Sr_{0.2}TiO_3$ thin films by a sol-gel process.–Jian-Gong Cheng, Jun Tang, Shao-Ling Guo, and Jun-Hao Chu; **16**(3), 778–783.

Cheng, Ju-Yin–Observations of structural order in ion-implanted amorphous silicon.–Ju-Yin Cheng, J.M. Gibson, and D.C. Jacobson; **16**(11), 3030–3033(L).

Cheng, S.D.–Preparation and characterization of nanocrystalline potassium lithium niobate powders and films.–H.X. Zhang, C.H. Kam, Y. Zhou, X.Q. Han, S.D. Cheng, C.Y. Chan, and Y.L. Lam; **16**(12), 3609–3613.

Cheng, Yi-Bing–Nonepitaxial heterogeneous nucleation of α-sialon in the Ca-doped system.–Ya-Wen Li, Pei-Ling Wang, Wei-Wu Chen, Jing-Wei Feng, Yi-Bing Cheng, and Dong-Sheng Yan; **16**(2), 578–582.

Chew, Chwee Har–Third-order nonlinear optical response in PbS-coated CdS nanocomposites.–Bing Liu, Chwee Har Chew, Leong Ming Gan, Guo Qin Xu, Heping Li, Yee Loy Lam, Chan Hin Kam, and Wen Xiu Que; **16**(6), 1644–1650.

Chhowalla, M.–Strongly adhering and thick highly tetrahedral amorphous carbon (ta–C) thin films via surface modification by implantation.–M. Chhowalla and G.A.J. Amaratunga; **16**(1), 5–8(L).

Chien, A.T.–Epitaxial growth of $PbZr_{0.5}Ti_{0.5}O_3$ thin films on $SrRuO_3/SrTiO_3$ substrates using chemical solution deposition: Microstructural and ferroelectric properties.–J.H. Kim, Youngman Kim, A.T. Chien, and F.F. Lange; **16**(6), 1739–1744.

Chin, T.S.–Electric properties of barium–strontium titanate thin films deposited by two-step radio-frequency sputtering.–J.S. Fang, C.T. Chang, and T.S. Chin; **16**(9), 2680–2686.

Chinh, N.Q.–Orientation dependence of Portevin–Le Châtelier plastic instabilities in depth-sensing microindentation.–Zs. Kovács, N.Q. Chinh, and J. Lendvai; **16**(4), 1171–1177.

Chiou, W-A.–Effect of annealing on microstructure, residual stress, and hardness of Al–Ti multilayered films.–R. Mitra, A. Madan, R.A. Hoffman, W-A. Chiou, and J.R. Weertman; **16**(7), 2064–2076.

Cho, Junghyun–Improved tensile creep properties of yttrium- and lanthanum-doped alumina: a solid solution effect.–Junghyun Cho, Chong Min Wang, Helen M. Chan, J.M. Rickman, and Martin P. Harmer; **16**(2), 425–429.

Cho, Nahmgyoo–Evaluation of the impactive-surface-fracture behavior of glass plates using a back-surface strain measurement.–Hyoung-Gu Kim, Nak-Sam Choi, and Nahmgyoo Cho; **16**(11), 3042–3045(L).

Cho, Y.W.–Photovoltaic effect of $Sn_2P_2S_6$ ferroelectric crystal and ceramics.–Y.W. Cho, S.K. Choi, and Yu.M. Vysochanskii; **16**(11), 3317–3322.

Choa, Yong-Ho–Effect of α/β phase ratio on microstructure and mechanical properties of silicon nitride ceramics.–Hirokazu Kawaoka, Tomohiko Adachi, Tohru Sekino, Yong-Ho Choa, Lian Gao, and Koichi Niihara; **16**(8), 2264–2270.

Choi, C.J.–Synthesis of $Nd_2Fe_{14}B$ powders by spray-drying and reduction–diffusion processes.–X.L. Dong, B.K. Kim, C.J. Choi, K.S. Park, and Z.D. Zhang; **16**(4), 1083–1089.

Choi, G.–Precipitation of icosahedral phase from amorphous $Zr_{65}Cu_{17.5-x}Al_{7.5}Ni_{10}Ag_x$ (x = 0, 5) alloys.–J.K. Lee, G. Choi, W.T. Kim, and D.H. Kim; **16**(5), 1311–1317.

Choi, In-Hoon–Low-temperature crystallization induced by excimer laser irradiation of $SrBi_2Ta_2O_9$ films.–Kwang Soo Seol, Hironao Hiramatsu, Yoshimichi Ohki, In-Hoon Choi, and Yong-Tea Kim; **16**(7), 1883–1886(L).

Choi, K.J.–Photoluminescence behavior of Al^{3+}, Pr^{3+} doped perovskite $La_{2/3}TiO_3$ and pyrochlore $La_2Ti_2O_7$.–J.K. Park, C.H. Kim, K.J. Choi, H.D. Park, and S.Y. Choi; **16**(9), 2568–2571.

Choi, Nak-Sam–Evaluation of the impactive-surface-fracture behavior of glass plates using a back-surface strain measurement.–Hyoung-Gu Kim, Nak-Sam Choi, and Nahmgyoo Cho; **16**(11), 3042–3045(L).

Choi, S.K.–Photovoltaic effect of $Sn_2P_2S_6$ ferroelectric crystal and ceramics.–Y.W. Cho, S.K. Choi, and Yu.M. Vysochanskii; **16**(11), 3317–3322.

Choi, S.Y.–Luminescence and decay behaviors of Tb-doped yttrium silicate.–Yoon Young Choi, Kee-Sun Sohn, Hee Dong Park, and Se Young Choi; **16**(3), 881–889.

–Photoluminescence behavior of Al^{3+}, Pr^{3+} doped perovskite $La_{2/3}TiO_3$ and pyrochlore $La_2Ti_2O_7$.–J.K. Park, C.H. Kim, K.J. Choi, H.D. Park, S.Y. Choi; **16**(9), 2568–2571.

Choi, Yoon Young–Luminescence and decay behaviors of Tb-doped yttrium silicate.–Yoon Young Choi, Kee-Sun Sohn, Hee Dong Park, and Se Young Choi; **16**(3), 881–889.

Chon, Uong–Formation and characteristics of highly c-axis-oriented $Bi_{3.25}La_{0.75}Ti_3O_{12}$ thin films on $SiO_2/Si(100)$ and $Pt/Ti/SiO_2/Si(100)$ substrates.–Uong Chon, Hyun M. Jang, Sun-Hwa Lee, and Gyu-Chul Yi; **16**(11), 3124–3132.

Chong, A.C.M.–Characterization and modeling of specific strain gradient modulus of epoxy.–D.C.C. Lam and A.C.M. Chong; **16**(2), 558–563.

–Torsion and bending of micron-scaled structures.–A.C.M. Chong, F. Yang, D.C.C. Lam, and P. Tong; **16**(4), 1052–1058.

Chong, T.C.–Formation of quasi-one-dimensional carbon chains in cubic nanocrystals by photon-breaking of C–S bonds in polythiophene.–Z.M. Ren, Y.F. Lu, H.W. Choy, T.C. Chong, S.C. Ng, and P. Miao; **16**(10), 2793–2797.

Chou, Chen-Chia–Ordered structure formation in the flux-grown $Ba(Mg_{1/3}Ta_{2/3})O_3$ single crystals.–Yu-Chang Lee, Chen-Chia Chou, and Dah-Shyang Tsai; **16**(6), 1593–1599.

Chou, Y.T.–Chemical stresses induced by grain-boundary diffusion in thin films.–W.L. Wang, Y.T. Chou, and Sanboh Lee; **16**(7), 1967–1974.

Chou, Yeong-Shyung–Mechanical and thermal properties of combustion-synthesized perovskites, $La_{1-x}Sr_xCr_{0.2}Fe_{0.8}O_3$.–Yeong-Shyung Chou, K. Kerstetter, L.R. Pederson, and R.E. Williford; **16**(12), 3545–3553.

Choy, C.L.–Relationship between the microstructure and nanoindentation hardness of thermally evaporated and magnetron-sputtered electrochromic tungsten oxide films.–C.W. Ong, H.Y. Wong, G.K.H. Pang, K.Z. Baba-Kishi, C.L. Choy; **16**(6), 1541–1548.

Choy, H.W.–Formation of quasi-one-dimensional carbon chains in cubic nanocrystals by photon-breaking of C–S bonds in polythiophene.–Z.M. Ren, Y.F. Lu, H.W. Choy, T.C. Chong, S.C. Ng, and P. Miao; **16**(10), 2793–2797.

Chrisey, D.B.–Dielectric properties of oxide structures by a laser-based direct-writing method.–D. Young, H.D. Wu, R.C.Y. Auyeung, R. Modi, J. Fitz-Gerald, A. Pique, D.B. Chrisey, P. Atanassova, and T. Kodas; **16**(6), 1720–1725.

–Direct writing of polymer thick film resistors using a novel laser transfer technique.–R. Modi, H.D. Wu, R.C.Y. Auyeung, C.M. Gilmore, D.B. Chrisey; **16**(11), 3214–3222.

Christ, Martin–Anelastic behavior of precursor-derived amorphous ceramics in the system Si–B–C–N.–Martin Christ, André Zimmermann, and Fritz Aldinger; **16**(7), 1994–1997.

Christen, D.K.–Growth and characterization of conductive $SrRuO_3$ and $LaNiO_3$ multilayers on textured Ni tapes for high-J_c $YBa_2Cu_3O_{7-\delta}$ coated conductors.–T. Aytug, B.W. Kang, C. Cantoni, E.D. Specht, M. Paranthaman, A. Goyal, D.K. Christen, D.T. Verebelyi, J.Z. Wu, R.E. Ericson, C.L. Thomas, C-Y.Yang, and S.E. Babcock; **16**(9), 2661–2669.

–Growth mechanism of superconducting MgB_2 films prepared by various methods.–H.Y. Zhai, H.M. Christen, L. Zhang, M. Paranthaman, C. Cantoni, B.C. Sales, P.H. Fleming, D.K. Christen, and D.H. Lowndes; **16**(10), 2759–2762(L).

Christen, H.M.–Growth mechanism of superconducting MgB_2 films prepared by various methods.–H.Y. Zhai, H.M. Christen, L. Zhang, M. Paranthaman, C. Cantoni, B.C. Sales, P.H. Fleming, D.K. Christen, and D.H. Lowndes; **16**(10), 2759–2762(L).

Chu, Hsu-Shen–Damping behavior of *in situ* Al–(graphite, Al_4C_3) composites produced by reciprocating extrusion.–Hsu-Shen Chu, Kuo-Shung Liu, and Jien-Wei Yeh; **16**(5), 1372–1380.

Chu, Jun-Hao–Low-temperature fabrication of pyroelectric $Ba_{0.8}Sr_{0.2}TiO_3$ thin films by a sol-gel process.–Jian-Gong Cheng, Jun Tang, Shao-Ling Guo, and Jun-Hao Chu; **16**(3), 778–783.

Chuang, C.M.–Effect of lead content on vibration fracture behavior of Pb–Sn eutectic solder.–C.M. Chuang, T.S. Lui, and L.H. Chen; **16**(9), 2644–2652.

Chumbley, L.S.–Analysis of interdiffusion of Dy, Nd, and Pr in Mg.–Y. Xu, L.S. Chumbley, G.A. Weigelt, and F.C. Laabs; **16**(11), 3287–3292.

Chung, D.D.L.–Rectifying and thermocouple junctions based on Portland cement.–Sihai Wen and D.D.L. Chung; **16**(7), 1989–1993.

Chung, Shyan-Lung–Combustion synthesis of aluminum nitride powder using additives.–Chun-Nan Lin and Shyan-Lung Chung; **16**(8), 2200–2208.

–Combustion synthesis method for synthesis of aluminum nitride powder using aluminum containers.–Chun-Nan Lin and Shyan-Lung Chung; **16**(12), 3518–3525.

Chung, Yong-Chae–Electrical transport properties of single-crystalline Mn–Zn ferrous ferrite.–Yong-Chae Chung and Han-Ill Yoo; **16**(3), 774–777.

Claeys, C.–Mechanical stress of the electrical performance of polycrystalline-silicon resistors.–N. Nakabayashi, H. Ohyama, E. Simoen, M. Ikegami, C. Claeys, K. Kobayashi, M. Yoneoka, and K. Miyahara; **16**(9), 2579–2582.

Clegg, W.J.–Deformation under nanoindents in Si, Ge, and GaAs examined through transmission electron microscopy.–S.J. Lloyd, J.M. Molina-Aldareguia, and W.J. Clegg; **16**(12), 3347–3350(L).

Clem, P.G.–High J_c $YBa_2Cu_3O_{7-\delta}$ films via rapid, low pO_2 pyrolysis.–J.T. Dawley, P.G. Clem, M.P. Siegal, and D.L. Overmyer; **16**(1), 13–16(L).

Cocco, G.–Combustion synthesis of mechanically activated powders in the Ti–Si system.–F. Maglia, U. Anselmi-Tamburini, G. Cocco, M. Monagheddu, N. Bertolino, and Z.A. Munir; **16**(4), 1074–1082.

–Mechanochemistry of the titanium–silicon system: Compositional effects.–S. Doppiu, M. Monagheddu, G. Cocco, F. Maglia, U. Anselmi-Tamburini, and Z.A. Munir; **16**(5), 1266–1279.

Cohen, L.F.–Magnetotransport properties of $La_{0.7}Ca_{0.3}MnO_3$ thick films prepared by spray pyrolysis.–F. Damay, J.L. MacManus-Driscoll, and L.F. Cohen; **16**(3), 784–789.

Colliex, Christian–Thermal stability of carbon nitride thin films.–Niklas Hellgren, Nian Lin, Esteban Broitman, Virginie Serin, Stefano E. Grillo, Ray Twesten, Ivan Petrov, Christian Colliex, Lars Hultman, and Jan-Eric Sundgren; **16**(11), 3188–3201.

Comini, E.–Production and characterization of titanium and iron oxide nano-sized thin films.–E. Comini, G. Sberveglieri, M. Ferroni, V. Guidi, C. Frigeri, and D. Boscarino; **16**(6), 1559–1564.

Compagnini, G.–Formation and characterization of high-density silver nanoparticles embedded in silica thin films by "*in situ*" self-reduction.–G. Compagnini, M.E. Fragalà, L. D'Urso, C. Spinella, and O. Puglisi; **16**(10), 2934–2938.

Conde, O.–Synthesis and properties of $B_xC_yN_z$ coatings.–M.N. Oliveira and O. Conde; **16**(3), 734–743.

Cook, Robert F.–Chemical vapor deposition of an aluminum nitride–diamond composite in a triple torch plasma reactor.–Marcus Assmann, Robert F. Cook, Joachim V. Heberlein, and Emil Pfender; **16**(2), 469–477.

Criado, José Manuel–Kinetic analysis of solid-state processes.–Jiří Málek, Takefumi Mitsuhashi, and José Manuel Criado; **16**(6), 1862–1871.

Cui, Bao-zhi–Effects of preparation processes on structure and magnetic properties of $Nd_2Fe_{14}B/\alpha$–Fe-type nanocomposite magnets.–Bao-zhi Cui, X.K. Sun, L.Y. Xiong, Wei Liu, Zhi-dong Zhang, Zhi-qing Yang, Ai-min Wang, and Jiang-ning Deng; **16**(3), 709–715.

Cui, H.–Study of the mechanism for controlled crystallization of BaF_2 under two kinds of monolayers.–L. Lu, H. Cui, W. Li, H. Zhang, and S. Xi; **16**(8), 2415–2420.

–Nucleation and growth of silicon nitride nanoneedles using microwave plasma heating.–H. Cui and B.R. Stoner; **16**(11), 3111–3115.

Cui, Jian-Jun–Electron microscopy of high-temperature and high-pressure as-grown diamond crystals.–Long-Wei Yin, Mu-Sen Li, Jian-Jun Cui, Bin Xu, Jian-Hong Gong, Zhao-Yin Hao, and Jiong-Fa Zhang; **16**(11), 3023–3026(L).

Cui, Suo-Jing–Enhanced crystallization and phase transformation of amorphous silicon nitride under high pressure.–Ya-Li Li, Yong Liang, Fen Zheng, Xian-Feng Ma, Suo-Jing Cui, and Liling Sun; **16**(1), 67–75.

Cumbrera, Francisco L.–Contact fracture of brittle bilayer coatings on soft substrates.–Pedro Miranda, Antonia Pajares, Fernando Guiberteau, Francisco L. Cumbrera, and Brian R. Lawn; **16**(1), 115–126.

D

Dahmen, K-H.–Effects of thermal annealing on the texture of $La_{0.67}Sr_{0.33}MnO_3$ thin films.–Lamartine Meda, LaQuita Kennon, Cristiane Bacaltchuk, Hamid Garmestani, Klaus H. Dahmen; **16**(7), 1887–1889(L).

–Microstructures of $La_{1-x}A_x$(A = Ca or Sr)$MnO_{3-\delta}$ thin films by liquid-delivery metalorganic chemical vapor deposition.–Y. Xin, K. Han, N. Mateeva, H. Garmestani, P.N. Kalu, and K-H. Dahmen; **16**(11), 3073–3083.

Dai, J.Y.–Coherent island formation of Cu_2O films grown by chemical vapor deposition on MgO(110).–P.R. Markworth, X. Liu, J.Y. Dai, W. Fan, T.J. Marks, and R.P.H. Chang; **16**(8), 2408–2414.

Dai, You Yuan–Blue photoluminescent properties of pure nanostructured γ–Al_2O_3.–Zhong Qing Yu, Dao Chang, Cun Li, Ning Zhang, Yu Ying Feng, and You Yuan Dai; **16**(7), 1890–1893(L).

Dallek, S.–Grain growth behavior of a nanostructured 5083 Al–Mg alloy.–V.L. Tellkamp, S. Dallek, D. Cheng, and E.J. Lavernia; **16**(4), 938–944.

–High grain size stability of nanocrystalline Al prepared by mechanical attrition.–F. Zhou, J. Lee, S. Dallek, and E.J. Lavernia; **16**(12), 3451–3458.

Damay, F.–Magnetotransport properties of $La_{0.7}Ca_{0.3}MnO_3$ thick films prepared by spray pyrolysis.–F. Damay, J.L. MacManus-Driscoll, and L.F. Cohen; **16**(3), 784–789.

Dann, Jeffrey N.–Solid-phase synthesis of cupric tungstate.–Leonid P. Dorfman, David L. Houck, Michael J. Scheithauer, Jeffrey N. Dann, and Harry O. Fassett; **16**(4), 1096–1102.

Dannenberg, Rand–Phenomenological description of grain growth stagnation for nanocrystalline films and powders.–Rand Dannenberg, Eric Stach, and Joanna R. Groza; **16**(4), 1090–1095.

Das, D.–Alternating current conductivity of the interfacial phase in copper oxide–silica gel nanocomposites.–D. Das and D. Chakravorty; **16**(4), 1047–1051.

Das, Swapan Kumar–Patterning of copper particles on polymeric surface.–Arvind Sinha, Swapan Kumar Das, V. Rao, and P. Ramachandrarao; **16**(5), 1354–1357.

Dasgupta, Arup–Development of *p*-type microcrystalline silicon carbon alloy films by the very high frequency plasma-enhanced chemical vapor deposition technique.–Tapati Jana, Arup Dasgupta, and Swati Ray; **16**(7), 2130–2135.

Dauskardt, Reinhold H.–Adhesion of benzocyclobutene-passivated silicon in epoxy layered structures.–Robert J. Hohlfelder, Daniel A. Maidenberg, Reinhold H. Dauskardt, Yueguang Wei, and John W. Hutchinson; **16**(1), 243–255.

Davies, I.J.–Microprobe fluorescence spectroscopy evaluation of stress fields developed along a propagating crack in an $Al_2O_3/CaO \cdot 6Al_2O_3$ ceramic composite.–O. Sbaizero, S. Maschio, G. Pezzotti, and I.J. Davies; **16**(10), 2798–2804.

Davies, Peter K.–Analysis of phase distributions in the Li_2O–Nb_2O_5–TiO_2 system by piezoresponse imaging.–Albina Y. Borisevich, Sergei V. Kalinin, Dawn A. Bonnell, and Peter K. Davies; **16**(2), 329–332(L).

Davis, N.G.–Solid-state foaming of titanium by superplastic expansion of argon-filled pores.–N.G. Davis, J. Teisen, C. Schuh, and D.C. Dunand; **16**(5), 1508–1519.

Dawley, J.T.–High J_c $YBa_2Cu_3O_{7-\delta}$ films via rapid, low pO_2 pyrolysis.–J.T. Dawley, P.G. Clem, M.P. Siegal, and D.L. Overmyer; **16**(1), 13–16(L).

–Properties of $YBa_2Cu_3O_{7-\delta}$ multilayer films from the fluoride-based sol-gel process.–M.P. Siegal, J.T. Dawley, and D.L. Overmyer; **16**(12), 3339–3342(L).

Deb, P.–Preparation of γ–Fe_2O_3 nanoparticles from a nonaqueous precursor.–P. Deb and A. Basumallick; **16**(12), 3471–3475.

Debnath, Radhaballabh–Thermally reversible γ-ray-induced redox reaction between substitutional iron and aluminum impurity centers in a silica glass.–Radhaballabh Debnath; **16**(1), 127–131.

De-Hazan, Y.–Entrapment of organosilicon molecules in nonhydrolytic alumina gels and thermal behavior of the resulting composite.–G.S. Grader, S.A. Melchior, Y. De-Hazan, S. Melamed, and G.E. Shter; **16**(5), 1413–1419.

De Hosson, J.Th.M.–Characterization of mechanical properties of tungsten carbide/carbon multilayers: Cross-sectional electron microscopy and nanoindentation observations.–N.J.M. Carvalho and J.Th.M. De Hosson; **16**(8), 2213–2222.

Dehm, C.–Phase formation and crystal growth of Sr–Bi–Ta–O thin films grown by metalorganic chemical vapor deposition.–H. Bachhofer, H. von Philipsborn, W. Hartner, C. Dehm, B. Jobst, A. Kiendl, H. Schroeder, and R. Waser; **16**(10), 2966–2973.

Delph, T.J.–Planar oxidation of strained silicon substrates.–M-T. Lin, R.J. Jaccodine, and T.J. Delph; **16**(3), 728–733.

Demirata, B.–Effect of composition on the thermal properties and spontaneous emission probabilities of Tm^{3+}-doped TeO_2–LiCl glass.–G. Özen, B. Demirata, and M.L. Öveçoğlu; **16**(5), 1381–1388.

Deng, B.–Preparation and phase control of nanocrystalline silver indium sulfides via a hydrothermal route.–J.Q. Hu, B. Deng, K.B. Tang, C.R. Wang, and Y.T. Qian; **16**(12), 3411–3415.

Deng, Jiang-ning–Effects of preparation processes on structure and magnetic properties of $Nd_2Fe_{14}B$/α–Fe-type nanocomposite magnets.–Bao-zhi Cui, X.K. Sun, L.Y. Xiong, Wei Liu, Zhi-dong Zhang, Zhi-qing Yang, Ai-min Wang, and Jiang-ning Deng; **16**(3), 709–715.

Deng, Tao–Fabrication and characterization of microscale sandwich beams.–Francisco Arias, Paul J.A. Kenis, Bing Xu, Tao Deng, Olivier J.A. Schueller, George M. Whitesides, Yuki Sugimura, and Anthony G. Evans; **16**(2), 597–605.

DePaula, R.F.–High critical current density $YBa_2Cu_3O_{7-\delta}$ thick films using ion beam assisted deposition MgO bi-axially oriented template layers on nickel-based superalloy substrates.–J.R. Groves, P.N. Arendt, S.R. Foltyn, Q.X. Jia, T.G. Holesinger, H. Kung, E.J. Peterson, R.F. DePaula, P.C. Dowden, L. Stan, L.A. Emmert; **16**(8), 2175–2178(L).

Depero, L.E.–X-ray reflectivity spectra of ultrathin films and nanometric multilayers: Experiment and simulation.–E. Bontempi, L.E. Depero, L. Sangaletti, F. Giorgis, and C.F. Pirri; **16**(9), 2556–2561.

Desnica-Franković, I.D.–Influence of compositional disorder on optical absorption processes in $Cu_6P(S_{1-x}Se_x)_5I$ crystals.–I.P. Studenyak, M. Kranjčec, Gy.Sh. Kovacs, I.D. Desnica-Franković, V.V. Panko, and V.Yu. Slivka; **16**(6), 1600–1608.

Dey, Sandwip K.–Highly (111)-oriented and conformal iridium films by liquid source metalorganic chemical vapor deposition.–Jaydeb Goswami, Chang-Gong Wang, Prashant Majhi, Yong-Wook Shin, Sandwip K. Dey; **16**(8), 2192–2195(L).

Di Giuseppe, Gianfranco–Anode-supported planar solid oxide fuel cells by plasma-enhanced metalorganic chemical vapor deposition (PE-MOCVD) and electrostatic spray deposition (ESD): Fabrication of dense thin layers of yttria-stabilized zirconia by PE-MOCVD.–Gianfranco Di Giuseppe and J. Robert Selman; **16**(10), 2983–2991.

Díaz-Parralejo, Antonio–Controlled preparation and characterization of multilayer sol-gel zirconia dip-coatings.–Ricardo Caruso, Antonio Díaz-Parralejo, Pedro Miranda, and Fernando Guiberteau; **16**(8), 2391–2398.

Dickey, Elizabeth C.–Metal–oxide films with magnetically-modulated nanoporous architectures.–Craig A. Grimes, R. Suresh Singh, Elizabeth C. Dickey, and Oomman K. Varghese; **16**(6), 1686–1693.

–Titanium oxide nanotube arrays prepared by anodic oxidation.–Dawei Gong, Craig A. Grimes, Oomman K. Varghese, R.S. Singh, Wenchong Hu, Zhi Chen, and Elizabeth C. Dickey; **16**(12), 3331–3334(L).

Ding, B.Z.–Preparation of superfine Fe-base alloy by liquidus casting.–X.F. Pan, H.F. Zhang, A.M. Wang, B.Z. Ding, and Z.Q. Hu; **16**(12), 3459–3463.

Ding, J.N.–Size effect on the mechanical properties of microfabricated polysilicon thin films.–J.N. Ding, Y.G. Meng, and S.Z. Wen; **16**(8), 2223–2228.

Dobal, P.S.–Raman spectroscopic determination of phase evolutions in $LiAl_xCo_{1-x}O_2$ battery materials.–P.S. Dobal, R.S. Katiyar, M.S. Tomar, and A. Hidalgo; **16**(1), 1–4(L).

–Synthesis of $Zn_{1-x}Mg_xO$ and its structural characterization.–M.S. Tomar, R. Melgarejo, P.S. Dobal, and R.S. Katiyar; **16**(4), 903–906(L).

Dodd, S.B.–Thermal analysis investigation of hydriding properties of nanocrystalline Mg–Ni- and Mg–Fe-based alloys prepared by high-energy ball milling.–L.E.A. Berlouis, E. Cabrera, E. Hall-Barientos, P.J. Hall, S.B. Dodd, S. Morris, and M.A. Imam; **16**(1), 45–57.

Dodelet, J-P.–Study of the activation process of Mg-based hydrogen storage materials modified by graphite and other carbonaceous compounds.–S. Bouaricha, J-P. Dodelet, D. Guay, J. Huot, and R. Schulz; **16**(10), 2893–2905.

Domansky, Karel–Chemical sensors based on dielectric response of functionalized mesoporous silica films.–Karel Domansky, Jun Liu, Li-Qiong Wang, Mark H. Engelhard, and Suresh Baskaran; **16**(10), 2810–2816.

Domínguez-Rodríguez, A.–Topological transformation of grains in three-dimensional normal grain growth.–F. Wakai, Y. Shinoda, S. Ishihara, and A. Domínguez-Rodríguez; **16**(7), 2136–2142.

Dong, Chuang–Formation rule for Al-based ternary quasi-crystals: Example of Al–Ni–Fe decagonal phase.–Jian-Bing Qiang, De-He Wang, Cui-Min Bao, Ying-Min Wang, Wei-Ping Xu, Mei-Li Song, and Chuang Dong; **16**(9), 2653–2660.

Dong, L.–Combined out-of-plane and in-plane texture control in thin films using ion beam assisted deposition.–L. Dong, D.J. Srolovitz, G.S. Was, Q. Zhao, and A.D. Rollett; **16**(1), 210–216.

Dong, M.–Ferroelectric $SrBi_2Ta_2O_9$ single-crystal growth and characterization.–B. Sih, J. Tang, M. Dong, and Z-G. Ye; **16**(6), 1726–1733.

Dong, Q.–Thermodynamic analysis of combustion synthesis of Al_2O_3–TiC–ZrO_2 nanoceramics.–Q. Dong, Q. Tang, W.C. Li, and D.Y. Wu; **16**(9), 2494–2498.

Dong, S.M.–Structure and the nonlinearity of lithium triborate studied by Raman and infrared reflectivity spectroscopy.–H.R. Xia, L.X. Li, H. Yu, S.M. Dong, J.Y. Wang, Q.M. Lu, C.Q. Ma, and X.N. Wang; **16**(12), 3464–3470.

Dong, X.L.–Synthesis of $Nd_2Fe_{14}B$ powders by spray-drying and reduction–diffusion processes.–X.L. Dong, B.K. Kim, C.J. Choi, K.S. Park, and Z.D. Zhang; **16**(4), 1083–1089.

Dong, Y.H.–Residual stress in fiber-textured thin films of cubic materials.–P. Scardi and Y.H. Dong; **16**(1), 233–242.

Donners, M.A.H.–Minima in the strength of MnZn ferrites.–M.A.H. Donners, L.J.M.G. Dortmans, G. de With, and M.J.M. de Graaf; **16**(12), 3575–3582.

Doppiu, S.–Mechanochemistry of the titanium–silicon system: Compositional effects.–S. Doppiu, M. Monagheddu, G. Cocco, F. Maglia, U. Anselmi-Tamburini, and Z.A. Munir; **16**(5), 1266–1279.

Doremus, Robert H.–Diffusion of oxygen and silicon in silicon: Silicon monoxide model.–Robert H. Doremus; **16**(1), 185–191.

Dorfman, Leonid P.–Solid-phase synthesis of cupric tungstate.–Leonid P. Dorfman, David L. Houck, Michael J. Scheithauer, Jeffrey N. Dann, and Harry O. Fassett; **16**(4), 1096–1102.

Dorosinez, V.–Preparation, structure, and magnetic properties of cobalt nanoparticles in carbon fibers.–I. Bashmakov, V. Dorosinez, M. Lukashevich, A. Mazanik, T. Tihonova, T. Zabel, B. Wiedenhorst, and H. Micklitz; **16**(10), 2832–2835.

Dortmans, L.J.M.G.–Minima in the strength of MnZn ferrites.–M.A.H. Donners, L.J.M.G. Dortmans, G. de With, and M.J.M. de Graaf; **16**(12), 3575–3582.

Dowden, P.C.–High critical current density $YBa_2Cu_3O_{7-\delta}$ thick films using ion beam assisted deposition MgO bi-axially oriented template layers on nickel-based superalloy substrates.–J.R. Groves, P.N. Arendt, S.R. Foltyn, Q.X. Jia, T.G. Holesinger, H. Kung, E.J. Peterson, R.F. DePaula, P.C. Dowden, L. Stan, L.A. Emmert; **16**(8), 2175–2178(L).

Drennan, John–Precursor scavenging of the resistive grain-boundary phase in 8 mol% yttria-stabilized zirconia: Effect of trace concentrations of SiO_2.–Jong-Heun Lee, Toshiyuki Mori, Ji-Guang Li, Takayasu Ikegami, John Drennan, and Doh-Yeon Kim; **16**(8), 2377–2383.

Dresselhaus, M.S.–Morphological effect on the electrochemical behavior of electric double-layer capacitors.–M. Endo, Y.J. Kim, T. Maeda, K. Koshiba, K. Katayam, and M.S. Dresselhaus; **16**(12), 3402–3410.

Drmanić, S.–Phase-transformation kinetics in triphasic cordierite gel.–R. Petrović, Dj. Janacković, S. Zec, S. Drmanić, and Lj. Kostić-Gvozdenović; **16**(2), 451–458.

Du, Binyang–Direct measurement of plowing friction and wear of a polymer thin film using the atomic force microscope.–Binyang Du, Mark R. VanLandingham, Qingling Zhang, and Tianbai He; **16**(5), 1487–1492.

Du, Tianbao–Piezoelectric actuation of crack growth along polymer–metal interfaces in adhesive bonds.–Tianbao Du, Ming Liu, Steve Seghi, K.J. Hsia, J. Economy, and J.K. Shang; **16**(10), 2885–2892.

Dunand, D.C.–Tensile fracture during transformation superplasticity of Ti–6Al–4V.–C. Schuh and D.C. Dunand; **16**(3), 865–875.

–Solid-state foaming of titanium by superplastic expansion of argon-filled pores.–N.G. Davis, J. Teisen, C. Schuh, and D.C. Dunand; **16**(5), 1508–1519.

Durán, P.–$BaTiO_3$ formation by thermal decomposition of a (BaTi)-citrate polyester resin in air.–P. Durán, F. Capel, J. Tartaj, and C. Moure; **16**(1), 197–209.

D'Urso, L.–Formation and characterization of high-density silver nanoparticles embedded in silica thin films by "*in situ*" self-reduction.–G. Compagnini, M.E. Fragalà, L. D'Urso, C. Spinella, and O. Puglisi; **16**(10), 2934–2938.

Dyck, J.S.–High-temperature thermoelectric properties of *n*-type $Ba_yNi_xCo_{4-x}Sb_{12}$.–X.F. Tang, L.M. Zhang, R.Z. Yuan, L.D. Chen, T. Goto, T. Hirai, J.S. Dyck, W. Chen, and C. Uher; **16**(12), 3343–3346(L).

E

Ea-Kim, B.–Oxygen transport during annealing of $Pb(Zr,Ti)O_3$ thin films in O_2 gas and its effect on their conductivity.–F. Ayguavives, B. Agius, B. Ea-Kim, and I. Vickridge; **16**(10), 3005–3008.

Economy, J.–Piezoelectric actuation of crack growth along polymer–metal interfaces in adhesive bonds.–Tianbao Du, Ming Liu, Steve Seghi, K.J. Hsia, J. Economy, and J.K. Shang; **16**(10), 2885–2892.

Edirisinghe, M.J.–Investigation of some phenomena occurring during continuous ink-jet printing of ceramics.–B.Y. Tay and M.J. Edirisinghe; **16**(2), 373–384.

Edwards, P.P.–Microstructure of laser-ablated superconducting $La_2CuO_4F_x$ thin films on $SrTiO_3$.–G. Kong, M.O. Jones, J.S. Abell, P.P. Edwards, S.T. Lees, K.E. Gibbons, I. Gameson, and M. Aindow; **16**(11), 3309–3316.

Einax, M.–Determination of the elastic properties of glasses and polymers exploiting the resonant characteristic of depth-sensing indentation tests.–D. Lorenz, W. Fränzel, M. Einax, P. Grau, and G. Berg; **16**(6), 1776–1783.

Eiras, J.A.–Structural and electrical properties of strontium barium niobate thin films crystallized by conventional furnace and rapid-thermal annealing process.–R.G. Mendes, E.B. Araújo, and J.A. Eiras; **16**(10), 3009–3013.

Eisenbraun, Eric T.–Metalorganic chemical vapor deposition of titanium oxide for microelectronics applications.–Kanchana Vydianathan, Guillermo Nuesca, Gregory Peterson, Eric T. Eisenbraun, Alain E. Kaloyeros, John J. Sullivan, and Bin Han; **16**(6), 1838–1849.

Eldred, B.T.–Wetting of mullite by Y_2O_3–Al_2O_3–SiO_2 and B_2O_3–SiO_2 glasses.–T.S. Huang, M.N. Rahaman, B.T. Eldred, and P.D. Ownby; **16**(11), 3223–3228.

El Khakani, M.A.–Highly textured nanostructure of pulsed laser deposited IrO_2 thin films as investigated by transmission electron microscopy.–A.M. Serventi, M.A. El Khakani, R.G. Saint-Jacques, and D.G. Rickerby; **16**(8), 2336–2342.

El-Ocker, M.–Optical and electrical properties of $Ge_{10+x}Se_{40}Te_{50-x}$ thin film.–S.A. Fayek, M. El-Ocker, and A.S. Hassanien; **16**(6), 1549–1553.

Emerson, S.C.–Hydrodynamic cavitation as a tool to control macro-, micro-, and nano-properties of inorganic materials.–J. Find, S.C. Emerson, I.M. Krausz, and W.R. Moser; **16**(12), 3503–3513.

Emmert, L.A.–High critical current density $YBa_2Cu_3O_{7-\delta}$ thick films using ion beam assisted deposition MgO bi-axially oriented template layers on nickel-based superalloy substrates.–J.R. Groves, P.N. Arendt, S.R. Foltyn, Q.X. Jia, T.G. Holesinger, H. Kung, E.J. Peterson, R.F. DePaula, P.C. Dowden, L. Stan, and L.A. Emmert; **16**(8), 2175–2178(L).

Endo, M.–Morphological effect on the electrochemical behavior of electric double-layer capacitors.–M. Endo, Y.J. Kim, T. Maeda, K. Koshiba, K. Katayam, and M.S. Dresselhaus; **16**(12), 3402–3410.

Engelhard, Mark H.–Chemical sensors based on dielectric response of functionalized mesoporous silica films.–Karel Domansky, Jun Liu, Li-Qiong Wang, Mark H. Engelhard, and Suresh Baskaran; **16**(10), 2810–2816.

Engemann, Jurgen–Comparison of hydrophilic properties of amorphous TiO_x films obtained by radio frequency sputtering and plasma-enhanced chemical vapor deposition.–Masatoshi Nakamura, Toru Aoki, Yoshinori Hatanaka, Dariusz Korzec, Jurgen Engemann; **16**(2), 621–626.

Erce-Montilla, R.–Control growth of PbS quantum dots doped sonoormosil.–R. Erce-Montilla, M. Piñero, N. de la Rosa-Fox, A. Santos, and L. Esquivias; **16**(9), 2572–2578.

Erhart, Jiří–Effective symmetry and physical properties of twinned perovskite ferroelectric single crystals.–Jiří Erhart and Wenwu Cao; **16**(2), 570–577.

Ericson, R.E.–Growth and characterization of conductive $SrRuO_3$ and $LaNiO_3$ multilayers on textured Ni tapes for high-J_c $YBa_2Cu_3O_{7-\delta}$ coated conductors.–T. Aytug, B.W. Kang, C. Cantoni, E.D. Specht, M. Paranthaman, A. Goyal, D.K. Christen, D.T. Verebelyi, J.Z. Wu, R.E. Ericson, C.L. Thomas, C-Y.Yang, and S.E. Babcock; **16**(9), 2661–2669.

Esaka, Takaò–Characterization of NO_x sensor using doped In_2O_3.–Shinichiro Tanaka and Takao Esaka; **16**(5), 1389–1395.

Esener, Sadik C.–Precipitate splitting in $Pb_{0.91}La_{0.09}Zr_{0.65}Ti_{0.35}O_3$ films.–Bahadir Tunaboylu, Ken Ring, Sadik C. Esener, Cengiz Ozkan, and Ali Ata; **16**(10), 2763–2766(L).

Esquivias, L.–Control growth of PbS quantum dots doped sonoormosil.–R. Erce-Montilla, M. Piñero, N. de la Rosa-Fox, A. Santos, L. Esquivias; **16**(9), 2572–2578.

Ethridge, Edwin C.–Explanation of the effects of gravity on crystallization of ZrF_2–BaF_2–LaF_3–AlF_3–NaF glass.–Dennis S. Tucker and Edwin C. Ethridge; **16**(11), 3027–3029(L).

Etz, Edgar S.–Correlation of the Raman spectra with the thermal conductivity of a set of diamond wafers prepared by chemical vapor deposition.–Edgar S. Etz, Wilbur S. Hurst, and Albert Feldman; **16**(6), 1694–1711.

Evans, A.G.–Fabrication and characterization of microscale sandwich beams.–Francisco Arias, Paul J.A. Kenis, Bing Xu, Tao Deng, Olivier J.A. Schueller, George M. Whitesides, Yuki Sugimura, and Anthony G. Evans; **16**(2), 597–605.

–Model for the robust mechanical behavior of nacre.–A.G. Evans, Z. Suo, R.Z. Wang, I.A. Aksay, M.Y. He, and J.W. Hutchinson; **16**(9), 2475–2484.

–Deformation mechanisms in nacre.–R.Z. Wang, Z. Suo, A.G. Evans, N. Yao, and I.A. Aksay; **16**(9), 2485–2493.

Evans, J.R.G.–Packing and solidification in ceramic injection moulding.–S. Krug, J.R.G. Evans, and J.H.H. ter Maat; **16**(6), 1829–1837.

Ewald, K.H.–Combustion of zirconium foils in oxygen.–K.H. Ewald, U. Anselmi-Tamburini, and Z.A. Munir; **16**(9), 2687–2694.

F

Faassen, E.E. van–Quantification and effects of molecular oxygen and water in zinc phthalocyanine layers.–H.R. Kerp, K.T. Westerduin, A.T. van Veen, and E.E. van Faassen; **16**(2), 503–511.

Fagherazzi, Giuliano–Fractal aggregates of lanthanide-doped Y_2O_3 nanoparticles obtained by propellant synthesis.–Stefano Polizzi, Giuliano Fagherazzi, Marino Battagliarin, Marco Bettinelli, and Adolfo Speghini; **16**(1), 146–154.

Fan, W.–Coherent island formation of Cu_2O films grown by chemical vapor deposition on MgO(110).–P.R. Markworth, X. Liu, J.Y. Dai, W. Fan, T.J. Marks, and R.P.H. Chang; **16**(8), 2408–2414.

Fang, J.S.–Electric properties of barium–strontium titanate thin films deposited by two-step radio-frequency sputtering.–J.S. Fang, C.T. Chang, and T.S. Chin; **16**(9), 2680–2686.

Fang, Yu-Ching–Devitrification kinetics and mechanism of Pyrex borosilicate glass.–Jau-Ho Jean and Yu-Ching Fang; **16**(6), 1752–1758.

Fanta, G.–Submicron-grained multiphase TiAlSi alloys: Processing, characterization, and microstructural design.–R. Bohn, G. Fanta, T. Klassen, and R. Bormann; **16**(6), 1850–1861.

Fantozzi, G.–Synthesis of Al_2O_3–SiC from kyanite precursor.–A. Amroune and G. Fantozzi; **16**(6), 1609–1613.

Fassett, Harry O.–Solid-phase synthesis of cupric tungstate.–Leonid P. Dorfman, David L. Houck, Michael J. Scheithauer, Jeffrey N. Dann, Harry O. Fassett; **16**(4), 1096–1102.

Fayad, W.R.–Modeling of the effects of crystallographic orientation on electromigration-limited reliability of interconnects with bamboo grain structures.–W.R. Fayad, V.K. Andleigh, and C.V. Thompson; **16**(2), 413–416.

Fayek, S.A.–Optical and electrical properties of $Ge_{10+x}Se_{40}Te_{50-x}$ thin film.–S.A. Fayek, M. El-Ocker, and A.S. Hassanien; **16**(6), 1549–1553.

Fè, L.–Growth of (111)-oriented $Pb(Zr,Ti)O_3$ layers on nanocrystalline RuO_2 electrodes using the sol-gel technique.–G.J. Norga, S. Jin, Laura Fè, D.J. Wouters, H. Bender, and H.E. Maes; **16**(3), 828–833.

–Chemical structure evolution and orientation selection in sol-gel-prepared ferroelectric $Pb(Zr,Ti)O_3$ thin films.–L. Fè, G.J. Norga, D.J. Wouters, H.E. Maes, and G. Maes; **16**(9), 2499–2504.

Feldman, A.–Thermal conductivity and thermal diffusivity of selected oxide single crystals.–A. Stanimirovic, N.M. Balzaretti, A. Feldman, and J.E. Graebner; **16**(3), 678–682.

–Correlation of the Raman spectra with the thermal conductivity of a set of diamond wafers prepared by chemical vapor deposition.–Edgar S. Etz, Wilbur S. Hurst, and Albert Feldman; **16**(6), 1694–1711.

Feng, A.–Modeling of wave configuration during electrically ignited combustion synthesis.–O.A. Graeve, E.M. Carrillo-Heian, A. Feng, and Z.A. Munir; **16**(1), 93–100.

Feng, Jing-Wei–Nonepitaxial heterogeneous nucleation of α-sialon in the Ca-doped system.–Ya-Wen Li, Pei-Ling Wang, Wei-Wu Chen, Jing-Wei Feng, Yi-Bing Cheng, and Dong-Sheng Yan; **16**(2), 578–582.

Feng, Wei–Fabrication of heteropolyoxometalate-based photochromic inorganic–organic nanocomposites.–Tie Rui Zhang, Wei Feng, Chun Yan Bao, Ran Lu, Xin Tong Zhang, Tie Jin Li, Ying Ying Zhao, and Jian Nian Yao; **16**(8), 2256–2263.

Feng, Yu Ying–Blue photoluminescent properties of pure nanostructured γ–Al_2O_3.–Zhong Qing Yu, Dao Chang, Cun Li, Ning Zhang, Yu Ying Feng, and You Yuan Dai; **16**(7), 1890–1893(L).

Ferreira, J.M.F.–Microstructure and formation mechanism of combustion-synthesized rodlike Ca α-sialon crystals.–Kexin Chen, Haibo Jin, M. Oliveira, Heping Zhou, J.M.F. Ferreira; **16**(7), 1928–1934.

Ferroni, M.–Production and characterization of titanium and iron oxide nano-sized thin films.–E. Comini, G. Sberveglieri, M. Ferroni, V. Guidi, C. Frigeri, and D. Boscarino; **16**(6), 1559–1564.

Field, D.P.–Electromigration properties of multigrain aluminum thin film conductors as influenced by grain boundary structure.–O.V. Kononenko, V.N. Matveev, and D.P. Field; **16**(7), 2124–2129.

Field, J.S.–Methods of correction for analysis of depth-sensing indentation test data for spherical indenters.–A.C. Fischer-Cripps, A. Bendeli, T.J. Bell, J.S. Field, and A.K. Jamting; **16**(8), 2244–2250.

Field, R.D.–Synthesis of silicon microwire.–J.J. Petrovic, R.C. Hoover, R.D. Field, and K. Han; **16**(10), 2777–2779(L).

Figueroa, O.L.–Study of the effects of low-energy electron bombardment during the chemical vapor deposition of diamond.–J.A. González, O.L. Figueroa, B.R. Weiner, and G. Morell; **16**(1), 293–295.

Find, J.–Hydrodynamic cavitation as a tool to control macro-, micro-, and nano-properties of inorganic materials.–J. Find, S.C. Emerson, I.M. Krausz, and W.R. Moser; **16**(12), 3503–3513.

Finegan, Ioana C.–Electrical conductivity of vapor-grown carbon fiber/thermoplastic composites.–Ioana C. Finegan and Gary G. Tibbetts; **16**(6), 1668–1674.

Fischer-Cripps, A.C.–Study of analysis methods of depth-sensing indentation test data for spherical indenters.–A.C. Fischer-Cripps; **16**(6), 1579–1584.

–Analysis of depth-sensing indentation tests with a Knoop indenter.–L. Riester, T.J. Bell, and A.C. Fischer-Cripps; **16**(6), 1660–1667.

–Simulation of sub-micron indentation tests with spherical and Berkovich indenters.–A.C. Fischer-Cripps; **16**(7), 2149–2157.

–Methods of correction for analysis of depth-sensing indentation test data for spherical indenters.–A.C. Fischer-Cripps, A. Bendeli, T.J. Bell, J.S. Field, and A.K. Jamting; **16**(8), 2244–2250.

–Use of combined elastic modulus in the analysis of depth-sensing indentation data.–A.C. Fischer-Cripps; **16**(11), 3050–3052(L).

Fitz-Gerald, J.–Dielectric properties of oxide structures by a laser-based direct-writing method.–D. Young, H.D. Wu, R.C.Y. Auyeung, R. Modi, J. Fitz-Gerald, A. Pique, D.B. Chrisey, P. Atanassova, and T. Kodas; **16**(6), 1720–1725.

Fleming, P.H.–Growth mechanism of superconducting MgB_2 films prepared by various methods.–H.Y. Zhai, H.M. Christen, L. Zhang, M. Paranthaman, C. Cantoni B.C. Sales, P.H. Fleming, D.K. Christen, and D.H. Lowndes; **16**(10), 2759–2762(L).

Flinn, B.D.–Biomimetic model of a sponge-spicular optical fiber—mechanical properties and structure.–M. Sarikaya, H. Fong, N. Sunderland, B.D. Flinn, G. Mayer, A. Mescher, and E. Gaino; **16**(5), 1420–1428.

Foltyn, S.R.–High critical current density $YBa_2Cu_3O_{7-\delta}$ thick films using ion beam assisted deposition MgO bi-axially oriented template layers on nickel-based superalloy substrates.–J.R. Groves, P.N. Arendt, S.R. Foltyn, Q.X. Jia, T.G. Holesinger, H. Kung, E.J. Peterson, R.F. DePaula, P.C. Dowden, L. Stan, and L.A. Emmert; **16**(8), 2175–2178(L).

Fong, H.–Biomimetic model of a sponge-spicular optical fiber—mechanical properties and structure.–M. Sarikaya, H. Fong, N. Sunderland, B.D. Flinn, G. Mayer, A. Mescher, and E. Gaino; **16**(5), 1420–1428.

Fortuna, S.V.–Mechanism of improvement of TiN-coated tool life by nitrogen implantation.–S.J. Bull, Yu.P. Sharkeev, S.V. Fortuna, I.A. Shulepov, and A.J. Perry; **16**(11), 3293–3303.

Fowlkes, J.D.–Laser-induced surface perturbations in silicon.–A.J. Pedraza, S. Jesse, Y.F. Guan, and J.D. Fowlkes; **16**(12), 3599–3608.

Fox, G.R.–Sintering of screen-printed platinum thick films for electrode applications.–J.B. Véchembre and G.R. Fox; **16**(4), 922–931.

Fragalà, M.E.–Formation and characterization of high-density silver nanoparticles embedded in silica thin films by "*in situ*" self-reduction.–G. Compagnini, M.E. Fragalà, L. D'Urso, C. Spinella, and O. Puglisi; **16**(10), 2934–2938.

Fränzel, W.–Determination of the elastic properties of glasses and polymers exploiting the resonant characteristic of depth-sensing indentation tests.–D. Lorenz, W. Fränzel, M. Einax, P. Grau, and G. Berg; **16**(6), 1776–1783.

Frazee, J. Wayne–Processing of mesoporous alumina from a powder precursor.–J. Wayne Frazee and Thomas M. Harris; **16**(11), 3262–3265.

Frigeri, C.–Production and characterization of titanium and iron oxide nano-sized thin films.–E. Comini, G. Sberveglieri, M. Ferroni, V. Guidi, C. Frigeri, and D. Boscarino; **16**(6), 1559–1564.

Fuentes, G.A.–Thermal and structural characterization of the $ZrO_{2-x}(OH)_{2x}$ to ZrO_2 transition.–E. Torres-García, A. Peláiz-Barranco, C. Vázquez-Ramos, and G.A. Fuentes; **16**(8), 2209–2212.

Fujii, Kanenaga–Coordination structures of implanted Fe, Co, and Ni ions in silica glass by x-ray absorption fine structure spectroscopy.–Kohei Fukumi, Akiyoshi Chayahara, Kohei Kadono, Hiroyuki Kageyama, Tomoko Akai, Hiroshi Mizoguchi, Naoyuki Kitamura, Masaki Makihara, Yuji Horino, and Kanenaga Fujii; **16**(1), 155–162.

Fujii, Tatsuo–Low-temperature growth of *c*-axis-oriented Y-type hexagonal ferrite thin films by the polymeric precursor method.–Tatsuo Fujii, Aiko Harano, Makoto Nakanishi, and Jun Takada; **16**(9), 2471–2474(L).

Fujimoto, Toshiyuki–Gas flow effects on the structure and composition of SiN_x/Si/SiN_x films prepared by radio-frequency magnetron sputtering.–Wentao Xu, Boquan Li, Toshiyuki Fujimoto, and Isao Kojima; **16**(1), 308–313.

Fukumi, Kohei–Coordination structures of implanted Fe, Co, and Ni ions in silica glass by x-ray absorption fine structure spectroscopy.–Kohei Fukumi, Akiyoshi Chayahara, Kohei Kadono, Hiroyuki Kageyama, Tomoko Akai, Hiroshi Mizoguchi, Naoyuki Kitamura, Masaki Makihara, Yuji Horino, and Kanenaga Fujii; **16**(1), 155–162.

Fukuyama, Seiji–Embedded-atom-method functions for the body-centered-cubic iron and hydrogen.–Mao Wen, Xue-Jun Xu, Seiji Fukuyama, and Kiyoshi Yokogawa; **16**(12), 3496–3502.

Funakubo, Hiroshi–Ferroelectric property of epitaxial $Bi_4Ti_3O_{12}$ films prepared by metalorganic chemical vapor deposition.–Takayuki Watanabe, Hiroshi Funakubo, and Keisuke Saito; **16**(1), 303–307.

Futakawa, Masatoshi–Identification of the constitutive equation by the indentation technique using plural indenters with different apex angles.–Masatoshi Futakawa, Takashi Wakui, Yuji Tanabe, and Ikuo Ioka; **16**(8), 2283–2292.

Futami, Takatoshi–Deformation-induced surface corrugation of superplastic ceramics.–Hiroyuki Muto, Takatoshi Futami, and Motosugu Sakai; **16**(7), 1879–1882(L).

G

Gaino, E.–Biomimetic model of a sponge-spicular optical fiber—mechanical properties and structure.–M. Sarikaya, H. Fong, N. Sunderland, B.D. Flinn, G. Mayer, A. Mescher, and E. Gaino; **16**(5), 1420–1428.

Galán, L.–X-ray photoelectron spectroscopy of electrodeposited cadmium mercury telluride thin films and their native surface oxides.–J. Ramiro, L. Galán, E. García Camarero, I. Montero, and Y. Laaziz; **16**(7), 1942–1952.

Galassi, C.–Rheological characteristics of slurry controlling the microstructure and the compressive strength behavior of biomimetic hydroxyapatite.–S. Guicciardi, C. Galassi, E. Landi, A. Tampieri, K. Satou, and G. Pezzotti; **16**(1), 163–170.

Gameson, I.–Microstructure of laser-ablated superconducting $La_2CuO_4F_x$ thin films on $SrTiO_3$.–G. Kong, M.O. Jones, J.S. Abell, P.P. Edwards, S.T. Lees, K.E. Gibbons, I. Gameson, and M. Aindow; **16**(11), 3309–3316.

Gan, Leong Ming–Third-order nonlinear optical response in PbS-coated CdS nanocomposites.–Bing Liu, Chwee Har Chew, Leong Ming Gan, Guo Qin Xu, Heping Li, Yee Loy Lam, Chan Hin Kam, and Wen Xiu Que; **16**(6), 1644–1650.

Gao, J.–Excellent buffer layer for growing high-quality Y–Ba–Cu–O thin films.–W.H. Tang, J. Gao, C.X. Liu, and Z.H. Mai; **16**(10), 2864–2868.

Gao, Jianrong–Metastable solidification of NdFeB alloys by drop-tube processing.–Jianrong Gao, Th. Volkmann, and D.M. Herlach; **16**(9), 2562–2567.

Gao, Lian–Effect of α/β phase ratio on microstructure and mechanical properties of silicon nitride ceramics.–Hirokazu Kawaoka, Tomohiko Adachi, Tohru Sekino, Yong-Ho Choa, Lian Gao, and Koichi Niihara; **16**(8), 2264–2270.

Garcia, J.A.–Deep center luminescence versus surface preparation of ZnSe single crystals.–J.A. Garcia, V. Muñoz, C. Martinez-Tomas, and J.J.S. Garitaonandia; **16**(5), 1245–1248(L).

Garcia, M.–Surface effects in field-assisted sintering.–J.R. Groza, M. Garcia, and J.A. Schneider; **16**(1), 286–292.

García, R.–New combustion synthesis technique for the production of $(In_xGa_{1-x})_2O_3$ powders: Hydrazine/metal nitrate method.–R. García, G.A. Hirata, and J. McKittrick; **16**(4), 1059–1065.

García-Serrano, J.–Determination of optical constants of Si/ZnO polycrystalline nanocomposites by spectroscopic ellipsometry.–J. García-Serrano, N. Koshizaki, T. Sasaki, G. Martínez-Montes, and U. Pal; **16**(12), 3554–3559.

Garitaonandia, J.J.S.–Deep center luminescence versus surface preparation of ZnSe single crystals.–J.A. Garcia, V. Muñoz, C. Martinez-Tomas, and J.J.S. Garitaonandia; **16**(5), 1245–1248(L).

Garmestani, H.–Effects of thermal annealing on the texture of $La_{0.67}Sr_{0.33}MnO_3$ thin films.–Lamartine Meda, LaQuita Kennon, Cristiane Bacaltchuk, Hamid Garmestani, and Klaus H. Dahmen; **16**(7), 1887–1889(L).

–Microstructures of $La_{1-x}A_x$(A = Ca or Sr)$MnO_{3-\delta}$ thin films by liquid-delivery metalorganic chemical vapor deposition.–Y. Xin, K. Han, N. Mateeva, H. Garmestani, P.N. Kalu, and K-H. Dahmen; **16**(11), 3073–3083.

Garníca-Romo, M.G.–Structure of heat-treated sol-gel SiO_2 glasses containing silver.–M.G. Garníca-Romo, J. González-Hernández, M.A. Hernández-Landaverde, Y.V. Vorobiev, F. Ruiz, and J.R. Martínez; **16**(7), 2007–2012.

Gasch, Matt J.–Consolidation and crystallization of Si_3N_4/SiC nanocomposites from a poly(urea–silazane) ceramic precursor.–Julin Wan, Matt J. Gasch, and Amiya K. Mukherjee; **16**(11), 3274–3286.

Gautrot, Sébastien–Characterization of bond formation in SiC and Si_3N_4 implanted with Ti, Fe, and Co.–Didier Zanghi, Agnès Traverse, Sébastien Gautrot, and Odile Kaïtasov; **16**(2), 512–523.

Gerberich, W.W.–Substrate effects on indentation plastic zone development in thin soft films.–D.E. Kramer, A.A. Volinsky, N.R. Moody, and W.W. Gerberich; **16**(11), 3150–3157.

Gerberich, William W.–Adhesion of polymer–inorganic interfaces by nanoindentation.–Min Li, C. Barry Carter, Marc A. Hillmyer, and William W. Gerberich; **16**(12), 3378–3388.

–Effect of ion implant dose on the mechanical properties of polyethersulfone films.–Manuel Luis B. Palacio, Yongquiang Wang, and William W. Gerberich; **16**(12), 3628–3635.

Ghica, C.–*In situ* transmission electron microscopy study of the silicidation process in Co thin films on patterned (001) Si substrates.–C. Ghica, L. Nistor, H. Bender, A. Steegen, A. Lauwers, K. Maex, and J. Van Landuyt; **16**(3), 701–708.

Gibala, R.–Microstructural and mechanical characterization of carbon coatings on SiC fibers.–K.L. Kendig, R. Gibala, and D.B. Miracle; **16**(12), 3366–3377.

Gibbons, K.E.–Microstructure of laser-ablated superconducting $La_2CuO_4F_x$ thin films on $SrTiO_3$.–G. Kong, M.O. Jones, J.S. Abell, P.P. Edwards, S.T. Lees, K.E. Gibbons, I. Gameson, and M. Aindow; **16**(11), 3309–3316.

Gibson, J.M.–Observations of structural order in ion-implanted amorphous silicon.–Ju-Yin Cheng, J.M. Gibson, and D.C. Jacobson; **16**(11), 3030–3033(L).

Gidley, David W.–Effect of material properties on integration damage in organosilicate glass films.–E. Todd Ryan, Jeremy Martin, Kurt Junker, Jeff Wetzel, David W. Gidley, and Jianing Sun; **16**(12), 3335–3338(L).

Gilmore, C.M.–Direct writing of polymer thick film resistors using a novel laser transfer technique.–R. Modi, H.D. Wu, R.C.Y. Auyeung, C.M. Gilmore, and D.B. Chrisey; **16**(11), 3214–3222.

Giorgis, F.–X-ray reflectivity spectra of ultrathin films and nanometric multilayers: Experiment and simulation.–E. Bontempi, L.E. Depero, L. Sangaletti, F. Giorgis, and C.F. Pirri; **16**(9), 2556–2561.

Gleiman, Seth–Low–power plasma torch method for the production of crystalline spherical ceramic particles.–Chun-Ku Chen, Seth Gleiman, and Jonathan Phillips; **16**(5), 1256–1265.

Goh, Jae-Mo–Photoluminescence spectra of undoped and Sm^{3+}-doped $BaAl_2S_4$ and $BaAl_2Se_4$ single crystals.–Moon-Seog Jin, Choong-Il Lee, Chang-Sun Yoon, Chang-Dae Kim, Jae-Mo Goh, and Wha-Tek Kim; **16**(5), 1520–1524.

Goldfarb, I.–Surface studies of phase formation in Co–Ge system: Reactive deposition epitaxy versus solid-phase epitaxy.–I. Goldfarb and G.A.D. Briggs; **16**(3), 744–752.

Gong, Dawei–Titanium oxide nanotube arrays prepared by anodic oxidation.–Dawei Gong, Craig A. Grimes, Oomman K. Varghese, R.S. Singh, Wenchong Hu, Zhi Chen, and Elizabeth C. Dickey; **16**(12), 3331–3334(L).

Gong, Jian-Hong–Electron microscopy of high-temperature and high-pressure as-grown diamond crystals.–Long-Wei Yin, Mu-Sen Li, Jian-Jun Cui, Bin Xu, Jian-Hong Gong, Zhao-Yin Hao, and Jiong-Fa Zhang; **16**(11), 3023–3026(L).

Gong, X.–Statistical behavior and misfit stresses in ceramic and metal laminated system.–D. Sherman and X. Gong; **16**(3), 721–727.

González, J.A.–Study of the effects of low-energy electron bombardment during the chemical vapor deposition of diamond.–J.A. González, O.L. Figueroa, B.R. Weiner, and G. Morell; **16**(1), 293–295.

González-Hernández, J.–Structure of heat-treated sol-gel SiO_2 glasses containing silver.–M.G. Garníca-Romo, J. González-Hernández, M.A. Hernández-Landaverde, Y.V. Vorobiev, F. Ruiz, and J.R. Martínez; **16**(7), 2007–2012.

Goodilin, E.A.–Formation of Nd_{1+x} $(Ba_{1-y}Sr_y)_{2-x}$ $Cu_3O_{7\pm\delta}$ solid solutions by crystal pulling.–Xin Yao, E.A. Goodilin, Teruo Izumi, and Yuh Shiohara; **16**(2), 529–533.

Goswami, Jaydeb–Highly (111)-oriented and conformal iridium films by liquid source metalorganic chemical vapor deposition.–Jaydeb Goswami, Chang-Gong Wang, Prashant Majhi, Yong-Wook Shin, and Sandwip K. Dey; **16**(8), 2192–2195(L).

Goto, T.–Effects of Ce filling fraction and Fe content on the thermoelectric properties of Co-rich $Ce_xFe_xCo_{4-x}Sb_{12}$.–Xinfeng Tang, Lidong Chen, Takashi Goto, and Toshio Hirai; **16**(3), 837–843.

–High-temperature thermoelectric properties of *n*-type $Ba_yNi_xCo_{4-x}Sb_{12}$.–X.F. Tang, L.M. Zhang, R.Z. Yuan, L.D. Chen, T. Goto, T. Hirai, J.S. Dyck, W. Chen, and C. Uher; **16**(12), 3343–3346(L).

Goyal, A.–Growth and characterization of conductive $SrRuO_3$ and $LaNiO_3$ multilayers on textured Ni tapes for high-J_c $YBa_2Cu_3O_{7-\delta}$ coated conductors.–T. Aytug, B.W. Kang, C. Cantoni, E.D. Specht, M. Paranthaman, A. Goyal, D.K. Christen, D.T. Verebelyi, J.Z. Wu, R.E. Ericson, C.L. Thomas, C-Y.Yang, and S.E. Babcock; **16**(9), 2661–2669.

Graaf, M.J.M. de–Minima in the strength of MnZn ferrites.–M.A.H. Donners, L.J.M.G. Dortmans, G. de With, and M.J.M. de Graaf; **16**(12), 3575–3582.

Grader, G.S.–Entrapment of organosilicon molecules in nonhydrolytic alumina gels and thermal behavior of the resulting composite.–G.S. Grader, S.A. Melchior, Y. De-Hazan, S. Melamed, and G.E. Shter; **16**(5), 1413–1419.

Graebner, J.E.–Thermal conductivity and thermal diffusivity of selected oxide single crystals.–A. Stanimirovic, N.M. Balzaretti, A. Feldman, and J.E. Graebner; **16**(3), 678–682.

Graeve, O.A.–Modeling of wave configuration during electrically ignited combustion synthesis.–O.A. Graeve, E.M. Carrillo-Heian, A. Feng, and Z.A. Munir; **16**(1), 93–100.

Grau, P.–Determination of the elastic properties of glasses and polymers exploiting the resonant characteristic of depth-sensing indentation tests.–D. Lorenz, W. Fränzel, M. Einax, P. Grau, and G. Berg; **16**(6), 1776–1783.

Grillo, Stefano E.–Thermal stability of carbon nitride thin films.–Niklas Hellgren, Nian Lin, Esteban Broitman, Virginie Serin, Stefano E. Grillo, Ray Twesten, Ivan Petrov, Christian Colliex, Lars Hultman, and Jan-Eric Sundgren; **16**(11), 3188–3201.

Grimes, Craig A.–Metal–oxide films with magnetically-modulated nanoporous architectures.–Craig A. Grimes, R. Suresh Singh, Elizabeth C. Dickey, and Oomman K. Varghese; **16**(6), 1686–1693.

–Titanium oxide nanotube arrays prepared by anodic oxidation.–Dawei Gong, Craig A. Grimes, Oomman K. Varghese, R.S. Singh, Wenchong Hu, Zhi Chen, and Elizabeth C. Dickey; **16**(12), 3331–3334(L).

Grivickas, Paulius–Carrier diffusion characterization in epitaxial 4H–SiC.–Paulius Grivickas, Jan Linnros, and Vytautas Grivickas; **16**(2), 524–528.

Grivickas, Vytautas–Carrier diffusion characterization in epitaxial 4H–SiC.–Paulius Grivickas, Jan Linnros, and Vytautas Grivickas; **16**(2), 524–528.

Grohe, B.–Additive controlled crystallization of barium titanate powders and their application for thin-film ceramic production: Part I. Powder Synthesis.–B. Grohe, G. Miehe, and G. Wegner; **16**(7), 1901–1910.

–Additive controlled crystallization of barium titanate powders and their application for thin-film ceramic production: Part II. From nano-sized powders to ceramic thin films.–B. Grohe, G. Miehe, and G. Wegner; **16**(7), 1911–1915.

Gronsky, R.–Epitaxial growth of skutterudite ($CoSb_3$) thin films on (001) InSb by pulsed laser deposition.–J.C. Caylor, M.S. Sander, A.M. Stacy, J.S. Harper, R. Gronsky, and T. Sands; **16**(9), 2467–2470(L).

Gross, M.–Characterization of GaN grown on sapphire by laser-induced molecular beam epitaxy.–H. Zhou, A. Rühm, N.Y. Jin-Phillipp, F. Phillipp, M. Gross, and H. Schröder; **16**(1), 261–267.

–Synthesis and processing of nanocrystalline Ag–Fe–Ni for low thermal expansion–high conductivity thermal management applications.–J. Stolk, M. Gross, D. Stolk, and A. Manthiram; **16**(2), 340–343(L).

Gross, Todd S.–Scanning probe microscopy generated out-of-plane deformation maps exhibiting heterogeneous nanoscale deformation resulting from thermal cycling of Cu–polyimide damascene interconnects.–Todd S. Gross, Nazri bin Kamsah, and I. Tsukrov; **16**(12), 3560–3566.

Groves, J.R.–High critical current density $YBa_2Cu_3O_{7-\delta}$ thick films using ion beam assisted deposition MgO bi-axially oriented template layers on nickel-based superalloy substrates.–J.R. Groves, P.N. Arendt, S.R. Foltyn, Q.X. Jia, T.G. Holesinger, H. Kung, E.J. Peterson, R.F. DePaula, P.C. Dowden, L. Stan, L.A. Emmert; **16**(8), 2175–2178(L).

Groza, J.R.–Surface effects in field-assisted sintering.–J.R. Groza, M. Garcia, and J.A. Schneider; **16**(1), 286–292.

–Phenomenological description of grain growth stagnation for nanocrystalline films and powders.–Rand Dannenberg, Eric Stach, and Joanna R. Groza; **16**(4), 1090–1095.

Gu, Mingyuan–Joining characteristics of oxidized SiC particles reinforced Al–Mg matrix composite prepared by reaction infiltration processing.–Zhongliang Shi, Shijiro Ochiai, Masaki Hojo, Jaechul Lee, Mingyuan Gu, and Hoin Lee; **16**(2), 400–406.

Guan, Y.F.–Laser-induced surface perturbations in silicon.–A.J. Pedraza, S. Jesse, Y.F. Guan, and J.D. Fowlkes; **16**(12), 3599–3608.

Guan, Zi-sheng–Photocatalytic activity of TiO_2 prepared at low temperature by a photo-assisted sol-gel method.–Zi-sheng Guan, Xin-tong Zhang, Ying Ma, Ya-an Cao, and Jian-nian Yao; **16**(4), 907–909(L).

–Effects of zinc(II) and iron(III) doping of titania films on their photoreactivity to decompose rhodamine B.–Ying Ma, Xin-tong Zhang, Zi-sheng Guan, Ya-an Cao, and Jian-nian Yao; **16**(10), 2928–2933.

Guanhu, He–The healing of quenched crack in 1045 steel under electropulsing.–Zhou Yizhou, Zeng You, He Guanhu, and Zhou Benlian; **16**(1), 17–19(L).

Guay, D.–Study of the activation process of Mg-based hydrogen storage materials modified by graphite and other carbonaceous compounds.–S. Bouaricha, J-P. Dodelet, D. Guay, J. Huot, and R. Schulz; **16**(10), 2893–2905.

Gui, Jianian–On some discrepancies in the literature about the formation of icosahedral quasi-crystal in Al–Cu–Fe alloys.–Jianian Gui, Jianbo Wang, Renhui Wang, Dahai Wang, Jing Liu, and Fangyu Chen; **16**(4), 1037–1046.

Guiberteau, Fernando–Contact fracture of brittle bilayer coatings on soft substrates.–Pedro Miranda, Antonia Pajares, Fernando Guiberteau, Francisco L. Cumbrera, and Brian R. Lawn; **16**(1), 115–126.

–Controlled preparation and characterization of multilayer sol-gel zirconia dip-coatings.–Ricardo Caruso, Antonio Díaz-Parralejo, Pedro Miranda, and Fernando Guiberteau; **16**(8), 2391–2398.

Guicciardi, S.–Rheological characteristics of slurry controlling the microstructure and the compressive strength behavior of biomimetic hydroxyapatite.–S. Guicciardi, C. Galassi, E. Landi, A. Tampieri, K. Satou, and G. Pezzotti; **16**(1), 163–170.

Guidi, V.–Production and characterization of titanium and iron oxide nano-sized thin films.–E. Comini, G. Sberveglieri, M. Ferroni, V. Guidi, C. Frigeri, and D. Boscarino; **16**(6), 1559–1564.

Guilemany, J.M.–Structural characterization of laser-treated Cr_3C_2–NiCr coatings.–P. Serra, J.M. Miguel, J.L. Morenza, and J.M. Guilemany; **16**(12), 3416–3422.

Gulliver, Eric–Mechanochemical-hydrothermal preparation of crystalline hydroxyapatite powders at room temperature.–Pavel Shuk, Wojciech L. Suchanek, Tian Hao, Eric Gulliver, Richard E. Riman, Mamoru Senna, Kevor S. TenHuisen, and Victor F. Janas; **16**(5), 1231–1234(L).

Guo, J.Q.–Single-crystal growth of the Al–Cu–Fe icosahedral quasicrystal from the ternary melt.–J.Q. Guo and A.P. Tsai; **16**(11), 3038–3041(L).

Guo, Jingkun–Formation of Al_2O_3 grains with different sizes and morphologies during the pulse electric current sintering process.–S.W. Wang, L.D. Chen, T. Hirai, and Jingkun Guo; **16**(12), 3514–3517.

Guo, Lin–Synthesis and characterization of antimony oxide nanoparticles.–Zaoli Zhang, Lin Guo, and Wendong Wang; **16**(3), 803–805.

Guo, Shao-Ling–Low-temperature fabrication of pyroelectric $Ba_{0.8}Sr_{0.2}TiO_3$ thin films by a sol-gel process.–Jian-Gong Cheng, Jun Tang, Shao-Ling Guo, and Jun-Hao Chu; **16**(3), 778–783.

Guo, Shuqi–Dependence of fracture stress on applied stress rate in a Yb_2O_3–SiO_2-doped hot-pressed silicon nitride ceramic.–Shuqi Guo, Naoto Hirosaki, Yoshinobu Yamamoto, Toshiyuki Nishimura, and Mamoru Mitomo; **16**(11), 3254–3261.

Guo, W.H.–Crystallization kinetics of amorphous nanostructured $Pd_{40.5}Ni_{40.5}P_{19}$ alloys.–H.W. Ngai, C.C. Leung, W.H. Guo, and H.W. Kui; **16**(3), 797–802.

Gustafson, D.E.–Formation of $NdBa_2Cu_3O_{7-\delta}$ amorphous phase by combining aero-acoustic levitation and splat quenching.–K. Nagashio, W.H. Hofmeister, D.E. Gustafson, A. Altgilbers, R.J. Bayuzick, and K. Kuribayashi; **16**(1), 138–145.

H

Haas, Dylan E.–Nondestructive measurement of striation defect spacing using laser diffraction.–Dylan E. Haas, Dunbar P. Birnie, III; **16**(12), 3355–3360.

Haeni, J.H.–Transmission electron microscopy study of $n = 1$–5 $Sr_{n+1}Ti_nO_{3n+1}$ epitaxial thin films.–W. Tian, X.Q. Pan, J.H. Haeni, and D.G. Schlom; **16**(7), 2013–2026.

Hall, P.J.–Thermal analysis investigation of hydriding properties of nanocrystalline Mg–Ni- and Mg–Fe-based alloys prepared by high-energy ball milling.–L.E.A. Berlouis, E. Cabrera, E. Hall-Barientos, P.J. Hall, S.B. Dodd, S. Morris, and M.A. Imam; **16**(1), 45–57.

Hall-Barientos, E.–Thermal analysis investigation of hydriding properties of nanocrystalline Mg–Ni- and Mg–Fe-based alloys prepared by high-energy ball milling.–L.E.A. Berlouis, E. Cabrera, E. Hall-Barientos, P.J. Hall, S.B. Dodd, S. Morris, and M.A. Imam; **16**(1), 45–57.

Han, Bao Shan–Plate domain structure of sintered NdFeB magnets and dependence on compacting mode.–Zhen Rong Zhang, Bao Shan Han, Ye Qing He, and Shou Zeng Zhou; **16**(10), 2992–2995.

Han, Bin–Metalorganic chemical vapor deposition of titanium oxide for microelectronics applications.–Kanchana Vydianathan, Guillermo Nuesca, Gregory Peterson, Eric T. Eisenbraun, Alain E. Kaloyeros, John J. Sullivan, and Bin Han; **16**(6), 1838–1849.

Han, Jiaping–Densification and grain growth of Al-doped ZnO.–Jiaping Han, P.Q. Mantas, and A.M.R. Senos; **16**(2), 459–468.

Han, K.–Synthesis of silicon microwire.–J.J. Petrovic, R.C. Hoover, R.D. Field, and K. Han; **16**(10), 2777–2779(L).

–Microstructures of $La_{1-x}A_x$(A = Ca or Sr)$MnO_{3-\delta}$ thin films by liquid-delivery metalorganic chemical vapor deposition.–Y. Xin, K. Han, N. Mateeva, H. Garmestani, P.N. Kalu, and K-H. Dahmen; **16**(11), 3073–3083.

Han, X.Q.–Preparation and characterization of nanocrystalline potassium lithium niobate powders and films.–H.X. Zhang, C.H. Kam, Y. Zhou, X.Q. Han, S.D. Cheng, C.Y. Chan, and Y.L. Lam; **16**(12), 3609–3613.

Han, Young Ki–Metalorganic chemical vapor deposition of very thin $Pb(Zr,Ti)O_3$ thin films at low temperatures for high-density ferroelectric memory applications.–Hye Ryoung Kim, Seehwa Jeong, Chung Bae Jeon, Oh Seong Kwon, Cheol Seong Hwang, Young Ki Han, Doo Young Yang, and Ki Young Oh; **16**(12), 3583–3591.

Haneda, Hajime–Oxygen self-diffusion in cerium oxide doped with Nd.–Michiyo Kamiya, Eriko Shimada, Yasuro Ikuma, Manabu Komatsu, Hajime Haneda, Soichiro Sameshima, and Yoshihiro Hirata; **16**(1), 179–184.

–Effect of the calcium dopant on oxide ion diffusion in yttria ceramics.–Noriko Saito, Hajime Haneda, Isao Sakaguchi, and Takayasu Ikegami; **16**(8), 2362–2368.

Hao, J.H.–Microstructure and misfit relaxation in $SrTiO_3/SrRuO_3$ bilayer films on $LaAlO_3$(100) substrates.–J.S. Wu, C.L. Jia, K. Urban, J.H. Hao, and X.X. Xi; **16**(12), 3443–3450.

Hao, Tian–Mechanochemical-hydrothermal preparation of crystalline hydroxyapatite powders at room temperature.–Pavel Shuk, Wojciech L. Suchanek, Tian Hao, Eric Gulliver, Richard E. Riman, Mamoru Senna, Kevor S. TenHuisen, and Victor F. Janas; **16**(5), 1231–1234(L).

Hao, Zhao-Yin–Electron microscopy of high-temperature and high-pressure as-grown diamond crystals.–Long-Wei Yin, Mu-Sen Li, Jian-Jun Cui, Bin Xu, Jian-Hong Gong, Zhao-Yin Hao, and Jiong-Fa Zhang; **16**(11), 3023–3026(L).

Harano, Aiko–Low-temperature growth of *c*-axis-oriented Y-type hexagonal ferrite thin films by the polymeric precursor method.–Tatsuo Fujii, Aiko Harano, Makoto Nakanishi, and Jun Takada; **16**(9), 2471–2474(L).

Hari Babu, N.–Growth of melt-textured Nd-123 by hot seeding under reduced oxygen partial pressure.–M. Kambara, N. Hari Babu, Y.H. Shi, and D.A. Cardwell; **16**(4), 1163–1170.

Hariharaputhiran, M.–Chemical–mechanical polishing of copper and tantalum with silica abrasives.–Y. Li, M. Hariharaputhiran, and S.V. Babu; **16**(4), 1066–1073.

Harmer, Martin P.–Improved tensile creep properties of yttrium- and lanthanum-doped alumina: a solid solution effect.–Junghyun Cho, Chong Min Wang, Helen M. Chan, J.M. Rickman, Martin P. Harmer; **16**(2), 425–429.

–Electron backscatter diffraction analysis of $Pb(Mg_{1/3}Nb_{2/3})O_3$–35mol%$PbTiO_3$ single crystals grown by seeded polycrystal conversion.–Ajmal Khan, Derrick T. Carpenter, Adam M. Scotch, Helen M. Chan, Martin P. Harmer; **16**(3), 694–700.

Harper, J.S.–Epitaxial growth of skutterudite ($CoSb_3$) thin films on (001) InSb by pulsed laser deposition.–J.C. Caylor, M.S. Sander, A.M. Stacy, J.S. Harper, R. Gronsky, and T. Sands; **16**(9), 2467–2470(L).

Harris, Thomas M.–Processing of mesoporous alumina from a powder precursor.–J. Wayne Frazee and Thomas M. Harris; **16**(11), 3262–3265.

Hartner, W.–Phase formation and crystal growth of Sr–Bi–Ta–O thin films grown by metalorganic chemical vapor deposition.–H. Bachhofer, H. von Philipsborn, W. Hartner, C. Dehm, B. Jobst, A. Kiendl, H. Schroeder, and R. Waser; **16**(10), 2966–2973.

Hartridge, A.–Synthesis and characterization of partially and fully stabilized zirconia fibers made from an inorganic precursor.–A. Hartridge, M.D. Taylor, and A.K. Bhattacharya; **16**(8), 2384–2390.

Hashimoto, Y.–Preparation of Cu(In,Ga)Se_2 thin films at low substrate temperatures.–S. Nishiwaki, T. Satoh, Y. Hashimoto, T. Negami, and T. Wada; **16**(2), 394–399.

Hass, Derek D.–Synthesis of open-cell metal foams by templated directed vapor deposition.–Douglas T. Queheillalt, Derek D. Hass, David J. Sypeck, and Haydn N.G. Wadley; **16**(4), 1028–1036.

Hassanien, A.S.–Optical and electrical properties of $Ge_{10+x}Se_{40}Te_{50-x}$ thin film.–S.A. Fayek, M. El-Ocker, and A.S. Hassanien; **16**(6), 1549–1553.

Hatanaka, Yoshinori–Comparison of hydrophilic properties of amorphous TiO_x films obtained by radio frequency sputtering and plasma-enhanced chemical vapor deposition.–Masatoshi Nakamura, Toru Aoki, Yoshinori Hatanaka, Dariusz Korzec, and Jurgen Engemann; **16**(2), 621–626.

Hatton, Benjamin D.–Dense, bubble-free ceramic deposits from aqueous suspensions by electrophoretic deposition.–Tetsuo Uchikoshi, Kiyoshi Ozawa, Benjamin D. Hatton, and Yoshio Sakka; **16**(2), 321–324(L).

Hawley, M.E.–Transmission electron microscopy study of (103)-oriented epitaxial $SrBi_2Nb_2O_9$ films grown on (111) $SrTiO_3$ and (111) $SrRuO_3$/(111) $SrTiO_3$.–M.A. Zurbuchen, J. Lettieri, Y. Jia, D.G. Schlom, S.K. Streiffer, and M.E. Hawley; **16**(2), 489–502.

Hay, J.L.–Small correction required when applying the Hertzian contact model to instrumented indentation data.–J.L. Hay and P.J. Wolff; **16**(5), 1280–1286.

Hay, Jack C.–Evaluation of the modified edge lift-off test for adhesion characterization in microelectronic multifilm applications.–Jack C. Hay, Eric G. Liniger, and Xiao Hu Liu; **16**(2), 385–393.

Hayashi, Kentaro–Novel hexagonal structure and ultrahigh strength of magnesium solid solution in the Mg–Zn–Y system.–Akihisa Inoue, Yoshihito Kawamura, Mitsuhide Matsushita, Kentaro Hayashi, and Junichi Koike; **16**(7), 1894–1900.

He, Duanwei–Effects of pressure on the solidification of Al–Mn alloy.–Duanwei He, M. He, C.S. Kiminami, F.X. Zhang, Y.F. Xu, W.K. Wang, and K.H. Kuo; **16**(4), 910–913(L).

He, Hongliang–Cubic silicon nitride embedded in amorphous silicon dioxide.–Ming Zhang, Hongliang He, F.F. Xu, T. Sekine, T. Kobayashi, and Y. Bando; **16**(8), 2179–2181(L).

He, Jianhong–Thermal stability of nanocrystalline WC–Co powder synthesized by using mechanical milling at low temperature.–Jianhong He, Leoanardo Ajdelsztajn, and Enrique J. Lavernia; **16**(2), 478–488.

–Development of nanocrystalline structure during cryomilling of Inconel 625.–Jianhong He and Enrique J. Lavernia; **16**(9), 2724–2732.

He, Jiawen–Elastic constants of polycrystalline Al and TiN calculated by an *ab initio* method within the local-density approximation.–Ming Zhang, Jiang Shen, and Jiawen He; **16**(8), 2293–2297.

–Fretting wear rate of sulphur deficient MoS_x coatings based on dissipated energy.–Xiaoling Zhang, W. Lauwerens, L. Stals, Jiawen He, and J-P. Celis; **16**(12), 3567–3574.

He, L.L.–Metal/ceramic interface in an *in situ* synthesized Ti/TiC_P composite coating by laser processing.–R. Yu, S. Zhang, L.L. He, W.T. Wu, and H.Q. Ye; **16**(1), 9–12(L).

–Shear-activated indentation crack in GaAs single crystal.–Z.C. Li, L. Liu, L.L. He, Y.B. Xu, and X. Wu; **16**(10), 2845–2849.

He, M.–Effects of pressure on the solidification of Al–Mn alloy.–Duanwei He, M. He, C.S. Kiminami, F.X. Zhang, Y.F. Xu, W.K. Wang, and K.H. Kuo; **16**(4), 910–913(L).

He, M.Y.–Model for the robust mechanical behavior of nacre.–A.G. Evans, Z. Suo, R.Z. Wang, I.A. Aksay, M.Y. He, and J.W. Hutchinson; **16**(9), 2475–2484.

He, Rongrui–Novel synthesis of AlN nanowires with controlled diameters.–Jun Liu, X. Zhang, Yingjiu Zhang, Rongrui He and Jing Zhu; **16**(11), 3133–3138.

He, Tianbai–Direct measurement of plowing friction and wear of a polymer thin film using the atomic force microscope.–Binyang Du, Mark R. VanLandingham, Qingling Zhang, and Tianbai He; **16**(5), 1487–1492.

He, Yanyan–Synthesis of $Ba_2Ti_9O_{20}$ via ethylenediaminetetraacetic acid precursor.–Yebin Xu, Yanyan He, and Liangbin Wang; **16**(4), 1195–1199.

He, Ye Qing–Plate domain structure of sintered NdFeB magnets and dependence on compacting mode.–Zhen Rong Zhang, Bao Shan Han, Ye Qing He, and Shou Zeng Zhou; **16**(10), 2992–2995.

Heberlein, Joachim V.–Chemical vapor deposition of an aluminum nitride–diamond composite in a triple torch plasma reactor.–Marcus Asmann, Robert F. Cook, Joachim V. Heberlein, and Emil Pfender; **16**(2), 469–477.

Helean, K.B.–Thermochemistry of rare-earth orthophosphates.–S.V. Ushakov, K.B. Helean, A. Navrotsky, and L.A. Boatner; **16**(9), 2623–2633.

–Enthalpies of formation of lanthanide oxyapatite phases.–A.S. Risbud, K.B. Helean, M.C. Wilding, P. Lu, and A. Navrotsky; **16**(10), 2780–2783(L).

Hellgren, Niklas–Thermal stability of carbon nitride thin films.–Niklas Hellgren, Nian Lin, Esteban Broitman, Virginie Serin, Stefano E. Grillo, Ray Twesten, Ivan Petrov, Christian Colliex, Lars Hultman, and Jan-Eric Sundgren; **16**(11), 3188–3201.

Heo, Jong–Enhancement of the 1.31-μm emission properties of Dy^{3+}-doped Ge–Ga–S glasses with the addition of alkali halides.–Yong Beom Shin, Jong Heo, and Hyoun Soo Kim; **16**(5), 1318–1324.

Herlach, D.M.–Metastable solidification of NdFeB alloys by drop-tube processing.–Jianrong Gao, Th. Volkmann, and D.M. Herlach; **16**(9), 2562–2567.

Hernández-Landaverde, M.A.–Structure of heat-treated sol-gel SiO_2 glasses containing silver.–M.G. Garníca-Romo, J. González-Hernández, M.A. Hernández-Landaverde, Y.V. Vorobiev, F. Ruiz, and J.R. Martínez; **16**(7), 2007–2012.

Herrero, Carlos P.–Quantum atomistic simulations of silicon and germanium.–Carlos P. Herrero; **16**(9), 2505–2512.

Hetzer, M.–Growth study of epitaxial $Fe_xZn_{1-x}F_2$ thin films.–J. McChesney, M. Hetzer, H. Shi, T. Charlton, and D. Lederman; **16**(6), 1769–1775.

Hidalgo, A.–Raman spectroscopic determination of phase evolutions in $LiAl_xCo_{1-x}O_2$ battery materials.–P.S. Dobal, R.S. Katiyar, M.S. Tomar, and A. Hidalgo; **16**(1), 1–4(L).

Higashi, Iwami–Atomic structure of YB_{56} studied by digital high-resolution electron microscopy and electron diffraction.–Takeo Oku, Jan-Olov Bovin, Iwami Higashi, Takaho Tanaka, and Yoshio Ishizawa; **16**(1), 101–107.

Higuchi, Atsushi–Single-layer submicron-thick $BaTiO_3$ coatings from poly(vinylpyrrolidone)-containing sols: Gel-to-ceramic film conversion, densification, and dielectric properties.–Hiromitsu Kozuka and Atsushi Higuchi; **16**(11), 3116–3123.

Hilborn, J.G.–Gradient porosity poly(dicyclopentadiene).–A. Della Martina and J.G. Hilborn; **16**(7), 2045–2052.

Hillmyer, Marc A.–Adhesion of polymer–inorganic interfaces by nanoindentation.–Min Li, C. Barry Carter, Marc A. Hillmyer, and William W. Gerberich; **16**(12), 3378–3388.

Hirai, T.–Effects of Ce filling fraction and Fe content on the thermoelectric properties of Co-rich $Ce_xFe_xCo_{4-x}Sb_{12}$.–Xinfeng Tang, Lidong Chen, Takashi Goto, and Toshio Hirai; **16**(3), 837–843.

–High-temperature thermoelectric properties of *n*-type $Ba_yNi_xCo_{4-x}Sb_{12}$.–X.F. Tang, L.M. Zhang, R.Z. Yuan, L.D. Chen, T. Goto, T. Hirai, J.S. Dyck, W. Chen, and C. Uher; **16**(12), 3343–3346(L).

–Formation of Al_2O_3 grains with different sizes and morphologies during the pulse electric current sintering process.–S.W. Wang, L.D. Chen, T. Hirai, and Jingkun Guo; **16**(12), 3514–3517.

Hiramatsu, Hironao–Low-temperature crystallization induced by excimer laser irradiation of $SrBi_2Ta_2O_9$ films.–Kwang Soo Seol, Hironao Hiramatsu, Yoshimichi Ohki, In-Hoon Choi, and Yong-Tea Kim; **16**(7), 1883–1886(L).

Hirano, Masahiro–Modification of sol–gel-derived amorphous Al_2O_3 thin films by F_2 excimer laser irradiation at ambient temperature.–Satoshi Takeda, Yoshiaki Ikuta, Masahiro Hirano, and Hideo Hosono; **16**(4), 1003–1009.

Hirano, Shin-ichi–Processing of highly oriented lithium niobate films through chemical solution deposition.–Satomi Ono and Shin-ichi Hirano; **16**(4), 1155–1162.

Hirao, K.–Relaxation of ultraviolet-radiation-induced structure and long-lasting phosphorescence in Eu^{2+}-doped strontium aluminosilicate glasses.–Jianrong Qiu, Y. Shimizugawa, K. Kojima, K. Tanaka, K. Hirao; **16**(1), 88–92.

Hirata, G.A.–New combustion synthesis technique for the production of $(In_xGa_{1-x})_2O_3$ powders: Hydrazine/metal nitrate method.–R. García, G.A. Hirata, and J. McKittrick; **16**(4), 1059–1065.

Hirata, Yoshihiro–Oxygen self-diffusion in cerium oxide doped with Nd.–Michiyo Kamiya, Eriko Shimada, Yasuro Ikuma, Manabu Komatsu, Hajime Haneda, Soichiro Sameshima, and Yoshihiro Hirata; **16**(1), 179–184.

Hirayama, Tsukasa–Influence of antiphase boundaries on critical current densities in $YBa_2Cu_3O_{7-x}$ single crystals.–Junko Shibata, Akihiro Oka, Teruo Izumi, Yuh Shiohara, Tsukasa Hirayama, and Yuichi Ikuhara; **16**(7), 1935–1941.

Hirosaki, Naoto–Dependence of fracture stress on applied stress rate in a Yb_2O_3–SiO_2-doped hot-pressed silicon nitride ceramic.–Shuqi Guo, Naoto Hirosaki, Yoshinobu Yamamoto, Toshiyuki Nishimura, and Mamoru Mitomo; **16**(11), 3254–3261.

Hirose, Yoichi–Misting-free diamond surface created by sheet electron beam irradiation.–Kazuya Oguri, Nobuhiro Iwataka, Akira Tonegawa, Yoichi Hirose, Kazuo Takayama, and Yoshitake Nishi; **16**(2), 553–557.

Hishiyama, Y.–Carbonization behavior of polyimide film containing iron complex in relation to magnetic properties.–Y. Kaburagi, T. Toriyama, A. Yoshida, H. Wakabayashi, Y. Hishiyama, and M. Inagaki; **16**(2), 352–365.

Hiura, Hidefumi–Generation of circular and hexagonal microholes in a graphite surface.–Hidefumi Hiura; **16**(5), 1287–1292.

Hoelzer, D.T.–Templated growth of a complex nitride island dispersion through an internal nitridation reaction.–M.P. Brady, D.T. Hoelzer, E.A. Payzant, P.F. Tortorelli, J.A. Horton, I.M. Anderson, L.R. Walker, and S.K. Wrobel; **16**(10), 2784–2787(L).

Hoffman, R.A.–Effect of process variables on the structure, residual stress, and hardness of sputtered nanocrystalline nickel films.–R. Mitra, R.A. Hoffman, A. Madan, and J.R. Weertman; **16**(4), 1010–1027.

–Effect of annealing on microstructure, residual stress, and hardness of Al–Ti multilayered films.–R. Mitra, A. Madan, R.A. Hoffman, W-A. Chiou, and J.R. Weertman; **16**(7), 2064–2076.

Hofmeister, W.H.–Formation of $NdBa_2Cu_3O_{7-\delta}$ amorphous phase by combining aero-acoustic levitation and splat quenching.–K. Nagashio, W.H. Hofmeister, D.E. Gustafson, A. Altgilbers, R.J. Bayuzick, and K. Kuribayashi; **16**(1), 138–145.

Högberg, H.–Deposition of epitaxial transition metal carbide films and superlattices by simultaneous direct current metal magnetron sputtering and C_{60} evaporation.–H. Högberg, J. Birch, M.P. Johansson, L. Hultman, and U. Jansson; **16**(3), 633–643.

–Growth, structure, and mechanical properties of transition metal carbide superlattices.–H. Högberg, J. Birch, M. Odén, J-O. Malm, L. Hultman, and U. Jansson; **16**(5), 1301–1310.

Hohlfelder, Robert J.–Adhesion of benzocyclobutene-passivated silicon in epoxy layered structures.–Robert J. Hohlfelder, Daniel A. Maidenberg, Reinhold H. Dauskardt, Yueguang Wei, and John W. Hutchinson; **16**(1), 243–255.

Hojo, Masaki–Joining characteristics of oxidized SiC particles reinforced Al–Mg matrix composite prepared by reaction infiltration processing.–Zhongliang Shi, Shijiro Ochiai, Masaki Hojo, Jaechul Lee, Mingyuan Gu, and Hoin Lee; **16**(2), 400–406.

Holc, Janez–Subsolidus phase relations in the La_2O_3–Fe_2O_3–Al_2O_3 system.–Danjela Kuščer, Slavko Bernik, Marko Hrovat, and Janez Holc; **16**(3), 822–827.

Holesinger, T.G.–High critical current density $YBa_2Cu_3O_{7-\delta}$ thick films using ion beam assisted deposition MgO bi-axially oriented template layers on nickel-based superalloy substrates.–J.R. Groves, P.N. Arendt, S.R. Foltyn, Q.X. Jia, T.G. Holesinger, H. Kung, E.J. Peterson, R.F. DePaula, P.C. Dowden, L. Stan, and L.A. Emmert; **16**(8), 2175–2178(L).

Hon, Min-Hsiung–Formation of intermetallic compounds at eutectic Sn–Zn–Al solder/Cu interface.–Shan-Pu Yu, Moo-Chin Wang, and Min-Hsiung Hon; **16**(1), 76–82.

Honda, S.–Nanocrystals in crystalline silicon: Void formation and hollow particles.–A. Meldrum, S. Honda, C.W. White, R.A. Zuhr, and L.A. Boatner; **16**(9), 2670–2679.

Hong, Kug Sun–Microwave dielectric properties of $(1 - x)Cu_3Nb_2O_8$–$xZn_3Nb_2O_8$ ceramics.–Dong-Wan Kim, In-Tae Kim, Byungwoo Park, Kug Sun Hong, and Jong-Hee Kim; **16**(5), 1465–1470.

Hong, S.I.–Superplasticicity of Cu–16 at.% Ag microcomposites.–S.I. Hong and H.J. Kwon; **16**(6), 1822–1828.

Hong, Soon H.–Analysis and modeling of residual stress in diamond thin film deposited by the hot-filament chemical vapor deposition process.–Seung I. Cha and Soon H. Hong; **16**(7), 1953–1959.

Hong, Sun Ig–Effects of strain hardenability and strain-rate sensitivity on the plastic flow and deformation homogeneity during equal channel angular pressing.–Hyoung Seop Kim, Sun Ig Hong, and Min Hong Seo; **16**(3), 856–864.

Hoover, R.C.–Synthesis of silicon microwire.–J.J. Petrovic, R.C. Hoover, R.D. Field, and K. Han; **16**(10), 2777–2779(L).

Horino, Yuji–Coordination structures of implanted Fe, Co, and Ni ions in silica glass by x-ray absorption fine structure spectroscopy.–Kohei Fukumi, Akiyoshi Chayahara, Kohei Kadono, Hiroyuki Kageyama, Tomoko Akai, Hiroshi Mizoguchi, Naoyuki Kitamura, Masaki Makihara, Yuji Horino, and Kanenaga Fujii; **16**(1), 155–162.

Horita, Zenji–Grain boundary structure in Al–Mg and Al–Mg–Sc alloys after equal-channel angular pressing.–Keiichiro Oh-ishi, Zenji Horita, David J. Smith, and Terence G. Langdon; **16**(2), 583–589.

Horton, J.A.–Templated growth of a complex nitride island dispersion through an internal nitridation reaction.–M.P. Brady, D.T. Hoelzer, E.A. Payzant, P.F. Tortorelli, J.A. Horton, I.M. Anderson, L.R. Walker, and S.K. Wrobel; **16**(10), 2784–2787(L).

Hoshi, Saburo–Preferential growth mechanism of $REBa_2Cu_3O_y$ (RE = Y, Nd) crystal on MgO substrate by liquid phase epitaxy.–Katsumi Nomura, Saburo Hoshi, Xin Yao, Kazuomi Kakimoto, Yuichi Nakamura, Teruo Izumi, and Yuh Shiohara; **16**(4), 979–989.

–Initial growth mechanism of $YBa_2Cu_3O_y$ crystal on MgO substrate by liquid-phase epitaxy.–Katsumi Nomura, Saburo Hoshi, Yuichi Nakamura, Teruo Izumi, and Yuh Shiohara; **16**(10), 2947–2958.

Hosono, Hideo–Modification of sol–gel-derived amorphous Al_2O_3 thin films by F_2 excimer laser irradiation at ambient temperature.–Satoshi Takeda, Yoshiaki Ikuta, Masahiro Hirano, and Hideo Hosono; **16**(4), 1003–1009.

Hou, Pengxiang–Purification of single-walled carbon nanotubes synthesized by the hydrogen arc-discharge method.–Pengxiang Hou, Chang Liu, Yu Tong, Shitao Xu, Min Liu, and Huiming Cheng; **16**(9), 2526–2529.

Houck, David L.–Solid-phase synthesis of cupric tungstate.–Leonid P. Dorfman, David L. Houck, Michael J. Scheithauer, Jeffrey N. Dann, and Harry O. Fassett; **16**(4), 1096–1102.

Hrovat, Marko–Subsolidus phase relations in the La_2O_3–Fe_2O_3–Al_2O_3 system.–Danjela Kuščer, Slavko Bernik, Marko Hrovat, and Janez Holc; **16**(3), 822–827.

Hsia, K.J.–Piezoelectric actuation of crack growth along polymer–metal interfaces in adhesive bonds.–Tianbao Du, Ming Liu, Steve Seghi, K.J. Hsia, J. Economy, and J.K. Shang; **16**(10), 2885–2892.

Hu, Hiu–Refractive index profile and attenuation measurement in $KTiOPO_4$ waveguide by megaelectronvolt He ions.–Ke-Ming Wang, Hiu Hu, Fei Lu, Feng Chen, Bo-Rong Shi, Yao-Gang Liu, Ding-Yu Shen, and Xie-Mei Wang; **16**(1), 276–279.

Hu, J.Q.–Preparation and phase control of nanocrystalline silver indium sulfides via a hydrothermal route.–J.Q. Hu, B. Deng, K.B. Tang, C.R. Wang, and Y.T. Qian; **16**(12), 3411–3415.

Hu, Wenchong–Titanium oxide nanotube arrays prepared by anodic oxidation.–Dawei Gong, Craig A. Grimes, Oomman K. Varghese, R.S. Singh, Wenchong Hu, Zhi Chen, and Elizabeth C. Dickey; **16**(12), 3331–3334(L).

Hu, X.–Effect of pressure on the structure of Fe–N alloys formed by solid-state reaction.–B. Yao, L. Liu, S.E. Liu, X. Hu, and W.H. Su; **16**(9), 2583–2590.

Hu, Xiaobo–Growth, defects, and properties of $GdCa_4O(BO_3)_3$ and $Nd:GdCa_4O(BO_3)_3$ crystals.–Jiyang Wang, Xiaobo Hu, Xin Yin, Renbo Song, Jingqian Wei, Zongsu Shao, Yaogang Liu, Minhua Jiang, Yulian Tian, Jianhua Jiang, and Wanxia Huang; **16**(3), 790–796.

Hu, Xiaozhi–Cracking of porcelain coatings bonded to metal substrates of different modulus and hardness.–Hong Zhao, Xiaozhi Hu, Mark B. Bush, and Brian R. Lawn; **16**(5), 1471–1478.

Hu, Z.Q.–Preparation of superfine Fe-base alloy by liquidus casting.–X.F. Pan, H.F. Zhang, A.M. Wang, B.Z. Ding, Z.Q. Hu; **16**(12), 3459–3463.

Huang, Feng–Ultrathin TiB_2 protective films.–Feng Huang, John A. Barnard, and Mark L. Weaver; **16**(4), 945–954.

Huang, Hsiang-Yuan–Silicalite/poly(dimethylsiloxane) nanocomposite pervaporation membranes for acetic acid/water separation.–Shih-Yuan Lu, Hsiang-Yuan Huang, and Kwen-Hua Wu; **16**(11), 3053–3059.

Huang, Jianyu–Structure and phase characteristics of amorphous boron–carbon–nitrogen under high pressure and high temperature.–Jianyu Huang, Yuntian T. Zhu, and Hirotaro Mori; **16**(4), 1178–1184.

Huang, Junchao–Preparation and characterization of nanocrystalline PbSe in poly(acrylic acid-*co*-styrene).–Yangyang Sun, Xuefeng Qian, Jie Yin, Junchao Huang, Xiaodong Ma, and Zikang Zhu; **16**(10), 2922–2927.

Huang, T.S.–Wetting of mullite by Y_2O_3–Al_2O_3–SiO_2 and B_2O_3–SiO_2 glasses.–T.S. Huang, M.N. Rahaman, B.T. Eldred, and P.D. Ownby; **16**(11), 3223–3228.

Huang, Wanxia–Growth, defects, and properties of $GdCa_4O(BO_3)_3$ and $Nd:GdCa_4O(BO_3)_3$ crystals.–Jiyang Wang, Xiaobo Hu, Xin Yin, Renbo Song, Jingqian Wei, Zongsu Shao, Yaogang Liu, Minhua Jiang, Yulian Tian, Jianhua Jiang, and Wanxia Huang; **16**(3), 790–796.

Huang, Z.P.–Growth and characterization of aligned carbon nanotubes from patterned nickel nanodots and uniform thin films.–J.G. Wen, Z.P. Huang, D.Z. Wang, J.H. Chen, S.X. Yang, Z.F. Ren, J.H. Wang, L.E. Calvet, J. Chen, J.F. Klemic, and M.A. Reed; **16**(11), 3246–3253.

Hugon, M.C.–^{18}O study of the oxidation of reactively sputtered $Ti_{1-x}Al_xN$ barrier.–M.C. Hugon, F. Varniere, F. Letendu, B. Agius, I. Vickridge, and A.I. Kingon; **16**(9), 2591–2599.

Hultman, L.–Deposition of epitaxial transition metal carbide films and superlattices by simultaneous direct current metal magnetron sputtering and C_{60} evaporation.–H. Högberg, J. Birch, M.P. Johansson, L. Hultman, and U. Jansson; **16**(3), 633–643.

–Growth, structure, and mechanical properties of transition metal carbide superlattices.–H. Högberg, J. Birch, M. Odén, J-O. Malm, L. Hultman, and U. Jansson; **16**(5), 1301–1310.

–Thermal stability of carbon nitride thin films.–Niklas Hellgren, Nian Lin, Esteban Broitman, Virginie Serin, Stefano E. Grillo, Ray Twesten, Ivan Petrov, Christian Colliex, Lars Hultman, and Jan-Eric Sundgren; **16**(11), 3188–3201.

Hung, Nguyen The–Electrical and microstructural characteristics of ZnO–Bi_2O_3-based varistors doped with rare-earth oxides.–Nguyen The Hung, Nguyen Dinh Quang, and Slavko Bernik; **16**(10), 2817–2823.

Huo, S.H.–Freeform fabrication of aluminum metal-matrix composites.–C.W. Souvignier, T.B. Sercombe, S.H. Huo, P. Calvert, and G.B. Schaffer; **16**(9), 2613–2618.

Huot, J.–Study of the activation process of Mg-based hydrogen storage materials modified by graphite and other carbonaceous compounds.–S. Bouaricha, J-P. Dodelet, D. Guay, J. Huot, and R. Schulz; **16**(10), 2893–2905.

Hurst, Wilbur S.–Correlation of the Raman spectra with the thermal conductivity of a set of diamond wafers prepared by chemical vapor deposition.–Edgar S. Etz, Wilbur S. Hurst, and Albert Feldman; **16**(6), 1694–1711.

Hussain, Zahid–Optical and electrochromic properties of heated and annealed MoO_3 thin films.–Zahid Hussain; **16**(9), 2695–2708.

Hutchinson, J.W.–Adhesion of benzocyclobutene-passivated silicon in epoxy layered structures.–Robert J. Hohlfelder, Daniel A. Maidenberg, Reinhold H. Dauskardt, Yueguang Wei, John W. Hutchinson; **16**(1), 243–255.

–Model for the robust mechanical behavior of nacre.–A.G. Evans, Z. Suo, R.Z. Wang, I.A. Aksay, M.Y. He, and J.W. Hutchinson; **16**(9), 2475–2484.

Hwang, Cheol Seong–Optimization of the annealing process for the (Ba,Sr)TiO_3 thin films grown by low-temperature (420 °C) metal-organic chemical vapor deposition.–Jaehoo Park, Cheol Seong Hwang, and Doo Young Yang; **16**(5), 1363–1371.

–Bulk- or interface-limited electrical conductions in IrO_2/(Ba,Sr)TiO_3/IrO_2 thin film capacitors.–Cheol Seong Hwang; **16**(12), 3476–3484.

–Metalorganic chemical vapor deposition of very thin Pb(Zr,Ti)O_3 thin films at low temperatures for high-density ferroelectric memory applications.–Hye Ryoung Kim, Seehwa Jeong, Chung Bae Jeon, Oh Seong Kwon, Cheol Seong Hwang, Young Ki Han, Doo Young Yang, and Ki Young Oh; **16**(12), 3583–3591.

Hwang, K.–Annealing effect on in-plane alignment and surface morphology of epitaxial $Bi_4Ti_3O_{12}$ thin films prepared by the chemical solution deposition.–K. Hwang and Y. Park; **16**(9), 2519–2525.

Hwu, R.J.–Investigation of crystal properties of TmP/GaAs and GaAs/TmP/GaAs heterostructures grown by molecular beam epitaxy.–C.H. Lin, R.J. Hwu, and L.P. Sadwick; **16**(11), 3266–3273.

Hyun, S.–Designing composite microstructures with targeted properties.–S. Hyun and S. Torquato; **16**(1), 280–285.

I

Iida, K.–Microstructure of (Nd, Eu, Gd)-123 matrix with (Nd, Eu, Gd)-211 inclusions.–M. Muralidhar, M. Jirsa, K. Iida, N. Sakai, and M. Murakami; **16**(2), 407–412.

Ikegami, M.–Mechanical stress of the electrical performance of polycrystalline-silicon resistors.–N. Nakabayashi, H. Ohyama, E. Simoen, M. Ikegami, C. Claeys, K. Kobayashi, M. Yoneoka, and K. Miyahara; **16**(9), 2579–2582.

Ikegami, Takayasu–Effect of the calcium dopant on oxide ion diffusion in yttria ceramics.–Noriko Saito, Hajime Haneda, Isao Sakaguchi, and Takayasu Ikegami; **16**(8), 2362–2368.

–Precursor scavenging of the resistive grain-boundary phase in 8 mol% yttria-stabilized zirconia: Effect of trace concentrations of SiO_2.–Jong-Heun Lee, Toshiyuki Mori, Ji-Guang Li, Takayasu Ikegami, John Drennan, and Doh-Yeon Kim; **16**(8), 2377–2383.

Ikuhara, Yuichi–Transient creep in fine-grained polycrystalline Al_2O_3 with Lu^{3+} ion segregation at the grain boundaries.–Hidehiro Yoshida, Yuichi Ikuhara, and Taketo Sakuma; **16**(3), 716–720.

–Influence of antiphase boundaries on critical current densities in $YBa_2Cu_3O_{7-y}$ single crystals.–Junko Shibata, Akihiro Oka, Teruo Izumi, Yuh Shiohara, Tsukasa Hirayama, and Yuichi Ikuhara; **16**(7), 1935–1941.

–Crystallography and structural evolution of $LiNbO_3$ and $LiNb_{1-x}Ta_xO_3$ films on sapphire prepared by high-rate thermal plasma spray chemical vapor deposition.–D.V. Shtansky, S.A. Kulinich, K. Terashima, T. Yoshida, Y. Ikuhara; **16**(8), 2271–2279.

Ikuma, Yasuro–Oxygen self-diffusion in cerium oxide doped with Nd.–Michiyo Kamiya, Eriko Shimada, Yasuro Ikuma, Manabu Komatsu, Hajime Haneda, Soichiro Sameshima, and Yoshihiro Hirata; **16**(1), 179–184.

Ikuta, Yoshiaki–Modification of sol–gel-derived amorphous Al_2O_3 thin films by F_2 excimer laser irradiation at ambient temperature.–Satoshi Takeda, Yoshiaki Ikuta, Masahiro Hirano, and Hideo Hosono; **16**(4), 1003–1009.

Im, Hyejin–Formation and characterization of crystalline iron oxide films on self-assembled organic monolayers and their *in situ* patterning.–Hyunjung Shin, Jong Up Jeon, Y. Eugene Pak, Hyejin Im, and Eung Soo Kim; **16**(2), 564–569.

Imafuku, Muneyuki–Change in local atomic structure during formation of the icosahedral quasicrystalline phase in $Zr_{70}Pd_{30}$ glassy alloy.–Muneyuki Imafuku, Junji Saida, and Akihisa Inoue; **16**(11), 3046–3049(L).

Imam, M.A.–Thermal analysis investigation of hydriding properties of nanocrystalline Mg–Ni- and Mg–Fe-based alloys prepared by high-energy ball milling.–L.E.A. Berlouis, E. Cabrera, E. Hall-Barientos, P.J. Hall, S.B. Dodd, S. Morris, and M.A. Imam; **16**(1), 45–57.

Inagaki, M.–Carbonization behavior of polyimide film containing iron complex in relation to magnetic properties.–Y. Kaburagi, T. Toriyama, A. Yoshida, H. Wakabayashi, Y. Hishiyama, and M. Inagaki; **16**(2), 352–365.

Inomata, Hiroshi–Valence variations in titanium-based perovskite oxides by high-pressure and high-temperature method.–Liping Li, Guangshe Li, Jipeng Miao, Wenhui Su, Hiroshi Inomata; **16**(2), 417–424.

–Solid solubility and transport properties of $Ce_{1-x}Nd_xO_{2-\delta}$ nanocrystalline solid solutions by a sol-gel route.–Liping Li, Xiaomin Lin, Guangshe Li, and Hiroshi Inomata; **16**(11), 3207–3213.

Inoue, A.–Formation of icosahedral quasicrystal by crystallization of $Zr_{70}(Ni, Cu, Pd)_{30}$ amorphous alloys.–T. Zhang, A. Inoue, M. Matsushita, and J. Saida; **16**(1), 20–23(L).

–Redistribution behavior of constitutional elements at an initial crystallization stage in the $Zr_{65}Al_{7.5}Ni_{10}Cu_{17.5}$ glassy alloy.–J. Saida, M. Matsushita, and A. Inoue; **16**(1), 28–31(L).

–Precipitation of icosahedral quasicrystalline phase in $Hf_{69.5}Al_{7.5}Ni_{11}Cu_{12}$ metallic glass.–Chunfei Li and Akihisa Inoue; **16**(4), 1190–1194.

–Novel hexagonal structure and ultrahigh strength of magnesium solid solution in the Mg–Zn–Y system.–Akihisa Inoue, Yoshihito Kawamura, Mitsuhide Matsushita, Kentaro Hayashi, and Junichi Koike; **16**(7), 1894–1900.

–Formation and mechanical properties of Cu–Hf–Ti bulk glassy alloys.–Akihisa Inoue, Wei Zhang, Tao Zhang, and Kei Kurosaka; **16**(10), 2836–2844.

–Change in local atomic structure during formation of the icosahedral quasicrystalline phase in $Zr_{70}Pd_{30}$ glassy alloy.–Muneyuki Imafuku, Junji Saida, and Akihisa Inoue; **16**(11), 3046–3049(L).

–Investigation of the stability of glassy state in the Zr- and Hf-based glassy alloys correlated with their transformation behavior.–Junji Saida, Chunfei Li, Mitsuhide Matsushita, and Akihisa Inoue; **16**(12), 3389–3401.

Inoue, N.–Chemical reaction at the interface between $(Hg_{0.9}Re_{0.1})$-$Ba_2CaCu_2O_y$ thin film and $SrTiO_3$ substrate.–Xiao-Jing Wu, N. Inoue, T. Sugano, T. Morishita, and K. Tanabe; **16**(1), 256–260.

Ioka, Ikuo–Identification of the constitutive equation by the indentation technique using plural indenters with different apex angles.–Masatoshi Futakawa, Takashi Wakui, Yuji Tanabe, and Ikuo Ioka; **16**(8), 2283–2292.

Ishihara, S.–Topological transformation of grains in three-dimensional normal grain growth.–F. Wakai, Y. Shinoda, S. Ishihara, and A. Domínguez-Rodríguez; **16**(7), 2136–2142.

Ishizawa, Yoshio–Atomic structure of YB_{56} studied by digital high-resolution electron microscopy and electron diffraction.–Takeo Oku, Jan-Olov Bovin, Iwami Higashi, Takaho Tanaka, Yoshio Ishizawa; **16**(1), 101–107.

Iwasaki, T.–Molecular dynamics analysis of adhesion strength of interfaces between thin films.–T. Iwasaki and H. Miura; **16**(6), 1789–1794.

Iwataka, Nobuhiro–Misting-free diamond surface created by sheet electron beam irradiation.–Kazuya Oguri, Nobuhiro Iwataka, Akira Tonegawa, Yoichi Hirose, Kazuo Takayama, and Yoshitake Nishi; **16**(2), 553–557.

Izumi, Teruo–Formation of $Nd_{1+x}(Ba_{1-y}Sr_y)_{2-3}Cu_3O_{7\pm\delta}$ solid solutions by crystal pulling.–Xin Yao, E.A. Goodilin, Teruo Izumi, and Yuh Shiohara; **16**(2), 529–533.

–Preferential growth mechanism of $REBa_2Cu_3O_y$ (RE = Y, Nd) crystal on MgO substrate by liquid phase epitaxy.–Katsumi Nomura, Saburo Hoshi, Xin Yao, Kazuomi Kakimoto, Yuichi Nakamura, Teruo Izumi, and Yuh Shiohara; **16**(4), 979–989.

–Influence of antiphase boundaries on critical current densities in $YBa_2Cu_3O_{7-y}$ single crystals.–Junko Shibata, Akihiro Oka, Teruo Izumi, Yuh Shiohara, Tsukasa Hirayama, and Yuichi Ikuhara; **16**(7), 1935–1941.

–Role of the primary phase particles during the peritectic solidification of Y-123 superconducting oxides.–M. Kambara, M. Yoshizumi, T. Umeda, K. Miyake, K. Murata, T. Izumi, and Y. Shiohara; **16**(8), 2229–2238.

–Initial growth mechanism of $YBa_2Cu_3O_y$ crystal on MgO substrate by liquid-phase epitaxy.–Katsumi Nomura, Saburo Hoshi, Yuichi Nakamura, Teruo Izumi, and Yuh Shiohara; **16**(10), 2947–2958.

J

Jaccodine, R.J.–Planar oxidation of strained silicon substrates.–M-T. Lin, R.J. Jaccodine, and T.J. Delph; **16**(3), 728–733.

Jachkin, V.A.–Electronic paramagnetic resonance study of Cu^{2+} ions in copper ion-exchanged layers of lithium niobate crystals.–F. Caccavale, C. Sada, F. Segato, L.D. Bogomolova, V.A. Jachkin, and N.A. Krasil'nikova; **16**(6), 1554–1558.

Jacobson, D.C.–Observations of structural order in ion-implanted amorphous silicon.–Ju-Yin Cheng, J.M. Gibson, and D.C. Jacobson; **16**(11), 3030–3033(L).

Jamting, A.K.–Methods of correction for analysis of depth-sensing indentation test data for spherical indenters.–A.C. Fischer-Cripps, A. Bendeli, T.J. Bell, J.S. Field, A.K. Jamting; **16**(8), 2244–2250.

Jana, Tapati–Development of *p*-type microcrystalline silicon carbon alloy films by the very high frequency plasma-enhanced chemical vapor deposition technique.–Tapati Jana, Arup Dasgupta, and Swati Ray; **16**(7), 2130–2135.

Janaković, Dj.–Phase-transformation kinetics in triphasic cordierite gel.–R. Petrović, Dj. Janaković, S. Zec, S. Drmanić, and Lj. Kostić-Gvozdenović; **16**(2), 451–458.

Janas, Victor F.–Mechanochemical-hydrothermal preparation of crystalline hydroxyapatite powders at room temperature.–Pavel Shuk, Wojciech L. Suchanek, Tian Hao, Eric Gulliver, Richard E. Riman, Mamoru Senna, Kevor S. TenHuisen, and Victor F. Janas; **16**(5), 1231–1234(L).

Jang, Hyun M.–Metal-organic vapor phase epitaxial growth of high-quality ZnO films on $Al_2O_3(00{\cdot}1)$.–W.I. Park, S-J. An, Gyu-Chul Yi, and Hyun M. Jang; **16**(5), 1358–1362.

–Formation and characteristics of highly *c*-axis-oriented $Bi_{3.25}La_{0.75}Ti_3O_{12}$ thin films on SiO_2/Si(100) and Pt/Ti/SiO_2/Si(100) substrates.–Uong Chon, Hyun M. Jang, Sun-Hwa Lee, and Gyu-Chul Yi; **16**(11), 3124–3132.

Jang, Jae Hyeok–Preparation and characteristics of seeded epitaxial $(Sr,Ba)Nb_2O_6$ optical waveguide thin films using sol-gel method.–Junmo Koo, Jae Hyeok Jang, and Byeong-Soo Bae; **16**(2), 430–436.

Jang, S.J.–Chemical-vapor-deposition growth and characterization of epitaxial 3C–SiC films on SOI substrates with thin silicon top layers.–C.K. Moon, H.J. Song, J.K. Kim, J.H. Park, S.J. Jang, J-B. Yoo, H-R. Park, and Byung-Teak Lee; **16**(1), 24–27(L).

Jankowski, A.F.–Processing and characterization of hydroxyapatite coatings on titanium produced by magnetron sputtering.–T.G. Nieh, A.F. Jankowski, and J. Koike; **16**(11), 3238–3245.

Jansson, U.–Deposition of epitaxial transition metal carbide films and superlattices by simultaneous direct current metal magnetron sputtering and C_{60} evaporation.–H. Högberg, J. Birch, M.P. Johansson, L. Hultman, U. Jansson; **16**(3), 633–643.

–Growth, structure, and mechanical properties of transition metal carbide superlattices.–H. Högberg, J. Birch, M. Odén, J-O. Malm, L. Hultman, and U. Jansson; **16**(5), 1301–1310.

Jayaram, V.–A new technique for pressureless infiltration of Al alloys into Al_2O_3 preforms.–B. Srinivasa Rao and V. Jayaram; **16**(10), 2906–2913.

Jean, Jau-Ho–Devitrification kinetics and mechanism of Pyrex borosilicate glass.–Jau-Ho Jean and Yu-Ching Fang; **16**(6), 1752–1758.

Jeon, Chung Bae–Metalorganic chemical vapor deposition of very thin $Pb(Zr,Ti)O_3$ thin films at low temperatures for high-density ferroelectric memory applications.–Hye Ryoung Kim, Seehwa Jeong, Chung Bae Jeon, Oh Seong Kwon, Cheol Seong Hwang, Young Ki Han, Doo Young Yang, and Ki Young Oh; **16**(12), 3583–3591.

Jeon, Jong Up–Formation and characterization of crystalline iron oxide films on self-assembled organic monolayers and their *in situ* patterning.–Hyunjung Shin, Jong Up Jeon, Y. Eugene Pak, Hyejin Im, and Eung Soo Kim; **16**(2), 564–569.

Jeong, Ha-Guk–Interface structure and solute segregation behavior in SiC/2124 and SiC/6061 Al composites exhibiting high-strain-rate superplasticity.–Woo-Jin Kim, Dong-Wha Kum, and Ha-Guk Jeong; **16**(8), 2429–2435.

Jeong, Seehwa–Metalorganic chemical vapor deposition of very thin $Pb(Zr,Ti)O_3$ thin films at low temperatures for high-density ferroelectric memory applications.–Hye Ryoung Kim, Seehwa Jeong, Chung Bae Jeon, Oh Seong Kwon, Cheol Seong Hwang, Young Ki Han, Doo Young Yang, and Ki Young Oh; **16**(12), 3583–3591.

Jesse, S.–Laser-induced surface perturbations in silicon.–A.J. Pedraza, S. Jesse, Y.F. Guan, and J.D. Fowlkes; **16**(12), 3599–3608.

Jia, C.L.–Microstructure and misfit relaxation in $SrTiO_3$/$SrRuO_3$ bilayer films on $LaAlO_3(100)$ substrates.–J.S. Wu, C.L. Jia, K. Urban, J.H. Hao, and X.X. Xi; **16**(12), 3443–3450.

Jia, Q.X.–High critical current density $YBa_2Cu_3O_{7-\delta}$ thick films using ion beam assisted deposition MgO bi-axially oriented template layers on nickel-based superalloy substrates.–J.R. Groves, P.N. Arendt, S.R. Foltyn, Q.X. Jia, T.G. Holesinger, H. Kung, E.J. Peterson, R.F. DePaula, P.C. Dowden, L. Stan, and L.A. Emmert; **16**(8), 2175–2178(L).

Jia, Y.–Transmission electron microscopy study of (103)-oriented epitaxial $SrBi_2Nb_2O_9$ films grown on (111) $SrTiO_3$ and (111) $SrRuO_3$/(111) $SrTiO_3$.–M.A. Zurbuchen, J. Lettieri, Y. Jia, D.G. Schlom, S.K. Streiffer, and M.E. Hawley; **16**(2), 489–502.

Jiang, Jianhua–Growth, defects, and properties of $GdCa_4O(BO_3)_3$ and Nd:$GdCa_4O(BO_3)_3$ crystals.–Jiyang Wang, Xiaobo Hu, Xin Yin, Renbo Song, Jingqian Wei, Zongsu Shao, Yaogang Liu, Minhua Jiang, Yulian Tian, Jianhua Jiang, and Wanxia Huang; **16**(3), 790–796.

Jiang, Minhua–Growth, defects, and properties of $GdCa_4O(BO_3)_3$ and Nd:$GdCa_4O(BO_3)_3$ crystals.–Jiyang Wang, Xiaobo Hu, Xin Yin, Renbo Song, Jingqian Wei, Zongsu Shao, Yaogang Liu, Minhua Jiang, Yulian Tian, Jianhua Jiang, and Wanxia Huang; **16**(3), 790–796.

Jiang, Q.–Comparison of different models for melting point change of metallic nanocrystals.–M. Zhao, X.H. Zhou, and Q. Jiang; **16**(11), 3304–3308.

Jiang, Yang–Preparation and characterization of $CuInS_2$ nanorods and nanotubes from an elemental solvothermal reaction.–Yang Jiang, Yue Wu, Shengwen Yuan, Bo Xie, Shuyuan Zhang, and Yitai Qian; **16**(10), 2805–2809.

Jin, C.Q.–Study of phase components of $La_{1.5}Ca_{1.5}Mn_2O_7$.–J.L. Zhu, R.C. Yu, F.Y. Li, C.Q. Jin, and Z. Zhang; **16**(7), 2027–2031.

Jin, Haibo–Microstructure and formation mechanism of combustion-synthesized rodlike Ca α-sialon crystals.–Kexin Chen, Haibo Jin, M. Oliveira, Heping Zhou, and J.M.F. Ferreira; **16**(7), 1928–1934.

Jin, Moon-Seog–Photoluminescence spectra of undoped and Sm^{3+}-doped $BaAl_2S_4$ and $BaAl_2Se_4$ single crystals.–Moon-Seog Jin, Choong-Il Lee, Chang-Sun Yoon, Chang-Dae Kim, Jae-Mo Goh, and Wha-Tek Kim; **16**(5), 1520–1524.

Jin, S.–Growth of (111)-oriented $Pb(Zr,Ti)O_3$ layers on nanocrystalline RuO_2 electrodes using the sol-gel technique.–G.J. Norga, S. Jin, Laura Fè, D.J. Wouters, H. Bender, and H.E. Maes; **16**(3), 828–833.

Jin-Phillipp, N.Y.–Characterization of GaN grown on sapphire by laser-induced molecular beam epitaxy.–H. Zhou, A. Rühm, N.Y. Jin-Phillipp, F. Phillipp, M. Gross, and H. Schröder; **16**(1), 261–267.

Jirsa, M.–Microstructure of (Nd, Eu, Gd)-123 matrix with (Nd, Eu, Gd)-211 inclusions.–M. Muralidhar, M. Jirsa, K. Iida, N. Sakai, and M. Murakami; **16**(2), 407–412.

Jobst, B.–Phase formation and crystal growth of Sr–Bi–Ta–O thin films grown by metalorganic chemical vapor deposition.–H. Bachhofer, H. von Philipsborn, W. Hartner, C. Dehm, B. Jobst, A. Kiendl, H. Schroeder, and R. Waser; **16**(10), 2966–2973.

Johansson, M.P.–Deposition of epitaxial transition metal carbide films and superlattices by simultaneous direct current metal magnetron sputtering and C_{60} evaporation.–H. Högberg, J. Birch, M.P. Johansson, L. Hultman, and U. Jansson; **16**(3), 633–643.

Johnson, Bradley R.–Crystallization kinetics of yttrium aluminum garnet ($Y_3Al_5O_{12}$).–Bradley R. Johnson and Waltraud M. Kriven; **16**(6), 1795–1805.

Johnson, W.L.–*In situ* transmission electron microscopy studies of shear bands in a bulk metallic glass based composite.–E. Pekarskaya, C.P. Kim, and W.L. Johnson; **16**(9), 2513–2518.

Jones, M.O.–Microstructure of laser-ablated superconducting $La_2CuO_4F_x$ thin films on $SrTiO_3$.–G. Kong, M.O. Jones, J.S. Abell, P.P. Edwards, S.T. Lees, K.E. Gibbons, I. Gameson, and M. Aindow; **16**(11), 3309–3316.

Josell, D.–Moving the pulsed heating technique beyond monolithic specimens: Experiments with coated wires.–D. Josell, D. Basak, J.L. McClure, U.R. Kattner, M.E. Williams, W.J. Boettinger, and M. Rappaz; **16**(8), 2421–2428.

Jung, Ji-In–Photoinduced condensation of sol-gel hybrid glass films doped with benzildimethylketal.–Oun-Ho Park, Ji-In Jung, and Byeong-Soo Bae; **16**(7), 2143–2148.

Junker, Kurt–Effect of material properties on integration damage in organosilicate glass films.–E. Todd Ryan, Jeremy Martin, Kurt Junker, Jeff Wetzel, David W. Gidley, and Jianing Sun; **16**(12), 3335–3338(L).

K

Kaburagi, Y.–Carbonization behavior of polyimide film containing iron complex in relation to magnetic properties.–Y. Kaburagi, T. Toriyama, A. Yoshida, H. Wakabayashi, Y. Hishiyama, and M. Inagaki; **16**(2), 352–365.

Kadono, Kohei–Coordination structures of implanted Fe, Co, and Ni ions in silica glass by x-ray absorption fine structure spectroscopy.–Kohei Fukumi, Akiyoshi Chayahara, Kohei Kadono, Hiroyuki Kageyama, Tomoko Akai, Hiroshi Mizoguchi, Naoyuki Kitamura, Masaki Makihara, Yuji Horino, and Kanenaga Fujii; **16**(1), 155–162.

Kagebayashi, Yoshio–Water-associated surface degradation of $CsLiB_6O_{10}$ crystal during harmonic generation in the ultraviolet region.–Yukihiro Morimoto, Shintaro Miyazawa, Yoshio Kagebayashi, Naoki Kitatochi, Toshio Yokota, and Jun Sakuma; **16**(7), 2082–2090.

Kageyama, Hiroyuki–Coordination structures of implanted Fe, Co, and Ni ions in silica glass by x-ray absorption fine structure spectroscopy.–Kohei Fukumi, Akiyoshi Chayahara, Kohei Kadono, Hiroyuki Kageyama, Tomoko Akai, Hiroshi Mizoguchi, Naoyuki Kitamura, Masaki Makihara, Yuji Horino, and Kanenaga Fujii; **16**(1), 155–162.

Kahn-Harari, A.–Phase transition, growth, and optical properties of $Nd_xLa_{1-x}Sc_3(BO_3)_4$ crystals.–Yunkui Li, G. Aga, A. Kahn-Harari, and D. Vivien; **16**(1), 38–44.

Kaïtasov, Odile–Characterization of bond formation in SiC and Si_3N_4 implanted with Ti, Fe, and Co.–Didier Zanghi, Agnès Traverse, Sébastien Gautrot, and Odile Kaïtasov; **16**(2), 512–523.

Kajihara, Koichi–Macroporous morphology of titania films prepared by sol-gel dip-coating method from a system containing poly(ethylene glycol) and poly(vinylpyrrolidone).–Koichi Kajihara and Kazuki Nakanishi; **16**(1), 58–66.

Kakimoto, Kazuomi–Preferential growth mechanism of $REBa_2Cu_3O_x$ (RE = Y, Nd) crystal on MgO substrate by liquid phase epitaxy.–Katsumi Nomura, Saburo Hoshi, Xin Yao, Kazuomi Kakimoto, Yuichi Nakamura, Teruo Izumi, and Yuh Shiohara; **16**(4), 979–989.

Kalidindi, S.R.–Finite element modeling of microscale thermal residual stresses in Al interconnects.–A. Saerens, P. Van Houtte, and S.R. Kalidindi; **16**(4), 1112–1122.

Kalinin, Sergei V.–Analysis of phase distributions in the Li_2O–Nb_2O_5–TiO_2 system by piezoresponse imaging.–Albina Y. Borisevich, Sergei V. Kalinin, Dawn A. Bonnell, and Peter K. Davies; **16**(2), 329–332(L).

Kaloyeros, Alain E.–Metalorganic chemical vapor deposition of titanium oxide for microelectronics applications.–Kanchana Vydianathan, Guillermo Nuesca, Gregory Peterson, Eric T. Eisenbraun, Alain E. Kaloyeros, John J. Sullivan, and Bin Han; **16**(6), 1838–1849.

Kalu, P.N.–Microstructures of $La_{1-x}A_xMnO_{3-\delta}$ (A = Ca or Sr) thin films by liquid-delivery metalorganic chemical vapor deposition.–Y. Xin, K. Han, N. Mateeva, H. Garmestani, P.N. Kalu, and K-H. Dahmen; **16**(11), 3073–3083.

Kam, C.H.–Third-order nonlinear optical response in PbS-coated CdS nanocomposites.–Bing Liu, Chwee Har Chew, Leong Ming Gan, Guo Qin Xu, Heping Li, Yee Loy Lam, Chan Hin Kam, and Wen Xiu Que; **16**(6), 1644–1650.

–Preparation and characterization of nanocrystalline potassium lithium niobate powders and films.–H.X. Zhang, C.H. Kam, Y. Zhou, X.Q. Han, S.D. Cheng, C.Y. Chan, and Y.L. Lam; **16**(12), 3609–3613.

Kambara, M.–Growth of melt-textured Nd-123 by hot seeding under reduced oxygen partial pressure.–M. Kambara, N. Hari Babu, Y.H. Shi, and D.A. Cardwell; **16**(4), 1163–1170.

–Role of the primary phase particles during the peritectic solidification of Y-123 superconducting oxides.–M. Kambara, M. Yoshizumi, T. Umeda, K. Miyake, K. Murata, T. Izumi, and Y. Shiohara; **16**(8), 2229–2238.

Kamiya, Michiyo–Oxygen self-diffusion in cerium oxide doped with Nd.–Michiyo Kamiya, Eriko Shimada, Yasuro Ikuma, Manabu Komatsu, Hajime Haneda, Soichiro Sameshima, and Yoshihiro Hirata; **16**(1), 179–184.

Kamsah, Nazri bin–Scanning probe microscopy generated out-of-plane deformation maps exhibiting heterogeneous nanoscale deformation resulting from thermal cycling of Cu–polyimide damascene interconnects.–Todd S. Gross, Nazri bin Kamsah, and I. Tsukrov; **16**(12), 3560–3566.

Kang, B.W.–Growth and characterization of conductive $SrRuO_3$ and $LaNiO_3$ multilayers on textured Ni tapes for high-J_c $YBa_2Cu_3O_{7-\delta}$ coated conductors.–T. Aytug, B.W. Kang, C. Cantoni, E.D. Specht, M. Paranthaman, A. Goyal, D.K. Christen, D.T. Verebelyi, J.Z. Wu, R.E. Ericson, C.L. Thomas, C-Y.Yang, and S.E. Babcock; **16**(9), 2661–2669.

Kang, H.C.–X-ray scattering study on the structural evolution of AlN/sapphire(0001) films during radiofrequency sputter growth.–H.C. Kang, S.H. Seo, and D.Y. Noh; **16**(6), 1814–1821.

Kang, Junyong–Threading dislocations with edge components in GaN epilayers grown on Al_2O_3 substrates.–Junyong Kang and Tomoya Ogawa; **16**(9), 2550–2555.

Kang, Shinhoo–Synthesis of $Zn_{2-x}Mn_xSiO_4$ phosphors using a hydrothermal technique.–Chulsoo Yoon and Shinhoo Kang; **16**(4), 1210–1216.

Kang, T.W.–Temperature dependence of the optical properties in p-$Cd_{0.96}Zn_{0.04}Te$ single crystals.–H.Y. Lee, T.W. Kang, and T.W. Kim; **16**(8), 2196–2199.

Karthikeyan, A.–Phase separation in SiO_2–TiO_2 gel and glassy films studied by atomic force microscopy and transmission electron microscopy.–A. Karthikeyan and Rui M. Almeida; **16**(6), 1626–1631.

Kasap, S.O.–Glass transformation in vitreous As_2Se_3 studied by conventional and temperature-modulated differential scanning calorimetry.–S.O. Kasap and D. Tonchev; **16**(8), 2399–2407.

Kassem, Magdy–Origins of stored enthalpy in cryomilled nanocrystalline Zn.–Xinghang Zhang, Haiyan Wang, Magdy Kassem, Jagdish Narayan, and Carl C. Koch; **16**(12), 3485–3495.

Kasuga, Toshihiro–Machinable calcium pyrophosphate glass-ceramics.–Toshihiro Kasuga, Miwako Terada, Masayuki Nogami, and Mitsuo Niinomi; **16**(3), 876–880.

Katayam, K.–Morphological effect on the electrochemical behavior of electric double-layer capacitors.–M. Endo, Y.J. Kim, T. Maeda, K. Koshiba, K. Katayam, and M.S. Dresselhaus; **16**(12), 3402–3410.

Katiyar, R.S.–Raman spectroscopic determination of phase evolutions in $LiAl_xCo_{1-x}O_2$ battery materials.–P.S. Dobal, R.S. Katiyar, M.S. Tomar, and A. Hidalgo; **16**(1), 1–4(L).

–Synthesis of $Zn_{1-x}Mg_xO$ and its structural characterization.–M.S. Tomar, R. Melgarejo, P.S. Dobal, and R.S. Katiyar; **16**(4), 903–906(L).

Kattner, U.R.–Moving the pulsed heating technique beyond monolithic specimens: Experiments with coated wires.–D. Josell, D. Basak, J.L. McClure, U.R. Kattner, M.E. Williams, W.J. Boettinger, and M. Rappaz; **16**(8), 2421–2428.

Kaul, Anupama B.–High-T_c superconducting NbN films with low particulate density grown at 25 °C using pulsed laser deposition.–Anupama B. Kaul, Timothy D. Sands, and Theodore Van Duzer; **16**(5), 1223–1226(L).

Kawamura, Yoshihito–Novel hexagonal structure and ultrahigh strength of magnesium solid solution in the Mg–Zn–Y system.–Akihisa Inoue, Yoshihito Kawamura, Mitsuhide Matsushita, Kentaro Hayashi, and Junichi Koike; **16**(7), 1894–1900.

Kawaoka, Hirokazu–Effect of α/β phase ratio on microstructure and mechanical properties of silicon nitride ceramics.–Hirokazu Kawaoka, Tomohiko Adachi, Tohru Sekino, Yong-Ho Choa, Lian Gao, and Koichi Niihara; **16**(8), 2264–2270.

Kay, J.P.–Thermal expansion and high-temperature phase transformation of the yttrium silicate Y_2SiO_5.–J.W. Nowok, J.P. Kay, and R.J. Kulas; **16**(8), 2251–2255.

Keast, V.J.–Compositional distributions in nanoscale metallic multilayers studied using x-ray mapping.–V.J. Keast, A. Misra, H. Kung, and T.E. Mitchell; **16**(7), 2032–2038.

Kendig, K.L.–Microstructural and mechanical characterization of carbon coatings on SiC fibers.–K.L. Kendig, R. Gibala, and D.B. Miracle; **16**(12), 3366–3377.

Kenis, Paul J.A.–Fabrication and characterization of microscale sandwich beams.–Francisco Arias, Paul J.A. Kenis, Bing Xu, Tao Deng, Olivier J.A. Schueller, George M. Whitesides, Yuki Sugimura, and Anthony G. Evans; **16**(2), 597–605.

Kennon, LaQuita–Effects of thermal annealing on the texture of $La_{0.67}Sr_{0.33}MnO_3$ thin films.–Lamartine Meda, LaQuita Kennon, Cristiane Bacaltchuk, Hamid Garmestani, and Klaus H. Dahmen; **16**(7), 1887–1889(L).

Kerp, H.R.–Quantification and effects of molecular oxygen and water in zinc phthalocyanine layers.–H.R. Kerp, K.T. Westerduin, A.T. van Veen, and E.E. van Faassen; **16**(2), 503–511.

Kerstetter, K.–Mechanical and thermal properties of combustion-synthesized perovskites, $La_{1-x}Sr_xCr_{0.2}Fe_{0.8}O_3$.–Yeong-Shyung Chou, K. Kerstetter, L.R. Pederson, and R.E. Williford; **16**(12), 3545–3553.

Ketterson, J.B.–Epitaxial stabilization of orthorhombic cuprous oxide films on MgO(110).–Paul R. Markworth, R.P.H. Chang, Y. Sun, G.K. Wong, J.B. Ketterson; **16**(4), 914–921.

Khan, Ajmal–Electron backscatter diffraction analysis of $Pb(Mg_{1/3}Nb_{2/3})O_3$–35mol%$PbTiO_3$ single crystals grown by seeded polycrystal conversion.–Ajmal Khan, Derrick T. Carpenter, Adam M. Scotch, Helen M. Chan, and Martin P. Harmer; **16**(3), 694–700.

Kiendl, A.–Phase formation and crystal growth of Sr–Bi–Ta–O thin films grown by metalorganic chemical vapor deposition.–H. Bachhofer, H. von Philipsborn, W. Hartner, C. Dehm, B. Jobst, A. Kiendl, H. Schroeder, and R. Waser; **16**(10), 2966–2973.

Kienzle, O.–Hardness–depth profile of a carbon-implanted Ti–6Al–4V alloy and its relation to composition and microstructure.–M. Kunert, O. Kienzle, B. Baretzky, S.P. Baker, and E.J. Mittemeijer; **16**(8), 2321–2335.

Kim, B.H.–Quasicrystalline phase formation in $Al_{62}Cu_{22.5}Fe_{12.5}$ and $Al_{55}Cu_{22.5}Fe_{12.5}Be_7$ alloys.–S.M. Lee, B.H. Kim, D.H. Kim, and W.T. Kim; **16**(6), 1535–1540.

Kim, B.K.–Synthesis of $Nd_2Fe_{14}B$ powders by spray-drying and reduction–diffusion processes.–X.L. Dong, B.K. Kim, C.J. Choi, K.S. Park, and Z.D. Zhang; **16**(4), 1083–1089.

Kim, C.H.–Photoluminescence behavior of Al^{3+}, Pr^{3+} doped perovskite $La_{2/3}TiO_3$ and pyrochlore $La_2Ti_2O_7$.–J.K. Park, C.H. Kim, K.J. Choi, H.D. Park, and S.Y. Choi; **16**(9), 2568–2571.

Kim, C.P.–*In situ* transmission electron microscopy studies of shear bands in a bulk metallic glass based composite.–E. Pekarskaya, C.P. Kim, and W.L. Johnson; **16**(9), 2513–2518.

Kim, Chang-Dae–Photoluminescence spectra of undoped and Sm^{3+}-doped $BaAl_2S_4$ and $BaAl_2Se_4$ single crystals.–Moon-Seog Jin, Choong-Il Lee, Chang-Sun Yoon, Chang-Dae Kim, Jae-Mo Goh, and Wha-Tek Kim; **16**(5), 1520–1524.

Kim, D.H.–Precipitation of icosahedral phase from amorphous $Zr_{65}Cu_{17.5-x}Al_{7.5}Ni_{10}Ag_x$ (x = 0, 5) alloys.–J.K. Lee, G. Choi, W.T. Kim, and D.H. Kim; **16**(5), 1311–1317.

–Quasicrystalline phase formation in $Al_{62}Cu_{22.5}Fe_{12.5}$ and $Al_{55}Cu_{22.5}Fe_{12.5}Be_7$ alloys.–S.M. Lee, B.H. Kim, D.H. Kim, and W.T. Kim; **16**(6), 1535–1540.

Kim, Doh-Yeon–Space-charge concepts on grain boundary impedance of a high-purity yttria-stabilized tetragonal zirconia polycrystal.–Jong-Sook Lee and Doh-Yeon Kim; **16**(9), 2739–2751.

–Precursor scavenging of the resistive grain-boundary phase in 8 mol% yttria-stabilized zirconia: Effect of trace concentrations of SiO_2.–Jong-Heun Lee, Toshiyuki Mori, Ji-Guang Li, Takayasu Ikegami, John Drennan, and Doh-Yeon Kim; **16**(8), 2377–2383.

Kim, Dong-Joo–Effect of hydrogen on true leakage current characteristics of $(Pb,La)(Zr,Ti)O_3$ thin-film capacitors with Pt- or Ir-based top electrodes.–Soon-Gil Yoon, Dwi Wicaksana, Dong-Joo Kim, Seung-Hyun Kim, and A.I. Kingon; **16**(4), 1185–1189.

Kim, Dong-Wan–Microwave dielectric properties of $(1-x)Cu_3Nb_2O_8$–$xZn_3Nb_2O_8$ ceramics.–Dong-Wan Kim, In-Tae Kim, Byungwoo Park, Kug Sun Hong, and Jong-Hee Kim; **16**(5), 1465–1470.

Kim, Eung Soo–Formation and characterization of crystalline iron oxide films on self-assembled organic monolayers and their *in situ* patterning.–Hyunjung Shin, Jong Up Jeon, Y. Eugene Pak, Hyejin Im, Eung Soo Kim; **16**(2), 564–569.

–Effect of bond valence on microwave dielectric properties of $(Pb_{1-x}Ca_x)(Mg_{0.33}Ta_{0.67})O_3$ ceramics.–Heung Soo Park, Ki Hyun Yoon, and Eung Soo Kim; **16**(3), 817–821.

Kim, Hae-Won–Improvement in oxidation resistance of TiB_2 by formation of protective SiO_2 layer on surface.–Young-Hag Koh, Hae-Won Kim, and Hyoun-Ee Kim; **16**(1), 132–137.

Kim, Hidong–Absorption spectra of Co^{2+} in $AgInS_2$ orthorhombic single crystals.–Hidong Kim, Seok-Joo Lee, Jae-Eun Kim, Hae Yong Park, Seok-Kyun Oh, and Wha-Tek Kim; **16**(4), 975–978.

Kim, Hwan–Experimental evidence for space charge segregation in Nb-doped $BaTiO_3$.–Seok Hyun Yoon and Hwan Kim; **16**(5), 1479–1486.

Kim, Hye Ryoung–Metalorganic chemical vapor deposition of very thin $Pb(Zr,Ti)O_3$ thin films at low temperatures for high-density ferroelectric memory applications.–Hye Ryoung Kim, Seehwa Jeong, Chung Bae Jeon, Oh Seong Kwon, Cheol Seong Hwang, Young Ki Han, Doo Young Yang, and Ki Young Oh; **16**(12), 3583–3591.

Kim, Hyoun-Ee–Improvement in oxidation resistance of TiB_2 by formation of protective SiO_2 layer on surface.–Young-Hag Koh, Hae-Won Kim, and Hyoun-Ee Kim; **16**(1), 132–137.

Kim, Hyoun Soo–Enhancement of the 1.31-μm emission properties of Dy^{3+}-doped Ge–Ga–S glasses with the addition of alkali halides.–Yong Beom Shin, Jong Heo, and Hyoun Soo Kim; **16**(5), 1318–1324.

Kim, Hyoung-Gu–Evaluation of the impactive-surface-fracture behavior of glass plates using a back-surface strain measurement.–Hyoung-Gu Kim, Nak-Sam Choi, and Nahmgyoo Cho; **16**(11), 3042–3045(L).

Kim, Hyoung Seop–Effects of strain hardenability and strain-rate sensitivity on the plastic flow and deformation homogeneity during equal channel angular pressing.–Hyoung Seop Kim, Sun Ig Hong, and Min Hong Seo; **16**(3), 856–864.

Kim, In-Tae–Microwave dielectric properties of $(1-x)Cu_3Nb_2O_8$–$xZn_3Nb_2O_8$ ceramics.–Dong-Wan Kim, In-Tae Kim, Byungwoo Park, Kug Sun Hong, and Jong-Hee Kim; **16**(5), 1465–1470.

Kim, J.H.–Epitaxial growth of $PbZr_{0.5}Ti_{0.5}O_3$ thin films on $SrRuO_3$/$SrTiO_3$ substrates using chemical solution deposition: Microstructural and ferroelectric properties.–J.H. Kim, Youngman Kim, A.T. Chien, and F.F. Lange; **16**(6), 1739–1744.

Kim, J.K.–Chemical-vapor-deposition growth and characterization of epitaxial 3C–SiC films on SOI substrates with thin silicon top layers.–C.K. Moon, H.J. Song, J.K. Kim, J.H. Park, S.J. Jang, J-B. Yoo, H-R. Park, and Byung-Teak Lee; **16**(1), 24–27(L).

Kim, Jae-Eun–Absorption spectra of Co^{2+} in $AgInS_2$ orthorhombic single crystals.–Hidong Kim, Seok-Joo Lee, Jae-Eun Kim, Hae Yong Park, Seok-Kyun Oh, and Wha-Tek Kim; **16**(4), 975–978.

Kim, Jong-Hee–Microwave dielectric properties of $(1-x)Cu_3Nb_2O_8$–$xZn_3Nb_2O_8$ ceramics.–Dong-Wan Kim, In-Tae Kim, Byungwoo Park, Kug Sun Hong, Jong-Hee Kim; **16**(5), 1465–1470.

Kim, Jun-Kyung–Silica particle growth in metastable supersaturation solution.–Kyung-Soo Kim, Jun-Kyung Kim, and Woo-Sik Kim; **16**(2), 545–552.

Kim, Kyung-Seok–Influence of sintering atmosphere on the fabrication of SiC ceramics with a powder mixture of sialon composition.–Jong-Kook Lee, Jong-Gon Park, Eun-Gu Lee, and Kyung-Seok Kim; **16**(6), 1784–1788.

Kim, Kyung-Soo–Silica particle growth in metastable supersaturation solution.–Kyung-Soo Kim, Jun-Kyung Kim, and Woo-Sik Kim; **16**(2), 545–552.

Kim, Seong-Ho–Analysis of defect formation in Nb-doped $SrTiO_3$ by impedance spectroscopy.–Seong-Ho Kim, Jung-Ho Moon, Jae-Hwan Park, Jae-Gwan Park, and Yoonho Kim; **16**(1), 192–196.

Kim, Seung-Hyun–Effect of hydrogen on true leakage current characteristics of $(Pb,La)(Zr,Ti)O_3$ thin-film capacitors with Pt- or Ir-based top electrodes.–Soon-Gil Yoon, Dwi Wicaksana, Dong-Joo Kim, Seung-Hyun Kim, and A.I. Kingon; **16**(4), 1185–1189.

Kim, Sun-Jae–Preparation of nanocrystalline nickel oxide–yttria-stabilized zirconia composite powder by solution combustion with ignition of glycine fuel.–Sun-Jae Kim, Wonhee Lee, Won-Jun Lee, Soon Dong Park, Jae Sung Song, and Eun Gu Lee; **16**(12), 3621–3627.

Kim, T.W.–Temperature dependence of the optical properties in $p\text{-}Cd_{0.96}Zn_{0.04}Te$ single crystals.–H.Y. Lee, T.W. Kang, and T.W. Kim; **16**(8), 2196–2199.

Kim, W.T.–Precipitation of icosahedral phase from amorphous $Zr_{65}Cu_{17.5-x}Al_{7.5}Ni_{10}Ag_x$ ($x = 0, 5$) alloys.–J.K. Lee, G. Choi, W.T. Kim, and D.H. Kim; **16**(5), 1311–1317.

–Quasicrystalline phase formation in $Al_{62}Cu_{22.5}Fe_{12.5}$ and $Al_{55}Cu_{22.5}Fe_{12.5}Be_7$ alloys.–S.M. Lee, B.H. Kim, D.H. Kim, and W.T. Kim; **16**(6), 1535–1540.

Kim, Wha-Tek–Absorption spectra of Co^{2+} in $AgInS_2$ orthorhombic single crystals.–Hidong Kim, Seok-Joo Lee, Jae-Eun Kim, Hae Yong Park, Seok-Kyun Oh, and Wha-Tek Kim; **16**(4), 975–978.

–Photoluminescence spectra of undoped and Sm^{3+}-doped $BaAl_2S_4$ and $BaAl_2Se_4$ single crystals.–Moon-Seog Jin, Choong-Il Lee, Chang-Sun Yoon, Chang-Dae Kim, Jae-Mo Goh, and Wha-Tek Kim; **16**(5), 1520–1524.

Kim, Wonjoong–Preferred orientation of beta-phase and its mechanisms in a fine-grained silicon-nitride-based ceramic.–Rong-Jun Xie, Mamoru Mitomo, Wonjoong Kim, Young-Wook Kim, and Guo-Dong Zhan; **16**(2), 590–596.

Kim, Woo-Jin–Interface structure and solute segregation behavior in SiC/2124 and SiC/6061 Al composites exhibiting high-strain-rate superplasticity.–Woo-Jin Kim, Dong-Wha Kum, and Ha-Guk Jeong; **16**(8), 2429–2435.

Kim, Woo-Sik–Silica particle growth in metastable supersaturation solution.–Kyung-Soo Kim, Jun-Kyung Kim, and Woo-Sik Kim; **16**(2), 545–552.

Kim, Y.J.–Morphological effect on the electrochemical behavior of electric double-layer capacitors.–M. Endo, Y.J. Kim, T. Maeda, K. Koshiba, K. Katayam, and M.S. Dresselhaus; **16**(12), 3402–3410.

Kim, Yong Kwan–Ferroelectric domain structure of epitaxial (Pb,Sr)TiO_3 thin films.–Yong Kwan Kim, Kyeong Seok Lee, and Sunggi Baik; **16**(9), 2463–2466(L).

Kim, Yong-Seog–Stability of channels at a scalloplike Cu_6Sn_5 layer in solder interconnections.–Jong-Hyun Lee, Jong-Hwan Park, Yong-Ho Lee, Yong-Seog Kim, and Dong Hyuk Shin; **16**(5), 1227–1230(L).

–Effects of Cu and Ni additions to eutectic Pb–Sn solders on Au embrittlement of solder interconnections.–Jong-Hyun Lee, Jong-Hwan Park, Yong-Ho Lee, and Yong-Seog Kim; **16**(5), 1249–1251(L).

–Effect of mechanical alloying on combustion synthesis of $MoSi_2$.–Hyung-Sang Park, Kwang-Seon Shin, and Yong-Seog Kim; **16**(11), 3060–3068.

Kim, Yong-Tea–Low-temperature crystallization induced by excimer laser irradiation of $SrBi_2Ta_2O_9$ films.–Kwang Soo Seol, Hironao Hiramatsu, Yoshimichi Ohki, In-Hoon Choi, Yong-Tea Kim; **16**(7), 1883–1886(L).

Kim, Yoonho–Analysis of defect formation in Nb-doped $SrTiO_3$ by impedance spectroscopy.–Seong-Ho Kim, Jung-Ho Moon, Jae-Hwan Park, Jae-Gwan Park, Yoonho Kim; **16**(1), 192–196.

Kim, Youngman–Epitaxial growth of $PbZr_{0.5}Ti_{0.5}O_3$ thin films on $SrRuO_3/SrTiO_3$ substrates using chemical solution deposition: Microstructural and ferroelectric properties.–J.H. Kim, Youngman Kim, A.T. Chien, and F.F. Lange; **16**(6), 1739–1744.

Kim, Young-Wook–Preferred orientation of beta-phase and its mechanisms in a fine-grained silicon-nitride-based ceramic.–Rong-Jun Xie, Mamoru Mitomo, Wonjoong Kim, Young-Wook Kim, and Guo-Dong Zhan; **16**(2), 590–596.

–Transmission electron microscopy observation in a liquid-phase-sintered SiC with oxynitride glass.–Guo-Dong Zhan, Mamoru Mitomo, Young-Wook Kim, Rong-Jun Xie, and Amiya K. Mukherjee; **16**(8), 2189–2191(L).

Kiminami, C.S.–Effects of pressure on the solidification of Al–Mn alloy.–Duanwei He, M. He, C.S. Kiminami, F.X. Zhang, Y.F. Xu, W.K. Wang, and K.H. Kuo; **16**(4), 910–913(L).

Kingon, A.I.–Effect of hydrogen on true leakage current characteristics of $(Pb,La)(Zr,Ti)O_3$ thin-film capacitors with Pt- or Ir-based top electrodes.–Soon-Gil Yoon, Dwi Wicaksana, Dong-Joo Kim, Seung-Hyun Kim, A.I. Kingon; **16**(4), 1185–1189.

–^{18}O study of the oxidation of reactively sputtered $Ti_{1-x}Al_xN$ barrier.–M.C. Hugon, F. Varniere, F. Letendu, B. Agius, I. Vickridge, and A.I. Kingon; **16**(9), 2591–2599.

Kisailus, David–Growth of epitaxial GaN on $LiGaO_2$ substrates via a reaction with ammonia.–David Kisailus and F.F. Lange; **16**(7), 2077–2081.

Kishio, K.–Melt processing of Ba_2CuO_3: Textured precursor for the fabrication of $HgBa_2CuO_x$ superconductor.–E. Sudhakar Reddy, T. Murakami, Y. Nakayama, J. Shimoyama, K. Kishio; **16**(6), 1759–1768.

Kitamura, Naoyuki–Coordination structures of implanted Fe, Co, and Ni ions in silica glass by x-ray absorption fine structure spectroscopy.–Kohei Fukumi, Akiyoshi Chayahara, Kohei Kadono, Hiroyuki Kageyama, Tomoko Akai, Hiroshi Mizoguchi, Naoyuki Kitamura, Masaki Makihara, Yuji Horino, and Kanenaga Fujii; **16**(1), 155–162.

Kitatochi, Naoki–Water-associated surface degradation of $CsLiB_6O_{10}$ crystal during harmonic generation in the ultraviolet region.–Yukihiro Morimoto, Shintaro Miyazawa, Yoshio Kagebayashi, Naoki Kitatochi, Toshio Yokota, and Jun Sakuma; **16**(7), 2082–2090.

Kivilahti, Jorma K.–Effect of oxygen on the reactions in the Si/Ta/Cu metallization system.–Tomi Laurila, Kejun Zeng, Jorma K. Kivilahti, Jyriki Molarius, and Ilkka Suni; **16**(10), 2939–2946.

Klassen, T.–Submicron-grained multiphase TiAlSi alloys: Processing, characterization, and microstructural design.–R. Bohn, G. Fanta, T. Klassen, and R. Bormann; **16**(6), 1850–1861.

Klemic, J.F.–Growth and characterization of aligned carbon nanotubes from patterned nickel nanodots and uniform thin films.–J.G. Wen, Z.P. Huang, D.Z. Wang, J.H. Chen, S.X. Yang, Z.F. Ren, J.H. Wang, L.E. Calvet, J. Chen, J.F. Klemic, and M.A. Reed; **16**(11), 3246–3253.

Kobayashi, K.–Mechanical stress of the electrical performance of polycrystalline-silicon resistors.–N. Nakabayashi, H. Ohyama, E. Simoen, M. Ikegami, C. Claeys, K. Kobayashi, M. Yoneoka, and K. Miyahara; **16**(9), 2579–2582.

Kobayashi, T.–Cubic silicon nitride embedded in amorphous silicon dioxide.–Ming Zhang, Hongliang He, F.F. Xu, T. Sekine, T. Kobayashi, and Y. Bando; **16**(8), 2179–2181(L).

Koch, C.C.–Mechanical properties of nanocrystalline and epitaxial TiN films on (100) silicon.–H. Wang, A. Sharma, A. Kvit, Q. Wei, X. Zhang, C.C. Koch, and J. Narayan; **16**(9), 2733–2738.

–Origins of stored enthalpy in cryomilled nanocrystalline Zn.–Xinghang Zhang, Haiyan Wang, Magdy Kassem, Jagdish Narayan, Carl C. Koch; **16**(12), 3485–3495.

Kodas, T.–Dielectric properties of oxide structures by a laser-based direct-writing method.–D. Young, H.D. Wu, R.C.Y. Auyeung, R. Modi, J. Fitz-Gerald, A. Pique, D.B. Chrisey, P. Atanassova, and T. Kodas; **16**(6), 1720–1725.

Koh, Young-Hag–Improvement in oxidation resistance of TiB_2 by formation of protective SiO_2 layer on surface.–Young-Hag Koh, Hae-Won Kim, and Hyoun-Ee Kim; **16**(1), 132–137.

Koike, J.–Novel hexagonal structure and ultrahigh strength of magnesium solid solution in the Mg–Zn–Y system.–Akihisa Inoue, Yoshihito Kawamura, Mitsuhide Matsushita, Kentaro Hayashi, Junichi Koike; **16**(7), 1894–1900.

–Processing and characterization of hydroxyapatite coatings on titanium produced by magnetron sputtering.–T.G. Nieh, A.F. Jankowski, and J. Koike; **16**(11), 3238–3245.

Kojima, Isao–Gas flow effects on the structure and composition of $SiN_x/Si/SiN_x$ films prepared by radio-frequency magnetron sputtering.–Wentao Xu, Boquan Li, Toshiyuki Fujimoto, and Isao Kojima; **16**(1), 308–313.

Kojima, K.–Relaxation of ultraviolet-radiation-induced structure and long-lasting phosphorescence in Eu^{2+}-doped strontium aluminosilicate glasses.–Jianrong Qiu, Y. Shimizugawa, K. Kojima, K. Tanaka, and K. Hirao; **16**(1), 88–92.

Kokorin, A.I.–Electrolyte electroreflectance study of TiO_2 films modified with metal nanoparticles.–A.I. Kulak, A.I. Kokorin, and D.V. Sviridov; **16**(8), 2357–2361.

Kololuoma, T.–Dye-doped sol-gel coatings for near-infrared laser protection.–T. Kololuoma, J.A.I. Oksanen, P. Raerinne, and J.T. Rantala; **16**(8), 2186–2188(L).

Komatsu, Manabu–Oxygen self-diffusion in cerium oxide doped with Nd.–Michiyo Kamiya, Eriko Shimada, Yasuro Ikuma, Manabu Komatsu, Hajime Haneda, Soichiro Sameshima, and Yoshihiro Hirata; **16**(1), 179–184.

Kondo, Naoki–High-strength porous silicon nitride fabricated by the sinter-forging technique.–Naoki Kondo, Yoshikazu Suzuki, and Tatsuki Ohji; **16**(1), 32–34(L).

–Improved creep resistance in anisotropic silicon nitride.–Naoki Kondo, Yoshikazu Suzuki, Manuel E. Brito, and Tatsuki Ohji; **16**(8), 2182–2185(L).

Kong, G.–Microstructure of laser-ablated superconducting $La_2CuO_4F_x$ thin films on $SrTiO_3$.–G. Kong, M.O. Jones, J.S. Abell, P.P. Edwards, S.T. Lees, K.E. Gibbons, I. Gameson, and M. Aindow; **16**(11), 3309–3316.

Kong, L.B.–$Pb(Zr_xTi_{1-x})O_3$ ceramics via reactive sintering of partially reacted mixture produced by a high-energy ball milling process.–L.B. Kong, J. Ma, T.S. Zhang, W. Zhu, and O.K. Tan; **16**(6), 1636–1643.

Kononenko, O.V.–Electromigration properties of multigrain aluminum thin film conductors as influenced by grain boundary structure.–O.V. Kononenko, V.N. Matveev, and D.P. Field; **16**(7), 2124–2129.

Koo, Junmo–Preparation and characteristics of seeded epitaxial $(Sr,Ba)Nb_2O_6$ optical waveguide thin films using sol-gel method.–Junmo Koo, Jae Hyeok Jang, and Byeong-Soo Bae; **16**(2), 430–436.

Korzec, Dariusz–Comparison of hydrophilic properties of amorphous TiO_x films obtained by radio frequency sputtering and plasma-enhanced chemical vapor deposition.–Masatoshi Nakamura, Toru Aoki, Yoshinori Hatanaka, Dariusz Korzec, and Jurgen Engemann; **16**(2), 621–626.

Koshiba, K.–Morphological effect on the electrochemical behavior of electric double-layer capacitors.–M. Endo, Y.J. Kim, T. Maeda, K. Koshiba, K. Katayam, and M.S. Dresselhaus; **16**(12), 3402–3410.

Koshizaki, N.–Parameter effect on the crystallization of Nd:yttrium aluminum garnet laser-ablated TiO_2 thin film.–Mrinal Pal, Aiko Narazaki, Takeshi Sasaki, and Naoto Koshizaki; **16**(11), 3158–3161.

–Determination of optical constants of Si/ZnO polycrystalline nanocomposites by spectroscopic ellipsometry.–J. García-Serrano, N. Koshizaki, T. Sasaki, G. Martínez-Montes, and U. Pal; **16**(12), 3554–3559.

Kostić-Gvozdenović, Lj.–Phase-transformation kinetics in triphasic cordierite gel.–R. Petrović, Dj. Janacković, S. Zec, S. Drmanić, Lj. Kostić-Gvozdenović; **16**(2), 451–458.

Kovacs, Gy.Sh.–Influence of compositional disorder on optical absorption processes in $Cu_6P(S_{1-x}Se_x)_5I$ crystals.–I.P. Studenyak, M. Kranjčec, Gy.Sh. Kovacs, I.D. Desnica-Franković, V.V. Panko, and V.Yu. Slivka; **16**(6), 1600–1608.

Kovács, Zs.–Orientation dependence of Portevin–Le Châtelier plastic instabilities in depth-sensing microindentation.–Zs. Kovács, N.Q. Chinh, and J. Lendvai; **16**(4), 1171–1177.

Kozuka, Hiromitsu–Single-layer submicron-thick $BaTiO_3$ coatings from poly(vinylpyrrolidone)-containing sols: Gel-to-ceramic film conversion, densification, and dielectric properties.–Hiromitsu Kozuka and Atsushi Higuchi; **16**(11), 3116–3123.

Kramer, D.E.–Substrate effects on indentation plastic zone development in thin soft films.–D.E. Kramer, A.A. Volinsky, N.R. Moody, and W.W. Gerberich; **16**(11), 3150–3157.

Kranjčec, M.–Influence of compositional disorder on optical absorption processes in $Cu_6P(S_{1-x}Se_x)_5I$ crystals.–I.P. Studenyak, M. Kranjčec, Gy.Sh. Kovacs, I.D. Desnica-Franković, V.V. Panko, and V.Yu. Slivka; **16**(6), 1600–1608.

Krasil'nikova, N.A.–Electronic paramagnetic resonance study of Cu^{2+} ions in copper ion-exchanged layers of lithium niobate crystals.–F. Caccavale, C. Sada, F. Segato, L.D. Bogomolova, V.A. Jachkin, and N.A. Krasil'nikova; **16**(6), 1554–1558.

Krausz, I.M.–Hydrodynamic cavitation as a tool to control macro-, micro-, and nano-properties of inorganic materials.–J. Find, S.C. Emerson, I.M. Krausz, and W.R. Moser; **16**(12), 3503–3513.

Kriven, Waltraud M.–Crystallization kinetics of yttrium aluminum garnet ($Y_3Al_5O_{12}$).–Bradley R. Johnson and Waltraud M. Kriven; **16**(6), 1795–1805.

Krug, S.–Packing and solidification in ceramic injection moulding.–S. Krug, J.R.G. Evans, and J.H.H. ter Maat; **16**(6), 1829–1837.

Krzesińska, M.–Elastic properties of anisotropic monolithic samples of compressed expanded graphite studied with ultrasounds.–M. Krzesińska, A. Celzard, J.F. Marêché, and S. Puricelli; **16**(2), 606–614.

Kubsky, S.–Characterization of the induction period in tricalcium silicate hydration by nuclear resonance reaction analysis.–R.A. Livingston, J.S. Schweitzer, C. Rolfs, H-W. Becker, S. Kubsky; **16**(3), 687–693.

Kui, H.W.–Crystallization kinetics of amorphous nanostructured $Pd_{40.5}Ni_{40.5}P_{19}$ alloys.–H.W. Ngai, C.C. Leung, W.H. Guo, and H.W. Kui; **16**(3), 797–802.

–Compaction of bulk ferromagnetic $Fe_{80}P_{13}C_7$ amorphous alloys.–F.W. Chan, N.G. Ma, and H.W. Kui; **16**(10), 2767–2769(L).

Kulak, A.I.–Electrolyte electroreflectance study of TiO_2 films modified with metal nanoparticles.–A.I. Kulak, A.I. Kokorin, and D.V. Sviridov; **16**(8), 2357–2361.

Kulas, R.J.–Thermal expansion and high-temperature phase transformation of the yttrium silicate Y_2SiO_5.–J.W. Nowok, J.P. Kay, and R.J. Kulas; **16**(8), 2251–2255.

Kulinich, S.A.–Crystallography and structural evolution of $LiNbO_3$ and $LiNb_{1-x}Ta_xO_3$ films on sapphire prepared by high-rate thermal plasma spray chemical vapor deposition.–D.V. Shtansky, S.A. Kulinich, K. Terashima, T. Yoshida, and Y. Ikuhara; **16**(8), 2271–2279.

Kum, Dong-Wha–Interface structure and solute segregation behavior in SiC/2124 and SiC/6061 Al composites exhibiting high-strain-rate superplasticity.–Woo-Jin Kim, Dong-Wha Kum, and Ha-Guk Jeong; **16**(8), 2429–2435.

Kunert, M.–Hardness–depth profile of a carbon-implanted Ti–6Al–4V alloy and its relation to composition and microstructure.–M. Kunert, O. Kienzle, B. Baretzky, S.P. Baker, and E.J. Mittemeijer; **16**(8), 2321–2335.

Kung, H.–Compositional distributions in nanoscale metallic multilayers studied using x-ray mapping.–V.J. Keast, A. Misra, H. Kung, and T.E. Mitchell; **16**(7), 2032–2038.

–High critical current density $YBa_2Cu_3O_{7-\delta}$ thick films using ion beam assisted deposition MgO bi-axially oriented template layers on nickel-based superalloy substrates.–J.R. Groves, P.N. Arendt, S.R. Foltyn, Q.X. Jia, T.G. Holesinger, H. Kung, E.J. Peterson, R.F. DePaula, P.C. Dowden, L. Stan, and L.A. Emmert; **16**(8), 2175–2178(L).

Kunita, M.H.–Low-resistance films of polyimides with impregnated copper sulfide.–R.V.A. Rowe, M.H. Kunita, M.F. Porto, E.C. Muniz, A.F. Rubira, R.C. Nery, E. Radovanovic, L.T. Taylor, and N. Nazem; **16**(11), 3097–3106.

Kuo, K.H.–Effects of pressure on the solidification of Al–Mn alloy.–Duanwei He, M. He, C.S. Kiminami, F.X. Zhang, Y.F. Xu, W.K. Wang, and K.H. Kuo; **16**(4), 910–913(L).

Kuribayashi, K.–Formation of $NdBa_2Cu_3O_{7-\delta}$ amorphous phase by combining aero-acoustic levitation and splat quenching.–K. Nagashio, W.H. Hofmeister, D.E. Gustafson, A. Altgilbers, R.J. Bayuzick, and K. Kuribayashi; **16**(1), 138–145.

Kuriger, Rex J.–Strength prediction of partially aligned discontinuous fiber-reinforced composites.–Rex J. Kuriger, M. Khairul Alam, and David P. Anderson; **16**(1), 226–232.

Kurosaka, Kei–Formation and mechanical properties of Cu–Hf–Ti bulk glassy alloys.–Akihisa Inoue, Wei Zhang, Tao Zhang, and Kei Kurosaka; **16**(10), 2836–2844.

Kuščer, Danjela–Subsolidus phase relations in the La_2O_3–Fe_2O_3–Al_2O_3 system.–Danjela Kuščer, Slavko Bernik, Marko Hrovat, and Janez Holc; **16**(3), 822–827.

Kuwabara, M.–Microstructural analysis of high-pressure compressed C_{60}.–K. Miyazawa, H. Satsuki, M. Kuwabara, and M. Akaishi; **16**(7), 1960–1966.

Kvit, A.–Mechanical properties of nanocrystalline and epitaxial TiN films on (100) silicon.–H. Wang, A. Sharma, A. Kvit, Q. Wei, X. Zhang, C.C. Koch, and J. Narayan; **16**(9), 2733–2738.

Kwon, Dongil–Derivation of plastic stress–strain relationship from ball indentations: Examination of strain definition and pileup effect.–Jeong-Hoon Ahn and Dongil Kwon; **16**(11), 3170–3178.

Kwon, H.J.–Superplasticicity of Cu–16 at.% Ag microcomposites.–S.I. Hong and H.J. Kwon; **16**(6), 1822–1828.

Kwon, Oh Seong–Metalorganic chemical vapor deposition of very thin $Pb(Zr,Ti)O_3$ thin films at low temperatures for high-density ferroelectric memory applications.–Hye Ryoung Kim, Seehwa Jeong, Chung Bae Jeon, Oh Seong Kwon, Cheol Seong Hwang, Young Ki Han, Doo Young Yang, and Ki Young Oh; **16**(12), 3583–3591.

L

Laabs, F.C.–Analysis of interdiffusion of Dy, Nd, and Pr in Mg.–Y. Xu, L.S. Chumbley, G.A. Weigelt, and F.C. Laabs; **16**(11), 3287–3292.

Laaziz, Y.–X-ray photoelectron spectroscopy of electrodeposited cadmium mercury telluride thin films and their native surface oxides.–J. Ramiro, L. Galán, E. García Camarero, I. Montero, Y. Laaziz; **16**(7), 1942–1952.

Lacout, J.L.–Preparation of calcium strontium hydroxyapatites by a new route involving calcium phosphate cements.–L. Leroux and J.L. Lacout; **16**(1), 171–178.

Lai, W.S.–Glass-forming ability of the Ni–Zr and Ni–Ti systems determined by interatomic potentials.–W.S. Lai and B.X. Liu; **16**(2), 446–450.

Lam, D.C.C.–Characterization and modeling of specific strain gradient modulus of epoxy.–D.C.C. Lam and A.C.M. Chong; **16**(2), 558–563.

–Torsion and bending of micron-scaled structures.–A.C.M. Chong, F. Yang, D.C.C. Lam, and P. Tong; **16**(4), 1052–1058.

Lam, Y.C.–Two-dimensional simulation of mass transport in polymer removal from a powder injection molding compact by thermal debinding.–Ying Shengjie, Y.C. Lam, S.C.M. Yu, and K.C. Tam; **16**(8), 2436–2451.

Lam, Y.L.–Third-order nonlinear optical response in PbS-coated CdS nanocomposites.–Bing Liu, Chwee Har Chew, Leong Ming Gan, Guo Qin Xu, Heping Li, Yee Loy Lam, Chan Hin Kam, and Wen Xiu Que; **16**(6), 1644–1650.

–Preparation and characterization of nanocrystalline potassium lithium niobate powders and films.–H.X. Zhang, C.H. Kam, Y. Zhou, X.Q. Han, S.D. Cheng, C.Y. Chan, and Y.L. Lam; **16**(12), 3609–3613.

Lanagan, Michael T.–Phase formation and reactions in the Bi_2O_3–ZnO–Nb_2O_5–Ag pyrochlore system.–Juan C. Nino, Michael T. Lanagan, and Clive A. Randall; **16**(5), 1460–1464.

Landi, E.–Rheological characteristics of slurry controlling the microstructure and the compressive strength behavior of biomimetic hydroxyapatite.–S. Guicciardi, C. Galassi, E. Landi, A. Tampieri, K. Satou, and G. Pezzotti; **16**(1), 163–170.

Langdon, Terence G.–Grain boundary structure in Al–Mg and Al–Mg–Sc alloys after equal-channel angular pressing.–Keiichiro Oh-ishi, Zenji Horita, David J. Smith, and Terence G. Langdon; **16**(2), 583–589.

Lange, F.F.–Epitaxial growth of $PbZr_{0.5}Ti_{0.5}O_3$ thin films on $SrRuO_3/SrTiO_3$ substrates using chemical solution deposition: Microstructural and ferroelectric properties.–J.H. Kim, Youngman Kim, A.T. Chien, and F.F. Lange; **16**(6), 1739–1744.

–Growth of epitaxial GaN on $LiGaO_2$ substrates via a reaction with ammonia.–David Kisailus and F.F. Lange; **16**(7), 2077–2081.

Lannutti, John–Phase transformation effects on the wear properties of alumina gel–polymer matrix nanocomposites.–Jiazhong Luo, John Lannutti, and Robert Seghi; **16**(6), 1680–1685.

–Increased fracture toughness in nanoporous silica–polyimide matrix composites.–Shiling Ruan, John J. Lannutti, Stan Prybyla, and Robert R. Seghi; **16**(7), 1975–1981.

Lau, Cheryl–Mechanistic studies in combustion synthesis of NiAl–TiB_2 composites: Effects of gravity.–Cheryl Lau, Alexander Mukasyan, Aleksey Pelekh, and Arvind Varma; **16**(6), 1614–1625.

Laurila, Tomi–Effect of oxygen on the reactions in the Si/Ta/Cu metallization system.–Tomi Laurila, Kejun Zeng, Jorma K. Kivilahti, Jyriki Molarius, and Ilkka Suni; **16**(10), 2939–2946.

Lauwerens, W.–Fretting wear rate of sulphur deficient MoS_x coatings based on dissipated energy.–Xiaoling Zhang, W. Lauwerens, L. Stals, Jiawen He, and J-P. Celis; **16**(12), 3567–3574.

Lauwers, A.–*In situ* transmission electron microscopy study of the silicidation process in Co thin films on patterned (001) Si substrates.–C. Ghica, L. Nistor, H. Bender, A. Steegen, A. Lauwers, K. Maex, and J. Van Landuyt; **16**(3), 701–708.

Lavernia, E.J.–Grain growth behavior of a nanostructured 5083 Al–Mg alloy.–V.L. Tellkamp, S. Dallek, D. Cheng, and E.J. Lavernia; **16**(4), 938–944.

–Thermal stability of nanocrystalline WC–Co powder synthesized by using mechanical milling at low temperature.–Jianhong He, Leoanardo Ajdelsztajn, and Enrique J. Lavernia; **16**(2), 478–488.

–Development of nanocrystalline structure during cryomilling of Inconel 625.–Jianhong He and Enrique J. Lavernia; **16**(9), 2724–2732.

–High grain size stability of nanocrystalline Al prepared by mechanical attrition.–F. Zhou, J. Lee, S. Dallek, and E.J. Lavernia; **16**(12), 3451–3458.

Lawn, Brian R.–Contact fracture of brittle bilayer coatings on soft substrates.–Pedro Miranda, Antonia Pajares, Fernando Guiberteau, Francisco L. Cumbrera, Brian R. Lawn; **16**(1), 115–126.

–Cracking of porcelain coatings bonded to metal substrates of different modulus and hardness.–Hong Zhao, Xiaozhi Hu, Mark B. Bush, and Brian R. Lawn; **16**(5), 1471–1478.

Lederman, D.–Growth study of epitaxial $Fe_xZn_{1-x}F_2$ thin films.–J. McChesney, M. Hetzer, H. Shi, T. Charlton, D. Lederman; **16**(6), 1769–1775.

Lee, Byung-Teak–Chemical-vapor-deposition growth and characterization of epitaxial 3C–SiC films on SOI substrates with thin silicon top layers.–C.K. Moon, H.J. Song, J.K. Kim, J.H. Park, S.J. Jang, J-B. Yoo, H-R. Park, and Byung-Teak Lee; **16**(1), 24–27(L).

Lee, Choong-Il–Photoluminescence spectra of undoped and Sm^{3+}-doped $BaAl_2S_4$ and $BaAl_2Se_4$ single crystals.–Moon-Seog Jin, Choong-Il Lee, Chang-Sun Yoon, Chang-Dae Kim, Jae-Mo Goh, and Wha-Tek Kim; **16**(5), 1520–1524.

Lee, Eun-Gu- Influence of sintering atmosphere on the fabrication of SiC ceramics with a powder mixture of sialon composition.–Jong-Kook Lee, Jong-Gon Park, Eun-Gu Lee, and Kyung-Seok Kim; **16**(6), 1784–1788.

–Preparation of nanocrystalline nickel oxide–yttria-stabilized zirconia composite powder by solution combustion with ignition of glycine fuel.–Sun-Jae Kim, Wonhee Lee, Won-Jun Lee, Soon Dong Park, Jae Sung Song, and Eun Gu Lee; **16**(12), 3621–3627.

Lee, H.Y.–Temperature dependence of the optical properties in p-$Cd_{0.96}Zn_{0.04}Te$ single crystals.–H.Y. Lee, T.W. Kang, and T.W. Kim; **16**(8), 2196–2199.

Lee, Hoin–Joining characteristics of oxidized SiC particles reinforced Al–Mg matrix composite prepared by reaction infiltration processing.–Zhongliang Shi, Shijiro Ochiai, Masaki Hojo, Jaechul Lee, Mingyuan Gu, and Hoin Lee; **16**(2), 400–406.

Lee, J.–High grain size stability of nanocrystalline Al prepared by mechanical attrition.–F. Zhou, J. Lee, S. Dallek, and E.J. Lavernia; **16**(12), 3451–3458.

Lee, J.K.–Precipitation of icosahedral phase from amorphous $Zr_{65}Cu_{17.5-x}Al_{7.5}Ni_{10}Ag_x$ (x = 0, 5) alloys.–J.K. Lee, G. Choi, W.T. Kim, and D.H. Kim; **16**(5), 1311–1317.

Lee, Jaechul–Joining characteristics of oxidized SiC particles reinforced Al–Mg matrix composite prepared by reaction infiltration processing.–Zhongliang Shi, Shijiro Ochiai, Masaki Hojo, Jaechul Lee, Mingyuan Gu, and Hoin Lee; **16**(2), 400–406.

Lee, Jim H.–Cure depth in photopolymerization: Experiments and theory.–Jim H. Lee, Robert K. Prud'homme, and Ilhan A. Aksay; **16**(12), 3536–3544.

Lee, Jong-Heun–Precursor scavenging of the resistive grain-boundary phase in 8 mol% yttria-stabilized zirconia: Effect of trace concentrations of SiO_2.–Jong-Heun Lee, Toshiyuki Mori, Ji-Guang Li, Takayasu Ikegami, John Drennan, and Doh-Yeon Kim; **16**(8), 2377–2383.

Lee, Jong-Hyun–Stability of channels at a scalloplike Cu_6Sn_5 layer in solder interconnections.–Jong-Hyun Lee, Jong-Hwan Park, Yong-Ho Lee, Yong-Seog Kim, and Dong Hyuk Shin; **16**(5), 1227–1230(L).

–Effects of Cu and Ni additions to eutectic Pb–Sn solders on Au embrittlement of solder interconnections.–Jong-Hyun Lee, Jong-Hwan Park, Yong-Ho Lee, and Yong-Seog Kim; **16**(5), 1249–1251(L).

Lee, Jong-Kook–Influence of sintering atmosphere on the fabrication of SiC ceramics with a powder mixture of sialon composition.–Jong-Kook Lee, Jong-Gon Park, Eun-Gu Lee, and Kyung-Seok Kim; **16**(6), 1784–1788.

Lee, Jong-Sook–Space-charge concepts on grain boundary impedance of a high-purity yttria-stabilized tetragonal zirconia polycrystal.–Jong-Sook Lee and Doh-Yeon Kim; **16**(9), 2739–2751.

Lee, K.L.–Texture analysis of grain refinement in undercooled $Ni_{99.45}B_{0.55}$.–K.L. Lee, C.H. Shek, and H. Yang; **16**(5), 1434–1438.

Lee, Kyeong Seok–Ferroelectric domain structure of epitaxial (Pb, Sr)TiO_3 thin films.–Yong Kwan Kim, Kyeong Seok Lee, and Sunggi Baik; **16**(9), 2463–2466(L).

Lee, S.M.–Quasicrystalline phase formation in $Al_{62}Cu_{22.5}Fe_{12.5}$ and $Al_{55}Cu_{22.5}Fe_{12.5}Be_7$ alloys.–S.M. Lee, B.H. Kim, D.H. Kim, and W.T. Kim; **16**(6), 1535–1540.

Lee, Sanboh–Chemical stresses induced by grain-boundary diffusion in thin films.–W.L. Wang, Y.T. Chou, and Sanboh Lee; **16**(7), 1967–1974.

Lee, Seok-Joo–Absorption spectra of Co^{2+} in $AgInS_2$ orthorhombic single crystals.–Hidong Kim, Seok-Joo Lee, Jae-Eun Kim, Hae Yong Park, Seok-Kyun Oh, and Wha-Tek Kim; **16**(4), 975–978.

Lee, Sun-Hwa–Formation and characteristics of highly *c*-axis-oriented $Bi_{3.25}La_{0.75}Ti_3O_{12}$ thin films on SiO_2/Si(100) and Pt/Ti/SiO_2/Si(100) substrates.–Uong Chon, Hyun M. Jang, Sun-Hwa Lee, and Gyu-Chul Yi; **16**(11), 3124–3132.

Lee, William E.–Relation between tolerance factor and T_c in Aurivillius compounds.–Donají Y. Suárez, Ian M. Reaney, and William E. Lee; **16**(11), 3139–3149.

Lee, Wonhee–Preparation of nanocrystalline nickel oxide–yttria-stabilized zirconia composite powder by solution combustion with ignition of glycine fuel.–Sun-Jae Kim, Wonhee Lee, Won-Jun Lee, Soon Dong Park, Jae Sung Song, and Eun Gu Lee; **16**(12), 3621–3627.

Lee, Won-Jun–Preparation of nanocrystalline nickel oxide–yttria-stabilized zirconia composite powder by solution combustion with ignition of glycine fuel.–Sun-Jae Kim, Wonhee Lee, Won-Jun Lee, Soon Dong Park, Jae Sung Song, and Eun Gu Lee; **16**(12), 3621–3627.

Lee, Yong-Ho–Stability of channels at a scalloplike Cu_6Sn_5 layer in solder interconnections.–Jong-Hyun Lee, Jong-Hwan Park, Yong-Ho Lee, Yong-Seog Kim, and Dong Hyuk Shin; **16**(5), 1227–1230(L).

–Effects of Cu and Ni additions to eutectic Pb–Sn solders on Au embrittlement of solder interconnections.–Jong-Hyun Lee, Jong-Hwan Park, Yong-Ho Lee, and Yong-Seog Kim; **16**(5), 1249–1251(L).

Lee, Yu-Chang–Ordered structure formation in the flux-grown $Ba(Mg_{1/3}Ta_{2/3})O_3$ single crystals.–Yu-Chang Lee, Chen-Chia Chou, and Dah-Shyang Tsai; **16**(6), 1593–1599.

Lees, S.T.–Microstructure of laser-ablated superconducting $La_2CuO_4F_x$ thin films on $SrTiO_3$.–G. Kong, M.O. Jones, J.S. Abell, P.P. Edwards, S.T. Lees, K.E. Gibbons, I. Gameson, and M. Aindow; **16**(11), 3309–3316.

Lei, Y.–Fabrication, characterization, and photoluminescence properties of highly ordered TiO_2 nanowire arrays.–Y. Lei and L.D. Zhang; **16**(4), 1138–1144.

Lendvai, J.–Orientation dependence of Portevin–Le Châtelier plastic instabilities in depth-sensing microindentation.–Zs. Kovács, N.Q. Chinh, and J. Lendvai; **16**(4), 1171–1177.

Leroux, L.–Preparation of calcium strontium hydroxyapatites by a new route involving calcium phosphate cements.–L. Leroux and J.L. Lacout; **16**(1), 171–178.

Letendu, F.–^{18}O study of the oxidation of reactively sputtered $Ti_{1-x}Al_xN$ barrier.–M.C. Hugon, F. Varniere, F. Letendu, B. Agius, I. Vickridge, and A.I. Kingon; **16**(9), 2591–2599.

Lettieri, J.–Transmission electron microscopy study of (103)-oriented epitaxial $SrBi_2Nb_2O_9$ films grown on (111) $SrTiO_3$ and (111) $SrRuO_3$/(111) $SrTiO_3$.–M.A. Zurbuchen, J. Lettieri, Y. Jia, D.G. Schlom, S.K. Streiffer, and M.E. Hawley; **16**(2), 489–502.

Leung, C.C.–Crystallization kinetics of amorphous nanostructured $Pd_{40.5}Ni_{40.5}P_{19}$ alloys.–H.W. Ngai, C.C. Leung, W.H. Guo, and H.W. Kui; **16**(3), 797–802.

Leventouri, Th.–Comparison of crystal structure parameters of natural and synthetic apatites from neutron powder diffraction.–Th. Leventouri, B.C. Chakoumakos, N. Papanearchou, and V. Perdikatsis; **16**(9), 2600–2606.

Li, A-D.–Processing- and composition-dependent characteristics of chemical solution deposited $Bi_{4-x}La_xTi_3O_{12}$ thin films.–Di Wu, Aidong Li, Tao Zhu, Zhifeng Li, Zhiguo Liu, and Naiben Ming; **16**(5), 1325–1332.

–Novel route for the epitaxial growth of $(SrBa)Nb_2O_6$ thick films by the sol-gel method using a self-template layer.–A-D. Li, C.L. Mak, K.H. Wong, D. Wu, and Naiben Ming; **16**(11), 3179–3183.

–Impacts of postannealing ambient atmospheres on Pt/$SrBi_{2.2}Ta_2O_9$/Pt capacitors.–Ai-Dong Li, Tao Yu, Hui-Qin Ling, Di Wu, Zhi-Guo Liu, and Nai-Ben Ming; **16**(12), 3526–3535.

Li, Boquan–Gas flow effects on the structure and composition of SiN_x/Si/SiN_x films prepared by radio-frequency magnetron sputtering.–Wentao Xu, Boquan Li, Toshiyuki Fujimoto, and Isao Kojima; **16**(1), 308–313.

Li, Chunfei–Precipitation of icosahedral quasicrystalline phase in $Hf_{69.5}Al_{7.5}Ni_{11}Cu_{12}$ metallic glass.–Chunfei Li and Akihisa Inoue; **16**(4), 1190–1194.

–Investigation of the stability of glassy state in the Zr- and Hf-based glassy alloys correlated with their transformation behavior.–Junji Saida, Chunfei Li, Mitsuhide Matsushita, and Akihisa Inoue; **16**(12), 3389–3401.

Li, Cun–Blue photoluminescent properties of pure nanostructured γ–Al_2O_3.–Zhong Qing Yu, Dao Chang, Cun Li, Ning Zhang, Yu Ying Feng, and You Yuan Dai; **16**(7), 1890–1893(L).

Li, D.X.–$L1_2$- and $L1_0$-like cation-ordered structures in ZrO_2–Y_2O_3 ceramics.–J.C. Rao, Y. Zhou, and D.X. Li; **16**(6), 1806–1813.

Li, Donglin–Twinning domain in $67Pb(Mg_{1/3}Nb_{2/3})O_3$–$33PbTiO_3$ ferroelectric complex perovskite crystal grown by the Bridgman method.–Donglin Li, Pingchu Wang, Xiaoming Pan, Haosu Luo, and Zhiwen Yin; **16**(5), 1252–1255(L).

Li, F.Y.–Study of phase components of $La_{1.5}Ca_{1.5}Mn_2O_7$.–J.L. Zhu, R.C. Yu, F.Y. Li, C.Q. Jin, and Z. Zhang; **16**(7), 2027–2031.

Li, G.L.–Microstructure studies of potassium hexatitanate whiskers.–G.L. Li, M. Liu, and G.H. Wang; **16**(12), 3614–3620.

Li, Guangshe–Valence variations in titanium-based perovskite oxides by high-pressure and high-temperature method.–Liping Li, Guangshe Li, Jipeng Miao, Wenhui Su, and Hiroshi Inomata; **16**(2), 417–424.

–Solid solubility and transport properties of $Ce_{1-x}Nd_xO_{2-\delta}$ nanocrystalline solid solutions by a sol-gel route.–Liping Li, Xiaomin Lin, Guangshe Li, and Hiroshi Inomata; **16**(11), 3207–3213.

Li, Heping–Third-order nonlinear optical response in PbS-coated CdS nanocomposites.–Bing Liu, Chwee Har Chew, Leong Ming Gan, Guo Qin Xu, Heping Li, Yee Loy Lam, Chan Hin Kam, and Wen Xiu Que; **16**(6), 1644–1650.

Li, J.C.M.–Impression creep of a viscous layer.–Hong Chen and J.C.M. Li; **16**(9), 2709–2715.

Li, Ji-Guang–Precursor scavenging of the resistive grain-boundary phase in 8 mol% yttria-stabilized zirconia: Effect of trace concentrations of SiO_2.–Jong-Heun Lee, Toshiyuki Mori, Ji-Guang Li, Takayasu Ikegami, John Drennan, and Doh-Yeon Kim; **16**(8), 2377–2383.

Li, L.X.–Structure and the nonlinearity of lithium triborate studied by Raman and infrared reflectivity spectroscopy.–H.R. Xia, L.X. Li, H. Yu, S.M. Dong, J.Y. Wang, Q.M. Lu, C.Q. Ma, and X.N. Wang; **16**(12), 3464–3470.

Li, Liping–Valence variations in titanium-based perovskite oxides by high-pressure and high-temperature method.–Liping Li, Guangshe Li, Jipeng Miao, Wenhui Su, and Hiroshi Inomata; **16**(2), 417–424.

–Solid solubility and transport properties of $Ce_{1-x}Nd_xO_{2-\delta}$ nanocrystalline solid solutions by a sol-gel route.–Liping Li, Xiaomin Lin, Guangshe Li, and Hiroshi Inomata; **16**(11), 3207–3213.

Li, Min–Adhesion of polymer–inorganic interfaces by nanoindentation.–Min Li, C. Barry Carter, Marc A. Hillmyer, and William W. Gerberich; **16**(12), 3378–3388.

Li, Mu-Sen–Electron microscopy of high-temperature and high-pressure as-grown diamond crystals.–Long-Wei Yin, Mu-Sen Li, Jian-Jun Cui, Bin Xu, Jian-Hong Gong, Zhao-Yin Hao, and Jiong-Fa Zhang; **16**(11), 3023–3026(L).

Li, Tie Jin–Fabrication of heteropolyoxometalate-based photochromic inorganic–organic nanocomposites.–Tie Rui Zhang, Wei Feng, Chun Yan Bao, Ran Lu, Xin Tong Zhang, Tie Jin Li, Ying Ying Zhao, and Jian Nian Yao; **16**(8), 2256–2263.

Li, W.–Study of the mechanism for controlled crystallization of BaF_2 under two kinds of monolayers.–L. Lu, H. Cui, W. Li, H. Zhang, and S. Xi; **16**(8), 2415–2420.

Li, W.C.–Thermodynamic analysis of combustion synthesis of Al_2O_3–TiC–ZrO_2 nanoceramics.–Q. Dong, Q. Tang, W.C. Li, and D.Y. Wu; **16**(9), 2494–2498.

Li, Wei–Novel photoluminescence from hydrogenated amorphous carbon films prepared by using xylene source.–Jun Xu, Wei Li, Tianfu Ma, Zhifeng Li, Li Wang, and Kunji Chen; **16**(2), 325–328(L).

Li, Y.–Chemical–mechanical polishing of copper and tantalum with silica abrasives.–Y. Li, M. Hariharaputhiran, and S.V. Babu; **16**(4), 1066–1073.

Li, Y.B.–Synthesis of α–SiO_2 nanowires using Au nanoparticle catalysts on a silicon substrate.–Z.Q. Liu, S.S. Xie, L.F. Sun, D.S. Tang, W.Y. Zhou, C.Y. Wang, W. Liu, Y.B. Li, X.P. Zou, and G. Wang; **16**(3), 683–686.

Li, Ya-Li–Enhanced crystallization and phase transformation of amorphous silicon nitride under high pressure.–Ya-Li Li, Yong Liang, Fen Zheng, Xian-Feng Ma, Suo-Jing Cui, and Liling Sun; **16**(1), 67–75.

Li, Ya-Wen–Nonepitaxial heterogeneous nucleation of α-sialon in the Ca-doped system.–Ya-Wen Li, Pei-Ling Wang, Wei-Wu Chen, Jing-Wei Feng, Yi-Bing Cheng, and Dong-Sheng Yan; **16**(2), 578–582.

Li, Yunkui–Phase transition, growth, and optical properties of $Nd_xLa_{1-x}Sc_3(BO_3)_4$ crystals.–Yunkui Li, G. Aga, A. Kahn-Harari, and D. Vivien; **16**(1), 38–44.

Li, Z.C.–Shear-activated indentation crack in GaAs single crystal.–Z.C. Li, L. Liu, L.L. He, Y.B. Xu, and X. Wu; **16**(10), 2845–2849.

Li, Zhenrong–Dielectric properties anomaly of (1–x)$Pb(Ni_{1/3}Nb_{2/3})$-O_3–x$PbTiO_3$ ceramics near the morphotropic phase boundary.–Zhenrong Li, Liangying Zhang, and Xi Yao; **16**(3), 834–836.

Li, Zhifeng–Novel photoluminescence from hydrogenated amorphous carbon films prepared by using xylene source.–Jun Xu, Wei Li, Tianfu Ma, Zhifeng Li, Li Wang, and Kunji Chen; **16**(2), 325–328(L).

–Processing- and composition-dependent characteristics of chemical solution deposited $Bi_{4-x}La_xTi_3O_{12}$ thin films–Di Wu, Aidong Li, Tao Zhu, Zhifeng Li, Zhiguo Liu, Naiben Ming; **16**(5), 1325–1332.

Liang, Ji–Aligned carbon nanotube growth under oxidative ambient.–Anyuan Cao, Xianfeng Zhang, Cailu Xu, Ji Liang, Dehai Wu, and Bingqing Wei; **16**(11), 3107–3110.

Liang, Yong–Enhanced crystallization and phase transformation of amorphous silicon nitride under high pressure.–Ya-Li Li, Yong Liang, Fen Zheng, Xian-Feng Ma, Suo-Jing Cui, and Liling Sun; **16**(1), 67–75.

–Corrosive wear of the Co–Cr–W alloy in liquid zinc.–Xibao Wang and Yong Liang; **16**(6), 1585–1592.

Lin, C.H.–Investigation of crystal properties of TmP/GaAs and GaAs/TmP/GaAs heterostructures grown by molecular beam epitaxy.–C.H. Lin, R.J. Hwu, and L.P. Sadwick; **16**(11), 3266–3273.

Lin, Chun-Nan–Combustion synthesis of aluminum nitride powder using additives.–Chun-Nan Lin and Shyan-Lung Chung; **16**(8), 2200–2208.

–Combustion synthesis method for synthesis of aluminum nitride powder using aluminum containers.–Chun-Nan Lin and Shyan-Lung Chung; **16**(12), 3518–3525.

Lin, M-T.–Planar oxidation of strained silicon substrates.–M-T. Lin, R.J. Jaccodine, and T.J. Delph; **16**(3), 728–733.

Lin, Nian–Thermal stability of carbon nitride thin films.–Niklas Hellgren, Nian Lin, Esteban Broitman, Virginie Serin, Stefano E. Grillo, Ray Twesten, Ivan Petrov, Christian Colliex, Lars Hultman, and Jan-Eric Sundgren; **16**(11), 3188–3201.

Lin, Xiaomin–Solid solubility and transport properties of $Ce_{1-x}Nd_xO_{2-\delta}$ nanocrystalline solid solutions by a sol-gel route.–Liping Li, Xiaomin Lin, Guangshe Li, and Hiroshi Inomata; **16**(11), 3207–3213.

Ling, Hui-Qin–Impacts of postannealing ambient atmospheres on Pt/$SrBi_{2.2}Ta_2O_9$/Pt capacitors.–Ai-Dong Li, Tao Yu, Hui-Qin Ling, Di Wu, Zhi-Guo Liu, and Nai-Ben Ming; **16**(12), 3526–3535.

Liniger, Eric G.–Evaluation of the modified edge lift-off test for adhesion characterization in microelectronic multifilm applications.–Jack C. Hay, Eric G. Liniger, and Xiao Hu Liu; **16**(2), 385–393.

Linnros, Jan–Carrier diffusion characterization in epitaxial 4H–SiC.–Paulius Grivickas, Jan Linnros, and Vytautas Grivickas; **16**(2), 524–528.

Liu, A.C.Y.–Defect formation due to the crystallization of deep amorphous volumes formed in silicon by mega electron volt (*MeV*) ion implantation.–A.C.Y. Liu, J.C. McCallum, and J. Wong-Leung; **16**(11), 3229–3237.

Liu, B.X.–Glass-forming ability of the Ni–Zr and Ni–Ti systems determined by interatomic potentials.–W.S. Lai and B.X. Liu; **16**(2), 446–450.

Liu, Bing–Third-order nonlinear optical response in PbS-coated CdS nanocomposites.–Bing Liu, Chwee Har Chew, Leong Ming Gan, Guo Qin Xu, Heping Li, Yee Loy Lam, Chan Hin Kam, and Wen Xiu Que; **16**(6), 1644–1650.

Liu, C.X.–Excellent buffer layer for growing high-quality Y–Ba–Cu–O thin films.–W.H. Tang, J. Gao, C.X. Liu, and Z.H. Mai; **16**(10), 2864–2868.

Liu, Chang–Purification of single-walled carbon nanotubes synthesized by the hydrogen arc-discharge method.–Pengxiang Hou, Chang Liu, Yu Tong, Shitao Xu, Min Liu, and Huiming Cheng; **16**(9), 2526–2529.

Liu, G.K.–Microscopic effects of self-radiation damage in ^{244}Cm-doped $LuPO_4$ crystals.–J.S. Luo and G.K. Liu; **16**(2), 366–372.

Liu, J-M.–Origin of the anomalous volume expansion in Al–Si alloys above liquidus.–W.M. Wang, X.F. Bian, H.R. Wang, Zhen Wang, L. Zhang, Z.G. Liu, and J-M. Liu; **16**(12), 3592–3598.

Liu, Jing–On some discrepancies in the literature about the formation of icosahedral quasi-crystal in Al–Cu–Fe alloys.–Jianian Gui, Jianbo Wang, Renhui Wang, Dahai Wang, Jing Liu, and Fangyu Chen; **16**(4), 1037–1046.

Liu, Jun–Chemical sensors based on dielectric response of functionalized mesoporous silica films.–Karel Domansky, Jun Liu, Li-Qiong Wang, Mark H. Engelhard, and Suresh Baskaran; **16**(10), 2810–2816.

–Novel synthesis of AlN nanowires with controlled diameters.–Jun Liu, X. Zhang, Yingjiu Zhang, Rongrui He, and Jing Zhu; **16**(11), 3133–3138.

Liu, K.W.–Formation of eutectic RuAl/Ru nanocomposite by mechanical alloying and subsequent annealing.–K.W. Liu, F. Mücklich, and R. Birringer; **16**(9), 2459–2462(L).

Liu, Kuo-Shung–Damping behavior of *in situ* Al–(graphite, Al_4C_3) composites produced by reciprocating extrusion.–Hsu-Shen Chu, Kuo-Shung Liu, and Jien-Wei Yeh; **16**(5), 1372–1380.

Liu, L.–Effect of pressure on the structure of Fe–N alloys formed by solid-state reaction.–B. Yao, L. Liu, S.E. Liu, X. Hu, and W.H. Su; **16**(9), 2583–2590.

–Shear-activated indentation crack in GaAs single crystal.–Z.C. Li, L. Liu, L.L. He, Y.B. Xu, and X. Wu; **16**(10), 2845–2849.

Liu, M.–Microstructure studies of potassium hexatitanate whiskers.–G.L. Li, M. Liu, and G.H. Wang; **16**(12), 3614–3620.

Liu, Min–Purification of single-walled carbon nanotubes synthesized by the hydrogen arc-discharge method.–Pengxiang Hou, Chang Liu, Yu Tong, Shitao Xu, Min Liu, and Huiming Cheng; **16**(9), 2526–2529.

Liu, Ming–Piezoelectric actuation of crack growth along polymer–metal interfaces in adhesive bonds.–Tianbao Du, Ming Liu, Steve Seghi, K.J. Hsia, J. Economy, and J.K. Shang; **16**(10), 2885–2892.

Liu, P.L.–Interfacial embrittlement by bismuth segregation in copper/tin–bismuth Pb-free solder interconnect.–P.L. Liu and J.K. Shang; **16**(6), 1651–1659.

Liu, S.E.–Effect of pressure on the structure of Fe–N alloys formed by solid-state reaction.–B. Yao, L. Liu, S.E. Liu, X. Hu, and W.H. Su; **16**(9), 2583–2590.

Lui, T.S.–Effect of lead content on vibration fracture behavior of Pb–Sn eutectic solder.–C.M. Chuang, T.S. Lui, and L.H. Chen; **16**(9), 2644–2652.

Liu, W.–Synthesis of α–SiO_2 nanowires using Au nanoparticle catalysts on a silicon substrate.–Z.Q. Liu, S.S. Xie, L.F. Sun, D.S. Tang, W.Y. Zhou, C.Y. Wang, W. Liu, Y.B. Li, X.P. Zou, and G. Wang; **16**(3), 683–686.

–Effect of a magnetic field on phase transformation of steel.–W. Liu, D.R. Ou, H.H. Zhou, G.Y. Tang, and F. Wu; **16**(8), 2280–2282.

Liu, Wei–Effects of preparation processes on structure and magnetic properties of $Nd_2Fe_{14}B/\alpha$–Fe-type nanocomposite magnets.–Baozhi Cui, X.K. Sun, L.Y. Xiong, Wei Liu, Zhi-dong Zhang, Zhi-qing Yang, Ai-min Wang, and Jiang-ning Deng; **16**(3), 709–715.

Liu, X.–Coherent island formation of Cu_2O films grown by chemical vapor deposition on MgO(110).–P.R. Markworth, X. Liu, J.Y. Dai, W. Fan, T.J. Marks, and R.P.H. Chang; **16**(8), 2408–2414.

Liu, Xiao Hu–Evaluation of the modified edge lift-off test for adhesion characterization in microelectronic multifilm applications.–Jack C. Hay, Eric G. Liniger, and Xiao Hu Liu; **16**(2), 385–393.

Liu, Yao-Gang–Refractive index profile and attenuation measurement in $KTiOPO_4$ waveguide by megaelectronvolt He ions.–Ke-Ming Wang, Hiu Hu, Fei Lu, Feng Chen, Bo-Rong Shi, Yao-Gang Liu, Ding-Yu Shen, and Xie-Mei Wang; **16**(1), 276–279.

Liu, Yaogang–Growth, defects, and properties of $GdCa_4O(BO_3)_3$ and $Nd:GdCa_4O(BO_3)_3$ crystals.–Jiyang Wang, Xiaobo Hu, Xin Yin, Renbo Song, Jingqian Wei, Zongsu Shao, Yaogang Liu, Minhua Jiang, Yulian Tian, Jianhua Jiang, and Wanxia Huang; **16**(3), 790–796.

Liu, Yuan-fang–Solvothermal route to Bi_3Se_4 nanorods at low temperature.–Yuan-fang Liu, Jing-hui Zeng, Wei-xin Zhang, Wei-chao Yu, Yi-tai Qian, Jin-bo Cao, and Wan-qun Zhang; **16**(12), 3361–3365.

Liu, Z.G.–Impacts of postannealing ambient atmospheres on $Pt/SrBi_{2.2}Ta_2O_9/Pt$ capacitors.–Ai-Dong Li, Tao Yu, Hui-Qin Ling, Di Wu, Zhi-Guo Liu, and Nai-Ben Ming; **16**(12), 3526–3535.

–Origin of the anomalous volume expansion in Al–Si alloys above liquidus.–W.M. Wang, X.F. Bian, H.R. Wang, Zhen Wang, L. Zhang, Z.G. Liu, and J-M. Liu; **16**(12), 3592–3598.

Liu, Z.Q.–Synthesis of α–SiO_2 nanowires using Au nanoparticle catalysts on a silicon substrate.–Z.Q. Liu, S.S. Xie, L.F. Sun, D.S. Tang, W.Y. Zhou, C.Y. Wang, W. Liu, Y.B. Li, X.P. Zou, and G. Wang; **16**(3), 683–686.

Liu, Zhiguo–Processing- and composition-dependent characteristics of chemical solution deposited $Bi_{4-x}La_xTi_3O_{12}$ thin films.–Di Wu, Aidong Li, Tao Zhu, Zhifeng Li, Zhiguo Liu, and Naiben Ming; **16**(5), 1325–1332.

Livingston, R.A.–Characterization of the induction period in tricalcium silicate hydration by nuclear resonance reaction analysis.–R.A. Livingston, J.S. Schweitzer, C. Rolfs, H-W. Becker, and S. Kubsky; **16**(3), 687–693.

Lloyd, Isabel K.–Microwave sintering of ZnO at ultra high heating rates.–Geng-fu Xu, Isabel K. Lloyd, Yuval Carmel, Tayo Olorunyolemi, Otto C. Wilson, Jr.; **16**(10), 2850–2858.

Lloyd, S.J.–Deformation under nanoindents in Si, Ge, and GaAs examined through transmission electron microscopy.–S.J. Lloyd, J.M. Molina-Aldareguia, and W.J. Clegg; **16**(12), 3347–3350(L).

Lo, W.–Microstructure and growth of joins in melt-textured $YBa_2Cu_3O_{7-\delta}$.–A.D. Bradley, W. Lo, M. Mironova, N.H. Babu, D.A. Cardwell, A.M. Campbell, and K. Salama; **16**(8), 2298–2305.

Lorenz, D.–Determination of the elastic properties of glasses and polymers exploiting the resonant characteristic of depth-sensing indentation tests.–D. Lorenz, W. Fränzel, M. Einax, P. Grau, and G. Berg; **16**(6), 1776–1783.

Loughran, Fiona–Influence of CaO–SiO_2 ratio on the chemistry of intergranular films in liquid-phase sintered alumina and implications for rate of erosive wear.–Rik Brydson, Peter C. Twigg, Fiona Loughran, and Frank L. Riley; **16**(3), 652–665.

Lowndes, D.H.–Growth mechanism of superconducting MgB_2 films prepared by various methods.–H.Y. Zhai, H.M. Christen, L. Zhang, M. Paranthaman, C. Cantoni, B.C. Sales, P.H. Fleming, D.K. Christen, and D.H. Lowndes; **16**(10), 2759–2762(L).

Lu, Fei–Refractive index profile and attenuation measurement in $KTiOPO_4$ waveguide by megaelectronvolt He ions.–Ke-Ming Wang, Hiu Hu, Fei Lu, Feng Chen, Bo-Rong Shi, Yao-Gang Liu, Ding-Yu Shen, and Xie-Mei Wang; **16**(1), 276–279.

Lu, L.–Study of the mechanism for controlled crystallization of BaF_2 under two kinds of monolayers.–L. Lu, H. Cui, W. Li, H. Zhang, and S. Xi; **16**(8), 2415–2420.

Lu, P.–Enthalpies of formation of lanthanide oxyapatite phases.–A.S. Risbud, K.B. Helean, M.C. Wilding, P. Lu, and A. Navrotsky; **16**(10), 2780–2783(L).

Lu, Q.M.–Structure and the nonlinearity of lithium triborate studied by Raman and infrared reflectivity spectroscopy.–H.R. Xia, L.X. Li, H. Yu, S.M. Dong, J.Y. Wang, Q.M. Lu, C.Q. Ma, and X.N. Wang; **16**(12), 3464–3470.

Lu, Ran–Fabrication of heteropolyoxometalate-based photochromic inorganic–organic nanocomposites.–Tie Rui Zhang, Wei Feng, Chun Yan Bao, Ran Lu, Xin Tong Zhang, Tie Jin Li, Ying Ying Zhao, and Jian Nian Yao; **16**(8), 2256–2263.

Lu, Shih-Yuan–Silicalite/poly(dimethylsiloxane) nanocomposite pervaporation membranes for acetic acid/water separation.–Shih-Yuan Lu, Hsiang-Yuan Huang, and Kwen-Hua Wu; **16**(11), 3053–3059.

Lu, X.J.–Dielectric properties of La-substituted $Pb_{0.5}Ca_{0.5}[(Mg_{1/3}Nb_{2/3})_{0.5}Ti_{0.5}]O_3$ ceramics.–X.J. Lu and X.M. Chen; **16**(7), 2053–2056.

Lu, Y.F.–Formation of quasi-one-dimensional carbon chains in cubic nanocrystals by photon-breaking of C–S bonds in polythiophene.–Z.M. Ren, Y.F. Lu, H.W. Choy, T.C. Chong, S.C. Ng, and P. Miao; **16**(10), 2793–2797.

Lucadamo, G.–Texture in Ti/Al and Nb/Al multilayer thin films: Role of Cu.–G. Lucadamo, K. Barmak, and K.P. Rodbell; **16**(5), 1449–1459.

Lukashevich, M.–Preparation, structure, and magnetic properties of cobalt nanoparticles in carbon fibers.–I. Bashmakov, V. Dorosinez, M. Lukashevich, A. Mazanik, T. Tihonova, T. Zabel, B. Wiedenhorst, and H. Micklitz; **16**(10), 2832–2835.

Lumpp, Janet K.–Microstructural studies of Cu brazing on AlN.–Chaoxian Cai and Janet K. Lumpp; **16**(3), 670–677.

Luo, Haosu–Domain configurations in relaxor ferroelectric single crystals $Pb(Mg_{1/3}Nb_{2/3})O_3$–$PbTiO_3$.–Guisheng Xu, Haosu Luo, Zhenyi Qi, Haiqing Xu, and Zhiwen Yin; **16**(4), 932–937.

–Twinning domain in $67Pb(Mg_{1/3}Nb_{2/3})O_3$–$33PbTiO_3$ ferroelectric complex perovskite crystal grown by the Bridgman method.–Donglin Li, Pingchu Wang, Xiaoming Pan, Haosu Luo, and Zhiwen Yin; **16**(5), 1252–1255(L).

Luo, J.S.–Microscopic effects of self-radiation damage in ^{244}Cm-doped $LuPO_4$ crystals.–J.S. Luo and G.K. Liu; **16**(2), 366–372.

Luo, Jiazhong–Phase transformation effects on the wear properties of alumina gel–polymer matrix nanocomposites.–Jiazhong Luo, John Lannutti, and Robert Seghi; **16**(6), 1680–1685.

Luo, Le–Effects of static thermal aging and thermal cycling on the microstructure and shear strength of $Sn_{95.5}Ag_{3.8}Cu_{0.7}$ solder joints.–Shawkret Ahat, Mei Sheng, and Le Luo; **16**(10), 2914–2921.

Luther-Davies, Barry–Direct laser writing of self-developed waveguides in benzyldimethylketal-doped sol-gel hybrid glass.–Byeong-Soo Bae, Oun-Ho Park, Robbie Charters, Barry Luther-Davies, and Graham R. Atkins; **16**(11), 3184–3187.

M

Ma, C.Q.–Structure and the nonlinearity of lithium triborate studied by Raman and infrared reflectivity spectroscopy.–H.R. Xia, L.X. Li, H. Yu, S.M. Dong, J.Y. Wang, Q.M. Lu, C.Q. Ma, and X.N. Wang; **16**(12), 3464–3470.

Ma, J.–$Pb(Zr_xTi_{1-x})O_3$ ceramics via reactive sintering of partially reacted mixture produced by a high-energy ball milling process.–L.B. Kong, J. Ma, T.S. Zhang, W. Zhu, and O.K. Tan; **16**(6), 1636–1643.

Ma, N.G.–Compaction of bulk ferromagnetic $Fe_{80}P_{13}C_7$ amorphous alloys.–F.W. Chan, N.G. Ma, and H.W. Kui; **16**(10), 2767–2769(L).

Ma, Tianfu–Novel photoluminescence from hydrogenated amorphous carbon films prepared by using xylene source.–Jun Xu, Wei Li, Tianfu Ma, Zhifeng Li, Li Wang, and Kunji Chen; **16**(2), 325–328(L).

Ma, Xian-Feng–Enhanced crystallization and phase transformation of amorphous silicon nitride under high pressure.–Ya-Li Li, Yong Liang, Fen Zheng, Xian-Feng Ma, Suo-Jing Cui, and Liling Sun; **16**(1), 67–75.

Ma, Xiaodong–Preparation and characterization of nanocrystalline PbSe in poly(acrylic acid-*co*-styrene).–Yangyang Sun, Xuefeng Qian, Jie Yin, Junchao Huang, Xiaodong Ma, and Zikang Zhu; **16**(10), 2922–2927.

Ma, Ying–Photocatalytic activity of TiO_2 prepared at low temperature by a photo-assisted sol-gel method.–Zi-sheng Guan, Xin-tong Zhang, Ying Ma, Ya-an Cao, and Jian-nian Yao; **16**(4), 907–909(L).

–Effects of zinc(II) and iron(III) doping of titania films on their photoreactivity to decompose rhodamine B.–Ying Ma, Xin-tong Zhang, Zi-sheng Guan, Ya-an Cao, and Jian-nian Yao; **16**(10), 2928–2933.

Maat, J.H.H. ter–Packing and solidification in ceramic injection moulding.–S. Krug, J.R.G. Evans, and J.H.H. ter Maat; **16**(6), 1829–1837.

MacManus-Driscoll, J.L.–Magnetotransport properties of $La_{0.7}Ca_{0.3}MnO_3$ thick films prepared by spray pyrolysis.–F. Damay, J.L. MacManus-Driscoll, and L.F. Cohen; **16**(3), 784–789.

Madan, A.–Effect of process variables on the structure, residual stress, and hardness of sputtered nanocrystalline nickel films.–R. Mitra, R.A. Hoffman, A. Madan, and J.R. Weertman; **16**(4), 1010–1027.

–Effect of annealing on microstructure, residual stress, and hardness of Al–Ti multilayered films.–R. Mitra, A. Madan, R.A. Hoffman, W-A. Chiou, and J.R. Weertman; **16**(7), 2064–2076.

Maeda, T.–Morphological effect on the electrochemical behavior of electric double-layer capacitors.–M. Endo, Y.J. Kim, T. Maeda, K. Koshiba, K. Katayam, and M.S. Dresselhaus; **16**(12), 3402–3410.

Maes, G.–Chemical structure evolution and orientation selection in sol-gel-prepared ferroelectric $Pb(Zr,Ti)O_3$ thin films.–L. Fè, G.J. Norga, D.J. Wouters, H.E. Maes, G. Maes; **16**(9), 2499–2504.

Maes, H.E.–Growth of (111)-oriented $Pb(Zr,Ti)O_3$ layers on nanocrystalline RuO_2 electrodes using the sol-gel technique.–G.J. Norga, S. Jin, Laura Fè, D.J. Wouters, H. Bender, and H.E. Maes; **16**(3), 828–833.

–Chemical structure evolution and orientation selection in sol-gel-prepared ferroelectric $Pb(Zr,Ti)O_3$ thin films.–L. Fè, G.J. Norga, D.J. Wouters, H.E. Maes, and G. Maes; **16**(9), 2499–2504.

Maex, K.–*In situ* transmission electron microscopy study of the silicidation process in Co thin films on patterned (001) Si substrates.–C. Ghica, L. Nistor, H. Bender, A. Steegen, A. Lauwers, K. Maex, and J. Van Landuyt; **16**(3), 701–708.

Maglia, F.–Field-activated combustion synthesis of Ta–Si intermetallic compounds.–F. Maglia, U. Anselmi-Tamburini, N. Bertolino, C. Milanese, and Z.A. Munir; **16**(2), 534–544.

–Mechanochemistry of the titanium–silicon system: Compositional effects.–S. Doppiu, M. Monagheddu, G. Cocco, F. Maglia, U. Anselmi-Tamburini, and Z.A. Munir; **16**(5), 1266–1279.

–Combustion synthesis of mechanically activated powders in the Ti–Si system.–F. Maglia, U. Anselmi-Tamburini, G. Cocco, M. Monagheddu, N. Bertolino, and Z.A. Munir; **16**(4), 1074–1082.

Mai, Z.H.–Excellent buffer layer for growing high-quality Y–Ba–Cu–O thin films.–W.H. Tang, J. Gao, C.X. Liu, and Z.H. Mai; **16**(10), 2864–2868.

Maidenberg, Daniel A.–Adhesion of benzocyclobutene-passivated silicon in epoxy layered structures.–Robert J. Hohlfelder, Daniel A. Maidenberg, Reinhold H. Dauskardt, Yueguang Wei, and John W. Hutchinson; **16**(1), 243–255.

Majhi, Prashant–Highly (111)-oriented and conformal iridium films by liquid source metalorganic chemical vapor deposition.–Jaydeb Goswami, Chang-Gong Wang, Prashant Majhi, Yong-Wook Shin, and Sandwip K. Dey; **16**(8), 2192–2195(L).

Mak, C.L.–Novel route for the epitaxial growth of $(SrBa)Nb_2O_6$ thick films by the sol-gel method using a self-template layer.–A-D. Li, C.L. Mak, K.H. Wong, D. Wu, and Naiben Ming; **16**(11), 3179–3183.

Makihara, Masaki–Coordination structures of implanted Fe, Co, and Ni ions in silica glass by x-ray absorption fine structure spectroscopy.–Kohei Fukumi, Akiyoshi Chayahara, Kohei Kadono, Hiroyuki Kageyama, Tomoko Akai, Hiroshi Mizoguchi, Naoyuki Kitamura, Masaki Makihara, Yuji Horino, and Kanenaga Fujii; **16**(1), 155–162.

Mal, Ajit–Characteristics of elastic waves generated by crack initiation in aluminum alloys under fatigue loading.–Kiwoo Nam and Ajit Mal; **16**(6), 1745–1751.

Málek, Jiří–Kinetic analysis of solid-state processes.–Jiří Málek, Takefumi Mitsuhashi, and José Manuel Criado; **16**(6), 1862–1871.

Malm, J-O.–Growth, structure, and mechanical properties of transition metal carbide superlattices.–H. Högberg, J. Birch, M. Odén, J-O. Malm, L. Hultman, and U. Jansson; **16**(5), 1301–1310.

Mantas, P.Q.–Densification and grain growth of Al-doped ZnO.–Jiaping Han, P.Q. Mantas, and A.M.R. Senos; **16**(2), 459–468.

Manthiram, A.–Synthesis and processing of nanocrystalline Ag–Fe–Ni for low thermal expansion–high conductivity thermal management applications.–J. Stolk, M. Gross, D. Stolk, and A. Manthiram; **16**(2), 340–343(L).

Marchand, R.–Calorimetric determination of the enthalpy of formation of InN and comparison with AlN and GaN.–M.R. Ranade, F. Tessier, A. Navrotsky, and R. Marchand; **16**(10), 2824–2831.

Marêché, J.F.–Elastic properties of anisotropic monolithic samples of compressed expanded graphite studied with ultrasounds.–M. Krzesińska, A. Celzard, J.F. Marêché, and S. Puricelli; **16**(2), 606–614.

Marks, T.J.–Coherent island formation of Cu_2O films grown by chemical vapor deposition on MgO(110).–P.R. Markworth, X. Liu, J.Y. Dai, W. Fan, T.J. Marks, and R.P.H. Chang; **16**(8), 2408–2414.

Markworth, P.R.–Epitaxial stabilization of orthorhombic cuprous oxide films on MgO(110).–Paul R. Markworth, R.P.H. Chang, Y. Sun, G.K. Wong, and J.B. Ketterson; **16**(4), 914–921.

–Coherent island formation of Cu_2O films grown by chemical vapor deposition on MgO(110).–P.R. Markworth, X. Liu, J.Y. Dai, W. Fan, T.J. Marks, and R.P.H. Chang; **16**(8), 2408–2414.

Martin, Jeremy–Effect of material properties on integration damage in organosilicate glass films.–E. Todd Ryan, Jeremy Martin, Kurt Junker, Jeff Wetzel, David W. Gidley, and Jianing Sun; **16**(12), 3335–3338(L).

Martina, A. Della–Gradient porosity poly(dicyclopentadiene).–A. Della Martina and J.G. Hilborn; **16**(7), 2045–2052.

Martínez, J.R.–Structure of heat-treated sol-gel SiO_2 glasses containing silver.–M.G. Garníca-Romo, J. González-Hernández, M.A. Hernández-Landaverde, Y.V. Vorobiev, F. Ruiz, and J.R. Martínez; **16**(7), 2007–2012.

Martínez, O.E.–Transient self-dewetting of steels after pulsed electron beam melting.–N. Mingolo, A.N. Roviglione, and O.E. Martínez; **16**(8), 2343–2349.

Martínez-Montes, G.–Determination of optical constants of Si/ZnO polycrystalline nanocomposites by spectroscopic ellipsometry.–J. García-Serrano, N. Koshizaki, T. Sasaki, G. Martínez-Montes, and U. Pal; **16**(12), 3554–3559.

Martinez-Tomas, C.–Deep center luminescence versus surface preparation of ZnSe single crystals.–J.A. Garcia, V. Muñoz, C. Martinez-Tomas, and J.J.S. Garitaonandia; **16**(5), 1245–1248(L).

Maschio, S.–Microprobe fluorescence spectroscopy evaluation of stress fields developed along a propagating crack in an Al_2O_3/CaO · $6Al_2O_3$ ceramic composite.–O. Sbaizero, S. Maschio, G. Pezzotti, and I.J. Davies; **16**(10), 2798–2804.

Mateeva, N.–Microstructures of $La_{1-x}A_x$(A = Ca or Sr)$MnO_{3-\delta}$ thin films by liquid-delivery metalorganic chemical vapor deposition.–Y. Xin, K. Han, N. Mateeva, H. Garmestani, P.N. Kalu, and K-H. Dahmen; **16**(11), 3073–3083.

Matikas, T.E.–Development of a model for the prediction of the fretting fatigue regimes.–T.E. Matikas and P.D. Nicolaou; **16**(9), 2716–2723.

Matsumoto, S.–Raman scattering of cubic boron nitride films deposited from the low-pressure gas phase.–W.J. Zhang and S. Matsumoto; **16**(12), 3430–3442.

Matsushita, M.–Formation of icosahedral quasicrystal by crystallization of Zr_{70}(Ni, Cu, Pd)$_{30}$ amorphous alloys.–T. Zhang, A. Inoue, M. Matsushita, and J. Saida; **16**(1), 20–23(L).

–Redistribution behavior of constitutional elements at an initial crystallization stage in the $Zr_{65}Al_{7.5}Ni_{10}Cu_{17.5}$ glassy alloy.–J. Saida, M. Matsushita, and A. Inoue; **16**(1), 28–31(L).

–Novel hexagonal structure and ultrahigh strength of magnesium solid solution in the Mg–Zn–Y system.–Akihisa Inoue, Yoshihito Kawamura, Mitsuhide Matsushita, Kentaro Hayashi, and Junichi Koike; **16**(7), 1894–1900.

–Investigation of the stability of glassy state in the Zr- and Hf-based glassy alloys correlated with their transformation behavior.–Junji Saida, Chunfei Li, Mitsuhide Matsushita, and Akihisa Inoue; **16**(12), 3389–3401.

Matveev, V.N.–Electromigration properties of multigrain aluminum thin film conductors as influenced by grain boundary structure.–O.V. Kononenko, V.N. Matveev, and D.P. Field; **16**(7), 2124–2129.

Mayer, G.–Biomimetic model of a sponge-spicular optical fiber—mechanical properties and structure.–M. Sarikaya, H. Fong, N. Sunderland, B.D. Flinn, G. Mayer, A. Mescher, and E. Gaino; **16**(5), 1420–1428.

Mazanik, A.–Preparation, structure, and magnetic properties of cobalt nanoparticles in carbon fibers.–I. Bashmakov, V. Dorosinez, M. Lukashevich, A. Mazanik, T. Tihonova, T. Zabel, B. Wiedenhorst, and H. Micklitz; **16**(10), 2832–2835.

McCallum, J.C.–Defect formation due to the crystallization of deep amorphous volumes formed in silicon by mega electron volt (*MeV*) ion implantation.–A.C.Y. Liu, J.C. McCallum, and J. Wong-Leung; **16**(11), 3229–3237.

McChesney, J.–Growth study of epitaxial $Fe_xZn_{1-x}F_2$ thin films.–J. McChesney, M. Hetzer, H. Shi, T. Charlton, and D. Lederman; **16**(6), 1769–1775.

McClure, J.L.–Moving the pulsed heating technique beyond monolithic specimens: Experiments with coated wires.–D. Josell, D. Basak, J.L. McClure, U.R. Kattner, M.E. Williams, W.J. Boettinger, and M. Rappaz; **16**(8), 2421–2428.

McCormick, Mark A.–Processing effects on the composition and dielectric properties of hydrothermally derived $Ba_xSr_{(1-x)}TiO_3$ thin films.–Mark A. McCormick, Ryan K. Roeder, and Elliott B. Slamovich; **16**(4), 1200–1209.

McGinn, P.J.–Combinatorial synthesis of oxide powders.–H.M. Reichenbach and P.J. McGinn; **16**(4), 967–974.

McKittrick, J.–New combustion synthesis technique for the production of $(In_xGa_{1-x})_2O_3$ powders: Hydrazine/metal nitrate method.–R. García, G.A. Hirata, and J. McKittrick; **16**(4), 1059–1065.

Meda, Lamartine–Effects of thermal annealing on the texture of $La_{0.67}Sr_{0.33}MnO_3$ thin films.–Lamartine Meda, LaQuita Kennon, Cristiane Bacaltchuk, Hamid Garmestani, and Klaus H. Dahmen; **16**(7), 1887–1889(L).

Meinders, Erwin R.–Measurement of the thermal conductivity of thin layers using a scanning thermal microscope.–Erwin R. Meinders; **16**(9), 2530–2543.

Melamed, S.–Entrapment of organosilicon molecules in nonhydrolytic alumina gels and thermal behavior of the resulting composite.–G.S. Grader, S.A. Melchior, Y. De-Hazan, S. Melamed, and G.E. Shter; **16**(5), 1413–1419.

Melchior, S.A.–Entrapment of organosilicon molecules in nonhydrolytic alumina gels and thermal behavior of the resulting composite.–G.S. Grader, S.A. Melchior, Y. De-Hazan, S. Melamed, and G.E. Shter; **16**(5), 1413–1419.

Meldrum, A.–Nanocrystals in crystalline silicon: Void formation and hollow particles.–A. Meldrum, S. Honda, C.W. White, R.A. Zuhr, and L.A. Boatner; **16**(9), 2670–2679.

Melgarejo, R.–Synthesis of $Zn_{1-x}Mg_xO$ and its structural characterization.–M.S. Tomar, R. Melgarejo, P.S. Dobal, and R.S. Katiyar; **16**(4), 903–906(L).

Mendes, R.G.–Structural and electrical properties of strontium barium niobate thin films crystallized by conventional furnace and rapid-thermal annealing process.–R.G. Mendes, E.B. Araújo, and J.A. Eiras; **16**(10), 3009–3013.

Meng, Y.G.–Size effect on the mechanical properties of microfabricated polysilicon thin films.–J.N. Ding, Y.G. Meng, and S.Z. Wen; **16**(8), 2223–2228.

Mescher, A.–Biomimetic model of a sponge-spicular optical fiber—mechanical properties and structure.–M. Sarikaya, H. Fong, N. Sunderland, B.D. Flinn, G. Mayer, A. Mescher, and E. Gaino; **16**(5), 1420–1428.

Miao, Jipeng–Valence variations in titanium-based perovskite oxides by high-pressure and high-temperature method.–Liping Li, Guangshe Li, Jipeng Miao, Wenhui Su, and Hiroshi Inomata; **16**(2), 417–424.

Miao, P.–Formation of quasi-one-dimensional carbon chains in cubic nanocrystals by photon-breaking of C–S bonds in polythiophene.–Z.M. Ren, Y.F. Lu, H.W. Choy, T.C. Chong, S.C. Ng, and P. Miao; **16**(10), 2793–2797.

Micklitz, H.–Preparation, structure, and magnetic properties of cobalt nanoparticles in carbon fibers.–I. Bashmakov, V. Dorosinez, M. Lukashevich, A. Mazanik, T. Tihonova, T. Zabel, B. Wiedenhorst, and H. Micklitz; **16**(10), 2832–2835.

Miehe, G.–Additive controlled crystallization of barium titanate powders and their application for thin-film ceramic production: Part I. Powder Synthesis.–B. Grohe, G. Miehe, and G. Wegner; **16**(7), 1901–1910.

–Additive controlled crystallization of barium titanate powders and their application for thin-film ceramic production: Part II. From nano-sized powders to ceramic thin films.–B. Grohe, G. Miehe, and G. Wegner; **16**(7), 1911–1915.

Miguel, J.M.–Structural characterization of laser-treated Cr_3C_2–NiCr coatings.–P. Serra, J.M. Miguel, J.L. Morenza, and J.M. Guilemany; **16**(12), 3416–3422.

Milanese, C.–Field-activated combustion synthesis of Ta–Si intermetallic compounds.–F. Maglia, U. Anselmi-Tamburini, N. Bertolino, C. Milanese, and Z.A. Munir; **16**(2), 534–544.

Ming, Naiben–Processing- and composition-dependent characteristics of chemical solution deposited $Bi_{4-x}La_xTi_3O_{12}$ thin films.–Di Wu, Aidong Li, Tao Zhu, Zhifeng Li, Zhiguo Liu, and Naiben Ming; **16**(5), 1325–1332.

–Novel route for the epitaxial growth of (SrBa)Nb_2O_6 thick films by the sol-gel method using a self-template layer.–A-D. Li, C.L. Mak, K.H. Wong, D. Wu, Naiben Ming; **16**(11), 3179–3183.

–Impacts of postannealing ambient atmospheres on Pt/$SrBi_{2.2}Ta_2O_9$/Pt capacitors.–Ai-Dong Li, Tao Yu, Hui-Qin Ling, Di Wu, Zhi-Guo Liu, and Nai-Ben Ming; **16**(12), 3526–3535.

Mingolo, N.–Transient self-dewetting of steels after pulsed electron beam melting.–N. Mingolo, A.N. Roviglione, and O.E. Martínez; **16**(8), 2343–2349.

Miracle, D.B.–Microstructural and mechanical characterization of carbon coatings on SiC fibers.–K.L. Kendig, R. Gibala, and D.B. Miracle; **16**(12), 3366–3377.

Miranda, Pedro–Contact fracture of brittle bilayer coatings on soft substrates.–Pedro Miranda, Antonia Pajares, Fernando Guiberteau, Francisco L. Cumbrera, and Brian R. Lawn; **16**(1), 115–126.

–Controlled preparation and characterization of multilayer sol-gel zirconia dip-coatings.–Ricardo Caruso, Antonio Díaz-Parralejo, Pedro Miranda, and Fernando Guiberteau; **16**(8), 2391–2398.

Mironova, M.–Microstructure and growth of joins in melt-textured $YBa_2Cu_3O_{7-\delta}$.–A.D. Bradley, W. Lo, M. Mironova, N.H. Babu, D.A. Cardwell, A.M. Campbell, and K. Salama; **16**(8), 2298–2305.

Misra, A.–Compositional distributions in nanoscale metallic multilayers studied using x-ray mapping.–V.J. Keast, A. Misra, H. Kung, and T.E. Mitchell; **16**(7), 2032–2038.

Mitchell, T.E.–Compositional distributions in nanoscale metallic multilayers studied using x-ray mapping.–V.J. Keast, A. Misra, H. Kung, and T.E. Mitchell; **16**(7), 2032–2038.

Mitomo, Mamoru–Preferred orientation of beta-phase and its mechanisms in a fine-grained silicon-nitride-based ceramic.–Rong-Jun Xie, Mamoru Mitomo, Wonjoong Kim, Young-Wook Kim, and Guo-Dong Zhan; **16**(2), 590–596.

–Transmission electron microscopy observation in a liquid-phase-sintered SiC with oxynitride glass.–Guo-Dong Zhan, Mamoru Mitomo, Young-Wook Kim, Rong-Jun Xie, and Amiya K. Mukherjee; **16**(8), 2189–2191(L).

–Dependence of fracture stress on applied stress rate in a Yb_2O_3–SiO_2-doped hot-pressed silicon nitride ceramic.–Shuqi Guo, Naoto Hirosaki, Yoshinobu Yamamoto, Toshiyuki Nishimura, Mamoru Mitomo; **16**(11), 3254–3261.

Mitra, R.–Effect of process variables on the structure, residual stress, and hardness of sputtered nanocrystalline nickel films.–R. Mitra, R.A. Hoffman, A. Madan, and J.R. Weertman; **16**(4), 1010–1027.

–Effect of annealing on microstructure, residual stress, and hardness of Al–Ti multilayered films.–R. Mitra, A. Madan, R.A. Hoffman, W-A. Chiou, and J.R. Weertman; **16**(7), 2064–2076.

Mitsuhashi, Takefumi–Kinetic analysis of solid-state processes.–Jiří Málek, Takefumi Mitsuhashi, and José Manuel Criado; **16**(6), 1862–1871.

Mittemeijer, E.J.–Hardness–depth profile of a carbon-implanted Ti–6Al–4V alloy and its relation to composition and microstructure.–M. Kunert, O. Kienzle, B. Baretzky, S.P. Baker, E.J. Mittemeijer; **16**(8), 2321–2335.

Miura, H.–Molecular dynamics analysis of adhesion strength of interfaces between thin films.–T. Iwasaki and H. Miura; **16**(6), 1789–1794.

Miyahara, K.–Mechanical stress of the electrical performance of polycrystalline-silicon resistors.–N. Nakabayashi, H. Ohyama, E. Simoen, M. Ikegami, C. Claeys, K. Kobayashi, M. Yoneoka, and K. Miyahara; **16**(9), 2579–2582.

Miyake, K.–Role of the primary phase particles during the peritectic solidification of Y-123 superconducting oxides.–M. Kambara, M. Yoshizumi, T. Umeda, K. Miyake, K. Murata, T. Izumi, and Y. Shiohara; **16**(8), 2229–2238.

Miyazawa, K.–Microstructural analysis of high-pressure compressed C_{60}.–K. Miyazawa, H. Satsuki, M. Kuwabara, and M. Akaishi; **16**(7), 1960–1966.

Miyazawa, Shintaro–Water-associated surface degradation of $CsLiB_6O_{10}$ crystal during harmonic generation in the ultraviolet region.–Yukihiro Morimoto, Shintaro Miyazawa, Yoshio Kagebayashi, Naoki Kitatochi, Toshio Yokota, and Jun Sakuma; **16**(7), 2082–2090.

Mizoguchi, Hiroshi–Coordination structures of implanted Fe, Co, and Ni ions in silica glass by x-ray absorption fine structure spectroscopy.–Kohei Fukumi, Akiyoshi Chayahara, Kohei Kadono, Hiroyuki Kageyama, Tomoko Akai, Hiroshi Mizoguchi, Naoyuki Kitamura, Masaki Makihara, Yuji Horino, and Kanenaga Fujii; **16**(1), 155–162.

Mo, Jimei–Synthesis of nano-AgI arrays and their optical properties.–Yinhai Wang, Jimei Mo, Weili Cai, Lianzeng Yao, and Lide Zhang; **16**(4), 990–992.

Modi, R.–Dielectric properties of oxide structures by a laser-based direct-writing method.–D. Young, H.D. Wu, R.C.Y. Auyeung, R. Modi, J. Fitz-Gerald, A. Pique, D.B. Chrisey, P. Atanassova, and T. Kodas; **16**(6), 1720–1725.

–Direct writing of polymer thick film resistors using a novel laser transfer technique.–R. Modi, H.D. Wu, R.C.Y. Auyeung, C.M. Gilmore, and D.B. Chrisey; **16**(11), 3214–3222.

Mohri, Tetsuo–Site preference determination in intermetallic compounds by thermal conductivity measurement.–Yoshihiro Terada, Kenji Ohkubo, Tetsuo Mohri, and Tomoo Suzuki; **16**(8), 2314–2320.

Molarius, Jyriki–Effect of oxygen on the reactions in the Si/Ta/Cu metallization system.–Tomi Laurila, Kejun Zeng, Jorma K. Kivilahti, Jyriki Molarius, and Ilkka Suni; **16**(10), 2939–2946.

Molina-Aldareguia, J.M.–Deformation under nanoindents in Si, Ge, and GaAs examined through transmission electron microscopy.–S.J. Lloyd, J.M. Molina-Aldareguia, and W.J. Clegg; **16**(12), 3347–3350(L).

Molotskii, M.–Polarization reversal and domain anisotropy in flux-grown $KTiOPO_4$ and isomorphic crystals.–P. Urenski, G. Rosenman, and M. Molotskii; **16**(5), 1493–1499.

Monagheddu, M.–Combustion synthesis of mechanically activated powders in the Ti–Si system.–F. Maglia, U. Anselmi-Tamburini, G. Cocco, M. Monagheddu, N. Bertolino, and Z.A. Munir; **16**(4), 1074–1082.

–Mechanochemistry of the titanium–silicon system: Compositional effects.–S. Doppiu, M. Monagheddu, G. Cocco, F. Maglia, U. Anselmi-Tamburini, and Z.A. Munir; **16**(5), 1266–1279.

Montero, I.–X-ray photoelectron spectroscopy of electrodeposited cadmium mercury telluride thin films and their native surface oxides.–J. Ramiro, L. Galán, E. García Camarero, I. Montero, and Y. Laaziz; **16**(7), 1942–1952.

Moodenbaugh, A.R.–Nucleation and growth of $YBa_2Cu_3O_x$ on $SrTiO_3$ and CeO_2 by a BaF_2 postdeposition reaction process.–L. Wu, Y. Zhu, V.F. Solovyov, H.J. Wiesmann, A.R. Moodenbaugh, R.L. Sabatini, and M. Suenaga; **16**(10), 2869–2884.

Moody, N.R.–Substrate effects on indentation plastic zone development in thin soft films.–D.E. Kramer, A.A. Volinsky, N.R. Moody, and W.W. Gerberich; **16**(11), 3150–3157.

Moon, C.K.–Chemical-vapor-deposition growth and characterization of epitaxial 3C–SiC films on SOI substrates with thin silicon top layers.–C.K. Moon, H.J. Song, J.K. Kim, J.H. Park, S.J. Jang, J-B. Yoo, H-R. Park, and Byung-Teak Lee; **16**(1), 24–27(L).

Moon, Jung-Ho–Analysis of defect formation in Nb-doped $SrTiO_3$ by impedance spectroscopy.–Seong-Ho Kim, Jung-Ho Moon, Jae-Hwan Park, Jae-Gwan Park, and Yoonho Kim; **16**(1), 192–196.

Morell, G.–Study of the effects of low-energy electron bombardment during the chemical vapor deposition of diamond.–J.A. González, O.L. Figueroa, B.R. Weiner, and G. Morell; **16**(1), 293–295.

Morenza, J.L.–Structural characterization of laser-treated Cr_3C_2–NiCr coatings.–P. Serra, J.M. Miguel, J.L. Morenza, and J.M. Guilemany; **16**(12), 3416–3422.

Mori, Hirotaro–Structure and phase characteristics of amorphous boron–carbon–nitrogen under high pressure and high temperature.–Jianyu Huang, Yuntian T. Zhu, and Hirotaro Mori; **16**(4), 1178–1184.

Mori, Toshiyuki–Precursor scavenging of the resistive grain-boundary phase in 8 mol% yttria-stabilized zirconia: Effect of trace concentrations of SiO_2.–Jong-Heun Lee, Toshiyuki Mori, Ji-Guang Li, Takayasu Ikegami, John Drennan, and Doh-Yeon Kim; **16**(8), 2377–2383.

Morimoto, Yukihiro–Water-associated surface degradation of $CsLiB_6O_{10}$ crystal during harmonic generation in the ultraviolet region.–Yukihiro Morimoto, Shintaro Miyazawa, Yoshio Kagebayashi, Naoki Kitatochi, Toshio Yokota, and Jun Sakuma; **16**(7), 2082–2090.

Morishita, T.–Chemical reaction at the interface between $(Hg_{0.9}Re_{0.1})$-$Ba_2CaCu_2O_x$ thin film and $SrTiO_3$ substrate.–Xiao-Jing Wu, N. Inoue, T. Sugano, T. Morishita, and K. Tanabe; **16**(1), 256–260.

Morris, S.–Thermal analysis investigation of hydriding properties of nanocrystalline Mg–Ni- and Mg–Fe-based alloys prepared by high-energy ball milling.–L.E.A. Berlouis, E. Cabrera, E. Hall-Barientos, P.J. Hall, S.B. Dodd, S. Morris, and M.A. Imam; **16**(1), 45–57.

Moser, W.R.–Hydrodynamic cavitation as a tool to control macro-, micro-, and nano-properties of inorganic materials.–J. Find, S.C. Emerson, I.M. Krausz, and W.R. Moser; **16**(12), 3503–3513.

Moure, C.–$BaTiO_3$ formation by thermal decomposition of a (BaTi)-citrate polyester resin in air.–P. Durán, F. Capel, J. Tartaj, and C. Moure; **16**(1), 197–209.

Mücklich, F.–Formation of eutectic RuAl/Ru nanocomposite by mechanical alloying and subsequent annealing.–K.W. Liu, F. Mücklich, and R. Birringer; **16**(9), 2459–2462(L).

Mukasyan, Alexander–Mechanistic studies in combustion synthesis of NiAl–TiB_2 composites: Effects of gravity.–Cheryl Lau, Alexander Mukasyan, Aleksey Pelekh, and Arvind Varma; **16**(6), 1614–1625.

Mukherjee, Amiya K.–Transmission electron microscopy observation in a liquid-phase-sintered SiC with oxynitride glass.–Guo-Dong Zhan, Mamoru Mitomo, Young-Wook Kim, Rong-Jun Xie, Amiya K. Mukherjee; **16**(8), 2189–2191(L).

–Consolidation and crystallization of Si_3N_4/SiC nanocomposites from a poly(urea–silazane) ceramic precursor.–Julin Wan, Matt J. Gasch, and Amiya K. Mukherjee; **16**(11), 3274–3286.

Munir, Z.A.–Modeling of wave configuration during electrically ignited combustion synthesis.–O.A. Graeve, E.M. Carrillo-Heian, A. Feng, and Z.A. Munir; **16**(1), 93–100.

–Field-activated combustion synthesis of Ta–Si intermetallic compounds.–F. Maglia, U. Anselmi-Tamburini, N. Bertolino, C. Milanese, Z.A. Munir; **16**(2), 534–544.

–Combustion synthesis of mechanically activated powders in the Ti–Si system.–F. Maglia, U. Anselmi-Tamburini, G. Cocco, M. Monagheddu, N. Bertolino, and Z.A. Munir; **16**(4), 1074–1082.

–Mechanochemistry of the titanium–silicon system: Compositional effects.–S. Doppiu, M. Monagheddu, G. Cocco, F. Maglia, U. Anselmi-Tamburini, and Z.A. Munir; **16**(5), 1266–1279.

–Synthesis of dense nanometric $MoSi_2$ through mechanical and field activation.–R. Orrù, J. Woolman, G. Cao, and Z.A. Munir; **16**(5), 1439–1448.

–Combustion of zirconium foils in oxygen.–K.H. Ewald, U. Anselmi-Tamburini, and Z.A. Munir; **16**(9), 2687–2694.

Muniz, E.C.–Low-resistance films of polyimides with impregnated copper sulfide.–R.V.A. Rowe, M.H. Kunita, M.F. Porto, E.C. Muniz, A.F. Rubira, R.C. Nery, E. Radovanovic, L.T. Taylor, and N. Nazem; **16**(11), 3097–3106.

Muñoz, V.–Deep center luminescence versus surface preparation of ZnSe single crystals.–J.A. Garcia, V. Muñoz, C. Martinez-Tomas, and J.J.S. Garitaonandia; **16**(5), 1245–1248(L).

Munroe, P.–Mechanical deformation in silicon by micro-indentation.–J.E. Bradby, J.S. Williams, J. Wong-Leung, M.V. Swain, P. Munroe; **16**(5), 1500–1507.

Murakami, M.–Microstructure of (Nd, Eu, Gd)-123 matrix with (Nd, Eu, Gd)-211 inclusions.–M. Muralidhar, M. Jirsa, K. Iida, N. Sakai, M. Murakami; **16**(2), 407–412.

Murakami, T.–Melt processing of Ba_2CuO_3: Textured precursor for the fabrication of $HgBa_2CuO_4$ superconductor.–E. Sudhakar Reddy, T. Murakami, Y. Nakayama, J. Shimoyama, and K. Kishio; **16**(6), 1759–1768.

Muralidhar, M.–Microstructure of (Nd, Eu, Gd)-123 matrix with (Nd, Eu, Gd)-211 inclusions.–M. Muralidhar, M. Jirsa, K. Iida, N. Sakai, and M. Murakami; **16**(2), 407–412.

Murata, K.–Role of the primary phase particles during the peritectic solidification of Y-123 superconducting oxides.–M. Kambara, M. Yoshizumi, T. Umeda, K. Miyake, K. Murata, T. Izumi, and Y. Shiohara; **16**(8), 2229–2238.

Muto, Hiroyuki–Deformation-induced surface corrugation of superplastic ceramics.–Hiroyuki Muto, Takatoshi Futami, and Motosugu Sakai; **16**(7), 1879–1882(L).

N

Nagashio, K.–Formation of $NdBa_2Cu_3O_{7-\delta}$ amorphous phase by combining aero-acoustic levitation and splat quenching.–K. Nagashio, W.H. Hofmeister, D.E. Gustafson, A. Altgilbers, R.J. Bayuzick, and K. Kuribayashi; **16**(1), 138–145.

Nainaparampil, J.J.–Lubricity of zinc oxide thin films: Study of deposition parameters and Si as an additive.–J.J. Nainaparampil and J.S. Zabinski; **16**(12), 3423–3429.

Nakabayashi, N.–Mechanical stress of the electrical performance of polycrystalline-silicon resistors.–N. Nakabayashi, H. Ohyama, E. Simoen, M. Ikegami, C. Claeys, K. Kobayashi, M. Yoneoka, and K. Miyahara; **16**(9), 2579–2582.

Nakamura, Masatoshi–Comparison of hydrophilic properties of amorphous TiO_x films obtained by radio frequency sputtering and plasma-enhanced chemical vapor deposition.–Masatoshi Nakamura, Toru Aoki, Yoshinori Hatanaka, Dariusz Korzec, and Jurgen Engemann; **16**(2), 621–626.

Nakamura, Yuichi–Preferential growth mechanism of $REBa_2Cu_3O_y$ (RE = Y, Nd) crystal on MgO substrate by liquid phase epitaxy.–Katsumi Nomura, Saburo Hoshi, Xin Yao, Kazuomi Kakimoto, Yuichi Nakamura, Teruo Izumi, and Yuh Shiohara; **16**(4), 979–989.

–Initial growth mechanism of $YBa_2Cu_3O_y$ crystal on MgO substrate by liquid-phase epitaxy.–Katsumi Nomura, Saburo Hoshi, Yuichi Nakamura, Teruo Izumi, and Yuh Shiohara; **16**(10), 2947–2958.

Nakanishi, Kazuki–Macroporous morphology of titania films prepared by sol-gel dip-coating method from a system containing poly(ethylene glycol) and poly(vinylpyrrolidone).–Koichi Kajihara and Kazuki Nakanishi; **16**(1), 58–66.

Nakanishi, Makoto–Low-temperature growth of *c*-axis-oriented Y-type hexagonal ferrite thin films by the polymeric precursor method.–Tatsuo Fujii, Aiko Harano, Makoto Nakanishi, and Jun Takada; **16**(9), 2471–2474(L).

Nakayama, Y.–Melt processing of Ba_2CuO_3: Textured precursor for the fabrication of $HgBa_2CuO_y$ superconductor.–E. Sudhakar Reddy, T. Murakami, Y. Nakayama, J. Shimoyama, and K. Kishio; **16**(6), 1759–1768.

Nam, Kiwoo–Characteristics of elastic waves generated by crack initiation in aluminum alloys under fatigue loading.–Kiwoo Nam and Ajit Mal; **16**(6), 1745–1751.

Narayan, J.–Mechanical properties of nanocrystalline and epitaxial TiN films on (100) silicon.–H. Wang, A. Sharma, A. Kvit, Q. Wei, X. Zhang, C.C. Koch, and J. Narayan; **16**(9), 2733–2738.

–Origins of stored enthalpy in cryomilled nanocrystalline Zn.–Xinghang Zhang, Haiyan Wang, Magdy Kassem, Jagdish Narayan, and Carl C. Koch; **16**(12), 3485–3495.

Narazaki, Aiko–Parameter effect on the crystallization of Nd:yttrium aluminum garnet laser-ablated TiO_2 thin film.–Mrinal Pal, Aiko Narazaki, Takeshi Sasaki, and Naoto Koshizaki; **16**(11), 3158–3161.

Navrotsky, A.–Thermochemistry of rare-earth orthophosphates.–S.V. Ushakov, K.B. Helean, A. Navrotsky, and L.A. Boatner; **16**(9), 2623–2633.

–Enthalpies of formation of lanthanide oxyapatite phases.–A.S. Risbud, K.B. Helean, M.C. Wilding, P. Lu, A. Navrotsky; **16**(10), 2780–2783(L).

–Calorimetric determination of the enthalpy of formation of InN and comparison with AlN and GaN.–M.R. Ranade, F. Tessier, A. Navrotsky, and R. Marchand; **16**(10), 2824–2831.

Nazem, N.–Low-resistance films of polyimides with impregnated copper sulfide.–R.V.A. Rowe, M.H. Kunita, M.F. Porto, E.C. Muniz, A.F. Rubira, R.C. Nery, E. Radovanovic, L.T. Taylor, and N. Nazem; **16**(11), 3097–3106.

Negami, T.–Preparation of $Cu(In,Ga)Se_2$ thin films at low substrate temperatures.–S. Nishiwaki, T. Satoh, Y. Hashimoto, T. Negami, and T. Wada; **16**(2), 394–399.

Nekvindova, P.–Erbium doping into lithium niobate and sapphire single crystal wafers.–P. Nekvindova, J. Spirkova-Hradilova, J. Schröfel, and V. Perina; **16**(2), 333–335(L).

Nery, R.C.–Low-resistance films of polyimides with impregnated copper sulfide.–R.V.A. Rowe, M.H. Kunita, M.F. Porto, E.C. Muniz, A.F. Rubira, R.C. Nery, E. Radovanovic, L.T. Taylor, and N. Nazem; **16**(11), 3097–3106.

Ng, S.C.–Preliminary study on alternating thienylene/phenylene copolymers functionalized with an electron-donating or -withdrawing group.–J.M. Xu, S.C. Ng, and H.S.O. Chan; **16**(5), 1235–1237(L).

–Formation of quasi-one-dimensional carbon chains in cubic nanocrystals by photon-breaking of C–S bonds in polythiophene.–Z.M. Ren, Y.F. Lu, H.W. Choy, T.C. Chong, S.C. Ng, and F. Miao; **16**(10), 2793–2797.

Ngai, H.W.–Crystallization kinetics of amorphous nanostructured $Pd_{40.5}Ni_{40.5}P_{19}$ alloys.–H.W. Ngai, C.C. Leung, W.H. Guo, and H.W. Kui; **16**(3), 797–802.

Ni, Xiao Dong–Site preference of alloying elements in Fe_3Al-based alloys.–Xiao Dong Ni, Nan Xian Chen, Jiang Shen, Zu Qing Sun, and Wang Yue Yang; **16**(2), 344–351.

Nicolaou, P.D.–Development of a model for the prediction of the fretting fatigue regimes.–T.E. Matikas and P.D. Nicolaou; **16**(9), 2716–2723.

Nieh, T.G.–Processing and characterization of hydroxyapatite coatings on titanium produced by magnetron sputtering.–T.G. Nieh, A.F. Jankowski, and J. Koike; **16**(11), 3238–3245.

Niihara, Koichi–Effect of α/β phase ratio on microstructure and mechanical properties of silicon nitride ceramics.–Hirokazu Kawaoka, Tomohiko Adachi, Tohru Sekino, Yong-Ho Choa, Lian Gao, and Koichi Niihara; **16**(8), 2264–2270.

Niinomi, Mitsuo–Machinable calcium pyrophosphate glass-ceramics.–Toshihiro Kasuga, Miwako Terada, Masayuki Nogami, and Mitsuo Niinomi; **16**(3), 876–880.

Nino, Juan C.–Phase formation and reactions in the Bi_2O_3–ZnO–Nb_2O_5–Ag pyrochlore system.–Juan C. Nino, Michael T. Lanagan, and Clive A. Randall; **16**(5), 1460–1464.

Nishi, Yoshitake–Misting-free diamond surface created by sheet electron beam irradiation.–Kazuya Oguri, Nobuhiro Iwataka, Akira Tonegawa, Yoichi Hirose, Kazuo Takayama, and Yoshitake Nishi; **16**(2), 553–557.

–High fracture resistance of carbon fiber treated by electron beam irradiation.–Yoshitake Nishi, Takashi Toriyama, Kazuya Oguri, Akira Tonegawa, and Kazuo Takayama; **16**(6), 1632–1635.

Nishimura, Toshiyuki–Dependence of fracture stress on applied stress rate in a Yb_2O_3–SiO_2-doped hot-pressed silicon nitride ceramic.–Shuqi Guo, Naoto Hirosaki, Yoshinobu Yamamoto, Toshiyuki Nishimura, and Mamoru Mitomo; **16**(11), 3254–3261.

Nishiwaki, S.–Preparation of $Cu(In,Ga)Se_2$ thin films at low substrate temperatures.–S. Nishiwaki, T. Satoh, Y. Hashimoto, T. Negami, and T. Wada; **16**(2), 394–399.

Nistor, L.–*In situ* transmission electron microscopy study of the silicidation process in Co thin films on patterned (001) Si substrates.–C. Ghica, L. Nistor, H. Bender, A. Steegen, A. Lauwers, K. Maex, and J. Van Landuyt; **16**(3), 701–708.

Nogami, Masayuki–Machinable calcium pyrophosphate glass-ceramics.–Toshihiro Kasuga, Miwako Terada, Masayuki Nogami, and Mitsuo Niinomi; **16**(3), 876–880.

Noh, D.Y.–X-ray scattering study on the structural evolution of AlN/sapphire(0001) films during radiofrequency sputter growth.–H.C. Kang, S.H. Seo, and D.Y. Noh; **16**(6), 1814–1821.

Nomura, Katsumi–Preferential growth mechanism of $REBa_2Cu_3O_y$ (RE = Y, Nd) crystal on MgO substrate by liquid phase epitaxy.–Katsumi Nomura, Saburo Hoshi, Xin Yao, Kazuomi Kakimoto, Yuichi Nakamura, Teruo Izumi, and Yuh Shiohara; **16**(4), 979–989.

–Initial growth mechanism of $YBa_2Cu_3O_y$ crystal on MgO substrate by liquid-phase epitaxy.–Katsumi Nomura, Saburo Hoshi, Yuichi Nakamura, Teruo Izumi, and Yuh Shiohara; **16**(10), 2947–2958.

Norga, G.J.–Growth of (111)-oriented $Pb(Zr,Ti)O_3$ layers on nanocrystalline RuO_2 electrodes using the sol-gel technique.–G.J. Norga, S. Jin, Laura Fè, D.J. Wouters, H. Bender, and H.E. Maes; **16**(3), 828–833.

–Chemical structure evolution and orientation selection in sol-gel-prepared ferroelectric $Pb(Zr,Ti)O_3$ thin films.–L. Fè, G.J. Norga, D.J. Wouters, H.E. Maes, and G. Maes; **16**(9), 2499–2504.

Noudem, J.G.–Single-domain $YBa_2Cu_3O_y$ thick films and fabrics prepared by an infiltration and growth process.–E. Sudhakar Reddy, J.G. Noudem, M. Tarka, and G.J. Schmitz; **16**(4), 955–966.

–Directional solidification and microstructural studies of the peritectic Y_2BaCuO_5 phase.–E. Sudhakar Reddy, J.G. Noudem, M. Tarka, and G.J. Schmitz; **16**(4), 1123–1134.

Nowok, J.W.–Thermal expansion and high-temperature phase transformation of the yttrium silicate Y_2SiO_5.–J.W. Nowok, J.P. Kay, and R.J. Kulas; **16**(8), 2251–2255.

Nuesca, Guillermo–Metalorganic chemical vapor deposition of titanium oxide for microelectronics applications.–Kanchana Vydianathan, Guillermo Nuesca, Gregory Peterson, Eric T. Eisenbraun, Alain E. Kaloyeros, John J. Sullivan, and Bin Han; **16**(6), 1838–1849.

O

Ochiai, Shijiro–Joining characteristics of oxidized SiC particles reinforced Al–Mg matrix composite prepared by reaction infiltration processing.–Zhongliang Shi, Shijiro Ochiai, Masaki Hojo, Jaechul Lee, Mingyuan Gu, and Hoin Lee; **16**(2), 400–406.

Odén, M.–Growth, structure, and mechanical properties of transition metal carbide superlattices.–H. Högberg, J. Birch, M. Odén, J-O. Malm, L. Hultman, and U. Jansson; **16**(5), 1301–1310.

Ogawa, Tomoya–Threading dislocations with edge components in GaN epilayers grown on Al_2O_3 substrates.–Junyong Kang and Tomoya Ogawa; **16**(9), 2550–2555.

Oguri, Kazuya–Misting-free diamond surface created by sheet electron beam irradiation.–Kazuya Oguri, Nobuhiro Iwataka, Akira Tonegawa, Yoichi Hirose, Kazuo Takayama, and Yoshitake Nishi; **16**(2), 553–557.

–High fracture resistance of carbon fiber treated by electron beam irradiation.–Yoshitake Nishi, Takashi Toriyama, Kazuya Oguri, Akira Tonegawa, and Kazuo Takayama; **16**(6), 1632–1635.

Oh, Ki Young–Metalorganic chemical vapor deposition of very thin $Pb(Zr,Ti)O_3$ thin films at low temperatures for high-density ferroelectric memory applications.–Hye Ryoung Kim, Seehwa Jeong, Chung Bae Jeon, Oh Seong Kwon, Cheol Seong Hwang, Young Ki Han, Doo Young Yang, and Ki Young Oh; **16**(12), 3583–3591.

Oh, Sang Ho–Growth behavior and defects in conductive $SrRuO_3$ thin films grown on a Si(100) substrate by sputtering.–Sang Ho Oh and Chan-Gyung Park; **16**(7), 1998–2006.

Oh, Seok-Kyun–Absorption spectra of Co^{2+} in $AgInS_2$ orthorhombic single crystals.–Hidong Kim, Seok-Joo Lee, Jae-Eun Kim, Hae Yong Park, Seok-Kyun Oh, and Wha-Tek Kim; **16**(4), 975–978.

Oh-ishi, Keiichiro–Grain boundary structure in Al–Mg and Al–Mg–Sc alloys after equal-channel angular pressing.–Keiichiro Oh-ishi, Zenji Horita, David J. Smith, and Terence G. Langdon; **16**(2), 583–589.

Ohji, Tatsuki–High-strength porous silicon nitride fabricated by the sinter-forging technique.–Naoki Kondo, Yoshikazu Suzuki, and Tatsuki Ohji; **16**(1), 32–34(L).

–Porosity and microstructure control of porous ceramics by partial hot pressing.–Jian-Feng Yang, Guo-Jun Zhang, and Tatsuki Ohji; **16**(7), 1916–1918.

–Improved creep resistance in anisotropic silicon nitride.–Naoki Kondo, Yoshikazu Suzuki, Manuel E. Brito, and Tatsuki Ohji; **16**(8), 2182–2185(L).

Ohki, Yoshimichi–Low-temperature crystallization induced by excimer laser irradiation of $SrBi_2Ta_2O_9$ films.–Kwang Soo Seol, Hironao Hiramatsu, Yoshimichi Ohki, In-Hoon Choi, and Yong-Tea Kim; **16**(7), 1883–1886(L).

Ohkubo, Kenji–Site preference determination in intermetallic compounds by thermal conductivity measurement.–Yoshihiro Terada, Kenji Ohkubo, Tetsuo Mohri, and Tomoo Suzuki; **16**(8), 2314–2320.

Ohyama, H.–Mechanical stress of the electrical performance of polycrystalline-silicon resistors.–N. Nakabayashi, H. Ohyama, E. Simoen, M. Ikegami, C. Claeys, K. Kobayashi, M. Yoneoka, and K. Miyahara; **16**(9), 2579–2582.

Oka, Akihiro–Influence of antiphase boundaries on critical current densities in $YBa_2Cu_3O_{7-\delta}$ single crystals.–Junko Shibata, Akihiro Oka, Teruo Izumi, Yuh Shiohara, Tsukasa Hirayama, and Yuichi Ikuhara; **16**(7), 1935–1941.

Oksanen, J.A.I.–Dye-doped sol-gel coatings for near-infrared laser protection.–T. Kololuoma, J.A.I. Oksanen, P. Raerinne, and J.T. Rantala; **16**(8), 2186–2188(L).

Oku, Takeo–Atomic structure of YB_{56} studied by digital high-resolution electron microscopy and electron diffraction.–Takeo Oku, Jan-Olov Bovin, Iwami Higashi, Takaho Tanaka, and Yoshio Ishizawa; **16**(1), 101–107.

Oliveira, M.N.–Synthesis and properties of $B_xC_yN_z$ coatings.–M.N. Oliveira and O. Conde; **16**(3), 734–743.

–Microstructure and formation mechanism of combustion-synthesized rodlike Ca α-sialon crystals.–Kexin Chen, Haibo Jin, M. Oliveira, Heping Zhou, and J.M.F. Ferreira; **16**(7), 1928–1934.

Oliver, W.C.–Alternative technique for analyzing instrumented indentation data.–W.C. Oliver; **16**(11), 3202–3206.

Olorunyolemi, Tayo–Microwave sintering of ZnO at ultra high heating rates.–Geng-fu Xu, Isabel K. Lloyd, Yuval Carmel, Tayo Olorunyolemi, Otto C. Wilson, Jr.; **16**(10), 2850–2858.

Ong, C.W.–Relationship between the microstructure and nanoindentation hardness of thermally evaporated and magnetron-sputtered electrochromic tungsten oxide films.–C.W. Ong, H.Y. Wong, G.K.H. Pang, K.Z. Baba-Kishi, and C.L. Choy; **16**(6), 1541–1548.

Ono, Satomi–Processing of highly oriented lithium niobate films through chemical solution deposition.–Satomi Ono and Shin-ichi Hirano; **16**(4), 1155–1162.

Orrù, R.–Synthesis of dense nanometric $MoSi_2$ through mechanical and field activation.–R. Orrù, J. Woolman, G. Cao, and Z.A. Munir; **16**(5), 1439–1448.

Ou, D.R.–Effect of a magnetic field on phase transformation of steel.–W. Liu, D.R. Ou, H.H. Zhou, G.Y. Tang, and F. Wu; **16**(8), 2280–2282.

Ovchar, Oleg V.–Solid-state reaction mechanism for the formation of $Ba_{6-x}Ln_{8+2\cdot x/3}Ti_{18}O_{54}$ (Ln = Nd, Sm) solid solutions.–Anatolii G. Belous, Oleg V. Ovchar, Matjaz Valant, and Danilo Suvorov; **16**(8), 2350–2356.

Öveçoğlu, M.L.–Effect of composition on the thermal properties and spontaneous emission probabilities of Tm^{3+}-doped TeO_2–LiCl glass.–G. Özen, B. Demirata, and M.L. Öveçoğlu; **16**(5), 1381–1388.

Overmyer, D.L.–High J_c $YBa_2Cu_3O_{7-\delta}$ films via rapid, low pO_2 pyrolysis.–J.T. Dawley, P.G. Clem, M.P. Siegal, and D.L. Overmyer; **16**(1), 13–16(L).

–Properties of $YBa_2Cu_3O_{7-\delta}$ multilayer films from the fluoride-based sol-gel process.–M.P. Siegal, J.T. Dawley, and D.L. Overmyer; **16**(12), 3339–3342(L).

Ownby, P.D.–Wetting of mullite by Y_2O_3–Al_2O_3–SiO_2 and B_2O_3–SiO_2 glasses.–T.S. Huang, M.N. Rahaman, B.T. Eldred, and P.D. Ownby; **16**(11), 3223–3228.

Ozawa, Kiyoshi–Dense, bubble-free ceramic deposits from aqueous suspensions by electrophoretic deposition.–Tetsuo Uchikoshi, Kiyoshi Ozawa, Benjamin D. Hatton, and Yoshio Sakka; **16**(2), 321–324(L).

Özen, G.–Effect of composition on the thermal properties and spontaneous emission probabilities of Tm^{3+}-doped TeO_2–LiCl glass.–G. Özen, B. Demirata, and M.L. Öveçoğlu; **16**(5), 1381–1388.

Ozkan, Cengiz–Precipitate splitting in $Pb_{0.91}La_{0.09}Zr_{0.65}Ti_{0.35}O_3$ films.–Bahadir Tunaboylu, Ken Ring, Sadik C. Esener, Cengiz Ozkan, and Ali Ata; **16**(10), 2763–2766(L).

P

Pajares, Antonia–Contact fracture of brittle bilayer coatings on soft substrates.–Pedro Miranda, Antonia Pajares, Fernando Guiberteau, Francisco L. Cumbrera, and Brian R. Lawn; **16**(1), 115–126.

Pak, Y. Eugene–Formation and characterization of crystalline iron oxide films on self-assembled organic monolayers and their *in situ* patterning.–Hyunjung Shin, Jong Up Jeon, Y. Eugene Pak, Hyejin Im, and Eung Soo Kim; **16**(2), 564–569.

Pal, Mrinal–Parameter effect on the crystallization of Nd:yttrium aluminum garnet laser-ablated TiO_2 thin film.–Mrinal Pal, Aiko Narazaki, Takeshi Sasaki, and Naoto Koshizaki; **16**(11), 3158–3161.

Pal, U.–Determination of optical constants of Si/ZnO polycrystalline nanocomposites by spectroscopic ellipsometry.–J. García-Serrano, N. Koshizaki, T. Sasaki, G. Martínez-Montes, U. Pal; **16**(12), 3554–3559.

Palacio, Manuel Luis B.–Effect of ion implant dose on the mechanical properties of polyethersulfone films.–Manuel Luis B. Palacio, Yongquiang Wang, and William W. Gerberich; **16**(12), 3628–3635.

Pan, M.X.–Formation and properties of $Zr_{48}Nb_8Fe_8Cu_{12}Be_{24}$ bulk metallic glass.–Yong Zhang, D.Q. Zhao, B.C. Wei, P. Wen, M.X. Pan, and W.H. Wang; **16**(6), 1675–1679.

Pan, X.F.–Preparation of superfine Fe-base alloy by liquidus casting.–X.F. Pan, H.F. Zhang, A.M. Wang, B.Z. Ding, and Z.Q. Hu; **16**(12), 3459–3463.

Pan, X.Q.–Transmission electron microscopy study of $n = 1$–5 $Sr_{n+1}Ti_nO_{3n+1}$ epitaxial thin films.–W. Tian, X.Q. Pan, J.H. Haeni, and D.G. Schlom; **16**(7), 2013–2026.

Pan, Xiaoming–Twinning domain in $67Pb(Mg_{1/3}Nb_{2/3})O_3$–$33PbTiO_3$ ferroelectric complex perovskite crystal grown by the Bridgman method.–Donglin Li, Pingchu Wang, Xiaoming Pan, Haosu Luo, and Zhiwen Yin; **16**(5), 1252–1255(L).

Pang, G.K.H.–Relationship between the microstructure and nanoindentation hardness of thermally evaporated and magnetron-sputtered electrochromic tungsten oxide films.–C.W. Ong, H.Y. Wong, G.K.H. Pang, K.Z. Baba-Kishi, and C.L. Choy; **16**(6), 1541–1548.

Pang, M.–Thin-film fracture during nanoindentation of a titanium oxide film–titanium system.–M. Pang and D.F. Bahr; **16**(9), 2634–2643.

Panko, V.V.–Influence of compositional disorder on optical absorption processes in $Cu_6P(S_{1-x}Se_x)_5I$ crystals.–I.P. Studenyak, M. Kranjčec, Gy.Sh. Kovacs, I.D. Desnica-Frankovič, V.V. Panko, and V.Yu. Slivka; **16**(6), 1600–1608.

Panneerselvam, M.–Translucent yttrium aluminum garnet: Microwave-assisted route to synthesis and processing.–M. Panneerselvam, G.N. Subanna, and K.J. Rao; **16**(10), 2773–2776(L).

Papanearchou, N.–Comparison of crystal structure parameters of natural and synthetic apatites from neutron powder diffraction.–Th. Leventouri, B.C. Chakoumakos, N. Papanearchou, and V. Perdikatsis; **16**(9), 2600–2606.

Paranthaman, M.–Growth and characterization of conductive Sr-RuO_3 and $LaNiO_3$ multilayers on textured Ni tapes for high-J_c $YBa_2Cu_3O_{7-\delta}$ coated conductors.–T. Aytug, B.W. Kang, C. Cantoni, E.D. Specht, M. Paranthaman, A. Goyal, D.K. Christen, D.T. Verebelyi, J.Z. Wu, R.E. Ericson, C.L. Thomas, C-Y.Yang, and S.E. Babcock; **16**(9), 2661–2669.

–Growth mechanism of superconducting MgB_2 films prepared by various methods.–H.Y. Zhai, H.M. Christen, L. Zhang, M. Paranthaman, C. Cantoni, B.C. Sales, P.H. Fleming, D.K. Christen, and D.H. Lowndes; **16**(10), 2759–2762(L).

Park, Byungwoo–Microwave dielectric properties of $(1-x)Cu_3Nb_2O_8$–$xZn_3Nb_2O_8$ ceramics.–Dong-Wan Kim, In-Tae Kim, Byungwoo Park, Kug Sun Hong, and Jong-Hee Kim; **16**(5), 1465–1470.

Park, Chan-Gyung–Growth behavior and defects in conductive $SrRuO_3$ thin films grown on a Si(100) substrate by sputtering.–Sang Ho Oh and Chan-Gyung Park; **16**(7), 1998–2006.

Park, H.D.–Luminescence and decay behaviors of Tb-doped yttrium silicate.–Yoon Young Choi, Kee-Sun Sohn, Hee Dong Park, and Se Young Choi; **16**(3), 881–889.

–Photoluminescence behavior of Al^{3+}, Pr^{3+} doped perovskite $La_{2/3}TiO_3$ and pyrochlore $La_2Ti_2O_7$.–J.K. Park, C.H. Kim, K.J. Choi, H.D. Park, and S.Y. Choi; **16**(9), 2568–2571.

Park, H-R.–Chemical-vapor-deposition growth and characterization of epitaxial 3C–SiC films on SOI substrates with thin silicon top layers.–C.K. Moon, H.J. Song, J.K. Kim, J.H. Park, S.J. Jang, J-B. Yoo, H-R. Park, and Byung-Teak Lee; **16**(1), 24–27(L).

Park, Hae Yong–Absorption spectra of Co^{2+} in $AgInS_2$ orthorhombic single crystals.–Hidong Kim, Seok-Joo Lee, Jae-Eun Kim, Hae Yong Park, Seok-Kyun Oh, and Wha-Tek Kim; **16**(4), 975–978.

Park, Heung Soo–Effect of bond valence on microwave dielectric properties of $(Pb_{1-x}Ca_x)(Mg_{0.33}Ta_{0.67})O_3$ ceramics.–Heung Soo Park, Ki Hyun Yoon, and Eung Soo Kim; **16**(3), 817–821.

Park, Hyung-Sang–Effect of mechanical alloying on combustion synthesis of $MoSi_2$.–Hyung-Sang Park, Kwang-Seon Shin, and Yong-Seog Kim; **16**(11), 3060–3068.

Park, J.H.–Chemical-vapor-deposition growth and characterization of epitaxial 3C–SiC films on SOI substrates with thin silicon top layers.–C.K. Moon, H.J. Song, J.K. Kim, J.H. Park, S.J. Jang, J-B. Yoo, H-R. Park, and Byung-Teak Lee; **16**(1), 24–27(L).

Park, J.K.–Photoluminescence behavior of Al^{3+}, Pr^{3+} doped perovskite $La_{2/3}TiO_3$ and pyrochlore $La_2Ti_2O_7$.–J.K. Park, C.H. Kim, K.J. Choi, H.D. Park, and S.Y. Choi; **16**(9), 2568–2571.

Park, Jae-Gwan–Analysis of defect formation in Nb-doped $SrTiO_3$ by impedance spectroscopy.–Seong-Ho Kim, Jung-Ho Moon, Jae-Hwan Park, Jae-Gwan Park, and Yoonho Kim; **16**(1), 192–196.

Park, Jaehoo–Optimization of the annealing process for the (Ba,Sr)TiO_3 thin films grown by low-temperature (420 °C) metalorganic chemical vapor deposition.–Jaehoo Park, Cheol Seong Hwang, and Doo Young Yang; **16**(5), 1363–1371.

Park, Jae-Hwan–Analysis of defect formation in Nb-doped $SrTiO_3$ by impedance spectroscopy.–Seong-Ho Kim, Jung-Ho Moon, Jae-Hwan Park, Jae-Gwan Park, and Yoonho Kim; **16**(1), 192–196.

Park, Jeong Hwan–Dependence of dielectric and piezoelectric properties on film thickness for highly {100}-oriented lead magnesium niobate–lead titanate (70/30) thin films.–Jeong Hwan Park and Susan Trolier-McKinstry; **16**(1), 268–275.

Park, Jong-Gon–Influence of sintering atmosphere on the fabrication of SiC ceramics with a powder mixture of sialon composition.–Jong-Kook Lee, Jong-Gon Park, Eun-Gu Lee, and Kyung-Seok Kim; **16**(6), 1784–1788.

Park, Jong-Hwan–Stability of channels at a scalloplike Cu_6Sn_5 layer in solder interconnections.–Jong-Hyun Lee, Jong-Hwan Park, Yong-Ho Lee, Yong-Seog Kim, and Dong Hyuk Shin; **16**(5), 1227–1230(L).

–Effects of Cu and Ni additions to eutectic Pb–Sn solders on Au embrittlement of solder interconnections.–Jong-Hyun Lee, Jong-Hwan Park, Yong-Ho Lee, and Yong-Seog Kim; **16**(5), 1249–1251(L).

Park, K.S.–Synthesis of $Nd_2Fe_{14}B$ powders by spray-drying and reduction–diffusion processes.–X.L. Dong, B.K. Kim, C.J. Choi, K.S. Park, and Z.D. Zhang; **16**(4), 1083–1089.

Park, Oun-Ho–Photoinduced condensation of sol-gel hybrid glass films doped with benzildimethylketal.–Oun-Ho Park, Ji-In Jung, and Byeong-Soo Bae; **16**(7), 2143–2148.

–Direct laser writing of self-developed waveguides in benzyldimethylketal-doped sol-gel hybrid glass.–Byeong-Soo Bae, Oun-Ho Park, Robbie Charters, Barry Luther-Davies, and Graham R. Atkins; **16**(11), 3184–3187.

Park, Soon Dong–Preparation of nanocrystalline nickel oxide–yttria-stabilized zirconia composite powder by solution combustion with ignition of glycine fuel.–Sun-Jae Kim, Wonhee Lee, Won-Jun Lee, Soon Dong Park, Jae Sung Song, and Eun Gu Lee; **16**(12), 3621–3627.

Park, W.I.–Metal-organic vapor phase epitaxial growth of high-quality ZnO films on Al_2O_3(00·1).–W.I. Park, S-J. An, Gyu-Chul Yi, and Hyun M. Jang; **16**(5), 1358–1362.

Park, Wounjhang–Eu^{+3} and Cr^{+3} doping for red cathodoluminescence in $ZnGa_2O_4$.–Philip D. Rack, Jeffrey J. Peterson, Michael D. Potter, and Wounjhang Park; **16**(5), 1429–1433.

Park, Y.–Annealing effect on in-plane alignment and surface morphology of epitaxial $Bi_4Ti_3O_{12}$ thin films prepared by the chemical solution deposition.–K. Hwang and Y. Park; **16**(9), 2519–2525.

Patil, R.C.–Piezoresistivity of conducting polyaniline/$BaTiO_3$ composites.–R.C. Patil, S. Radhakrishnan, Sushama Pethkar, and K. Vijaymohanan; **16**(7), 1982–1988.

Payzant, E.A.–Templated growth of a complex nitride island dispersion through an internal nitridation reaction.–M.P. Brady, D.T. Hoelzer, E.A. Payzant, P.F. Tortorelli, J.A. Horton, I.M. Anderson, L.R. Walker, and S.K. Wrobel; **16**(10), 2784–2787(L).

Pederson, L.R.–Mechanical and thermal properties of combustion-synthesized perovskites, $La_{1-x}Sr_xCr_{0.2}Fe_{0.8}O_3$.–Yeong-Shyung Chou, K. Kerstetter, L.R. Pederson, and R.E. Williford; **16**(12), 3545–3553.

Pedraza, A.J.–Laser-induced surface perturbations in silicon.–A.J. Pedraza, S. Jesse, Y.F. Guan, and J.D. Fowlkes; **16**(12), 3599–3608.

Peelamedu, Ramesh D.–Reaction kinetics and anisothermal effects in microwave fields: The System Y_2O_3–Fe_3O_4.–Ramesh D. Peelamedu, Rustum Roy, and Dinesh K. Agrawal; **16**(10), 2770–2772(L).

Pei, Z.L.–Dependence of structural, electrical, and optical properties of ZnO:Al films on substrate temperature.–M. Chen, Z.L. Pei, X. Wang, C. Sun, and L.S. Wen; **16**(7), 2118–2123.

Pekarskaya, E.–*In situ* transmission electron microscopy studies of shear bands in a bulk metallic glass based composite.–E. Pekarskaya, C.P. Kim, and W.L. Johnson; **16**(9), 2513–2518.

Peláiz-Barranco, A.–Thermal and structural characterization of the $ZrO_{2-x}(OH)_{2x}$ to ZrO_2 transition.–E. Torres-García, A. Peláiz-Barranco, C. Vázquez-Ramos, and G.A. Fuentes; **16**(8), 2209–2212.

Pelekh, Aleksey–Mechanistic studies in combustion synthesis of NiAl–TiB_2 composites: Effects of gravity.–Cheryl Lau, Alexander Mukasyan, Aleksey Pelekh, and Arvind Varma; **16**(6), 1614–1625.

Peng, Hsin-Wei–Crystallization and dielectric properties of SrO–BaO–Nb_2O_5–GeO_2 tungsten–bronze glass–ceramics.–Jiin-Jyh Shyu and Hsin-Wei Peng; **16**(7), 2057–2063.

Perdikatsis, V.–Comparison of crystal structure parameters of natural and synthetic apatites from neutron powder diffraction.–Th. Leventouri, B.C. Chakoumakos, N. Papanearchou, and V. Perdikatsis; **16**(9), 2600–2606.

Pérez, E.–Influence of thermal history on morphology and viscoelastic behavior of ethylene–1-octene copolymers synthesized with metallocene catalysts.–M.L. Cerrada, R. Benavente, and E. Pérez; **16**(4), 1103–1111.

Pérez-Pariente, J.–Textural properties of $SiO_2 \cdot CaO \cdot P_2O_5$ glasses prepared by the sol-gel method.–F. Balas, D. Arcos, J. Pérez-Pariente, and M. Vallet-Regí; **16**(5), 1345–1348.

Perina, V.–Erbium doping into lithium niobate and sapphire single crystal wafers.–P. Nekvindova, J. Spirkova-Hradilova, J. Schröfel, and V. Perina; **16**(2), 333–335(L).

Perry, A.J.–Mechanism of improvement of TiN-coated tool life by nitrogen implantation.–S.J. Bull, Yu.P. Sharkeev, S.V. Fortuna, I.A. Shulepov, A.J. Perry; **16**(11), 3293–3303.

Peterson, E.J.–High critical current density $YBa_2Cu_3O_{7-\delta}$ thick films using ion beam assisted deposition MgO bi-axially oriented template layers on nickel-based superalloy substrates.–J.R. Groves, P.N. Arendt, S.R. Foltyn, Q.X. Jia, T.G. Holesinger, H. Kung, E.J. Peterson, R.F. DePaula, P.C. Dowden, L. Stan, and L.A. Emmert; **16**(8), 2175–2178(L).

Peterson, Gregory–Metalorganic chemical vapor deposition of titanium oxide for microelectronics applications.–Kanchana Vydianathan, Guillermo Nuesca, Gregory Peterson, Eric T. Eisenbraun, Alain E. Kaloyeros, John J. Sullivan, and Bin Han; **16**(6), 1838–1849.

Peterson, Jeffrey J.–Eu^{+3} and Cr^{+3} doping for red cathodoluminescence in $ZnGa_2O_4$.–Philip D. Rack, Jeffrey J. Peterson, Michael D. Potter, and Wounjhang Park; **16**(5), 1429–1433.

Pethkar, Sushama–Piezoresistivity of conducting polyaniline/$BaTiO_3$ composites.–R.C. Patil, S. Radhakrishnan, Sushama Pethkar, and K. Vijaymohanan; **16**(7), 1982–1988.

Petrov, Ivan–Thermal stability of carbon nitride thin films.–Niklas Hellgren, Nian Lin, Esteban Broitman, Virginie Serin, Stefano E. Grillo, Ray Twesten, Ivan Petrov, Christian Colliex, Lars Hultman, and Jan-Eric Sundgren; **16**(11), 3188–3201.

Petrovic, J.J.–Synthesis of silicon microwire.–J.J. Petrovic, R.C. Hoover, R.D. Field, and K. Han; **16**(10), 2777–2779(L).

Petrović, R.–Phase-transformation kinetics in triphasic cordierite gel.–R. Petrović, Dj. Janacković, S. Zec, S. Drmanić, and Lj. Kostić-Gvozdenović; **16**(2), 451–458.

Pezzotti, G.–Rheological characteristics of slurry controlling the microstructure and the compressive strength behavior of biomimetic hydroxyapatite.–S. Guicciardi, C. Galassi, E. Landi, A. Tampieri, K. Satou, and G. Pezzotti; **16**(1), 163–170.

–Microprobe fluorescence spectroscopy evaluation of stress fields developed along a propagating crack in an $Al_2O_3/CaO \cdot 6Al_2O_3$ ceramic composite.–O. Sbaizero, S. Maschio, G. Pezzotti, and I.J. Davies; **16**(10), 2798–2804.

Pfender, Emil–Chemical vapor deposition of an aluminum nitride–diamond composite in a triple torch plasma reactor.–Marcus Assmann, Robert F. Cook, Joachim V. Heberlein, and Emil Pfender; **16**(2), 469–477.

Pharr, G.M.–Measurement of residual stress by load and depth sensing indentation with spherical indenters.–J.G. Swadener, B. Taljat, and G.M. Pharr; **16**(7), 2091–2102.

Philipsborn, H. von–Phase formation and crystal growth of Sr–Bi–Ta–O thin films grown by metalorganic chemical vapor deposition.–H. Bachhofer, H. von Philipsborn, W. Hartner, C. Dehm, B. Jobst, A. Kiendl, H. Schroeder, and R. Waser; **16**(10), 2966–2973.

Phillipp, F.–Characterization of GaN grown on sapphire by laser-induced molecular beam epitaxy.–H. Zhou, A. Rühm, N.Y. Jin-Phillipp, F. Phillipp, M. Gross, and H. Schröder; **16**(1), 261–267.

Phillips, Jonathan–Low-power plasma torch method for the production of crystalline spherical ceramic particles.–Chun-Ku Chen, Seth Gleiman, and Jonathan Phillips; **16**(5), 1256–1265.

Piñero, M.–Control growth of PbS quantum dots doped sonoormosil.–R. Erce-Montilla, M. Piñero, N. de la Rosa-Fox, A. Santos, and L. Esquivias; **16**(9), 2572–2578.

Pique, A.–Dielectric properties of oxide structures by a laser-based direct-writing method.–D. Young, H.D. Wu, R.C.Y. Auyeung, R. Modi, J. Fitz-Gerald, A. Pique, D.B. Chrisey, P. Atanassova, and T. Kodas; **16**(6), 1720–1725.

Pirri, C.F.–X-ray reflectivity spectra of ultrathin films and nanometric multilayers: Experiment and simulation.–E. Bontempi, L.E. Depero, L. Sangaletti, F. Giorgis, C.F. Pirri; **16**(9), 2556–2561.

Polizzi, Stefano–Fractal aggregates of lanthanide-doped Y_2O_3 nanoparticles obtained by propellant synthesis.–Stefano Polizzi, Giuliano Fagherazzi, Marino Battagliarin, Marco Bettinelli, and Adolfo Speghini; **16**(1), 146–154.

Poortmans, Jef–Effect of *in situ* boron doping on properties of silicon germanium films deposited by chemical vapor deposition at 400 °C.–Sherif Sedky, Ann Witvrouw, Annelies Saerens, Paul Van Houtte, Jef Poortmans, and Kris Baert; **16**(9), 2607–2612.

Porto, M.F.–Low-resistance films of polyimides with impregnated copper sulfide.–R.V.A. Rowe, M.H. Kunita, M.F. Porto, E.C. Muniz, A.F. Rubira, R.C. Nery, E. Radovanovic, L.T. Taylor, and N. Nazem; **16**(11), 3097–3106.

Potter, Michael D.–Eu^{+3} and Cr^{+3} doping for red cathodoluminescence in $ZnGa_2O_4$.–Philip D. Rack, Jeffrey J. Peterson, Michael D. Potter, and Wounjhang Park; **16**(5), 1429–1433.

Prud'homme, Robert K.–Cure depth in photopolymerization: Experiments and theory.–Jim H. Lee, Robert K. Prud'homme, and Ilhan A. Aksay; **16**(12), 3536–3544.

Prybyla, Stan–Increased fracture toughness in nanoporous silica–polyimide matrix composites.–Shiling Ruan, John J. Lannutti, Stan Prybyla, and Robert R. Seghi; **16**(7), 1975–1981.

Puglisi, O.–Formation and characterization of high-density silver nanoparticles embedded in silica thin films by "*in situ*" self-reduction.–G. Compagnini, M.E. Fragalà, L. D'Urso, C. Spinella, O. Puglisi; **16**(10), 2934–2938.

Pullar, R.C.–Halide removal from BaM ($BaFe_{12}O_{19}$) and SrM ($SrFe_{12}O_{19}$) ferrite fibers via a steaming process.–R.C. Pullar, M.D. Taylor, and A.K. Bhattacharya; **16**(11), 3162–3169.

Pun, Edwin Yue Bun–Investigation of optical waveguide formed in Er:Yb:phosphate glass by MeV He^+ implantation.–Zhuang Zhuo, Edwin Yue Bun Pun, Sun Fat Wong, and Ying Zhou; **16**(4), 1135–1137.

Puricelli, S.–Elastic properties of anisotropic monolithic samples of compressed expanded graphite studied with ultrasounds.–M. Krzesińska, A. Celzard, J.F. Marêché, and S. Puricelli; **16**(2), 606–614.

Q

Qi, Zhenyi–Domain configurations in relaxor ferroelectric single crystals $Pb(Mg_{1/3}Nb_{2/3})O_3$–$PbTiO_3$.–Guisheng Xu, Haosu Luo, Zhenyi Qi, Haiqing Xu, and Zhiwen Yin; **16**(4), 932–937.

Qian, Xuefeng–Preparation and characterization of nanocrystalline PbSe in poly(acrylic acid-*co*-styrene).–Yangyang Sun, Xuefeng Qian, Jie Yin, Junchao Huang, Xiaodong Ma, and Zikang Zhu; **16**(10), 2922–2927.

Qian, Y.T.–Preparation and characterization of $CuInS_2$ nanorods and nanotubes from an elemental solvothermal reaction.–Yang Jiang, Yue Wu, Shengwen Yuan, Bo Xie, Shuyuan Zhang, and Yitai Qian; **16**(10), 2805–2809.

–Solvothermal route to Bi_2Se_4 nanorods at low temperature.–Yuanfang Liu, Jing-hui Zeng, Wei-xin Zhang, Wei-chao Yu, Yi-tai Qian, Jin-bo Cao, and Wan-qun Zhang; **16**(12), 3361–3365.

–Preparation and phase control of nanocrystalline silver indium sulfides via a hydrothermal route.–J.Q. Hu, B. Deng, K.B. Tang, C.R. Wang, Y.T. Qian; **16**(12), 3411–3415.

Qiang, Jian-Bing–Formation rule for Al-based ternary quasi-crystals: Example of Al–Ni–Fe decagonal phase.–Jian-Bing Qiang, De-He Wang, Cui-Min Bao, Ying-Min Wang, Wei-Ping Xu, Mei-Li Song, and Chuang Dong; **16**(9), 2653–2660.

Qiu, Jianrong–Relaxation of ultraviolet-radiation-induced structure and long-lasting phosphorescence in Eu^{2+}-doped strontium aluminosilicate glasses.–Jianrong Qiu, Y. Shimizugawa, K. Kojima, K. Tanaka, and K. Hirao; **16**(1), 88–92.

Quang, Nguyen Dinh–Electrical and microstructural characteristics of ZnO–Bi_2O_3-based varistors doped with rare-earth oxides.–Nguyen The Hung, Nguyen Dinh Quang, and Slavko Bernik; **16**(10), 2817–2823.

Que, Wen Xiu–Third-order nonlinear optical response in PbS-coated CdS nanocomposites.–Bing Liu, Chwee Har Chew, Leong Ming Gan, Guo Qin Xu, Heping Li, Yee Loy Lam, Chan Hin Kam, and Wen Xiu Que; **16**(6), 1644–1650.

Queheillalt, Douglas T.–Synthesis of open-cell metal foams by templated directed vapor deposition.–Douglas T. Queheillalt, Derek D. Hass, David J. Sypeck, and Haydn N.G. Wadley; **16**(4), 1028–1036.

R

Rack, Philip D.–Eu^{+3} and Cr^{+3} doping for red cathodoluminescence in $ZnGa_2O_4$.–Philip D. Rack, Jeffrey J. Peterson, Michael D. Potter, and Wounjhang Park; **16**(5), 1429–1433.

Radhakrishnan, S.–Piezoresistivity of conducting polyaniline/$BaTiO_3$ composites.–R.C. Patil, S. Radhakrishnan, Sushama Pethkar, and K. Vijaymohanan; **16**(7), 1982–1988.

Radovanovic, E.–Low-resistance films of polyimides with impregnated copper sulfide.–R.V.A. Rowe, M.H. Kunita, M.F. Porto, E.C. Muniz, A.F. Rubira, R.C. Nery, E. Radovanovic, L.T. Taylor, and N. Nazem; **16**(11), 3097–3106.

Raerinne, P.–Dye-doped sol-gel coatings for near-infrared laser protection.–T. Kololuoma, J.A.I. Oksanen, P. Raerinne, and J.T. Rantala; **16**(8), 2186–2188(L).

Rahaman, M.N.–Wetting of mullite by Y_2O_3–Al_2O_3–SiO_2 and B_2O_3–SiO_2 glasses.–T.S. Huang, M.N. Rahaman, B.T. Eldred, and P.D. Ownby; **16**(11), 3223–3228.

Rainho, J.P.–^{29}Si nuclear-magnetic-resonance and vibrational spectroscopy studies of SiO_2–TiO_2 powders prepared by the sol-gel process.–J.P. Rainho, J. Rocha, L.D. Carlos, and R.M. Almeida; **16**(8), 2369–2376.

Ramachandrarao, P.–Patterning of copper particles on polymeric surface.–Arvind Sinha, Swapan Kumar Das, V. Rao, and P. Ramachandrarao; **16**(5), 1354–1357.

Ramamoorthy, R.–Sintering and microstructure of glass-coated nanocrystalline yttria-stabilized tetragonal zirconia powder: Effect of the glass.–R. Ramamoorthy and R. Chaim; **16**(1), 296–302.

Ramiro, J.–X-ray photoelectron spectroscopy of electrodeposited cadmium mercury telluride thin films and their native surface oxides.–J. Ramiro, L. Galán, E. García Camarero, I. Montero, and Y. Laaziz; **16**(7), 1942–1952.

Ramos, A.Y.–CsCl-modified Ga_2S_3–La_2S_3 glasses: Structural approach by x-ray absorption spectroscopy.–A.Y. Ramos, M. Grisolía Cardona, H.C.N. Tolentino, M.C.M. Alves, N. Watanabe, O.L. Alves, and L.C. Barbosa; **16**(5), 1349–1353.

Ranade, M.R.–Calorimetric determination of the enthalpy of formation of InN and comparison with AlN and GaN.–M.R. Ranade, F. Tessier, A. Navrotsky, and R. Marchand; **16**(10), 2824–2831.

Randall, Clive A.–Phase formation and reactions in the Bi_2O_3–ZnO–Nb_2O_5–Ag pyrochlore system.–Juan C. Nino, Michael T. Lanagan, and Clive A. Randall; **16**(5), 1460–1464.

Ranganathan, S.–Microstructural characterization of rapidly solidified Al–Fe–Si, Al–V–Si, and Al–Fe–V–Si alloys.–A.K. Srivastava and S. Ranganathan; **16**(7), 2103–2117.

Rantala, J.T.–Dye-doped sol-gel coatings for near-infrared laser protection.–T. Kololuoma, J.A.I. Oksanen, P. Raerinne, and J.T. Rantala; **16**(8), 2186–2188(L).

Rao, B. Srinivasa–A new technique for pressureless infiltration of Al alloys into Al_2O_3 preforms.–B. Srinivasa Rao and V. Jayaram; **16**(10), 2906–2913.

Rao, J.C.–$L1_2$- and $L1_0$-like cation-ordered structures in ZrO_2–Y_2O_3 ceramics.–J.C. Rao, Y. Zhou, and D.X. Li; **16**(6), 1806–1813.

Rao, K.J.–Translucent yttrium aluminum garnet: Microwave-assisted route to synthesis and processing.–M. Panneerselvam, G.N. Subanna, and K.J. Rao; **16**(10), 2773–2776(L).

Rao, V.–Patterning of copper particles on polymeric surface.–Arvind Sinha, Swapan Kumar Das, V. Rao, and P. Ramachandrarao; **16**(5), 1354–1357.

Rappaz, M.–Moving the pulsed heating technique beyond monolithic specimens: Experiments with coated wires.–D. Josell, D. Basak, J.L. McClure, U.R. Kattner, M.E. Williams, W.J. Boettinger, and M. Rappaz; **16**(8), 2421–2428.

Ray, Swati–Development of *p*-type microcrystalline silicon carbon alloy films by the very high frequency plasma-enhanced chemical vapor deposition technique.–Tapati Jana, Arup Dasgupta, and Swati Ray; **16**(7), 2130–2135.

Reaney, Ian M.–Relation between tolerance factor and T_c in Aurivillius compounds.–Donají Y. Suárez, Ian M. Reaney, and William E. Lee; **16**(11), 3139–3149.

Reddy, E. Sudhakar–Single-domain $YBa_2Cu_3O_y$ thick films and fabrics prepared by an infiltration and growth process.–E. Sudhakar Reddy, J.G. Noudem, M. Tarka, and G.J. Schmitz; **16**(4), 955–966.

–Directional solidification and microstructural studies of the peritectic Y_2BaCuO_5 phase.–E. Sudhakar Reddy, J.G. Noudem, M. Tarka, and G.J. Schmitz; **16**(4), 1123–1134.

–Melt processing of Ba_2CuO_3: Textured precursor for the fabrication of $HgBa_2CuO_y$ superconductor.–E. Sudhakar Reddy, T. Murakami, Y. Nakayama, J. Shimoyama, and K. Kishio; **16**(6), 1759–1768.

Reece, M.J.–Direct measurement of mechanical properties of (Pb,La)TiO_3 ferroelectric thin films using nanoindentation techniques.–M. Algueró, A.J. Bushby, and M.J. Reece; **16**(4), 993–1002.

Reed, M.A.–Growth and characterization of aligned carbon nanotubes from patterned nickel nanodots and uniform thin films. –J.G. Wen, Z.P. Huang, D.Z. Wang, J.H. Chen, S.X. Yang, Z.F. Ren, J.H. Wang, L.E. Calvet, J. Chen, J.F. Klemic, and M.A. Reed; **16**(11), 3246–3253.

Rehn, L.E.–Mass density of glassy $Pd_{80}Si_{20}$ during low-temperature light ion irradiation.–G. Schumacher, R.C. Birtcher, and L.E. Rehn; **16**(10), 2788–2792.

Reichenbach, H.M.–Combinatorial synthesis of oxide powders.–H.M. Reichenbach and P.J. McGinn; **16**(4), 967–974.

Ren, Z.F.–Growth and characterization of aligned carbon nanotubes from patterned nickel nanodots and uniform thin films.–J.G. Wen, Z.P. Huang, D.Z. Wang, J.H. Chen, S.X. Yang, Z.F. Ren, J.H. Wang, L.E. Calvet, J. Chen, J.F. Klemic, and M.A. Reed; **16**(11), 3246–3253.

Ren, Z.M.–Formation of quasi-one-dimensional carbon chains in cubic nanocrystals by photon-breaking of C–S bonds in polythiophene.–Z.M. Ren, Y.F. Lu, H.W. Choy, T.C. Chong, S.C. Ng, and P. Miao; **16**(10), 2793–2797.

Rickerby, D.G.–Highly textured nanostructure of pulsed laser deposited IrO_2 thin films as investigated by transmission electron microscopy.–A.M. Serventi, M.A. El Khakani, R.G. Saint-Jacques, and D.G. Rickerby; **16**(8), 2336–2342.

Rickman, J.M.–Improved tensile creep properties of yttrium- and lanthanum-doped alumina: a solid solution effect.–Junghyun Cho, Chong Min Wang, Helen M. Chan, J.M. Rickman, and Martin P. Harmer; **16**(2), 425–429.

Riester, L.–Analysis of depth-sensing indentation tests with a Knoop indenter.–L. Riester, T.J. Bell, and A.C. Fischer-Cripps; **16**(6), 1660–1667.

Riley, Frank L.–Influence of CaO–SiO_2 ratio on the chemistry of intergranular films in liquid-phase sintered alumina and implications for rate of erosive wear.–Rik Brydson, Peter C. Twigg, Fiona Loughran, and Frank L. Riley; **16**(3), 652–665.

Riman, Richard E.–Mechanochemical-hydrothermal preparation of crystalline hydroxyapatite powders at room temperature.–Pavel Shuk, Wojciech L. Suchanek, Tian Hao, Eric Gulliver, Richard E. Riman, Mamoru Senna, Kevor S. TenHuisen, and Victor F. Janas; **16**(5), 1231–1234(L).

Ring, Ken–Precipitate splitting in $Pb_{0.91}La_{0.09}Zr_{0.65}Ti_{0.35}O_3$ films.–Bahadir Tunaboylu, Ken Ring, Sadik C. Esener, Cengiz Ozkan, and Ali Ata; **16**(10), 2763–2766(L).

Risbud, A.S.–Enthalpies of formation of lanthanide oxyapatite phases.–A.S. Risbud, K.B. Helean, M.C. Wilding, P. Lu, and A. Navrotsky; **16**(10), 2780–2783(L).

Rocha, J.–^{29}Si nuclear-magnetic-resonance and vibrational spectroscopy studies of SiO_2–TiO_2 powders prepared by the sol-gel process.–J.P. Rainho, J. Rocha, L.D. Carlos, and R.M. Almeida; **16**(8), 2369–2376.

Rodbell, K.P.–Texture in Ti/Al and Nb/Al multilayer thin films: Role of Cu.–G. Lucadamo, K. Barmak, and K.P. Rodbell; **16**(5), 1449–1459.

Roeder, Ryan K.–Processing effects on the composition and dielectric properties of hydrothermally derived $Ba_xSr_{(1-x)}TiO_3$ thin films.–Mark A. McCormick, Ryan K. Roeder, and Elliott B. Slamovich; **16**(4), 1200–1209.

Rogers, John A.–Optical evaluation of the flexural rigidity and residual stress in thin membranes: Picosecond transient grating measurements of the dispersion of the lowest-order Lamb acoustic waveguide mode.–John A. Rogers and Greg R. Bogart; **16**(1), 217–225.

Rolfs, C.–Characterization of the induction period in tricalcium silicate hydration by nuclear resonance reaction analysis.–R.A. Livingston, J.S. Schweitzer, C. Rolfs, H-W. Becker, and S. Kubsky; **16**(3), 687–693.

Rollett, A.D.–Combined out-of-plane and in-plane texture control in thin films using ion beam assisted deposition.–L. Dong, D.J. Srolovitz, G.S. Was, Q. Zhao, A.D. Rollett; **16**(1), 210–216.

Rosa-Fox, N. de la–Control growth of PbS quantum dots doped sonoormosil.–R. Erce-Montilla, M. Piñero, N. de la Rosa-Fox, A. Santos, and L. Esquivias; **16**(9), 2572–2578.

Rosenman, G.–Polarization reversal and domain anisotropy in flux-grown $KTiOPO_4$ and isomorphic crystals.–P. Urenski, G. Rosenman, and M. Molotskii; **16**(5), 1493–1499.

Roviglione, A.N.–Transient self-dewetting of steels after pulsed electron beam melting.–N. Mingolo, A.N. Roviglione, and O.E. Martínez; **16**(8), 2343–2349.

Rowe, R.V.A.–Low-resistance films of polyimides with impregnated copper sulfide.–R.V.A. Rowe, M.H. Kunita, M.F. Porto, E.C. Muniz, A.F. Rubira, R.C. Nery, E. Radovanovic, L.T. Taylor, and N. Nazem; **16**(11), 3097–3106.

Roy, Rustum–Reaction kinetics and anisothermal effects in microwave fields: The System Y_2O_3–Fe_3O_4.–Ramesh D. Peelamedu, Rustum Roy, and Dinesh K. Agrawal; **16**(10), 2770–2772(L).

Ruan, Shiling–Increased fracture toughness in nanoporous silica–polyimide matrix composites.–Shiling Ruan, John J. Lannutti, Stan Prybyla, and Robert R. Seghi; **16**(7), 1975–1981.

Rubira, A.F.–Low-resistance films of polyimides with impregnated copper sulfide.–R.V.A. Rowe, M.H. Kunita, M.F. Porto, E.C. Muniz, A.F. Rubira, R.C. Nery, E. Radovanovic, L.T. Taylor, and N. Nazem; **16**(11), 3097–3106.

Rühm, A.–Characterization of GaN grown on sapphire by laser-induced molecular beam epitaxy.–H. Zhou, A. Rühm, N.Y. Jin-Phillipp, F. Phillipp, M. Gross, and H. Schröder; **16**(1), 261–267.

Ruiz, F.–Structure of heat-treated sol-gel SiO_2 glasses containing silver.–M.G. Garníca-Romo, J. González-Hernández, M.A. Hernández-Landaverde, Y.V. Vorobiev, F. Ruiz, and J.R. Martínez; **16**(7), 2007–2012.

Rusakova, Irene A.–Thermodynamic stability of tetragonal zirconia nanocrystallites.–Nae-Lih Wu, Ton-Fon Wu, and Irene A. Rusakova; **16**(3), 666–669.

Ryan, E. Todd–Effect of material properties on integration damage in organosilicate glass films.–E. Todd Ryan, Jeremy Martin, Kurt Junker, Jeff Wetzel, David W. Gidley, and Jianing Sun; **16**(12), 3335–3338(L).

S

Sabatini, R.L.–Nucleation and growth of $YBa_2Cu_3O_x$ on $SrTiO_3$ and CeO_2 by a BaF_2 postdeposition reaction process.–L. Wu, Y. Zhu, V.F. Solovyov, H.J. Wiesmann, A.R. Moodenbaugh, R.L. Sabatini, and M. Suenaga; **16**(10), 2869–2884.

Sada, C.–Electronic paramagnetic resonance study of Cu^{2+} ions in copper ion-exchanged layers of lithium niobate crystals.–F. Caccavale, C. Sada, F. Segato, L.D. Bogomolova, V.A. Jachkin, and N.A. Krasil'nikova; **16**(6), 1554–1558.

Sadoway, Donald R.–Synthesis of nanoscale particles of Ta and Nb_3Al by homogeneous reduction in liquid ammonia.–Hongmin Zhu and Donald R. Sadoway; **16**(9), 2544–2549.

Sadwick, L.P.–Investigation of crystal properties of TmP/GaAs and GaAs/TmP/GaAs heterostructures grown by molecular beam epitaxy.–C.H. Lin, R.J. Hwu, and L.P. Sadwick; **16**(11), 3266–3273.

Saerens, A.–Finite element modeling of microscale thermal residual stresses in Al interconnects.–A. Saerens, P. Van Houtte, and S.R. Kalidindi; **16**(4), 1112–1122.

–Effect of *in situ* boron doping on properties of silicon germanium films deposited by chemical vapor deposition at 400 °C.–Sherif Sedky, Ann Witvrouw, Annelies Saerens, Paul Van Houtte, Jef Poortmans, and Kris Baert; **16**(9), 2607–2612.

Saida, J.–Formation of icosahedral quasicrystal by crystallization of $Zr_{70}(Ni, Cu, Pd)_{30}$ amorphous alloys.–T. Zhang, A. Inoue, M. Matsushita, and J. Saida; **16**(1), 20–23(L).

–Redistribution behavior of constitutional elements at an initial crystallization stage in the $Zr_{65}Al_{7.5}Ni_{10}Cu_{17.5}$ glassy alloy.–J. Saida, M. Matsushita, and A. Inoue; **16**(1), 28–31(L).

–Change in local atomic structure during formation of the icosahedral quasicrystalline phase in $Zr_{70}Pd_{30}$ glassy alloy.–Muneyuki Imafuku, Junji Saida, and Akihisa Inoue; **16**(11), 3046–3049(L).

–Investigation of the stability of glassy state in the Zr- and Hf-based glassy alloys correlated with their transformation behavior.–Junji Saida, Chunfei Li, Mitsuhide Matsushita, and Akihisa Inoue; **16**(12), 3389–3401.

Saint-Jacques, R.G.–Highly textured nanostructure of pulsed laser deposited IrO_2 thin films as investigated by transmission electron microscopy.–A.M. Serventi, M.A. El Khakani, R.G. Saint-Jacques, and D.G. Rickerby; **16**(8), 2336–2342.

Saito, Keisuke–Ferroelectric property of epitaxial $Bi_4Ti_3O_{12}$ films prepared by metalorganic chemical vapor deposition.–Takayuki Watanabe, Hiroshi Funakubo, and Keisuke Saito; **16**(1), 303–307.

Saito, Noriko–Effect of the calcium dopant on oxide ion diffusion in yttria ceramics.–Noriko Saito, Hajime Haneda, Isao Sakaguchi, and Takayasu Ikegami; **16**(8), 2362–2368.

Sakaguchi, Isao–Effect of the calcium dopant on oxide ion diffusion in yttria ceramics.–Noriko Saito, Hajime Haneda, Isao Sakaguchi, and Takayasu Ikegami; **16**(8), 2362–2368.

Sakai, Motosugu–Deformation-induced surface corrugation of superplastic ceramics.–Hiroyuki Muto, Takatoshi Futami, and Motosugu Sakai; **16**(7), 1879–1882(L).

Sakai, N.–Microstructure of (Nd, Eu, Gd)-123 matrix with (Nd, Eu, Gd)-211 inclusions.–M. Muralidhar, M. Jirsa, K. Iida, N. Sakai, and M. Murakami; **16**(2), 407–412.

Sakka, Yoshio–Dense, bubble-free ceramic deposits from aqueous suspensions by electrophoretic deposition.–Tetsuo Uchikoshi, Kiyoshi Ozawa, Benjamin D. Hatton, and Yoshio Sakka; **16**(2), 321–324(L).

Sakuma, Jun–Water-associated surface degradation of $CsLiB_6O_{10}$ crystal during harmonic generation in the ultraviolet region.–Yukihiro Morimoto, Shintaro Miyazawa, Yoshio Kagebayashi, Naoki Kitatochi, Toshio Yokota, and Jun Sakuma; **16**(7), 2082–2090.

Sakuma, Taketo–Transient creep in fine-grained polycrystalline Al_2O_3 with Lu^{3+} ion segregation at the grain boundaries.–Hidehiro Yoshida, Yuichi Ikuhara, and Taketo Sakuma; **16**(3), 716–720.

Salama, K.–Microstructure and growth of joins in melt-textured $YBa_2Cu_3O_{7-\delta}$.–A.D. Bradley, W. Lo, M. Mironova, N.H. Babu, D.A. Cardwell, A.M. Campbell, and K. Salama; **16**(8), 2298–2305.

Salem, Jon–Creep and toughness of cryomilled NiAl containing Cr.–J. Daniel Whittenberger, Beverly Aikin, and Jon Salem; **16**(5), 1333–1344.

Sales, B.C.–Growth mechanism of superconducting MgB_2 films prepared by various methods.–H.Y. Zhai, H.M. Christen, L. Zhang, M. Paranthaman, C. Cantoni, B.C. Sales, P.H. Fleming, D.K. Christen, and D.H. Lowndes; **16**(10), 2759–2762(L).

Sameshima, Soichiro–Oxygen self-diffusion in cerium oxide doped with Nd.–Michiyo Kamiya, Eriko Shimada, Yasuro Ikuma, Manabu Komatsu, Hajime Haneda, Soichiro Sameshima, and Yoshihiro Hirata; **16**(1), 179–184.

Sander, M.S.–Epitaxial growth of skutterudite ($CoSb_3$) thin films on (001) InSb by pulsed laser deposition.–J.C. Caylor, M.S. Sander, A.M. Stacy, J.S. Harper, R. Gronsky, and T. Sands; **16**(9), 2467–2470(L).

Sands, T.–High-T_c superconducting NbN films with low particulate density grown at 25 °C using pulsed laser deposition.–Anupama B. Kaul, Timothy D. Sands, and Theodore Van Duzer; **16**(5), 1223–1226(L).

–Epitaxial growth of skutterudite ($CoSb_3$) thin films on (001) InSb by pulsed laser deposition.–J.C. Caylor, M.S. Sander, A.M. Stacy, J.S. Harper, R. Gronsky, and T. Sands; **16**(9), 2467–2470(L).

Sangaletti, L.–X-ray reflectivity spectra of ultrathin films and nanometric multilayers: Experiment and simulation.–E. Bontempi, L.E. Depero, L. Sangaletti, F. Giorgis, and C.F. Pirri; **16**(9), 2556–2561.

Santos, A.–Control growth of PbS quantum dots doped sonoormosil.–R. Erce-Montilla, M. Piñero, N. de la Rosa-Fox, A. Santos, and L. Esquivias; **16**(9), 2572–2578.

Sarikaya, M.–Biomimetic model of a sponge-spicular optical fiber—mechanical properties and structure.–M. Sarikaya, H. Fong, N. Sunderland, B.D. Flinn, G. Mayer, A. Mescher, and E. Gaino; **16**(5), 1420–1428.

Sasaki, T.–Parameter effect on the crystallization of Nd:yttrium aluminum garnet laser-ablated TiO_2 thin film.–Mrinal Pal, Aiko Narazaki, Takeshi Sasaki, and Naoto Koshizaki; **16**(11), 3158–3161.

–Determination of optical constants of Si/ZnO polycrystalline nanocomposites by spectroscopic ellipsometry.–J. García-Serrano, N. Koshizaki, T. Sasaki, G. Martínez-Montes, and U. Pal; **16**(12), 3554–3559.

Satoh, T.–Preparation of $Cu(In,Ga)Se_2$ thin films at low substrate temperatures.–S. Nishiwaki, T. Satoh, Y. Hashimoto, T. Negami, and T. Wada; **16**(2), 394–399.

Satou, K.–Rheological characteristics of slurry controlling the microstructure and the compressive strength behavior of biomimetic hydroxyapatite.–S. Guicciardi, C. Galassi, E. Landi, A. Tampieri, K. Satou, and G. Pezzotti; **16**(1), 163–170.

Satsuki, H.–Microstructural analysis of high-pressure compressed C_{60}.–K. Miyazawa, H. Satsuki, M. Kuwabara, and M. Akaishi; **16**(7), 1960–1966.

Sawa, Takeshi–Simplified method for analyzing nanoindentation data and evaluating performance of nanoindentation instruments.–Takeshi Sawa and Kohichi Tanaka; **16**(11), 3084–3096.

Sbaizero, O.–Microprobe fluorescence spectroscopy evaluation of stress fields developed along a propagating crack in an Al_2O_3/CaO · $6Al_2O_3$ ceramic composite.–O. Sbaizero, S. Maschio, G. Pezzotti, and I.J. Davies; **16**(10), 2798–2804.

Sberveglieri, G.–Production and characterization of titanium and iron oxide nano-sized thin films.–E. Comini, G. Sberveglieri, M. Ferroni, V. Guidi, C. Frigeri, and D. Boscarino; **16**(6), 1559–1564.

Scardi, P.–Residual stress in fiber-textured thin films of cubic materials.–P. Scardi and Y.H. Dong; **16**(1), 233–242.

Schaffer, G.B.–Freeform fabrication of aluminum metal-matrix composites.–C.W. Souvignier, T.B. Sercombe, S.H. Huo, P. Calvert, G.B. Schaffer; **16**(9), 2613–2618.

Scheithauer, Michael J.–Solid-phase synthesis of cupric tungstate.–Leonid P. Dorfman, David L. Houck, Michael J. Scheithauer, Jeffrey N. Dann, and Harry O. Fassett; **16**(4), 1096–1102.

Schlom, D.G.–Transmission electron microscopy study of (103)-oriented epitaxial $SrBi_2Nb_2O_9$ films grown on (111) $SrTiO_3$ and (111) $SrRuO_3$/(111) $SrTiO_3$.–M.A. Zurbuchen, J. Lettieri, Y. Jia, D.G. Schlom, S.K. Streiffer, and M.E. Hawley; **16**(2), 489–502.

–Transmission electron microscopy study of $n = 1$–5 $Sr_{n+1}Ti_nO_{3n+1}$ epitaxial thin films.–W. Tian, X.Q. Pan, J.H. Haeni, and D.G. Schlom; **16**(7), 2013–2026.

Schlumm, D.–Analysis of a ceramic/metal laminate under thermal shock.–D. Sherman and D. Schlumm; **16**(3), 753–764.

Schmitz, G.J.–Single-domain $YBa_2Cu_3O_y$ thick films and fabrics prepared by an infiltration and growth process.–E. Sudhakar Reddy, J.G. Noudem, M. Tarka, and G.J. Schmitz; **16**(4), 955–966.

–Directional solidification and microstructural studies of the peritectic Y_2BaCuO_5 phase.–E. Sudhakar Reddy, J.G. Noudem, M. Tarka, and G.J. Schmitz; **16**(4), 1123–1134.

Schneider, J.A.–Surface effects in field-assisted sintering.–J.R. Groza, M. Garcia, and J.A. Schneider; **16**(1), 286–292.

Schröder, H.–Characterization of GaN grown on sapphire by laser-induced molecular beam epitaxy.–H. Zhou, A. Rühm, N.Y. Jin-Phillipp, F. Phillipp, M. Gross, and H. Schröder; **16**(1), 261–267.

Schroeder, H.–Phase formation and crystal growth of Sr–Bi–Ta–O thin films grown by metalorganic chemical vapor deposition.–H. Bachhofer, H. von Philipsborn, W. Hartner, C. Dehm, B. Jobst, A. Kiendl, H. Schroeder, and R. Waser; **16**(10), 2966–2973.

Schröfel, J.–Erbium doping into lithium niobate and sapphire single crystal wafers.–P. Nekvindova, J. Spirkova-Hradilova, J. Schröfel, and V. Perina; **16**(2), 333–335(L).

Schubert, M.–Infrared optical properties of aged porous GaAs.–S. Zangooie, M. Schubert, T.E. Tiwald, and J.A. Woollam; **16**(5), 1241–1244(L).

Schueller, Olivier J.A.–Fabrication and characterization of microscale sandwich beams.–Francisco Arias, Paul J.A. Kenis, Bing Xu, Tao Deng, Olivier J.A. Schueller, George M. Whitesides, Yuki Sugimura, and Anthony G. Evans; **16**(2), 597–605.

Schuh, C.–Tensile fracture during transformation superplasticity of Ti–6Al–4V.–C. Schuh and D.C. Dunand; **16**(3), 865–875.

–Solid-state foaming of titanium by superplastic expansion of argon-filled pores.–N.G. Davis, J. Teisen, C. Schuh, and D.C. Dunand; **16**(5), 1508–1519.

Schulz, R.–Study of the activation process of Mg-based hydrogen storage materials modified by graphite and other carbonaceous compounds.–S. Bouaricha, J-P. Dodelet, D. Guay, J. Huot, R. Schulz; **16**(10), 2893–2905.

Schumacher, G.–Mass density of glassy $Pd_{80}Si_{20}$ during low-temperature light ion irradiation.–G. Schumacher, R.C. Birtcher, and L.E. Rehn; **16**(10), 2788–2792.

Schweitzer, J.S.–Characterization of the induction period in tricalcium silicate hydration by nuclear resonance reaction analysis.–R.A. Livingston, J.S. Schweitzer, C. Rolfs, H-W. Becker, and S. Kubsky; **16**(3), 687–693.

Sciti, D.–Influence of annealing treatments on microstructure and toughness of liquid-phase-sintered silicon carbide.–D. Sciti and A. Bellosi; **16**(3), 806–816.

Scotch, Adam M.–Electron backscatter diffraction analysis of $Pb(Mg_{1/3}Nb_{2/3})O_3$–35mol%$PbTiO_3$ single crystals grown by seeded polycrystal conversion.–Ajmal Khan, Derrick T. Carpenter, Adam M. Scotch, Helen M. Chan, and Martin P. Harmer; **16**(3), 694–700.

Sedky, Sherif–Effect of *in situ* boron doping on properties of silicon germanium films deposited by chemical vapor deposition at 400 °C.–Sherif Sedky, Ann Witvrouw, Annelies Saerens, Paul Van Houtte, Jef Poortmans, and Kris Baert; **16**(9), 2607–2612.

Segato, F.–Electronic paramagnetic resonance study of Cu^{2+} ions in copper ion-exchanged layers of lithium niobate crystals.–F. Caccavale, C. Sada, F. Segato, L.D. Bogomolova, V.A. Jachkin, and N.A. Krasil'nikova; **16**(6), 1554–1558.

Seghi, Robert–Phase transformation effects on the wear properties of alumina gel–polymer matrix nanocomposites.–Jiazhong Luo, John Lannutti, and Robert Seghi; **16**(6), 1680–1685.

–Increased fracture toughness in nanoporous silica–polyimide matrix composites.–Shiling Ruan, John J. Lannutti, Stan Prybyla, and Robert R. Seghi; **16**(7), 1975–1981.

Seghi, Steve–Piezoelectric actuation of crack growth along polymer–metal interfaces in adhesive bonds.–Tianbao Du, Ming Liu, Steve Seghi, K.J. Hsia, J. Economy, and J.K. Shang; **16**(10), 2885–2892.

Sekine, T.–Cubic silicon nitride embedded in amorphous silicon dioxide.–Ming Zhang, Hongliang He, F.F. Xu, T. Sekine, T. Kobayashi, and Y. Bando; **16**(8), 2179–2181(L).

Sekino, Tohru–Effect of α/β phase ratio on microstructure and mechanical properties of silicon nitride ceramics.–Hirokazu Kawaoka, Tomohiko Adachi, Tohru Sekino, Yong-Ho Choa, Lian Gao, and Koichi Niihara; **16**(8), 2264–2270.

Selman, J. Robert–Anode-supported planar solid oxide fuel cells by plasma-enhanced metalorganic chemical vapor deposition (PE-MOCVD) and electrostatic spray deposition (ESD): Fabrication of dense thin layers of yttria-stabilized zirconia by PE-MOCVD.–Gianfranco Di Giuseppe and J. Robert Selman; **16**(10), 2983–2991.

Senna, Mamoru–Mechanochemical-hydrothermal preparation of crystalline hydroxyapatite powders at room temperature.–Pavel Shuk, Wojciech L. Suchanek, Tian Hao, Eric Gulliver, Richard E. Riman, Mamoru Senna, Kevor S. TenHuisen, and Victor F. Janas; **16**(5), 1231–1234(L).

Senos, A.M.R.–Densification and grain growth of Al-doped ZnO.–Jiaping Han, P.Q. Mantas, and A.M.R. Senos; **16**(2), 459–468.

Seo, Min Hong–Effects of strain hardenability and strain-rate sensitivity on the plastic flow and deformation homogeneity during equal channel angular pressing.–Hyoung Seop Kim, Sun Ig Hong, and Min Hong Seo; **16**(3), 856–864.

Seo, S.H.–X-ray scattering study on the structural evolution of AlN/sapphire(0001) films during radiofrequency sputter growth.–H.C. Kang, S.H. Seo, and D.Y. Noh; **16**(6), 1814–1821.

Seol, Kwang Soo–Low-temperature crystallization induced by excimer laser irradiation of $SrBi_2Ta_2O_9$ films.–Kwang Soo Seol, Hironao Hiramatsu, Yoshimichi Ohki, In-Hoon Choi, and Yong-Tea Kim; **16**(7), 1883–1886(L).

Sercombe, T.B.–Freeform fabrication of aluminum metal-matrix composites.–C.W. Souvignier, T.B. Sercombe, S.H. Huo, P. Calvert, and G.B. Schaffer; **16**(9), 2613–2618.

Serin, Virginie–Thermal stability of carbon nitride thin films.–Niklas Hellgren, Nian Lin, Esteban Broitman, Virginie Serin, Stefano E. Grillo, Ray Twesten, Ivan Petrov, Christian Colliex, Lars Hultman, and Jan-Eric Sundgren; **16**(11), 3188–3201.

Serra, P.–Structural characterization of laser-treated Cr_3C_2–NiCr coatings.–P. Serra, J.M. Miguel, J.L. Morenza, and J.M. Guilemany; **16**(12), 3416–3422.

Serventi, A.M.–Highly textured nanostructure of pulsed laser deposited IrO_2 thin films as investigated by transmission electron microscopy.–A.M. Serventi, M.A. El Khakani, R.G. Saint-Jacques, and D.G. Rickerby; **16**(8), 2336–2342.

Sevillano, J. Gil–Size effects in powder compaction.–J. Gil Sevillano; **16**(5), 1238–1240(L).

–Size effects in powder compaction.–J. Gil Sevillano; **16**(6), 1872(E).

Shang, J.K.–Interfacial embrittlement by bismuth segregation in copper/tin–bismuth Pb-free solder interconnect.–P.L. Liu and J.K. Shang; **16**(6), 1651–1659.

–Piezoelectric actuation of crack growth along polymer–metal interfaces in adhesive bonds.–Tianbao Du, Ming Liu, Steve Seghi, K.J. Hsia, J. Economy, and J.K. Shang; **16**(10), 2885–2892.

Shao, Zongsu–Growth, defects, and properties of $GdCa_4O(BO_3)_3$ and Nd:$GdCa_4O(BO_3)_3$ crystals.–Jiyang Wang, Xiaobo Hu, Xin Yin, Renbo Song, Jingqian Wei, Zongsu Shao, Yaogang Liu, Minhua Jiang, Yulian Tian, Jianhua Jiang, and Wanxia Huang; **16**(3), 790–796.

Sharkeev, Yu.P.–Mechanism of improvement of TiN-coated tool life by nitrogen implantation.–S.J. Bull, Yu.P. Sharkeev, S.V. Fortuna, I.A. Shulepov, and A.J. Perry; **16**(11), 3293–3303.

Sharma, A.–Mechanical properties of nanocrystalline and epitaxial TiN films on (100) silicon.–H. Wang, A. Sharma, A. Kvit, Q. Wei, X. Zhang, C.C. Koch, and J. Narayan; **16**(9), 2733–2738.

Shek, C.H.–Texture analysis of grain refinement in undercooled $Ni_{99.45}B_{0.55}$.–K.L. Lee, C.H. Shek, and H. Yang; **16**(5), 1434–1438.

Shen, Bao-Gen–Magnetic properties, domain structure, and microstructure of anisotropic $SmCo_{6.5}Zr_{0.5}$ ribbons with C addition.–A-Ru Yan, Zhi-Gang Sun, Wen-Yong Zhang, Hong-Wei Zhang, Bao-Gen Shen; **16**(3), 629–632(L).

Shen, Ding-Yu–Refractive index profile and attenuation measurement in $KTiOPO_4$ waveguide by megaelectronvolt He ions.–Ke-Ming Wang, Hiu Hu, Fei Lu, Feng Chen, Bo-Rong Shi, Yao-Gang Liu, Ding-Yu Shen, and Xie-Mei Wang; **16**(1), 276–279.

Shen, Jiang–Site preference of alloying elements in Fe_3Al-based alloys.–Xiao Dong Ni, Nan Xian Chen, Jiang Shen, Zu Qing Sun, and Wang Yue Yang; **16**(2), 344–351.

–Elastic constants of polycrystalline Al and TiN calculated by an *ab initio* method within the local-density approximation.–Ming Zhang, Jiang Shen, and Jiawen He; **16**(8), 2293–2297.

Sheng, Mei–Effects of static thermal aging and thermal cycling on the microstructure and shear strength of $Sn_{95.5}Ag_{3.8}Cu_{0.7}$ solder joints.–Shawkret Ahat, Mei Sheng, and Le Luo; **16**(10), 2914–2921.

Shengjie, Ying–Two-dimensional simulation of mass transport in polymer removal from a powder injection molding compact by thermal debinding.–Ying Shengjie, Y.C. Lam, S.C.M. Yu, and K.C. Tam; **16**(8), 2436–2451.

Sherman, D.–Statistical behavior and misfit stresses in ceramic and metal laminated system.–D. Sherman and X. Gong; **16**(3), 721–727.

–Analysis of a ceramic/metal laminate under thermal shock.–D. Sherman and D. Schlumm; **16**(3), 753–764.

Shi, Bo-Rong–Refractive index profile and attenuation measurement in $KTiOPO_4$ waveguide by megaelectronvolt He ions.–Ke-Ming Wang, Hiu Hu, Fei Lu, Feng Chen, Bo-Rong Shi, Yao-Gang Liu, Ding-Yu Shen, and Xie-Mei Wang; **16**(1), 276–279.

Shi, H.–Growth study of epitaxial $Fe_xZn_{1-x}F_2$ thin films.–J. McChesney, M. Hetzer, H. Shi, T. Charlton, and D. Lederman; **16**(6), 1769–1775.

Shi, Y.H.–Growth of melt-textured Nd-123 by hot seeding under reduced oxygen partial pressure.–M. Kambara, N. Hari Babu, Y.H. Shi, and D.A. Cardwell; **16**(4), 1163–1170.

Shi, Zhongliang–Joining characteristics of oxidized SiC particles reinforced Al–Mg matrix composite prepared by reaction infiltration processing.–Zhongliang Shi, Shijiro Ochiai, Masaki Hojo, Jaechul Lee, Mingyuan Gu, and Hoin Lee; **16**(2), 400–406.

Shibata, Junko–Influence of antiphase boundaries on critical current densities in $YBa_2Cu_3O_{7-y}$ single crystals.–Junko Shibata, Akihiro Oka, Teruo Izumi, Yuh Shiohara, Tsukasa Hirayama, and Yuichi Ikuhara; **16**(7), 1935–1941.

Shimada, Eriko–Oxygen self-diffusion in cerium oxide doped with Nd.–Michiyo Kamiya, Eriko Shimada, Yasuro Ikuma, Manabu Komatsu, Hajime Haneda, Soichiro Sameshima, and Yoshihiro Hirata; **16**(1), 179–184.

Shimizugawa, Y.–Relaxation of ultraviolet-radiation-induced structure and long-lasting phosphorescence in Eu^{2+}-doped strontium aluminosilicate glasses.–Jianrong Qiu, Y. Shimizugawa, K. Kojima, K. Tanaka, and K. Hirao; **16**(1), 88–92.

Shimoyama, J.–Melt processing of Ba_2CuO_3: Textured precursor for the fabrication of $HgBa_2CuO_y$ superconductor.–E. Sudhakar Reddy, T. Murakami, Y. Nakayama, J. Shimoyama, and K. Kishio; **16**(6), 1759–1768.

Shin, Dong Hyuk–Stability of channels at a scalloplike Cu_6Sn_5 layer in solder interconnections.–Jong-Hyun Lee, Jong-Hwan Park, Yong-Ho Lee, Yong-Seog Kim, Dong Hyuk Shin; **16**(5), 1227–1230(L).

Shin, Hyunjung–Formation and characterization of crystalline iron oxide films on self-assembled organic monolayers and their *in situ* patterning.–Hyunjung Shin, Jong Up Jeon, Y. Eugene Pak, Hyejin Im, and Eung Soo Kim; **16**(2), 564–569.

Shin, Kwang-Seon–Effect of mechanical alloying on combustion synthesis of $MoSi_2$.–Hyung-Sang Park, Kwang-Seon Shin, and Yong-Seog Kim; **16**(11), 3060–3068.

Shin, Yong Beom–Enhancement of the 1.31-μm emission properties of Dy^{3+}-doped Ge–Ga–S glasses with the addition of alkali halides.–Yong Beom Shin, Jong Heo, and Hyoun Soo Kim; **16**(5), 1318–1324.

Shin, Yong-Wook–Highly (111)-oriented and conformal iridium films by liquid source metalorganic chemical vapor deposition.–Jaydeb Goswami, Chang-Gong Wang, Prashant Majhi, Yong-Wook Shin, and Sandwip K. Dey; **16**(8), 2192–2195(L).

Shinoda, Y.–Topological transformation of grains in three-dimensional normal grain growth.–F. Wakai, Y. Shinoda, S. Ishihara, and A. Domínguez-Rodríguez; **16**(7), 2136–2142.

Shiohara, Y.–Formation of $Nd_{1+x}(Ba_{1-y}Sr_y)_{2-x}Cu_3O_{7\pm\delta}$ solid solutions by crystal pulling.–Xin Yao, E.A. Goodilin, Teruo Izumi, and Yuh Shiohara; **16**(2), 529–533.

–Preferential growth mechanism of $REBa_2Cu_3O_y$ (RE = Y, Nd) crystal on MgO substrate by liquid phase epitaxy.–Katsumi Nomura, Saburo Hoshi, Xin Yao, Kazuomi Kakimoto, Yuichi Nakamura, Teruo Izumi, and Yuh Shiohara; **16**(4), 979–989.

–Influence of antiphase boundaries on critical current densities in $YBa_2Cu_3O_{7-y}$ single crystals.–Junko Shibata, Akihiro Oka, Teruo Izumi, Yuh Shiohara, Tsukasa Hirayama, and Yuichi Ikuhara; **16**(7), 1935–1941.

–Role of the primary phase particles during the peritectic solidification of Y-123 superconducting oxides.–M. Kambara, M. Yoshizumi, T. Umeda, K. Miyake, K. Murata, T. Izumi, and Y. Shiohara; **16**(8), 2229–2238.

–Initial growth mechanism of $YBa_2Cu_3O_y$ crystal on MgO substrate by liquid-phase epitaxy.–Katsumi Nomura, Saburo Hoshi, Yuichi Nakamura, Teruo Izumi, Yuh Shiohara; **16**(10), 2947–2958.

Shtansky, D.V.–Crystallography and structural evolution of $LiNbO_3$ and $LiNb_{1-x}Ta_xO_3$ films on sapphire prepared by high-rate thermal plasma spray chemical vapor deposition.–D.V. Shtansky, S.A. Kulinich, K. Terashima, T. Yoshida, and Y. Ikuhara; **16**(8), 2271–2279.

Shter, G.E.–Entrapment of organosilicon molecules in nonhydrolytic alumina gels and thermal behavior of the resulting composite.–G.S. Grader, S.A. Melchior, Y. De-Hazan, S. Melamed, G.E. Shter; **16**(5), 1413–1419.

Shuk, Pavel–Mechanochemical-hydrothermal preparation of crystalline hydroxyapatite powders at room temperature.–Pavel Shuk, Wojciech L. Suchanek, Tian Hao, Eric Gulliver, Richard E. Riman, Mamoru Senna, Kevor S. TenHuisen, and Victor F. Janas; **16**(5), 1231–1234(L).

Shulepov, I.A.–Mechanism of improvement of TiN-coated tool life by nitrogen implantation.–S.J. Bull, Yu.P. Sharkeev, S.V. Fortuna, I.A. Shulepov, and A.J. Perry; **16**(11), 3293–3303.

Shyu, Jiin-Jyh–Crystallization and dielectric properties of SrO–BaO–Nb_2O_5–GeO_2 tungsten–bronze glass–ceramics.–Jiin-Jyh Shyu and Hsin-Wei Peng; **16**(7), 2057–2063.

Siegal, M.P.–High J_c $YBa_2Cu_3O_{7-\delta}$ films via rapid, low pO_2 pyrolysis.–J.T. Dawley, P.G. Clem, M.P. Siegal, and D.L. Overmyer; **16**(1), 13–16(L).

–Properties of $YBa_2Cu_3O_{7-\delta}$ multilayer films from the fluoride-based sol-gel process.–M.P. Siegal, J.T. Dawley, and D.L. Overmyer; **16**(12), 3339–3342(L).

Sih, B.–Ferroelectric $SrBi_2Ta_2O_9$ single-crystal growth and characterization.–B. Sih, J. Tang, M. Dong, and Z-G. Ye; **16**(6), 1726–1733.

Simoen, E.–Mechanical stress of the electrical performance of polycrystalline-silicon resistors.–N. Nakabayashi, H. Ohyama, E. Simoen, M. Ikegami, C. Claeys, K. Kobayashi, M. Yoneoka, and K. Miyahara; **16**(9), 2579–2582.

Singh, R.S.–Metal–oxide films with magnetically-modulated nanoporous architectures.–Craig A. Grimes, R. Suresh Singh, Elizabeth C. Dickey, and Oomman K. Varghese; **16**(6), 1686–1693.

–Titanium oxide nanotube arrays prepared by anodic oxidation.–Dawei Gong, Craig A. Grimes, Oomman K. Varghese, R.S. Singh, Wenchong Hu, Zhi Chen, and Elizabeth C. Dickey; **16**(12), 3331–3334(L).

Sinha, Arvind–Patterning of copper particles on polymeric surface.–Arvind Sinha, Swapan Kumar Das, V. Rao, and P. Ramachandrarao; **16**(5), 1354–1357.

Slamovich, Elliott B.–Processing effects on the composition and dielectric properties of hydrothermally derived $Ba_xSr_{(1-x)}TiO_3$ thin films.–Mark A. McCormick, Ryan K. Roeder, and Elliott B. Slamovich; **16**(4), 1200–1209.

Slivka, V.Yu.–Influence of compositional disorder on optical absorption processes in $Cu_6P(S_{1-x}Se_x)_5I$ crystals.–I.P. Studenyak, M. Kranjčec, Gy.Sh. Kovacs, I.D. Desnica-Franković, V.V. Panko, and V.Yu. Slivka; **16**(6), 1600–1608.

Smith, David J.–Grain boundary structure in Al–Mg and Al–Mg–Sc alloys after equal-channel angular pressing.–Keiichiro Oh-ishi, Zenji Horita, David J. Smith, and Terence G. Langdon; **16**(2), 583–589.

Sohn, Kee-Sun–Luminescence and decay behaviors of Tb-doped yttrium silicate.–Yoon Young Choi, Kee-Sun Sohn, Hee Dong Park, and Se Young Choi; **16**(3), 881–889.

Solovyov, V.F.–Nucleation and growth of $YBa_2Cu_3O_x$ on $SrTiO_3$ and CeO_2 by a BaF_2 postdeposition reaction process.–L. Wu, Y. Zhu, V.F. Solovyov, H.J. Wiesmann, A.R. Moodenbaugh, R.L. Sabatini, and M. Suenaga; **16**(10), 2869–2884.

Song, H.J.–Chemical-vapor-deposition growth and characterization of epitaxial 3C–SiC films on SOI substrates with thin silicon top layers.–C.K. Moon, H.J. Song, J.K. Kim, J.H. Park, S.J. Jang, J-B. Yoo, H-R. Park, and Byung-Teak Lee; **16**(1), 24–27(L).

Song, Jae Sung–Preparation of nanocrystalline nickel oxide–yttria-stabilized zirconia composite powder by solution combustion with ignition of glycine fuel.–Sun-Jae Kim, Wonhee Lee, Won-Jun Lee, Soon Dong Park, Jae Sung Song, and Eun Gu Lee; **16**(12), 3621–3627.

Song, Mei-Li–Formation rule for Al-based ternary quasi-crystals: Example of Al–Ni–Fe decagonal phase.–Jian-Bing Qiang, De-He Wang, Cui-Min Bao, Ying-Min Wang, Wei-Ping Xu, Mei-Li Song, and Chuang Dong; **16**(9), 2653–2660.

Song, Renbo–Growth, defects, and properties of $GdCa_4O(BO_3)_3$ and $Nd:GdCa_4O(BO_3)_3$ crystals.–Jiyang Wang, Xiaobo Hu, Xin Yin, Renbo Song, Jingqian Wei, Zongsu Shao, Yaogang Liu, Minhua Jiang, Yulian Tian, Jianhua Jiang, and Wanxia Huang; **16**(3), 790–796.

Souvignier, C.W.–Freeform fabrication of aluminum metal-matrix composites.–C.W. Souvignier, T.B. Sercombe, S.H. Huo, P. Calvert, and G.B. Schaffer; **16**(9), 2613–2618.

Specht, E.D.–Growth and characterization of conductive $SrRuO_3$ and $LaNiO_3$ multilayers on textured Ni tapes for high-J_c $YBa_2Cu_3O_{7-\delta}$ coated conductors.–T. Aytug, B.W. Kang, C. Cantoni, E.D. Specht, M. Paranthaman, A. Goyal, D.K. Christen, D.T. Verebelyi, J.Z. Wu, R.E. Ericson, C.L. Thomas, C-Y.Yang, and S.E. Babcock; **16**(9), 2661–2669.

Speghini, Adolfo–Fractal aggregates of lanthanide-doped Y_2O_3 nanoparticles obtained by propellant synthesis.–Stefano Polizzi, Giuliano Fagherazzi, Marino Battagliarin, Marco Bettinelli, Adolfo Speghini; **16**(1), 146–154.

Spence, J.C.H.–Microstructure of $La_{1-x}Ca_xMnO_3$ studied by transmission electron microscopy.–Q. Chen, J. Tao, J.M. Zuo, and J.C.H. Spence; **16**(10), 2959–2965.

Spinella, C.–Formation and characterization of high-density silver nanoparticles embedded in silica thin films by "*in situ*" self-reduction.–G. Compagnini, M.E. Fragalà, L. D'Urso, C. Spinella, and O. Puglisi; **16**(10), 2934–2938.

Spirkova-Hradilova, J.–Erbium doping into lithium niobate and sapphire single crystal wafers.–P. Nekvindova, J. Spirkova-Hradilova, J. Schröfel, and V. Perina; **16**(2), 333–335(L).

Srivastava, A.K.–Microstructural characterization of rapidly solidified Al–Fe–Si, Al–V–Si, and Al–Fe–V–Si alloys.–A.K. Srivastava and S. Ranganathan; **16**(7), 2103–2117.

Srolovitz, D.J.–Combined out-of-plane and in-plane texture control in thin films using ion beam assisted deposition.–L. Dong, D.J. Srolovitz, G.S. Was, Q. Zhao, and A.D. Rollett; **16**(1), 210–216.

Stach, Eric–Phenomenological description of grain growth stagnation for nanocrystalline films and powders.–Rand Dannenberg, Eric Stach, and Joanna R. Groza; **16**(4), 1090–1095.

Stacy, A.M.–Epitaxial growth of skutterudite ($CoSb_3$) thin films on (001) InSb by pulsed laser deposition.–J.C. Caylor, M.S. Sander, A.M. Stacy, J.S. Harper, R. Gronsky, and T. Sands; **16**(9), 2467–2470(L).

Stals, L.–Fretting wear rate of sulphur deficient MoS_x coatings based on dissipated energy.–Xiaoling Zhang, W. Lauwerens, L. Stals, Jiawen He, and J-P. Celis; **16**(12), 3567–3574.

Stan, L.–High critical current density $YBa_2Cu_3O_{7-\delta}$ thick films using ion beam assisted deposition MgO bi-axially oriented template layers on nickel-based superalloy substrates.–J.R. Groves, P.N. Arendt, S.R. Foltyn, Q.X. Jia, T.G. Holesinger, H. Kung, E.J. Peterson, R.F. DePaula, P.C. Dowden, L. Stan, and L.A. Emmert; **16**(8), 2175–2178(L).

Stanimirovic, A.–Thermal conductivity and thermal diffusivity of selected oxide single crystals.–A. Stanimirovic, N.M. Balzaretti, A. Feldman, and J.E. Graebner; **16**(3), 678–682.

Steegen, A.–*In situ* transmission electron microscopy study of the silicidation process in Co thin films on patterned (001) Si substrates.–C. Ghica, L. Nistor, H. Bender, A. Steegen, A. Lauwers, K. Maex, and J. Van Landuyt; **16**(3), 701–708.

Stolk, D.–Synthesis and processing of nanocrystalline Ag–Fe–Ni for low thermal expansion–high conductivity thermal management applications.–J. Stolk, M. Gross, D. Stolk, and A. Manthiram; **16**(2), 340–343(L).

Stolk, J.–Synthesis and processing of nanocrystalline Ag–Fe–Ni for low thermal expansion–high conductivity thermal management applications.–J. Stolk, M. Gross, D. Stolk, and A. Manthiram; **16**(2), 340–343(L).

Stoner, B.R.–Nucleation and growth of silicon nitride nanoneedles using microwave plasma heating.–H. Cui and B.R. Stoner; **16**(11), 3111–3115.

Streiffer, S.K.–Transmission electron microscopy study of (103)-oriented epitaxial $SrBi_2Nb_2O_9$ films grown on (111) $SrTiO_3$ and (111) $SrRuO_3$/(111) $SrTiO_3$.–M.A. Zurbuchen, J. Lettieri, Y. Jia, D.G. Schlom, S.K. Streiffer, and M.E. Hawley; **16**(2), 489–502.

Studenyak, I.P.–Influence of compositional disorder on optical absorption processes in $Cu_6P(S_{1-x}Se_x)_5I$ crystals.–I.P. Studenyak, M. Kranjčec, Gy.Sh. Kovacs, I.D. Desnica-Franković, V.V. Panko, and V.Yu. Slivka; **16**(6), 1600–1608.

Stuerga, D.–Flash synthesis of zirconia nanoparticles by microwave forced hydrolysis.–K. Bellon, D. Chaumont, and D. Stuerga; **16**(9), 2619–2622.

Su, W.H.–Effect of pressure on the structure of Fe–N alloys formed by solid-state reaction.–B. Yao, L. Liu, S.E. Liu, X. Hu, W.H. Su; **16**(9), 2583–2590.

Su, Wenhui–Valence variations in titanium-based perovskite oxides by high-pressure and high-temperature method.–Liping Li, Guangshe Li, Jipeng Miao, Wenhui Su, and Hiroshi Inomata; **16**(2), 417–424.

Suárez, Donají Y.–Relation between tolerance factor and T_c in Aurivillius compounds.–Donají Y. Suárez, Ian M. Reaney, and William E. Lee; **16**(11), 3139–3149.

Subkanna, G.N.–Translucent yttrium aluminum garnet: Microwave-assisted route to synthesis and processing.–M. Panneerselvam, G.N. Subanna, and K.J. Rao; **16**(10), 2773–2776(L).

Suchanek, Wojciech L.–Mechanochemical-hydrothermal preparation of crystalline hydroxyapatite powders at room temperature.–Pavel Shuk, Wojciech L. Suchanek, Tian Hao, Eric Gulliver, Richard E. Riman, Mamoru Senna, Kevor S. TenHuisen, and Victor F. Janas; **16**(5), 1231–1234(L).

Suenaga, M.–Nucleation and growth of $YBa_2Cu_3O_x$ on $SrTiO_3$ and CeO_2 by a BaF_2 postdeposition reaction process.–L. Wu, Y. Zhu, V.F. Solovyov, H.J. Wiesmann, A.R. Moodenbaugh, R.L. Sabatini, and M. Suenaga; **16**(10), 2869–2884.

Sugano, T.–Chemical reaction at the interface between $(Hg_{0.9}Re_{0.1})Ba_2CaCu_2O_y$ thin film and $SrTiO_3$ substrate.–Xiao-Jing Wu, N. Inoue, T. Sugano, T. Morishita, and K. Tanabe; **16**(1), 256–260.

Sugimura, Yuki–Fabrication and characterization of microscale sandwich beams.–Francisco Arias, Paul J.A. Kenis, Bing Xu, Tao Deng, Olivier J.A. Schueller, George M. Whitesides, Yuki Sugimura, and Anthony G. Evans; **16**(2), 597–605.

Suhir, E.–Thermal stress in a polymer-coated optical glass fiber with a low-modulus coating at the ends.–E. Suhir; **16**(10), 2996–3004.

Sullivan, John J.–Metalorganic chemical vapor deposition of titanium oxide for microelectronics applications.–Kanchana Vydianathan, Guillermo Nuesca, Gregory Peterson, Eric T. Eisenbraun, Alain E. Kaloyeros, John J. Sullivan, and Bin Han; **16**(6), 1838–1849.

Sun, C.–Dependence of structural, electrical, and optical properties of ZnO:Al films on substrate temperature.–M. Chen, Z.L. Pei, X. Wang, C. Sun, and L.S. Wen; **16**(7), 2118–2123.

Sun, Jianing–Effect of material properties on integration damage in organosilicate glass films.–E. Todd Ryan, Jeremy Martin, Kurt Junker, Jeff Wetzel, David W. Gidley, and Jianing Sun; **16**(12), 3335–3338(L).

Sun, L.F.–Synthesis of α–SiO_2 nanowires using Au nanoparticle catalysts on a silicon substrate.–Z.Q. Liu, S.S. Xie, L.F. Sun, D.S. Tang, W.Y. Zhou, C.Y. Wang, W. Liu, Y.B. Li, X.P. Zou, and G. Wang; **16**(3), 683–686.

Sun, Liling–Enhanced crystallization and phase transformation of amorphous silicon nitride under high pressure.–Ya-Li Li, Yong Liang, Fen Zheng, Xian-Feng Ma, Suo-Jing Cui, and Liling Sun; **16**(1), 67–75.

Sun, X.K.–Effects of preparation processes on structure and magnetic properties of $Nd_2Fe_{14}B$/α–Fe-type nanocomposite magnets.–Baozhi Cui, X.K. Sun, L.Y. Xiong, Wei Liu, Zhi-dong Zhang, Zhi-qing Yang, Ai-min Wang, and Jiang-ning Deng; **16**(3), 709–715.

Sun, Y.–Epitaxial stabilization of orthorhombic cuprous oxide films on MgO(110).–Paul R. Markworth, R.P.H. Chang, Y. Sun, G.K. Wong, and J.B. Ketterson; **16**(4), 914–921.

Sun, Yangyang–Preparation and characterization of nanocrystalline PbSe in poly(acrylic acid-*co*-styrene).–Yangyang Sun, Xuefeng Qian, Jie Yin, Junchao Huang, Xiaodong Ma, and Zikang Zhu; **16**(10), 2922–2927.

Sun, Zhi-Gang–Magnetic properties, domain structure, and microstructure of anisotropic $SmCo_{6.5}Zr_{0.5}$ ribbons with C addition.–A-Ru Yan, Zhi-Gang Sun, Wen-Yong Zhang, Hong-Wei Zhang, and Bao-Gen Shen; **16**(3), 629–632(L).

Sun, Zu Qing–Site preference of alloying elements in Fe_3Al-based alloys.–Xiao Dong Ni, Nan Xian Chen, Jiang Shen, Zu Qing Sun, and Wang Yue Yang; **16**(2), 344–351.

Sundararajan, Sriram–Development of a continuous microscratch technique in an atomic force microscope and its application to study scratch resistance of ultrathin hard amorphous carbon coatings.–Sriram Sundararajan and Bharat Bhushan; **16**(2), 437–445.

Sunderland, N.–Biomimetic model of a sponge-spicular optical fiber—mechanical properties and structure.–M. Sarikaya, H. Fong, N. Sunderland, B.D. Flinn, G. Mayer, A. Mescher, and E. Gaino; **16**(5), 1420–1428.

Sundgren, Jan-Eric–Thermal stability of carbon nitride thin films.–Niklas Hellgren, Nian Lin, Esteban Broitman, Virginie Serin, Stefano E. Grillo, Ray Twesten, Ivan Petrov, Christian Colliex, Lars Hultman, and Jan-Eric Sundgren; **16**(11), 3188–3201.

Sung, Yun-Mo–Nonisothermal phase formation kinetics in sol-gel-derived strontium bismuth tantalate.–Yun-Mo Sung; **16**(7), 2039–2044.

Suni, Ilkka–Effect of oxygen on the reactions in the Si/Ta/Cu metallization system.–Tomi Laurila, Kejun Zeng, Jorma K. Kivilahti, Jyriki Molarius, Ilkka Suni; **16**(10), 2939–2946.

Suo, Z.–Model for the robust mechanical behavior of nacre.–A.G. Evans, Z. Suo, R.Z. Wang, I.A. Aksay, M.Y. He, and J.W. Hutchinson; **16**(9), 2475–2484.

–Deformation mechanisms in nacre.–R.Z. Wang, Z. Suo, A.G. Evans, N. Yao, and I.A. Aksay; **16**(9), 2485–2493.

Suvorov, Danilo–Solid-state reaction mechanism for the formation of $Ba_{6-x}Ln_{8+2x/3}Ti_{18}O_{54}$ (Ln = Nd, Sm) solid solutions.–Anatolii G. Belous, Oleg V. Ovchar, Matjaz Valant, and Danilo Suvorov; **16**(8), 2350–2356.

Suzuki, Minoru–Effects of whisker content and dimensions on the *R*-curve behavior of an alumina matrix composite reinforced with silicon carbide whiskers.–Takashi Akatsu, Minoru Suzuki, Yasuhiro Tanabe, and Eiichi Yasuda; **16**(7), 1919–1927.

Suzuki, Tomoo–Site preference determination in intermetallic compounds by thermal conductivity measurement.–Yoshihiro Terada, Kenji Ohkubo, Tetsuo Mohri, and Tomoo Suzuki; **16**(8), 2314–2320.

Suzuki, Yoshikazu–High-strength porous silicon nitride fabricated by the sinter-forging technique.–Naoki Kondo, Yoshikazu Suzuki, and Tatsuki Ohji; **16**(1), 32–34(L).

–Improved creep resistance in anisotropic silicon nitride.–Naoki Kondo, Yoshikazu Suzuki, Manuel E. Brito, and Tatsuki Ohji; **16**(8), 2182–2185(L).

Sviridov, D.V.–Electrolyte electroreflectance study of TiO_2 films modified with metal nanoparticles.–A.I. Kulak, A.I. Kokorin, and D.V. Sviridov; **16**(8), 2357–2361.

Swadener, J.G.–Measurement of residual stress by load and depth sensing indentation with spherical indenters.–J.G. Swadener, B. Taljat, and G.M. Pharr; **16**(7), 2091–2102.

Swain, M.V.–Mechanical deformation in silicon by micro-indentation.–J.E. Bradby, J.S. Williams, J. Wong-Leung, M.V. Swain, and P. Munroe; **16**(5), 1500–1507.

Sypeck, D.J.–Multifunctional microtruss laminates: Textile synthesis and properties.–D.J. Sypeck and H.N.G. Wadley; **16**(3), 890–897.

–Synthesis of open-cell metal foams by templated directed vapor deposition.–Douglas T. Queheillalt, Derek D. Hass, David J. Sypeck, and Haydn N.G. Wadley; **16**(4), 1028–1036.

T

Takada, Jun–Low-temperature growth of *c*-axis-oriented Y-type hexagonal ferrite thin films by the polymeric precursor method.–Tatsuo Fujii, Aiko Harano, Makoto Nakanishi, and Jun Takada; **16**(9), 2471–2474(L).

Takagi, Yoshiki–*In situ* analysis of gaseous species for chemical vapor deposition diamond synthesis and the possible reaction model.–Mayu Uede and Yoshiki Takagi; **16**(11), 3069–3072.

Takayama, Kazuo–Misting-free diamond surface created by sheet electron beam irradiation.–Kazuya Oguri, Nobuhiro Iwataka, Akira Tonegawa, Yoichi Hirose, Kazuo Takayama, and Yoshitake Nishi; **16**(2), 553–557.

–High fracture resistance of carbon fiber treated by electron beam irradiation.–Yoshitake Nishi, Takashi Toriyama, Kazuya Oguri, Akira Tonegawa, Kazuo Takayama; **16**(6), 1632–1635.

Takeda, Satoshi–Modification of sol–gel-derived amorphous Al_2O_3 thin films by F_2 excimer laser irradiation at ambient temperature.–Satoshi Takeda, Yoshiaki Ikuta, Masahiro Hirano, and Hideo Hosono; **16**(4), 1003–1009.

Taljat, B.–Measurement of residual stress by load and depth sensing indentation with spherical indenters.–J.G. Swadener, B. Taljat, and G.M. Pharr; **16**(7), 2091–2102.

Tam, K.C.–Two-dimensional simulation of mass transport in polymer removal from a powder injection molding compact by thermal debinding.–Ying Shengjie, Y.C. Lam, S.C.M. Yu, and K.C. Tam; **16**(8), 2436–2451.

Tampieri, A.–Rheological characteristics of slurry controlling the microstructure and the compressive strength behavior of biomimetic hydroxyapatite.–S. Guicciardi, C. Galassi, E. Landi, A. Tampieri, K. Satou, and G. Pezzotti; **16**(1), 163–170.

Tan, O.K.–$Pb(Zr_xTi_{1-x})O_3$ ceramics via reactive sintering of partially reacted mixture produced by a high-energy ball milling process.–L.B. Kong, J. Ma, T.S. Zhang, W. Zhu, O.K. Tan; **16**(6), 1636–1643.

Tanabe, K.–Chemical reaction at the interface between $(Hg_{0.9}Re_{0.1})$-$Ba_2CaCu_2O_y$ thin film and $SrTiO_3$ substrate.–Xiao-Jing Wu, N. Inoue, T. Sugano, T. Morishita, K. Tanabe; **16**(1), 256–260.

Tanabe, Yasuhiro–Effects of whisker content and dimensions on the *R*-curve behavior of an alumina matrix composite reinforced with silicon carbide whiskers.–Takashi Akatsu, Minoru Suzuki, Yasuhiro Tanabe, and Eiichi Yasuda; **16**(7), 1919–1927.

Tanabe, Yuji–Identification of the constitutive equation by the indentation technique using plural indenters with different apex angles.–Masatoshi Futakawa, Takashi Wakui, Yuji Tanabe, and Ikuo Ioka; **16**(8), 2283–2292.

Tanaka, K.–Relaxation of ultraviolet-radiation-induced structure and long-lasting phosphorescence in Eu^{2+}-doped strontium aluminosilicate glasses.–Jianrong Qiu, Y. Shimizugawa, K. Kojima, K. Tanaka, and K. Hirao; **16**(1), 88–92.

Tanaka, Kohichi–Simplified method for analyzing nanoindentation data and evaluating performance of nanoindentation instruments.–Takeshi Sawa and Kohichi Tanaka; **16**(11), 3084–3096.

Tanaka, Shinichiro–Characterization of NO_x sensor using doped In_2O_3.–Shinichiro Tanaka and Takao Esaka; **16**(5), 1389–1395.

Tanaka, Takaho–Atomic structure of YB_{56} studied by digital high-resolution electron microscopy and electron diffraction.–Takeo Oku, Jan-Olov Bovin, Iwami Higashi, Takaho Tanaka, and Yoshio Ishizawa; **16**(1), 101–107.

Tanaka, Yasuo–Spectroscopic study of a cryptomelane-type manganic acid exchanged by divalent transition-metal cations.–Masamichi Tsuji and Yasuo Tanaka; **16**(1), 108–114.

Tang, D.S.–Synthesis of α–SiO_2 nanowires using Au nanoparticle catalysts on a silicon substrate.–Z.Q. Liu, S.S. Xie, L.F. Sun, D.S. Tang, W.Y. Zhou, C.Y. Wang, W. Liu, Y.B. Li, X.P. Zou, and G. Wang; **16**(3), 683–686.

Tang, G.Y.–Effect of a magnetic field on phase transformation of steel.–W. Liu, D.R. Ou, H.H. Zhou, G.Y. Tang, and F. Wu; **16**(8), 2280–2282.

Tang, J.–Ferroelectric $SrBi_2Ta_2O_9$ single-crystal growth and characterization.–B. Sih, J. Tang, M. Dong, and Z-G. Ye; **16**(6), 1726–1733.

Tang, Jun–Low-temperature fabrication of pyroelectric $Ba_{0.8}Sr_{0.2}TiO_3$ thin films by a sol-gel process.–Jian-Gong Cheng, Jun Tang, Shao-Ling Guo, and Jun-Hao Chu; **16**(3), 778–783.

Tang, K.B.–Preparation and phase control of nanocrystalline silver indium sulfides via a hydrothermal route.–J.Q. Hu, B. Deng, K.B. Tang, C.R. Wang, and Y.T. Qian; **16**(12), 3411–3415.

Tang, Q.–Thermodynamic analysis of combustion synthesis of Al_2O_3–TiC–ZrO_2 nanoceramics.–Q. Dong, Q. Tang, W.C. Li, and D.Y. Wu; **16**(9), 2494–2498.

Tang, W.H.–Excellent buffer layer for growing high-quality Y–Ba–Cu–O thin films.–W.H. Tang, J. Gao, C.X. Liu, and Z.H. Mai; **16**(10), 2864–2868.

Tang, X.F.–High-temperature thermoelectric properties of *n*-type $Ba_yNi_xCo_{4-x}Sb_{12}$.–X.F. Tang, L.M. Zhang, R.Z. Yuan, L.D. Chen, T. Goto, T. Hirai, J.S. Dyck, W. Chen, and C. Uher; **16**(12), 3343–3346(L).

Tang, Xinfeng–Effects of Ce filling fraction and Fe content on the thermoelectric properties of Co-rich $Ce_xFe_xCo_{4-x}Sb_{12}$.–Xinfeng Tang, Lidong Chen, Takashi Goto, and Toshio Hirai; **16**(3), 837–843.

Tao, J.–Microstructure of $La_{1-x}Ca_xMnO_3$ studied by transmission electron microscopy.–Q. Chen, J. Tao, J.M. Zuo, and J.C.H. Spence; **16**(10), 2959–2965.

Tarka, M.–Single-domain $YBa_2Cu_3O_y$ thick films and fabrics prepared by an infiltration and growth process.–E. Sudhakar Reddy, J.G. Noudem, M. Tarka, and G.J. Schmitz; **16**(4), 955–966.

–Directional solidification and microstructural studies of the peritectic Y_2BaCuO_5 phase.–E. Sudhakar Reddy, J.G. Noudem, M. Tarka, and G.J. Schmitz; **16**(4), 1123–1134.

Tartaj, J.–$BaTiO_3$ formation by thermal decomposition of a (BaTi)-citrate polyester resin in air.–P. Durán, F. Capel, J. Tartaj, and C. Moure; **16**(1), 197–209.

Tay, B.Y.–Investigation of some phenomena occurring during continuous ink-jet printing of ceramics.–B.Y. Tay and M.J. Edirisinghe; **16**(2), 373–384.

Taylor, L.T.–Low-resistance films of polyimides with impregnated copper sulfide.–R.V.A. Rowe, M.H. Kunita, M.F. Porto, E.C. Muniz, A.F. Rubira, R.C. Nery, E. Radovanovic, L.T. Taylor, and N. Nazem; **16**(11), 3097–3106.

Taylor, M.D.–Synthesis and characterization of partially and fully stabilized zirconia fibers made from an inorganic precursor.–A. Hartridge, M.D. Taylor, and A.K. Bhattacharya; **16**(8), 2384–2390.

–Halide removal from BaM ($BaFe_{12}O_{19}$) and SrM ($SrFe_{12}O_{19}$) ferrite fibers via a steaming process.–R.C. Pullar, M.D. Taylor, and A.K. Bhattacharya; **16**(11), 3162–3169.

Teisen, J.–Solid-state foaming of titanium by superplastic expansion of argon-filled pores.–N.G. Davis, J. Teisen, C. Schuh, and D.C. Dunand; **16**(5), 1508–1519.

Tellkamp, V.L.–Grain growth behavior of a nanostructured 5083 Al–Mg alloy.–V.L. Tellkamp, S. Dallek, D. Cheng, and E.J. Lavernia; **16**(4), 938–944.

TenHuisen, Kevor S.–Mechanochemical-hydrothermal preparation of crystalline hydroxyapatite powders at room temperature.–Pavel Shuk, Wojciech L. Suchanek, Tian Hao, Eric Gulliver, Richard E. Riman, Mamoru Senna, Kevor S. TenHuisen, and Victor F. Janas; **16**(5), 1231–1234(L).

Terada, Miwako–Machinable calcium pyrophosphate glass-ceramics.–Toshihiro Kasuga, Miwako Terada, Masayuki Nogami, and Mitsuo Niinomi; **16**(3), 876–880.

Terada, Yoshihiro–Site preference determination in intermetallic compounds by thermal conductivity measurement.–Yoshihiro Terada, Kenji Ohkubo, Tetsuo Mohri, and Tomoo Suzuki; **16**(8), 2314–2320.

Terashima, K.–Crystallography and structural evolution of $LiNbO_3$ and $LiNb_{1-x}Ta_xO_3$ films on sapphire prepared by high-rate thermal plasma spray chemical vapor deposition.–D.V. Shtansky, S.A. Kulinich, K. Terashima, T. Yoshida, and Y. Ikuhara; **16**(8), 2271–2279.

Tessier, F.–Calorimetric determination of the enthalpy of formation of InN and comparison with AlN and GaN.–M.R. Ranade, F. Tessier, A. Navrotsky, and R. Marchand; **16**(10), 2824–2831.

Thomas, C.L.–Growth and characterization of conductive $SrRuO_3$ and $LaNiO_3$ multilayers on textured Ni tapes for high-J_c $YBa_2Cu_3O_{7-\delta}$ coated conductors.–T. Aytug, B.W. Kang, C. Cantoni, E.D. Specht, M. Paranthaman, A. Goyal, D.K. Christen, D.T. Verebelyi, J.Z. Wu, R.E. Ericson, C.L. Thomas, C-Y.Yang, and S.E. Babcock; **16**(9), 2661–2669.

Thompson, C.V.–Modeling of the effects of crystallographic orientation on electromigration-limited reliability of interconnects with bamboo grain structures.–W.R. Fayad, V.K. Andleigh, and C.V. Thompson; **16**(2), 413–416.

Tian, W.–Transmission electron microscopy study of $n = 1$–5 $Sr_{n+1}Ti_nO_{3n+1}$ epitaxial thin films.–W. Tian, X.Q. Pan, J.H. Haeni, and D.G. Schlom; **16**(7), 2013–2026.

Tian, Yulian–Growth, defects, and properties of $GdCa_4O(BO_3)_3$ and $Nd:GdCa_4O(BO_3)_3$ crystals.–Jiyang Wang, Xiaobo Hu, Xin Yin, Renbo Song, Jingqian Wei, Zongsu Shao, Yaogang Liu, Minhua Jiang, Yulian Tian, Jianhua Jiang, and Wanxia Huang; **16**(3), 790–796.

Tibbetts, Gary G.–Electrical conductivity of vapor-grown carbon fiber/thermoplastic composites.–Ioana C. Finegan and Gary G. Tibbetts; **16**(6), 1668–1674.

Tihonova, T.–Preparation, structure, and magnetic properties of cobalt nanoparticles in carbon fibers.–I. Bashmakov, V. Dorosinez, M. Lukashevich, A. Mazanik, T. Tihonova, T. Zabel, B. Wiedenhorst, and H. Micklitz; **16**(10), 2832–2835.

Ting, Chu-Chi–Influence of ligand groups in Ti precursors on phase transformation and microstructural evolution of TiO_2 thin films prepared by the wet chemical process.–Chu-Chi Ting and San-Yuan Chen; **16**(6), 1712–1719.

Tiwald, T.E.–Infrared optical properties of aged porous GaAs.–S. Zangooie, M. Schubert, T.E. Tiwald, and J.A. Woollam; **16**(5), 1241–1244(L).

Tolentino, H.C.N.–CsCl-modified Ga_2S_3–La_2S_3 glasses: Structural approach by x-ray absorption spectroscopy.–A.Y. Ramos, M. Grisolía Cardona, H.C.N. Tolentino, M.C.M. Alves, N. Watanabe, O.L. Alves, and L.C. Barbosa; **16**(5), 1349–1353.

Tomar, M.S.–Raman spectroscopic determination of phase evolutions in $LiAl_xCo_{1-x}O_2$ battery materials.–P.S. Dobal, R.S. Katiyar, M.S. Tomar, and A. Hidalgo; **16**(1), 1–4(L).

–Synthesis of $Zn_{1-x}Mg_xO$ and its structural characterization.–M.S. Tomar, R. Melgarejo, P.S. Dobal, and R.S. Katiyar; **16**(4), 903–906(L).

Tonchev, D.–Glass transformation in vitreous As_2Se_3 studied by conventional and temperature-modulated differential scanning calorimetry.–S.O. Kasap and D. Tonchev; **16**(8), 2399–2407.

Tonegawa, Akira–Misting-free diamond surface created by sheet electron beam irradiation.–Kazuya Oguri, Nobuhiro Iwataka, Akira Tonegawa, Yoichi Hirose, Kazuo Takayama, and Yoshitake Nishi; **16**(2), 553–557.

–High fracture resistance of carbon fiber treated by electron beam irradiation.–Yoshitake Nishi, Takashi Toriyama, Kazuya Oguri, Akira Tonegawa, and Kazuo Takayama; **16**(6), 1632–1635.

Tong, P.–Torsion and bending of micron-scaled structures.–A.C.M. Chong, F. Yang, D.C.C. Lam, and P. Tong; **16**(4), 1052–1058.

Tong, Yu–Purification of single-walled carbon nanotubes synthesized by the hydrogen arc-discharge method.–Pengxiang Hou, Chang Liu, Yu Tong, Shitao Xu, Min Liu, and Huiming Cheng; **16**(9), 2526–2529.

Toriyama, T.–Carbonization behavior of polyimide film containing iron complex in relation to magnetic properties.–Y. Kaburagi, T. Toriyama, A. Yoshida, H. Wakabayashi, Y. Hishiyama, and M. Inagaki; **16**(2), 352–365.

Toriyama, Takashi–High fracture resistance of carbon fiber treated by electron beam irradiation.–Yoshitake Nishi, Takashi Toriyama, Kazuya Oguri, Akira Tonegawa, and Kazuo Takayama; **16**(6), 1632–1635.

Torquato, S.–Designing composite microstructures with targeted properties.–S. Hyun and S. Torquato; **16**(1), 280–285.

Torres-García, E.–Thermal and structural characterization of the $ZrO_{2-x}(OH)_{2x}$ to ZrO_2 transition.–E. Torres-García, A. Peláiz-Barranco, C. Vázquez-Ramos, and G.A. Fuentes; **16**(8), 2209–2212.

Tortorelli, P.F.–Templated growth of a complex nitride island dispersion through an internal nitridation reaction.–M.P. Brady, D.T. Hoelzer, E.A. Payzant, P.F. Tortorelli, J.A. Horton, I.M. Anderson, L.R. Walker, and S.K. Wrobel; **16**(10), 2784–2787(L).

Traverse, Agnès–Characterization of bond formation in SiC and Si_3N_4 implanted with Ti, Fe, and Co.–Didier Zanghi, Agnès Traverse, Sébastien Gautrot, and Odile Kaïtasov; **16**(2), 512–523.

Trolier-McKinstry, Susan–Dependence of dielectric and piezoelectric properties on film thickness for highly {100}-oriented lead magnesium niobate–lead titanate (70/30) thin films.–Jeong Hwan Park and Susan Trolier-McKinstry; **16**(1), 268–275.

Tsai, A.P.–Single-crystal growth of the Al–Cu–Fe icosahedral quasicrystal from the ternary melt.–J.Q. Guo and A.P. Tsai; **16**(11), 3038–3041(L).

Tsai, Dah-Shyang–Ordered structure formation in the flux-grown $Ba(Mg_{1/3}Ta_{2/3})O_3$ single crystals.–Yu-Chang Lee, Chen-Chia Chou, and Dah-Shyang Tsai; **16**(6), 1593–1599.

Tsuji, Masamichi–Spectroscopic study of a cryptomelane-type manganic acid exchanged by divalent transition-metal cations.–Masamichi Tsuji and Yasuo Tanaka; **16**(1), 108–114.

Tsukrov, I.–Scanning probe microscopy generated out-of-plane deformation maps exhibiting heterogeneous nanoscale deformation resulting from thermal cycling of Cu–polyimide damascene interconnects.–Todd S. Gross, Nazri bin Kamsah, and I. Tsukrov; **16**(12), 3560–3566.

Tucker, Dennis S.–Explanation of the effects of gravity on crystallization of ZrF_2–BaF_2–LaF_3–AlF_3–NaF glass.–Dennis S. Tucker and Edwin C. Ethridge; **16**(11), 3027–3029(L).

Tunaboylu, Bahadir–Precipitate splitting in $Pb_{0.91}La_{0.09}Zr_{0.65}Ti_{0.35}O_3$ films.–Bahadir Tunaboylu, Ken Ring, Sadik C. Esener, Cengiz Ozkan, and Ali Ata; **16**(10), 2763–2766(L).

Twesten, Ray–Thermal stability of carbon nitride thin films.–Niklas Hellgren, Nian Lin, Esteban Broitman, Virginie Serin, Stefano E. Grillo, Ray Twesten, Ivan Petrov, Christian Colliex, Lars Hultman, and Jan-Eric Sundgren; **16**(11), 3188–3201.

Twigg, Peter C.–Influence of $CaO–SiO_2$ ratio on the chemistry of intergranular films in liquid-phase sintered alumina and implications for rate of erosive wear.–Rik Brydson, Peter C. Twigg, Fiona Loughran, and Frank L. Riley; **16**(3), 652–665.

U

Uchikoshi, Tetsuo–Dense, bubble-free ceramic deposits from aqueous suspensions by electrophoretic deposition.–Tetsuo Uchikoshi, Kiyoshi Ozawa, Benjamin D. Hatton, and Yoshio Sakka; **16**(2), 321–324(L).

Uede, Mayu–*In situ* analysis of gaseous species for chemical vapor deposition diamond synthesis and the possible reaction model.–Mayu Uede and Yoshiki Takagi; **16**(11), 3069–3072.

Uher, C.–High-temperature thermoelectric properties of *n*-type $Ba_yNi_xCo_{4-x}Sb_{12}$.–X.F. Tang, L.M. Zhang, R.Z. Yuan, L.D. Chen, T. Goto, T. Hirai, J.S. Dyck, W. Chen, and C. Uher; **16**(12), 3343–3346(L).

Umeda, T.–Role of the primary phase particles during the peritectic solidification of Y-123 superconducting oxides.–M. Kambara, M. Yoshizumi, T. Umeda, K. Miyake, K. Murata, T. Izumi, and Y. Shiohara; **16**(8), 2229–2238.

Urban, K.–Microstructure and misfit relaxation in $SrTiO_3/SrRuO_3$ bilayer films on $LaAlO_3(100)$ substrates.–J.S. Wu, C.L. Jia, K. Urban, J.H. Hao, and X.X. Xi; **16**(12), 3443–3450.

Urenski, P.–Polarization reversal and domain anisotropy in flux-grown $KTiOPO_4$ and isomorphic crystals.–P. Urenski, G. Rosenman, and M. Molotskii; **16**(5), 1493–1499.

Ushakov, S.V.–Thermochemistry of rare-earth orthophosphates.–S.V. Ushakov, K.B. Helean, A. Navrotsky, and L.A. Boatner; **16**(9), 2623–2633.

V

Valant, Matjaz–Solid-state reaction mechanism for the formation of $Ba_{6-x}Ln_{8+2x/3}Ti_{18}O_{54}$ (Ln = Nd, Sm) solid solutions.–Anatolii G. Belous, Oleg V. Ovchar, Matjaz Valant, and Danilo Suvorov; **16**(8), 2350–2356.

Vallet-Regí, M.–Textural properties of $SiO_2 \cdot CaO \cdot P_2O_5$ glasses prepared by the sol-gel method.–F. Balas, D. Arcos, J. Pérez-Pariente, and M. Vallet-Regí; **16**(5), 1345–1348.

Van Der Biest, O.–Transformation behavior of yttria stabilized tetragonal zirconia polycrystal–TiB_2 composites.–B. Basu, J. Vleugels, and O. Van Der Biest; **16**(7), 2158–2169.

Van der Giessen, E.–Delamination of a strong film from a ductile substrate during indentation unloading.–A. Abdul-Baqi and E. Van der Giessen; **16**(5), 1396–1407.

Van Duzer, Theodore–High-T_c superconducting NbN films with low particulate density grown at 25 °C using pulsed laser deposition.–Anupama B. Kaul, Timothy D. Sands, and Theodore Van Duzer; **16**(5), 1223–1226(L).

Van Houtte, P.–Finite element modeling of microscale thermal residual stresses in Al interconnects.–A. Saerens, P. Van Houtte, and S.R. Kalidindi; **16**(4), 1112–1122.

–Effect of *in situ* boron doping on properties of silicon germanium films deposited by chemical vapor deposition at 400 °C.–Sherif Sedky, Ann Witvrouw, Annelies Saerens, Paul Van Houtte, Jef Poortmans, and Kris Baert; **16**(9), 2607–2612.

Van Landuyt, J.–*In situ* transmission electron microscopy study of the silicidation process in Co thin films on patterned (001) Si substrates.–C. Ghica, L. Nistor, H. Bender, A. Steegen, A. Lauwers, K. Maex, and J. Van Landuyt; **16**(3), 701–708.

VanLandingham, Mark R.–Direct measurement of plowing friction and wear of a polymer thin film using the atomic force microscope.–Binyang Du, Mark R. VanLandingham, Qingling Zhang, and Tianbai He; **16**(5), 1487–1492.

Varghese, Oomman K.–Metal–oxide films with magnetically-modulated nanoporous architectures.–Craig A. Grimes, R. Suresh Singh, Elizabeth C. Dickey, and Oomman K. Varghese; **16**(6), 1686–1693.

–Titanium oxide nanotube arrays prepared by anodic oxidation.–Dawei Gong, Craig A. Grimes, Oomman K. Varghese, R.S. Singh, Wenchong Hu, Zhi Chen, and Elizabeth C. Dickey; **16**(12), 3331–3334(L).

Varma, Arvind–Mechanistic studies in combustion synthesis of NiAl–TiB_2 composites: Effects of gravity.–Cheryl Lau, Alexander Mukasyan, Aleksey Pelekh, and Arvind Varma; **16**(6), 1614–1625.

Varniere, F.–^{18}O study of the oxidation of reactively sputtered $Ti_{1-x}Al_xN$ barrier.–M.C. Hugon, F. Varniere, F. Letendu, B. Agius, I. Vickridge, and A.I. Kingon; **16**(9), 2591–2599.

Vázquez-Ramos, C.–Thermal and structural characterization of the $ZrO_{2-x}(OH)_{2x}$ to ZrO_2 transition.–E. Torres-García, A. Peláiz-Barranco, C. Vázquez-Ramos, and G.A. Fuentes; **16**(8), 2209–2212.

Véchembre, J.B.–Sintering of screen-printed platinum thick films for electrode applications.–J.B. Véchembre and G.R. Fox; **16**(4), 922–931.

Veen, A.T. van–Quantification and effects of molecular oxygen and water in zinc phthalocyanine layers.–H.R. Kerp, K.T. Westerduin, A.T. van Veen, and E.E. van Faassen; **16**(2), 503–511.

Verebelyi, D.T.–Growth and characterization of conductive $SrRuO_3$ and $LaNiO_3$ multilayers on textured Ni tapes for high-J_c $YBa_2Cu_3O_{7-\delta}$ coated conductors.–T. Aytug, B.W. Kang, C. Cantoni, E.D. Specht, M. Paranthaman, A. Goyal, D.K. Christen, D.T. Verebelyi, J.Z. Wu, R.E. Ericson, C.L. Thomas, C-Y.Yang, and S.E. Babcock; **16**(9), 2661–2669.

Vickridge, I.–^{18}O study of the oxidation of reactively sputtered $Ti_{1-x}Al_xN$ barrier.–M.C. Hugon, F. Varniere, F. Letendu, B. Agius, I. Vickridge, and A.I. Kingon; **16**(9), 2591–2599.

–Oxygen transport during annealing of $Pb(Zr,Ti)O_3$ thin films in O_2 gas and its effect on their conductivity.–F. Ayguavives, B. Agius, B. Ea-Kim, and I. Vickridge; **16**(10), 3005–3008.

Vijaymohanan, K.–Piezoresistivity of conducting polyaniline/$BaTiO_3$ composites.–R.C. Patil, S. Radhakrishnan, Sushama Pethkar, and K. Vijaymohanan; **16**(7), 1982–1988.

Vivien, D.–Phase transition, growth, and optical properties of $Nd_xLa_{1-x}Sc_3(BO_3)_4$ crystals.–Yunkui Li, G. Aga, A. Kahn-Harari, and D. Vivien; **16**(1), 38–44.

Vlassak, Joost J.–Numerical study on the measurement of thin film mechanical properties by means of nanoindentation.–Xi Chen and Joost J. Vlassak; **16**(10), 2974–2982.

Vleugels, J.–Transformation behavior of yttria stabilized tetragonal zirconia polycrystal–TiB_2 composites.–B. Basu, J. Vleugels, and O. Van Der Biest; **16**(7), 2158–2169.

Volinsky, A.A.–Substrate effects on indentation plastic zone development in thin soft films.–D.E. Kramer, A.A. Volinsky, N.R. Moody, and W.W. Gerberich; **16**(11), 3150–3157.

Volkmann, Th.–Metastable solidification of NdFeB alloys by drop-tube processing.–Jianrong Gao, Th. Volkmann, and D.M. Herlach; **16**(9), 2562–2567.

Vorobiev, Y.V.–Structure of heat-treated sol-gel SiO_2 glasses containing silver.–M.G. Garníca-Romo, J. González-Hernández, M.A. Hernández-Landaverde, Y.V. Vorobiev, F. Ruiz, and J.R. Martínez; **16**(7), 2007–2012.

Vydianathan, Kanchana–Metalorganic chemical vapor deposition of titanium oxide for microelectronics applications.–Kanchana Vydianathan, Guillermo Nuesca, Gregory Peterson, Eric T. Eisenbraun, Alain E. Kaloyeros, John J. Sullivan, and Bin Han; **16**(6), 1838–1849.

Vysochanskii, Yu.M.–Photovoltaic effect of $Sn_2P_2S_6$ ferroelectric crystal and ceramics.–Y.W. Cho, S.K. Choi, and Yu.M. Vysochanskii; **16**(11), 3317–3322.

W

Wada, K.–Synthesis of coaxial nanotubes: Titanium oxide sheathed with silicon oxide.–Ming Zhang, Y. Bando, and K. Wada; **16**(5), 1408–1412.

Wada, T.–Preparation of Cu(In,Ga)Se_2 thin films at low substrate temperatures.–S. Nishiwaki, T. Satoh, Y. Hashimoto, T. Negami, T. Wada; **16**(2), 394–399.

Wadley, H.N.G.–Multifunctional microtruss laminates: Textile synthesis and properties.–D.J. Sypeck and H.N.G. Wadley; **16**(3), 890–897.

–Synthesis of open-cell metal foams by templated directed vapor deposition.–Douglas T. Queheillalt, Derek D. Hass, David J. Sypeck, and Haydn N.G. Wadley; **16**(4), 1028–1036.

Wakabayashi, H.–Carbonization behavior of polyimide film containing iron complex in relation to magnetic properties.–Y. Kaburagi, T. Toriyama, A. Yoshida, H. Wakabayashi, Y. Hishiyama, and M. Inagaki; **16**(2), 352–365.

Wakai, F.–Topological transformation of grains in three-dimensional normal grain growth.–F. Wakai, Y. Shinoda, S. Ishihara, and A. Domínguez-Rodríguez; **16**(7), 2136–2142.

Wakui, Takashi–Identification of the constitutive equation by the indentation technique using plural indenters with different apex angles.–Masatoshi Futakawa, Takashi Wakui, Yuji Tanabe, and Ikuo Ioka; **16**(8), 2283–2292.

Walker, L.R.–Templated growth of a complex nitride island dispersion through an internal nitridation reaction.–M.P. Brady, D.T. Hoelzer, E.A. Payzant, P.F. Tortorelli, J.A. Horton, I.M. Anderson, L.R. Walker, and S.K. Wrobel; **16**(10), 2784–2787(L).

Wan, Julin–Consolidation and crystallization of Si_3N_4/SiC nanocomposites from a poly(urea–silazane) ceramic precursor.–Julin Wan, Matt J. Gasch, and Amiya K. Mukherjee; **16**(11), 3274–3286.

Wan, Shan–Modeling of electric field induced texture in lead zirconate titanate ceramics.–Shan Wan and Keith Bowman; **16**(8), 2306–2313.

Wang, A.M.–Effects of preparation processes on structure and magnetic properties of $Nd_2Fe_{14}B$/α–Fe-type nanocomposite magnets.–Bao-zhi Cui, X.K. Sun, L.Y. Xiong, Wei Liu, Zhi-dong Zhang, Zhi-qing Yang, Ai-min Wang, and Jiang-ning Deng; **16**(3), 709–715.

–Preparation of superfine Fe-base alloy by liquidus casting.–X.F. Pan, H.F. Zhang, A.M. Wang, B.Z. Ding, and Z.Q. Hu; **16**(12), 3459–3463.

Wang, C.R.–Preparation and phase control of nanocrystalline silver indium sulfides via a hydrothermal route.–J.Q. Hu, B. Deng, K.B. Tang, C.R. Wang, and Y.T. Qian; **16**(12), 3411–3415.

Wang, C.Y.–Synthesis of α–SiO_2 nanowires using Au nanoparticle catalysts on a silicon substrate.–Z.Q. Liu, S.S. Xie, L.F. Sun, D.S. Tang, W.Y. Zhou, C.Y. Wang, W. Liu, Y.B. Li, X.P. Zou, and G. Wang; **16**(3), 683–686.

Wang, Chang-Gong–Highly (111)-oriented and conformal iridium films by liquid source metalorganic chemical vapor deposition.–Jaydeb Goswami, Chang-Gong Wang, Prashant Majhi, Yong-Wook Shin, and Sandwip K. Dey; **16**(8), 2192–2195(L).

Wang, Chong Min–Improved tensile creep properties of yttrium- and lanthanum-doped alumina: a solid solution effect.–Junghyun Cho, Chong Min Wang, Helen M. Chan, J.M. Rickman, and Martin P. Harmer; **16**(2), 425–429.

Wang, D.Z.–Growth and characterization of aligned carbon nanotubes from patterned nickel nanodots and uniform thin films.–J.G. Wen, Z.P. Huang, D.Z. Wang, J.H. Chen, S.X. Yang, Z.F. Ren, J.H. Wang, L.E. Calvet, J. Chen, J.F. Klemic, and M.A. Reed; **16**(11), 3246–3253.

Wang, Dahai–On some discrepancies in the literature about the formation of icosahedral quasi-crystal in Al–Cu–Fe alloys.–Jianian Gui, Jianbo Wang, Renhui Wang, Dahai Wang, Jing Liu, and Fangyu Chen; **16**(4), 1037–1046.

Wang, De-He–Formation rule for Al-based ternary quasi-crystals: Example of Al–Ni–Fe decagonal phase.–Jian-Bing Qiang, De-He Wang, Cui-Min Bao, Ying-Min Wang, Wei-Ping Xu, Mei-Li Song, and Chuang Dong; **16**(9), 2653–2660.

Wang, G.–Synthesis of α–SiO_2 nanowires using Au nanoparticle catalysts on a silicon substrate.–Z.Q. Liu, S.S. Xie, L.F. Sun, D.S. Tang, W.Y. Zhou, C.Y. Wang, W. Liu, Y.B. Li, X.P. Zou, and G. Wang; **16**(3), 683–686.

Wang, G.H.–Microstructure studies of potassium hexatitanate whiskers.–G.L. Li, M. Liu, and G.H. Wang; **16**(12), 3614–3620.

Wang, H.–Mechanical properties of nanocrystalline and epitaxial TiN films on (100) silicon.–H. Wang, A. Sharma, A. Kvit, Q. Wei, X. Zhang, C.C. Koch, and J. Narayan; **16**(9), 2733–2738.

–Origins of stored enthalpy in cryomilled nanocrystalline Zn.–Xinghang Zhang, Haiyan Wang, Magdy Kassem, Jagdish Narayan, and Carl C. Koch; **16**(12), 3485–3495.

Wang, H.R.–Origin of the anomalous volume expansion in Al–Si alloys above liquidus.–W.M. Wang, X.F. Bian, H.R. Wang, Zhen Wang, L. Zhang, Z.G. Liu, and J-M. Liu; **16**(12), 3592–3598.

Wang, Hong–Structure and dielectric properties of pyrochlore–fluorite biphase ceramics in the Bi_2O_3–ZnO–Nb_2O_5 system.–Hong Wang and Xi Yao; **16**(1), 83–87.

Wang, J.–Structural and dielectric characterization of $Ba_4Nd_2Ti_{4+x}Ta_{6-x}O_{30-x/2}$ nonstoichiometric ceramics.–X.M. Chen, X.H. Zheng, and J. Wang; **16**(10), 2859–2863.

Wang, J.H.–Growth and characterization of aligned carbon nanotubes from patterned nickel nanodots and uniform thin films.–J.G. Wen, Z.P. Huang, D.Z. Wang, J.H. Chen, S.X. Yang, Z.F. Ren, J.H. Wang, L.E. Calvet, J. Chen, J.F. Klemic, M.A. Reed; **16**(11), 3246–3253.

Wang, J.Y.–Structure and the nonlinearity of lithium triborate studied by Raman and infrared reflectivity spectroscopy.–H.R. Xia, L.X. Li, H. Yu, S.M. Dong, J.Y. Wang, Q.M. Lu, C.Q. Ma, and X.N. Wang; **16**(12), 3464–3470.

Wang, Jianbo–On some discrepancies in the literature about the formation of icosahedral quasi-crystal in Al–Cu–Fe alloys.–Jianian Gui, Jianbo Wang, Renhui Wang, Dahai Wang, Jing Liu, and Fangyu Chen; **16**(4), 1037–1046.

Wang, Jiyang–Growth, defects, and properties of $GdCa_4O(BO_3)_3$ and Nd:$GdCa_4O(BO_3)_3$ crystals.–Jiyang Wang, Xiaobo Hu, Xin Yin, Renbo Song, Jingqian Wei, Zongsu Shao, Yaogang Liu, Minhua Jiang, Yulian Tian, Jianhua Jiang, and Wanxia Huang; **16**(3), 790–796.

Wang, Ke-Ming–Refractive index profile and attenuation measurement in $KTiOPO_4$ waveguide by megaelectronvolt He ions.–Ke-Ming Wang, Hiu Hu, Fei Lu, Feng Chen, Bo-Rong Shi, Yao-Gang Liu, Ding-Yu Shen, and Xie-Mei Wang; **16**(1), 276–279.

Wang, Li–Novel photoluminescence from hydrogenated amorphous carbon films prepared by using xylene source.–Jun Xu, Wei Li, Tianfu Ma, Zhifeng Li, Li Wang, and Kunji Chen; **16**(2), 325–328(L).

Wang, Liangbin–Synthesis of $Ba_2Ti_9O_{20}$ via ethylenediaminetetraacetic acid precursor.–Yebin Xu, Yanyan He, and Liangbin Wang; **16**(4), 1195–1199.

Wang, Li-Qiong–Chemical sensors based on dielectric response of functionalized mesoporous silica films.–Karel Domansky, Jun Liu, Li-Qiong Wang, Mark H. Engelhard, and Suresh Baskaran; **16**(10), 2810–2816.

Wang, Mingtai–Precipitation of multilayered core–shell TiO_2 composite nanoparticles onto polymer layers.–Mingtai Wang and Lide Zhang; **16**(3), 765–773.

Wang, Moo-Chin–Formation of intermetallic compounds at eutectic Sn–Zn–Al solder/Cu interface.–Shan-Pu Yu, Moo-Chin Wang, and Min-Hsiung Hon; **16**(1), 76–82.

Wang, Pei-Ling–Nonepitaxial heterogeneous nucleation of α-sialon in the Ca-doped system.–Ya-Wen Li, Pei-Ling Wang, Wei-Wu Chen, Jing-Wei Feng, Yi-Bing Cheng, and Dong-Sheng Yan; **16**(2), 578–582.

Wang, Pingchu–Twinning domain in $67Pb(Mg_{1/3}Nb_{2/3})O_3$–$33PbTiO_3$ ferroelectric complex perovskite crystal grown by the Bridgman method.–Donglin Li, Pingchu Wang, Xiaoming Pan, Haosu Luo, and Zhiwen Yin; **16**(5), 1252–1255(L).

Wang, R.Z.–Model for the robust mechanical behavior of nacre.–A.G. Evans, Z. Suo, R.Z. Wang, I.A. Aksay, M.Y. He, and J.W. Hutchinson; **16**(9), 2475–2484.

–Deformation mechanisms in nacre.–R.Z. Wang, Z. Suo, A.G. Evans, N. Yao, and I.A. Aksay; **16**(9), 2485–2493.

Wang, Renhui–On some discrepancies in the literature about the formation of icosahedral quasi-crystal in Al–Cu–Fe alloys.–Jianian Gui, Jianbo Wang, Renhui Wang, Dahai Wang, Jing Liu, and Fangyu Chen; **16**(4), 1037–1046.

Wang, S.W.–Formation of Al_2O_3 grains with different sizes and morphologies during the pulse electric current sintering process.–S.W. Wang, L.D. Chen, T. Hirai, and Jingkun Guo; **16**(12), 3514–3517.

Wang, W.H.–Formation and properties of $Zr_{48}Nb_8Fe_8Cu_{12}Be_{24}$ bulk metallic glass.–Yong Zhang, D.Q. Zhao, B.C. Wei, P. Wen, M.X. Pan, and W.H. Wang; **16**(6), 1675–1679.

Wang, W.K.–Effects of pressure on the solidification of Al–Mn alloy.–Duanwei He, M. He, C.S. Kiminami, F.X. Zhang, Y.F. Xu, W.K. Wang, and K.H. Kuo; **16**(4), 910–913(L).

Wang, W.L.–Chemical stresses induced by grain-boundary diffusion in thin films.–W.L. Wang, Y.T. Chou, and Sanboh Lee; **16**(7), 1967–1974.

Wang, W.M.–Origin of the anomalous volume expansion in Al–Si alloys above liquidus.–W.M. Wang, X.F. Bian, H.R. Wang, Zhen Wang, L. Zhang, Z.G. Liu, and J-M. Liu; **16**(12), 3592–3598.

Wang, Wendong–Synthesis and characterization of antimony oxide nanoparticles.–Zaoli Zhang, Lin Guo, and Wendong Wang; **16**(3), 803–805.

Wang, X.–Dependence of structural, electrical, and optical properties of ZnO:Al films on substrate temperature.–M. Chen, Z.L. Pei, X. Wang, C. Sun, and L.S. Wen; **16**(7), 2118–2123.

Wang, X.N.–Structure and the nonlinearity of lithium triborate studied by Raman and infrared reflectivity spectroscopy.–H.R. Xia, L.X. Li, H. Yu, S.M. Dong, J.Y. Wang, Q.M. Lu, C.Q. Ma, and X.N. Wang; **16**(12), 3464–3470.

Wang, Xibao–Corrosive wear of the Co–Cr–W alloy in liquid zinc.–Xibao Wang and Yong Liang; **16**(6), 1585–1592.

Wang, Xie-Mei–Refractive index profile and attenuation measurement in $KTiOPO_4$ waveguide by megaelectronvolt He ions.–Ke-Ming Wang, Hiu Hu, Fei Lu, Feng Chen, Bo-Rong Shi, Yao-Gang Liu, Ding-Yu Shen, and Xie-Mei Wang; **16**(1), 276–279.

Wang, Ying-Min–Formation rule for Al-based ternary quasi-crystals: Example of Al–Ni–Fe decagonal phase.–Jian-Bing Qiang, De-He Wang, Cui-Min Bao, Ying-Min Wang, Wei-Ping Xu, Mei-Li Song, and Chuang Dong; **16**(9), 2653–2660.

Wang, Yinhai–Synthesis of nano-AgI arrays and their optical properties.–Yinhai Wang, Jimei Mo, Weili Cai, Lianzeng Yao, and Lide Zhang; **16**(4), 990–992.

Wang, Yongquiang–Effect of ion implant dose on the mechanical properties of polyethersulfone films.–Manuel Luis B. Palacio, Yongquiang Wang, and William W. Gerberich; **16**(12), 3628–3635..

Wang, Zhen–Origin of the anomalous volume expansion in Al–Si alloys above liquidus.–W.M. Wang, X.F. Bian, H.R. Wang, Zhen Wang, L. Zhang, Z.G. Liu, and J-M. Liu; **16**(12), 3592–3598.

Was, G.S.–Combined out-of-plane and in-plane texture control in thin films using ion beam assisted deposition.–L. Dong, D.J. Srolovitz, G.S. Was, Q. Zhao, and A.D. Rollett; **16**(1), 210–216.

Waser, R.–Phase formation and crystal growth of Sr–Bi–Ta–O thin films grown by metalorganic chemical vapor deposition.–H. Bachhofer, H. von Philipsborn, W. Hartner, C. Dehm, B. Jobst, A. Kiendl, H. Schroeder, and R. Waser; **16**(10), 2966–2973.

Watanabe, N.–CsCl-modified Ga_2S_3–La_2S_3 glasses: Structural approach by x-ray absorption spectroscopy.–A.Y. Ramos, M. Grisolía Cardona, H.C.N. Tolentino, M.C.M. Alves, N. Watanabe, O.L. Alves, and L.C. Barbosa; **16**(5), 1349–1353.

Watanabe, Takayuki–Ferroelectric property of epitaxial $Bi_4Ti_3O_{12}$ films prepared by metalorganic chemical vapor deposition.–Takayuki Watanabe, Hiroshi Funakubo, and Keisuke Saito; **16**(1), 303–307.

Weaver, Mark L.–Ultrathin TiB_2 protective films.–Feng Huang, John A. Barnard, and Mark L. Weaver; **16**(4), 945–954.

Weertman, J.R.–Effect of process variables on the structure, residual stress, and hardness of sputtered nanocrystalline nickel films.–R. Mitra, R.A. Hoffman, A. Madan, and J.R. Weertman; **16**(4), 1010–1027.

–Effect of annealing on microstructure, residual stress, and hardness of Al–Ti multilayered films.–R. Mitra, A. Madan, R.A. Hoffman, W-A. Chiou, J.R. Weertman; **16**(7), 2064–2076.

Wegner, G.–Additive controlled crystallization of barium titanate powders and their application for thin-film ceramic production: Part I. Powder Synthesis.–B. Grohe, G. Miehe, and G. Wegner; **16**(7), 1901–1910.

–Additive controlled crystallization of barium titanate powders and their application for thin-film ceramic production: Part II. From nano-sized powders to ceramic thin films.–B. Grohe, G. Miehe, and G. Wegner; **16**(7), 1911–1915.

Wei, B.C.–Formation and properties of $Zr_{48}Nb_8Fe_8Cu_{12}Be_{24}$ bulk metallic glass.–Yong Zhang, D.Q. Zhao, B.C. Wei, P. Wen, M.X. Pan, and W.H. Wang; **16**(6), 1675–1679.

Wei, Bingqing–Aligned carbon nanotube growth under oxidative ambient.–Anyuan Cao, Xianfeng Zhang, Cailu Xu, Ji Liang, Dehai Wu, and Bingqing Wei; **16**(11), 3107–3110.

Wei, Jingqian–Growth, defects, and properties of $GdCa_4O(BO_3)_3$ and $Nd:GdCa_4O(BO_3)_3$ crystals.–Jiyang Wang, Xiaobo Hu, Xin Yin, Renbo Song, Jingqian Wei, Zongsu Shao, Yaogang Liu, Minhua Jiang, Yulian Tian, Jianhua Jiang, and Wanxia Huang; **16**(3), 790–796.

Wei, Q.–Mechanical properties of nanocrystalline and epitaxial TiN films on (100) silicon.–H. Wang, A. Sharma, A. Kvit, Q. Wei, X. Zhang, C.C. Koch, and J. Narayan; **16**(9), 2733–2738.

Wei, Yueguang–Adhesion of benzocyclobutene-passivated silicon in epoxy layered structures.–Robert J. Hohlfelder, Daniel A. Maidenberg, Reinhold H. Dauskardt, Yueguang Wei, and John W. Hutchinson; **16**(1), 243–255.

Weigelt, G.A.–Analysis of interdiffusion of Dy, Nd, and Pr in Mg.–Y. Xu, L.S. Chumbley, G.A. Weigelt, and F.C. Laabs; **16**(11), 3287–3292.

Weiner, B.R.–Study of the effects of low-energy electron bombardment during the chemical vapor deposition of diamond.–J.A. González, O.L. Figueroa, B.R. Weiner, and G. Morell; **16**(1), 293–295.

Wen, J.G.–Growth and characterization of aligned carbon nanotubes from patterned nickel nanodots and uniform thin films.–J.G. Wen, Z.P. Huang, D.Z. Wang, J.H. Chen, S.X. Yang, Z.F. Ren, J.H. Wang, L.E. Calvet, J. Chen, J.F. Klemic, and M.A. Reed; **16**(11), 3246–3253.

Wen, L.S.–Dependence of structural, electrical, and optical properties of ZnO:Al films on substrate temperature.–M. Chen, Z.L. Pei, X. Wang, C. Sun, L.S. Wen; **16**(7), 2118–2123.

Wen, Mao–Embedded-atom-method functions for the body-centered-cubic iron and hydrogen.–Mao Wen, Xue-Jun Xu, Seiji Fukuyama, and Kiyoshi Yokogawa; **16**(12), 3496–3502.

Wen, P.–Formation and properties of $Zr_{48}Nb_8Fe_8Cu_{12}Be_{24}$ bulk metallic glass.–Yong Zhang, D.Q. Zhao, B.C. Wei, P. Wen, M.X. Pan, and W.H. Wang; **16**(6), 1675–1679.

Wen, S.Z.–Size effect on the mechanical properties of microfabricated polysilicon thin films.–J.N. Ding, Y.G. Meng, and S.Z. Wen; **16**(8), 2223–2228.

Wen, Sihai–Rectifying and thermocouple junctions based on Portland cement.–Sihai Wen and D.D.L. Chung; **16**(7), 1989–1993.

Westerduin, K.T.–Quantification and effects of molecular oxygen and water in zinc phthalocyanine layers.–H.R. Kerp, K.T. Westerduin, A.T. van Veen, and E.E. van Faassen; **16**(2), 503–511.

Wetzel, Jeff–Effect of material properties on integration damage in organosilicate glass films.–E. Todd Ryan, Jeremy Martin, Kurt Junker, Jeff Wetzel, David W. Gidley, and Jianing Sun; **16**(12), 3335–3338(L).

White, C.W.–Nanocrystals in crystalline silicon: Void formation and hollow particles.–A. Meldrum, S. Honda, C.W. White, R.A. Zuhr, and L.A. Boatner; **16**(9), 2670–2679.

Whitesides, George M.–Fabrication and characterization of microscale sandwich beams.–Francisco Arias, Paul J.A. Kenis, Bing Xu, Tao Deng, Olivier J.A. Schueller, George M. Whitesides, Yuki Sugimura, and Anthony G. Evans; **16**(2), 597–605.

Whittenberger, J. Daniel–Creep and toughness of cryomilled NiAl containing Cr.–J. Daniel Whittenberger, Beverly Aikin, and Jon Salem; **16**(5), 1333–1344.

Wicaksana, Dwi–Effect of hydrogen on true leakage current characteristics of $(Pb,La)(Zr,Ti)O_3$ thin-film capacitors with Pt- or Ir-based top electrodes.–Soon-Gil Yoon, Dwi Wicaksana, Dong-Joo Kim, Seung-Hyun Kim, and A.I. Kingon; **16**(4), 1185–1189.

Wiedenhorst, B.–Preparation, structure, and magnetic properties of cobalt nanoparticles in carbon fibers.–I. Bashmakov, V. Dorosinez, M. Lukashevich, A. Mazanik, T. Tihonova, T. Zabel, B. Wiedenhorst, and H. Micklitz; **16**(10), 2832–2835.

Wiesmann, H.J.–Nucleation and growth of $YBa_2Cu_3O_x$ on $SrTiO_3$ and CeO_2 by a BaF_2 postdeposition reaction process.–L. Wu, Y. Zhu, V.F. Solovyov, H.J. Wiesmann, A.R. Moodenbaugh, R.L. Sabatini, and M. Suenaga; **16**(10), 2869–2884.

Wilding, M.C.–Enthalpies of formation of lanthanide oxyapatite phases.–A.S. Risbud, K.B. Helean, M.C. Wilding, P. Lu, and A. Navrotsky; **16**(10), 2780–2783(L).

Williams, J.S.–Mechanical deformation in silicon by microindentation.–J.E. Bradby, J.S. Williams, J. Wong-Leung, M.V. Swain, and P. Munroe; **16**(5), 1500–1507.

Williams, M.E.–Moving the pulsed heating technique beyond monolithic specimens: Experiments with coated wires.–D. Josell, D. Basak, J.L. McClure, U.R. Kattner, M.E. Williams, W.J. Boettinger, and M. Rappaz; **16**(8), 2421–2428.

Williford, R.E.–Mechanical and thermal properties of combustion-synthesized perovskites, $La_{1-x}Sr_xCr_{0.2}Fe_{0.8}O_3$.–Yeong-Shyung Chou, K. Kerstetter, L.R. Pederson, and R.E. Williford; **16**(12), 3545–3553.

Wilson, Jr., Otto C.–Microwave sintering of ZnO at ultra high heating rates.–Geng-fu Xu, Isabel K. Lloyd, Yuval Carmel, Tayo Olorunyolemi, Otto C. Wilson, Jr.; **16**(10), 2850–2858.

With, G. de–Minima in the strength of MnZn ferrites.–M.A.H. Donners, L.J.M.G. Dortmans, G. de With, and M.J.M. de Graaf; **16**(12), 3575–3582.

Witvrouw, Ann–Effect of *in situ* boron doping on properties of silicon germanium films deposited by chemical vapor deposition at 400 °C.–Sherif Sedky, Ann Witvrouw, Annelies Saerens, Paul Van Houtte, Jef Poortmans, and Kris Baert; **16**(9), 2607–2612.

Wolff, P.J.–Small correction required when applying the Hertzian contact model to instrumented indentation data.–J.L. Hay and P.J. Wolff; **16**(5), 1280–1286.

Wong, G.K.–Epitaxial stabilization of orthorhombic cuprous oxide films on MgO(110).–Paul R. Markworth, R.P.H. Chang, Y. Sun, G.K. Wong, and J.B. Ketterson; **16**(4), 914–921.

Wong, H.Y.–Relationship between the microstructure and nanoindentation hardness of thermally evaporated and magnetron-sputtered electrochromic tungsten oxide films.–C.W. Ong, H.Y. Wong, G.K.H. Pang, K.Z. Baba-Kishi, and C.L. Choy; **16**(6), 1541–1548.

Wong, K.H.–Novel route for the epitaxial growth of $(SrBa)Nb_2O_6$ thick films by the sol-gel method using a self-template layer.–A-D. Li, C.L. Mak, K.H. Wong, D. Wu, and Naiben Ming; **16**(11), 3179–3183.

Wong, Sun Fat–Investigation of optical waveguide formed in Er:Yb: phosphate glass by MeV He^+ implantation.–Zhuang Zhuo, Edwin Yue Bun Pun, Sun Fat Wong, and Ying Zhou; **16**(4), 1135–1137.

Wong-Leung, J.–Mechanical deformation in silicon by microindentation.–J.E. Bradby, J.S. Williams, J. Wong-Leung, M.V. Swain, and P. Munroe; **16**(5), 1500–1507.

–Defect formation due to the crystallization of deep amorphous volumes formed in silicon by mega electron volt (*MeV*) ion implantation.–A.C.Y. Liu, J.C. McCallum, and J. Wong-Leung; **16**(11), 3229–3237.

Woollam, J.A.–Infrared optical properties of aged porous GaAs.–S. Zangooie, M. Schubert, T.E. Tiwald, and J.A. Woollam; **16**(5), 1241–1244(L).

Woolman, J.–Synthesis of dense nanometric $MoSi_2$ through mechanical and field activation.–R. Orrù, J. Woolman, G. Cao, and Z.A. Munir; **16**(5), 1439–1448.

Wouters, D.J.–Growth of (111)-oriented $Pb(Zr,Ti)O_3$ layers on nanocrystalline RuO_2 electrodes using the sol-gel technique.–G.J. Norga, S. Jin, Laura Fè, D.J. Wouters, H. Bender, and H.E. Maes; **16**(3), 828–833.

–Chemical structure evolution and orientation selection in sol-gel-prepared ferroelectric $Pb(Zr,Ti)O_3$ thin films.–L. Fè, G.J. Norga, D.J. Wouters, H.E. Maes, and G. Maes; **16**(9), 2499–2504.

Wrobel, S.K.–Templated growth of a complex nitride island dispersion through an internal nitridation reaction.–M.P. Brady, D.T. Hoelzer, E.A. Payzant, P.F. Tortorelli, J.A. Horton, I.M. Anderson, L.R. Walker, and S.K. Wrobel; **16**(10), 2784–2787(L).

Wu, L.–Nucleation and growth of $YBa_2Cu_3O_x$ on $SrTiO_3$ and CeO_2 by a BaF_2 postdeposition reaction process.–L. Wu, Y. Zhu, V.F. Solovyov, H.J. Wiesmann, A.R. Moodenbaugh, R.L. Sabatini, and M. Suenaga; **16**(10), 2869–2884.

Wu, D.–Processing- and composition-dependent characteristics of chemical solution deposited $Bi_{4-x}La_xTi_3O_{12}$ thin films.–Di Wu, Aidong Li, Tao Zhu, Zhifeng Li, Zhiguo Liu, and Naiben Ming; **16**(5), 1325–1332.

–Novel route for the epitaxial growth of $(SrBa)Nb_2O_6$ thick films by the sol-gel method using a self-template layer.–A-D. Li, C.L. Mak, K.H. Wong, D. Wu, and Naiben Ming; **16**(11), 3179–3183.

–Impacts of postannealing ambient atmospheres on $Pt/SrBi_{2.2}Ta_2O_9/Pt$ capacitors.–Ai-Dong Li, Tao Yu, Hui-Qin Ling, Di Wu, Zhi-Guo Liu, and Nai-Ben Ming; **16**(12), 3526–3535.

Wu, D.Y.–Thermodynamic analysis of combustion synthesis of Al_2O_3–TiC–ZrO_2 nanoceramics.–Q. Dong, Q. Tang, W.C. Li, and D.Y. Wu; **16**(9), 2494–2498.

Wu, Dehai–Aligned carbon nanotube growth under oxidative ambient.–Anyuan Cao, Xianfeng Zhang, Cailu Xu, Ji Liang, Dehai Wu, and Bingqing Wei; **16**(11), 3107–3110.

Wu, F.–Effect of a magnetic field on phase transformation of steel.–W. Liu, D.R. Ou, H.H. Zhou, G.Y. Tang, F. Wu; **16**(8), 2280–2282.

Wu, H.D.–Dielectric properties of oxide structures by a laser-based direct-writing method.–D. Young, H.D. Wu, R.C.Y. Auyeung, R. Modi, J. Fitz-Gerald, A. Pique, D.B. Chrisey, P. Atanassova, and T. Kodas; **16**(6), 1720–1725.

–Direct writing of polymer thick film resistors using a novel laser transfer technique.–R. Modi, H.D. Wu, R.C.Y. Auyeung, C.M. Gilmore, and D.B. Chrisey; **16**(11), 3214–3222.

Wu, J.S.–Microstructure and misfit relaxation in $SrTiO_3/SrRuO_3$ bilayer films on $LaAlO_3(100)$ substrates.–J.S. Wu, C.L. Jia, K. Urban, J.H. Hao, and X.X. Xi; **16**(12), 3443–3450.

Wu, J.Z.–Growth and characterization of conductive $SrRuO_3$ and $LaNiO_3$ multilayers on textured Ni tapes for high-J_c $YBa_2Cu_3O_{7-\delta}$ coated conductors.–T. Aytug, B.W. Kang, C. Cantoni, E.D. Specht, M. Paranthaman, A. Goyal, D.K. Christen, D.T. Verebelyi, J.Z. Wu, R.E. Ericson, C.L. Thomas, C-Y.Yang, and S.E. Babcock; **16**(9), 2661–2669.

Wu, Jeffrey C.S.–Sol-gel-derived photosensitive TiO_2 and Cu/TiO_2 using homogeneous hydrolysis technique.–Jeffrey C.S. Wu and Chih-Yang Yeh; **16**(2), 615–620.

Wu, Kwen-Hua–Silicalite/poly(dimethylsiloxane) nanocomposite pervaporation membranes for acetic acid/water separation.–Shih-Yuan Lu, Hsiang-Yuan Huang, and Kwen-Hua Wu; **16**(11), 3053–3059.

Wu, Nae-Lih–Thermodynamic stability of tetragonal zirconia nanocrystallites.–Nae-Lih Wu, Ton-Fon Wu, and Irene A. Rusakova; **16**(3), 666–669.

Wu, Ton-Fon–Thermodynamic stability of tetragonal zirconia nanocrystallites.–Nae-Lih Wu, Ton-Fon Wu, and Irene A. Rusakova; **16**(3), 666–669.

Wu, W.T.–Metal/ceramic interface in an *in situ* synthesized Ti/TiC_P composite coating by laser processing.–R. Yu, S. Zhang, L.L. He, W.T. Wu, and H.Q. Ye; **16**(1), 9–12(L).

Wu, X.–Shear-activated indentation crack in GaAs single crystal.–Z.C. Li, L. Liu, L.L. He, Y.B. Xu, X. Wu; **16**(10), 2845–2849.

Wu, Xiao-Jing–Chemical reaction at the interface between $(Hg_{0.9}Re_{0.1})Ba_2CaCu_2O_y$ thin film and $SrTiO_3$ substrate.–Xiao-Jing Wu, N. Inoue, T. Sugano, T. Morishita, and K. Tanabe; **16**(1), 256–260.

Wu, Yong Jun–Structures and microwave dielectric properties of $Ba_{6-3x}(Nd,Bi_y)_{8+2x}Ti_{18}O_{54}$ ($x = \frac{2}{3}$) solid solution.–Yong Jun Wu and Xiang Ming Chen; **16**(6), 1734–1738.

Wu, Yue–Preparation and characterization of $CuInS_2$ nanorods and nanotubes from an elemental solvothermal reaction.–Yang Jiang, Yue Wu, Shengwen Yuan, Bo Xie, Shuyuan Zhang, and Yitai Qian; **16**(10), 2805–2809.

X

Xi, S.–Study of the mechanism for controlled crystallization of BaF_2 under two kinds of monolayers.–L. Lu, H. Cui, W. Li, H. Zhang, S. Xi; **16**(8), 2415–2420.

Xi, X.X.–Microstructure and misfit relaxation in $SrTiO_3/SrRuO_3$ bilayer films on $LaAlO_3(100)$ substrates.–J.S. Wu, C.L. Jia, K. Urban, J.H. Hao, X.X. Xi; **16**(12), 3443–3450.

Xia, H.R.–Structure and the nonlinearity of lithium triborate studied by Raman and infrared reflectivity spectroscopy.–H.R. Xia, L.X. Li, H. Yu, S.M. Dong, J.Y. Wang, Q.M. Lu, C.Q. Ma, and X.N. Wang; **16**(12), 3464–3470.

Xie, Bo–Preparation and characterization of $CuInS_2$ nanorods and nanotubes from an elemental solvothermal reaction.–Yang Jiang, Yue Wu, Shengwen Yuan, Bo Xie, Shuyuan Zhang, and Yitai Qian; **16**(10), 2805–2809.

Xie, Rong-Jun–Preferred orientation of beta-phase and its mechanisms in a fine-grained silicon-nitride-based ceramic.–Rong-Jun Xie, Mamoru Mitomo, Wonjoong Kim, Young-Wook Kim, and Guo-Dong Zhan; **16**(2), 590–596.

–Transmission electron microscopy observation in a liquid-phase-sintered SiC with oxynitride glass.–Guo-Dong Zhan, Mamoru Mitomo, Young-Wook Kim, Rong-Jun Xie, and Amiya K. Mukherjee; **16**(8), 2189–2191(L).

Xie, S.S.–Synthesis of α–SiO_2 nanowires using Au nanoparticle catalysts on a silicon substrate.–Z.Q. Liu, S.S. Xie, L.F. Sun, D.S. Tang, W.Y. Zhou, C.Y. Wang, W. Liu, Y.B. Li, X.P. Zou, and G. Wang; **16**(3), 683–686.

Xin, Y.–Microstructures of $La_{1-x}A_x(A = Ca \text{ or } Sr)MnO_{3-\delta}$ thin films by liquid-delivery metalorganic chemical vapor deposition.–Y. Xin, K. Han, N. Mateeva, H. Garmestani, P.N. Kalu, and K-H. Dahmen; **16**(11), 3073–3083.

Xiong, L.Y.–Effects of preparation processes on structure and magnetic properties of $Nd_2Fe_{14}B/\alpha$–Fe-type nanocomposite magnets.–Bao-zhi Cui, X.K. Sun, L.Y. Xiong, Wei Liu, Zhi-dong Zhang, Zhi-qing Yang, Ai-min Wang, and Jiang-ning Deng; **16**(3), 709–715.

Xu, Bin–Electron microscopy of high-temperature and high-pressure as-grown diamond crystals.–Long-Wei Yin, Mu-Sen Li, Jian-Jun Cui, Bin Xu, Jian-Hong Gong, Zhao-Yin Hao, and Jiong-Fa Zhang; **16**(11), 3023–3026(L).

Xu, Bing–Fabrication and characterization of microscale sandwich beams.–Francisco Arias, Paul J.A. Kenis, Bing Xu, Tao Deng, Olivier J.A. Schueller, George M. Whitesides, Yuki Sugimura, and Anthony G. Evans; **16**(2), 597–605.

Xu, Cailu–Aligned carbon nanotube growth under oxidative ambient.–Anyuan Cao, Xianfeng Zhang, Cailu Xu, Ji Liang, Dehai Wu, and Bingqing Wei; **16**(11), 3107–3110.

Xu, F.F.–Cubic silicon nitride embedded in amorphous silicon dioxide.–Ming Zhang, Hongliang He, F.F. Xu, T. Sekine, T. Kobayashi, and Y. Bando; **16**(8), 2179–2181(L).

Xu, Geng-fu–Microwave sintering of ZnO at ultra high heating rates.–Geng-fu Xu, Isabel K. Lloyd, Yuval Carmel, Tayo Olorunyolemi, Otto C. Wilson, Jr.; **16**(10), 2850–2858.

Xu, Guisheng–Domain configurations in relaxor ferroelectric single crystals $Pb(Mg_{1/3}Nb_{2/3})O_3$–$PbTiO_3$.–Guisheng Xu, Haosu Luo, Zhenyi Qi, Haiqing Xu, and Zhiwen Yin; **16**(4), 932–937.

Xu, Guo Qin–Third-order nonlinear optical response in PbS-coated CdS nanocomposites.–Bing Liu, Chwee Har Chew, Leong Ming Gan, Guo Qin Xu, Heping Li, Yee Loy Lam, Chan Hin Kam, and Wen Xiu Que; **16**(6), 1644–1650.

Xu, Haiqing–Domain configurations in relaxor ferroelectric single crystals $Pb(Mg_{1/3}Nb_{2/3})O_3$–$PbTiO_3$.–Guisheng Xu, Haosu Luo, Zhenyi Qi, Haiqing Xu, and Zhiwen Yin; **16**(4), 932–937.

Xu, J.M.–Preliminary study on alternating thienylene/phenylene copolymers functionalized with an electron-donating or -withdrawing group.–J.M. Xu, S.C. Ng, and H.S.O. Chan; **16**(5), 1235–1237(L).

Xu, Jun–Novel photoluminescence from hydrogenated amorphous carbon films prepared by using xylene source.–Jun Xu, Wei Li, Tianfu Ma, Zhifeng Li, Li Wang, and Kunji Chen; **16**(2), 325–328(L).

Xu, Shitao–Purification of single-walled carbon nanotubes synthesized by the hydrogen arc-discharge method.–Pengxiang Hou, Chang Liu, Yu Tong, Shitao Xu, Min Liu, and Huiming Cheng; **16**(9), 2526–2529.

Xu, Wei-Ping–Formation rule for Al-based ternary quasi-crystals: Example of Al–Ni–Fe decagonal phase.–Jian-Bing Qiang, De-He Wang, Cui-Min Bao, Ying-Min Wang, Wei-Ping Xu, Mei-Li Song, and Chuang Dong; **16**(9), 2653–2660.

Xu, Wentao–Gas flow effects on the structure and composition of $SiN_x/Si/SiN_x$ films prepared by radio-frequency magnetron sputtering.–Wentao Xu, Boquan Li, Toshiyuki Fujimoto, and Isao Kojima; **16**(1), 308–313.

Xu, Xue-Jun–Embedded-atom-method functions for the body-centered-cubic iron and hydrogen.–Mao Wen, Xue-Jun Xu, Seiji Fukuyama, and Kiyoshi Yokogawa; **16**(12), 3496–3502.

Xu, Y.–Analysis of interdiffusion of Dy, Nd, and Pr in Mg.–Y. Xu, L.S. Chumbley, G.A. Weigelt, and F.C. Laabs; **16**(11), 3287–3292.

Xu, Y.B.–Shear-activated indentation crack in GaAs single crystal.–Z.C. Li, L. Liu, L.L. He, Y.B. Xu, and X. Wu; **16**(10), 2845–2849.

Xu, Y.F.–Effects of pressure on the solidification of Al–Mn alloy.–Duanwei He, M. He, C.S. Kiminami, F.X. Zhang, Y.F. Xu, W.K. Wang, and K.H. Kuo; **16**(4), 910–913(L).

Xu, Yebin–Synthesis of $Ba_2Ti_9O_{20}$ via ethylenediaminetetraacetic acid precursor.–Yebin Xu, Yanyan He, and Liangbin Wang; **16**(4), 1195–1199.

Y

Yamamoto, Yoshinobu–Dependence of fracture stress on applied stress rate in a Yb_2O_3–SiO_2-doped hot-pressed silicon nitride ceramic.–Shuqi Guo, Naoto Hirosaki, Yoshinobu Yamamoto, Toshiyuki Nishimura, and Mamoru Mitomo; **16**(11), 3254–3261.

Yan, A-Ru–Magnetic properties, domain structure, and microstructure of anisotropic $SmCo_{6.5}Zr_{0.5}$ ribbons with C addition.–A-Ru Yan, Zhi-Gang Sun, Wen-Yong Zhang, Hong-Wei Zhang, and Bao-Gen Shen; **16**(3), 629–632(L).

Yan, Dong-Sheng–Nonepitaxial heterogeneous nucleation of α-sialon in the Ca-doped system.–Ya-Wen Li, Pei-Ling Wang, Wei-Wu Chen, Jing-Wei Feng, Yi-Bing Cheng, and Dong-Sheng Yan; **16**(2), 578–582.

Yang, C-Y.–Growth and characterization of conductive $SrRuO_3$ and $LaNiO_3$ multilayers on textured Ni tapes for high-J_c $YBa_2Cu_3O_{7-\delta}$ coated conductors.–T. Aytug, B.W. Kang, C. Cantoni, E.D. Specht, M. Paranthaman, A. Goyal, D.K. Christen, D.T. Verebelyi, J.Z. Wu, R.E. Ericson, C.L. Thomas, C-Y.Yang, and S.E. Babcock; **16**(9), 2661–2669.

Yang, Doo Young–Optimization of the annealing process for the (Ba,Sr)TiO_3 thin films grown by low-temperature (420 °C) metal-organic chemical vapor deposition.–Jaehoo Park, Cheol Seong Hwang, and Doo Young Yang; **16**(5), 1363–1371.

–Metalorganic chemical vapor deposition of very thin Pb(Zr,Ti)O_3 thin films at low temperatures for high-density ferroelectric memory applications.–Hye Ryoung Kim, Seehwa Jeong, Chung Bae Jeon, Oh Seong Kwon, Cheol Seong Hwang, Young Ki Han, Doo Young Yang, and Ki Young Oh; **16**(12), 3583–3591.

Yang, F.–Torsion and bending of micron-scaled structures.–A.C.M. Chong, F. Yang, D.C.C. Lam, and P. Tong; **16**(4), 1052–1058.

Yang, H.–Texture analysis of grain refinement in undercooled $Ni_{99.45}B_{0.55}$.–K.L. Lee, C.H. Shek, and H. Yang; **16**(5), 1434–1438.

Yang, Jian-Feng–Porosity and microstructure control of porous ceramics by partial hot pressing.–Jian-Feng Yang, Guo-Jun Zhang, and Tatsuki Ohji; **16**(7), 1916–1918.

Yang, Wang Yue–Site preference of alloying elements in Fe_3Al-based alloys.–Xiao Dong Ni, Nan Xian Chen, Jiang Shen, Zu Qing Sun, Wang Yue Yang; **16**(2), 344–351.

Yang, Zhi-qing–Effects of preparation processes on structure and magnetic properties of $Nd_2Fe_{14}B$/α–Fe-type nanocomposite magnets.–Bao-zhi Cui, X.K. Sun, L.Y. Xiong, Wei Liu, Zhi-dong Zhang, Zhi-qing Yang, Ai-min Wang, and Jiang-ning Deng; **16**(3), 709–715.

Yao, B.–Effect of pressure on the structure of Fe–N alloys formed by solid-state reaction.–B. Yao, L. Liu, S.E. Liu, X. Hu, and W.H. Su; **16**(9), 2583–2590.

Yao, Jian Nian–Fabrication of heteropolyoxometalate-based photochromic inorganic–organic nanocomposites.–Tie Rui Zhang, Wei Feng, Chun Yan Bao, Ran Lu, Xin Tong Zhang, Tie Jin Li, Ying Ying Zhao, and Jian Nian Yao; **16**(8), 2256–2263.

Yao, Jian-nian–Photocatalytic activity of TiO_2 prepared at low temperature by a photo-assisted sol-gel method.–Zi-sheng Guan, Xin-tong Zhang, Ying Ma, Ya-an Cao, Jian-nian Yao; **16**(4), 907–909(L).

–Effects of zinc(II) and iron(III) doping of titania films on their photoreactivity to decompose rhodamine B.–Ying Ma, Xin-tong Zhang, Zi-sheng Guan, Ya-an Cao, Jian-nian Yao; **16**(10), 2928–2933.

Yao, Lianzeng–Synthesis of nano-AgI arrays and their optical properties.–Yinhai Wang, Jimei Mo, Weili Cai, Lianzeng Yao, and Lide Zhang; **16**(4), 990–992.

Yao, N.–Deformation mechanisms in nacre.–R.Z. Wang, Z. Suo, A.G. Evans, N. Yao, and I.A. Aksay; **16**(9), 2485–2493.

Yao, Xi–Structure and dielectric properties of pyrochlore–fluorite biphase ceramics in the Bi_2O_3–ZnO–Nb_2O_5 system.–Hong Wang and Xi Yao; **16**(1), 83–87.

–Dielectric properties anomaly of (1–x)Pb($Ni_{1/3}Nb_{2/3}$)O_3–x$PbTiO_3$ ceramics near the morphotropic phase boundary.–Zhenrong Li, Liangying Zhang, and Xi Yao; **16**(3), 834–836.

Yao, Xin–Formation of Nd_{1+x} $(Ba_{1-y}Sr_y)_{2-x}$ $Cu_3O_{7\pm\delta}$ solid solutions by crystal pulling.–Xin Yao, E.A. Goodilin, Teruo Izumi, and Yuh Shiohara; **16**(2), 529–533.

–Preferential growth mechanism of $REBa_2Cu_3O_y$ (RE = Y, Nd) crystal on MgO substrate by liquid phase epitaxy.–Katsumi Nomura, Saburo Hoshi, Xin Yao, Kazuomi Kakimoto, Yuichi Nakamura, Teruo Izumi, and Yuh Shiohara; **16**(4), 979–989.

Yasuda, Eiichi–Effects of whisker content and dimensions on the *R*-curve behavior of an alumina matrix composite reinforced with silicon carbide whiskers.–Takashi Akatsu, Minoru Suzuki, Yasuhiro Tanabe, and Eiichi Yasuda; **16**(7), 1919–1927.

Ye, H.Q.–Metal/ceramic interface in an *in situ* synthesized Ti/TiC_P composite coating by laser processing.–R. Yu, S. Zhang, L.L. He, W.T. Wu, H.Q. Ye; **16**(1), 9–12(L).

Ye, Jinhua–Optical and structural properties of solid oxide photocatalyst Bi_2FeNbO_7.–Zhigang Zou, Jinhua Ye, and Hironori Arakawa; **16**(1), 35–37(L).

Ye, Z-G.–Ferroelectric $SrBi_2Ta_2O_9$ single-crystal growth and characterization.–B. Sih, J. Tang, M. Dong, and Z-G. Ye; **16**(6), 1726–1733.

Yeh, Chih-Yang–Sol-gel-derived photosensitive TiO_2 and Cu/TiO_2 using homogeneous hydrolysis technique.–Jeffrey C.S. Wu and Chih-Yang Yeh; **16**(2), 615–620.

Yeh, Jien-Wei–Damping behavior of *in situ* Al–(graphite, Al_4C_3) composites produced by reciprocating extrusion.–Hsu-Shen Chu, Kuo-Shung Liu, and Jien-Wei Yeh; **16**(5), 1372–1380.

Yi, Gyu-Chul–Metal-organic vapor phase epitaxial growth of high-quality ZnO films on Al_2O_3(00·1).–W.I. Park, S-J. An, Gyu-Chul Yi, and Hyun M. Jang; **16**(5), 1358–1362.

–Formation and characteristics of highly *c*-axis-oriented $Bi_{3.25}La_{0.75}Ti_3O_{12}$ thin films on SiO_2/Si(100) and Pt/Ti/SiO_2/Si(100) substrates.–Uong Chon, Hyun M. Jang, Sun-Hwa Lee, and Gyu-Chul Yi; **16**(11), 3124–3132.

Yin, Jie–Preparation and characterization of nanocrystalline PbSe in poly(acrylic acid-*co*-styrene).–Yangyang Sun, Xuefeng Qian, Jie Yin, Junchao Huang, Xiaodong Ma, and Zikang Zhu; **16**(10), 2922–2927.

Yin, Long-Wei–Electron microscopy of high-temperature and high-pressure as-grown diamond crystals.–Long-Wei Yin, Mu-Sen Li, Jian-Jun Cui, Bin Xu, Jian-Hong Gong, Zhao-Yin Hao, and Jiong-Fa Zhang; **16**(11), 3023–3026(L).

Yin, Xin–Growth, defects, and properties of $GdCa_3O(BO_3)_3$ and Nd:$GdCa_4O(BO_3)_3$ crystals.–Jiyang Wang, Xiaobo Hu, Xin Yin, Renbo Song, Jingqian Wei, Zongsu Shao, Yaogang Liu, Minhua Jiang, Yulian Tian, Jianhua Jiangm and Wanxia Huang; **16**(3), 790–796.

Yin, Zhiwen–Domain configurations in relaxor ferroelectric single crystals Pb($Mg_{1/3}Nb_{2/3}$)O_3–$PbTiO_3$.–Guisheng Xu, Haosu Luo, Zhenyi Qi, Haiqing Xu, Zhiwen Yin; **16**(4), 932–937.

–Twinning domain in 67Pb($Mg_{1/3}Nb_{2/3}$)O_3–33$PbTiO_3$ ferroelectric complex perovskite crystal grown by the Bridgman method.–Donglin Li, Pingchu Wang, Xiaoming Pan, Haosu Luo, Zhiwen Yin; **16**(5), 1252–1255(L).

Yizhou, Zhou–The healing of quenched crack in 1045 steel under electropulsing.–Zhou Yizhou, Zeng You, He Guanhu, and Zhou Benlian; **16**(1), 17–19(L).

Yokogawa, Kiyoshi–Embedded-atom-method functions for the body-centered-cubic iron and hydrogen.–Mao Wen, Xue-Jun Xu, Seiji Fukuyama, and Kiyoshi Yokogawa; **16**(12), 3496–3502.

Yokota, Toshio–Water-associated surface degradation of $CsLiB_6O_{10}$ crystal during harmonic generation in the ultraviolet region.–Yukihiro Morimoto, Shintaro Miyazawa, Yoshio Kagebayashi, Naoki Kitatochi, Toshio Yokota, and Jun Sakuma; **16**(7), 2082–2090.

Yoneoka, M.–Mechanical stress of the electrical performance of polycrystalline-silicon resistors.–N. Nakabayashi, H. Ohyama, E. Simoen, M. Ikegami, C. Claeys, K. Kobayashi, M. Yoneoka, and K. Miyahara; **16**(9), 2579–2582.

Yoo, Han-Ill–Electrical transport properties of single-crystalline Mn–Zn ferrous ferrite.–Yong-Chae Chung and Han-Ill Yoo; **16**(3), 774–777.

Yoo, J-B.–Chemical-vapor-deposition growth and characterization of epitaxial 3C–SiC films on SOI substrates with thin silicon top layers.–C.K. Moon, H.J. Song, J.K. Kim, J.H. Park, S.J. Jang, J-B. Yoo, H-R. Park, and Byung-Teak Lee; **16**(1), 24–27(L).

Yoon, Chang-Sun–Photoluminescence spectra of undoped and Sm^{3+}-doped $BaAl_2S_4$ and $BaAl_2Se_4$ single crystals.–Moon-Seog Jin, Choong-Il Lee, Chang-Sun Yoon, Chang-Dae Kim, Jae-Mo Goh, and Wha-Tek Kim; **16**(5), 1520–1524.

Yoon, Chulsoo–Synthesis of $Zn_{2-x}Mn_xSiO_4$ phosphors using a hydrothermal technique.–Chulsoo Yoon and Shinhoo Kang; **16**(4), 1210–1216.

Yoon, Jong-Hwan–Intrinsic microcrystalline silicon by postgrowth anneals.–Jong-Hwan Yoon; **16**(6), 1531–1534(L).

Yoon, Ki Hyun–Effect of bond valence on microwave dielectric properties of $(Pb_{1-x}Ca_x)(Mg_{0.33}Ta_{0.67})O_3$ ceramics.–Heung Soo Park, Ki Hyun Yoon, and Eung Soo Kim; **16**(3), 817–821.

Yoon, Seok Hyun–Experimental evidence for space charge segregation in Nb-doped $BaTiO_3$.–Seok Hyun Yoon and Hwan Kim; **16**(5), 1479–1486.

Yoon, Soon-Gil–Effect of hydrogen on true leakage current characteristics of $(Pb,La)(Zr,Ti)O_3$ thin-film capacitors with Pt- or Ir-based top electrodes.–Soon-Gil Yoon, Dwi Wicaksana, Dong-Joo Kim, Seung-Hyun Kim, and A.I. Kingon; **16**(4), 1185–1189.

Yoshida, A.–Carbonization behavior of polyimide film containing iron complex in relation to magnetic properties.–Y. Kaburagi, T. Toriyama, A. Yoshida, H. Wakabayashi, Y. Hishiyama, and M. Inagaki; **16**(2), 352–365.

Yoshida, Hidehiro–Transient creep in fine-grained polycrystalline Al_2O_3 with Lu^{3+} ion segregation at the grain boundaries.–Hidehiro Yoshida, Yuichi Ikuhara, and Taketo Sakuma; **16**(3), 716–720.

Yoshida, T.–Crystallography and structural evolution of $LiNbO_3$ and $LiNb_{1-x}Ta_xO_3$ films on sapphire prepared by high-rate thermal plasma spray chemical vapor deposition.–D.V. Shtansky, S.A. Kulinich, K. Terashima, T. Yoshida, and Y. Ikuhara; **16**(8), 2271–2279.

Yoshizumi, M.–Role of the primary phase particles during the peritectic solidification of Y-123 superconducting oxides.–M. Kambara, M. Yoshizumi, T. Umeda, K. Miyake, K. Murata, T. Izumi, and Y. Shiohara; **16**(8), 2229–2238.

You, Zeng–The healing of quenched crack in 1045 steel under electropulsing.–Zhou Yizhou, Zeng You, He Guanhu, and Zhou Benlian; **16**(1), 17–19(L).

Young, D.–Dielectric properties of oxide structures by a laser-based direct-writing method.–D. Young, H.D. Wu, R.C.Y. Auyeung, R. Modi, J. Fitz-Gerald, A. Pique, D.B. Chrisey, P. Atanassova, and T. Kodas; **16**(6), 1720–1725.

Yu, H.–Structure and the nonlinearity of lithium triborate studied by Raman and infrared reflectivity spectroscopy.–H.R. Xia, L.X. Li, H. Yu, S.M. Dong, J.Y. Wang, Q.M. Lu, C.Q. Ma, and X.N. Wang; **16**(12), 3464–3470.

Yu, R.–Metal/ceramic interface in an *in situ* synthesized Ti/TiC_p composite coating by laser processing.–R. Yu, S. Zhang, L.L. He, W.T. Wu, and H.Q. Ye; **16**(1), 9–12(L).

Yu, R.C.–Study of phase components of $La_{1.5}Ca_{1.5}Mn_2O_7$.–J.L. Zhu, R.C. Yu, F.Y. Li, C.Q. Jin, and Z. Zhang; **16**(7), 2027–2031.

Yu, S.C.M.–Two-dimensional simulation of mass transport in polymer removal from a powder injection molding compact by thermal debinding.–Ying Shengjie, Y.C. Lam, S.C.M. Yu, and K.C. Tam; **16**(8), 2436–2451.

Yu, Shan-Pu–Formation of intermetallic compounds at eutectic Sn–Zn–Al solder/Cu interface.–Shan-Pu Yu, Moo-Chin Wang, and Min-Hsiung Hon; **16**(1), 76–82.

Yu, Tao–Impacts of postannealing ambient atmospheres on $Pt/SrBi_{2.2}Ta_2O_9/Pt$ capacitors.–Ai-Dong Li, Tao Yu, Hui-Qin Ling, Di Wu, Zhi-Guo Liu, and Nai-Ben Ming; **16**(12), 3526–3535.

Yu, Wei-chao–Solvothermal route to Bi_2Se_4 nanorods at low temperature.–Yuan-fang Liu, Jing-hui Zeng, Wei-xin Zhang, Wei-chao Yu, Yi-tai Qian, Jin-bo Cao, and Wan-qun Zhang; **16**(12), 3361–3365.

Yu, Zhong Qing–Blue photoluminescent properties of pure nanostructured γ–Al_2O_3.–Zhong Qing Yu, Dao Chang, Cun Li, Ning Zhang, Yu Ying Feng, and You Yuan Dai; **16**(7), 1890–1893(L).

Yuan, R.Z.–High-temperature thermoelectric properties of *n*-type $Ba_yNi_xCo_{4-x}Sb_{12}$.–X.F. Tang, L.M. Zhang, R.Z. Yuan, L.D. Chen, T. Goto, T. Hirai, J.S. Dyck, W. Chen, and C. Uher; **16**(12), 3343–3346(L).

Yuan, Shengwen–Preparation and characterization of $CuInS_2$ nanorods and nanotubes from an elemental solvothermal reaction.–Yang Jiang, Yue Wu, Shengwen Yuan, Bo Xie, Shuyuan Zhang, and Yitai Qian; **16**(10), 2805–2809.

Z

Zabel, T.–Preparation, structure, and magnetic properties of cobalt nanoparticles in carbon fibers.–I. Bashmakov, V. Dorosinez, M. Lukashevich, A. Mazanik, T. Tihonova, T. Zabel, B. Wiedenhorst, and H. Micklitz; **16**(10), 2832–2835.

Zabinski, J.S.–Lubricity of zinc oxide thin films: Study of deposition parameters and Si as an additive.–J.J. Nainaparampil and J.S. Zabinski; **16**(12), 3423–3429.

Zanghi, Didier–Characterization of bond formation in SiC and Si_3N_4 implanted with Ti, Fe, and Co.–Didier Zanghi, Agnès Traverse, Sébastien Gautrot, and Odile Kaïtasov; **16**(2), 512–523.

Zangooie, S.–Infrared optical properties of aged porous GaAs.–S. Zangooie, M. Schubert, T.E. Tiwald, and J.A. Woollam; **16**(5), 1241–1244(L).

Zec, S.–Phase-transformation kinetics in triphasic cordierite gel.–R. Petrović, Dj. Janacković, S. Zec, S. Drmanić, and Lj. Kostić-Gvozdenović; **16**(2), 451–458.

Zeng, Jing-hui–Solvothermal route to Bi_2Se_4 nanorods at low temperature.–Yuan-fang Liu, Jing-hui Zeng, Wei-xin Zhang, Wei-chao Yu, Yi-tai Qian, Jin-bo Cao, and Wan-qun Zhang; **16**(12), 3361–3365.

Zeng, Kejun–Effect of oxygen on the reactions in the Si/Ta/Cu metallization system.–Tomi Laurila, Kejun Zeng, Jorma K. Kivilahti, Jyriki Molarius, and Ilkka Suni; **16**(10), 2939–2946.

Zexian, Cao–Ion energy dependence of film properties for diamond-like carbon prepared with plasma-assisted deposition.–Cao Zexian; **16**(11), 3034–3037(L).

Zhai, H.Y.–Growth mechanism of superconducting MgB_2 films prepared by various methods.–H.Y. Zhai, H.M. Christen, L. Zhang, M. Paranthaman, C. Cantoni, B.C. Sales, P.H. Fleming, D.K. Christen, and D.H. Lowndes; **16**(10), 2759–2762(L).

Zhan, Guo-Dong–Preferred orientation of beta-phase and its mechanisms in a fine-grained silicon-nitride-based ceramic.–Rong-Jun Xie, Mamoru Mitomo, Wonjoong Kim, Young-Wook Kim, Guo-Dong Zhan; **16**(2), 590–596.

–Transmission electron microscopy observation in a liquid-phase-sintered SiC with oxynitride glass.–Guo-Dong Zhan, Mamoru Mitomo, Young-Wook Kim, Rong-Jun Xie, and Amiya K. Mukherjee; **16**(8), 2189–2191(L).

Zhang, F.X.–Effects of pressure on the solidification of Al–Mn alloy.–Duanwei He, M. He, C.S. Kiminami, F.X. Zhang, Y.F. Xu, W.K. Wang, and K.H. Kuo; **16**(4), 910–913(L).

Zhang, Guo-Jun–Porosity and microstructure control of porous ceramics by partial hot pressing.–Jian-Feng Yang, Guo-Jun Zhang, and Tatsuki Ohji; **16**(7), 1916–1918.

Zhang, H.–Study of the mechanism for controlled crystallization of BaF_2 under two kinds of monolayers.–L. Lu, H. Cui, W. Li, H. Zhang, and S. Xi; **16**(8), 2415–2420.

Zhang, H.F.–Preparation of superfine Fe-base alloy by liquidus casting.–X.F. Pan, H.F. Zhang, A.M. Wang, B.Z. Ding, and Z.Q. Hu; **16**(12), 3459–3463.

Zhang, H.X.–Preparation and characterization of nanocrystalline potassium lithium niobate powders and films.–H.X. Zhang, C.H. Kam, Y. Zhou, X.Q. Han, S.D. Cheng, C.Y. Chan, and Y.L. Lam; **16**(12), 3609–3613.

Zhang, Hong-Wei–Magnetic properties, domain structure, and microstructure of anisotropic $SmCo_{6.5}Zr_{0.5}$ ribbons with C addition.–A-Ru Yan, Zhi-Gang Sun, Wen-Yong Zhang, Hong-Wei Zhang, and Bao-Gen Shen; **16**(3), 629–632(L).

Zhang, Jiong-Fa–Electron microscopy of high-temperature and high-pressure as-grown diamond crystals.–Long-Wei Yin, Mu-Sen Li, Jian-Jun Cui, Bin Xu, Jian-Hong Gong, Zhao-Yin Hao, and Jiong-Fa Zhang; **16**(11), 3023–3026(L).

Zhang, L.–Growth mechanism of superconducting MgB_2 films prepared by various methods.–H.Y. Zhai, H.M. Christen, L. Zhang, M. Paranthaman, C. Cantoni, B.C. Sales, P.H. Fleming, D.K. Christen, and D.H. Lowndes; **16**(10), 2759–2762(L).

–Origin of the anomalous volume expansion in Al–Si alloys above liquidus.–W.M. Wang, X.F. Bian, H.R. Wang, Zhen Wang, L. Zhang, Z.G. Liu, and J-M. Liu; **16**(12), 3592–3598.

Zhang, L.D.–Fabrication, characterization, and photoluminescence properties of highly ordered TiO_2 nanowire arrays.–Y. Lei and L.D. Zhang; **16**(4), 1138–1144.

Zhang, L.M.–High-temperature thermoelectric properties of *n*-type $Ba_yNi_xCo_{4-x}Sb_{12}$.–X.F. Tang, L.M. Zhang, R.Z. Yuan, L.D. Chen, T. Goto, T. Hirai, J.S. Dyck, W. Chen, and C. Uher; **16**(12), 3343–3346(L).

Zhang, Liangying–Dielectric properties anomaly of $(1-x)Pb(Ni_{1/3}Nb_{2/3})O_3$–$xPbTiO_3$ ceramics near the morphotropic phase boundary.–Zhenrong Li, Liangying Zhang, and Xi Yao; **16**(3), 834–836.

Zhang, Lide–Precipitation of multilayered core–shell TiO_2 composite nanoparticles onto polymer layers.–Mingtai Wang and Lide Zhang; **16**(3), 765–773.

–Synthesis of nano-AgI arrays and their optical properties.–Yinhai Wang, Jimei Mo, Weili Cai, Lianzeng Yao, Lide Zhang; **16**(4), 990–992.

Zhang, Ming–Synthesis of coaxial nanotubes: Titanium oxide sheathed with silicon oxide.–Ming Zhang, Y. Bando, and K. Wada; **16**(5), 1408–1412.

–Cubic silicon nitride embedded in amorphous silicon dioxide.–Ming Zhang, Hongliang He, F.F. Xu, T. Sekine, T. Kobayashi, and Y. Bando; **16**(8), 2179–2181(L).

–Elastic constants of polycrystalline Al and TiN calculated by an *ab initio* method within the local-density approximation.–Ming Zhang, Jiang Shen, and Jiawen He; **16**(8), 2293–2297.

Zhang, Ning–Blue photoluminescent properties of pure nanostructured γ–Al_2O_3.–Zhong Qing Yu, Dao Chang, Cun Li, Ning Zhang, Yu Ying Feng, and You Yuan Dai; **16**(7), 1890–1893(L).

Zhang, Qingling–Direct measurement of plowing friction and wear of a polymer thin film using the atomic force microscope.–Binyang Du, Mark R. VanLandingham, Qingling Zhang, and Tianbai He; **16**(5), 1487–1492.

Zhang, S.–Metal/ceramic interface in an *in situ* synthesized Ti/TiC_P composite coating by laser processing.–R. Yu, S. Zhang, L.L. He, W.T. Wu, and H.Q. Ye; **16**(1), 9–12(L).

Zhang, Shuyuan–Preparation and characterization of $CuInS_2$ nanorods and nanotubes from an elemental solvothermal reaction.–Yang Jiang, Yue Wu, Shengwen Yuan, Bo Xie, Shuyuan Zhang, and Yitai Qian; **16**(10), 2805–2809.

Zhang, T.–Formation of icosahedral quasicrystal by crystallization of $Zr_{70}(Ni, Cu, Pd)_{30}$ amorphous alloys.–T. Zhang, A. Inoue, M. Matsushita, and J. Saida; **16**(1), 20–23(L).

–Formation and mechanical properties of Cu–Hf–Ti bulk glassy alloys.–Akihisa Inoue, Wei Zhang, Tao Zhang, and Kei Kurosaka; **16**(10), 2836–2844.

Zhang, T.S.–$Pb(Zr_xTi_{1-x})O_3$ ceramics via reactive sintering of partially reacted mixture produced by a high-energy ball milling process.–L.B. Kong, J. Ma, T.S. Zhang, W. Zhu, and O.K. Tan; **16**(6), 1636–1643.

Zhang, Tie Rui–Fabrication of heteropolyoxometalate-based photochromic inorganic–organic nanocomposites.–Tie Rui Zhang, Wei Feng, Chun Yan Bao, Ran Lu, Xin Tong Zhang, Tie Jin Li, Ying Ying Zhao, and Jian Nian Yao; **16**(8), 2256–2263.

Zhang, W.J.–Raman scattering of cubic boron nitride films deposited from the iow-pressure gas phase.–W.J. Zhang and S. Matsumoto; **16**(12), 3430–3442.

Zhang, Wan-qun–Solvothermal route to Bi_3Se_4 nanorods at low temperature.–Yuan-fang Liu, Jing-hui Zeng, Wei-xin Zhang, Wei-chao Yu, Yi-tai Qian, Jin-bo Cao, and Wan-qun Zhang; **16**(12), 3361–3365.

Zhang, Wei–Formation and mechanical properties of Cu–Hf–Ti bulk glassy alloys.–Akihisa Inoue, Wei Zhang, Tao Zhang, and Kei Kurosaka; **16**(10), 2836–2844.

Zhang, Wei-xin–Solvothermal route to Bi_3Se_4 nanorods at low temperature.–Yuan-fang Liu, Jing-hui Zeng, Wei-xin Zhang, Wei-chao Yu, Yi-tai Qian, Jin-bo Cao, and Wan-qun Zhang; **16**(12), 3361–3365.

Zhang, Wen-Yong–Magnetic properties, domain structure, and microstructure of anisotropic $SmCo_{6.5}Zr_{0.5}$ ribbons with C addition.–A-Ru Yan, Zhi-Gang Sun, Wen-Yong Zhang, Hong-Wei Zhang, and Bao-Gen Shen; **16**(3), 629–632(L).

Zhang, X.–Mechanical properties of nanocrystalline and epitaxial TiN films on (100) silicon.–H. Wang, A. Sharma, A. Kvit, Q. Wei, X. Zhang, C.C. Koch, and J. Narayan; **16**(9), 2733–2738.

–Novel synthesis of AlN nanowires with controlled diameters.–Jun Liu, X. Zhang, Yingjiu Zhang, Rongrui He, and Jing Zhu; **16**(11), 3133–3138.

Zhang, Xianfeng–Aligned carbon nanotube growth under oxidative ambient.–Anyuan Cao, Xianfeng Zhang, Cailu Xu, Ji Liang, Dehai Wu, and Bingqing Wei; **16**(11), 3107–3110.

Zhang, Xiaoling–Fretting wear rate of sulphur deficient MoS_x coatings based on dissipated energy.–Xiaoling Zhang, W. Lauwerens, L. Stals, Jiawen He, and J-P. Celis; **16**(12), 3567–3574.

Zhang, Xinghang–Origins of stored enthalpy in cryomilled nanocrystalline Zn.–Xinghang Zhang, Haiyan Wang, Magdy Kassem, Jagdish Narayan, and Carl C. Koch; **16**(12), 3485–3495.

Zhang, Xin-tong–Photocatalytic activity of TiO_2 prepared at low temperature by a photo-assisted sol-gel method.–Zi-sheng Guan, Xin-tong Zhang, Ying Ma, Ya-an Cao, and Jian-nian Yao; **16**(4), 907–909(L).

–Fabrication of heteropolyoxometalate-based photochromic inorganic–organic nanocomposites.–Tie Rui Zhang, Wei Feng, Chun Yan Bao, Ran Lu, Xin Tong Zhang, Tie Jin Li, Ying Ying Zhao, and Jian Nian Yao; **16**(8), 2256–2263.

–Effects of zinc(II) and iron(III) doping of titania films on their photoreactivity to decompose rhodamine B.–Ying Ma, Xin-tong Zhang, Zi-sheng Guan, Ya-an Cao, and Jian-nian Yao; **16**(10), 2928–2933.

Zhang, Yingjiu–Novel synthesis of AlN nanowires with controlled diameters.–Jun Liu, X. Zhang, Yingjiu Zhang, Rongrui He, and Jing Zhu; **16**(11), 3133–3138.

Zhang, Yong–Formation and properties of $Zr_{48}Nb_8Fe_8Cu_{12}Be_{24}$ bulk metallic glass.–Yong Zhang, D.Q. Zhao, B.C. Wei, P. Wen, M.X. Pan, and W.H. Wang; **16**(6), 1675–1679.

Zhang, Z.–Synthesis and characterization of antimony oxide nanoparticles.–Zaoli Zhang, Lin Guo, and Wendong Wang; **16**(3), 803–805.

–Study of phase components of $La_{1.5}Ca_{1.5}Mn_2O_7$.–J.L. Zhu, R.C. Yu, F.Y. Li, C.Q. Jin, Z. Zhang; **16**(7), 2027–2031.

Zhang, Z.D.–Synthesis of $Nd_2Fe_{14}B$ powders by spray-drying and reduction–diffusion processes.–X.L. Dong, B.K. Kim, C.J. Choi, K.S. Park, Z.D. Zhang; **16**(4), 1083–1089.

Zhang, Zhen Rong–Plate domain structure of sintered NdFeB magnets and dependence on compacting mode.–Zhen Rong Zhang, Bao Shan Han, Ye Qing He, and Shou Zeng Zhou; **16**(10), 2992–2995.

Zhang, Zhi-dong–Effects of preparation processes on structure and magnetic properties of $Nd_2Fe_{14}B/\alpha$–Fe-type nanocomposite magnets.–Bao-zhi Cui, X.K. Sun, L.Y. Xiong, Wei Liu, Zhi-dong Zhang, Zhi-qing Yang, Ai-min Wang, and Jiang-ning Deng; **16**(3), 709–715.

Zhao, D.Q.–Formation and properties of $Zr_{48}Nb_8Fe_8Cu_{12}Be_{24}$ bulk metallic glass.–Yong Zhang, D.Q. Zhao, B.C. Wei, P. Wen, M.X. Pan, and W.H. Wang; **16**(6), 1675–1679.

Zhao, Hong–Cracking of porcelain coatings bonded to metal substrates of different modulus and hardness.–Hong Zhao, Xiaozhi Hu, Mark B. Bush, and Brian R. Lawn; **16**(5), 1471–1478.

Zhao, Ji-Cheng–A combinatorial approach for efficient mapping of phase diagrams and properties.–Ji-Cheng Zhao; **16**(6), 1565–1578.

Zhao, M.–Comparison of different models for melting point change of metallic nanocrystals.–M. Zhao, X.H. Zhou, and Q. Jiang; **16**(11), 3304–3308.

Zhao, Q.–Combined out-of-plane and in-plane texture control in thin films using ion beam assisted deposition.–L. Dong, D.J. Srolovitz, G.S. Was, Q. Zhao, and A.D. Rollett; **16**(1), 210–216.

Zhao, Ying Ying–Fabrication of heteropolyoxometalate-based photochromic inorganic–organic nanocomposites.–Tie Rui Zhang, Wei Feng, Chun Yan Bao, Ran Lu, Xin Tong Zhang, Tie Jin Li, Ying Ying Zhao, and Jian Nian Yao; **16**(8), 2256–2263.

Zheng, Fen–Enhanced crystallization and phase transformation of amorphous silicon nitride under high pressure.–Ya-Li Li, Yong Liang, Fen Zheng, Xian-Feng Ma, Suo-Jing Cui, and Liling Sun; **16**(1), 67–75.

Zheng, X.H.–Structural and dielectric characterization of $Ba_4Nd_2Ti_{4+x}Ta_{6-x}O_{30-x/2}$ nonstoichiometric ceramics.–X.M. Chen, X.H. Zheng, and J. Wang; **16**(10), 2859–2863.

Zhou, F.–High grain size stability of nanocrystalline Al prepared by mechanical attrition.–F. Zhou, J. Lee, S. Dallek, and E.J. Lavernia; **16**(12), 3451–3458.

Zhou, H.–Characterization of GaN grown on sapphire by laser-induced molecular beam epitaxy.–H. Zhou, A. Rühm, N.Y. Jin-Phillipp, F. Phillipp, M. Gross, and H. Schröder; **16**(1), 261–267.

–Microstructure and formation mechanism of combustion-synthesized rodlike Ca α-sialon crystals.–Kexin Chen, Haibo Jin, M. Oliveira, Heping Zhou, and J.M.F. Ferreira; **16**(7), 1928–1934.

Zhou, H.H.–Effect of a magnetic field on phase transformation of steel.–W. Liu, D.R. Ou, H.H. Zhou, G.Y. Tang, and F. Wu; **16**(8), 2280–2282.

Zhou, Shou Zeng–Plate domain structure of sintered NdFeB magnets and dependence on compacting mode.–Zhen Rong Zhang, Bao Shan Han, Ye Qing He, and Shou Zeng Zhou; **16**(10), 2992–2995.

Zhou, W.Y.–Synthesis of α–SiO_2 nanowires using Au nanoparticle catalysts on a silicon substrate.–Z.Q. Liu, S.S. Xie, L.F. Sun, D.S. Tang, W.Y. Zhou, C.Y. Wang, W. Liu, Y.B. Li, X.P. Zou, and G. Wang; **16**(3), 683–686.

Zhou, X.H.–Comparison of different models for melting point change of metallic nanocrystals.–M. Zhao, X.H. Zhou, and Q. Jiang; **16**(11), 3304–3308.

Zhou, Y.–$L1_2$- and $L1_0$-like cation-ordered structures in ZrO_2–Y_2O_3 ceramics.–J.C. Rao, Y. Zhou, and D.X. Li; **16**(6), 1806–1813.

–Preparation and characterization of nanocrystalline potassium lithium niobate powders and films.–H.X. Zhang, C.H. Kam, Y. Zhou, X.Q. Han, S.D. Cheng, C.Y. Chan, and Y.L. Lam; **16**(12), 3609–3613.

Zhou, Ying–Investigation of optical waveguide formed in Er:Yb: phosphate glass by MeV He^+ implantation.–Zhuang Zhuo, Edwin Yue Bun Pun, Sun Fat Wong, and Ying Zhou; **16**(4), 1135–1137.

Zhu, Hongmin–Synthesis of nanoscale particles of Ta and Nb_3Al by homogeneous reduction in liquid ammonia.–Hongmin Zhu and Donald R. Sadoway; **16**(9), 2544–2549.

Zhu, J.L.–Study of phase components of $La_{1.5}Ca_{1.5}Mn_2O_7$.–J.L. Zhu, R.C. Yu, F.Y. Li, C.Q. Jin, and Z. Zhang; **16**(7), 2027–2031.

Zhu, Jing–Novel synthesis of AlN nanowires with controlled diameters.–Jun Liu, X. Zhang, Yingjiu Zhang, Rongrui He and Jing Zhu; **16**(11), 3133–3138.

Zhu, Tao–Processing- and composition-dependent characteristics of chemical solution deposited $Bi_{4-x}La_xTi_3O_{12}$ thin films.–Di Wu, Aidong Li, Tao Zhu, Zhifeng Li, Zhiguo Liu, and Naiben Ming; **16**(5), 1325–1332.

Zhu, W.–$Pb(Zr_xTi_{1-x})O_3$ ceramics via reactive sintering of partially reacted mixture produced by a high-energy ball milling process.–L.B. Kong, J. Ma, T.S. Zhang, W. Zhu, and O.K. Tan; **16**(6), 1636–1643.

Zhu, Y.–Nucleation and growth of $YBa_2Cu_3O_x$ on $SrTiO_3$ and CeO_2 by a BaF_2 postdeposition reaction process.–L. Wu, Y. Zhu, V.F. Solovyov, H.J. Wiesmann, A.R. Moodenbaugh, R.L. Sabatini, and M. Suenaga; **16**(10), 2869–2884.

Zhu, Yuntian T.–Structure and phase characteristics of amorphous boron–carbon–nitrogen under high pressure and high temperature.–Jianyu Huang, Yuntian T. Zhu, and Hirotaro Mori; **16**(4), 1178–1184.

Zhu, Zikang–Preparation and characterization of nanocrystalline PbSe in poly(acrylic acid-*co*-styrene).–Yangyang Sun, Xuefeng Qian, Jie Yin, Junchao Huang, Xiaodong Ma, and Zikang Zhu; **16**(10), 2922–2927.

Zhuo, Zhuang–Investigation of optical waveguide formed in Er:Yb: phosphate glass by MeV He^+ implantation.–Zhuang Zhuo, Edwin Yue Bun Pun, Sun Fat Wong, and Ying Zhou; **16**(4), 1135–1137.

Zimmermann, André–Anelastic behavior of precursor-derived amorphous ceramics in the system Si–B–C–N.–Martin Christ, André Zimmermann, and Fritz Aldinger; **16**(7), 1994–1997.

Zou, X.P.–Synthesis of α–SiO_2 nanowires using Au nanoparticle catalysts on a silicon substrate.–Z.Q. Liu, S.S. Xie, L.F. Sun, D.S. Tang, W.Y. Zhou, C.Y. Wang, W. Liu, Y.B. Li, X.P. Zou, and G. Wang; **16**(3), 683–686.

Zou, Zhigang–Optical and structural properties of solid oxide photocatalyst Bi_2FeNbO_7.–Zhigang Zou, Jinhua Ye, and Hironori Arakawa; **16**(1), 35–37(L).

Zuhr, R.A.–Nanocrystals in crystalline silicon: Void formation and hollow particles.–A. Meldrum, S. Honda, C.W. White, R.A. Zuhr, and L.A. Boatner; **16**(9), 2670–2679.

Zuo, J.M.–Microstructure of $La_{1-x}Ca_xMnO_3$ studied by transmission electron microscopy.–Q. Chen, J. Tao, J.M. Zuo, and J.C.H. Spence; **16**(10), 2959–2965.
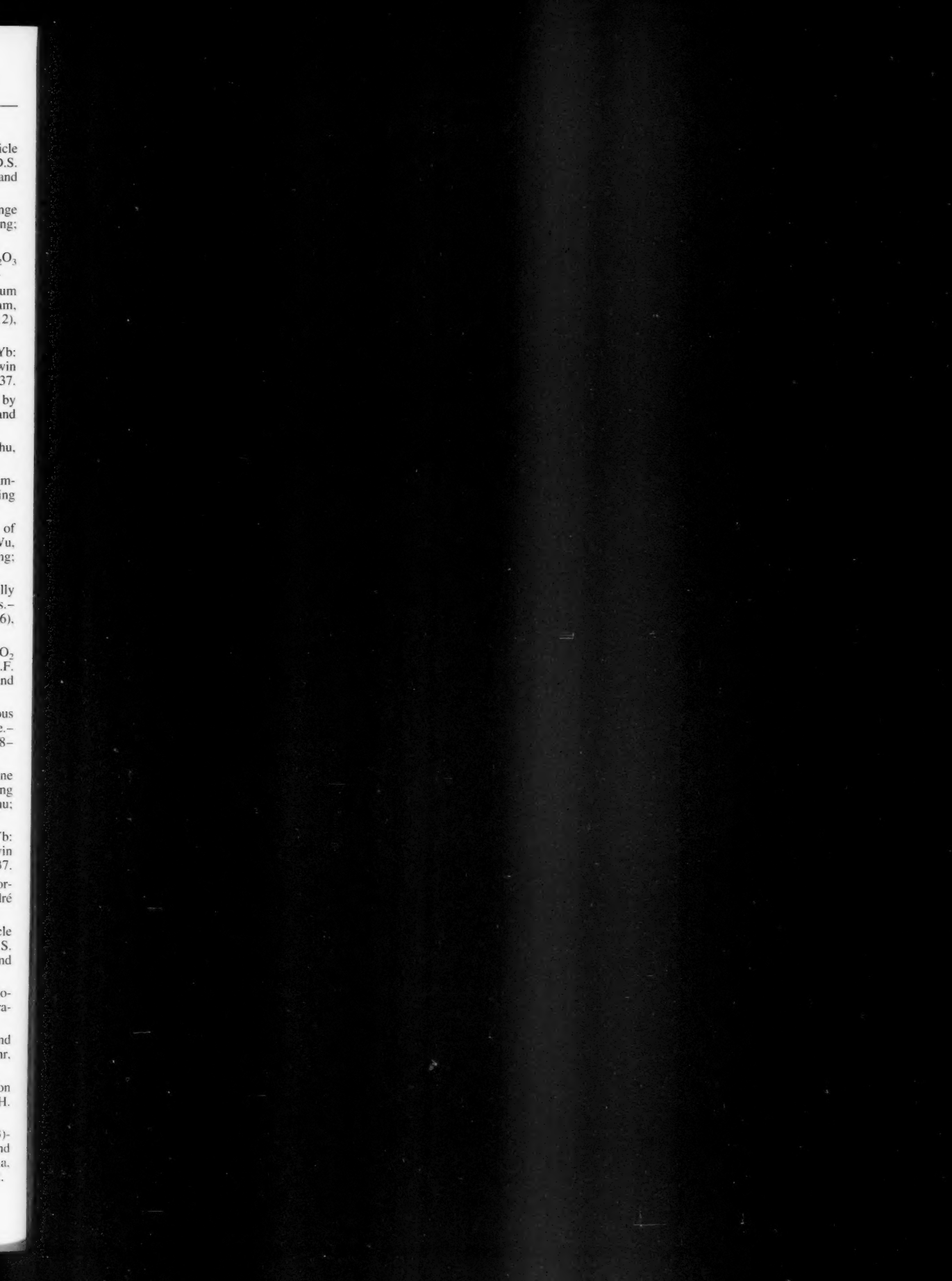
Zurbuchen, M.A.–Transmission electron microscopy study of (103)-oriented epitaxial $SrBi_2Nb_2O_9$ films grown on (111) $SrTiO_3$ and (111) $SrRuO_3$/(111) $SrTiO_3$.–M.A. Zurbuchen, J. Lettieri, Y. Jia, D.G. Schlom, S.K. Streiffer, and M.E. Hawley; **16**(2), 489–502.